Instituto de Catálisis y Petroleoquímica (CSIC)
Universidad Autónoma de Madrid
(Departamento de Biología Molecular)

TESIS DOCTORAL

Evolución Dirigida de la Peroxidasa Versátil para el Diseño de una Levadura de Podredumbre Blanca

---

David González Pérez

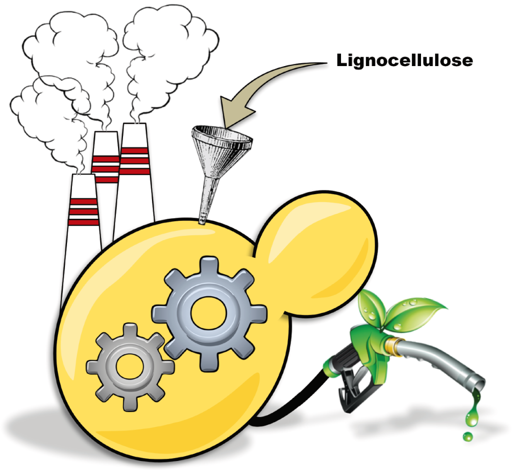

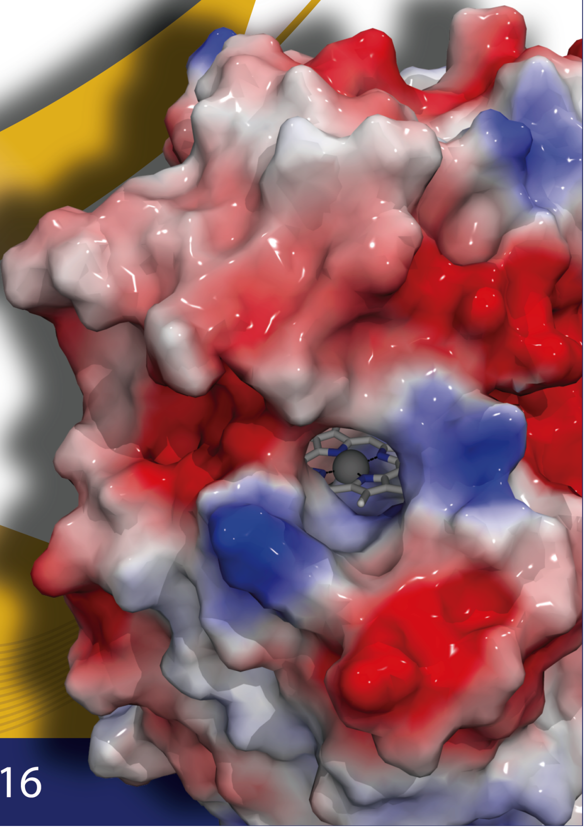

Madrid, 2016

Universidad Autónoma de Madrid
Facultad de Ciencias, Departamento de Biología Molecular

EVOLUCIÓN DIRIGIDA DE LA PEROXIDASA VERSÁTIL PARA EL DISEÑO DE UNA LEVADURA DE PODREDUMBRE BLANCA

MEMORIA

Para optar al grado de Doctor en Bioquímica, Biología Molecular, Biomedicina y Biotecnología (Biociencias Moleculares) por la Universidad Autónoma de Madrid.

Presentada por:

DAVID GONZÁLEZ PÉREZ

Madrid, 2016

EVOLUCIÓN DIRIGIDA DE LA PEROXIDASA VERSÁTIL PARA EL DISEÑO DE UNA LEVADURA DE PODREDUMBRE BLANCA

MEMORIA

Para optar al grado de Doctor en Bioquímica, Biología Molecular, Biomedicina y Biotecnología (Biociencias Moleculares) por la Universidad Autónoma de Madrid.

Presentada por:

DAVID GONZÁLEZ PÉREZ

Director de Tesis:

Dr. Miguel Alcalde Galeote
Instituto de Catálisis y Petroleoquímica
Departamento de Biocatálisis
Consejo Superior de Investigaciones Científicas, Madrid

ICP
INSTITUTO DE CATÁLISIS Y PETROLEOQUÍMICA

CSIC
CONSEJO SUPERIOR DE INVESTIGACIONES CIENTÍFICAS

Tutora académica:
Dra. María Fernández Lobato
Universidad Autónoma de Madrid
Facultad de Ciencias, Departamento de Biología Molecular

UAM
UNIVERSIDAD AUTONOMA
DE MADRID

Madrid, 2016

ICP
INSTITUTO DE CATÁLISIS Y PETROLEOQUÍMICA

CSIC
CONSEJO SUPERIOR DE INVESTIGACIONES CIENTÍFICAS

Miguel Alcalde Galeote, en calidad de Dr. en Ciencias Biológicas, Investigador Científico del CSIC

CERTIFICA:

Que el presente trabajo "*Evolución dirigida de la peroxidasa versátil para el diseño de una levadura de podredumbre blanca*" constituye la Memoria que presenta el Licenciado en Bioquímica por la Universidad Autónoma de Madrid, David González Pérez, para optar al grado de Doctor, y que ha sido realizado bajo su dirección en el departamento de Biocatálisis del Instituto de Catálisis y Petroleoquímica del CSIC, Campus de Excelencia Internacional UAM + CSIC, Madrid.

Y para que conste, firma el presente certificado en Madrid, a 15 de Octubre de 2016.

Dr. Miguel Alcalde Galeote

A mis padres
A mi familia
A Carina

“*Most of innovations are not obvious to other people at the time. You have to believe in yourself. If you’ve got a good idea, follow it even when others say it’s not*”

- Frances H. Arnold -
Directed Evolution of Enzymes

AGRADECIMIENTOS

Como dice un proverbio hebreo: "*El que da, no debe volver a acordarse; pero el que recibe nunca debe olvidar*". Es por esto por lo que me gustaría agradecer a todas las personas, instituciones, organismos y servicios que han contribuido en mayor o menor medida en la realización de la presente Tesis Doctoral desarrollada en el Departamento de Biocatálisis del Instituto de Catálisis y Petroleoquímica del CSIC.

En primer lugar me gustaría agradecer la financiación recibida a través de proyectos nacionales e internacionales que me han permitido llevar a cabo el trabajo de esta Tesis Doctoral. En particular, a los proyectos europeos "*Novel and more robust fungal peroxidases as industrial biocatalysts*" (Peroxicats - http://www.peroxicats.org/ - ; Ref: FP7-KBBE-2010-4-265337), "*Optimized oxidoreductases for medium and large scale industrial biotransformations*" (Indox - http://www.indoxproject.eu -; Ref: FP7-KBBE-2013-7-613549) ; así como a los proyectos nacionales "*Evolución molecular dirigida de factorías celulares ligninolíticas en Saccharomyces cerevisiae. Aplicaciones medioambientales, industriales y energéticas*" (Evofacel; Ref: BIO2010-19697) y "*Evolución dirigida de oxidoreductasas ligninolíticas modernas y ancestrales para el diseño de una levadura de podredumbre blanca*" (Dewry; Ref: BIO2013-43407-R).

También quisiera agradecer el apoyo económico del programa "*Short-Term Scientific Missions (STSMs)*", perteneciente a la red Europea COST (http://www.cost.eu/), por financiar parcialmente mi estancia de 3 meses en la Universidad de Sheffield (Reino Unido), concretamente en el laboratorio del Dr. Tuck Seng Wong. Asimismo, también quiero agradecer el apoyo de las acciones de esta red Europea dedicadas a la formación de jóvenes investigadores que he tenido la oportunidad de disfrutar en numerosos simposios y escuelas de verano ("*Cascade Chemo-Enzymatic Processes: new synergies between chemistry and biochemistry (CASCAT)*", Ref: CM0701. *COST Action* (*European Cooperation in the Field of Scientific and Technical Research*) y "*Systems Biocatalysis*", Ref: CM1303. *COST Action* (*European Cooperation in the Field of Scientific and Technical Research*). Quiero agradecer también al Instituto de Catálisis y Petroleoquímica del CSIC, y a la Universidad Autónoma de Madrid (UAM), por proporcionarme el apoyo administrativo e infraestructuras necesarias para el desarrollo de la Tesis.

El capital humano ha sido a mi entender, el factor más importante a la hora de la realización de la Tesis Doctoral. Por ello, me gustaría agradecer a todas las personas que han contribuido en diferentes aspectos al desarrollo de este trabajo.

Al Dr. Miguel Alcalde, mi director de Tesis y amigo. Muchas gracias por la gran confianza que has depositado en mí en todo momento durante estos 6 años, por haber sido mi referencia a seguir, por saber exprimir mis ganas de hacer ciencia y por enseñarme a ser exigente conmigo mismo. Gracias también por demostrarme que se pueden hacer presentaciones serias, incluso haciendo guiños de Star Wars para relajar el ambiente.

A la Dra. María Fernández, mi cotutora de Tesis y antigua supervisora. Muchas gracias por aceptarme en tu grupo de investigación y permitirme comenzar mi carrera investigadora en tu laboratorio. Gracias por tu apoyo incondicional a lo largo de todos estos años de amistad.

Al Dr. Francisco Plou, gran científico y amante de la literatura científica. Muchas gracias por contar conmigo para ayudarte en tu labor divulgativa, y por las numerosas charlas científicas que tanto me han ayudado durante la Tesis. Espero que tu libro *"¿Qué sabemos de? Las enzimas"*, del que me invitaste a formar parte, sea todo un *best seller* muy pronto.

Al Dr. Antonio Ballesteros, por su gran experiencia investigadora y paciencia. Muchas gracias por tu ayuda y consejo científico durante el desarrollo de la Tesis, especialmente durante la etapa de escritura ayudándome a gestionar los detalles más difíciles con lo que lidiar.

A los Dres. Ángel Martínez y Francisco Javier Ruiz, ambos del CIB (Centro de Investigaciones Biológicas del CSIC). Al Dr. Ángel Martínez, por ser el coordinador de los proyectos europeos en los que me he visto inmerso, por darme su apoyo científico y por contribuir a mejorar la calidad de mis artículos. Al Dr. Francisco Javier Ruiz, por su ayuda técnica a la hora de realizar experimentos y por sus consejos que tanto me han valido a la hora de entender la difícil VP.

To Dr. Tuck Seng Wong, from University of Sheffield (UK). Thank you for accepting me in your research group, thank you for giving me the opportunity to have one of the best experiences in my life, and teaching me how to make good science with positive attitude. I really had a good time during my stay in your research group. In addition, I would like to thank Dr. Kang Lang, Abdu, Yomi, Miriam, Pawel, Inas, Zaki, James and Hosam. Thanks everybody!, you made me feel like if I were at home… I could not be happier during my stay at CBE. Special thanks to Abdu, who spent a lot of time showing me how to eat food from many different countries, it was yummy!. Finally, I would like to thank the friendly people from my office there: Tomas, Esther, Mariona, Anne, Casia, Dave, etc…

Es importante resaltar que todo esto no hubiera sido posible sin la inestimable colaboración de todos y cada uno de mis compañeros de laboratorio, que tan amena me han hecho esta etapa. Eva, Diana, Patri, Alina, Javi, Berni, Xavi, Ivan, Isa, Pati, Luci, Paloma y Noa. Muchas gracias a todos por haberme hecho sentir tan bien y orgulloso de estar en un grupo tan unido pudiendo hacer buena ciencia al mismo tiempo. A Eva, por su tiempo y dedicación aun cuando yo no sabía lo que era una VP, por su alegría y motivación a la hora de enseñar. A Diana, por su ayuda y apoyo incondicional, por animarme y por mostrarme el apasionante mundo de las lacasas con todos sus buenos momentos. A Patri, por todo lo que me ha ayudado en nuestra labor conjunta como *lab managers*, por enseñarme que no se puede hacer una miniprep en 30 minutos, y por toda su ayuda y apoyo a lo largo de la Tesis. A Alina, por haberme ayudado en los inicios de esta Tesis, y por su alegría. A Javi y Berni, el dúo perfecto que hizo mucho más divertido el trabajo en el laboratorio haciéndonos reír con sus bromas, ¡sois los mejores!. Al Xaba, por ser mí joven padawan y ayudarme a desarrollar las ideas locas que me surgen en el laboratorio. A Ivan, por su amabilidad y estar siempre dispuesto a colaborar, y por enseñarme palabras en el difícil lenguaje croata. A Isa, por enseñarme que se puede ser fuerte en ciencia y nunca rendirse; ¡tú siempre has sido una Wisinner!. A Pati, por su positivismo y alegría en el laboratorio, por creer siempre en mí cuando me has pedido consejo. A Luci, gracias por ser mi compi de oficina y estar siempre dispuesta a ayudarme. A Paloma, gracias por estar siempre dispuesta a ayudar y guiarme en el difícil proceso del COST. A Noa, gracias por tus bromas que tanto nos hacen reír. Gracias también a todas las personas que han estado de paso por nuestro laboratorio enseñándonos nuevas cosas y transmitiéndonos su alegría (Mohammad, Pamela, Mar y Joan, Carmen, Adela y Valeria, Azar, Elvin, Macarena y Antonio Javier, Katarina, Miguelito, Berndjan, etc.).

Quisiera dar gracias también a las personas que formaron parte del grupo de María Fernández Lobato durante mi paso por allí. Miguel, Mike, Lola, Patricia, Brian, Asun, Marta, María, etc, ¡gracias a todos!. Y en especial al Dr. Miguel Álvaro por dirigirme y enseñarme durante el tiempo que estuve aprendiendo allí. Gracias también al Dr. Aurelio Hidalgo del CBM (Centro de Biología Molecular Severo Ocho), por creer en mí y estar dispuesto a ayudarme en mi carrera investigadora.

Gracias a todos los *partners* de los proyectos europeos en los que he participado, así como a la gente del CIB e IRNAS (Instituto de Recursos Naturales y Agrobiología de Sevilla) con la que hemos compartido muy buenos momentos (especialmente en los viajes y reuniones internacionales; gracias también a las Dras. Marta Pérez Boada y Susana Camarero, y a todo el grupo de Biotecnología para la Biomasa Lignocelulósica del CIB, así como al grupo de los Dres. Ana Gutiérrez y José Carlos del Rio del IRNAS de Sevilla.

A los Dres. Vivian de los Ríos y Francisco García Tabares del CIB, por los análisis de MALDI-TOF y geles bidimensionales. Gracias al Dr. Juan Román Luque Ortega, del servicio de Centrifugación analítica del CIB, por la determinación de coeficientes de sedimentación en las muestras de VP.

No podría acabar de dar las gracias a mis compañeros del ámbito científico sin antes nombrar al Dr. Manuel Ferrer y a su grupo de investigación (Mónica, Mercedes, Rafa, Cristina, etc...). Gracias porque siempre habéis estado ahí cuando hemos necesitado cualquier favor permitiéndonos seguir hacia delante sin tener que esperar a la llegada de nuevo material. ¡Muchas gracias chic@s!.

A los Dres. Antonio López y Marcos Pita por su ayuda y buena disposición a la hora de trabajar en colaboración. Gracias también a todas aquellas personas de los servicios del ICP de almacén, secretaria, recursos humanos, mantenimiento, informática, etc… que hacen que el Instituto siga funcionando día a día resolviendo todos los problemas inesperados.

Como no podría ser de otra manera, he dejado para lo último aquellas personas más cercanas a mí, y a las que agradezco enormemente que me hayan acompañado durante todos estos años.

Gracias a todos mis amigos (Josemi y Kate, David, Álvaro y Alba, Ricardo, Jorge, Borja, Dani, Angelina, Jessica y Andoni, Adri, Xumi y Ángel, Guada y Nacho, Hairen, Came, Oze, Jesús, Chus, Laura, Raúl, Carlos, María, etc…) por haberme hecho sentir tan bien, y por los buenos momentos y risas compartidas. ¡Gracias por ayudarme a llegar hasta aquí!.

Muchas gracias también a toda mi familia por haberme apoyado y creer en mí durante todos estos años, ¡por ser la mejor familia del mundo!. Gracias por ayudarme en todo lo que he necesitado y por hacer este viaje mucho más fácil. En especial quiero dar gracias a mis padres, Julio y Margarita, **MUCHAS GRACIAS** (y gritado en voz alta) por haber creído siempre en mí, por haberme apoyado en cualquier cosa que hiciera falta, por haberme dado ánimos siempre para que continuara el camino que yo eligiera, y por esperar tanto que llegara este momento.

El último lugar y más especial, lo he dejado para mi compañera de aventuras, Carina. Muchas gracias por estos últimos años de felicidad, cariño y apoyo que me has dado en todo momento. Gracias por tu paciencia y ánimos, porque aunque a veces la situación parezca difícil, estoy seguro que nos espera un futuro lleno de esperanzas.

ESTRUCTURA GENERAL DE LA TESIS

La presente Tesis Doctoral se encuentra estructurada en los siguientes capítulos:

- **Capítulo 1**: Introducción y objetivos.

- **Capítulo 2**: Publicación científica; "***Directed evolution of a temperature-, peroxide- and alkaline pH-tolerant versatile peroxidase***" (2012). Authors: Garcia-Ruiz, E., Gonzalez-Perez, D., Ruiz-Dueñas, F.J., Martínez, A.T. and Alcalde, M. *Biochem J* **441**, 487-498. DOI: 10.1042/BJ20111199.

- **Capítulo 3**: Publicación científica; "***Structural determinants of oxidative stabilization in an evolved versatile peroxidase***" (2014). Authors: Gonzalez-Perez, D., Garcia-Ruiz, E., Ruiz-Dueñas, F.J., Martínez, A.T., and Alcalde, M. *ACS Catal* **4**, 3891-3901. DOI: 10.1021/cs501218v.

- **Capítulo 4**: Publicación científica; "***Mutagenic Organized Recombination Process by Homologous In vivo Grouping (MORPHING) for Directed Enzyme Evolution***" (2014). Authors: Gonzalez-Perez, D., Molina-Espeja, P., Garcia-Ruiz, E., and Alcalde, M. *Plos one* **9**, e90919. DOI: 10.1371/journal.pone.0090919.

- **Capítulo 5**: Publicación científica; "***Alkaline versatile peroxidase by directed evolution***" (2016). Authors: Gonzalez-Perez, D., Mateljak, I., Garcia-Ruiz, E., Ruiz-Dueñas, F.J., Martínez, A.T., and Alcalde, M. *Catal Sci Technol* **6**, 6625-6636. DOI: 10.1039/C6CY01044J.

- **Capítulo 6**: Revisión científica; "***Saccharomyces cerevisiae in directed evolution: An efficient tool to improve enzymes***" (2012). Authors: Gonzalez-Perez, D., Garcia-Ruiz, E., and Alcalde, M. *Bioeng Bugs* **3**, 172-177. DOI: 10.4161/bbug.19544.

- **Capítulo 7**: Publicación científica; "***Assembly of evolved ligninolytic genes in Saccharomyces cerevisiae***" (2014). Authors: Gonzalez-Perez, D., and Alcalde, M. *Bioengineered* **5**, 1-10. DOI: 10.4161/bioe.29167.

- **Capítulo 8**: Discusión general de resultados.

- **Capítulo 9**: Conclusiones. Escritas en español e inglés.

- **Capítulo 10:** Referencias bibliográficas.

- **Capítulo 11**: Anexos I y II. El Anexo I incluye las secuencias de las VPs evolucionadas y la producción científica del doctorando durante el desarrollo de la presente Tesis Doctoral. El Anexo II incluye una tabla de aminoácidos con sus características principales y un mapa del código genético.

Los **capítulos del 2 al 7** corresponden a la producción científica de esta Tesis Doctoral, y se encuentran escritos en su lengua original (inglés) manteniendo el formato de las revistas científicas. El **capítulo 2** describe la evolución dirigida de la peroxidasa versátil (VP) del hongo *Pleurotus eryngii* hacia expresión funcional y termoestabilidad. El **capítulo 3** describe la evolución dirigida de la VP para resistencia a H_2O_2. El **capítulo 4** explica la puesta a punto de un método para la creación de diversidad (MORPHING) enfocada a experimentos de evolución dirigida. El **capítulo 5** detalla la evolución dirigida de la VP hacia actividad a pH alcalino. El **capítulo 6** revisa el uso de la levadura *S. cerevisiae* como hospedador heterólogo y herramienta de creación de diversidad en experimentos de evolución dirigida. Finalmente, el **capítulo 7** muestra el diseño de un prototipo inicial de levadura de podredumbre blanca mediante la co-expresión de una VP y una lacasa evolucionadas.

ÍNDICE DE CONTENIDOS

LISTADO DE ABREVIATURAS Y ACRÓNIMOS

Abreviatura/Acrónimo	**Descriptor: Español / *English***
2,5-DMBQ	2,5-dimetoxibenzoquinona / *2,5-dimethoxybenzoquinone*
2,5-DMHQ	2,5-dimetoxihidroquinona / *2,5-dimethoxyhydroquinone*
2-1B	Mutante de termoestabilidad / *Thermostability mutant*
AAD	Aril-alcohol deshidrogenasa / *Aryl-alcohol dehydrogenase*
AAO	Aril-alcohol oxidasa / *Aryl-alcohol oxidase*
ABTS	2,2´-azino-bis(3-etilbenzotiazolin-6-sulfonato) / *2,2´-azino-bis(3-ethyl-benzothiazoline-6-sulfonate)*
ApX	Ascorbato peroxidasa / *Ascorbate peroxidase*
ARP	Peroxidasa de *Arthromyces ramosus* / *Arthromyces ramosus peroxidase*
AT-AT	Mutante de estabilidad oxidativa / *Oxidative stability mutant*
BB-8	Mutante de actividad alcalina / *Alkaline activity mutant*
CBM	Módulo de unión a celulosa / *Cellulose binding module*
CCP	Citocromo C peroxidasa / *Cytochrome C peroxidase*
CDH	Celobiosa deshidrogenasa / *Cellobiose dehydrogenase*
CFCs	Compuestos clorofluorocarbonados / *Chlorofluorocarbon compounds*
CiP	Peroxidasa de *Coprinus cinerea* / *Coprinus cinerea peroxidase*
Compuesto I (C-I)	Compuesto IA + IB / *Compound IA + IB*
Compuesto IA	Compuesto intermediario del ciclo catalítico de la VP con dos deficiencias electrónicas / *Intermediary compound from VP cycle with a two-electron deficiency*
Compuesto IB	Compuesto intermediario del ciclo catalítico de la VP con una deficiencia electrónica en el Trp catalítico y un radical oxiferrilo / *Intermediary compound from VP cycle with a single electron deficiency at the catalytic tryptophan and a oxyferryl radical*
Compuesto II (C-II)	Compuesto IIA + IIB / *Compound IIA + IIB*
Compuesto IIA	Compuesto intermediario del ciclo catalítico de la VP con una deficiencia electrónica / *Intermediary compound from VP cycle with a single electron deficiency*
Compuesto IIB	Compuesto intermediario del ciclo catalítico de la VP con una deficiencia electrónica en el Trp catalítico / *Intermediary compound from VP cycle with a single electron deficiency at the catalytic tryptophan*
CRS	Escenarios de barreras de coral / *Coral reefs scenario*
CSM	Mutagénesis combinatorial saturada / *Combinatorial Saturation mutagenesis*
CT	Banda de transferencia de carga / *Charge transference band*
DFAD	4-[(3,5-difluoro-4-hidroxifenil)azo] bencensulfonato; tinte aniónico / *4-[(3,5-difluoro-4-hydroxyphenyl)azo] benzene sulfonate; anionic dye*
DMP	2,6-dimetoxifenol / *2,6-dimethoxyphenol*
DNA shuffling	Barajado del DNA
DNA$_{\text{puzzle}}$	Puzzle de DNA
dNTPs	Desoxirribonucleótidos / *deoxyribonucleotides*
DOE	Departamento de Energía de EEUU / *Department of Energy from USA*
DyP	Peroxidasa decolorante de tintes / *Dye-decolorizing peroxidase*
E^o	Potencial redox estándar / *Standard redox-potential*
epPCR	PCR propensa a error / *error-prone PCR*
EPR	Resonancia paramagnética electrónica / *Electron paramagnetic resonance*
FACS	Clasificación celular activada por fluorescencia / *Fluorescence-*

	activated cell sorting
FCBM	Microorganismo que proporciona un proceso completo y consolidado / *Full-consolidate bioprocessing microbe*
GHG	Gases de efecto invernadero / *Green house gases*
GLX	Glioxal oxidasa / *Glyoxal oxidase*
GMC	Familia glucosa-metanol-colina / *Glucose-methanol-choline family*
GOX	Glucosa oxidasa / *Glucose oxidase*
GP	Peroxidasa genérica / *Generic peroxidase*
$\mathbf{H_2O_2}$ $\boldsymbol{t_{1/2}}$	Vida media frente a H_2O_2 / *Half-life against* H_2O_2
HPLC	Cromatografía líquida de alta resolución / *High-performance liquid chromatography*
HRP	Peroxidasa de rábano / *Horseradish peroxidase*
HRPL	Lacasa de alto potencial redox / *High-redox potential laccase*
HTP	Peroxidasa hemotiolada / *Heme-thiolate peroxidase*
HTS	Ensayo de cribado de alta capacidad / *High-throughput screening*
***Iv*AM**	Ensamblaje *in vivo* de librerías mutagénicas con distinto espectro mutacional / *In vivo assembly of mutant libraries with different mutational spectra*
IVOE	Solapamiento *in vivo* por extensión / *In vivo overlap extension*
JGI	Instituto de genoma colectivo (EEUU) / *Joint Genome Institute (USA)*
$\boldsymbol{k_{cat}}$	Número de recambio / *Turnover rate*
$\mathbf{K_m}$	Constante de Michaelis-Menten / *Michaelis-Menten constant*
$\boldsymbol{k_{cat}}/\mathbf{K_m}$	Eficiencia catalítica / *Catalityc efficiency*
Lac	Lacasa / *Laccase*
LiP	Lignina peroxidasa / *Lignin peroxidase*
LPMO	Monooxigenasa degradadora de polisacáridos */ Lytic polysaccharide Monooxygenase*
LRET	Ruta de transferencia electrónica de largo recorrido / *Large-range electron transfer pathway*
MALDI-TOF	Desorción/ionización mediante láser asistida por matriz acoplada a timpo de vuelo / *Matrix-assisted laser desorption/ionization-time of flight*
MnP	Manganeso peroxidasa / *Manganese peroxidase*
MORPHING	Proceso de recombinación mutagénico de manera organizada mediante agrupamiento *in vivo* / *Mutagenic Organized Recombination Process by Homologous IN vivo Grouping*
MOX	Metanol oxidasa / *Methanol oxidase*
NBD	5-nitro-1,3-benzodioxol / *5-nitro-1,3-benzodioxole*
OD	Densidad óptica / *Optical density*
ODC	Oxalato descarboxilasa / *Oxalate decarboxylase*
P2O	Piranosa 2-oxidasa / *Pyranose 2-oxidase*
***p*-Aa**	Alcohol *p*-anisílico / *p-anisyl alcohol*
PAH	Hidrocarburos aromáticos policíclicos / *Polycyclic aromatic hydrocarbons*
PcL	Lacasa de *Pycnoporus cinnabarinus* / *Pycnoporus cinnabarinus laccase*
PCR	Reacción en cadena de la polimerasa / *Polymerase chain reaction*
PDB	Base de datos de proteínas / *Protein data bank*
***p*I**	Punto isoeléctrico / *Isoelectric point*
$\mathbf{p}\boldsymbol{K}_\mathbf{a}$	Fuerza relativa de un ácido / *Relative force of an acid*
POD	Peroxidasa ligninolítica / *Ligninolytic peroxidase*
QR	Quinona reductasa / *Quinone reductase*
R4	Mutante de secreción / *Secretion mutant*
RB5	Reactivo negro 5 / *Reactive black 5*
ROS	Especies reactivas de oxígeno / *Reactive oxygen species*

RS	Estado de reposo de la VP / *Resting state of VP*
R_z	Valor de Reinheitszahl */ Reinheitszahl value*
SDS-PAGE	Gel de electroforesis de poliacrilamida con dodecilsulfato sódico / *Sodium dodecyl sulfate-polyacrylamide gel eletrophoresis*
$\mathbf{SI^{th}}$	Mutante de estabilidad oxidativa / *Oxidative stability mutant*
SOE	Empalme mediante solapado y extensión / *Splice by overlap extension*
***St*Ep**	Proceso de extensión escalonado / *Staggered extension process*
T_{50}	Temperatura a la cual la enzima conserva el 50% de su actividad tras una incubación de 10 min / *Temperature at which the enzyme keeps 50 % of its activity after incubation for 10 min*
TAI	Mejora sobre la actividad total / *Total activity improvement*
Taq	Polimerasa de *Thermus aquaticus* / *Thermus aquaticus polymerase*
TMB	3,3′,5,5′-Tetrametilbencidina / *3,3′,5,5′-Tetramethylbenzidine*
Ts	Transición / *Transition*
Tv	Transversión / *Transversion*
Unidades G	Unidad guayacilo de lignina */ Guaiacyl unit of lignin*
Unidades H	Unidad *p*-hidroxifenilo de lignina */ p-hydroxyphenyl unit of lignin*
Unidades S	Unidad siringilo de lignina */ Syringyl unit of lignin*
UPO	Peroxigenasa inespecífica / *Unspecific peroxygenase*
VA	Alcohol veratrílico / *Veratryl alcohol*
VP	Peroxidasa versátil / *Versatile peroxidase*
WRY	Levadura de podredumbre blanca / *White-rot yeast*
$\Delta t_{1/2}$	Incremento de vida media / *Increment of half-life*

ÍNDICE DE FIGURAS

Capítulo 1

"Introducción y objetivos"

Capítulo 2

"Directed evolution of a temperature-, peroxide- and alkaline pH-tolerant versatile peroxidase"

Capítulo 3

"Structural determinants of oxidative stabilization in an evolved versatile peroxidase"

Capítulo 4

"Mutagenic Organized Recombination Process by Homologous In vivo Grouping (MORPHING) for directed enzyme evolution"

Capítulo 5

"Alkaline versatile peroxidase by directed evolution"

Capítulo 6

"Saccharomyces cerevisiae in directed evolution: an efficient tool to improve enzymes"

Capítulo 7

"Assembly of evolved ligninolytic genes in Saccharomyces cerevisiae"

Capítulo 8

"Discusión general de resultados"

ÍNDICE DE TABLAS

Capítulo 1

"Introducción y objetivos"

Capítulo 2

"Directed evolution of a temperature-, peroxide- and alkaline pH-tolerant versatile peroxidase"

Capítulo 3

"Structural determinants of oxidative stabilization in an evolved versatile peroxidase"

Capítulo 4

"Mutagenic Organized Recombination Process by Homologous In vivo Grouping (MORPHING) for directed enzyme evolution"

Capítulo 5

"Alkaline versatile peroxidase by directed evolution"

Capítulo 8

"Discusión general de resultados"

Summary

The role of versatile peroxidase (VP) during lignin depolymerization has arisen a huge biotechnological interest for its potential application in the pre-treatment of lignocellulosic biomass. VPs are haem-containing proteins dependent of H_2O_2 which show a high substrate promiscuity thanks to their ability to oxidize a wide range of phenolic and non-phenolic compounds ranging from low-, medium-, to high-redox potentials. The structure of VP is stabilized by the presence of two structural calcium ions which maintain VP activity in its three oxidation sites including a haem access channel, the Mn^{2+} oxidation site, and an oxidation site governed by a superficial catalytic tryptophan. These structural features have been acquired during the natural evolution of VP from an atypical MnP (Manganese peroxidase) with Paleozoic origin.

In order to improve VP properties for application in lignocellulosic biorefineries, its heterologous functional expression in suitable hosts for directed evolution becomes a crucial factor. Secondly, among the features that require attention in VP are its low oxidative stability towards H_2O_2 (a common process for all haem-containing peroxidases which is mechanism-based) and the lack of activity and stability at neutral/alkaline pH. The latter is the result of the natural selection of VPs to work under acidic environments during natural lignin decay.

By performing directed evolution in *Saccharomyces cerevisiae* as heterologous host, the VP from *Pleurotus eryngii* was evolved towards functional expression, and afterwards, for thermostabilization. The R4 mutant enhanced its secretion levels ~129-fold in yeast with respect to parental type, while the thermostability mutant (2-1B variant) improved its thermostability by 8 ºC. Surprisingly, R4 mutant also showed a higher oxidative stability, hence it was chosen as departure point to tailor resistance against H_2O_2. Within this approach, different *in vivo* and *in vitro* directed evolution tools were used to create mutagenic libraries including two new methods referred as MORPHING and DNA_{puzzle}. MORPHING protocol was based on focusing specifically random mutagenesis and recombination over three regions involved in H_2O_2 inactivation. DNA_{puzzle} was used as the last evolution step to select the best combination of mutations through the *in vivo* recombination of evolved sequence blocks. Finally, two variant (AT-AT and SI^{th}) were obtained with 7 and 8 mutations each, which improved their half-lives from 3 min (parent) to 18 and 35 min, respectively, in presence of 3,000 equivalents of H_2O_2. In addition, SI^{th} mutant enhanced its thermostability around 6 ºC. The mutations found in this work were analyzed together with other resistant peroxidases highlighting possible mechanisms and pathways to improve oxidative stability.

On the other hand, the thermostable mutant 2-1B showed an unusual high stability under alkaline pHs after evolution as result of a stabilizing mutational backbone which is composed by three mutations that help to avoid the structural calcium leakage under alkaline pH. Although 2-1B variant was stable at alkaline pH, it did not show measurable activity beyond pH 5.0. Harnessing its alkaline stability, 2-1B mutant was subjected to new evolution rounds to achieve activity at neutral/alkaline pH. The final variant (BB-8) accumulated three mutations which conferred activity under neutral/alkaline pH with different low redox-potential substrates at the haem access channel, and the Mn^{2+} binding site. However, the catalytic Trp remained inactive at alkaline pH because of the strong dependency of its ionic state and redox potential at acid pH. The introduction of a single mutation in the surroundings of Mn^{2+} binding site, affected negatively the

catalytic properties in this site while allowing, for the first time, the direct oxidation of ABTS at alkaline pH in the Mn^{2+} binding pocket. In addition, it was observed a hyperactivation effect after incubating BB-8 variant at alkaline pH.

Finally, the thermoestable variant 2-1B and a high-redox potential laccase (evolved for functional expression in *S. cerevisiae*, and later towards tolerance to human blood) were co-expressed in *S. cerevisiae* with the aim of designing an initial prototype of white-rot yeast (WRY). The co-expression of both genes was carried out both in microplate and flask formats by using different construction based on bi-directional vectors under the control of distinct expression cassettes (GAL1/CYC1 and GAL10/ADH1). The main outcome from this work showed that is possible to co-express both ligninases in *S. cerevisiae* without significant interferences with cell metabolism. The co-expression of both enzymes decreased by 4- and 10-fold (depending of enzyme tested and culture format) comparing with their counterparts single expression cassettes. The best result in terms of co-expression was achieved with the construction GAL1/VP/CYC1-GAL10/Laccase/ADH1 where activities towards ABTS as substrate of ~ 175 U/L (microplate) and 30 U/L (flask) were observed, for VP and laccase, respectively. This WRY prototype could be improved in the near future by including new ligninases along with an autonomous cellulolytic apparatus, which would allow the design of a synthetic microorganism capable of converting lignocellulosic materials into biofuels or added-value compounds. From a more basic point of view, this microorganism could be also useful as model of study to understand the complex mechanism of selective/simultaneous white-rotting fungi.

Resumen

El papel que desempeña la peroxidasa versátil (VP) en el proceso de despolimerización de la lignina ha despertado un gran interés biotecnológico para su aplicación en el pre-tratamiento de la biomasa lignocelulósica. Las VPs son hemoproteínas dependientes de H_2O_2 que presentan una alta promiscuidad de sustrato, pudiendo oxidar un amplio rango de compuestos fenólicos y no fenólicos de alto, medio y bajo potencial redox. La estructura de la VP se encuentra estabilizada por la presencia de dos calcios estructurales que mantienen la actividad de sus tres sitios catalíticos: un canal principal de acceso al grupo hemo, un sitio de oxidación de Mn^{2+} y un sitio de oxidación gobernado por un triptófano catalítico superficial. Estas características estructurales parecen haber sido adquiridas durante la evolución natural de la VP a partir de MnP (Manganeso peroxidasa) atípicas de origen Paleozoico.

Con el fin de mejorar las propiedades de la VP para sus posibles aplicaciones en el contexto de las biorefinerías lignocelulósicas, la expresión funcional heteróloga de la VP en hospedadores apropiados de evolución dirigida es fundamental. En segundo lugar, entre las características que requieren una urgente revisión en la VP se encuentran su pobre estabilidad oxidativa frente a H_2O_2 (un proceso común a todas las hemo-peroxidasas, que es dependiente del mecanismo de acción de la enzima) y su nula actividad y estabilidad a pH neutro/alcalino, como consecuencia del proceso de selección natural que han cursado para funcionar en ambientes ácidos durante la degradación de lignina.

Haciendo uso de la evolución dirigida en la levadura *Saccharomyces cerevisiae* como hospedador heterólogo, se diseñó la VP de *Pleurotus eryngii* hacia expresión funcional, y seguidamente hacia termoestabilidad. El mutante R4 aumentó sus niveles de secreción en levadura ~129 veces (22 mg/L) respecto al parental, mientras que el mutante de termoestabilidad (variante 2-1B) incrementó su termoestabilidad en 8 ºC. Inesperadamente, R4 también mostró un aumento en su estabilidad oxidativa, por lo que fue seleccionado como punto de partida para mejorar su resistencia a H_2O_2. Para ello, se utilizaron diferentes herramientas *in vivo* e *in vitro* durante la generación de las librerías mutagénicas, incluyendo dos nuevas técnicas llamas MORPHING y DNA_{puzzle}. El protocolo de MORPHING consistió en enfocar la carga mutagénica y los eventos de recombinación, específicamente sobre tres regiones potencialmente implicadas en la inactivación por peróxidos, mientras que el DNA_{puzzle} se aplicó como último paso de evolución con la idea de seleccionar la mejor combinación de mutaciones encontradas, mediante la recombinación de bloques de secuencia evolucionados en diferentes estadios. Finalmente se obtuvieron dos variantes (AT-AT y SI^{th}) con 7 y 8 mutaciones cada una que mejoraron sus vidas medias de 3 min (parental) hasta 18 y 35 min, respectivamente, en presencia de 3000 equivalentes de H_2O_2. Además, el mutante SI^{th}, también aumentó su termoestabilidad en 6 ºC. Las mutaciones encontradas en este trabajo se analizaron junto con otras peroxidasas resistentes a peróxidos, proponiendo posibles mecanismos y vías de estabilización oxidativa.

Por otro lado, el mutante de termoestabilidad 2-1B presentó una inusual elevada estabilidad frente a pHs alcalinos tras el proceso de evolución como consecuencia de un eje estabilizante constituido por tres mutaciones, que favorecieron la conservación de los calcios estructurales bajo pH alcalinos. A pesar de que 2-1B fue estable a pH alcalino, no mostró actividad detectable más allá de pH 5.0. Tomando ventaja de su estabilidad alcalina, 2-1B fue evolucionado hacia actividad a pH neutro/alcalino. El mutante resultante de dicha proceso (variante BB-8), acumuló tres

mutaciones que le dotaron de actividad a pHs neutros/alcalinos frente a diferentes sustratos de bajo potencial redox, tanto en el canal del hemo como en el sitio del Mn^{2+}, mientras que el Trp catalítico fue inactivo a pH alcalino debido a que su funcionamiento es dependiente de su estado de ionización y potencial redox a pH ácidos. La incorporación de una mutación en las proximidades del sitio de unión de Mn^{2+}, afectó negativamente las propiedades catalíticas de este sitio, efecto que se vio compensado por la capacidad de oxidar ABTS a pH alcalino en dicho centro catalítico de manera directa, lo cual nunca antes había sido reportado en la VP. Además, también se detectó un fenómeno de hiperactivación enzimática tras la incubación de BB-8 a pH alcalino.

Por último, el mutante termoestable 2-1B y una lacasa de alto potencial redox previamente evolucionada (primero hacia expresión funcional en *S. cerevisiae*, y más tarde hacia tolerancia a sangre humana), fueron co-expresados en *S. cerevisiae* con la intención de crear un prototipo inicial de levadura de podredumbre blanca (WRY). La co-expresión de ambos genes se llevó a cabo en formato de microplaca y matraz, mediante el uso de construcciones basadas en vectores bi-direccionales controlados por diferentes *cassettes* de expresión (GAL1/CYC1 y GAL10/ADH1). Los resultados de este trabajo mostraron la posibilidad de co-expresar ambos genes en *S. cerevisiae* sin interferir significativamente el metabolismo de la célula. Se comprobó que la co-expresión de ambas enzimas en levadura se ve disminuida entre 4 y 10 veces (dependiendo de la enzima y el formato de cultivo) frente a la expresión individual de cada una de ellas. En cualquier caso, los niveles de co-expresión más altos y equitativos, para VP y lacasa, se obtuvieron con la construcción GAL1/VP/CYC1-GAL10/Lacasa/ADH1, donde las actividades reportadas fueron ~ 175 U/L (microplaca) y 30 U/L (matraz) para la VP y la lacasa, respectivamente. Este prototipo de WRY podría ser mejorado en un futuro próximo incorporando un aparato ligninolítico más elaborado que, junto con un aparato celulolítico, permitiese abordar el diseño de un organismo sintético capaz de transformar el material lignocelulósico en biocombustibles o compuestos químicos de alto valor añadido. Desde una perspectiva fundamental, podría servir además de modelo de estudio aplicado a hongos de podredumbre blanca selectivos y/o simultáneos.

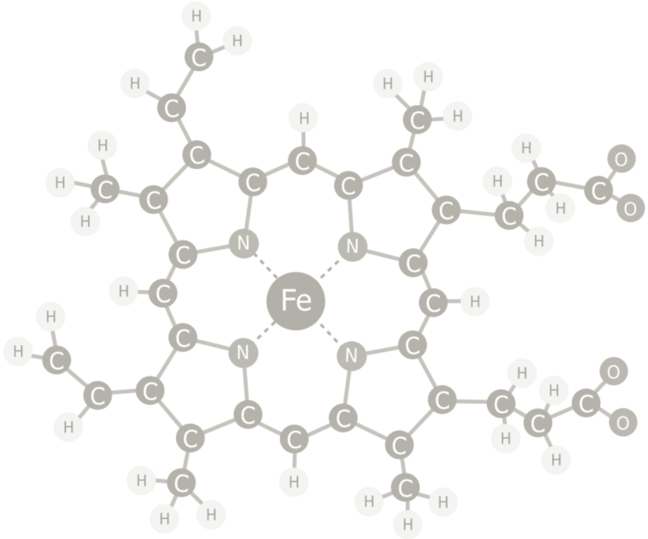

Capítulo 1:

Introducción y objetivos

La peroxidasa versátil es una oxidorreductasa ligninolítica con numerosas aplicaciones potenciales en diferentes sectores biotecnológicos. En este capítulo se revisa su origen y función biológica, así como sus principales ventajas y limitaciones. Además se describe el papel fundamental de la levadura Saccharomyces cerevisiae como hospedador heterólogo en experimentos de evolución dirigida. Finalmente se comenta el interés biotecnológico que suscita el diseño de una levadura sintética de podredumbre blanca como base para el estudio del aprovechamiento de la biomasa vegetal, y su uso como modelo de organismo ligninolítico.

1. La biorefinería como un modelo de sostenibilidad energética

1.1. Concepto de biorefinería

El uso globalizado de energías basadas en combustibles fósiles ha provocado a largo plazo un aumento progresivo de las concentraciones atmosféricas de gases con efecto invernadero (GHG, *greenhouse gases*), entre los que se encuentran fundamentalmente el CO_2, NO_2, y CH_4.

La acumulación de los GHG en la atmósfera produce un efecto pantalla frente al calor generado por la radiación infrarroja solar, provocando que la temperatura global del planeta sufra un incremento considerable. Este fenómeno se conoce como efecto invernadero, y entre otras consecuencias, puede derivar en la fusión gradual de los polos, el aumento del nivel del mar, y desastres como inundaciones o anegaciones de tierras de cultivo.

Con una concentración atmosférica próxima a las 400 ppm, se estima que el CO_2 es el principal agente responsable del efecto invernadero en la Tierra (Solomon *et al.*, 2009, **Figura 1A**). Se ha determinado que de las emisiones de CO_2 de origen antropogénico, alrededor del 25% son asimiladas por los mares en forma de H_2CO_3, lo que genera su acidificación y consiguiente reducción de la biodisponibilidad de carbonato en dicho ecosistema. Ambos factores afectan negativamente a los arrecifes de coral y a la biodiversidad marina del entorno (Hoegh-Guldberg *et al.*, 2007, **Figura 1B**).

Asimismo, tanto la lluvia ácida como la desaparición de la capa de ozono son importantes fenómenos derivados del impacto de los GHG en la atmósfera (Dincer and Ronsen, 1998). La lluvia ácida sucede como resultado del exceso de emisiones industriales de SO_2 y NO_x. Ambos gases ascienden hasta la troposfera, donde sufren un proceso de oxidación fotoquímica, acumulándose en forma de nubes que posteriormente dan lugar a precipitaciones que acidifican lagos y aguas freáticas para el consumo humano. Por otro lado, el papel protector de la capa de ozono en la Tierra es muy importante, ya que actúa como un filtro frente a la radiación ultravioleta solar. Una disminución considerable de esta capa daría acceso directo a la radiación ultravioleta aumentando el riesgo de padecer cáncer de piel y daño ocular, entre otras afecciones (Dincer and Ronsen, 1998; Rowland, 2006). En este sentido, la destrucción de la capa de ozono se produce por el efecto de las emisiones de NO_x y compuestos clorofluorocarbonados (o CFCs). La formación de la capa de ozono tiene lugar a partir de átomos de oxígeno que reaccionan entre sí en presencia de radiación solar ultravioleta generando O_3. Sin embargo, tanto el NO_x como los CFCs son capaces de reaccionar con el O_3 ya formado, produciendo O_2, óxidos de cloro y nitrógeno que descomponen la capa.

En conclusión, se puede decir acertadamente que el efecto perjudicial que generan las emisiones de los combustibles fósiles ha generado una necesidad urgente de implantar nuevas tecnologías que sean más limpias y respetuosas con el medio ambiente, como por ejemplo, el aprovechamiento de la abundante biomasa vegetal.

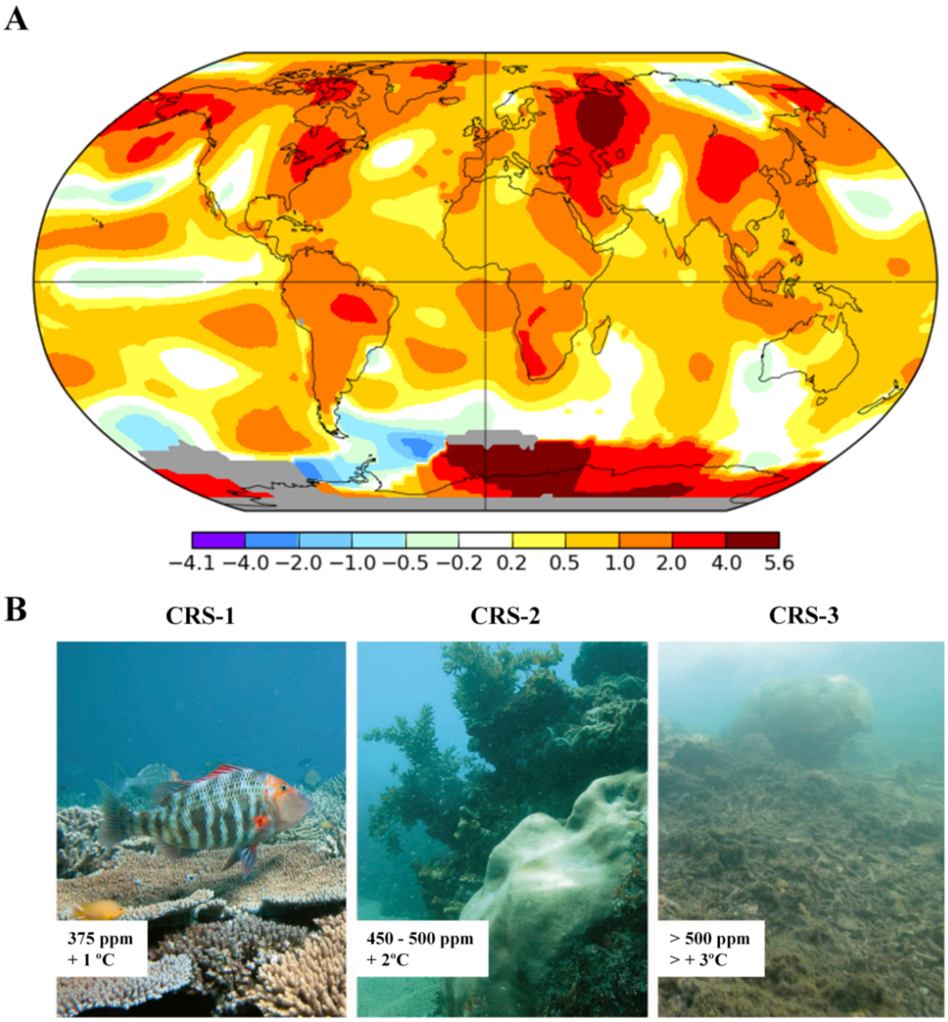

Figura 1. Incidencia de las emisiones de CO_2 sobre el cambio climático y los mares.
(**A**) Diferencia de temperatura en ºC (como anomalía de temperatura) registrada en 2016 con respecto al período comprendido entre los años 1950-2000 (imagen obtenida a través de la página web: http://data.giss.nasa.gov/gistemp/maps/). (**B**) Simulación del efecto de la concentración de CO_2 en diferentes escenarios de barreras de coral (CRS). CRS-1, barrera de coral en *Heron island*. CRS-2, barrera de coral en *Bees island*. CRS-3, barrera de coral en *Low isles*. Las imágenes corresponden a la gran barrera de coral australiana. Los números indican la concentración de CO_2 atmosférico en ppm y el incremento de temperatura en ºC respecto al valor normal (Hoegh-Guldberg *et al.*, 2007).

En este contexto, la Unión Europea ha lanzado un programa energético denominado "*2050 Energy strategy*" (https://ec.europa.eu/energy/en/topics/energy-strategy/2050-energy-strategy) cuya finalidad es disminuir las emisiones de GHG. Como objetivo a largo plazo, se pretenden reducir los valores de emisión de estos gases entre el 80-95% a efectos del año 2050 con respecto a los valores obtenidos en el año 1990. Dicha reducción se plantea llevar a cabo mediante el uso de energías renovables más eficientes, limpias y sostenibles con el medio ambiente. Recientemente, el Departamento de Energía de los Estados Unidos (DOE) también se ha unido a esta iniciativa energética concediendo cuantiosas financiaciones (de hasta 90 millones de dólares) a proyectos enfocados hacia el diseño, construcción y aplicación de biorefinerías integradas.

Las biorefinerías integradas operan de un modo similar a las clásicas refinerías petrolíferas. Sin embargo, las primeras emplean como materia prima la biomasa lignocelulósica para la obtención de biocombustibles y productos químicos derivados, a través del aprovechamiento integral de cada uno de los constituyentes básicos del material lignocelulósico.

Debido a su alto contenido en polisacáridos, la mayor parte de la biomasa lignocelulósica se destina a la producción de bioetanol de segunda generación (*i.e.* a partir de residuos agrícolas o de otros orígenes), mientras que el contenido remanente de lignina y parte de la hemicelulosa se emplean en la producción de productos químicos con valor añadido (*p. ej.* adhesivos y surfactantes) que aseguran la sostenibilidad económica de la factoría, permitiendo ajustar los costes de producción (Azapagic, 2014; Cherubini, 2010; Liao *et al.*, 2016; Upton and Kasko, 2016). La lignina remanente del proceso puede ser también incinerada para generar calor y/o energía con el fin de autoabastecer a la biorefinería integral.

Se ha estimado que el balance entre el carbono fijado en la biomasa lignocelulósica, y el liberado durante la producción de biocombustibles y compuestos químicos en la biorefinería, es próximo a cero (*i.e.* idealmente el CO_2 liberado por la biorefinería será fijado nuevamente por las plantas mediante la fotosíntesis) (Martínez *et al.*, 2009a). De este modo se establece un proceso cíclico e iterativo proporcionando un modelo ecológico y sostenible que contribuye a reducir las emisiones antropogénicas de CO_2 (**Figura 2**).

Figura 2. Representación del proceso de reciclado del CO_2 en una biorefinería integral.

1.2. Aprovechamiento y estructura de la biomasa lignocelulósica

1.2.1. Aprovechamiento de la biomasa lignocelulósica

Una biorefinería integral funciona a través de cuatro etapas fundamentales. La primera de ellas es la recogida y almacenaje de la biomasa vegetal, la cual puede proceder de fuentes muy diversas como, por ejemplo, residuos forestales o aquellos generados en el entorno urbano (**Tabla 1**).

Tabla 1. Clasificación y cantidades de material lignocelulósico en función de su origen.

Biomasa lignocelulósica	Millones de toneladas (peso seco / año)
Residuos agrícolas	428
Residuos forestales	370
Residuos de cultivos destinados a energía	377
Residuos procedentes de cereales y maíz	87
Residuos municipales e industriales	58
Otros (*p. ej.* cultivos oleaginosos)	48
Total	**1.368**

Tabla adaptada de Limayem and Ricke, 2012.

El segundo paso consiste en el pre-tratamiento de la biomasa con el fin de retirar la lignina y facilitar el acceso a los polisacáridos para continuar con la siguiente etapa. Dependiendo de la naturaleza del material lignocelulósico, este proceso puede requerir un pre-tratamiento mecánico, químico, físico o bien una combinación de todos ellos (Jonsson and Martin, 2016; **Tablas 1** y **2**).

Tabla 2. Composición de la biomasa lignocelulósica -en función de su origen- destinada a la biorefinería.

Materia prima	Celulosa (%)	Hemicelulosa (%)	Lignina (%)	Cenizas y otros (%)
Residuos agrícolas	37-50	25-50	5-15	12-16
Angiospermas	45-47	25-40	20-25	0,8
Gimnospermas	40-45	25-29	30-60	0,5
Gramíneas	25-40	35-50	-	-
Residuos del blanqueo de papel	50-70	12-20	6-10	-
Periódicos	40-55	25-40	18-30	-
Panicum virgatum (*Switch grass*)	40-45	30-35	12	-

Las cantidades están expresadas como porcentaje de biomasa en peso seco. Tabla adaptada de Limayem and Ricke, 2012.

En este punto, se puede abordar además la extracción de compuestos de alto valor añadido presentes en la biomasa de manera natural como fragancias, flavorizantes y compuestos nutracéuticos.

El tercer paso comienza con el proceso de sacarificación de la biomasa utilizando enzimas capaces de hidrolizar los polisacáridos en sus subunidades monoméricas (glucosa, galactosa, fructosa, xilano, etc.). A partir de éstas, se lleva a cabo el proceso de fermentación microbiana hacía la producción de biocombustibles como el biobutanol y el bioetanol, siendo este último una molécula central del metabolismo fermentativo para su biotransformación hacia otros productos de interés como glicerol o sorbitol (estos dos alcoholes se han clasificado por el DOE dentro de los 12 productos químicos con mayor interés industrial derivados de la biomasa vegetal). Otros productos químicos de alto valor añadido que se pueden extraer en esta última etapa son, por ejemplo, el hidroximetilfurfural o los ácidos levulínico, succínico y fumárico, los cuales se obtienen a partir del metabolismo de microorganismos específicos o bien empleando cócteles enzimáticos (Ragauskas *et al.*, 2014).

1.2.2. Estructura de la lignocelulosa

Con una producción anual estimada en más de 1.000 millones de toneladas métricas, y una representación cercana al 70% frente a la biomasa vegetal de la Tierra, la lignocelulosa es la materia prima más abundante de la esfera terrestre (Moreno *et al.*, 2015; Octave and Thomas, 2009). La lignocelulosa está formada por tres componentes principales: celulosa (35-50%), hemicelulosa (25-40%) y lignina (10-25%). Aunque en menor proporción, también se encuentran otros elementos incluyendo cenizas, pectinas, proteínas y otros compuestos extraíbles de naturaleza tanto orgánica como inorgánica (He *et al.*, 2014; Limayem and Ricke, 2012; Quiroz-Castañeda and Folch-Mallol, 2010; Xiao and Anderson, 2013, **Figura 3**).

La celulosa es el polisacárido más abundante de la Tierra y el principal componente de las paredes celulares vegetales. Su estructura primaria se encuentra formando cadenas lineales de β-D-glucopiranosa unidas entre sí mediante enlaces glucosídicos β-1,4. La longitud de sus cadenas puede variar presentando un grado de polimerización que oscila entre 2.000 a 25.000 unidades de β-D-glucopiranosa (Delmer and Amor, 1995). Las cadenas lineales de celulosa interaccionan consigo mismas y con otras cadenas adyacentes mediante puentes de hidrógeno e interacciones de Van der Waals, formando microfibras de celulosa que a su vez se agrupan para compactarse en forma de paquetes de fibras. Aunque la mayor parte de este polímero se dispone formando una estructura cristalina ordenada, también presenta en menor proporción regiones amorfas que son más susceptibles a la degradación enzimática (Beguin, 1994; Pérez *et al.*, 2002). En las plantas, la celulosa se encuentra asociada con la hemicelulosa y lignina constituyendo una pared vegetal robusta que proporciona sustento y rigidez (**Figura 3**).

A diferencia de la celulosa, la hemicelulosa es un heteropolísacarido que presenta un mayor grado de complejidad estructural, ya que contiene numerosas ramificaciones y modificaciones (*p. ej.* O-acetilaciones). Estas últimas pueden encontrarse distribuidas a lo largo de la cadena principal así como en las ramificaciones. Dependiendo del tipo de hemicelulosa, su cadena principal puede estar compuesta principalmente de pentosas (D-xilosa), y/o hexosas (D-glucosa, D-manosa). Al igual que en la celulosa, las unidades que componen dicha cadena se encuentran unidas mediante enlaces β-1,4-glucosídicos. Por otra parte, las moléculas que forman las ramificaciones de la hemicelulosa suelen ser L-arabinosa, L-fructosa, D-galactosa, ácido 4-O-metilglucurónico, ácido D-galacturónico, ácido D-glucurónico y ácido ferúlico, entre otros. Para facilitar la clasificación de las diferentes hemicelulosas, éstas se han agrupado en cinco subtipos diferentes: xiloglucanos (cadena principal formada por D-glucosa con ramificaciones de D-xilosa), glucuronoxilano (cadena principal formada de D-xilosa con ramificaciones de ácido glucurónico), glucuronoarabinoxilano (cadena principal formada de D-xilosa con ramificaciones de tipo ácido glucurónico y L-arabinosa), galactomanano (cadena principal compuesta de D-manosa con ramificaciones de D-galactosa) y galactoglucomanano (cadena principal formada de D-manosa y D-glucosa dispuestas de manera alterna con ramificaciones de ácido galacturónico). De manera excepcional, se ha descrito que la cadena lineal de la hemicelulosa también puede encontrarse unida mediante enlaces β-1,3 y β-1,4-glucosídicos alternados, como es el caso de plantas dentro del orden Poales (Quiroz-Castañeda and Folch-Mallol, 2010; Scheller and Ulvskov, 2010).

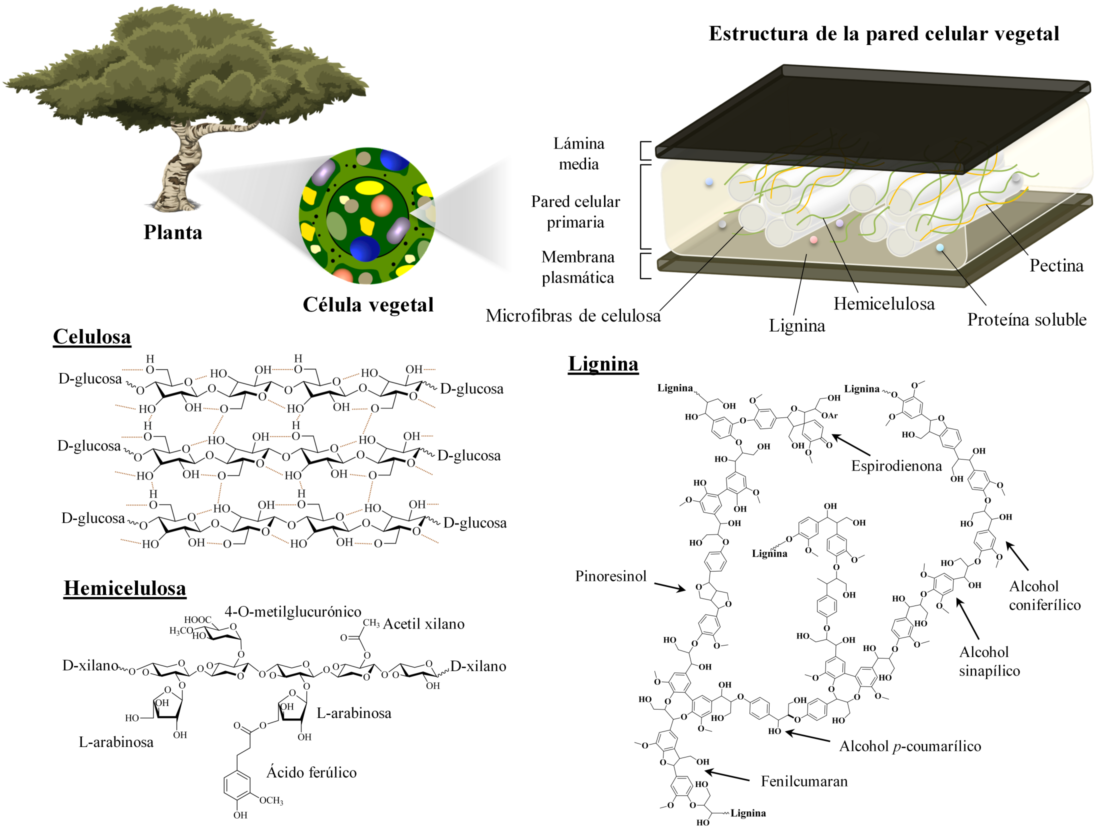

Figura 3. Composición de la biomasa lignocelulósica.

El tercer componente de la lignocelulosa, la lignina, es un polímero aromático complejo que se encuentra localizado principalmente en la pared vegetal primaria, entre la lámina media y la membrana plasmática (**Figura 3**). Tras la celulosa, la lignina es el compuesto más abundante en la biomasa terrestre, y su función biológica consiste en recubrir la celulosa y hemicelulosa creando una barrera biológica protectora frente al ataque microbiano, al tiempo que actúa a modo de cemento molecular imbricándose entre las fibras y aportando solidez. En torno al 20% del CO_2 fijado mediante el proceso de fotosíntesis se deposita en forma de lignina, lo cual supone un alto contenido en carbono aprovechable en la biomasa (Ruiz-Dueñas and Martínez, 2009a). La lignina se genera a través de la polimerización deshidrogenativa al azar de tres precursores fenólicos conocidos como alcoholes *p*-hidroxicinamílicos (*p*-coumarílico, sinapílico y coniferílico), los cuales son sintetizados a través de la ruta del ácido siquímico (Vanholme *et al.*, 2010). Cada uno de estos monolignones, tras su oxidación, da lugar a los correspondientes radicales fenoxilo que reaccionan entre sí a través de procesos de acoplamiento molecular formando las unidades fenilpropanoides constitutivas de la lignina, y que se clasifican en tres grupos: unidades H (*p*-hidroxifenilo; derivado del alcohol *p*-coumarílico), unidades G (guayacilo; derivado del alcohol coniferílico) y unidades S (siringilo; derivado del alcohol sinapílico). La presencia y distribución de estas unidades definen el tipo de lignina que compone el tejido vegetal (Martínez *et al.*, 2005; 2008; Ralph *et al.*, 2004; Ruiz-Dueñas and Martínez, 2009a). En la estructura de la lignina, alrededor de un 90% de los enlaces intermoleculares que la componen son de tipo no fenólico, predominando las uniones β-O-4 (Camarero *et al.*, 1994). Sin embargo, también se distribuyen en menor porcentaje enlaces de tipo β-5-fenilcumaran, β,β'-pinoresinol, 4-O-5-difeniléter y β-1-difenil-metano (Munk *et al.*, 2015; Xu *et al.*, 2014, **Figura 4**).

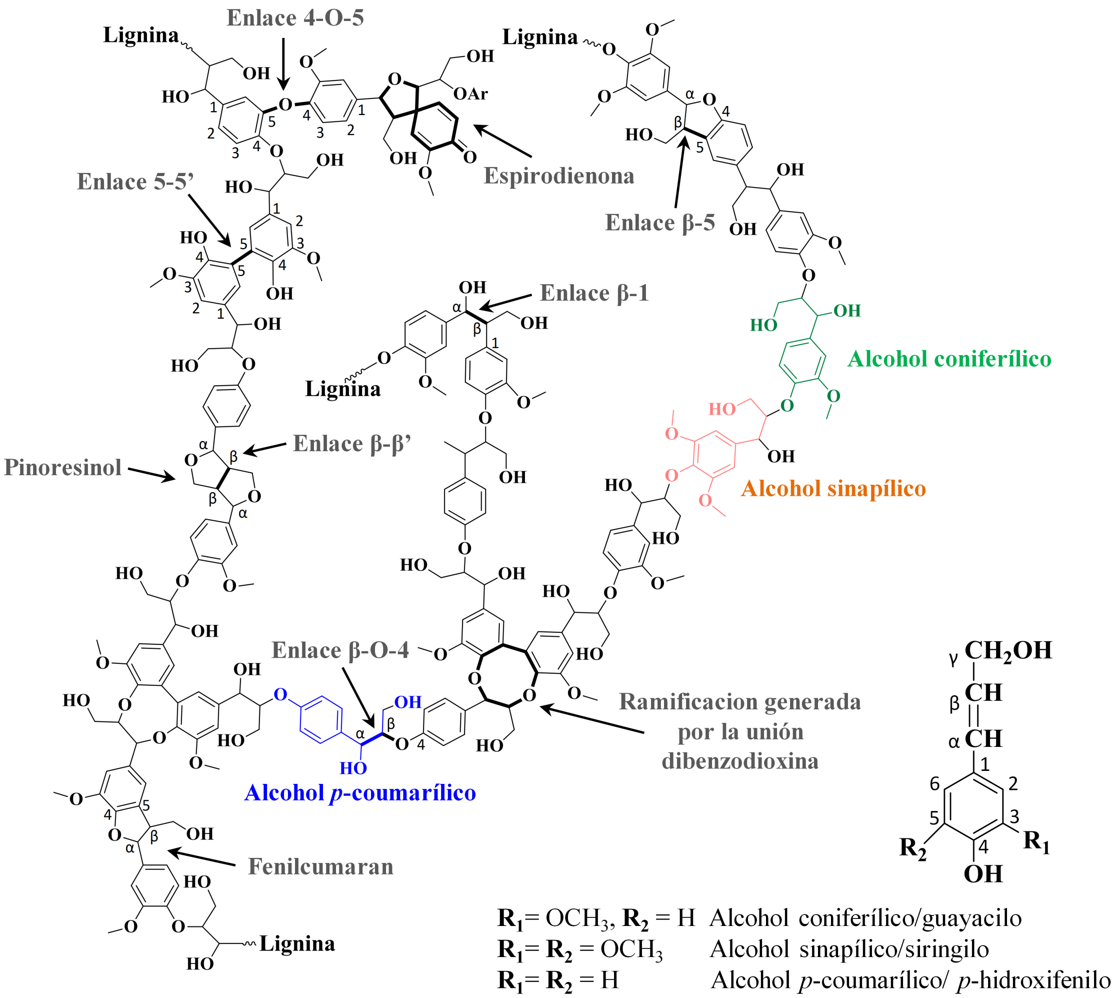

Figura 4. Estructura de un modelo de lignina con sus unidades fenilpropanoides y los enlaces principales. La estructura representada en la parte inferior derecha muestra los tres monolignones de lignina.

El contenido y composición en lignina del tejido vegetal presenta variaciones dependiendo del tipo de planta y su estado de desarrollo. En el caso de las gimnospermas la lignina se encuentra representada en mayor proporción que en angiospermas con una elevada predominancia en unidades G frente a unidades H (*ca.* 90%). En cambio, la lignina en angiospermas posee una proporción de unidades G y S que se distribuyen de manera más equitativa (*ca.* 50%). A diferencia de éstas, en herbáceas las tres unidades (H, G y S) se pueden encontrar en muy diferentes proporciones (Munk *et al.*, 2015; Novaes *et al.*, 2010; Zakzeski *et al.*, 2010). Particularmente, la relación S/G resulta muy útil a la hora de clasificar el tipo de material lignocelulósico que se va a tratar en la biorefinería, ya que puede dar una idea de la dificultad de degradación que va a requerir ese material en cuestión. Por ejemplo, relaciones mayores de 1 expresan altos contenidos en unidades S, lo cual es indicativo de una mayor susceptibilidad a la degradación.

La despolimerización de lignina es un proceso complejo debido a su elevada naturaleza recalcitrante. Es por ello, que se han desarrollado herramientas de bioingeniería de plantas para facilitar dicha transformación. Entre las técnicas más tradicionales utilizadas se encuentran: la represión de genes implicados en la biosíntesis de lignina, la búsqueda e identificación de polimorfismos que modifiquen el patrón de lignina desarrollado, y la ingeniería de RNA de interferencia que silencien genes específicos. Sin embargo, estas estrategias afectan a nivel general la estructura de la planta con la consiguiente pérdida de rigidez y protección frente a patógenos, llegando a provocar en algunos casos interferencias metabólicas. Las nuevas tecnologías en estado de desarrollo incluyen el uso de promotores específicos de tejido mediante editado del genoma vegetal, de manera que se pueda controlar la expresión de los transgenes implicados en la biosíntesis de lignina, dependiendo del estado de desarrollo de la planta. Además, se están intentando reemplazar los monolignones tradicionales por otros como, por ejemplo, el coniferil ferulato, la clovamida o ácido rosmarínico que faciliten una mayor degradación de la lignina y/o limiten la longitud de sus cadenas (Eudes *et al.*, 2014).

Sin lugar a dudas, para un buen aprovechamiento de la biomasa vegetal, la combinación de la bioingeniería de lignina con otras aproximaciones surgidas del auge de la biología sintética, la ingeniería de proteínas y la ingeniería metabólica, pueden contribuir a crear un modelo eficiente de degradación apoyado por herramientas de pre-tratamiento mecánico y/o físico-químico del material lignocelulósico.

Aunque se han dedicado muchos esfuerzos para facilitar el trabajo en las biorefinerías integrales, éstas han de recorrer todavía un largo camino hasta que puedan reemplazar a las tradicionales refinerías petrolíferas y se instauren como modelo económico sostenible. Dejando a un lado los problemas mecánicos inherentes a la materia prima vegetal (que incluye numerosos residuos y arenas que obstruyen las tuberías de la biorefinería, encareciendo y limitando el proceso), el principal obstáculo deriva de una ineficaz despolimerización de lignina. Dentro de las alternativas en estudio más pioneras se incluyen aquellos microorganismos capaces de mineralizar la lignina hasta CO_2, y el empleo de consorcios enzimáticos ligninolíticos (secretomas). En las siguientes secciones, se pasara a comentar los organismos implicados en el proceso de degradación de lignina, así como sus actividades enzimáticas con potencial uso en el pre-tratamiento del material lignocelulósico.

2. Organismos implicados en la degradación de lignina

Actualmente, existe una batería de pre-tratamientos mecánicos, físicos y químicos con los que se puede procesar la biomasa vegetal antes de ser sometida al tratamiento enzimático con celulasas, y finalmente al proceso fermentativo con diversos microorganismos. Sin embargo, en la mayoría de los casos suelen ser procesos muy costosos energéticamente, poco respetuosos con el medio ambiente y que generan subproductos que inhiben las rutas fermentativas (Jonsson and Martin, 2016). Como alternativa, se pueden aprovechar determinados sistemas biológicos, que han evolucionado de manera natural durante millones de años, y que se han especializado para desempeñar un papel fundamental en el reciclado del carbono en la biosfera. Se ha estimado que el contenido en lignina de las plantas comenzó a decrecer de manera abrupta con la aparición de los primeros hongos degradadores de lignina ya en el período del Carbonífero (hace unos 320 millones de años) (Floudas *et al.*, 2012). El contenido en lignina descendió desde mitad del Paleozoico (hace 350-250 millones de años), donde la lignina representaba en torno al 30-50% del peso total de la planta, hasta un 30% en el Mesozoico (hace 250-65 millones de años). En la actualidad, se ha determinado que el contenido medio en lignina de las plantas modernas ha disminuido hasta un 20% frente al peso total de la planta (Novaes *et al.*, 2010).

Los hongos capaces de despolimerizar la lignina sustancialmente en la naturaleza pertenecen a la división *Basidiomycota*, aunque también hay hongos de la división *Ascomycota* y bacterias capaces de modificar la lignina en un grado muy inferior (Abdel-Hamid *et al.*, 2013; Regalado *et al.*, 1997; Shary *et al.*, 2007). Dentro de los basidiomicetes, se pueden distinguir dos tipos de hongos según sus estrategias de degradación: los hongos de la podredumbre blanca y los hongos de la podredumbre parda. Los primeros secretan un conjunto de enzimas que tienen actividades inespecíficas capaces de descomponer la matriz de la lignina hasta CO_2 y agua, dando acceso a la celulosa y hemicelulosa. A diferencia de estos, los hongos de la podredumbre parda pueden modificar la lignina en un menor grado, pero suficiente como para poder acceder a los polisacáridos contenidos en la madera y utilizarlos como fuente de carbono. Evolutivamente, se ha descrito que los hongos de la podredumbre parda proceden de hongos de la podredumbre blanca simultáneos ancestrales que perdieron posteriormente sus actividades enzimáticas destinadas a la degradación específica de lignina. Este fenómeno ocurrió como un medio para reducir excesivo consumo energético asociado a la expresión de la gran batería de enzimas ligninolíticas, para centrarse en aquellas enzimas implicadas en la utilización de los polisacáridos (Eastwood *et al.*, 2011).

En la naturaleza, se pueden distinguir estos dos tipos de hongos porque mientras que los de la podredumbre blanca degradan la lignina dejando expuesta la celulosa no consumida con un característico color blanquecino en la madera, los hongos de la podredumbre parda dejan en la madera un depósito residual de lignina modificada que presenta color marrón o parduzco (Arantes *et al.*, 2012, **Figura 5**).

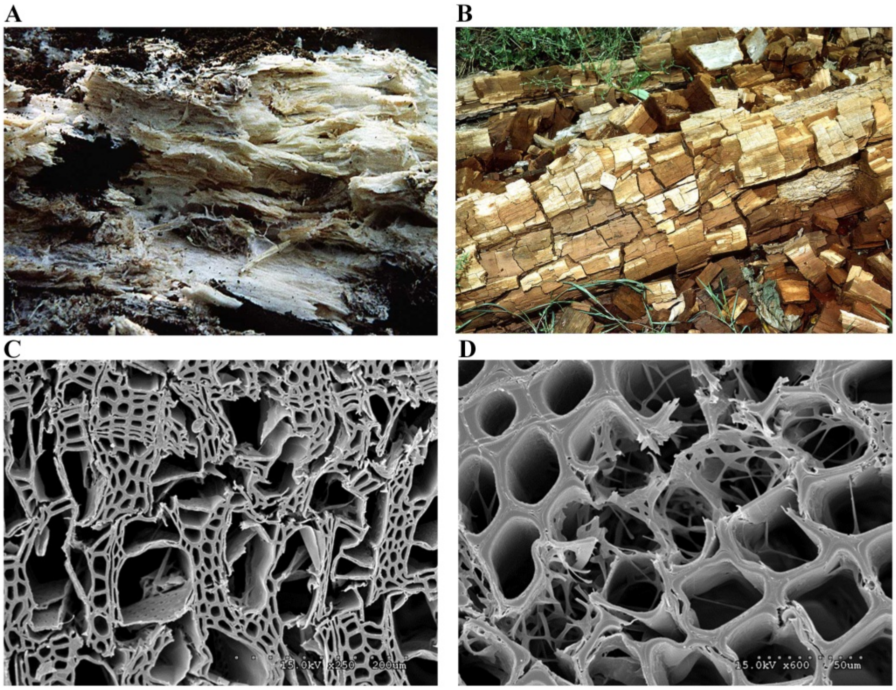

Figura 5. Patrones de degradación de lignina de hongos de la podredumbre blanca y parda. (**A**) y (**B**) muestran los depósitos que presenta la madera tras la actividad de hongos de podredumbre blanca (**A**) y parda (**B**). En (**C**) y (**D**) se muestran imágenes obtenidas con microscopia electrónica de barrido de diferentes materiales lignocelulósicos después de su tratamiento con *Botryobasidium botryosum* (**C**) y *Jaapia argillacea* (**D**), ambos hongos de podredumbre blanca. Se puede observar la degradación de lignina, celulosa y hemicelulosa en varias zonas del tejido vegetal. (Imágenes procedentes del *Joint Genome Institute*).

De manera general, los hongos de la podredumbre blanca se suelen encontrar colonizando especies de angiospermas donde el contenido en lignina es en torno al 20% (Couturier *et al.*, 2015, **Tabla 2**), mientras que los hongos de la podredumbre parda colonizan especies de gimnospermas, donde el contenido en lignina es mayor (30-60%) y su estructura presenta una alta cantidad de unidades G (Ferrer *et al.*, 2008; Martínez *et al.*, 2005; Schmidt, 2006).

Según la base de datos *MycoCosm-The Fungal Genomics Resource* (http://genome.jgi.doe.gov/programs/fungi/index.jsf) desarrollada por el *Joint Genome Institute* (JGI, USA), actualmente hay secuenciados 622 genomas de hongos de los cuales 215 pertenecen a basidiomicetes. Dichas secuencias proporcionan una enorme fuente de actividades ligninolíticas de gran interés con aplicación potencial dentro del campo de las biorefinerías.

2.1. Mecanismos de los hongos de la podredumbre parda

Las vías de despolimerización de lignina en los hongos de la podredumbre parda han sido ampliamente estudiadas en los organismos modelo *Gloephyllum trabeum* y *Postia placenta* (Daniel *et al.*, 2007; Jensen *et al.*, 2001; Martínez *et al.*, 2009b; Vanden Wymelenberg *et al.*, 2011). Sin embargo, el mecanismo específico de degradación por el cual se rigen este tipo de hongos es todavía una incógnita. De manera unánime entre los autores se ha llegado a un consenso acerca del papel relevante que desempeña la reacción de Fenton ($Fe^{2+} + H_2O_2 \rightarrow Fe^{3+} + OH^- + OH^\bullet$) durante el proceso de degradación mediado por radicales hidroxilo. Así, la reacción de Fenton se ha consolidado como el mecanismo subyacente a la despolimerización de lignina en hongos de podredumbre parda tanto para estadios tempranos como avanzados (Arantes *et al.*, 2012, **Figura 6A**). En efecto, se considera que la procedencia de los reactantes de Fenton (Fe^{2+} y H_2O_2) determina el mecanismo principal de degradación de la lignina. En este sentido, la mayoría de las rutas descritas tienen como denominador común la obtención de Fe^{2+} a partir de la reducción de depósitos naturales de Fe^{3+}. Además, se conoce que la solubilización del Fe^{3+} tiene lugar a través de su quelación con ácidos procedentes del metabolismo del hongo como el oxálico o el malónico. El gradiente de pH creado por la concentración de ácido oxálico (junto con la actividad tamponante de oxalato descarboxilasas) y la formación del complejo Fe^{3+}-oxalato evita la reducción del Fe^{3+} en las proximidades de la hifa del hongo protegiéndolo del daño oxidativo generado por la reacción de Fenton (Hyde and Wood, 1997; Varela and Tien, 2003). En cuanto a la producción de H_2O_2, se han descrito tres posibles vías diferentes incluyendo: (i) la actividad biológica de celobiosa deshidrogenasas (CDH), (ii) la actividad de metanol oxidasas (MOX) y, (iii) la vía no enzimática mediada por queladores/reductores de hierro o quinonas que son más fácilmente difusibles (Arantes *et al.*, 2012; Cameron and Aust, 1999; Zhu *et al.*, 2016).

2.2. Mecanismos de los hongos de la podredumbre blanca

Los hongos de la podredumbre blanca se dividen a su vez en dos categorías dependientes de las actividades codificantes en su genoma. Aquellos que son capaces de degradar la lignina selectivamente, pero no pueden utilizar los polisacáridos (celulosa y hemicelulosa) como fuente de carbono y energía, se denominan degradadores selectivos. Representantes de este tipo de hongos son *Pleurotus eryngii* y *Ceriporiopsis subvermispora* (Fernández-Fueyo *et al.*, 2012; Martínez *et al.*, 1994). Si la maquinaria presente en el hongo permite degradar la lignina al tiempo que hidrolizar los polisacáridos, se denominan degradadores simultáneos. Ejemplo de ello son *Phanerochaete chrysosporium* y *Trametes versicolor* (Goodell *et al.*, 2008; Martínez *et al.*, 2005; Tanaka *et al.*, 1999). Como ya se ha descrito anteriormente en el **apartado 1.2.2**, la estructura de la lignina no tiene un patrón específico de formación y presenta una diversidad de enlaces que hace aún más difícil su despolimerización. Como mecanismo de respuesta a dicha complejidad estructural, los hongos de podredumbre blanca han desarrollado un consorcio extracelular multienzimático constituido por diversas oxidorreductasas altamente inespecíficas y por norma general, con elevado potencial redox. Este secretoma ligninolítico se complementa con diversos metabolitos difusibles que contribuyen al proceso de mineralización de la lignina (Kirk and Farrell, 1987, Martinez *et al.*, 2005; Ruiz-Dueñas and Martínez, 2009a). Entre las principales oxidorreductasas ligninolíticas (también conocidas como ligninasas) implicadas en la combustión enzimática de la lignina podemos encontrar lacasas, peroxidasas, peroxigenasas inespecíficas, peroxidasas decolorantes de tintes y enzimas auxiliares (estas últimas suministran H_2O_2 tanto a las peroxidasas/peroxigenasas como a la reacción de Fenton) (Abdel-Hamid *et al.*, 2013; Liers *et al.*, 2011; Wong, 2009, **Figura 6B**). En lo referente a los metabolitos difusibles, su función biológica es de gran importancia ya que solventan las limitaciones estéricas que encuentran las enzimas debido a la compleja estructura del entramado lignocelulósico.

Dichos metabolitos actúan como transportadores (mediadores redox) difusibles, que tras ser oxidados por la ligninasa, pueden difundir en su forma radicalaria a través de la estructura interna de la lignina favoreciendo la despolimerización interna. Los mediadores redox pueden proceder de diferentes fuentes como, por ejemplo, el entorno donde se encuentra la hifa del hongo (depósitos de Mn^{2+} en la madera), del propio metabolismo fúngico (alcohol veratrílico), o bien de subproductos derivados de la degradación temprana de lignina (siringaldehído, vanillina, acetosiringona, etc). (Camarero *et al.*, 1996; Cañas and Camarero, 2010; Goodwin *et al.*, 1995; Harvey *et al.*, 1986). La actuación coordinada de las ligninasas y los mediadores redox genera una población de radicales aromáticos que desencadenan una cascada de reacciones de tipo no enzimático, que son responsables de la ruptura de numerosos enlaces de la lignina, como los enlaces β-O-4, las uniones Cα-Cβ (reacciones que liberan mediadores redox), además de promover desmetoxilaciones de unidades G y S (Martínez *et al.*, 2005, **Figura 6**). Asimismo, se han descrito péptidos de bajo peso molecular (desde 1,5 kDa hasta 12 kDa) capaces de generar radicales hidroxilo mediante reacciones acopladas de reducción/oxidación, siendo una vía complementaria de degradación de lignina a la acción de las ligninasas y los mediadores difusibles (Dashtban *et al.*, 2010).

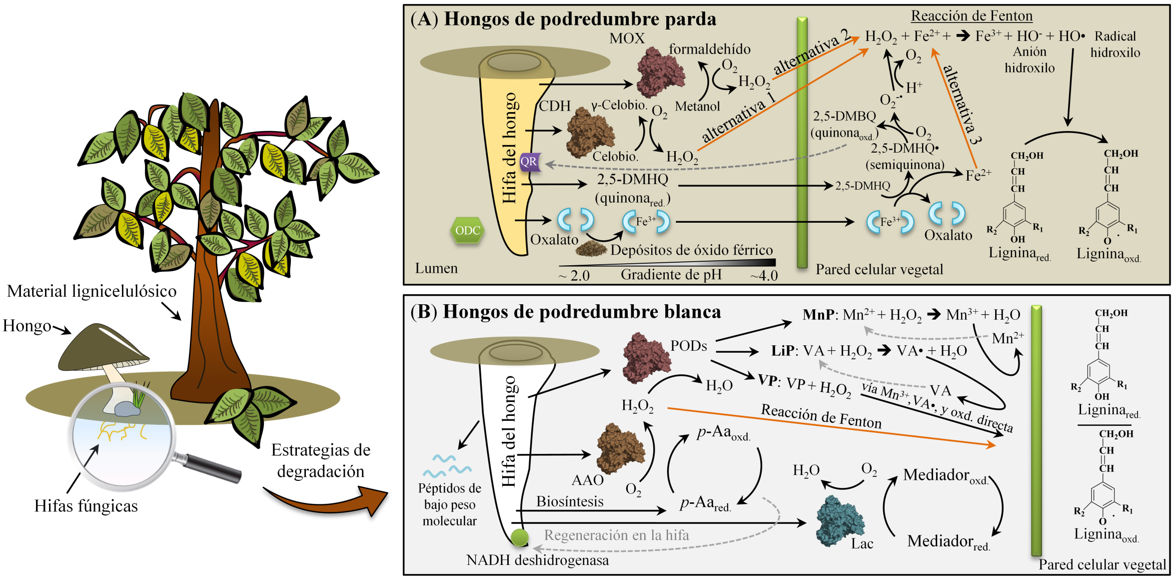

Figura 6. Mecanismos de degradación de lignina de hongos de la podredumbre parda y blanca. En (**A**) y (**B**) se muestran los mecanismos de degradación de lignina de los hongos de la podredumbre parda y blanca, respectivamente. También se incluyen las actividades de las enzimas y/o metabolitos implicados en el proceso. Las rutas de regeneración se indican con línea punteada gris. Las flechas negras indican la dirección de la reacción. AAO: aril-alcohol oxidasa, CDH: celobiosa deshidrogenasa, Lac: lacasa, LiP: lignina peroxidasa, MnP: manganeso peroxidasa, MOX: metanol oxidasa, ODC: oxalato descarboxilasa, *p*-Aa: alcohol *p*-anisílico, PODs: peroxidasas ligninolíticas, QR: quinona reductasa, VA: alcohol veratrílico y VP: peroxidasa versátil.

A continuación se describen brevemente las características de las principales oxidorreductasas que componen el consorcio ligninolítico de los hongos de la podredumbre blanca:

Las **lacasas fúngicas** (EC 1.10.3.2) pertenecen al grupo de las oxidasas multicobre y se caracterizan por presentar en su centro activo cuatro átomos de cobre agrupados en un cobre de tipo T1, y un cluster trinuclear T2/T3 (Matera *et al.*, 2008). Estas enzimas pueden oxidar un amplio espectro de compuestos incluyendo fenoles, polifenoles, anilinas y benzotioles dando lugar a la reducción del oxígeno molecular para formar agua como único subproducto (Baldrian, 2006; Cañas and Camarero, 2010; Xu, 1996). Debido a su limitado potencial redox (0,5-0,8V), las lacasas necesitan de mediadores para que actúen como intermediarios de la reacción difundiendo y aumentando dicho potencial mediante los conocidos sistemas lacasa-mediador (Cañas and Camarero, 2010; Morozova *et al.*, 2007). En presencia de mediadores, las lacasas pueden llevar a cabo la despolimerización de lignina a través de la ruptura de enlaces entre subunidades no fenólicas que presentan un alto potencial redox (~1,5 V). Sin embargo, en ausencia de mediador sólo pueden limitarse a oxidar subunidades fenólicas de lignina ya que muestran menor potencial redox (0,5-1,0 V; Munk *et al.*, 2015).

Las **peroxidasas ligninolíticas** (EC 1.11.1.x), a diferencia de las lacasas, son hemoproteínas dependientes de H_2O_2 y tienen un potencial redox que varía desde 0,9 hasta 1,5 V. Según su espectro de oxidación se pueden clasificar en cuatro grupos diferenciados: lignina peroxidasa (LiP), manganeso peroxidasa (MnP), peroxidasa versátil (VP) y peroxidasas genéricas (GP) (Floudas *et al.*, 2012; Kellner *et al.*, 2014). La LiP es capaz de oxidar compuestos no fenólicos presentes en la estructura de la lignina además de un amplio rango de compuestos fenólicos en presencia de alcohol veratrílico (Harvey and Palmer, 1990; Koduri and Tien, 1995; Wong, 2009). La localización estratégica de un triptófano catalítico en la superficie de la LiP, la permite modificar la lignina directamente aunque también puede usar el alcohol veratrílico como mediador redox -de corto recorrido- para este fin (Floudas *et al.*, 2012; Hammel and Moen, 1991). La MnP, a diferencia de la LiP, posee un canal lateral que permite la oxidación de Mn^{2+} a Mn^{3+}, el cual es quelado mediante ácidos orgánicos secretados por el propio hongo con lo que finalmente puede difundir penetrando en el entramado molecular de la lignina más fácilmente. Al formarse el complejo quelado el potencial redox natural del Mn^{3+} (0,7-0,9V) decae, y esto hace que solo pueda oxidar subunidades no fenólicas de lignina (Hofrichter, 2002; Nousiainen *et al.*, 2014). Sin embargo, dicho complejo es capaz de oxidar también subunidades fenólicas de lignina a través de un segundo mediador redox (como ácidos orgánicos o ácidos grasos poliinsaturados) generado por peroxidación de lípidos, radicales de ácido acético, radicales superóxido y radicales de formato (Bao *et al.*, 1994; Dashtban *et al.*, 2010; Hofrichter *et al.*, 1998). Las peroxidasas genéricas por su parte, se caracterizan por tener un canal de acceso al hemo y bajo potencial redox ~0,9 V. Estas características sólo las permiten oxidar ciertos fenoles y dímeros de lignina que sean accesibles por el canal de acceso al grupo hemo (Floudas *et al.*, 2012). Finalmente, las VPs comparten las características estructurales de la LiP, MnP y GPs (Camarero *et al.*, 1999; Floudas *et al.*, 2012; Ruiz-Dueñas *et al.*, 2009b). Esto significa que son capaces de oxidar Mn^{2+} como hace la MnP, alcohol veratrílico como la LiP y fenoles como las GPs. Además de oxidar subunidades fenólicas y no fenólicas de lignina, las VPs también pueden actuar sobre otros sustratos como tintes de alto potencial redox (*p. ej.* el *Reactive black 5*, RB5) que no son oxidados por la MnP ni la LiP en ausencia de mediadores. La VP se ha descrito principalmente en los géneros de hongos degradadores selectivos como *Bjerkandera spp.* y *Pleurotus spp.*, pero no en degradadores simultáneos como *P. chrysosporium* (Coconi-Linares *et al.*, 2014; Jarosz-Wilkołazka *et al.*, 2009; Ruiz-Dueñas *et al.*, 2001).

Las **enzimas supletorias de H_2O_2** (EC 1.1.3.x), son oxidorreductasas que reducen alcoholes derivados de la despolimerización de lignina (como el metilglioxal), o procedentes del metabolismo del hongo (como el alcohol *p*-anisílico), produciendo H_2O_2 y aldehídos a partir de O_2 molecular (Hernández-Ortega *et al.*, 2012; Kersten and Cullen, 2007; Ruiz-Dueñas and Martínez, 2009a). Entre los representantes de este grupo de enzimas se incluyen las flavoxidasas (pertenecientes a la familia glucosa-metanol-colina; GMC) aril-alcohol oxidasa (AAO; ampliamente estudiada en el género *Pleurotus*; Guillén *et al.*, 1990), piranosa 2-oxidasa (Leitner *et al.*, 2001) y metanol oxidasa (Linke *et al.*, 2014), así como la radical-cobre oxidasa glioxal oxidasa (Kersten and Kirk, 1987). El H_2O_2 producido por estas enzimas alimenta de manera lateral a la reacción de Fenton, siendo también esta vía una de las alternativas adoptada para la generación de H_2O_2 en los hongos de la podredumbre parda (**Figura 6A**).

Recientemente, también se han descrito nuevas enzimas del consorcio ligninolítico que han obligado a crear nuevas superfamilias debido a sus diferencias estructurales y catalíticas. Estos miembros son las peroxidasas decolorantes de tintes y las peroxigenasas inespecíficas que se comentan a continuación:

Las DyP (EC 1.11.1.19), también conocidas como peroxidasas decolorantes de tintes, presentan un alto potencial redox de ~1,2 V (Hofrichter *et al.*, 2010) y al igual que las peroxidasas ligninolíticas mencionadas, son capaces de oxidar sustratos tales como el alcohol veratrílico, RB5, Mn^{2+} y dímeros modelo no fenólicos de lignina (Fernández-Fueyo *et al.*, 2015; Liers *et al.*, 2013; Salvachúa *et al.*, 2013). En la DyP, de modo similar a la LiP y VP, se ha descrito una ruta de transferencia electrónica que conecta el grupo hemo con un residuo de Tyr en la superficie de la proteína que actúa en forma de radical (Colpa *et al.*, 2014; Strittmatter *et al.*, 2013a). A pesar de que la función biológica de las DyP no está clara por el momento, se ha postulado que pueden estar implicadas en la degradación de lignocelulosa, así como en la detoxificación y defensa inespecífica en el hongo (Liers *et al.*, 2011; 2013).

La UPO o peroxigenasa inespecífica (EC 1.11.2.1) pertenece a la superfamilia de las peroxidasas hemotioladas (HTP) mostrando tanto actividad peroxidasa (reacción de oxidación de un electrón) como peroxigenasa (reacción de oxidación de dos electrones). Es esta segunda actividad la que mayor relevancia biotecnológica adquiere, debido a su capacidad para realizar oxifuncionalizaciones de enlaces C-H con una alta selectividad sobre una gran variedad de compuestos orgánicos. Aunque su papel en la despolimerización de la lignina no está del todo claro, su actividad frente a compuestos modelo de lignina no fenólicos la atribuyen una implicación razonable (Kinne *et al.*, 2011; Liers *et al.*, 2011; Ullrich *et al.*, 2004; Wang *et al.*, 2015).

Por último, es importante mencionar que todas estas enzimas principales, también coexisten junto con otros miembros como las aril-alcohol deshidrogenasas (AAD) y quinona reductasas (QR), las cuales ayudan al reciclado de las reacciones redox creando un sistema mucho más autónomo. A modo de ilustrar el proceso de degradación de lignina, en la **Figura 7** se detallan las reacciones más probables que puede llevarse a cabo por el consorcio ligninolítico en la naturaleza.

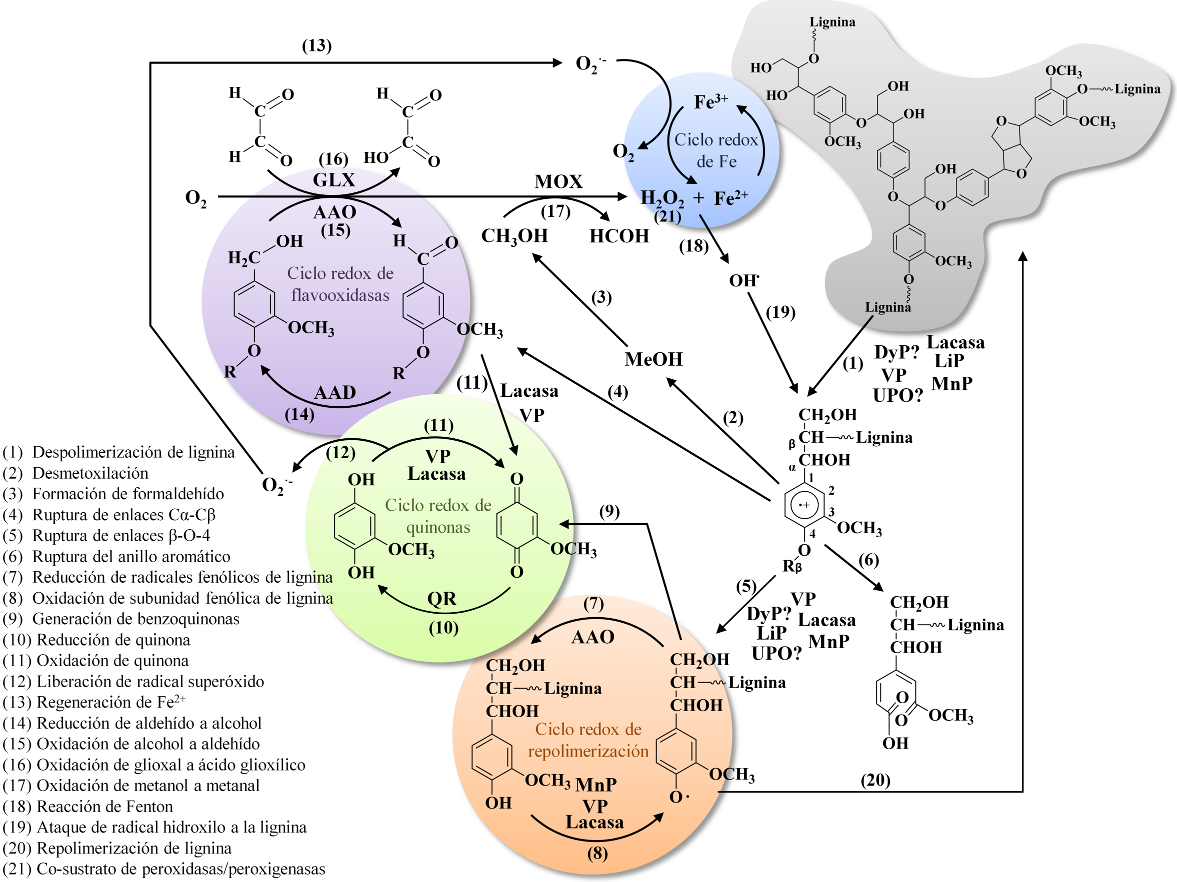

(1) Despolimerización de lignina
(2) Desmetoxilación
(3) Formación de formaldehído
(4) Ruptura de enlaces Cα-Cβ
(5) Ruptura de enlaces β-O-4
(6) Ruptura del anillo aromático
(7) Reducción de radicales fenólicos de lignina
(8) Oxidación de subunidad fenólica de lignina
(9) Generación de benzoquinonas
(10) Reducción de quinona
(11) Oxidación de quinona
(12) Liberación de radical superóxido
(13) Regeneración de Fe^{2+}
(14) Reducción de aldehído a alcohol
(15) Oxidación de alcohol a aldehído
(16) Oxidación de glioxal a ácido glioxílico
(17) Oxidación de metanol a metanal
(18) Reacción de Fenton
(19) Ataque de radical hidroxilo a la lignina
(20) Repolimerización de lignina
(21) Co-sustrato de peroxidasas/peroxigenasas

Figura 7. Detalle de las reacciones implicadas en la despolimerización de lignina por el consorcio ligninolítico.

Los números indican el tipo de reacción, mientras que en cada reacción se incluyen las enzimas más probablemente implicadas en los diferentes procesos. En azul se resalta el ciclo redox de la regeneración de hierro para la reacción de Fenton, en morado se detalla el ciclo redox de producción de H_2O_2, en verde el ciclo redox de quinonas, y en naranja el ciclo de redox que da lugar a la repolimerización de lignina. AAD: aril-alcohol deshidrogenasa, AAO: aril-alcohol oxidasa, DyP: peroxidasa decolorante de tintes, GLX: glioxal oxidasa, LiP: lignina peroxidasa, MOX: metanol oxidasa, MnP: manganeso peroxidasa, QR: quinona reductasa, UPO: peroxigenasa inespecífica y VP: peroxidasa versátil.

3. Peroxidasas ligninolíticas

3.1. Clasificación, generalidades y estructura

Las peroxidasas, como ya se ha mencionado en el apartado anterior, son oxidorreductasas que catalizan la oxidación de diferentes sustratos tras su activación mediada por H_2O_2. Su distribución biológica es ubicua en todos los reinos de la vida, y se cuenta con más de 13.000 secuencias que han sido recogidas hasta la fecha en una base de datos denominada PeroxiBase (Fawal *et al.*, 2013, http://peroxibase.toulouse.inra.fr/). Taxonómicamente, las peroxidasas se pueden clasificar en dos grandes grupos: peroxidasas que contienen un cofactor de tipo hemo (la mayoría de ellas), o peroxidasas que usan otros elementos como cofactor entre las que se encuentran la vanadio haloperoxidasa, manganeso catalasa, tiol peroxidasa o la alquil hidroperoxidasa (Butler and Carter-Franklin, 2004; Flohe *et al.*, 2011; Guimaraes *et al.*, 2005; Whittaker, 2012). Las peroxidasas ligninolíticas (conocidas como PODs) se clasifican dentro del grupo de las peroxidasas que contienen grupo hemo, y se pueden encontrar en un número limitado de organismos (hongos y bacterias). Dentro de las hemoperoxidasas se describen seis superfamilias diferentes, entre las que se incluye la superfamilia de peroxidasas no animales. Dicha superfamilia se divide a su vez en tres clases donde se recogen las peroxidasas intracelulares o bacterianas (Clase I), peroxidasas fúngicas (Clase II, en este grupo se encuentran las PODs) y las peroxidasas de plantas (Clase III).

A diferencia de las peroxidasas de Clase II, las DyPs y las UPOs presentan diferencias estructurales que hacen necesaria su agrupación en otras superfamilias (Hofrichter *et al.*, 2010; Zamocky *et al.*, 2014). En el siguiente esquema se muestra la clasificación de las PODs (resaltadas en negrita):

Peroxidasas (EC 1.11.x)

- Peroxidasas que no contienen hemo (5 superfamilias)
- Peroxidasas que contienen hemo (6 superfamilias)
  - Peroxidasa-ciclooxigenasas (7 clases, *p. ej.* peroxidasa tiroidea, EC 1.11.1.8)
  - Hemo peroxidasas no animales (3 clases)
    - Clase I (peroxidasas intracelulares y/o bacterianas, *p. ej.* APx, EC 1.11.1.11)
    - **Clase II (peroxidasas secretadas por hongos)**
      - **GP (peroxidasas genéricas, *p. ej.* CiP, EC 1.11.1.7)**
      - **MnP (manganeso peroxidasa, EC 1.11.1.13)**
      - **LiP (lignina peroxidasa, EC 1.11.1.14)**
      - **VP (peroxidasa versátil, EC 1.11.1.16)**
    - Clase III (peroxidasas de plantas, EC 1.11.1.7)
  - Catalasas (EC 1.11.1.6)
- Di-hemo citocromo c peroxidasa (EC 1.11.1.5)
- **DyP (peroxidasa decolorante de tintes, EC 1.11.1.x)**
  - Familia 1 (DyPs bacterianas y fúngicas)
    - Subfamilia 1A (DyPs fúngicas)
    - Subfamilia 1B (DyPs bacterianas)
  - Familia 2 (DyPs bacterianas y de *Ascomicetos*)
    - Subfamilia 2A (Tat-DyPs bacterianas)
    - Subfamilia 2B (TyrA y BtDyP homólogas a DyPs)
- Peroxidasas hemotioladas (“Haloperoxidasas”)
  - CPO (Cloroperoxidasas de *Caldariomyces fumago*, EC 1.11.1.10)
  - **UPO (*p. ej.* peroxigenasa inespecífica de *Agrocybe aegerita*, EC 1.11.2.1)**

Las peroxidasas ligninolíticas se describieron por primera vez en cultivos de *P. chrysosporium*, donde la adición de catalasa a los medios de cultivo disminuyó drásticamente la tasa de despolimerización de lignina (Faison and Kirk, 1983). Este hecho correlacionó la existencia de las peroxidasas a la presencia de H_2O_2. A partir de entonces se descubrieron la MnP y la LiP en *P. chrysosporium*, y más tarde la VP en los géneros *Pleurotus* y *Bjerkandera* (Martínez, 2002). La LiP H8 (denominada así por la fracción en la que eluyó durante su purificación; Rothschild *et al.*, 1997) y la MnP1 de *P. chrysosporium* fueron las primeras peroxidasas ligninolíticas en resolverse cristalográficamente (Piontek *et al.*, 1993; Sundaramoorthy *et al.*, 1994). Tras ello la estructura de la VP de *P. eryngii* también fue resuelta (PDB: 3FJW). Además de estas estructuras, también se han cristalizado otras peroxidasas genéricas como la CiP (*Coprinus cinerea* peroxidasa) y la ARP (*Arthromyces ramosus* peroxidasa) (Kunishima *et al.*, 1994; Petersen *et al.*, 1994).

Los estudios desarrollados a partir de las estructuras resueltas de las PODs, han proporcionado valiosa información que ha permitido la caracterización de los cuatro grupos ya comentados en la sección anterior (**Tabla 3**).

Tabla 3. Características de las peroxidasas ligninolíticas.

Enzima	Numero EC	Potencial redox (V)	Peso molecular (kDa)	Punto isoeléctrico	Mediadores redox	Degradación de lignina
LiP	1.11.1.14	1,4-1,5	38-46	3,2-4,0	Alcohol veratrílico$^{+\bullet}$	Subunidades no fenólicas
MnP	1.11.1.13	1,0-1,2	38-62	3,1-4,8	Mn^{3+}	Subunidades fenólicas y no fenólicas
VP	1.11.1.16	~1,4-1,5	39-43	3,5-4,6	Alcohol veratrílico$^{+\bullet}$ y Mn^{3+}	Subunidades fenólicas y no fenólicas
GP	1.11.1.7	~0,9-1,1	42	3,5	-	Compuestos fenólicos

Tabla realizada a partir de (Hofrichter *et al.*, 2010 and Wong, 2009).

En cuanto a su estructura molecular, las PODs muestran una forma globular compuesta en su mayoría por 11-12 α-hélices, que se nombran por orden alfabético de la A a la J incluyendo B', según la numeración que ya se aplicó anteriormente para la citocromo C peroxidasa (CCP, la primera peroxidasa resuelta cristalográficamente; Finzel *et al.*, 1984). La estructura de las PODs se mantiene estable gracias a la presencia de cuatro puentes disulfuro (cinco en las MnPs; el quinto situado en el C-terminal) y dos iones calcio localizados por encima y por debajo del plano del hemo (Martínez, 2002). A partir de esta estructura molecular básica cada una de las PODs ha desarrollado de uno a tres sitios activos que determinan sus principales diferencias catalíticas. Todas ellas presentan un canal de acceso a un grupo hemo, el cual es de tipo b y está formado por la unión de cuatro anillos pirrólicos (protoporfirina IX) más un ion férrico en su estado basal. El plano creado por el grupo hemo divide la proteína en dos dominios diferenciados: el dominio situado en la parte superior del hemo recibe el nombre dominio distal, mientras que el dominio situado en la parte inferior del mismo se denomina dominio proximal. A excepción de las peroxidasas genéricas que sólo presentan el canal de acceso al grupo hemo, el resto de PODs pueden mostrar un sitio de unión a Mn^{2+} como la MnP, un triptófano catalítico en la superficie de la proteína como la LiP o ambos sitios catalíticos como la VP (**Figura 8**).

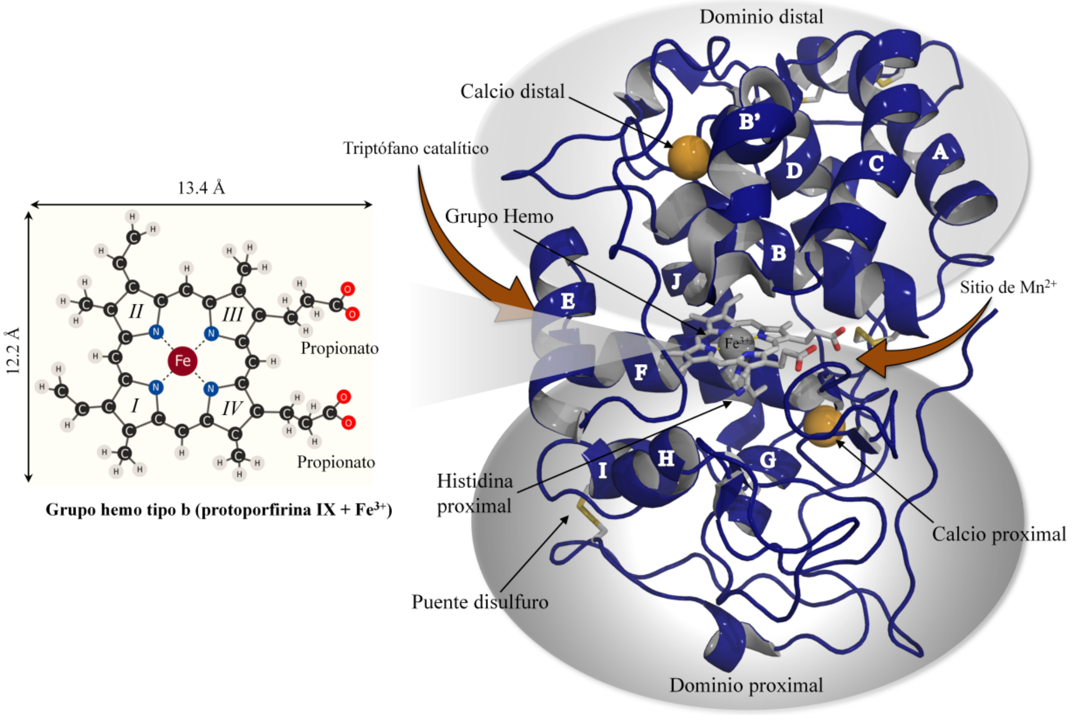

Grupo hemo tipo b (protoporfirina IX + Fe^{3+})

Figura 8. Estructura general de las PODs.
A la izquierda se muestra el detalle del grupo prostético hemo de tipo b. En la parte derecha se detalla la estructura de las PODs resaltando la posición de los calcios estructurales, los sitios catalíticos alternativos (para LiP, VP y MnP), los puentes disulfuro y los dominios que las caracterizan. Las letras indicadas en el modo *cartoon* corresponden a la numeración de las alfa hélices en la estructura.

3.2. Peroxidasa versátil

La peroxidasa versátil (VP) secretada por el hongo de podredumbre blanca *Pleurotus eryngii* ha sido el objeto de estudio de la presente Tesis Doctoral. Esta enzima se descubrió en 1996 asignándose como MnP, y más tarde como una peroxidasa híbrida con actividad MnP y LiP (Camarero *et al.*, 1999; Martínez *et al.*, 1996; Ruiz-Dueñas *et al.*, 1999; 2001). La VP se encuentra en el genoma de *P. eryngii* en forma de tres variantes alélicas denominadas *vpl1*, *vpl2*, y *vpl3,* siendo la isoforma VPl2 (GeneBank-AF007224; UniProtKB-O94753) la más estudiada hasta el momento. La VP es una proteína de 361 aminoácidos, y en *P. eryngii* porta una secuencia señal de 30 aminoácidos extra que es escindida antes de su exportación. El contenido en carbohidratos de la VP es de ~7% y su peso molecular total ronda los 43 kDa (Ruiz-Dueñas *et al.*, 1999). Debido a la presencia de tres sitios de oxidación (canal de acceso al hemo, sitio de oxidación de Mn^{2+} y triptófano catalítico en superficie), la VP está capacitada para catalizar -tras su activación mediada por H_2O_2- la oxidación de compuestos aromáticos tanto fenólicos como no fenólicos, tintes de alto potencial redox, e incluso el polímero de lignina directamente o de forma mediada (Morales *et al.*, 2012; Pérez-Boada *et al.*, 2005; Sáez-Jiménez *et al.*, 2015b).

En las próximas secciones se detallarán los determinantes estructurales, mecanismo catalítico, características de los sitios de oxidación, así como las potenciales aplicaciones y limitaciones biotecnológicas de las VPs.

3.2.1. Disposición estructural del grupo hemo

Se han identificado al menos diez residuos conservados que definen la reactividad y funcionalidad de la VP, los cuales se dividen en dos grupos de cinco ubicándose en los lados proximal y distal, respectivamente. La contribución de estos residuos se describe a continuación empleando la numeración de la VP de *P. eryngii* (**Figura 9**).

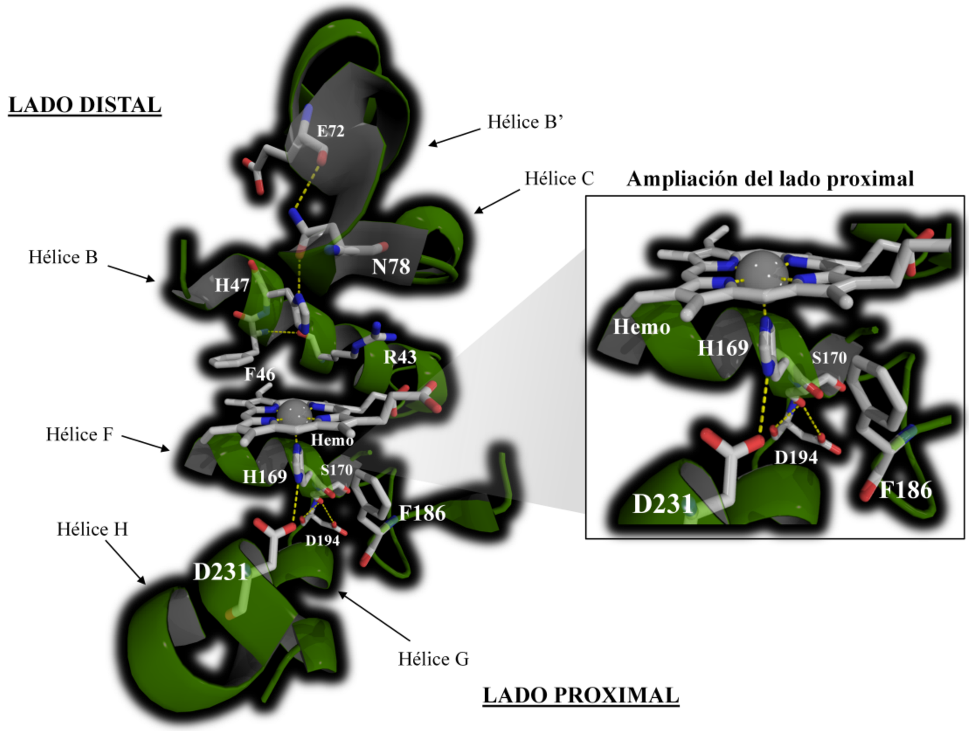

Figura 9. Residuos conservados en las PODs en los lados proximal y distal.

En el lado proximal (por debajo del plano del hemo) se encuentra la His169 (histidina proximal) que actúa como quinto ligando axial en la coordinación del Fe^{3+} contenido en el hemo. En estado de reposo, el Fe^{3+} se encuentra en forma de alto spin mediante la coordinación de los cuatro nitrógenos del anillo pirrólico, más la quinta coordinación del N_{ε} de esta histidina proximal.

Se ha postulado que la distancia entre la histidina proximal y el Fe^{3+} modula el potencial redox de la enzima, ya que cuanto mayor es esta distancia en la coordinación axial, mayor es el potencial redox siguiendo el orden LiP~VP>MnP>GP (Banci *et al.*, 1993). Además, se piensa que el factor responsable de dicha distancia se localiza en una red de puentes de hidrógeno establecida entre la His169 y los residuos Ser170, Asp194 y Asp231 (Piontek *et al.*, 1993).

En el lado proximal también se localiza la Phe186, con función no determinada, pero cuya sustitución facilita la perdida de los calcios estructurales comprometiendo la estabilidad de la proteína (Kishi *et al.*, 1997). Sin embargo, esta posición se encuentra ocupada por un residuo de triptófano en las peroxidasas de clase I como la CCP.

En el lado distal de la proteína (por encima del plano del hemo) se encuentra la histidina distal (His47) que junto con la Arg43 tiene un papel fundamental en la ruptura heterolítica del H_2O_2 (Erman *et al.*, 1993; Vitello *et al.*, 1993). Además, en este mismo lado se encuentran la Phe46, el Glu72 y la Asn78, que establecen una red de puentes de hidrógeno que ayudan a mantener la posición relativa de las ya mencionadas His47 y Arg43 (Martínez, 2002).

3.2.2 Calcios estructurales

En la estructura de VP (y por extensión en las PODs) se pueden encontrar dos calcios estructurales que se localizan en el domino proximal (calcio proximal) y en el domino distal (calcio distal). Ambos iones calcio se encuentran unidos a la proteína mediante siete enlaces de coordinación establecidos con átomos de oxígeno pertenecientes a residuos colindantes o moléculas de agua. El calcio proximal se encuentra sumergido en la estructura de la VP y fuertemente unido por la presencia de cinco residuos colocados estratégicamente (Ser170, Asp187, Thr189, Val192 y Asp194). Sin embargo, el calcio distal se encuentra más expuesto al solvente y coordinado por la acción de cuatro residuos (Asp48, Gly60, Asp62 y Ser64) y dos moléculas de agua (**Figura 10**).

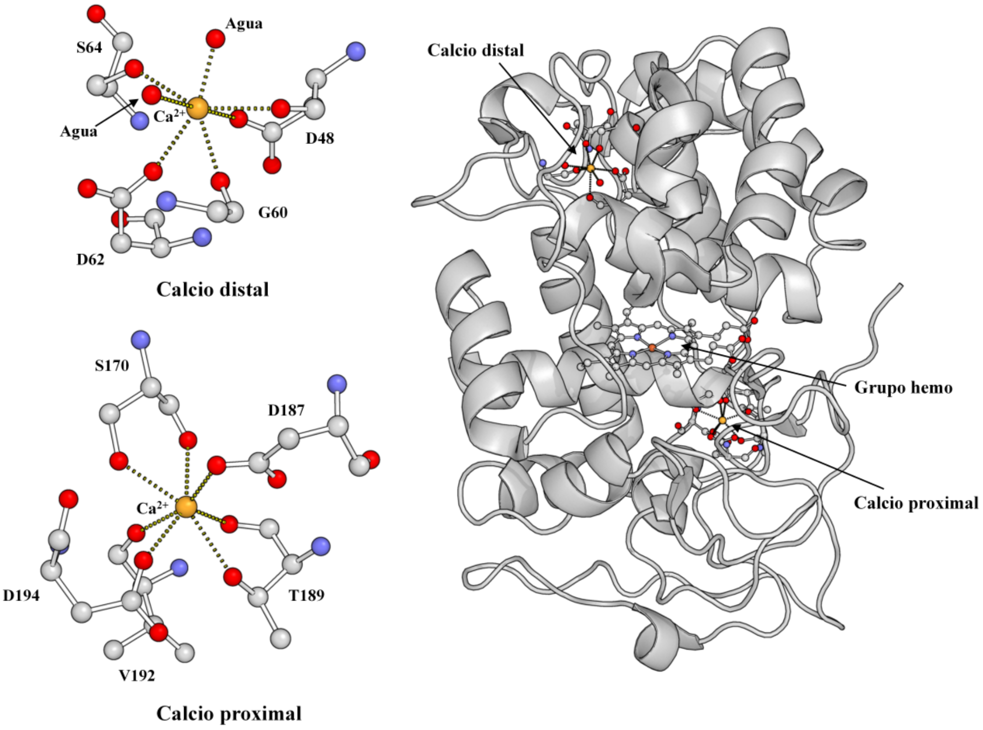

Figura 10. Interacción de los calcios estructurales en la VP de *P. eryngii*.

3.2.3 Mecanismo catalítico y características espectroscópicas

El primer paso del ciclo catalítico general de las PODs comienza con una activación por H_2O_2. El hierro del grupo hemo (en forma de Fe^{3+} en su estado basal), es capaz de unir el H_2O_2 haciendo que la His47 y la Arg43 puedan llevar a cabo la ruptura heterolítica del mismo. Esto ocurre mediante la acción ácido-base de la His47 que retira un protón del oxígeno α del H_2O_2, mientras que la cadena lateral de la Arg43 estabiliza la carga negativa del oxígeno β del mismo. Seguidamente, la His47 transfiere el protón sustraído hasta el oxígeno β dando lugar a la ruptura del enlace O-O con la correspondiente liberación de una molécula de agua (Hiner *et al.*, 2002, **Figura 11**).

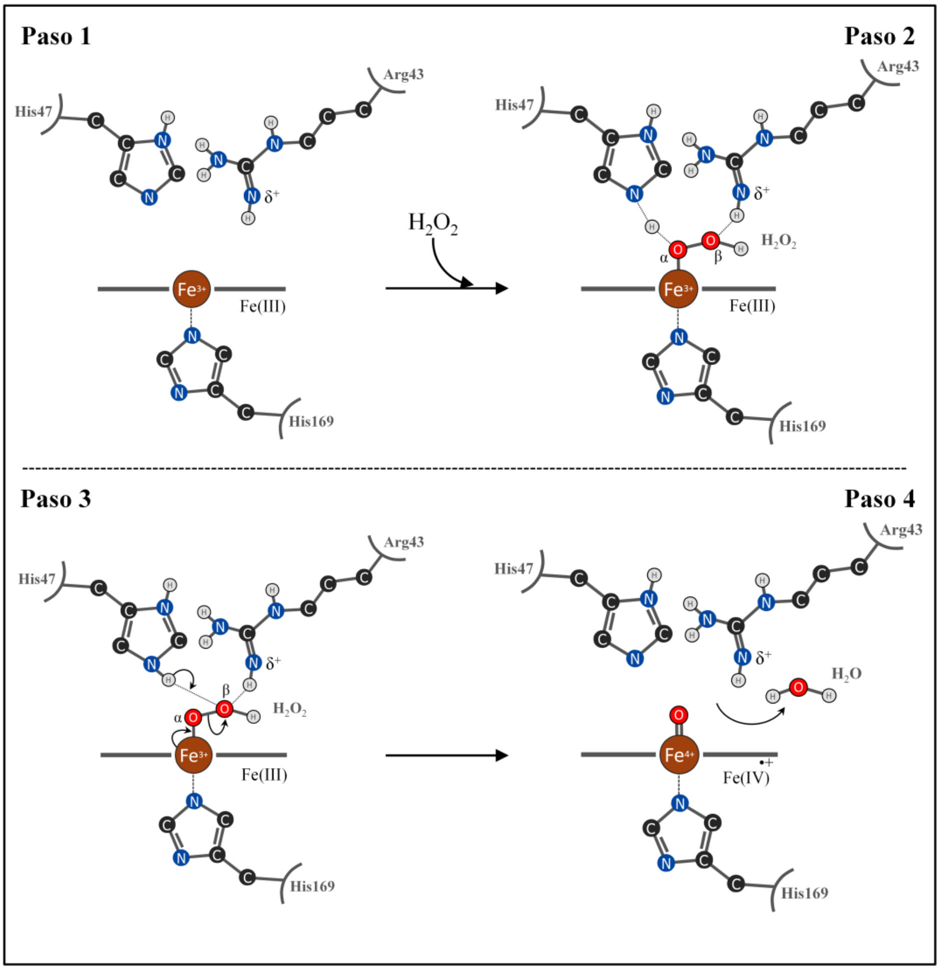

Figura 11. Mecanismo de ruptura heterolítica de la molécula de H_2O_2 en la VP.

En esta situación, la enzima se encuentra en su forma activada (*i.e.* ha perdido dos electrones) y puede llevar a cabo la oxidación sucesiva de dos moléculas de sustrato para recuperar su estado de reposo. Durante este ciclo catalítico se pueden distinguir dos intermediarios denominados compuesto I y compuesto II (Gumiero *et al.*, 2011; Pérez-Boada *et al.*, 2005, **Figura 12**). La formación del compuesto I tiene lugar justo después de la activación por el H_2O_2. Esta especie catalítica se caracteriza por tener dos deficiencias electrónicas localizadas en el hierro del hemo en forma de radical oxoferrilo ($Fe^{4+}=O$), y en el anillo de la porfirina como radical catiónico-π. Tras la oxidación de una primera molécula de sustrato, la deficiencia de la porfirina se satisface y se forma el compuesto II (que sigue portando el radical oxoferrilo). Finalmente, el compuesto II oxida una segunda molécula de sustrato liberando una molécula de H_2O y devolviendo la enzima a su estado basal (con el ion hierro en estado férrico).

En el caso de la VP, el ciclo catalítico es más complicado ya que al tener tres sitios de oxidación diferentes (canal del hemo, Trp catalítico y sitio de unión de Mn^{2+}) existen múltiples rutas e intermediarios catalíticos. Entre estos intermediarios se encuentran dos nuevas especies catalíticas, compuesto IB y compuesto IIB que designan el porcentaje de enzima en que el residuo Trp164 se encuentra en forma de radical. Ambas especies son capaces de oxidar compuestos de alto potencial redox a través de una ruta de transferencia electrónica interna de largo recorrido, y están en equilibrio con los compuestos I y II que ahora pasan a llamarse IA y IIA (Morales *et al.*, 2012; Pérez-Boada *et al.*, 2005). Se ha determinado que los porcentajes de las especies IB y IIB (según las condiciones experimentales en los ensayo de EPR) corresponden al 25% del Compuesto I y al 3% del Compuesto II, respectivamente (Ruiz-Dueñas *et al.*, 2009c, **Figura 12**).

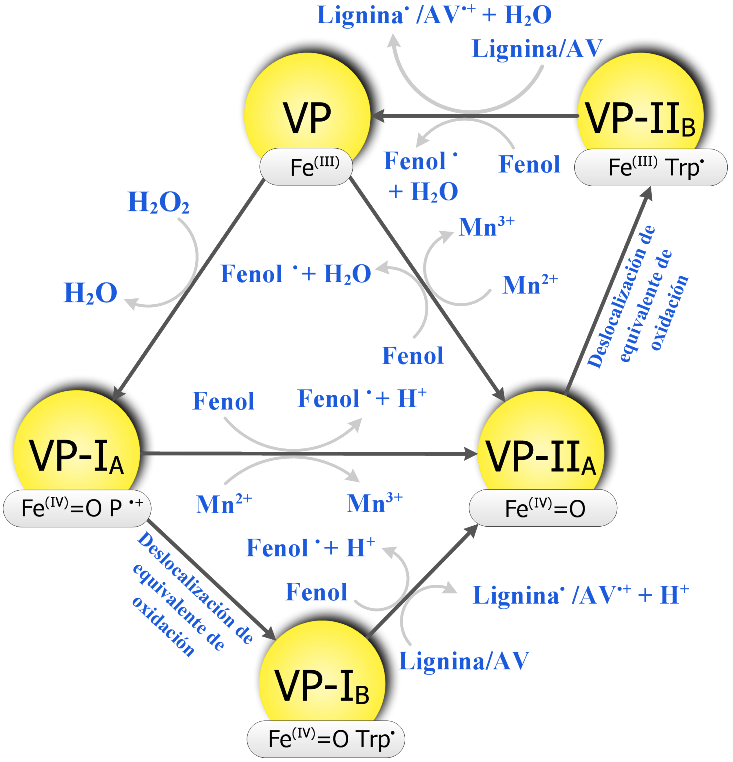

Figura 12. Ciclo catalítico de la VP.

El análisis de las características espectroscópicas de la VP en su estado basal (determinado por técnicas de *stopped flow*) indica la presencia de un pico de absorción a 407 nm (conocido como banda Soret), y dos picos más discretos a 505 nm (banda de transferencia de carga 2, CT2) y 637 nm (banda de transferencia de carga 1, CT1). Además, también aparecen dos bandas muy discretas a 532 y 560 nm correspondientes a las bandas β y α, respectivamente. El lugar de aparición e intensidad de estos cuatro últimos picos da una idea del estado electrónico en el que se encuentra el Fe^{3+} unido al hemo (en el estado de reposo el Fe^{3+} se encuentra en forma de alto spin y pentacoordinado, **Figura 13**).

Cuando la enzima entra en compuesto I tras su activación, el espectro de absorción muestra un desplazamiento de la banda Soret con un máximo a 403 nm, sumado a una disminución en su intensidad relativa. Además, las bandas CT sufren modificaciones mostrando hombros de mayor intensidad que el estado basal a 532, 560 y 651nm (**Figura 13A**). A diferencia del compuesto I, el compuesto II muestra un desplazamiento de la banda Soret hacia el lado opuesto (máximo a 417 nm), junto con dos hombros a 530 y 552 nm (**Figura 13B**).

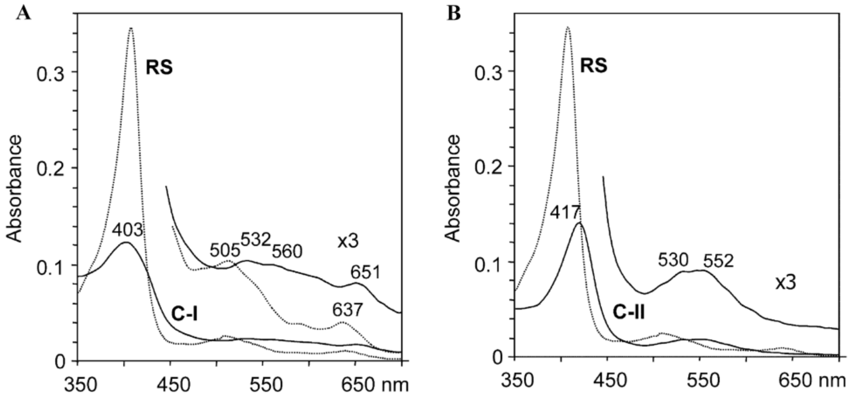

Figura 13. Características espectroscópicas de los diferentes intermediarios catalíticos de la VP. En (**A**) se muestran RS (estado de reposo) y C-I (compuesto I) y en (**B**) se muestran RS (estado de reposo) y C-II (compuesto II). Imagen adaptada de Pérez-Boada *et al.*, 2005.

3.2.4 Sitios catalíticos en la VP

A) Canal principal de acceso al grupo hemo

El canal principal de acceso al hemo se encuentra comunicado con el solvente y permite la oxidación de sustratos de bajo potencial redox en contacto directo con la denominada arista δ-*meso* del grupo hemo (arista superior). Además de ser un canal característico de las peroxidasas ligninolíticas, también se encuentra en el resto de hemoperoxidasas como la peroxidasa de rábano (HRP, Clase III), la ascorbato peroxidasa (ApX, Clase I) o la CCP (Finzel *et al.*, 1984; Gajhede *et al.*, 1997; Sharp *et al.*, 2003). Por este canal también accede la molécula de H_2O_2 donde sufre la ruptura heterolítica llevando a cabo la activación de la enzima (Hiner *et al.*, 2002, véase **apartado 3.2.3**).

Como se muestra en la **Figura 14**, el canal de las diferentes PODs presenta variaciones en cuanto a su tamaño y morfología que determinarán la oxidación de los diferentes sustratos (todos ellos de bajo potencial redox) como por ejemplo, compuestos fenólicos, quinonas, y otras moléculas sintéticas como el ABTS (2,2´azino-bis(3-etil-benzotiazolin-6-sulfonato) (Morales *et al.*, 2012). Se han llevado a cabo diferentes estudios en la CiP y VP basándose en la oxidación de *p*-fenoles substituidos en este canal, que muestran que la CiP es más eficiente en la oxidación de estos sustratos que la VP (Ayala *et al.*, 2007a; Liers *et al.*, 2014). Este efecto puede correlacionarse con el tamaño del canal que presentan ambas PODs, y que curiosamente sigue la misma relación que la oxidación de *p*-fenoles (CiP>VP). Probablemente, debido al tamaño reducido del canal de acceso de la LiP, ésta sólo puede oxidar determinados sustratos como el tinte aniónico DFAD (4-[(3,5-difluoro-4-hidroxyfenil)azo] bencenosulfonato) (Doyle *et al.*, 1998). En efecto, a pesar de que existen diferencias en las cargas locales de los residuos que conforman el canal de las diferentes PODs, no son tan críticas como lo es el tamaño de los residuos que lo componen (Morales *et al.*, 2012; Ruiz-Dueñas *et al.*, 2009b; **Figura 14**).

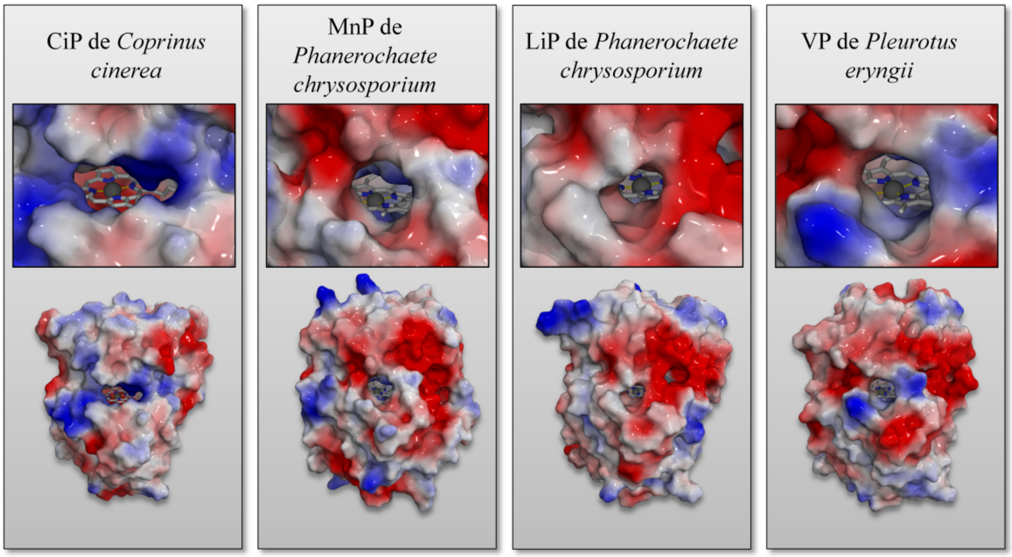

Figura 14. Tamaño y cargas locales del canal de acceso al grupo hemo en las diferentes PODs. CiP (PDB: 1H3J), MnP (PDB: 1MNP), LiP (PDB: 1LGA) y VP (PDB: 3FJW).

B) Entorno del triptófano catalítico

El sitio de oxidación de compuestos de alto potencial redox en la VP se localiza en la superficie de la proteína, y además de sustratos de alto potencial redox también puede oxidar compuestos de bajo y medio potencial con una mayor eficiencia que en el propio canal del hemo (Morales *et al.*, 2012; Pérez-Boada *et al.*, 2005). Dicho sitio de oxidación está gobernado por un triptófano catalítico (Trp164), que se localiza en un microambiente característico proporcionado por los residuos circundantes y que conecta catalíticamente con el hemo a través de una ruta interna de transferencia electrónica de largo recorrido (Martínez, 2002; Pérez-Boada *et al.*, 2005; Ruiz-Dueñas *et al.*, 2008). Una vez la enzima entra en compuesto I (véase **apartado 3.2.3**), una de las dos deficiencias electrónicas generadas en el hemo se pueden deslocalizar al triptófano catalítico a través de la ruta de transferencia electrónica formando un radical catiónico (compuestos IB y IIB en el ciclo catalítico, **Figura 12**, Ruiz-Dueñas *et al.*, 2009c). Es importante resaltar que, además del radical catiónico del Trp164, también se ha descrito en la VP la presencia de este residuo en forma de radical neutro mediante técnicas de EPR, aunque aún se desconocen las diferencias catalíticas entre ambas especies (Pogni *et al.*, 2006).

La transferencia de electrones desde el grupo hemo hasta el triptófano catalítico, y viceversa, ha sido caracterizada tanto en la VP como en la LiP teniendo lugar vía Trp164-Leu165-Hemo y Trp171-(Met172 o Leu172)-Hemo para VP y LiP (LiPH8 y LiPH2), respectivamente (Blodig *et al.*, 1998; Doyle *et al.*, 1998; Pérez-Boada *et al.*, 2005, **Figura 15**). A pesar de que ambas enzimas poseen una ruta de transferencia de electrones similar, presentan características muy diferentes. En la LiP por ejemplo, el C_β del triptófano catalítico se encuentra hidroxilado (Choinowski *et al.*, 1999), mientras que en la VP no se ha detectado todavía ninguna hidroxilación en dicha posición (Pérez-Boada *et al.*, 2005). Por otra parte, el entorno del triptófano catalítico de la LiP se encuentra rodeado por residuos ácidos que estabilizan el radical catiónico del alcohol veratrílico debido a su corta vida media ($t_{1/2}$ ~ 60 ms a pH 3) (Candeias and Harvey, 1995). A diferencia de la LiP, el entorno del Trp164 en la VP es más básico, impidiendo estabilizar el radical del alcohol veratrílico (aunque lo puede oxidar), pero permitiendo la oxidación de otros compuestos como el colorante de tipo azo RB5 de manera directa (Pérez-Boada *et al.*, 2005).

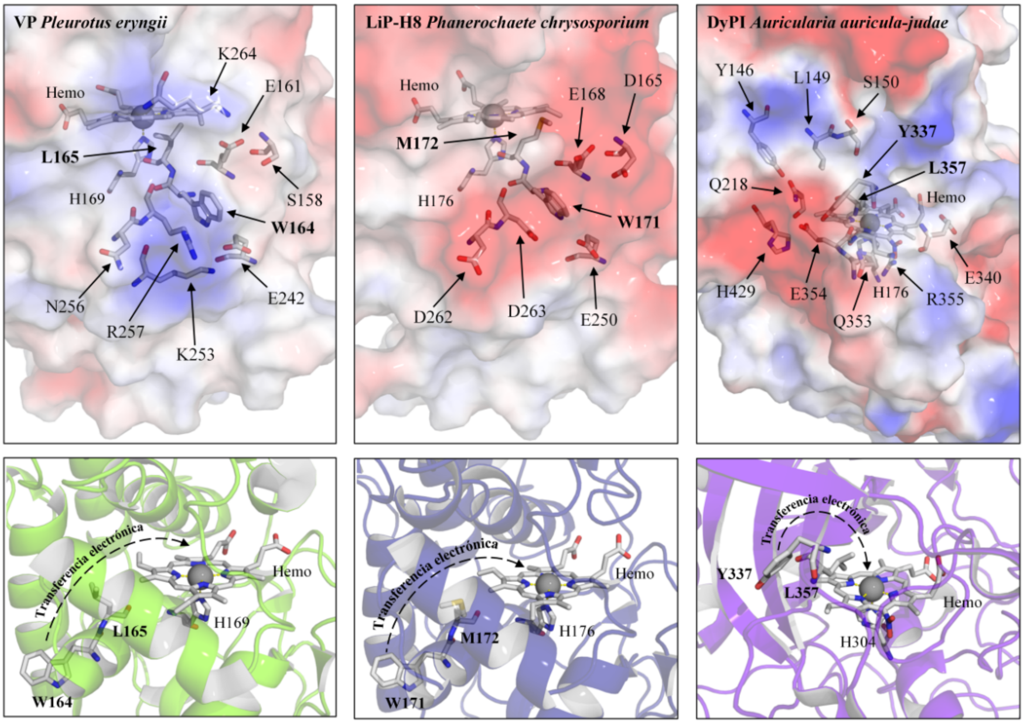

Figura 15. Entornos del triptófano catalítico en la VP y la LiP y de la tirosina catalítica en la DyPI. En la parte superior de la figura se detallan los aminoácidos que forman el entorno del triptófano (VP y LiP) o la tirosina (DyPI) catalíticos. Se puede apreciar que el entrono en la VP es básico, en la LiP ácido y en la DyPI ácido/básico. VP (PDB: 3FJW), LiP-H8 (PDB: 1LGA) y DyPI (PDB: 5AG1).

Aunque los residuos de triptófano actúan como centros catalíticos en LiP y VP, también se han descrito residuos de tirosina catalíticos en la LiP de *Trametes cervina* e incluso en la DyPI de *Auricularia auricula-judae* (Colpa *et al.*, 2014; Miki *et al.*, 2009; Strittmatter *et al.*, 2013b). El entorno catalítico de esta última le permite oxidar RB5 y otros compuestos de alto potencial redox como el alcohol veratrílico (Liers *et al.*, 2010), probablemente debido a su similitud con el entorno del Trp164 de la VP (**Figura 15**).

Por último, es importante resaltar que la transferencia de este sitio catalítico a las PODs es posible mediante un diseño adecuado. Dicho fenómeno ha sido comprobado en una MnP dotándola de actividad tipo LiP (Timofeevski *et al.*, 1999).

C) Sitio de oxidación de Mn^{2+}

El sitio de oxidación de Mn^{2+} fue descrito por primera vez en la MnP1 de *P. chrysosporium* (Sundaramoorthy *et al.*, 1994). Del mismo modo que en ésta, la oxidación de Mn^{2+} a Mn^{3+} en la VP se lleva a cabo en un canal localizado en el lateral de la estructura y que da acceso a uno de los propionatos internos del hemo. En efecto, en la coordinación del ion Mn^{2+} participan las cadenas laterales de tres residuos carboxílicos situados de manera enfrentada y uno de los propionatos internos del hemo. Dichos residuos (Glu36, Glu40 y Asp175 en la VP y Glu35, Glu39 y Asp179 en la MnP1) tienen unos valores de pK_a de cadena lateral de ~ 3,8-4,3, por lo que la coordinación de la esfera de Mn^{2+} y su oxidación ocurre de manera más eficiente a pH ~ 5 (*i.e.* donde los carboxilos están desprotonados). Esto difiere del pH óptimo de actividad que presenta el triptófano catalítico de la VP (pH 3,0). Dicho efecto se produce porque a pHs más ácidos el potencial redox del radical triptófano es más alto, pudiendo oxidar con mayor facilidad sustratos de alto potencial (Morozova and Yurkovskaya, 2015).

Se ha determinado que este sitio de Mn^{2+} puede encontrarse en dos configuraciones diferentes durante el ciclo catalítico: i) en ausencia de Mn^{2+}, los residuos Glu36 y Glu40 de la VP se orientan hacia el solvente aliviando el exceso de carga negativa en el centro activo. Esta conformación define la configuración de canal abierto siendo el residuo Glu36 el responsable de la apertura y cierre de dicho canal. Al encontrarse ausente el Mn^{2+}, una molécula de agua se sitúa en el sitio de oxidación estabilizando la estructura de la VP; ii) en presencia de Mn^{2+}, los tres residuos ácidos se reorientan para coordinar la esfera de Mn^{2+} produciendo el cierre del canal, y tras su coordinación, el propionato interno del hemo abstrae un electrón del Mn^{2+} dando lugar a Mn^{3+}. Esta configuración se denomina de puerta cerrada (Ruiz-Dueñas *et al.*, 2007; 2009b, **Figura 16**).

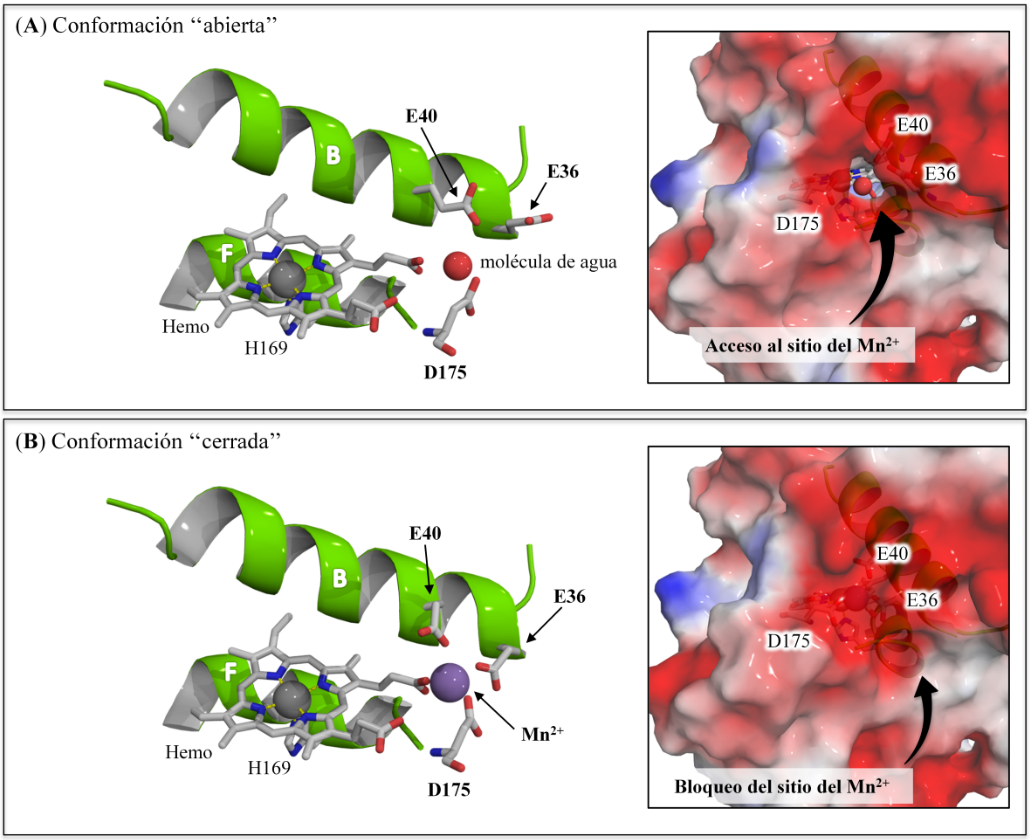

Figura 16. Sitio de oxidación del Mn^{2+} en la VP.

A pesar de que los sitios de oxidación de Mn^{2+} en la MnP1 y VP actúan de manera similar, existen diferencias en cuanto a su topología y mecanismo catalítico. Así, la MnP necesita de Mn^{2+} para reducir el compuesto II y regenerar el estado de reposo de la enzima (véase ciclo catalítico **apartado 3.2.3**). Sin embargo, en la VP la reducción de compuesto II puede llevarse a cabo tanto por Mn^{2+} como a través de compuestos oxidados en el canal del hemo o en triptófano catalítico (Morales *et al.*, 2012).

Mediante estudios de mutagénesis dirigida sobre la VP, se ha demostrado que su sitio de oxidación es más eficiente que el de la MnP1 aun cuando solo uno de los ácidos se encuentra presente. Además, la substitución de los residuos que componen el sitio catalítico en la VP por aspárticos, reveló que la topología de dicho sitio en la VP tiene una mayor plasticidad que el de la MnP1 (Ruiz-Dueñas *et al.*, 2007; 2009b).

La transferencia de este sitio de oxidación es posible incluso en otras peroxidasas no ligninolíticas, como ya se hizo en la CCP de *S. cerevisiae* (Hosseinzadeh *et al.*, 2016; Pfister *et al.*, 2007). La enzima resultante fue capaz de degradar compuestos fenólicos modelos de lignina, así como lignina kraft imitando el mecanismo de la MnP nativa.

3.3. Aplicaciones y limitaciones biotecnológicas de la VP

Debido a su elevado potencial redox y promiscuidad de sustrato, la VP puede encontrar aplicaciones potenciales en un amplio rango de procesos biotecnológicos como el blanqueo de la pasta de papel, la biorremediación enzimática (incluyendo la degradación de compuestos que interfieren en el sistema endocrino animal, tintes industriales, compuestos farmacéuticos activos, hidrocarburos aromáticos policíclicos (PAHs), pesticidas y otros xenobióticos), producción de compuestos flavorizantes aromáticos para la industria alimentaria, desarrollo de biosensores, y procesos diversos de síntesis orgánica incluyendo la preparación de homo- y heteropolímeros (Knop *et al.*, 2015; Mendonça Maciel *et al.*, 2010; Pizzul *et al.*, 2009; Sáez-Jiménez *et al.*, 2015b; Taboada-Puig *et al.*, 2011; Touahar *et al.*, 2014; Yadav and Yadav, 2015).

Sin embargo, el gran potencial biotecnológico que ofrece la VP se encuentra mermado por una serie de limitaciones que dificultan su aplicación como biocatalizadores industriales en diferentes procesos. Entre estos inconvenientes destacan fundamentalmente: i) la escasez de hospedadores apropiados para su expresión funcional heteróloga, ii) su baja estabilidad frente a diferentes agentes como la temperatura o la presencia de H_2O_2, y iii) su nula actividad (y estabilidad) a pH neutros o alcalinos.

La presente Tesis Doctoral se ha centrado en el estudio y la mejora de algunas de estas limitaciones mediante técnicas de evolución molecular dirigida aplicadas a la VP de *P. eryngii*.

3.3.1. Expresión funcional y termoestabilidad

La expresión funcional heteróloga de la VP es un factor limitante a la hora de afrontar su diseño mediante herramientas de evolución dirigida, así como para poder producirlas a mayor escala. Las VPs, al igual que otras PODs, son difíciles de expresar funcionalmente ya que requieren una maquinaria celular especializada que permita llevar a cabo numerosas modificaciones post-traduccionales que faciliten el correcto plegamiento de la proteína. En los sistemas procariotas modelo como *Escherichia coli*, la expresión de la VP requiere, en el mejor de los escenarios proteínas de fusión, ya que en ausencia de ellas se producen cuerpos de inclusión que deben ser solubilizados y replegados posteriormente (Bao *et al.*, 2012; Pérez-Boada *et al.*, 2002). Así, la expresión heteróloga y funcional de la VP únicamente se ha conseguido en los hongos *Aspergillus nidulans* y *P. chrysosporium* (Coconi-Linares *et al.*, 2015; Lu-Chau *et al.*, 2004). Sin embargo, la difícil manipulación genética en estos organismos dificulta enormemente su uso como hospedador heterólogo en procesos de evolución dirigida. En este punto, *Saccharomcyes cerevisiae* puede ser una atractiva alternativa ya que además de poder llevar a cabo el correcto procesado de las proteínas eucariotas, su similitud con *Pichia pastoris* puede permitir su uso como sistemas de expresión en tándem usando *S. cerevisiae* durante la evolución dirigida, y *P. pastoris* para la sobreproducción de las variantes mejoradas. Este sistema en tándem ha sido validado con éxito en estudios recientes utilizando lacasas de alto potencial redox y UPOs (Mate *et al.*, 2013b; Molina-Espeja *et al.*, 2015).

Por otro lado, la mejora de la termoestabilidad de estas enzimas para su aplicación industrial también es un factor importante, ya que la VP no tolera elevadas temperaturas que de modo ordinario afectan a la pérdida de los calcios estructurales comprometiendo la integridad estructural de la enzima. Este fenómeno también transcurre cuando la enzima se incuba a pHs alcalinos (Plieth and Vollbehr, 2012; Sutherland and Aust, 1996; véase también **apartado 3.3.3**).

3.3.2. Inactivación mediada por H_2O_2

La VP es posiblemente la peroxidasa conocida con menor estabilidad oxidativa frente al H_2O_2. El fenómeno por el cual ocurre este proceso tiene lugar se denomina "inactivación suicida" (donde paradójicamente, el H_2O_2 es el co-sustrato de la enzima pero también un fuerte inhibidor), y es responsable del daño oxidativo irreparable que ha suscitado un gran interés durante décadas de investigación con ésta y otras peroxidasas (Cherry *et al.*, 1999; Miyazaki and Takahashi, 2001; Miyazaki-Imamura *et al.*, 2003; Morawsky *et al.*, 2001; Ogola *et al.*, 2010; Valderrama *et al.*, 2002).

En general, el daño oxidativo de proteínas es un proceso complejo del que aún se conoce muy poco. Además de ser un mecanismo que limita notablemente el uso industrial de las peroxidasas, también es la causa que está detrás de diferentes enfermedades como el Alzheimer (Zhao and Zhao, 2013). En el caso particular de las peroxidasas, es un problema universal que se encuentra asociado al mecanismo de acción de la enzima. En efecto, durante el ciclo catalítico, el compuesto II en presencia de H_2O_2 puede derivar en un intermediario no natural del ciclo que es altamente reactivo (Wariishi and Gold, 1989), pero inactivo catalíticamente, y que se denomina compuesto III (Valderrama *et al.*, 2002; 2010, **Figura 17**).

Dicho compuesto III se caracteriza por presentar un radical superóxido unido al Fe^{3+} y se puede formar tanto en presencia como en ausencia de sustrato reductor, siempre que el H_2O_2 se encuentre en el medio de reacción (Hernández-Ruiz *et al.*, 2001). Así, la formación del compuesto III depende considerablemente de factores como el pH, la temperatura y la relación molar H_2O_2/enzima (Böckle *et al.*, 1999; Hiner *et al.*, 2001).

Algunos autores han puesto de manifiesto que la formación del compuesto III se debe a que la constante de reducción del compuesto II hacia el estado nativo es muy lenta, considerándose la etapa limitante en la catálisis de las peroxidasas. En consecuencia, el compuesto II puede acumularse de manera espontánea reaccionando con una nueva molécula de H_2O_2 para dar compuesto III (Gil-Rodríguez *et al.*, 2008). Una vez formado, el compuesto III puede seguir diferentes rutas (Valderrama *et al.*, 2002, **Figura 17**):

i) El radical superóxido presente en el compuesto III puede reaccionar atacando a los aminoácidos más próximos al grupo hemo. Una vez modificados, se producen cambios conformacionales que abren nuevos espacios en la estructura de la proteína haciéndola más susceptible a la sobreoxidación. Esto ocurre principalmente por la modificación de metioninas (a metionina sulfona y metionina sulfóxido) y cisteínas (a cistina). Además de estos aminoácidos, hay otros que también son fácilmente oxidables como triptófanos, tirosinas e histidinas (Kim *et al.*, 2001; Sáez-Jiménez *et al.*, 2015a; Valderrama *et al.*, 2002). Aunque la enzima finalmente puede retornar a su estado basal, el daño oxidativo se acumula de manera irreparable hasta la completa inactivación tras varios ciclos catalíticos.

ii) El radical superóxido del compuesto III puede atacar al anillo de la porfirina dada su proximidad, lo que provoca su ruptura con la consiguiente inactivación irreversible de la enzima (blanqueo de la peroxidasa). Este proceso libera biliverdina y Fe^{3+}.

iii) El compuesto III puede desaparecer mediante la descomposición unimolecular del radical superóxido generando especies reactivas de oxigeno (ROS). Entre los ROS liberados se encuentran los radicales hidroxilo que son aún más reactivos que el propio radical superóxido. De hecho, se considera que el daño que provocan es incluso mayor que en las rutas i y ii, porque tanto los radicales hidroxilo como otros ROS generados son capaces de oxidar distintas regiones de la proteína (incluso a distancia del hemo).

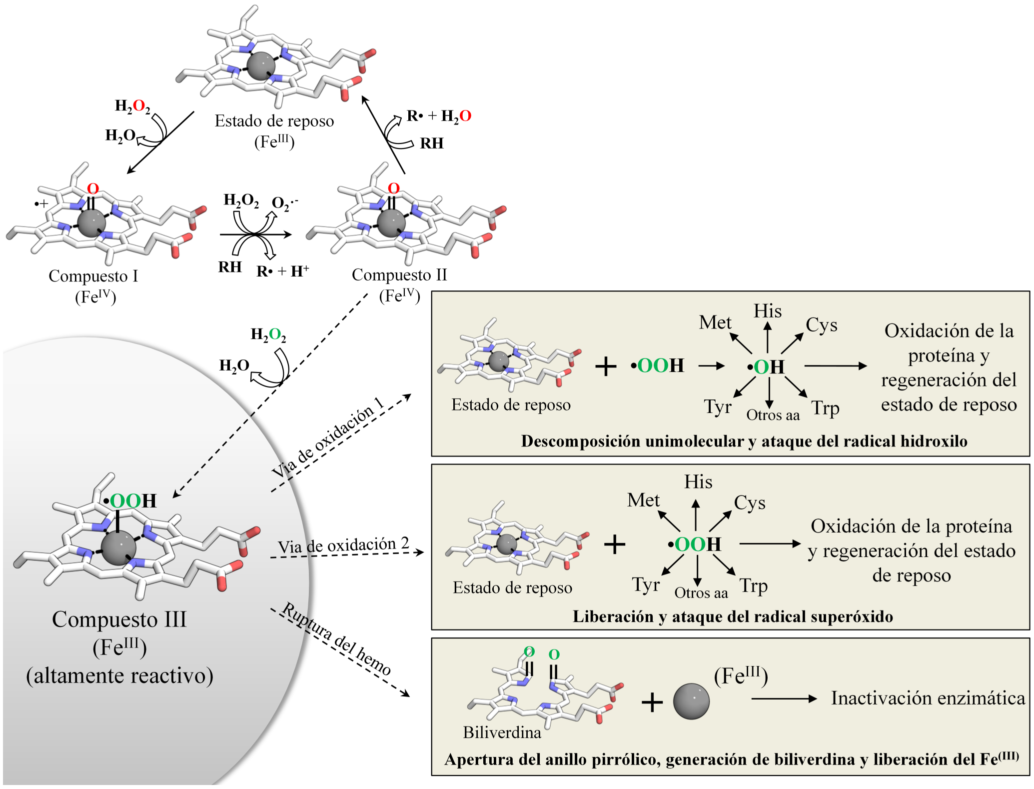

Figura 17. Mecanismo de inactivación suicida en las peroxidasas.
En recuadros marrones se detallan las vías que puede seguir el compuesto III provocando daño oxidativo a la proteína, o bien inactivación enzimática mediante la apertura del grupo hemo; aa: aminoácidos.

Existen algunas estrategias para reducir el daño oxidativo en las peroxidasas. La más rudimentaria, pero no por ello menos eficaz, consiste en dosificar el suministro de H_2O_2 (haciendo uso de bombas peristálticas, o con sistemas enzimáticos en cascada, (*p. ej.* con AAO o glucosas oxidasas) donde se genere *in situ* el H_2O_2) para reducir, en la medida de lo posible, la formación del compuesto III (Carro *et al.*, 2015; Hernández *et al.*, 2012; Pezzotti *et al.*, 2004). Otra alternativa válida es la inclusión en la mezcla de reacción de moléculas estabilizantes como el polietilenglicol y aminoácidos (Hernández *et al.*, 2012; Mao *et al.*, 2013). Por último, se ha descrito también que la presencia de los radicales catiónicos que forman algunos sustratos como el alcohol veratrílico o el 1,2,4,5-tetrametoxibenceno (TMB) son capaces de revertir el compuesto III, devolviendo la enzima al estado de reposo aunque sumando daño oxidativo, como se vio en estudios realizados con la LiP (Barr and Aust, 1994).

Sin embargo, son las técnicas de ingeniería de proteínas las que pueden hacer frente a este problema de una manera más precisa y eficaz, como se ha descrito en numerosos estudios orientados a la sustitución de residuos altamente oxidables por otros menos propensos a la oxidación y con bajo potencial redox como alaninas, fenilalaninas, leucinas o isoleucinas (Bao *et al.*, 2014; Miyazaki and Takahashi, 2001; Ogola *et al.*, 2010; Ryan and O'Fagain, 2007; Sáez-Jiménez *et al.*, 2015a).

A pesar de todos estos esfuerzos, todavía existe una gran incertidumbre en torno al futuro uso de la VP en procesos industriales. En efecto, su baja estabilidad oxidativa se debe a la presencia de sus varios sitios catalíticos y canales por donde difunden con facilidad las ROS, lo que obstaculiza su aplicación en numerosos procesos biotecnológicos.

Así pues uno de los objetivos prioritarios en esta Tesis Doctoral ha sido la exploración de varias regiones de la VP de *P. eryngii*, haciendo uso de un amplio abanico de herramientas de evolución dirigida y/o enfocada, con la intención de desenmascarar nuevos determinantes estructurales que aporten conocimiento al mecanismo de inactivación suicida.

3.3.3. Actividad y estabilidad a pHs alcalinos

La estabilidad y actividad a pH neutros o alcalinos de la VP, y por extensión de las peroxidasas ligninolíticas, es otro de los mayores inconvenientes a la hora de utilizarlas como biocatalizadores industriales. Aunque estas condiciones se requieren para muchos procesos (*p. ej.* determinadas etapas de blanqueo de la pasta de papel, procesos de síntesis orgánica, etc.), desafortunadamente estas enzimas no son activas a valores a pHs neutros o alcalinos. Esto puede ser debido a que el consorcio ligninolítico se ha especializado durante miles de años de evolución a funcionar a pHs ácidos, como consecuencia directa de la producción de ácidos orgánicos por parte del hongo de podredumbre blanca durante el proceso de degradación del material lignocelulósico.

Es conocido que la actividad y estabilidad a pHs alcalinos de la VP se encuentra condicionada a la retención de los iones calcio en la estructura de la enzima (George *et al.*, 1999; Lu-Chau *et al.*, 2004; Youngs *et al.*, 2000). Particularmente, la unión más débil del calcio distal (véase **Figura 10**) bajo condiciones alcalinas, hace que se libere con mayor facilidad que el calcio proximal provocando que el domino distal se relaje colapsando la cavidad del hemo. En dicha distensión, la histidina distal (contenida en la hélice B, véase **Figura 8**) se aproxima al Fe^{3+} interaccionando con él y formándose un complejo hexacoordinado con el hemo que causa la inactivación de la enzima (Banci *et al.*, 1999; George *et al.*, 1999; Laberge *et al.*, 2003). Este complejo se caracteriza por unas características espectroscópicas muy concretas que incluyen un desplazamiento en la banda Soret (413-420 nm), y la aproximación de las bandas CT (CT2: 505 nm; CT1: 637 nm) a 546 y 581 nm, respectivamente.

La presencia de este complejo hexacoordinado se ha descrito en multitud de trabajos con peroxidasas por las limitaciones que supone para las PODs a pHs alcalinos (Ferrer *et al.*, 1994; George *et al.*, 1999; Howes *et al.*, 2001; Kishi *et al.*, 1997; Lu-Chau *et al.*, 2004; Youngs *et al.*, 2000), aunque la formación de un hemo hexacoordinado también se ha descrito de manera funcional en hemoglobinas y citocromos (Uzan *et al.*, 2004).

El proceso de inactivación a pH alcalino de las PODs ha sido estudiado en la VP, y los resultados mostraron que en determinadas condiciones se puede revertir el complejo hexacoordinado (*i.e.* a pH 5,0 y en presencia de 1,6 mM de calcio). No obstante, la adición de calcio tras incubación a pH alcalino sólo permite una recuperación parcial de la enzima que depende también del tiempo que ha permanecido inactiva (Lu-Chau *et al.*, 2004), hecho que también ha sido descrito en la LiP de *P. chrysosporium* (George *et al.*, 1999).

Aunque se han llevado a cabo algunos estudios de ingeniería con la VP para emular las interacciones estabilizantes de una MnP4 de *Pleurotus ostreatus* (Sáez-Jiménez *et al.*, 2015c), no se había detectado aún actividad alcalina en ninguna peroxidasa ligninolítica. Por esta razón, otro de los objetivos de esta Tesis Doctoral fue someter a evolución dirigida la VP de *P. eryngii* para dotarla de actividad a pH neutro/alcalino.

4. Evolución dirigida de enzimas ligninolíticas en *Saccharomyces cerevisiae*

La evolución dirigida de enzimas es una poderosa herramienta que permite la obtención de biocatalizadores a medida para diferentes aplicaciones biotecnológicas (Bloom and Arnold, 2009; Packer and Liu, 2015; Porter *et al.*, 2016). El impacto que ha supuesto el desarrollo de la evolución dirigida es tal, que sus descubridores Frances H. Arnold y Willem P. Stemmer, fueron galardonados con el "*Charles Stark Draper Prize*" otorgado por la Academia Nacional de Ingeniería de los Estados Unidos (premio equivalente al Nobel de Ingeniería). En el presente año, la Dra. Arnold ha sido también galardonada con el "*Millennium Technology Prize*", considerado como el Nobel de Tecnología, y que premia únicamente a invenciones que suponen un impacto en la vida de la sociedad como lo fue, por ejemplo, la invención de la "*World Wide Web*". En efecto, pocos pueden dudar tras 25 años de desarrollo de esta herramienta, de su robustez, fiabilidad y rapidez para el diseño de enzimas, rutas metabólicas e incluso microorganismos completos.

El éxito de la evolución dirigida se basa principalmente en su capacidad para recrear el proceso de la evolución natural (*i.e.* mutación/recombinación y selección), pero aplicándolo a procesos que la naturaleza puede no haberse planteado nunca antes, permitiendo reescribir el código de la vida hacia funciones biotecnológicas muy dispares. Haciendo un uso adecuado de la evolución dirigida se pueden mejorar diferentes propiedades de las enzimas, aun cuando exista un limitado conocimiento de la característica potencialmente evolucionable. Entre las propiedades que se pueden mejorar, se encuentran aquellas que condicionan de ordinario la funcionalidad de las enzimas en procesos biotecnológicos como son la estabilidad (frente a temperatura, presión, pHs extremos, presencia de co-solventes orgánicos, etc.), actividad, especificidad y selectividad, resistencia a inhibidores o expresión funcional (Bornscheuer *et al.*, 2012; Cherry *et al.*, 1999; Dalby, 2003; Miyazaki-Imamura *et al.*, 2003; Ryu *et al.*, 2008; Sun *et al.*, 2016; Williams *et al.*, 2007). Es más, actualmente nos encontramos en disposición de transgredir los límites establecidos por la propia naturaleza, e ir incluso más allá, explorando la actividad de las enzimas en ambientes fuera de su contexto biológico, o bien llevando a cabo reacciones no naturales nunca antes descritas por las enzimas encontradas hasta el momento en nuestro planeta (Arnold, 2015; Molina-Espeja *et al.*, 2016b; Renata *et al.*, 2015).

El proceso de evolución dirigida consiste en mutagenizar (y recombinar) de forma aleatoria genes completos, regiones y/o posiciones del mismo, creando librerías de mutantes que son exploradas mediante herramientas de alta capacidad (*i.e.* mediante "*high-throughput screening -HTS-*", o incluso más recientemente *ultra-high-througput screening*). Para que el análisis rápido y simultáneo de las variantes de la librería sea efectivo, se requiere de un hospedador heterólogo adecuado.

En el caso de las ligninasas, al tratarse de proteínas eucariotas extracelulares, se hace necesaria una maquinaria celular capaz de llevar a cabo el plegamiento y las modificaciones post-traduccionales pertinentes (glicosilación, procesamiento de péptidos señales o formación de puentes disulfuro entre otras) que faciliten una exocitosis exitosa (todos los intentos descritos hasta la fecha para expresar funcionalmente ligninasas en *E. coli* han conducido a plegamientos incorrectos con la formación de cuerpos de inclusión).

Así, en la última década, nuestro laboratorio ha construido y empleado de manera eficaz una plataforma de evolución dirigida para ligninasas basada en la levadura panadera *Saccharomyces cerevisiae* como hospedador heterólogo (Alcalde, 2015; Garcia-Ruiz *et al.*, 2014; Mate *et al.*, 2016a; Viña-Gonzalez *et al.*, 2016, **Figura 18**). El uso de *S. cerevisiae* en evolución dirigida de genes ligninolíticos permite un procesamiento adecuado debido a la similitud existente entre la fisiología de la levadura y la del hongo nativo, si bien el alcanzar niveles de expresión funcional suficientes en formato HTS se antoja complicado. Por este motivo, de ordinario se requiere evolucionar la expresión funcional antes de afrontar nuevos desafíos (*p. ej.* actividad con sustratos complejos o en medios artificiales). Por otro lado, la elevada tasa de recombinación homóloga de S. *cerevisiae* junto con su preciso mecanismo corrector, hace de este microorganismo un vehículo versátil en la preparación de métodos de creación diversidad genética (véase **Capítulo 6** de la Tesis Doctoral).

De esta manera, los principales representantes del consorcio ligninolítico que han sido evolucionados hacia diferentes fines tomando ventaja de la plataforma de *S. cerevisiae* construida en nuestro laboratorio son:

i) **Incremento de la expresión funcional**:
   Lacasa de *Myceliopthora thermophila* (Bulter *et al.*, 2003)
   Lacasa del basidiomicete PM1 (Mate *et al.*, 2010)
   Lacasa de *Pycnoporus cinnabarinus* (PcL; Camarero *et al.*, 2012)
   UPO de *Agrocybe aegerita* (Molina-Espeja *et al.*, 2014)
   AAO de *P. eryngii* (Viña-Gonzalez *et al.*, 2015)

ii) **Actividad en ambientes no naturales**
   Lacasa del basidiomicete PM1 (tolerancia a sangre humana; Mate *et al.*, 2013a)
   Lacasa de *Myceliopthora thermophila* (actividad en medio alcalino; Torres-Salas *et al.*, 2013)
   Lacasa de *Myceliopthora thermophila* (actividad en disolventes orgánicos; Zumárraga *et al.*, 2007)

iii) **Incremento de actividad**
   UPO de *Agrocybe aegerita* (síntesis de 1-naftol a partir de naftaleno; Molina-Espeja *et al.*, 2016a)
   UPO de *Agrocybe aegerita* (síntesis de 5'-OH propranolol; material sin publicar).
   Lacasa quimérica para la oxidación de ácido sinápico (Pardo *et al.*, 2015; 2016)
   AAO de *P. eryngii* (oxidación de alcoholes secundarios; material sin publicar)
   Lacasa de *Myceliopthora thermophila* (síntesis de colorantes heteropoliméricos; Vicente *et al.*, 2016)

iv) **Lacasa quiméricas**
   Lacasas quiméricas de PcL y PM1 con propiedades combinadas (Pardo *et al.*, 2012)

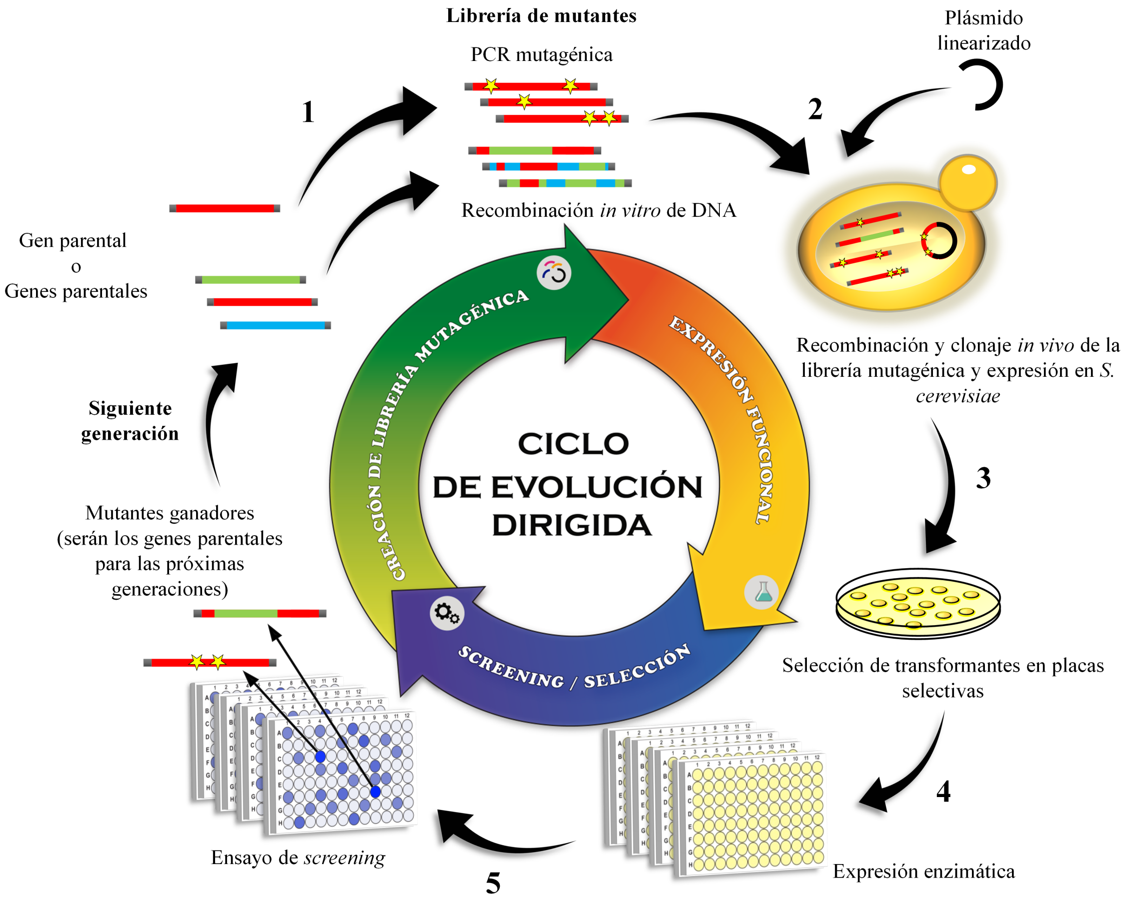

Figura 18. Plataforma de evolución dirigida basada en *S. cerevisiae* y su eficiente maquinaria de recombinación homóloga de DNA.

(**1**) A partir de un gen parental, o varios genes (con una cierta identidad de secuencia), se generan las librerías mutagénicas por PCR propensa a error o recombinación de DNA. (**2**) Las librerías se co-transforman en la levadura con el plásmido linearizado (que porta extremos solapantes para los insertos) y se seleccionan los clones positivos. (**3**) Estos clones se transfieren individualmente a placas de 96 pocillos y se procede con la expresión de las diferentes variantes. (**4**) Finalmente, se realiza el proceso de cribado en el que seleccionarán las variantes mejoradas que superen el proceso de "*screening*" aplicado. (**5**) Dichas variantes se pueden volver a usar como parentales para llevar a cabo nuevas rondas de evolución. Este proceso se puede repetir tantas veces como se necesite hasta obtener la propiedad deseada.

5. *Saccharomyces cerevisiae* como prototipo de levadura de podredumbre blanca

El uso de *S. cerevisiae* para la fermentación del pan, la cerveza o el vino se remonta a más de 7.000 años A.C. (Legras *et al.*, 2007), lo que ha dado lugar a su amplio uso y estudio permitiendo conocer su fisiología y desarrollar una infinidad de protocolos para su manipulación. Cuenta de ello son el gran número de patentes registradas en el empleo de *S. cerevisiae* como factoría celular para la obtención de productos industriales como insulina, vacunas contra la hepatitis o el papiloma humano, nutracéuticos (*p. ej.* resveratrol), ácido láctico o glicerol (Hong and Nielsen, 2012). Además, su capacidad para llevar a cabo la transformación de azúcares en etanol para la producción de biocombustibles ha suscitado un gran interés en los últimos años. En este sentido, se han realizado muchos esfuerzos en la mejora de *S. cerevisiae* como organismo fermentador a partir de material lignocelulósico, entre los que destacan estudios de ingeniería metabólica para evitar la acumulación de glicerol, controlar el balance NAD^+/NADH, así como promover el consumo de pentosas (Nielsen *et al.*, 2013). Sin embargo, todos estos estudios requieren de una etapa inicial (pre-tratamiento) orientada a retirar el contenido de lignina y facilitar el acceso a los azúcares para su consiguiente fermentación. Si *S. cerevisiae* tuviera la capacidad de despolimerizar la lignina se estaría dando un paso al frente en el diseño de un FCBM (del inglés *full consolidated bioprocessing microbe*) como base para el estudio del aprovechamiento de la biomasa vegetal, además de su uso como modelo de organismo ligninolítico (Hasunuma and Kondo, 2012; Huang *et al.*, 2014).

Este concepto de “superlevadura” planteado en nuestro laboratorio propone el empleo de *S. cerevisiae* como organismo sintético capaz de imitar los mecanismos naturales de los hongos de podredumbre blanca de una manera simplificada. El desarrollo de este chasis de levadura de la podredumbre blanca requeriría por tanto de dos “*gadgets*” fundamentales: un sistema para hidrolizar celulosa y hemicelulosa, y otro que le permita despolimerizar lignina.

En cuanto al aparato degradador de celulosa, ya se han llevado a cabo muchos abordajes de ingeniería metabólica en los que se han expresado heterólogamente una serie de celulasas dando rendimientos de producción de bioetanol entre 1-17 g/L (Hasunuma and Kondo, 2012). Para poder degradar celulosa es necesaria la actividad coordinada de endoglucanasas, exoglucanasas y β-glucosidasas. Este consorcio de celulasas puede expresarse de forma soluble o bien ensamblarse en un minicelulosoma localizado en la superficie de la levadura. Este último abordaje se suele llevar a cabo en presencia de una proteína de soporte, que contiene un módulo de unión a celulosa (CBM), y unas proteínas conectoras llamadas cohesinas donde se anclan las celulasas. Estas últimas enzimas pueden ser expresadas por la propia célula o bien añadidas como un cóctel enzimático previamente producido por otro(s) organismo(s) heterólogo(s). El anclaje de las celulasas en el minicelulosoma requiere de su expresión en forma de proteínas de fusión con dockerinas que mediarán la unión específica con las cohesinas. Este modelo de organización está inspirado en el celulosoma natural de *Clostridium cellulolyticum,* el cual es altamente eficiente (Fan *et al.*, 2012; Gilmore *et al.*, 2015; Hasunuma and Kondo, 2012; Huang *et al.*, 2014; Kim *et al.*, 2013, **Figura 19A-B**). Recientemente, se ha estudiado la eficiencia en la degradación de celulosa mediante celulasas secretadas al medio de cultivo en *S. cerevisiae*, así como en forma de minicelulosoma ensamblado en la superficie de la levadura (Liu *et al.*, 2016; **Figura 19C-F**).

En efecto, la estructura del celulosoma permite que las celulasas se encuentren muy cercanas entre sí potenciando sinergias en la degradación de la celulosa, lo que parece convertirle en el modelo más adecuado para su uso potencial en biorefinerías integradas (Liu *et al.*, 2016, **Figura 19C**). En un futuro próximo, es muy probable que este sistema de minicelulosoma incorpore un nuevo tipo de enzimas llamadas LPMO (del inglés *Lytic Polysaccharides MonoOxygenases*). Las LPMO han atraído un gran interés biotecnológico en los últimos años por su implicación en el aprovechamiento de la biomasa lignocelulósica, ya que actúan digiriendo las regiones cristalinas de la celulosa para facilitar el ataque hidrolítico de celulasas. En particular, además de su actividad sobre celulosa, también son capaces de actuar sobre quitina, xilanos, xiloglucanos, glucomananos, liquenanos, β-glucanos, y almidón (Hemsworth *et al.*, 2015; Martínez, 2016).

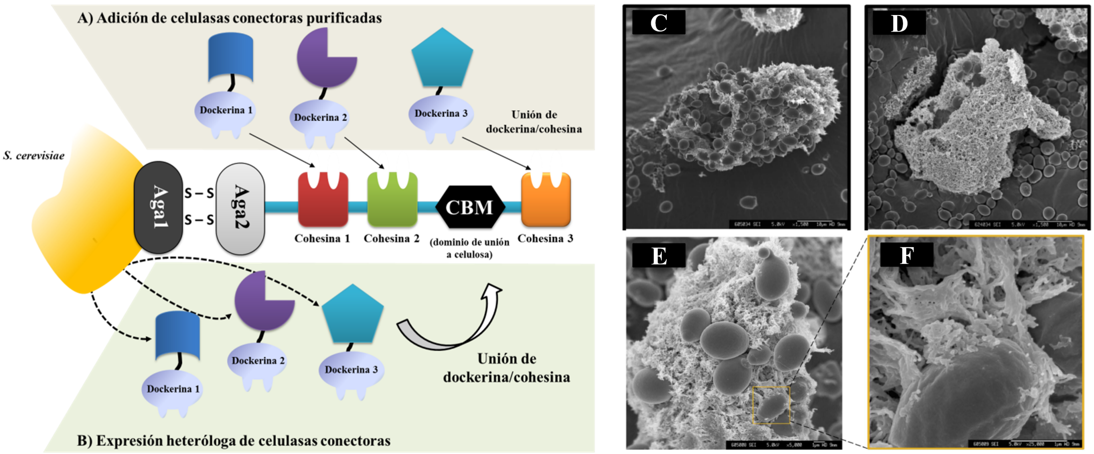

Figura 19. Estructura del minicelulosoma y degradación de celulosa con *S. cerevisiae*.
En la parte izquierda de la imagen se muestra la estructura del minicelulosoma para *S. cerevisiae*. Mediante la expresión de una proteína de soporte (mini CipA, barra turquesa) se pueden anclar las diferentes actividades para la degradación de celulosa. La proteína soporte contiene un módulo de unión a celulosa (CBM), una serie de cohesinas (cajas de colores) y una proteína intermediaria de unión a la membrana de la levadura (Aga2). La expresión de Aga1 en la superficie de *S. cerevisiae* permite el anclaje del minicelulosoma por Aga2. La producción de las celulasas necesarias (endocelulasa, exocelulasa, y β-glucosidasa; formas geométricas azul, morada y turquesa, respectivamente) se realiza como proteínas de fusión unidas a dockerinas (ligando de las cohesinas). Estas construcciones se pueden expresar en otros organismos, purificarlas y añadirlas al medio de cultivo de *S. cerevisiae* (**A**), o bien se puede expresar en la propia levadura (**B**). En la parte derecha de la imagen se puede ver la diferencia entre la expresión de las celulasas en forma de minicelulosoma (**C**), o en forma secretada (**D**). La ausencia de minicelulosoma impide la unión directa de la levadura a la celulosa. En (**E**) y (**F**) se muestra el detalle de la interacción de *S. cerevisiae* con la celulosa cuando se expresa el minicelulosoma en superficie. Las figuras (**C**), (**D**), (**E**) y (**F**) han sido adaptadas de Liu *et al.*, 2016.

A pesar de que se ha prestado mucha atención al desarrollo de celulosomas en *S. cerevisiae* para la producción de etanol, no hay ningún estudio que se dirija hacia el pre-tratamiento de la biomasa lignocelulósica con este microorganismo. La expresión de un “minisecretoma” ligninolítico en *S. cerevisiae* abriría la puerta a un modelo de estudio para comprender mejor el mecanismo de degradación de lignina, al tiempo que podría tener un marcado carácter industrial, lo cual es otro de los objetivos de esta Tesis Doctoral.

6. Objetivos de la Tesis Doctoral

A pesar del elevado potencial biotecnológico que tiene la VP para su aplicación industrial, existen una serie de limitaciones prácticas que necesitan ser solucionadas para transformarla en un biocatalizador robusto. Entre ellas se incluyen la falta de expresión funcional en hospedadores empleados en evolución dirigida, una alta susceptibilidad al daño oxidativo y la ausencia de actividad a pH neutro y/o alcalino. Por otro lado, al disponer de varios bolsillos catalíticos en una única cadena polipeptídica, la VP es capaz de emular la función conjunta de MnPs y LiPs reduciendo el consumo energético del hospedador. En este sentido, se podría tomar ventaja de las características de la VP para su co-expresión junto con una lacasa de alto potencial redox, en la construcción de un prototipo inicial de levadura de podredumbre de blanca con potencial uso para el pre-tratamiento en las biorefinerías integrales.

Así pues, los principales objetivos de esta Tesis Doctoral fueron:

- Evolución dirigida de la VP hacia expresión funcional/termoestabilidad. Se llevó a cabo una exhaustiva caracterización bioquímica de los mutantes obtenidos con el fin de seleccionar los parentales más adecuados para mejorar tanto la estabilidad oxidativa de la VP, como su actividad en condiciones de pH neutro/alcalino.

- Diseño de una VP resistente al H_2O_2. Para ello se hizo uso de la plataforma de evolución dirigida desarrollada en levadura y se diseñaron diferentes herramientas de creación de diversidad genética *in vivo*. Para la exploración de las librerías se puso a punto un método HTS que permitió detectar las mejoras implicadas en la estabilidad oxidativa, incluyendo la medición de las vidas medias frente a H_2O_2.

- Evolución dirigida de una VP activa y estable a pH neutro/alcalino. En esta nueva ruta evolutiva se combinaron diferentes herramientas de creación de diversidad junto con aproximaciones híbridas. Como criterio HTS se promovió la ampliación del perfil de pH junto con un incremento gradual de la presión selectiva hacia el rango alcalino.

- Diseño de un prototipo inicial de levadura de podredumbre blanca (*white-rot yeast*, WRY) mediante la co-expresión heteróloga de mutantes evolucionados de VP y lacasa. Se evaluó la co-expresión simultánea de dichos mutantes con diferentes *cassettes* de expresión (incluyendo diversas combinaciones de promotores y terminadores), además de testarse distintas condiciones de cultivo tanto a escala de microfermentación como de matraz.

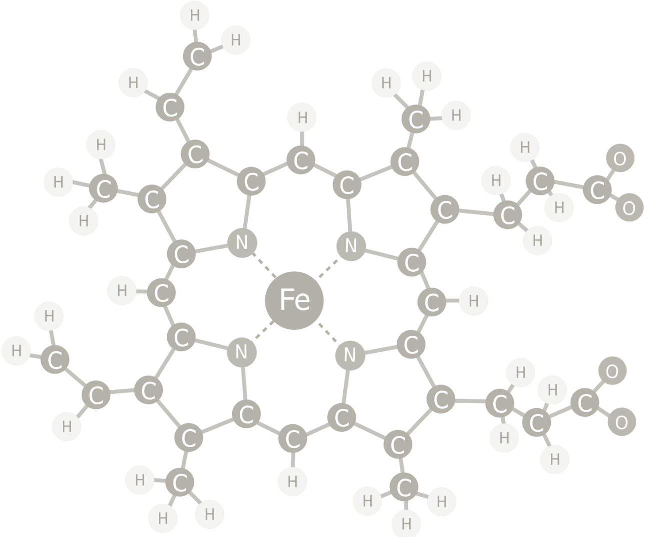

Capítulo 2:

Directed evolution of a temperature-, peroxide- and alkaline pH tolerant versatile peroxidase

---

En este capítulo se describe la obtención de la expresión funcional de la peroxidasa versátil (VP) por primera vez en levadura de forma soluble, altamente activa y termoestable, estableciendo una plataforma de evolución dirigida para su futura ingeniería hacia diversos fines.

BJ www.biochemj.org

BJ Structure

Biochem. J. (2012) **441**, 487–498 (Printed in Great Britain) doi:10.1042/BJ20111199

online data

Directed evolution of a temperature-, peroxide- and alkaline pH-tolerant versatile peroxidase

Eva GARCIA-RUIZ*, David GONZALEZ-PEREZ*, Francisco J. RUIZ-DUEÑAS†, Angel T. MARTÍNEZ† and Miguel ALCALDE*[1]

*Department of Biocatalysis, Institute of Catalysis, CSIC, Cantoblanco, 28049 Madrid, Spain, and †Center for Biological Investigations, CSIC, Ramiro de Maeztu 9, 28040 Madrid, Spain

The VPs (versatile peroxidases) secreted by white-rot fungi are involved in the natural decay of lignin. In the present study, a fusion gene containing the VP from *Pleurotus eryngii* was subjected to six rounds of directed evolution, achieving a level of secretion in *Saccharomyces cerevisiae* (21 mg/l) as yet unseen for any ligninolytic peroxidase. The evolved variant for expression harboured four mutations and increased its total VP activity 129-fold. The signal leader processing by the *STE13* protease at the Golgi compartment changed as a consequence of overexpression, retaining the additional N-terminal sequence Glu-Ala-Glu-Ala that enhanced secretion. The engineered N-terminally truncated variant displayed similar biochemical properties to those of the non-truncated counterpart in terms of kinetics, stability and spectroscopic features. Additional cycles of evolution raised the T_{50} 8 °C and significantly increased the enzyme's stability at alkaline pHs. In addition, the K_m for H_2O_2 was enhanced up to 15-fold while the catalytic efficiency was maintained, and there was an improvement in peroxide stability (with half-lives for H_2O_2 of 43 min at a H_2O_2/enzyme molar ratio of 4000:1). Overall, the directed evolution approach described provides a set of strategies for selecting VPs with improvements in secretion, activity and stability.

Key words: α-factor prepro-leader, directed evolution, enzyme promiscuity, *Saccharomyces cerevisiae*, versatile peroxidase.

INTRODUCTION

The ligninolytic enzymatic consortium secreted by white-rot fungi represents a remarkable example of a highly efficient oxidative system [1]. For decades, the complex interactions and synergies between enzymes and diffusible electron carriers generated by the wood-decaying fungi during lignin combustion have constituted a hot topic of research [2]. Typically formed by different oxidoreductases (mostly laccases, peroxidases and H_2O_2-supplying oxidases), this lignin-degrading array of enzymes have potential applications in the production of second-generation biofuels, pulp biobleaching, the design of nanobiodevices (biosensors and biofuel cells), organic synthesis and bioremediation, to name a few [3–6]. Among these enzymes, the high-redox potential VP (versatile peroxidase) is arousing great interest because of its catalytic promiscuity, being mainly described in *Pleurotus*, *Bjerkandera* and some other basidiomycete species [7–13].

As a protein, VP is classified by its structural properties and sequence information in Class II, corresponding to fungal secreted haem-containing peroxidases. As an enzyme, it is presented as a high-redox-potential substrate and Mn^{2+}-oxidizing peroxidase (E.C. 1.11.1.6) [14]. VPs combine the general catalytic features of other haem-containing enzymes (in terms of substrate specificity and reaction mechanisms), such as the high-redox-potential ligninolytic peroxidases, LiP (lignin peroxidase) and MnP (manganese peroxidase), with those of peroxidases with a lower redox potential, such as HRP (horseradish peroxidase) and CIP (*Coprinopsis cinerea* peroxidase) [15]. The VP's substrate promiscuity is associated with a high redox potential ($E° > +1.4$ V) and the presence of different catalytic sites for the oxidation of low- and high-redox-potential compounds [14,16]. Comprehensive structure–function studies have helped to reveal the mechanisms underlying the complex activity of these enzymes, which is governed by a haem domain located in the middle of a structure formed by 12 helices and that is connected to the protein surface by two small channels. In a scaffold of ~300 amino acids, VPs contain three carboxy residues implicated in the co-ordination of Mn^{2+} and one catalytic tryptophan residue involved in the oxidation of high-redox-potential compounds through a long-range electron-transfer pathway. In addition, VP has an oxidation site for low–medium-redox-potential compounds (0.6–0.8 V) associated with the main haem-access channel [17–19]. Thus VP behaves as a generalist biocatalyst, readily oxidizing VA (veratryl alcohol), methoxybenzenes or non-phenolic lignin model compounds (such as LiP); Mn^{2+} to Mn^{3+} (such as MnP), the latter able to act as diffusible oxidizer; and phenolic compounds (such as HRP and CIP). Furthermore, and unlike laccases that require the help of redox mediators [20], VPs can oxidize high-redox-potential compounds alone, such as polycyclic aromatic hydrocarbons, azo-dyes and many other complex recalcitrant molecules that LiP only oxidizes in the presence of VA [16].

Despite its broad catalytic promiscuity, the lack of a suitable heterologous host to functionally express VPs has impeded their engineering by directed evolution. Their extreme structural complexity (four disulfide bridges, two structural Ca^{2+}, the haem prosthetic group) often hampers proper folding and functional expression at reasonable levels. Indeed, when *Emericella nidulans*

Abbreviations used: ABTS, 2,2′-azinobis-(3-ethylbenzothiazoline-6-sulfonic acid); CIP, *Coprinopsis cinerea* peroxidase; DMP, 2,6-dimethoxyphenol; HRP, horseradish peroxidase; IvAM, *in vivo* assembly of mutant libraries constructed with different mutational spectra; IVOE, *in vivo* overlap extension; LiP, lignin peroxidase; MALDI–TOF-MS, matrix-assisted laser-desorption ionization–time-of-flight MS; MnP, manganese peroxidase; RB5, Reactive Black 5; StEP, staggered extension process; TAI, total activity improvement; VA, veratryl alcohol; VP, versatile peroxidase.

[1] To whom correspondence should be addressed (email malcalde@icp.csic.es).

or *Aspergillus niger* have been tested as hosts, VP expression was similar to that achieved from the homologous VP in *Pleurotus eryngii* (~0.4 mg/l) [21]. Moreover, further optimization by engineering only slightly improved the yields of secretion up to 2 mg/l [22,23]. When *Escherichia coli* has been used (one of the favourite hosts for directed evolution along with *Saccharomyces cerevisiae*), inclusion bodies were generally formed, and when a soluble enzyme was obtained, its atypical properties were related to improper folding [24]. In *E. coli*, the *in vitro* refolding from inclusion bodies can be attempted [25], which, although useful for structure–function studies [17–19], is not appropriate for high-throughput screening or directed evolution experiments. Rather than facing the shortcomings found for correct VP folding in bacteria (from different codon usage to the lack of post-translational modifications and missing chaperones), we circumvented these bottlenecks by engineering strategies to perform laboratory evolution of VP in *S. cerevisiae*. In the present paper, we report for the first time an evolved VP produced heterologously and functionally in a soluble, active and stable form. To extract further benefits from this system, additional rounds of molecular evolution were carried out to tailor a highly stable enzyme. The laboratory evolution approach based on the yeast eukaryotic machinery is discussed in detail, together with the properties of a set of novel VPs that include strong functional expression and improved stability against temperature, alkaline pH and inactivation by H_2O_2. A comprehensive biochemical analysis of the VP variants is provided.

EXPERIMENTAL

Laboratory evolution: general aspects

The original parental *α-vpl2* fusion gene was constructed as described in the Supplementary Experimental section at http://www.BiochemJ.org/bj/441/bj4410487add.htm. In each generation, PCR fragments were cleaned, concentrated and loaded on to a low-melting-point preparative agarose gel for purification using the Zymoclean gel DNA recovery kit (Zymo Research). PCR products were cloned under the control of GAL1p in the pJRoC30 expression shuttle vector, replacing the native gene in pJRoC30. The pJRoC30 plasmid was linearized with XhoI and BamHI to remove the native gene, and the linear plasmid was concentrated and purified as described above for the PCR fragments.

Evolution for secretion: first generation

A mutagenic library (~1400 clones) was constructed by error-prone PCR using the following primers for amplification: RMLN sense primer, 5′-CCTCTATACTTTAACGTCAAGG-3′, which binds to bp 160–181 of pJRoC30-*αvpl2*; and RMLC antisense primer, 5′-GGGAGGGCGTGAATGTAAGC-3′, which binds to bp 1532–1551 of pJRoC30-*αvpl2*. To promote *in vivo* ligation, overhangs of 40 and 66 bp homologous with the linear vector were designed. The reaction mixture was prepared in a final volume of 50 μl containing 90 nM RMLN primer, 90 nM RMLC primer, 0.1 ng/μl pJRoC30-*αvpl2*, 0.3 mM dNTPs (0.075 mM each), 3 % DMSO, 1.5 mM $MgCl_2$ and 0.05 unit/μl Taq DNA polymerase (Sigma). Different concentrations of $MnCl_2$ were tested to estimate the appropriate mutation rate before adopting 0.01 mM as the final concentration. Error-prone PCR was carried out on a gradient thermocycler (MyCycler, Bio-Rad Laboratories) using the following programme: 95 °C for 2 min (1 cycle); 94 °C for 0.45 min, 53 °C for 0.45 min, 74 °C for 3 min (28 cycles); and 74 °C for 10 min (1 cycle).The PCR product (400 ng) was mixed with the linearized vector (100 ng) and transformed into competent cells using the yeast transformation kit (Sigma). Transformed cells were plated in SC (synthetic complete) drop-out plates and incubated for 3 days at 30 °C. Colonies containing the whole autonomously replicating vector were picked and screened, and then subjected to additional screenings as described in the Supplementary Experimental section. From the first to the fourth round of evolution, the libraries were explored for improvements in total activity. From the fourth round onwards, libraries were explored for improvements in thermostability. Here and in other parts of the study, VP activity was measured by oxidation of 2 mM ABTS [2,2′-azinobis-(3-ethylbenzothiazoline-6-sulfonic acid)] ($\varepsilon_{\mathrm{ABTS}}{}^{\bullet+} = 36\,000\ \mathrm{M}^{-1}\cdot\mathrm{cm}^{-1}$) in 100 mM sodium tartrate buffer, pH 3.5 (the optimum ABTS oxidation value for the VPL2 parent) in the presence of 0.1 mM H_2O_2.

Evolution for secretion: second generation

The best secretion variants from the first round (11H10, 15G9, 4B5 and 4B1; Figure 1) were subjected to Taq/$MnCl_2$ amplification and recombined further by *in vivo* DNA shuffling (~1800 clones). The Taq/$MnCl_2$ amplifications were prepared as described above for the first round. Mutated PCR products were mixed in equimolar amounts and transformed along with the linearized vector into yeast (4:1 ratio of PCR products/vector).

Evolution for secretion: third generation

The best secretion variants of the second round (16E12, 19C2, 20D1 and 13G1; Figure 1) were subjected to Taq/$MnCl_2$ amplification and recombined by *in vivo* DNA shuffling (~1100 clones) as described for the second generation.

Evolution for secretion and thermostability: fourth generation

The best secretion variants of the third round (10C3, 6B1, 13E4, 6E7 and 11F3; Figure 1) were subjected to mutagenic StEP (staggered extension process) and *in vivo* DNA shuffling (~2000 clones). StEP was performed as reported previously [26] with some modifications. In order to favour random mutagenesis during StEP, Taq DNA polymerase was employed for the PCR reaction along with a low template concentration to promote the introduction of point mutations during amplification. The PCRs were performed in a final volume of 50 μl containing 90 nM RMLN primer, 90 nM RMLC primer, 0.3 mM dNTPs, 3 % DMSO, 0.05 unit/μl of Taq polymerase (Sigma), 1.5 mM $MgCl_2$ and 0.1 ng/μl of the 10C3, 6B1, 13E4, 6E7 and 11F3 DNA-template mixture. The thermal cycling programme for StEP was: 95 °C for 5 min (1 cycle), and 94 °C for 30 s and 55 °C for 20 s (90 cycles). Purified PCR products were recombined further by *in vivo* DNA shuffling as described for earlier generations. A thermostability assay was incorporated to screen this and future generations (see the Supplementary Experimental section for details). The temperature established to screen this generation was 60 °C.

Evolution for thermostability: fifth generation

A library of ~1400 clones was built by IvAM (*in vivo* assembly of mutant libraries constructed with different mutational spectra) [27]. The 24E10 thermostable mutant was used as the parental type (Figure 1), and Taq/$MnCl_2$ (Sigma) and Mutazyme libraries (Stratagene) were mixed in equimolar amounts, and they were transformed into competent *S. cerevisiae* cells along with the linearized vector as described above (4:1 ratio of library/vector). The library was explored by thermostability screening as described in the Supplementary Experimental section. The temperature established to screen this generation was 80 °C.

Evolution for thermostability: sixth generation

The best thermostable variants of the former round (3H9 and 15B4; Figure 1) were subjected to Taq/$MnCl_2$ amplification and recombined by *in vivo* DNA shuffling (~1400 clones) as described for the third generation. The library was screened as described for the previous generation with the screening temperature established as 90 °C.

Engineering truncated variants

In order to remove the extra N-terminal sequence, the best secretion mutant (R4, fourth generation) was subjected to deletion mutagenesis by IVOE (*in vivo* overlap extension) [28] (see details in the Supplementary Experimental section).

High-throughput screening

Activity and thermostability screening assays were performed as indicated in the Supplementary Experimental section. Selected mutants were produced, purified and characterized as described in the Supplementary Experimental section.

RESULTS AND DISCUSSION

Directed evolution strategy

Our starting point in the present study was the cDNA of the high-redox potential VP from the white-rot fungus *P. eryngii* (allelic variant *vpl2*). This gene encodes a mature protein of 331 amino acids, with a 30-amino-acid signal leader that directs its secretion. Initially, the native VP signal leader was replaced by the α-factor prepro-leader from *S. cerevisiae*, a commonly used signal peptide for heterologous protein expression in yeast [29]. The fusion gene constructed (α-*vpl2*) was cloned into the corresponding shuttle vector and was shown to be functionally expressed in *S. cerevisiae* (120 ABTS units/l of culture flask). The medium composition (haem supply, ethanol content and $CaCl_2$ content) and the culture conditions (temperature, pH, oxygen uptake and shaking) were optimized for microcultures of *S. cerevisiae* in 96-well plates (see the Supplementary Experimental section). Several specific substrates for different VP catalytic sites were tested to design a suitable screening assay for VP evolution: ABTS, RB5 (Reactive Black 5), VA, Mn^{2+} and DMP (2,6-dimethoxyphenol). In terms of reliability, signal stability and interference with the supernatant from the culture broth, ABTS appeared to be the most appropriate. It is worth noting that this molecule can be very efficiently oxidized by VP at the catalytic tryptophan residue, Trp^{164}, and less efficiently in the haem channel [16]. The ABTS colorimetric assay was adjusted and validated (limit of sensitivity ~5 n-units/ml, coefficient of variance <13 %) to screen for total activity (i.e. the product of functional expression and specific activity for ABTS), and later in the evolution process, this colorimetric assay was adapted to a high-throughput protocol to screen for thermostability [30].

Approximately 9000 clones were explored in six rounds of molecular evolution to improve functional expression and thermostability (Figure 1 and Supplementary Table S1 at http://www.BiochemJ.org/bj/441/bj4410487add.htm). Following a general premise, the whole α-*vpl2* fusion gene was targeted for random mutagenesis and DNA recombination to improve secretion and activity. Once the secretion levels had been considerably improved, mutants were screened at high temperatures in an attempt to transform the VP into a more stable enzyme. Most of the tools employed for library construction were based on *S. cerevisiae* physiology, encouraged by our previous results when using the *in vivo* gap-repair mechanism of this yeast coupled to its high frequency of homologous DNA recombination [31–33]. *In vivo* cloning and/or repair of mutagenic products was tackled by engineering specific overhangs with homologous regions of 30–60 bp that annealed to the linearized vector without altering the ORF (open reading frame). *In vivo* DNA shuffling, IvAM or deletion mutagenesis by IVOE to construct truncated variants were the preferred DNA recombination tools [27,28,34]. Accordingly, error-prone PCR was combined with the aforementioned *in vivo* strategies, which was particularly helpful to overcome the characteristic trade-off between activity and stability when evolving towards thermal stability [35,36]. In order to enhance further the complexity of the library (i.e. the frequency of crossover events between mutant templates), *in vitro* and *in vivo* recombination tools were mixed in the same cycle of evolution (e.g. by combining mutagenic StEP with *in vivo* DNA shuffling). Up to three re-screenings were incorporated in the evolution protocol to rule out the presence of false positives.

Directed evolution for functional expression

The first four cycles of evolution aimed to enhance the secretion of the VP in *S. cerevisiae* (Figure 1 and Supplementary Table S1). The TAI (total activity improvement) over the parental VPL2 obtained from large-scale fermentations was ~129-fold (the TAI value represents the enhancement of both ABTS specific activity and secretion; Supplementary Table S2 at http://www.BiochemJ.org/bj/441/bj4410487add.htm). The breakdown of the TAI value reflected a 51.6-fold improvement in functional expression and a 2.5-fold increase in ABTS oxidation activity with respect to the parental enzyme. The secretion of the most strongly expressed variant (R4 mutant) was 21.6 mg/l, to the best of our knowledge the highest functional expression reported to date for a high-redox potential peroxidase (from ligninolytic fungi).

During evolution, several mutations were introduced in the α-factor prepro-leader (up to eight mutations that included two synonymous ones, four in the pre-leader and four in the pro-leader), although consecutive cycles of DNA recombination ruled out all of them (Figure 1 and Supplementary Table S1). Hence the native signal sequence of the α-factor appeared to drive efficient secretion of the mature R4 mutant in yeast and it did not need further adjustment to successfully export the VP polypeptide. The mutation rate coupled with DNA recombination was highly tuned to generate approximately one mutation per round of evolution on average (i.e. the R4 expression mutant harboured four mutations after four cycles of evolution; Figure 1). Therefore the accumulation of neutral or deleterious mutations was almost completely avoided, which was advantageous in terms of identifying the roles of specific mutations. The four mutations E37K, V160A, T184M and Q202L harboured in the R4 mutant provided an amino acidic backbone responsible for the enhancement in functional expression and ABTS oxidation activity. Three of these four mutations (E37K, V160A and T184M) were introduced independently in different first generation mutants (the 11H10, 15G9 and 4B1 variants

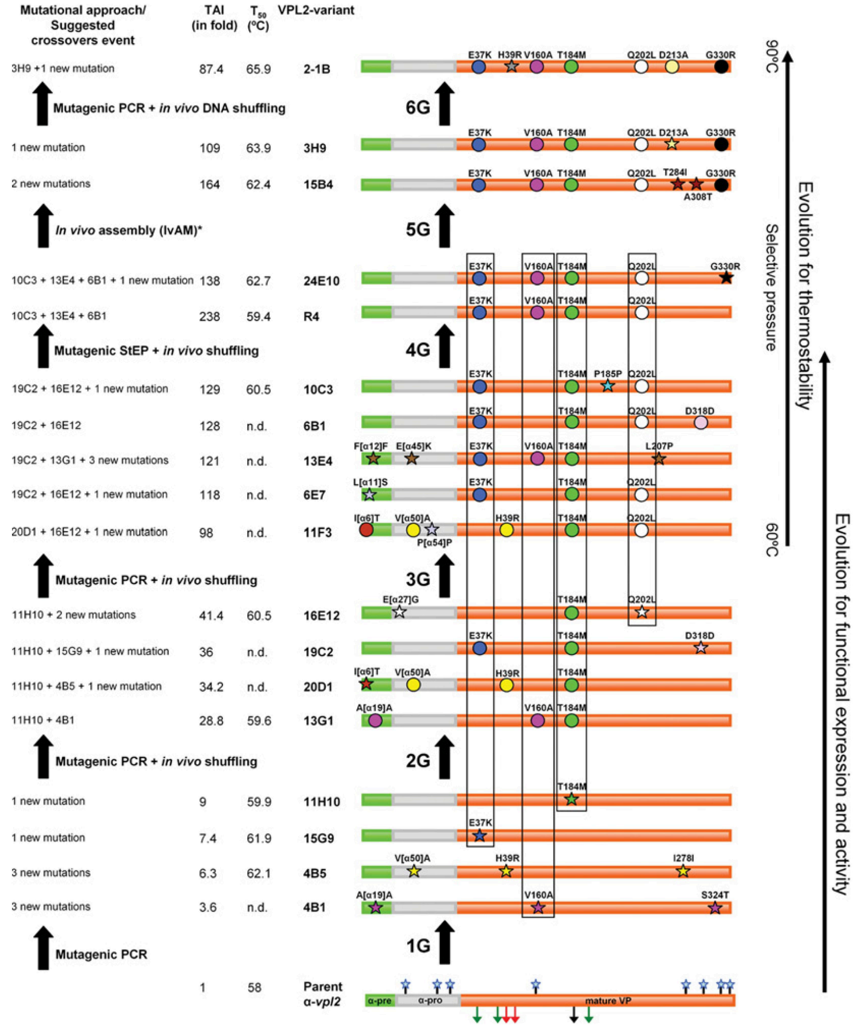

Figure 1 Laboratory evolution of the α-*vpl2* fusion gene

The properties targeted for evolution were secretion (from first to fourth generation) and thermal stability (from fourth to sixth generation). In the fourth generation, secretion and thermal stability were combined during the screening. The α-factor pre-leader is represented in green, the α-factor pro-leader is in grey, and the mature VP is in orange. In the parent α-*vpl2*, the glycosylation sites are represented as blue stars, the Mn^{2+}-binding site (Glu^{36}, Glu^{40} and Asp^{175}) is indicated by green arrows, the catalytic Trp^{164} is marked by a black arrow and the H_2O_2-binding site (from the distal side, Arg^{43} and His^{47}) is shown by red arrows. New mutations are depicted as stars and accumulated mutations are shown as circles. The amino acid backbone for secretion is highlighted in boxes. TAI indicates the improvement in VP activity detected in *S. cerevisiae* microcultures for each mutant when compared with the parental α-*vpl2*. The breakdown of the TAI into specific activity and expression for the best secretion variant is represented in Supplementary Table S2 at http://www.BiochemJ.org/bj/441/bj4410487add.htm. The suggested crossover events and the T_{50} values are included (n.d., not determined). See also Supplementary Table S1 at http://www.BiochemJ.org/bj/441/bj4410487add.htm.

that had TAI values ranging from 9- to 3.6-fold over parental type), whereas Q202L came from the best mutant of the second generation, the 16E12 variant. The DNA recombination approach enabled us to recreate crossover events in such a way that these mutations, discovered early in the evolution pathway, represented a common and well-conserved scaffold on which new thermostable variants could be constructed from the fourth round onwards.

The extra N-terminal sequence

The α-factor prepro-leader fusion proteins are processed in yeast by: (i) a signal peptidase acting on the pre-leader during the translocation of the nascent secretory protein at the endoplasmic reticulum membrane; and (ii) the action of *STE13* and *KEX2* proteases in the Golgi compartment to remove the pro-leader (Supplementary Figure S1A at http://www.BiochemJ.org/bj/441/bj4410487add.htm) [29,37,38].

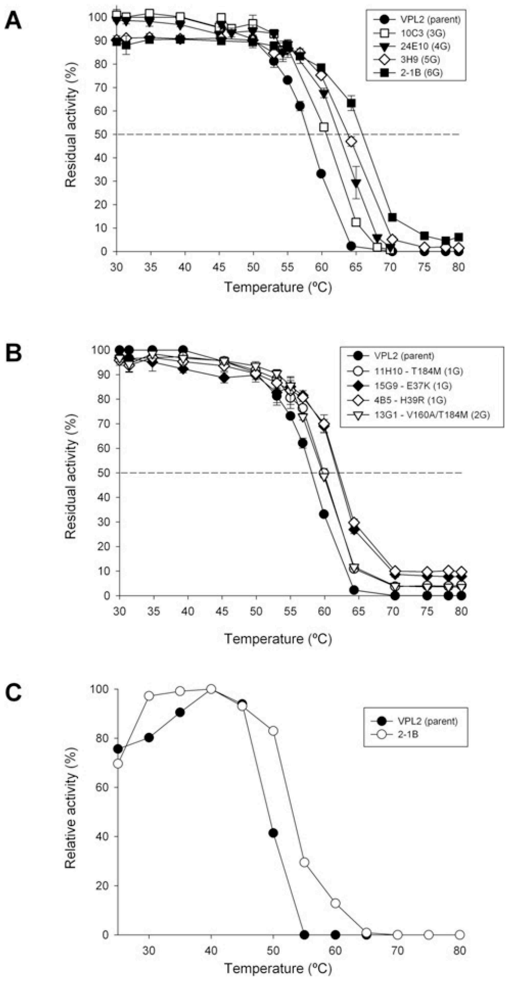

Figure 2 Thermostability of evolved VPs

(**A**) T_{50} profiles of mutants from the third to sixth generations. (**B**) T_{50} profiles of mutants from the first and second generations. (**C**) Thermo-activity (optimum temperature for activity) of parental VPL2 and the 2-1B mutant. Results are means ± S.D. for three independent experiments.

It has been reported that when high levels of fusion protein secretion are achieved with the α-factor prepro-leader, alternative processing occurs such that extracellular proteins contain a dipeptide spacer sequence linked to the N-terminus. This effect is attributed to the fact that the yeast produced insufficient *STE13* protease to process the high levels of heterologous proteins expressed from these synthetic genes. When we sequenced the N-terminal end of the R4 mutant overexpressed by *S. cerevisiae*, an extra acidic N-terminal sequence (EAEA, Glu-Ala-Glu-Ala) led the original mature protein, confirming that *STE13* failed to adequately process the pro-leader (Supplementary Figure S1B).

We decided to delete the portion of our synthetic gene encoding the spacer dipeptide (Supplementary Figure S1C), engineering a truncated version of the R4 mutant by IVOE deletion mutagenesis [28]. This strategy took advantage of the eukaryotic *S. cerevisiae* machinery by designing specific overhangs between fragments with homologous regions that tolerated the splicing of the truncated products between each other and with the linearized vector, giving rise to an autonomously replicating plasmid (see the Supplementary Experimental section and Supplementary Figure S2 at http://www.BiochemJ.org/bj/441/bj4410487add.htm). The new variant was produced and purified, and the N-terminus was sequenced to verify that it was correctly processed and secreted without the *STE13* cleavage site (i.e. only through *KEX2* protease activity; Supplementary Figure S1C). However, the secretion levels were reduced ~60 % upon deletion of the EAEA sequence (Supplementary Table S3 at http://www.BiochemJ.org/bj/441/bj4410487add.htm). Since the removal of the charged spacer peptide linked the fusion directly to the Lys-Arg processing site, making it a poor substrate for the *KEX2* protease, an acidic environment in the proximity of the *KEX2* cleavage site would appear to be important for secretion. Similar effects have been observed with other fusions, such as the α-factor leader–interferon-α1, in which the intracellular accumulation and secretion of unprocessed and partially processed forms occurred [39]. The truncated R4 variant behaved similarly to its extra N-terminal sequence counterpart in terms of spectroscopic characteristics, kinetic parameters and stability (including pH-activity profiles and temperature or pH stability), indicating that the N-terminal extension had little or no impact on the biochemical properties of the mutant VPs (Table 1, Figure 3, Supplementary Table S3 and Supplementary Figure S3 at http://www.BiochemJ.org/bj/441/bj4410487add.htm). Therefore the R4 mutant containing the N-terminal sequence was subjected to further engineering.

Directed evolution for thermal stability

After considerably augmenting the levels of secretion by evolution, our next goal was to tailor a more thermostable VP. Accordingly, further rounds of evolution were carried out and screened with a high-throughput thermostability assay, based on the ratio of residual activity/initial activity in combination with the estimated T_{50} values [30] (see the Supplementary Experimental section for details). The selection pressure was progressively increased from 60 °C (fourth cycle) to 80 °C and 90 °C in the fifth and sixth generations respectively. This approach was possible because the improvements accomplished in each generation were sufficient to retain >30 % of residual activity making them suitable to evolve stability. The T_{50} (i.e. the temperature at which the enzyme retains 50 % of its activity after 10 min of incubation) shifted ~2 °C per round of evolution for thermostability (Figure 2A), attaining a final T_{50} of 66 °C in the most thermostable mutant, the 2-1B variant (with a global improvement in T_{50} of 8 °C over the parental VPL2). Interestingly, an improvement of ~2 °C in T_{50} was detected in the third generation 10C3 mutant when compared with the original parental VPL2, despite the fact that the thermal stability was not targeted during the first three rounds of evolution, only secretion (Figures 1 and 2A). Hence some of the mutations discovered during the *in vitro* evolution for expression also displayed improved stability.

Intrigued by this result, we evaluated the T_{50} values in several variants of the first and second generation that harboured beneficial mutations finally inherited by the 10C3 mutant. The improvements in stability could be precisely attributed to each mutation under study as, at this primary stage of evolution, most of the mutations appeared individually in the mutants or in combination with other mutations that were either silent or located at the signal leader, and that did not affect stability (Figure 1 and Supplementary Table S1). Accordingly, the T_{50} of the 11H10

Table 1 Kinetic parameters for parent type and evolved variants of VPL2 expressed in *S. cerevisiae*

Kinetic constants were estimated in 100 mM sodium tartrate buffer containing 0.1 mM H_2O_2 at pH 3.5 for ABTS, DMP and RB5, and at pH 5.0 for Mn^{2+}. H_2O_2 kinetic constants were estimated using ABTS as reducing substrate at the corresponding saturated conditions and taking into account the reaction stoichiometry (one H_2O_2 molecule is reduced for oxidation of two ABTS molecules).

Substrate	Kinetic constants	VPL2 parent type	R4 mutant	2-1B mutant
ABTS (low efficiency)	K_m (mM)	0.54 ± 0.05	0.056 ± 0.003	0.034 ± 0.004
	k_{cat} (s^{-1})	220 ± 30	365 ± 6	850 ± 40
	k_{cat}/K_m ($mM^{-1} \cdot s^{-1}$)	410 ± 30	6480 ± 280	25000 ± 2100
DMP (low efficiency)	K_m (mM)	32 ± 6	6.5 ± 0.5	2.5 ± 0.2
	k_{cat} (s^{-1})	98 ± 7	58 ± 1	97 ± 1
	k_{cat}/K_m ($mM^{-1} \cdot s^{-1}$)	3.1 ± 0.4	9.1 ± 0.5	39 ± 2
RB5	K_m (mM)	0.007 ± 0.0007	0.0066 ± 0.0004	0.0055 ± 0.0006
	k_{cat} (s^{-1})	11.8 ± 0.5	10.6 ± 0.2	9.4 ± 0.4
	k_{cat}/K_m ($mM^{-1} \cdot s^{-1}$)	1670 ± 100	1600 ± 65	1700 ± 140
Mn^{2+}	K_m (mM)	0.045 ± 0.007	0.12 ± 0.01	4.3 ± 0.3
	k_{cat} (s^{-1})	54 ± 1	75 ± 1	98 ± 2
	k_{cat}/K_m ($mM^{-1} \cdot s^{-1}$)	1190 ± 180	630 ± 50	23 ± 1
H_2O_2	K_m (mM)	0.051 ± 0.009	0.20 ± 0.02	0.8 ± 0.1
	k_{cat} (s^{-1})	135 ± 5	490 ± 15	1720 ± 70
	k_{cat}/K_m ($mM^{-1} \cdot s^{-1}$)	2650 ± 370	2400 ± 160	2260 ± 305

Table 2 Biochemical features of parent and evolved variants

n.d., not determined.

Biochemical and spectroscopic feature	VPL2	R4 mutant	2-1B mutant
Molecular mass (Da)*	35257.6	35243.7	35317.9
Molecular mass (Da)†	38618.4	38600.0	38761.4
Degree of glycosylation (%)	9	9	9
Thermal stability, T_{50} (°C)	58	59.4	65.9
pI	4.6	4.6	4.6
Optimum pH	3.0	3.5	4.0
R_Z (A_{410}/A_{280})	2	4	4
Soret region (nm)	407	407	407
Charge transference band, CT1 (nm)	n.d.	504	503
Charge transference band, CT2 (nm)	631	638	638

*Estimated from amino acid composition.
†Estimated by MALDI–TOF-MS.

mutant containing the T184M mutation and the 15G9 mutant containing the E37K mutation improved 2–4 °C over VPL2, which corroborated the stabilizing effect of T184M and E37K mutations (Figures 1 and 2B). The T_{50} remained constant when the 13G1 mutant from the second generation was compared with 11H10, indicating that the V160A mutation did not affect thermal stability. It is also notable that the H39R mutation (found for the first time in the 4B5 mutant from the first generation) was lost during the recombination events that took place in the fourth round, although it was rediscovered in the final cycle for thermal stability (in the 2-1B mutant; Figure 1). The T_{50} of the 4B5 mutant was 4 °C higher than that of the parental type, which confirmed that the H39R mutation also had a strong influence on protein stability during secretion (Figure 2B).

Enhanced thermostability often coincides with improved thermo-activity (T_a) and/or a widening of the T_a range [40]. The 2-1B mutant had the same T_a (defined as the optimal temperature for activity) as the parental VPL2 at 40 °C, although the range of temperature at which the enzyme is highly active was broader after artificial selection (2-1B retaining over 80 % of relative activity in the range from 30 to 50 °C as opposed to the range from 30 to 45 °C for the parental type; Figure 2C). Thus the relative activity at 50 °C of the 2-1B mutant was double that of the parental type at the same temperature. Generally, when thermostability is improved, there is an inherent trade-off between stability and activity, with the concomitant detrimental effect on the specific activity. This is basically due to the fact that stabilizing mutations are not necessarily beneficial for activity, but, rather, they may confer robustness on the protein structure that compromises flexibility in some cases and, consequently, turnover rates. Indeed, the TAI was reduced from 129-fold (10C3 mutant, 3G) to 87-fold (2-1B mutant, 6G) from the fourth to sixth round of evolution (Figure 1). However, as might be expected, this reduction did not drastically affect the kinetics, but, rather, expression above all. With all of the substrates tested (except for Mn^{2+}, where several stabilizing mutations were located around the Mn^{2+}-binding site, see below), the catalytic efficiencies were either improved (at the haem channel site, with ~4-fold improvements for ABTS or DMP) or conserved (at the catalytic Trp^{164}) when compared with the R4 mutant (Table 1).

In general terms, the secretion backbone generated for functional expression helped tolerate the introduction of a new set of stabilizing mutations during evolution towards thermal stability without compromising the kinetics. This was particularly noticeable in the fourth generation when screening for total activity and thermostability was combined in the same cycle (Figure 1). For the first time, all of the fourth generation VPL2 variants selected bought together the E37K, V160A, T184M and Q202L mutations to produce the most active mutant R4. The related 24E10 mutant also selected harboured an additional G330R mutation that, while impeding large gains in total ABTS oxidation activity, increased its thermostability by >2 °C (Figure 1). The DNA recombination method used in this cycle (mutagenic StEP in combination with *in vivo* DNA shuffling) favoured the joining of the four mutations beneficial for total activity, which buffered the effect of incorporating the stabilizing mutation G330R in the same template. Therefore a more thermostable mutant with activity similar to that of the parental types was created.

Characterization of evolved VPs

The parental and evolved R4 and 2-1B VPs were purified and their averaged molecular masses were measured by MALDI–TOF-MS (matrix-assisted laser-desorption ionization–time-of-flight MS) and found to marginally differ from their

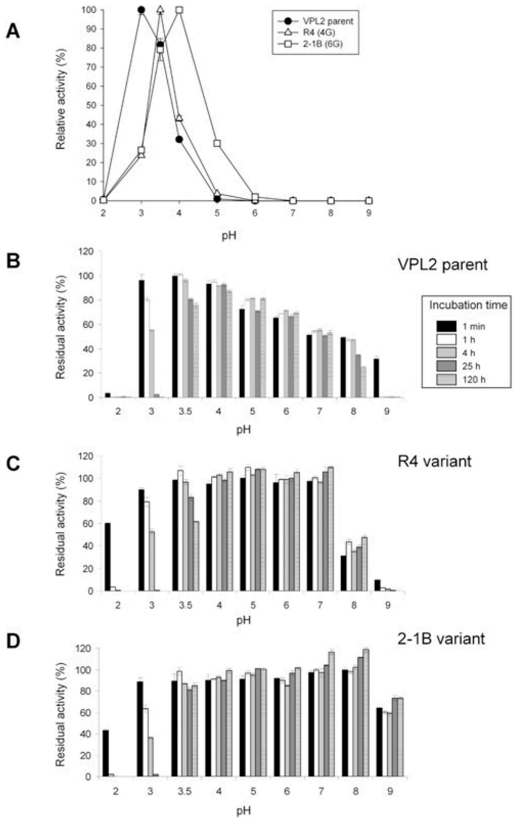

Figure 3 Activity and stability against pH

(**A**) pH-activity profile for the parental VPL2, R4 and 2-1B mutants. Activities were measured in 100 mM B&R (Britton and Robinson) buffer at different pHs with 2 mM ABTS and 0.1 mM H_2O_2. VP activity was normalized to the optimum activity value, and results are means $\pm$ S.D. for three independent experiments. pH stability of the parental VPL2 (**B**), the R4 (**C**) and the 2-1B mutants (**D**). Enzyme samples were incubated in 100 mM B&R buffer at different pH values, and the residual activity was measured in 100 mM sodium tartrate buffer (pH 3.5) containing 2 mM ABTS and 0.1 mM H_2O_2. Results are means $\pm$ S.D. for three independent experiments. See also Table 2 and Supplementary Figure S4 at http://www.BiochemJ.org/bj/441/bj4410487add.htm.

expected masses (Table 2). The other biochemical features (pI 4.6; ~9 % glycosylation) also remained unchanged in the mutant VPs (Table 2 and Supplementary Figure S4 at http://www.BiochemJ.org/bj/441/bj4410487add.htm). Unlike other proteins expressed heterologously in *S. cerevisiae* that are hyperglycosylated upon secretion, the low sugar content of the parental VPL2 and the mutants probably reflects the short residence in the Golgi compartment that is associated with the ease of exocytosis by yeast. The spectroscopic characteristics of VP variants expressed by *S. cerevisiae* were similar to those of VP from *P. eryngii* or the *in vitro* refolded VP from *E. coli* inclusion bodies (Table 2 and Supplementary Figure S4D). Thus the absorption spectrum showed a maximum in the Soret region and two charge transference bands (CT1 and CT2) that are characteristic of Fe^{3+} in a high-spin state. The pH-activity profile was shifted in the course of evolution and while the parental VPL2 displayed an optimum pH for activity at 3.0, this value rose to 3.5 and 4.0 for the R4 and 2-1B variants respectively (Figure 3A). Together with this unexpected change, the stability at alkaline pH values was notably improved in the thermostable 2-1B variant (Figures 3B–3D). When maintained for 120 h at pH 9.0, the 2-1B variant conserved ~60 % of its residual activity as it was very stable in the pH range 3.5–9. In contrast, the parental VPL2 (from yeast) was very unstable at pH 9.0, losing nearly all of its residual activity after 1 h at this pH. Similar alkaline instability has been reported for the wild-type VP produced by *P. eryngii* as well as for the *Aspergillus*-expressed recombinant enzyme, being related to the loss of structural Ca^{2+} ions (as shown by enzyme stability in Ca^{2+}-containing buffer) [23].

Kinetic constants were assessed using an array of substrates that bind to the different catalytic sites of VP (Table 1). The substrates ABTS and DMP are both oxidized with high efficiency at the catalytic Trp^{164} and less efficiently at the haem channel site. Substrate RB5 is exclusively oxidized at Trp^{164}, whereas the substrate Mn^{2+} is only oxidized at the Mn^{2+} oxidation site [16]. The R4 mutant had an improved affinity for ABTS and DMP at the haem channel with a 10-fold lower K_m and almost 2-fold higher k_{cat} for ABTS that enhanced its k_{cat}/K_m 16-fold compared with VPL2. This improvement prevented the measurement of ABTS oxidation at the catalytic Trp^{164} since the kinetics of ABTS oxidation at the haem channel masked the plots for its oxidation at this site. However, the k_{cat}/K_m values for RB5 at the catalytic Trp^{164} were readily measured and they were similar to those of the parental VPL2 (~1600 $mM^{-1} \cdot s^{-1}$), indicating that the improvement in activity was mainly concentrated at the haem channel site. Similar behaviour was detected for the thermostable 2-1B mutant with RB5 as substrate, yet the k_{cat}/K_m for ABTS was much improved at the haem channel site (over 61-fold better than the parental type). In contrast, and even though the k_{cat} for Mn^{2+} was slightly improved over the course of evolution, the Mn^{2+}-binding site was negatively affected by the mutations (see the structural analysis of the mutations below), with a 2.6- and 94-fold enhancement of the K_m for Mn^{2+} for R4 and 2-1B respectively. We chose ABTS for the screening as this molecule can be oxidized at both the haem channel site and the catalytic tryptophan residue, thereby avoiding the tendency to lose performance at the different catalytic sites. Indeed, activity at both sites was fairly well conserved or even substantially improved during evolution. The fall in Mn^{2+} activity underscores the fact that all of the properties not addressed in the screen could drift. For future applications in which Mn^{2+} activity might be required, the kinetics of the enzyme with this specific substrate can be enhanced by directed evolution or semi-rational approaches.

Stability of the evolved VPs against peroxide

Peroxidases are inhibited by excess of H_2O_2 and the *Pleurotus* VP is no exception [41]. Although this inhibition is caused by relatively large molar excesses of H_2O_2 (with respect to enzyme concentration), it results in substantial activity losses when the enzyme is in the absence of a reducing substrate. The explanation for such inhibition is found in the peroxidase catalytic cycle, which includes a highly reactive two-electron oxidized species (compound I, a porphyrin radical Fe^{4+}=O complex) that, under turnover conditions, is reduced back to the resting state (via compound II, Fe^{4+}=O haem). In the absence of reducing substrate, compound I reacts with H_2O_2, resulting in compound III (a Fe^{3+}–superoxide complex) formation and then in irreversible inactivation due to the haem/protein oxidative degradation, as reported for ligninolytic and other peroxidases [42,43]. Comparing peroxide stability between different peroxidases is not straightforward because the process is strongly dependent on

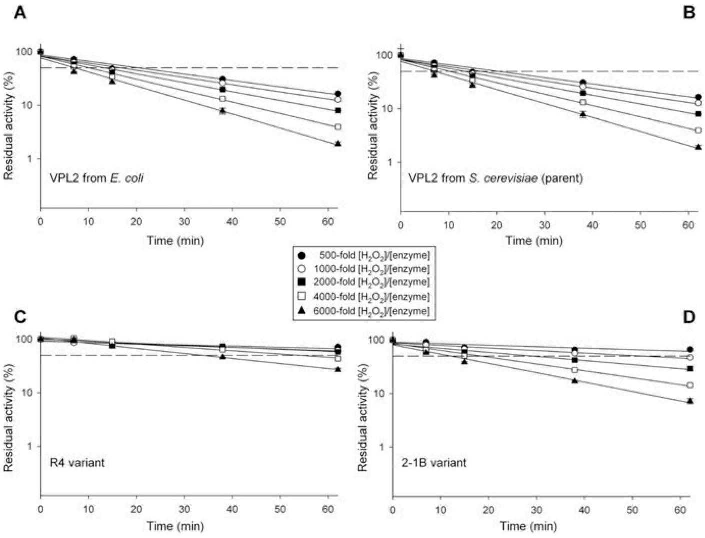

Figure 4 Inactivation of parental and VP mutants at different H_2O_2/enzyme ratios

(**A**) VPL2 from *E. coli* after *in vitro* refolding. (**B**) Functional expression in *S. cerevisiae* of the parental VPL2, (**C**) the R4 and (**D**) 2-1B mutant. The purified VPs (0.06 μM) were incubated at room temperature (24°C) in 20 mM B&R (Britton and Robinson) buffer containing different H_2O_2 concentrations. The following [H_2O_2]/[VP] molar ratios were assayed: ●, 500-fold; ○, 1000-fold; ■, 2000-fold; □, 4000-fold; ▲, 6000-fold. The residual activity was measured with 2 mM ABTS and 0.1 mM H_2O_2 in 100 mM sodium tartrate buffer (pH 3.5). The residual activity refers to the corresponding VP variant incubated in the absence of H_2O_2, taking into account the final concentration of H_2O_2 for each assay. Results are means ± S.D. for three independent experiments. The broken line indicates 50 % of the residual activity. See also Supplementary Figure S5 at http://www.BiochemJ.org/bj/441/bj4410487add.htm.

pH; nevertheless, wild-type VP susceptibility would be of the same order as other ligninolytic peroxidases (60 % inactivation after 1 h of incubation with 250 H_2O_2 equivalents at pH 4.5, and 90 % inactivation at pH 3.0) [41]. Inactivation by their oxidizing substrate is an important problem to be overcome for biotechnological application of peroxidases, since some loss of activity is produced by H_2O_2 even under steady-state operation conditions, and in this context has been referred to as a suicide inactivation of the enzyme [43–45]. Although this problem has yet to be fully resolved, it has been examined by controlling the addition of H_2O_2 by sensors, by co-immobilization with glucose oxidase to generate H_2O_2 *in situ* coupled to the oxidation of glucose, as well as through site-directed mutagenesis and directed evolution (with low- and high-redox potential peroxidases, but not VPs) [46–53].

In the course of evolution, we detected a dramatic shift in the K_m for H_2O_2. The peroxide k_{cat} was inferred from ABTS oxidation at the haem channel site (taking into account the stoichiometry of the reaction: one molecule of H_2O_2 is reduced by oxidizing two substrate molecules; Table 1 and Supplementary Figure S5 at http://www.BiochemJ.org/bj/441/bj4410487add.htm). Indeed, the R4 and 2-1B mutants reduced their affinity for H_2O_2 4- and 15-fold respectively, without the catalytic efficiency being modified. This means that the evolved VP can operate at higher H_2O_2 concentrations with a significant improvement in turnover rates (k_{cat}, molecules of peroxide reduced per molecule of VP per s) from 135 s^{-1} for VPL2 to 1720 s^{-1} for 2-1B. In contrast, the 2–7-fold increases in K_m for H_2O_2 attained by engineering H_2O_2 stability in bacterial dye-decolorizing peroxidases by site-directed mutagenesis of methionine residues resulted in reductions in k_{cat} and subsequent catalytic efficiency k_{cat}/K_m [53]. Thus R4 and 2-1B worked efficiently in the presence of high concentrations of H_2O_2, showing specific activities with ABTS as high as 3530 and 11 300 units/mg respectively, when estimated using saturating H_2O_2 conditions (i.e. at concentrations of 2.0 and 7.6 mM for R4 and 2-1B respectively, representing 10-fold the H_2O_2 K_m of each variant). Under these conditions, the total ABTS-oxidation activity of the R4 mutant secreted into the culture broth was ~57 000 units/l, to date the highest value reported for any peroxidase as far as we are aware.

The half lives in the presence of H_2O_2 ($t_{1/2}$ H_2O_2) were assessed at several H_2O_2/enzyme molar ratios (Figure 4). Both the R4 and 2-1B mutants significantly improved their peroxide stability relative to VPL2. The $t_{1/2}$ H_2O_2 of R4 and 2-1B at a H_2O_2/enzyme molar ratio of 4000:1 was enhanced from 10 min for VPL2 to 53 and 19 min respectively (Figure 4). In contrast, the K_m for H_2O_2 for 2-1B was 4- and 16-fold higher than for R4 and VPL2 (Table 1). This apparent catalytic inconsistency is probably a consequence of the different experimental conditions used to measure K_m for H_2O_2 (steady-state conditions in the presence of both peroxidase oxidizing and reducing substrates) and $t_{1/2}$ H_2O_2 (no reducing substrate present). The enhanced K_m for H_2O_2 detected in R4 and 2-1B suggests that the kinetic constants of the transient state has been altered by directed evolution of VP, the estimation of which could provide additional information on the mechanisms underlying peroxide stability. These changes may affect different stages of the VP catalytic cycle (i.e. from the resting state to compound I, or its derivative compound II). In fact, any subtle modification in the balance between these intermediates could vary the overall catalytic cycle, affecting the formation of compound III, which is the main precursor for peroxidase inactivation by H_2O_2, as described above. Possibly, the improved oxidative stability is a side effect of laboratory evolution, suggesting a potential use of our mutants to further select for VP variants with improved stability against H_2O_2.

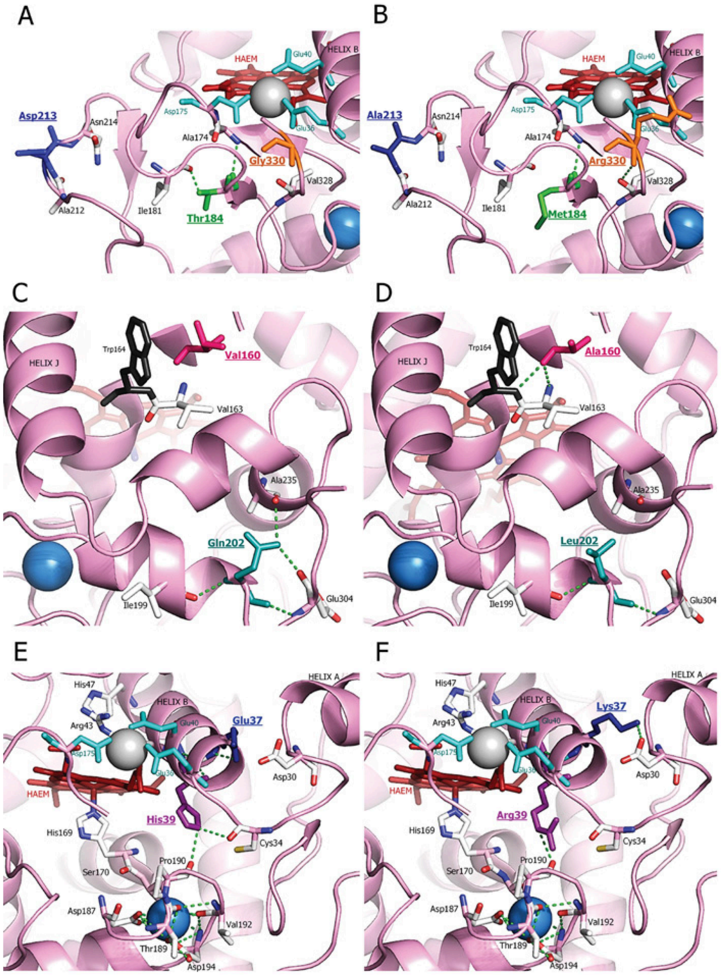

Figure 5 Structural examination of the selected mutations in VPL2

The haem group is represented in red, the catalytic Trp^{164} is in black, and the Mn^{2+}-binding site formed by acidic residues Glu^{36}, Glu^{40} and Asp^{175} is in blue. Grey sphere, Mn^{2+}; blue sphere, Ca^{2+}. (**A** and **B**) Mutations G330R (in orange and underlined), D213A (in blue and underlined) and T184M (in green and underlined). (**C** and **D**) Mutations V160A (in red and underlined) and Q202L (in green and underlined). (**E** and **F**) Mutations H39R (in violet and underlined) and E37K (in blue and underlined). The residues involved in the co-ordination of the proximal Ca^{2+} (Ser^{170}, Asp^{187}, Thr^{189}, Val^{192} and Asp^{194}) are highlighted. Based on PDB code 3FJW (parental VPL2) and modelled with the mutations introduced by directed evolution.

Structural analysis of mutations

The mutations introduced by directed evolution were mapped using the crystal structure of glycosylated VP isolated from *P. eryngii* (PDB code 3FJW; Supplementary Figure S6 at http://www.BiochemJ.org/bj/441/bj4410487add.htm). In this structure, Thr^{184}, Glu^{37} and Val^{160} mutated in R4 are partially exposed to the solvent and distributed in different regions of the protein (Supplementary Figure S6). In contrast, the mutated Leu^{202} occupies an internal position in the VP molecule. Upon inspection of the VP structure, the Thr^{184} mutation may interrupt a hydrogen bond with the neighbouring Ile^{181}, relieving possible structural tension in this region (Figures 5A and 5B). This change might also cause reorientation of the hydrogen-bonded Ala^{174} and adjoining Asp^{175} that constitutes one of the three carboxy residues of the Mn^{2+}-binding site, possibly explaining the increased K_m for Mn^{2+} by R4 (Table 1). The Q202L mutation may interrupt two hydrogen bonds with Ala^{235} and Glu^{304}. This residue is located deep in the protein, at the end of the last β-strand in the enzyme, which is followed by a long C-terminal tail (Supplementary Figure S6). The possible changes in the hydrogen-bonding structure provoked by the Q202L mutation in this area might enhance the structural flexibility of the protein, improving its secretion (Figures 5C and 5D). The E37K mutation increased the T_{50} by 4 °C (Figure 2B). The side-chain carboxy group of Glu^{37} is hydrogen-bonded to the backbone amide proton of Glu^{36} (both residues located in helix B; Figures 5E and 5F). However, inspection of the protein model suggests that the resulting Lys^{37} may establish a salt bridge with the adjacent Asp^{30} of helix A. This new interaction could pack the two neighbouring A and B helices more tightly, which may improve stability [54]. Moreover, Glu^{36} is one of the three acidic residues forming the Mn^{2+}-binding site, and it seems plausible that helix B could shift slightly due to this mutation, varying the relative position of Glu^{36} with respect to the other two acidic residues. This shift could ultimately affect the geometry of the co-ordination sphere of the Mn^{2+} ion and, consequently, the affinity for this substrate [18] (Table 1). Interestingly, helix B also harbours the residues involved in H_2O_2 binding (His^{47} and Arg^{43}). Any subtle change in the position of this helix relative to the haem cofactor could affect peroxide binding, and, indeed, the K_m for H_2O_2 in the R4 mutant was 15-fold higher than that of the parental VPL2 (Table 1 and Supplementary Figure S5). Finally, the V160A mutation seems to create two new hydrogen bonds (with Trp^{164} and Val^{163}; Figures 5C and 5D), without affecting either the kinetics at the catalytic Trp^{164} (Table 1) or stability (Figure 2B). The change in this position could be related with more correct polypeptide maturation in *S. cerevisiae*.

The remaining mutations discovered during the evolution to improve thermal stability were also located at the surface of the protein (G330R, D213A and H39R). Gly^{330} is situated at the C-terminal tail of VP, the most mobile region in the protein (Supplementary Figure S6). According to our model, the G330R mutation seems to produce a new hydrogen bond with Val^{328} (Figures 5A and 5B), which could stabilize this area (the T_{50} was enhanced by 2.2 °C upon mutation; Figure 1). Asp^{213} is very exposed to solvent in the most external part of the haem channel (Figures 5A and 5B). The change of a negative residue for a neutral one at this position would help VP to accommodate negatively charged substrates, like ABTS, to be oxidized at the haem edge. It is likely that a change in the polarity of this region might suppress unfolding at higher temperatures. The H39R mutation was discovered at different points of the evolution route and indeed, the secretion mutant 4B5 and the final 2-1B thermostable variant incorporated this mutation in the first and last cycle of evolution respectively. As discussed above, this mutation considerably enhances the stability of the enzyme, improving secretion and thermal stability (Figures 1 and 2B). In native VP, His^{39} is hydrogen-bond to Pro^{190}, acting as a bridge between helix B and the loop containing the proximal Ca^{2+} ion (one of the two structural Ca^{2+} conserved in all Class-II peroxidases [10]). In fact, this proline residue is contiguous with Thr^{189}, one of the five residues involved in the co-ordination of the proximal Ca^{2+} ion in VP (together with Ser^{170}, Asp^{187}, Val^{192} and Asp^{194}). Differences in the strength of the hydrogen bonds between His^{39} and Pro^{190} in native VP and between Arg^{39} and Pro^{190} in 2-1B (Figures 5E and 5F) could be related to the improvement in thermal (and alkaline) resistance of the latter variant by modifying the stability of the proximal Ca^{2+}-binding site. This effect is supported by the fact that the first-generation 4B5 variant (containing only the H39R beneficial mutation) also showed improved stability (Figures 1 and 2B).The suggested changes in the proximal Ca^{2+} loop after mutation are in good agreement with the reported role for the protein stability of the two structural Ca^{2+} ions, as for LiP and VP among other Class-II peroxidases [13,55,56]. The H39R mutation may also break down the hydrogen bond with Cys^{34} (Figures 5E and 5F), which in turn could affect the distance between helix B and the haem domain, modifying the binding of peroxide (Supplementary Figure S5). It is also worth noting that this mutation may affect the oxidation of Mn^{2+} in the 2-1B variant (exhibiting a K_m value 100-fold higher than that of the parental VPL2), enhancing the effect previously described for the E37K mutation since both Arg^{39} and Lys^{37} are contiguous with Glu^{40}, which, along with Glu^{36} and Asp^{175}, contributes to the Mn^{2+}-binding site (Table 1). A summary of the different characteristics (such as location, distance to the catalytic sites and interactions affected) of the seven residues that were mutated during VP directed evolution is provided in Supplementary Table S4 at http://www.BiochemJ.org/bj/441/bj4410487add.htm.

Conclusions

VPs are a typical example of generalist enzymes with phylogenetic sequence comparisons indicating that they are related to MnP and LiP. In principle, VP has adapted through natural selection to combine many catalytic phenotypes from its related peroxidases. Indeed, modern VPs probably possess a broader substrate specificity than their ancestral progenitors [14]. Given their intrinsic enzymatic promiscuity, it is likely that VPs have the capacity to evolve novel catalytic properties, making them a potentially powerful model enzyme to engineer by molecular evolution towards specialized functions. *S. cerevisiae* is considered by many to be the preferred eukaryotic model organism for molecular and cell biology, with this versatility making it a highly useful expression host in directed protein evolution studies [28,46,57]. Indeed, in the present study, we have demonstrated the usefulness of *S. cerevisiae* for evolving VP variants via laboratory evolution strategies to select for more stable and active forms, possibly serving as a suitable platform to tailor VPs with targeted catalytic attributes [58]. Recently, new laccases have been engineered by artificial evolution, strengthening the array of ligninolytic enzymes available for different potential applications [31,59]. These evolutionary models could be employed as a biomolecular toolbox in order to address both traditional problems and new challenges in synthetic biology that have so far hindered the practical use of VPs and other high-redox-potential oxidoreductases: from inactivation by H_2O_2 to the construction of artificial operons of evolved laccases and VPs for the directed evolution of whole ligninolytic cell factories in yeast.

AUTHOR CONTRIBUTION

Eva Garcia-Ruiz carried out all of the laboratory evolution experiments. David Gonzalez-Perez helped in the biochemical characterization of evolved variants. Francisco Ruiz-Dueñas and Angel Martínez contributed to the structure–function analysis of the mutations and helped with the writing and the revision of the paper. Miguel Alcalde conceived the project, supervised its development and wrote the paper.

ACKNOWLEDGEMENTS

We thank Rita Getzlaff from the Helmholtz Centre for Infection Research (HZI, Braunschweig, Germany) for sequence analyses. We thank Dr Francisco J. Plou from the ICP (CSIC, Madrid, Spain) for assistance with the HPLC purification.

FUNDING

This study is based upon work funded by European Union Projects [grant numbers NMP2-CT-2006-026456-Biorenew, FP7-KBBE-2010-4-26537-Peroxicats and COST Action CM0701] and National projects [grant numbers BIO2010-19697 and BIO2008-01533]. We also thank NeuronBiopharma for financial support through Research Contracts [grant numbers 020401070029, Profit Program and 020401070004, Idea Program]. E.G.-R. was supported by a Biorenew grant, D.G.-P. was supported by a Peroxicats contract, and F.J.R.-D. was supported by the Ministerio de Cienca e Innovación (MICINN) Ramón y Cajal Program.

REFERENCES

1 Martínez, A. T., Ruiz-Dueñas, F. J., Martínez, M. J., del Río, J. C. and Gutiérrez, A. (2009) Enzymatic delignification of plant cell-wall: from nature to mill. Curr. Opin. Biotechnol. **20**, 348–357

2 Ruiz-Dueñas, F. J. and Martínez, A. T. (2009) Microbial degradation of lignin: how a bulky recalcitrant polymer is efficiently recycled in nature and how we can take advantage of this. Microbial Biotechnol. **2**, 164–177

3 Kamm, B. and Kamm, M. (2007) Biorefineries: multi product processes. Adv. Biochem. Eng./Biotechnol. **105**, 175–204

4 Orts, W. J., Imam, S., Glenn, G. M., Inglesby, M., Wong, D., Guttman, M. and Samac, D. A. (2004) Envisioning biorefineries based on utilization of lignocellulosic straws and bagasses. 227th National Meeting of the American Chemical Society, Anaheim, CA, U.S.A., 28 March–1 April 2004, Abstract Cell 192

5 Alcalde, M., Ferrer, M., Plou, F. J. and Ballesteros, A. (2006) Environmental biocatalysis: from remediation with enzymes to novel green processes. Trends Biotechnol. **24**, 281–287

6 Xu, F. (2005) Applications of oxidoreductases: recent progress. Industr. Biotechnol. **1**, 38–50

7 Camarero, S., Sarkar, S., Ruiz-Dueñas, F. J., Martínez, M. J. and Martínez, A. T. (1999) Description of a versatile peroxidase involved in natural degradation of lignin that has both Mn-peroxidase and lignin-peroxidase substrate binding sites. J. Biol. Chem. **274**, 10324–10330

8 Martínez, M. J., Ruiz-Dueñas, F. J., Guillén, F. and Martínez, A. T. (1996) Purification and catalytic properties of two manganese-peroxidase isoenzymes from *Pleurotus eryngii*. Eur. J. Biochem. **237**, 424–432

9 Ruiz-Dueñas, F. J., Martínez, M. J. and Martínez, A. T. (1999) Molecular characterization of a novel peroxidase isolated from the ligninolytic fungus *Pleurotus eryngii*. Mol. Microbiol. **31**, 223–236

10 Martínez, A. T. (2002) Molecular biology and structure–function of lignin-degrading heme peroxidases. Enzyme Microb. Technol. **30**, 425–444

11 Rainio, A., Maijala, P., Hildén, K. and Hatakka, A. (2008) A novel peroxidase from the white-rot fungus *Cerrena unicolor*. Peroxidase 2008, Tampere, Finland 20–23 August 2008, Abstract PX-S10-5

12 Moreria, P. R., Duez, C., Dehareng, D., Antunes, A., Almeida-Vara, E., Frère, J.-M., Malcata, F. X. and Duarte, J. C. (2005) Molecular characterisation of a versatile peroxidase from a *Bjerkandera* strain. J. Biotechnol. **118**, 339–352

13 Verdín, J., Pogni, R., Baeza, A., Baratto, M. C., Basosi, R. and Vázquez-Duhalt, R. (2006) Mechanism of versatile peroxidase inactivation by Ca^{2+} depletion. Biophys. Chem. **121**, 163–170

14 Hofrichter, M., Ullrich, R., Pecyna, M. J., Liers, C. and Lundell, T. (2010) New and classic families of secreted fungal heme peroxidases. Appl. Microbiol. Biotechnol. **87**, 871–897

15 Martínez, A. T. (2007) High redox potential peroxidases. In Industrial Enzymes: Structure, Function and Applications (Polaina, J. and MacCabe, A. P., eds), pp. 475–486, Springer, Berlin

16 Ruiz-Dueñas, F. J., Morales, M., García, E., Miki, Y., Martínez, M. J. and Martínez, A. T. (2009) Substrate oxidation sites in versatile peroxidase and other basidiomycete peroxidases. J. Exp. Bot. **60**, 441–452

17 Ruiz-Dueñas, F. J., Morales, M., Mate, M. J., Romero, A., Martínez, M. J., Smith, A. T. and Martínez, A. T. (2008) Site-directed mutagenesis of the catalytic tryptophan environment in *Pleurotus eryngii* versatile peroxidase. Biochemistry **47**, 1685–1695

18 Ruiz-Dueñas, F. J., Morales, M., Pérez-Boada, M., Choinowski, T., Martínez, M. J., Piontek, K. and Martínez, A. T. (2007) Manganese oxidation site in *Pleurotus eryngii* versatile peroxidase: a site-directed mutagenesis, kinetic and crystallographic study. Biochemistry **46**, 66–77

19 Ruiz-Dueñas, F. J., Pogni, R., Morales, M., Giansanti, S., Mate, M. J., Romero, A., Martínez, M. J., Basosi, R. and Martínez, A. T. (2009) Protein radicals in fungal versatile peroxidase: catalytic tryptophan radical in both Compound I and Compound II and studies on W164Y, W164H and W164S variants. J. Biol. Chem. **284**, 7986–7994

20 Cañas, A. and Camarero, S. (2010) Laccases and their natural mediators: biotechnological tools for sustainable eco-friendly processes. Biotechnol. Adv. **28**, 694–705

21 Ruiz-Dueñas, F. J., Martínez, M. J. and Martínez, A. T. (1999) Heterologous expression of *Pleurotus eryngii* peroxidase confirms its ability to oxidize Mn^{2+} and different aromatic substrates. Appl. Environ. Microbiol. **65**, 4705–4707

22 Eibes, G. M., Lu-Chau, T. A., Ruiz-Dueñas, F. J., Feijoo, G., Martínez, M. J., Martínez, A. T. and Lema, J. M. (2009) Effect of culture temperature on the heterologous expression of *Pleurotus eryngii* versatile peroxidase in *Aspergillus* hosts. Bioprocess Biosyst. Eng. **32**, 129–134

23 Lú-Chau, T. A., Ruiz-Dueñas, F. J., Camarero, S., Feijoo, G., Martínez, M. J., Lema, J. M. and Martínez, A. T. (2004) Effect of pH on the stability of *Pleurotus eryngii* versatile peroxidase during heterologous production in *Emericella nidulans*. Bioprocess Biosyst. Eng. **26**, 287–293

24 Mohorcic, M., Bencina, M., Friedrich, J. and Jerala, R. (2009) Expression of soluble versatile peroxidase of *Bjerkandera adusta* in *Escherichia coli*. Bioresour. Technol. **100**, 851–858

25 Pérez-Boada, M., Doyle, W. A., Ruiz-Dueñas, F. J., Martínez, M. J., Martínez, A. T. and Smith, A. T. (2002) Expression of *Pleurotus eryngii* versatile peroxidase in *Escherichia coli* and optimisation of *in vitro* folding. Enzyme Microb. Technol. **30**, 518–524

26 Zhao, H. M., Giver, L., Shao, Z. X., Affholter, J. A. and Arnold, F. H. (1998) Molecular evolution by staggered extension process (StEP) *in vitro* recombination. Nat. Biotechnol. **16**, 258–261

27 Zumárraga, M., Camarero, S., Shleev, S., Martínez-Arias, A., Ballesteros, A., Plou, F. J. and Alcalde, M. (2008) Altering the laccase functionality by *in vivo* assembly of mutant libraries with different mutational spectra. Proteins **71**, 250–260

28 Alcalde, M. (2010) Mutagenesis protocols in *Saccharomyces cerevisiae* by *in vivo* overlap extension. Methods Mol. Biol. **634**, 3–14

29 Brake, A. J. (1990) α-Factor leader-directed secretion of heterologous proteins from yeast. Methods Enzymol. **185**, 408–421

30 García-Ruiz, E., Maté, D., Ballesteros, A., Martínez, A. T. and Alcalde, M. (2010) Evolving thermostability in mutant libraries of ligninolytic oxidoreductases expressed in yeast. Microb. Cell Fact. **9**, 17

31 Mate, D., Garcia-Burgos, C., Garcia-Ruiz, E., Ballesteros, A. O., Camarero, S. and Alcalde, M. (2010) Laboratory evolution of high-redox potential laccases. Chem. Biol. **17**, 1030–1041

32 Zumárraga, M., Bulter, T., Shleev, S., Polaina, J., Martínez-Arias, A., Plou, F. J., Ballesteros, A. and Alcalde, M. (2007) *In vitro* evolution of a fungal laccase in high concentrations of organic cosolvents. Chem. Biol. **14**, 1052–1064

33 Bulter, T., Alcalde, M., Sieber, V., Meinhold, P., Schlachtbauer, C. and Arnold, F. H. (2003) Functional expression of a fungal laccase in *Saccharomyces cerevisiae* by directed evolution. Appl. Environ. Microbiol. **69**, 987–995

34 Alcalde, M., Zumárraga, M., Polaina, J., Ballesteros, A. and Plou, F. J. (2006) Combinatorial saturation mutagenesis by *in vivo* overlap extension for the engineering of fungal laccases. Comb. Chem. High Throughput Screening **9**, 719–727

35 Bloom, J. D. and Arnold, F. H. (2009) In the light of directed evolution: pathways of adaptive protein evolution. Proc. Natl. Acad. Sci. U.S.A. **106**, 9995–10000

36 Romero, P. A. and Arnold, F. H. (2009) Exploring protein fitness landscapes by directed evolution. Nat. Rev. Mol. Cell Biol. **10**, 866–876

37 Brake, A. J., Merryweather, J. P., Coit, D. G., Heberlein, U. A., Masiarz, F. R., Mullenbach, G. T., Urdea, M. S., Valenzuela, P. and Barr, P. J. (1984) α-Factor-directed synthesis and secretion of mature foreign proteins in *Saccharomyces cerevisiae*. Proc. Natl. Acad. Sci. U.S.A. **81**, 4642–4646

38 Romanos, M. A., Scorer, C. A. and Clare, J. J. (1992) Foreign gene expression in yeast: a review. Yeast **8**, 423–488

39 Zsebo, K. M., Lu, H. S., Fieschko, J. C., Goldstein, L., Davis, J., Duker, K., Suggs, S. V., Lai, P. H. and Bitter, G. A. (1986) Protein secretion from *Saccharomyces cerevisiae* directed by the prepro-α-factor leader region. J. Biol. Chem. **261**, 5858–5865

40 Cirino, P. C. and Georgescu, R. (2003) Screening for thermostability. Methods Mol. Biol. **230**, 117–125

41 Böckle, B., Martínez, M. J., Guillén, F. and Martínez, A. T. (1999) Mechanism of peroxidase inactivation in liquid cultures of the ligninolytic fungus *Pleurotus pulmonarius*. Appl. Environ. Microbiol. **65**, 923–928

42 Wariishi, H. and Gold, M. H. (1989) Lignin peroxidase compound III: formation, inactivation, and conversion to the native enzyme. FEBS Lett. **243**, 165–168

43 Valderrama, B., Ayala, M. and Vázquez-Duhalt, R. (2002) Suicide inactivation of peroxidases and the challenge of engineering more robust enzymes. Chem. Biol. **9**, 555–565

44 Timofeevski, S. L., Reading, N. S. and Aust, S. D. (1998) Mechanisms for protection against inactivation of manganese peroxidase by hydrogen peroxide. Arch. Biochem. Biophys. **356**, 287–295

45 Hernández-Ruiz, J., Arnao, M. B., Hiner, A. N. P., García-Canovas, F. and Acosta, M. (2001) Catalase-like activity of horseradish peroxidase: relationship to enzyme inactivation by H_2O_2. Biochem. J. **354**, 107–114

46 Cherry, J. R., Lamsa, M. H., Schneider, P., Vind, J., Svendsen, A., Jones, A. and Pedersen, A. H. (1999) Directed evolution of a fungal peroxidase. Nat. Biotechnol. **17**, 379–384

47 Morawski, B., Quan, S. and Arnold, F. H. (2001) Functional expression and stabilization of horseradish peroxidase by directed evolution in *Saccharomyces cerevisiae*. Biotechnol. Bioeng. **76**, 99–107

48 Miyazaki-Imamura, C., Oohira, K., Kitagawa, R., Nakano, H., Yamane, T. and Takahashi, H. (2003) Improvement of H_2O_2 stability of manganese peroxidase by combinatorial mutagenesis and high-throughput screening using *in vitro* expression with protein disulfide isomerase. Protein Eng. **16**, 423–428

49 Ryu, K., Hwang, S. Y., Kim, K. H., Kang, J. H. and Lee, E. K. (2008) Functionality improvement of fungal lignin peroxidase by DNA shuffling for 2,4-dichlorophenol degradability and H_2O_2 stability. J. Biotechnol. **133**, 110–115

50 Ryu, K., Kang, J. H., Wang, L. S. and Lee, E. K. (2008) Expression in yeast of secreted lignin peroxidase with improved 2,4-dichlorophenol degradability by DNA shuffling. J. Biotechnol. **135**, 241–246

51 Miyazaki, C. and Takahashi, H. (2001) Engineering of the H_2O_2-binding pocket region of a recombinant manganese peroxidase to be resistant to H_2O_2. FEBS Lett. **509**, 111–114
52 Ryan, B. J. and O'Fagain, C. (2007) Effects of single mutations on the stability of horseradish peroxidase to hydrogen peroxide. Biochimie **89**, 1029–1032
53 Ogola, H. J.O., Hashimoto, N., Miyabe, S., Ashida, H., Ishikawa, T., Shibata, H. and Sawa, Y. (2010) Enhancement of hydrogen peroxide stability of a novel *Anabaena* sp. DyP-type peroxidase by site-directed mutagenesis of methionine residues. Appl. Microbiol. Biotechnol. **87**, 1727–1736
54 Musafia, B., Buchner, V. and Arad, D. (1995) Complex salt bridges in proteins: statistical analysis of structure and function. J. Mol. Biol. **254**, 761–770
55 Nie, G. J. and Aust, S. D. (1997) Effect of calcium on the reversible thermal inactivation of lignin peroxidase. Arch. Biochem. Biophys. **337**, 225–231
56 George, S. J., Kvaratskhelia, M., Dilworth, M. J. and Thorneley, R. N. F. (1999) Reversible alkaline inactivation of lignin peroxidase involves the release of both the distal and proximal site calcium ions and bishistidine co-ordination of the haem. Biochem. J. **344**, 237–244
57 Okkels, J. S. (2004) *In vivo* gene shuffling in yeast: a fast and easy method for directed evolution of enzymes. In Enzyme Functionality: Design, Engineering, and Screening (Svendsen, A., ed.), pp. 378–389, Marcel Dekker, New York
58 García, E., Martínez, F. J., Ruiz-Dueñas, F. J., Martínez, A. T. and Alcalde, M. (2010) High redox potential peroxidases designed by directed evolution. Int. Pat. WO/2010/130862
59 Camarero, S., Cañas, A., Martínez, M. J., Martínez, A. T., Ballesteros, A., Plou, F. J., Record, E., Asther, M. and Alcalde, M. (2010) Laccases having high redox potential obtained through directed evolution. Int. Pat. WO/2010/058057

Received 5 July 2011/7 October 2011; accepted 7 October 2011
Published as BJ Immediate Publication 7 October 2011, doi:10.1042/BJ20111199

Supplemental data chapter 2

Directed evolution of a temperature-, peroxide-, and alkaline pH tolerant versatile peroxidase

Authors: Garcia-Ruiz, E., González-Perez, D., Ruiz-Dueñas, F.J., Martínez, A.T., and Alcalde, M.

Biochem J (2012) **441**, 487-498.

Biochem. J. (2012) **441**, 487–498 (Printed in Great Britain) doi:10.1042/BJ20111199

SUPPLEMENTARY ONLINE DATA

Directed evolution of a temperature-, peroxide- and alkaline pH-tolerant versatile peroxidase

Eva GARCIA-RUIZ*, David GONZALEZ-PEREZ*, Francisco J. RUIZ-DUEÑAS†, Angel T. MARTÍNEZ† and Miguel ALCALDE*[1]
*Department of Biocatalysis, Institute of Catalysis, CSIC, Cantoblanco, 28049 Madrid, Spain, and †Center for Biological Investigations, CSIC, Ramiro de Maeztu 9, 28040 Madrid, Spain

EXPERIMENTAL

Reagents and enzymes

ABTS, DMP, VA, RB5, haemoglobin from bovine blood, Taq DNA polymerase for random mutagenesis, StEP and the *S. cerevisiae* transformation kit were purchased from Sigma–Aldrich. The *E. coli* XL2-Blue competent cells and the Genemorph II random mutagenesis kit were obtained from Stratagene. The protease-deficient *S. cerevisiae* strain BJ5465 was from LGC Promochem, the uracil-independent and ampicillin-resistance shuttle vector pJRoC30 was a gift from Professor E. H. Arnold at the California Institute of Technology (Caltech), whereas the pGAPZαA vector containing α-factor prepro-leader and the Taq DNA polymerase used to construct the α-*vpl2* fusion were from Invitrogen. The Zymoprep yeast plasmid miniprep kit, Zymoclean gel DNA-recovery kit and the DNA clean and concentrator TM-5 kit were all from Zymo Research. The NucleoSpin® plasmid kit was purchased from Macherey-Nagel and the restriction enzymes BamHI, XhoI, EcoRI and NotI were from New England Biolabs. VPL2 from *E. coli* was prepared by *in vitro* refolding from inclusion bodies as reported previously [25]. All chemicals were reagent-grade purity.

Culture media

Minimal medium contained 100 ml of 6.7 % sterile yeast nitrogen base, 100 ml of 19.2 g/l sterile yeast synthetic drop-out medium supplement without uracil, 100 ml of sterile 20 % raffinose, 1 ml of 25 g/l chloramphenicol and 700 ml of sterile double-distilled water. YP medium contained 10 g of yeast extract, 20 g of peptone and double-distilled water to 650 ml. Flask expression medium contained 720 ml of YP medium, 67 ml of 1 M potassium phosphate buffer (pH 6.0), 111 ml of 20 % galactose, 25 g/l ethanol, 500 mg/l bovine haemoglobin, 1 mM $CaCl_2$, 1 ml of 25 g/l chloramphenicol and double-distilled water to 1 litre. Microplate expression medium contained 720 ml of YP medium, 67 ml of 1 M potassium phosphate buffer (pH 6.0), 111 ml of 20 % galactose, 100 mg/l bovine haemoglobin, 1 ml of 25 g/l chloramphenicol and double-distilled water to 1 litre. YPD solution contained 10 g of yeast extract, 20 g of peptone, 100 ml of 20 % sterile glucose, 1 ml of 25 g/l chloramphenicol and double-distilled water to 1 litre. SC (synthetic complete) drop-out plates contained 100 ml of 6.7 % sterile yeast nitrogen base, 100 ml of 19.2 g/l sterile yeast synthetic drop-out medium supplement without uracil, 20 g of Bacto agar, 100 ml of 20 % sterile glucose, 1 ml of 25 g/l chloramphenicol and double-distilled water to 1 litre.

Construction of pJRoC30-α-*vpl2*

The pGAPZ-αA vector was used as a template to fuse the native *vpl2* with the α-factor prepro-leader. First, the cDNA from *vpl2* (996 bp) excluding the native signal leader was amplified using the following primers: NtEcoRI-direct (5′-CGGAATTCGCAACTTGCGACGACGGACGC-3′) and CtNotl-reverse (5′-AAGGAAAAAAGCGGCCGCTTACGATC-CAGGGACGGGAGG-3′). The target sequences for EcoRI and Notl are underlined. PCRs were performed in a final volume of 50 μl containing 400 nM NecoRI-direct, 400 nM CtNotl-reverse, 0.25 mM dNTPs, 0.05 unit/μl Taq DNA polymerase (Invitrogen), 4 mM $MgCl_2$ and 0.5 ng/μl *vpl2* cDNA. The thermal cycling programme was: 94 °C for 5 min, 55 °C for 5 min, 72 °C for 5 min (1 cycle); 95 °C for 0.35 min, 50 °C for 2 min, 72 °C for 4 min (25 cycles); and 72 °C for 10 min (1 cycle). The amplified *vpl2* was purified by low-melting-point gel extraction and recovered with Zymoclean gel DNA-recovery kit. The *vpl2* product and the pGAPZαA vector were both digested with EcoRI and Notl, and ligated, giving rise to pGAPZ-α-*vpl2*. This construct was used to transform *E. coli* XL2-Blue cells and the product was prepared in large amounts. The pGAPZα-*vpl2* was used to amplify the α-*vpl2* fusion gene with the following primers: NtpJRBamHI-direct (5′-CGCGGATCCATGAGATTTCCTTC-AATTTTTACTGC-3′), which included the BamHI target (underlined); and CtNotL-reverse sequences. PCRs were performed in a final volume of 50 μl containing 400 nM NtpJRBamHI-direct, 400 nM CtNotl-reverse, 0.25 mM dNTPs, 0.05 unit/μl Taq DNA polymerase (Invitrogen), 4 mM $MgCl_2$ and 0.4 ng/μl pGAPZ-α-*vpl2*. The amplified α-*vpl2* fusion was purified and cleaned as described above and then cloned into the pJRoC30 episomal shuttle vector. Both α-*vpl2* and pJRoC30 were linearized with BamHI and NotI, and ligated to generate pJRoC30-α-*vpl2*.

Truncated variant

The extra N-terminal sequence was removed by deletion mutagenesis (R4DEL variant) using IVOE (as summarized in Figure S2 [28]). For the R4DEL mutant, the primers for PCR 1 were RMLN and IVΔSTE13 R (5′-GCAGCATTTGCG-GTGGTGCGTCCGTCGTCGCAAGTTGCTCTTTTCTCGAG-AGATACCCCTTC-3′ which binds to positions 441–465 of pJRoC30-αPM1). The primers for PCR 2 were IVΔEcoRI F (5′-GCAACTTGCGACGACGGACGC-3′ which binds to positions 483–503 of pJRoC30-α-*vpl2*) and RMLC. The products from PCR 1 and PCR 2 have overhangs with homologous regions of 38 bp between each other, and of 40 and 66 bp with the linearized

---

[1] To whom correspondence should be addressed (email malcalde@icp.csic.es).

vector for *in vivo* cloning. The linearized plasmid (100 ng) was mixed with products from PCR 1 and PCR 2 (400 ng each) and transformed into competent *S. cerevisiae* cells. Individual clones were picked and cultured in 96-well plates (Greiner Bio-One) containing 50 μl of minimal medium per well and subjected to the screening procedure described below. Positive clones were re-screened (see below), the *in vivo* repaired plasmid was recovered, and the truncated fusion gene was confirmed by DNA sequencing.

High-throughput screening assays

Owing to the low levels of secretion, longer induction times in expression medium were used in the first round of evolution (up to 72 h). From the second cycle onwards, expression was sufficiently strong that the time required for protein induction was reduced to 24 h. Moreover, in the first two cycles, the screening was carried out in end-point mode after incubating the supernatants for several hours in the presence of ABTS. As a consequence of the high levels of secretion achieved, from the third generation on the supernatants were diluted 1:10 before screening.

High-throughput screening assays for secretion (total activity)

Individual clones were picked and cultured in 96-well plates (Greiner Bio-One) containing 50 μl of minimal medium per well. In each plate, column number 6 was inoculated with the parental type and one well (H1-control) was inoculated with non-transformed yeast cells as a negative control. The plates were sealed to prevent evaporation and incubated at 30 °C, 225 rev./min and 80 % relative humidity in a humid shaker (Minitron-INFORS, Biogen). After 48 h, 160 μl of expression medium was added to each well and the plates were incubated for 24 h. The plates (master plates) were centrifuged at 3000 ***g*** for 5 min at 4 °C (Eppendorf 5810R centrifuge), and 20 μl of supernatant was transferred from the master plate on to a replica plate using a robot (Liquid Handler Quadra 96-320, Tomtec). The replica plate was filled with 180 μl of 100 mM sodium tartrate buffer (pH 3.5) containing 2 mM ABTS and 0.1 mM H_2O_2. The plates were stirred briefly and the absorption at 418 nm ($\varepsilon_{\mathrm{ABTS}}{}^{\bullet +} = 36\,000$ $M^{-1} \cdot cm^{-1}$) was recorded in the plate reader (SpectraMax Plus 384, Molecular Devices). The plates were incubated at room temperature until the colour developed and the absorption was measured again. Relative activities were calculated from the difference between the absorption after incubation and that of the initial measurement normalized against the parental type and used as a reference in the corresponding plate (the reference parental types were as follows: 1G, α-VPL2; 2G, 11H10; 3G, 16E12; 4G, 10C3; 5G, 24E10; 6G, 3H9).

High-throughput screening assay for thermostability

From the fourth generation onwards, a thermostability assay was incorporated, as described previously [30] with minor modifications. Accordingly, 20 μl of supernatant was transferred to the replica plate from the master plate using the robot. Subsequently, 180 μl of stability buffer (10 mM sodium tartrate buffer, pH 5.0) was added to each replica and they were stirred briefly. The replica plate was duplicated with the help of the robot by transferring 50 μl of the mixtures to a thermocycler plate (Multiply PCR plate without skirt, neutral, Sarstedt) and 20 μl to the initial activity plate. Thermocycler plates were sealed with thermoresistant film (Deltalab) and incubated at the corresponding temperature in a thermocycler (MyCycler, Bio-Rad Laboratories). The incubation took place over 10 min so that the activity assessed was reduced to two-thirds of the initial activity. Afterwards, the thermocycler plates were placed on ice for 10 min and incubated further for 5 min at room temperature. Subsequently, 20 μl of the supernatants were transferred from both the thermocycler and the initial activity plates to new plates to estimate the initial and residual activities in ABTS buffer. The plates were stirred briefly and the ABTS oxidation activity was measured as described in the previous section. The plates were incubated at room temperature until a green colour developed and the absorbance was measured again. The same experiment was performed for both the initial activity plate and the residual activity plate. The relative activity was calculated from the difference between the absorbance after incubation and that of the initial measurement normalized against the parental type in the corresponding plate. Thermostability values were taken as the ratio between the residual and initial activity.

Re-screening

To rule out false positives, two consecutive re-screenings were carried out according to an earlier protocol with some modifications [30]. A third rescreening was incorporated to calculate the T_{50} of the mutants selected from the thermostability assay.

First re-screening. Aliquots (5 μl) of the best clones were removed from the master plates to inoculate minimal medium (50 μl) in new 96-well plates. Columns 1 and 12 (rows A and H) were not used to prevent the appearance of false positives. After 24 h of incubation at 30 °C and 225 rev./min, an aliquot (5 μl) was transferred to the adjacent wells and incubated further for 24 h. Finally, expression medium (160 μl) was added and the plates were incubated for 24 h. Thus each mutant was grown in four wells. The parental types were subjected to the same procedure (lane D, wells 7–11) and the plates were assessed using the same protocol as that used for the screenings described above.

Second re-screening. An aliquot from the wells with the best clones from the first re-screening was inoculated in YPD medium (3 ml), incubated at 30 °C and 225 rev./min for 24 h, and the plasmids from these cultures were recovered (Zymoprep yeast plasmid miniprep kit). As the product of the Zymoprep was very impure and the DNA concentration extracted was very low, the shuttle vectors were transformed into super-competent *E. coli* XL2-Blue cells and plated on to LB (Luria–Bertani)-amp (ampicillin) plates. Single colonies were picked and used to inoculate LB-amp medium (5 ml) and they were grown overnight at 37 °C and 225 rev./min. The plasmids were then extracted (NucleoSpin® plasmid kit) and *S. cerevisiae* was transformed with plasmids from the best mutants and the parental type. Five colonies for each mutant were picked and re-screened as described above.

Third re-screening for thermostability (T_{50}). Fresh transformants of selected mutants and of the parental types were cultured (10 ml) in a 100 ml flask for VP production. The supernatants were assayed for thermostability to accurately estimate their T_{50} using 96/384-well gradient thermocyclers. Appropriate dilutions of supernatants were prepared with the help of the robot such that aliquots (20 μl) produced a linear response in kinetic mode, and for each point in the gradient scale, aliquots (50 μl) from both selected mutants and the parental types were used. A temperature gradient profile ranging from 30 to 80 °C was established and, after 10 min of incubation, samples were chilled on ice for 10 min and incubated further at room temperature for 5 min. Finally, aliquots (20 μl) were removed and subjected to the same ABTS-based colorimetric assay described above for the screening. Thermostability values were deduced from the ratio between the residual activities incubated at different temperatures and the initial activity at room temperature.

Production and purification of VP variants

Production of VPs in *S. cerevisiae*

A single colony from the *S. cerevisiae* clone containing the parental or mutant *vp* gene was picked from a SC drop-out plate, inoculated in minimal medium (10 ml) and incubated for 48 h at 30 °C and 225 rev./min (Micromagmix shaker). An aliquot of cells was removed and used to inoculate minimal medium (50 ml) in a 500 ml flask (at a D_{600} of 0.25). The cells completed two growth phases (6–8 h) and then expression medium (450 ml) was inoculated with the pre-culture (50 ml) in a 2 litre baffled flask (D_{600} of 0.1). After incubating for 48 h at 30 °C and 225 rev./min (maximal VP activity; $D_{600} = 28$–30), the cells were recovered by centrifugation at 4600 ***g*** for 15 min at 4 °C on an Avanti J-E centrifuge, Beckman Coulter) and the supernatant was double-filtered (through both a glass filter and then a nitrocellulose membrane of 0.45 μm pore size).

Purification

VPs were purified by FPLC (fast protein liquid chromatography) (LCC-500CI instrument, GE Healthcare) and HPLC [Waters 600E System with a Varian PDA (photodiode array) detector]. The crude extract was first submitted to a fractional precipitation with ammonium sulfate (50 %, first cut) and after removing the pellet, the supernatant was again precipitated with ammonium sulfate (65 %, second cut). The final pellet was recovered in 20 mM piperazine buffer (buffer P, pH 5.5), and the sample was filtered and loaded on to the FPLC coupled with a strong anion-exchange column (HiTraP QFF, GE Healthcare) pre-equilibrated with buffer P. The proteins were eluted with a linear gradient from 0 to 1 M of NaCl in two phases at a flow rate of 1 ml/min: from 0 to 25 % over 50 min and from 25 to 100 % over 10 min. Fractions with VP activity were pooled, concentrated, dialysed against buffer P and purified further by HPLC–PDA coupled with a 10 μm high-resolution anion-exchange Biosuite Q (Waters) pre-equilibrated with buffer P. The proteins were eluted on a linear gradient from 0 to 1 M NaCl at a flow rate of 1 ml/min in two phases: from 0 to 6 % in 65 min and from 6 to 100 % in 10 min.

For R4DEL, the non-retained fraction (with VP activity) was dialysed against 20 mM Bis-Tris buffer (buffer BT, pH 6.5) and purified by HPLC–PDA coupled with a 10 μm high-resolution anion-exchange Biosuite Q pre-equilibrated with buffer BT. The proteins were eluted with a linear gradient from 0 to 1 M NaCl at a flow rate of 1 ml/min in three phases: from 0 to 7 % in 25 min, from 7 to 9 % in 65 min and from 9 to 100 % in 10 min. The fractions with VP activity were pooled, dialysed against buffer BT and purified by HPLC–PDA under the same conditions described above until Reinheitszahl values (*Rz*) ~4 were attained. The fractions with VP activity were pooled, dialysed against 10 mM sodium tartrate buffer (pH 5.0), concentrated and stored at −20 °C. Throughout the purification protocol, the fractions were analysed by SDS/PAGE on 12 % gels and the proteins were stained with colloidal Coomassie Blue (Protoblue Safe, National Diagnostics). The concentrations of all crude protein extracts were determined using the Bio-Rad protein reagent and BSA as a standard. Purified VP concentrations were determined by measuring the absorbance at 407 nm ($\varepsilon_{\mathrm{VP}} = 150000\ \mathrm{M^{-1} \cdot cm^{-1}}$).

MALDI–TOF-MS analysis

The MALDI–TOF-MS experiments were performed on an Autoflex III MALDI-TOF-TOF instrument with a smartbeam laser (Bruker Daltonics). The spectra were acquired using a laser power just above the ionization threshold, and the samples were analysed in the positive-ion detection and delayed extraction linear mode. Typically, 1000 laser shots were summed into a single mass spectrum. External calibration was performed, using the BSA from Bruker, covering the range 15 000–70 000 Da. The 2,5-DHAP (2,5-dihydroxyacetophenone) matrix solution was prepared by dissolving 7.6 mg (50 μmol) of 2,5-DHAP in 375 μl of ethanol followed by the addition of 125 μl of 80 mM diammonium hydrogen citrate aqueous solution. To prepare the samples, 2.0 μl of purified enzyme was diluted with 2.0 μl of 2 % trifluoroacetic acid aqueous solution and 2.0 μl of the matrix solution. An aliquot (1.0 μl) of this mixture was spotted on to the stainless steel target and allowed to dry at room temperature.

pI determination

Purified VPs (8 μg each) were subjected to two-dimensional electrophoresis at the Proteomic and Genomic Services from CIB (CSIC, Spain).

N-terminal analysis

Purified VPs were subjected to SDS/PAGE, and the protein bands were blotted on to PVDF membranes. The PVDF membranes were stained with Coomassie Brilliant Blue R-250, after which the enzyme bands were excised and processed for N-terminal amino acid sequencing on a precise sequencer at the Core facilities of the Helmholtz Centre for Infection Research.

Determination of thermostability (T_{50})

The thermostability of the different VP samples was estimated by assessing their T_{50} values using 96/384-well gradient thermocyclers. Appropriate VP dilutions were prepared with the robot such that the aliquots (20 μl) gave rise to a linear response in the kinetic mode. The samples (50 μl) were then used for each point in the gradient scale and a temperature gradient profile ranging from 30 to 80 °C was established as follows: 30.0, 31.4, 34.8, 39.3, 45.3, 49.9, 53, 55, 56.8, 59.9, 64.3, 70.3, 75, 78.1 and 80 °C. After 10 min of incubation, samples were chilled on ice for 10 min and incubated further at room temperature for 5 min. Afterwards, aliquots (20 μl) were subjected to the ABTS-based colorimetric assay described above for screening. The thermostability values were deduced from the ratio between the residual activities incubated at different temperatures and the initial activity at room temperature.

Kinetic parameters

As reported previously [17], steady-state enzyme kinetics were determined using the following molar absorption coefficients: ABTS product, $\varepsilon_{418} = 36000\ \mathrm{M^{-1} \cdot cm^{-1}}$; DMP product, $\varepsilon_{469} = 27500\ \mathrm{M^{-1} \cdot cm^{-1}}$ (in reference to the substrate concentration); RB5, $\varepsilon_{598} = 50000\ \mathrm{M^{-1} \cdot cm^{-1}}$; $\mathrm{Mn^{3+}}$-tartrate, $\varepsilon_{238} = 6500\ \mathrm{M^{-1} \cdot cm^{-1}}$.

DNA sequencing

Plasmids containing VP variants were sequenced with an ABI 3730 DNA Analyzer/Applied Biosystems Automatic

Sequencer from Secugen. The primers were designed with Fast-PCR software (University of Helsinki) as follows: RMLN; 3R-direct (5′-GTTCCATCATCGCGTTCG-3′); 5F-reverse (5′-GGATTCCTTTCTTCTTGG-3′) and RMLC.

Protein modelling

The structural model of wild-type VPL2 (purified from *P. eryngii* culture) at a resolution of 2.8 Å (1 Å = 0.1 nm) (PDB code 3FJW) was used to map the mutations, and the 1.33 Å crystal structure of non-glycosylated VP from *E. coli* (PDB code 2BOQ) was used for comparison (only 0.36 Å root mean square distance between 319 Cα). Mutations selected upon VP evolution were analysed by DeepView/Swiss-Pdb Viewer (GlaxoSmithKline) and the PyMOL Viewer (DeLano Scientific; http://www.pymol.org), and evolved VP variants were modelled using the Swiss-Model protein automated modelling server (http://swissmodel.expasy.org/).

RESULTS

Table S1 Mutations introduced in the directed evolution of α-*vpl2*

Silent mutations are indicated in bold; ○, accumulated mutation; ●, new mutation. Subscript indicates codon usage in *S. cerevisiae*. n.d., not determined.

Mutation		Round of evolution . . .	1G				2G				3G					4G		5G		6G
Amino acid	Codon		11H10	15G9	4B5	4B1	16E12	19C2	20D1	13G1	10C3	6B1	13E4	6E7	11F3	R4	24E10	3H9	15B4	2-1B
I(α6)T	ATT/ACT								●						○					
L(α11)S	TTA/TCA													●						
F(α12)F	TTC_{18}/TTT_{26}												●							
A(α19)A	GCT_{21}/GCC_{12}					●				○										
E(α27)G	GAA/GGA						●													
E(α45)K	GAA/AAA												●							
V(α50)A	GTT/GCT				●				○						○					
P(α54)P	CCA_{18}/CCT_{13}														●					
E37K	GAG/AAG			●				○			○	○	○	○		○	○	○	○	○
H39R	CAC/CGC				●				○						○					●
V160A	GTC/GCC					●				○			○			○	○	○	○	○
T184M	ACG/ATG		●				○	○	○	○	○	○	○	○	○	○	○	○	○	○
P185P	CCA_{18}/CCG_{5}										●									
Q202L	CAA/CTA						●				○	○		○	○	○	○	○	○	○
L207P	CTC/CCC												●							
D213A	GAC/GCC																	●		○
I278I	ATT_{30}/ATC_{17}				●															
T284I	ACC/ATC																		●	
A308T	GCC/ACC																		●	
D318D	GAC_{20}/GAT_{38}							●				○								
S324T	TCC/ACC					●														
G330R	GGA/AGA																●	○	○	○
TAI (fold increase) mutant/parent			9	7.4	6.3	3.6	41.5	36	34.2	28.8	129	128	121	118	98	238	138	109	164	87.4
Thermostability (T_{50}, °C)			59.9	61.9	62.1	n.d.	60.5	n.d.	n.d.	59.6	60.5	n.d.	n.d.	n.d.	n.d.	59.4	62.7	63.9	62.4	65.9

Table S2 Dissection of specific activity and secretion

Total activities and TAI values are calculated from large-scale fermentation experiments. Activities were assessed in 100 mM sodium tartrate buffer (pH 3.5) containing 2 mM ABTS and 0.1 mM H_2O_2.

					Improvement dissection	
Enzyme	Total activity (units/l)	TAI (fold increase)	Units/mg	Secretion levels (mg/l)	Specific activity (fold)	Expression (fold)
VPL2 parent	120	1	283	0.42	1	1
R4 mutant (fourth generation)	15500	129	717	21.6	2.5	51.6

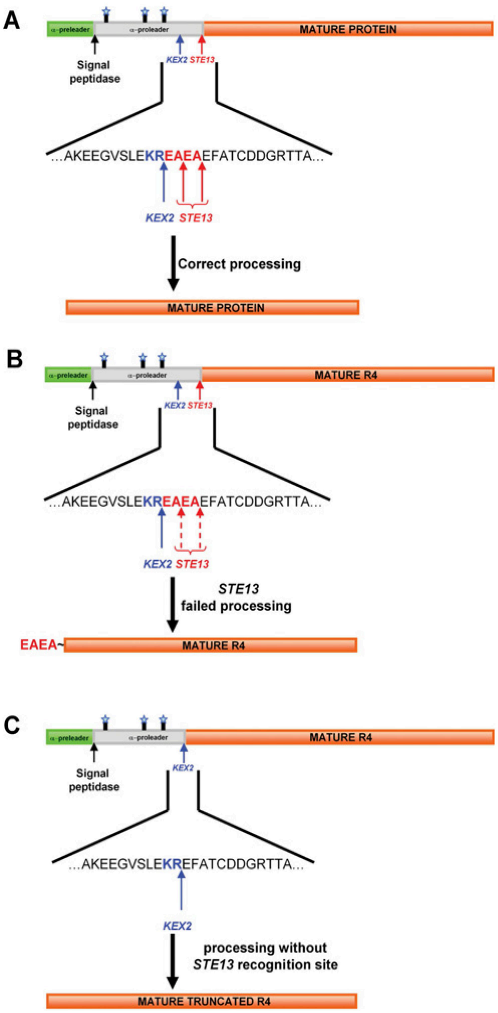

Figure S1 Overexpression of the R4 mutant and the engineering of a truncated variant

(**A**) Correct processing of the α-factor prepro-leader by the signal peptidase, the *KEX2* and *STE13* proteases, during the heterologous expression of a foreign protein in yeast. (**B**) Failed processing of *STE13* and the secretion of mature R4 with an extra N-terminal sequence (in red). (**C**) Fusion construct without the EAEA cleavage site and the action of *KEX2* in mature R4 secretion. The α-factor pre-leader is in green, the α-factor pro-leader is in grey and the mature VP is in orange. Blue stars indicate the glycosylation sites in the pro-leader.

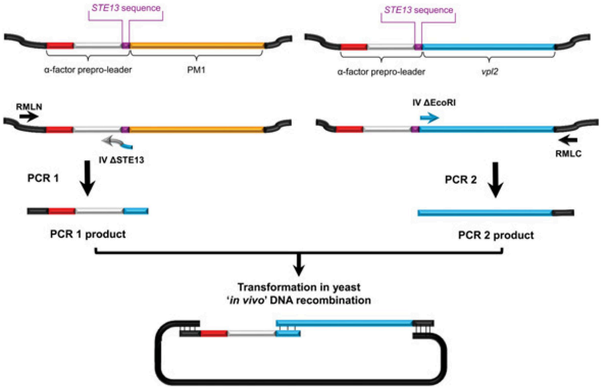

Figure S2 Deletion mutagenesis by IVOE to engineer truncated variants

To amplify the whole α-factor prepro-leader without the *STE13* motif, a construction containing the *PM1* gene instead of the original α-*vpl2* was used as the template to avoid loops and mismatching during PCR with the overhang of the reverse primer IVΔSTE13. The α-factor pre-leader is in red, the α-factor pro-leader is in grey, the *STE13* cleavage site is in purple, the *vpl2* gene is in blue, the *PM1* gene is in orange, and the shuttle vector is in black.

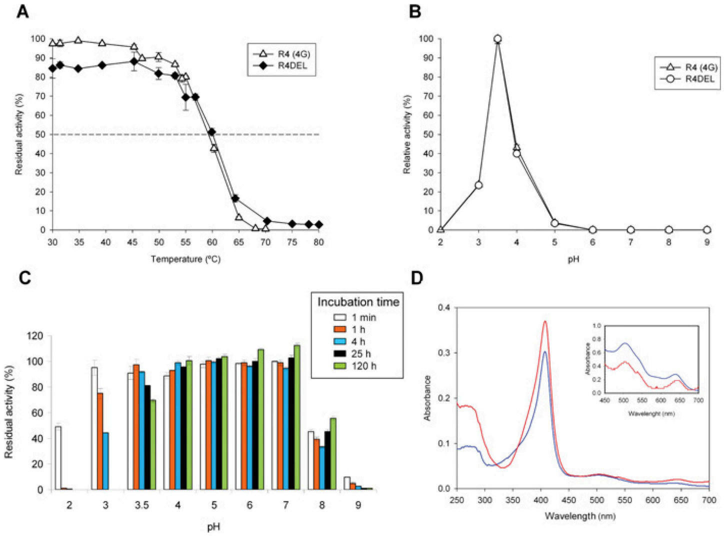

Figure S3 Biochemical characteristics of the R4 truncated variant

(**A**) Thermostability (T_{50}) of the R4 and R4DEL (truncated) mutant. Results are means ± S.D. for three independent experiments. (**B**) The pH-activity profile for R4 and R4DEL. Activities were measured in 100 mM B&R (Britton and Robinson) buffer at different pH values with 2 mM ABTS and 0.1 mM H_2O_2. VP activity was normalized to the optimum activity value, and results are means ± S.D. for three independent experiments. (**C**) pH stabilities of R4DEL. Enzyme samples were incubated in 100 mM B&R buffer at different pH values, and the residual activity was measured in 100 mM sodium tartrate buffer (pH 3.5) containing 2 mM ABTS and 0.1 mM H_2O_2. Results are means ± S.D. for three independent experiments. (**D**) Spectroscopic characteristics of R4 (blue line) and R4DEL (red line). See also Table 1 and Figure 3 of the main text and Table S3.

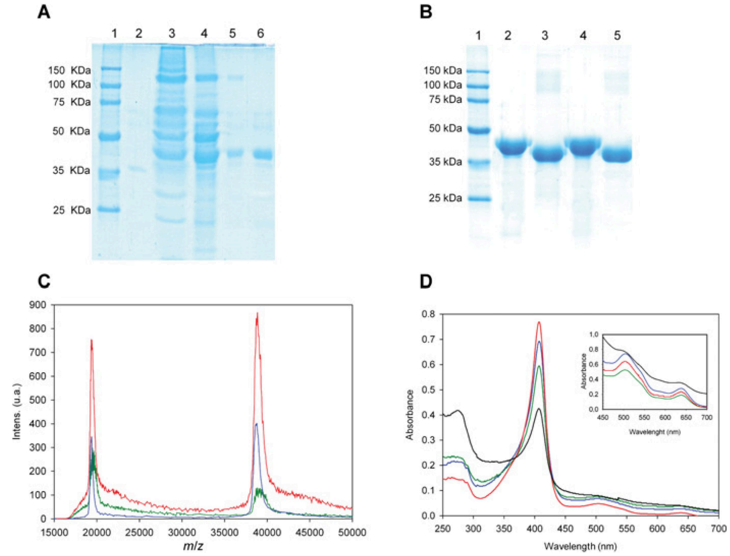

Figure S4 Biochemical characterization of the parental VP and evolved variants

(**A**) SDS/PAGE of the purified R4 mutant. Lanes: 1, protein ladder; 2, VPL2 from *E. coli* after *in vitro* refolding; 3, culture filtrate; 4, $(NH_4)_2SO_4$ precipitate; 5, anion exchange (HiTraP Q FF); 6, high-resolution anion exchange (Biosuite Q). (**B**) N-deglycosylation of R4 and 2-1B variants. Lanes: 1, protein ladder; 2, R4; 3, deglycosylated R4; 4, 2-1B; 5, deglycosylated 2-1B. The purified enzymes were deglycosylated using PNGase F (peptide N-glycosidase F). Samples were resolved by SDS/PAGE (12 % gels) and stained with colloidal Coomassie Blue stain. (**C**) MALDI–TOF mass spectra of VP purified variants (VPL2, green line; R4, blue line; 2-1B, red line). (**D**) Spectroscopic characteristics of VP variants. VPL2 from *S. cerevisiae*, black line; VPL2 from *E. coli* after *in vitro* refolding, red line; R4 variant, blue line; 2-1B variant, green line. See also Table S3.

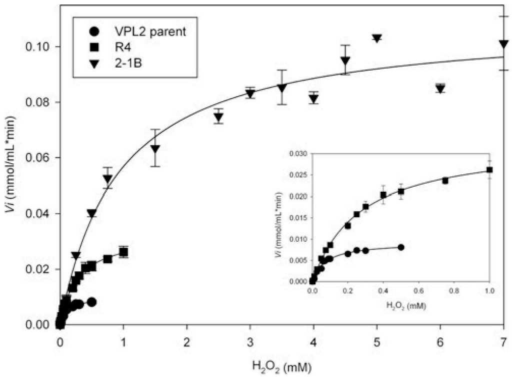

Figure S5 Kinetics for H_2O_2

Estimation of steady-state kinetic constants for H_2O_2 of VPL2, R4 mutant and 2-1B mutant using ABTS as a reducing substrate. The inset shows the low-concentration detail for VPL2 and R4 kinetics, and results are means ± S.D. of three measurements. Measurements were carried out in 100 mM sodium tartrate buffer (pH 3.5) using 5×10^{-4} μM enzyme and ABTS at concentrations of 5.5 mM (for parental VPL2 and VPL2 from *E. coli* after *in vitro* refolding), 0.6 mM (for the R4 mutant) and 0.5 mM (for the 2-1B mutant).

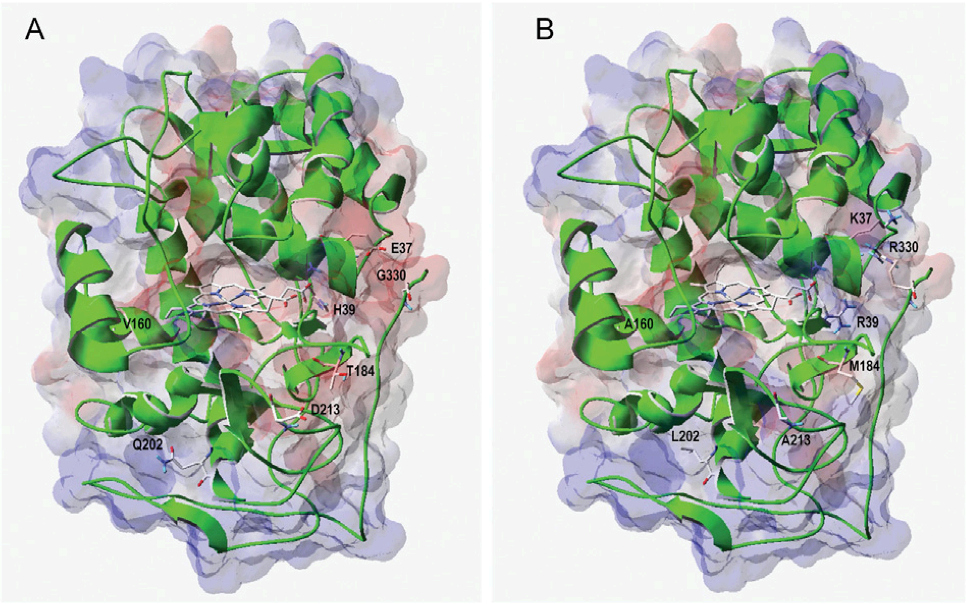

Figure S6 Wild-type VP and 2-1B variant molecular structure

(**A**) Wild-type VPL2 isolated from *P. eryngii* (PDB code 3FJW) indicating the seven residues that were seen to be modified during directed evolution. (**B**) Model for the 2-1B evolved variant including the seven mutations selected. The secondary protein structure (dominated by helices), the position of the haem cofactor [CPK (Corey–Pauling–Koltun) sticks] and the solvent-access surfaces of both proteins (in partially transparent electrostatic-potential colours) are shown.

Table S3 Characteristics of the R4 truncated mutant

Biochemical, spectroscopic and kinetic feature	Value
Molecular mass (Da)*	34567
Molecular mass (Da)†	38100
Degree of glycosylation (%)	9
Thermal stability, T_{50} (°C)	60
Optimum pH	3.5
pI	4.9
R_Z (A_{410}/A_{280})	4
Soret region (nm)	407
Charge transference band, CT1 (nm)	504
Charge transference band, CT2 (nm)	643
Total activity (units/l)‡	4670
Secretion levels (mg/l)	8.84
Kinetics for ABTS (low efficiency)	
K_m (mM)	0.052 ± 0.005
k_{cat} (s^{-1})	520 ± 20
k_{cat}/K_m ($mM^{-1} \cdot s^{-1}$)	9880 ± 620
Kinetics for RB5	
K_m (mM)	0.0043 ± 0.0004
k_{cat} (s^{-1})	10.5 ± 0.3
k_{cat}/K_m ($mM^{-1} \cdot s^{-1}$)	2440 ± 170

*Estimated from amino acid composition.

†Estimated by MALDI–TOF-MS.

‡Activities were assessed in 100 mM sodium tartrate buffer (pH 3.5) containing 2 mM ABTS and 0.1 mM H_2O_2.

Table S4 Mutations in evolved VPs

							Interactions with surrounding residues*	
Mutation	Domain	Secondary structure	Location	Distance to Fe^{3+} (Å)	Distance to Mn^{2+} oxidation site (Å)	Distance to Trp^{164} (Å)	Before mutation	After mutation
E37K	Distal	Helix B	Near Mn^{2+} site	14.29	7.61	21.86	$\underline{\mathrm{Glu}^{36}}$, 2×($\mathrm{Ser}^{41}$)	**Asp^{30}**, 2×(Ser^{41})
H39R	Distal	Helix B	Near Mn^{2+} site	9.71	6.74	16.69	$\underline{\mathrm{Cys}^{34}}$, Gly^{35}, Glu^{36}, Leu^{42}, Arg^{43}, $\underline{\mathrm{Pro}^{190}}$	Gly^{35}, Glu^{36}, Leu^{42}, Arg^{43}, **Pro^{190}**
V160A	Distal	Helix F	Near Trp^{164}	15.87	25.52	6.52	–	**Val^{163}, Trp^{164}**
T184M	Proximal	β-Sheet	Near Mn^{2+} site	13.03	8.62	21.86	Ala^{174}, $\underline{\mathrm{Ile}^{181}}$	Ala^{174}
Q202L	Proximal	β-Sheet	Buried	17.14	22.9	15.85	Ile^{199}, $\underline{\mathrm{Ala}^{235}}$, 2×($\mathrm{Glu}^{\underline{304}}$)	Ile^{199}, Glu^{304}
D213A	Proximal	Coil	Haem channel	20.25	20.31	29.46	–	–
G330R	C-terminus	Coil	Surface	18.09	8.57	27.07	–	**Val^{328}**

*Underlined residues indicate those involved in bonds interrupted after mutation; residues in bold indicate those involved in newly formed bonds after mutation.

Received 5 July 2011/7 October 2011; accepted 7 October 2011
Published as BJ Immediate Publication 7 October 2011, doi:10.1042/BJ20111199

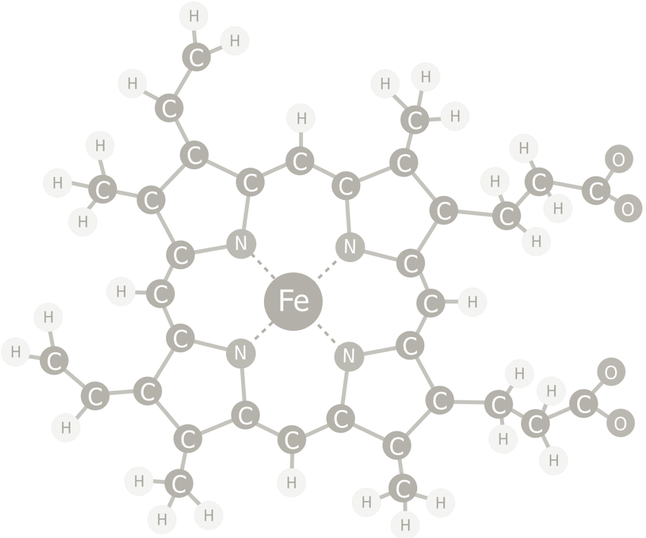

Capítulo 3:

Structural determinants of oxidative stabilization in an evolved versatile peroxidase

---

En este capítulo se describe la evolución dirigida de la VP para incrementar su estabilidad hacia peróxido de hidrógeno, en el que se obtuvieron dos variantes evolucionas que revelaron determinantes estructurales detrás del mecanismo de inactivación. Estos nuevos cambios pueden ayudar a entender el mecanismo de inactivación y ser trasladados a otras peroxidasas con el mismo fin.

ACS Catalysis

Research Article

pubs.acs.org/acscatalysis

Structural Determinants of Oxidative Stabilization in an Evolved Versatile Peroxidase

David Gonzalez-Perez,[†] Eva Garcia-Ruiz,[‡] Francisco Javier Ruiz-Dueñas,[§] Angel T. Martinez,[§] and Miguel Alcalde*[,†]

[†]Department of Biocatalysis, Institute of Catalysis, CSIC, Marie Curie 2, Cantoblanco, 28049 Madrid, Spain

[‡]Department of Chemical and Biomolecular Engineering, University of Illinois at Urbana−Champaign, 600 South Mathews Avenue, Urbana, Illinois 61801, United States

[§]Biological Research Centre, CSIC, Ramiro de Maeztu 9, 28040 Madrid, Spain

Ⓢ *Supporting Information*

ABSTRACT: Versatile peroxidases (VP) are promiscuous biocatalysts with the highest fragility to hydroperoxides yet reported due to a complex molecular architecture, with three catalytic sites and several oxidation pathways. To improve the VP resistance to H_2O_2, an evolved version of this enzyme was subjected to a range of directed evolution and hybrid strategies in *Saccharomyces cerevisiae*. After five generations of random, saturation, and domain mutagenesis, together with in vivo DNA recombination, several structural determinants behind the oxidative destabilization of the enzyme were unmasked. To establish a balance between activity and stability, selected beneficial mutations were introduced into novel mutational environments by the in vivo exchange of sequence blocks, promoting epistatic interactions. The best variant of this process accumulated 8 mutations that increased the half-life of the protein from 3 (parental type) to 35 min in the presence of 3000 equiv of H_2O_2 and with a 6 °C upward shift in thermostability. Multiple structural alignment with other H_2O_2-tolerant heme peroxidases help to understand the possible roles played by the new mutations in the overall oxidative stabilization of these enzymes.

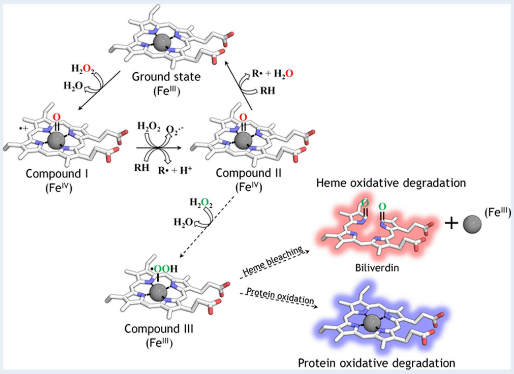

KEYWORDS: *versatile peroxidase, oxidative stability, directed evolution, rational design, Saccharomyces cerevisiae, in vivo DNA recombination*

■ INTRODUCTION

As well as being quite broadly distributed in nature, peroxidases (EC 1.11.1) are an important group of oxidoreductases that are capable of oxidizing a wide variety of substrates in the presence of peroxides.[1] Heme-containing peroxidases catalyze the successive removal of two electrons from two individual reducing substrates via a *ping-pong* mechanism. In its ferric resting state, the enzyme is activated by H_2O_2 to yield one molecule of water and an oxidized reactive intermediate (an oxoferryl (IV) porphyrin π cation-radical complex, $Fe^{IV}{=}O\cdot P^{\bullet+}$) called compound I. After the generation of compound I, the first reducing substrate molecule is oxidized so that the enzyme switches to the second catalytic intermediate, called compound II ($Fe^{IV}{=}O$), which in turn returns to the ground state (Fe^{III}) after the oxidation of a new reducing substrate and the release of a second water molecule.[2−4]

Although there are many applications for peroxidases, ranging from bioremediation to organic synthesis, their poor oxidative stability in the presence of modest concentrations of H_2O_2 precludes their use in many areas of biotechnology.[5−9] Indeed, for decades, the oxidative damage to peroxidases provoked by H_2O_2 has been considered a hot research topic, given that the complex inhibitory process (referred to as suicide inactivation) is not yet fully understood. This irreversible inactivation occurs either in the presence of the reducing substrate (with an excess of H_2O_2) or in its absence (at catalytic concentrations of H_2O_2), whereby the reaction of compound II with a second peroxide molecule generates compound III, an iron(III) superoxide radical complex that finally fosters inactivation through at least two different pathways: (i) heme bleaching (i.e., protoporphyrin ring cleavage into biliverdin plus Fe^{III}); and/or (ii) protein damage due to the interaction with the reactive oxygen species (ROS) that are generated.[10−13]

Received: August 19, 2014
Revised: September 21, 2014

dx.doi.org/10.1021/cs501218v | *ACS Catal.* 2014, 4, 3891−3901

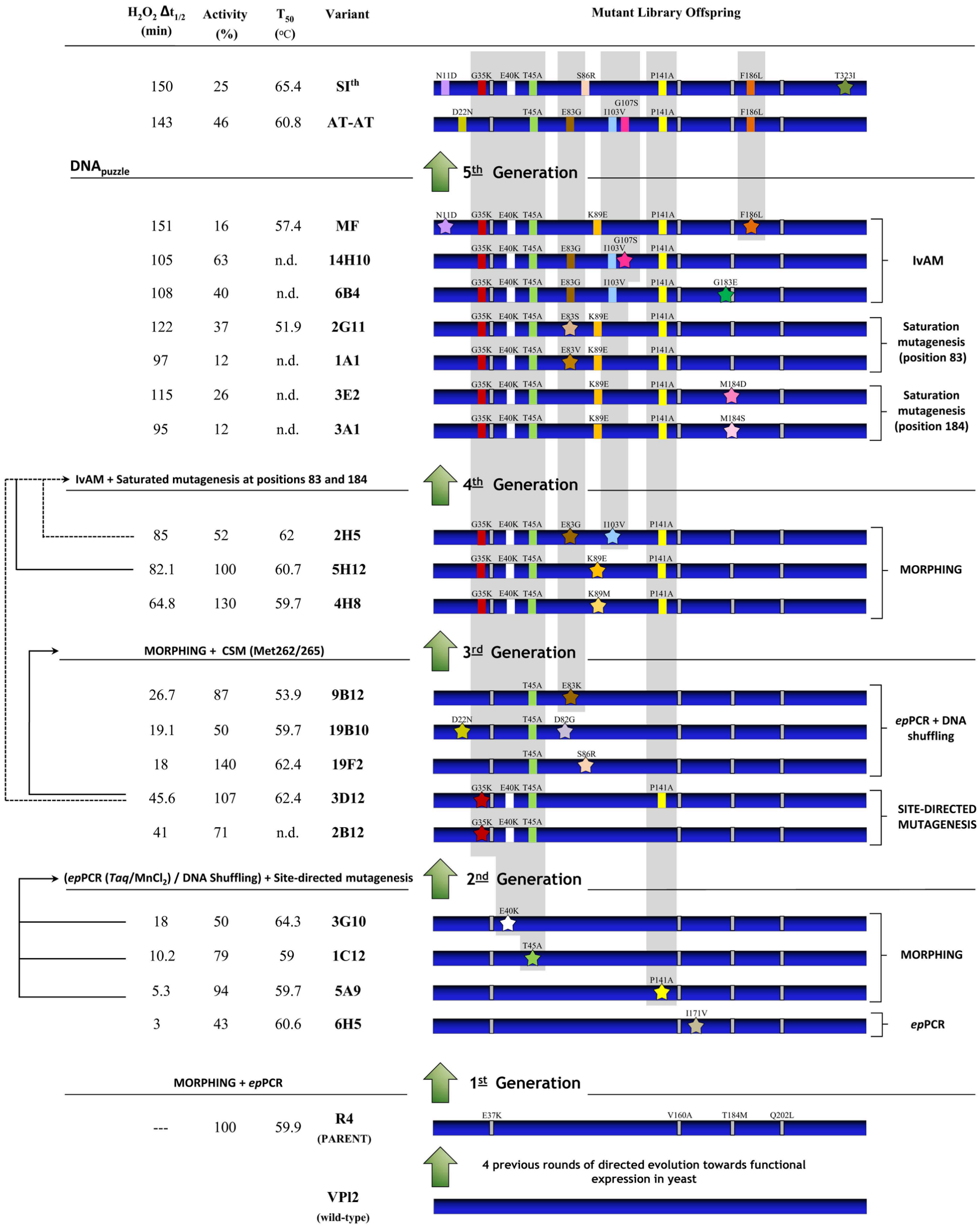

Figure 1. Evolutionary pathway for VP oxidative stability. New mutations are depicted as stars, and accumulated mutation are shown as squares. The amino acid backbone for secretion and activity is indicated by thin gray rectangles. $\Delta t_{1/2}$, the increase in the apparent half-life in the presence of H_2O_2 compared to the R4-parental type calculated from *S. cerevisiae* supernatants. Activity (%), ABTS-activity improvement (given in %) vs the R4-parental type detected in *S. cerevisiae* microcultures. T_{50}, temperature at which the enzyme retains 50% of its activity after a 10 min incubation. MORPHING, mutagenic organized recombination by homologous in vivo grouping; *ep*PCR, error-prone PCR; IvAM, in vivo assembly of mutant libraries; CSM, combinatorial saturation mutagenesis.

Even though some peroxidases are naturally resistant to high concentrations of H_2O_2, unfortunately they are poorly expressed and/or their sequences are not available to perform deeper structure−function studies.[14] To enhance the oxidative stability of heme peroxidases, protein engineering can focus on site-directed mutagenesis to replace the most oxidizable residues (Met, Cys, Trp, His, and Tyr) with lower-redox-potential/less-oxidizable amino acids, as well as performing directed evolution.[15−20] The joint use of these approaches is highly advisable when exploring different intrinsic- and mechanism-based problems, such as the modification of enantio- and stereoselectivity, the creation of novel substrate specificities, or conferring resistance toward different types of inhibitors.[21−23] By contrast, little attention has been paid to the combination of evolutionary and rational/hybrid strategies to engineer H_2O_2 stability in heme peroxidases.

Here, we have used a ligninolytic versatile peroxidase (VP, EC 1.11.1.16) that had been previously evolved in the laboratory for improved expression and activity as the point of departure to tailor oxidative stability.[24] VP are highly promiscuous biocatalysts that share catalytic attributes with lignin peroxidases (LiP), manganese peroxidases (MnP), and generic peroxidases (GP).[25−28] With one of the highest redox potentials found in nature (>+1.4 V), this promiscuous enzyme is capable of oxidizing low-, medium-, and high-redox-potential compounds. Due to a unique structure (with three different catalytic sites and two access channels to the heme domain), VP promiscuity is associated with extreme fragility when confronted by peroxides, making them a challenging model to study suicide inactivation. In the present work, we prepared several strategies that take advantage of the recombination apparatus of *Saccharomyces cerevisiae* to generate DNA diversity and engineer VP, including a *one-pot* random mutagenic method for defined domains, as well as in vivo recombination of a pool of short sequence mutagenized blocks. Enriched mutant libraries with different mutational loads were explored with the help of a sensitive high-throughput screening assay based on an estimated H_2O_2/enzyme molar ratio and the enhanced half-live in the presence of H_2O_2. By combining rational/hybrid and laboratory evolution approaches, several structural determinants involved in oxidative damage were identified. The best VP variants were characterized biochemically and the mutations analyzed by multiple structural alignment in order to shed light on the mechanism underlying oxidative stabilization of heme-peroxidases.

■ RESULTS AND DISCUSSION

The starting point of this study was the VP from *Pleurotus eryngii* (R4 mutant) that was a product of four generations of directed evolution to improve secretion and activity in the yeast *S. cerevisiae*.[24] The amino acid backbone of the R4 mutant contains the E37K, V160A, T184M, and Q202L mutations that promote the secretion of the enzyme by yeast (~22 mg/L) in conjunction with an 129-fold improvement in total activity. The K_m for H_2O_2 of the R4 mutant also increased 4-fold, allowing the variant to show high specific activities under saturating conditions. In order to engineer oxidative stability in the R4 mutant, a colorimetric high-throughput screening assay was adjusted for the different mutant libraries constructed in yeast. Because the molar excess of H_2O_2 applied in the screening leads to different responses in function of the activity and secretion of each variant, we carefully chose the H_2O_2/enzyme molar ratio so that the parental types in each generation were capable of maintaining at least 1/3 of their initial activity after a given period in the presence of H_2O_2. Accordingly, the process of evolution was accelerated by progressively enhancing the oxidative stress applied in each generation (up to 0.6 mM of H_2O_2, see Supporting Materials and Methods for details). ABTS (2, 2′-azino-bis(3-ethylbenzothiazoline-6-sulfonic acid)) was used as a reporter, ensuring the screening assay was very reliable with a coefficient of variance ~12%. Selected clones were subjected to several consecutive rescreenings and in particular, the increase in the apparent half-life in the presence of H_2O_2 compared to the parental type ($\Delta t_{1/2}$) and the kinetic thermostability (based on the T_{50} defined as the temperature at which the enzyme retains 50% of its activity after a 10 min incubation) were both assessed in a third rescreening to rule out the selection of false positives.

Evolutionary and Hybrid Strategy. Approximately 15 000 clones were explored in five generations of laboratory evolution and semirational experiments (Figures 1, S1). Several mutant libraries were constructed in the first round of directed evolution, targeting either the whole VP gene for random mutagenesis or restricting the mutational load to specific regions of 30 to 69 amino acids. The latter approach was performed with the help of an ad hoc domain mutagenesis method known as MORPHING (mutagenic organized recombination process by homologous in vivo grouping) that introduces mutations and promotes recombination in small protein segments.[29] MORPHING took advantage of the high frequency of homologous recombination in *S. cerevisiae*, facilitating the *one-pot* construction of mutant libraries affecting defined regions without altering the remaining parts of the gene.[30] After running multiple structural alignments to identify putative H_2O_2-sensitive regions in VP, the 30 amino acid distal His environment (Leu28-Gly57), the 26 amino acid proximal His environment (Leu149-Ala174), and the 69 amino acid Met environment (Ile199-Leu268) were chosen for MORPHING. The three best variants produced in this generation came from random mutagenesis at the distal and proximal His environments. Given that no beneficial mutations were located in the Met environment, the three oxidizable Met residues in this area (Met247, Met262, and Met265) may not be implicated in the oxidative destabilization of VP (as confirmed by combinatorial saturation mutagenesis, see below). The 3G10 variant (E40K mutation) had a $\Delta t_{1/2}$ of 18 min and a 5 °C improved T_{50} over the parental type, albeit at the cost of a 50% decrease in its activity. By contrast, the 1C12 variant (T45A mutation) had a $\Delta t_{1/2}$ ~10 min, maintaining ~80% of its activity and a similar T_{50} as the parental type (~60 °C). In addition, the 5A9 variant (P141A mutation) had a $\Delta t_{1/2}$ ~5 min, retaining most of its activity and with the same T_{50} as the parental type.

Taking into account that recombination between the E40K and T45A mutations was very unlikely, second generation double and triple mutants (including P141A) were constructed by site-directed mutagenesis. Both the double and the triple variants (2B12 and 3D12, respectively) incorporated the G35K mutation due to a PCR amplification error, which was conserved during the remaining evolution. The 2B12 and 3D12 variants displayed similar improvements in the $\Delta t_{1/2}$ (ranging from 41 to 46 min) while they retained most of their activity. In parallel, the 3G10, 1C12, and 5A9 mutants from the first generation were randomly mutated and further subjected to in vivo DNA shuffling. From this library, the 9B12 variant (T45A-$\underline{\text{E83K}}$), 19B10 ($\underline{\text{D22N}}$-T45A-$\underline{\text{D82G}}$), and 19F2 (T45A-$\underline{\text{S86R}}$) were selected, with $\Delta t_{1/2}$'s ranging from 27 to 18 min

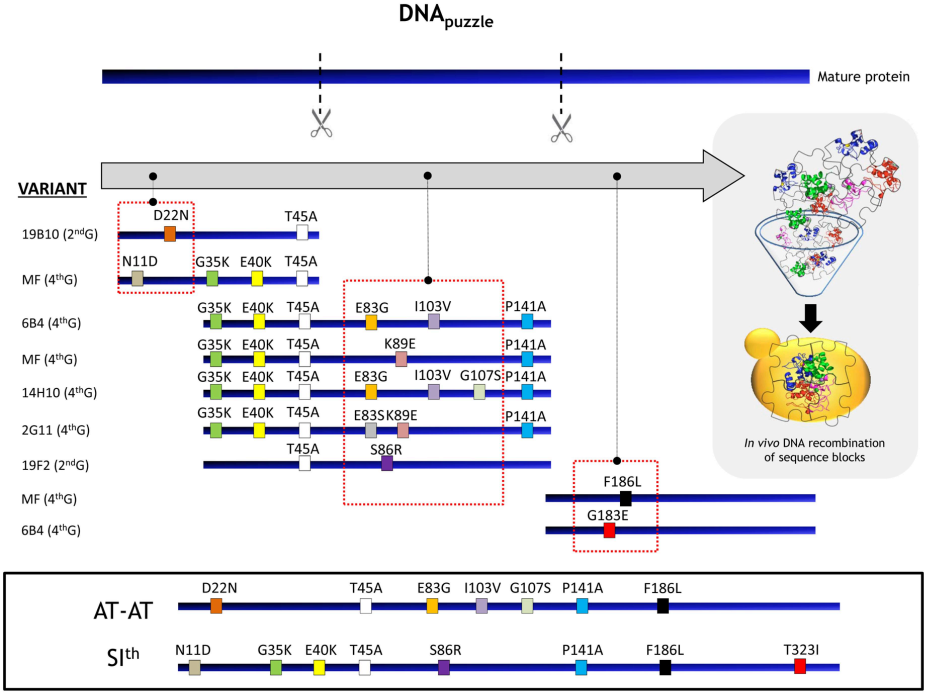

Figure 2. Fifth generation by DNA puzzle. The whole VP fusion gene (including the α-factor prepro-leader for secretion) was fragmented by high fidelity PCR in three independent segments containing overlapping areas flanking each end (the mutations under study are framed with red-dotted lines). The evolved sequence blocks were obtained from different templates from the 2nd and 4th generation. The pool of segments was shuffled and cloned in vivo into *S. cerevisiae* (sequence blocks are represented as pieces of a puzzle). Functional sequences were sorted through the screening assay in terms of $\Delta t_{1/2}$, T_{50}, and total activity values. The T323I mutation of the SIth variant was introduced during the PCR amplification of segment 151–331.

and displaying 50 to 140% of the parental activity. These three variants were exclusive offspring of the 1C12 parental VP (T45A), because the T45A mutation appeared in each, along with the new point mutations underlined. As predicted, crossover events between E40K and T45A did not take place; however, combined site-directed mutagenesis gave us the possibility to assess the effect of these two mutations together.

The best variant of this second generation (3D12) was used as the starting point for a third round of semirational experiments. No improvements were produced when Met262 and Met265 were subjected to combinatorial saturation mutagenesis, confirming the results obtained when the mutant library at the Met environment was explored in the first generation. In fact, ~95% of the clones in the mutagenic landscapes were inactive, indicating that these positions are highly conserved and they barely tolerate modifications. At this point, it is important to note that three of the four new mutations introduced by mutagenic PCR/DNA shuffling in the second generation were located between positions 82 and 86 (i.e., D82G, E83K, S86R), highlighting the interest in this region for further engineering. Hence, a new library comprising the two helices between residues Gly63-Lys94 (32 amino acids long) was constructed by MORPHING, again mutating Glu83 but this time, to a nonpolar residue (E83G in 2H5 mutant), a position further explored by saturation mutagenesis in generation 4 (see below). Accordingly, two new positions were unmasked: Lys89, with substitutions K89M and K89E in the 4H8 and 5H12 mutants, respectively; and I103V in the 2H5 mutant that was in the overlapping recombination area between fragments. With respect to the parental protein, the new mutants 2H5, 4H8, and 5H12 had a $\Delta t_{1/2}$ from ~65 to 85 min, retaining 50 to 130% of their activity, and a T_{50} enhanced by 3 °C in the case of 2H5.

In the fourth generation, IvAM (in vivo assembly of mutant libraries[31]) was carried out using 5H12 and 2H5 mutants from the previous round as the parental variants, along with 3D12 from the second round for backcrossing recombination. In this set of experiments, 4H8 was discarded as a parental type due to its reduced thermal and oxidative stability, despite the single mutation at the same position as 5H12 (K89M and K89E for 4H8 and 5H12, respectively). Three new improved variants were identified in this generation (MF, 6B4 and 14H10), the most stable of which was the MF mutant (with a $\Delta t_{1/2}$ = 151 min but a significant decrease in activity) due to the incorporation of two new mutations (N11D and F186L) into 5H12. Moreover, 6B4 and 14H10 (with a $\Delta t_{1/2}$ of 108 and 105 min, respectively) were generated by introducing the G183E and G107S mutations into 2H5, respectively. In parallel, positions 83 and 184 were analyzed individually by saturation mutagenesis of the 5H12 mutant. Glu83 showed mutational redundancy through the second and third generations (i.e., E83K in the 9B12 mutant of the second generation and E83G

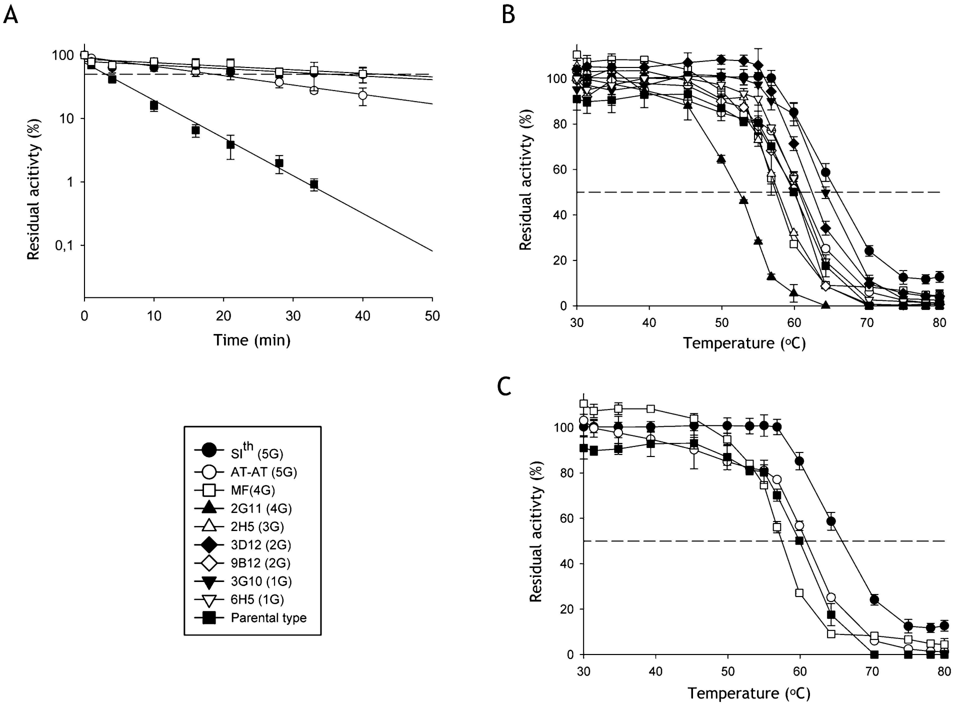

Figure 3. Oxidative and kinetic stabilities. (A) The $t_{1/2}$ H_2O_2. The purified VP samples (1 μM final concentration) were incubated for 90 min in a thermocycler at 25 °C in 100 mM phosphate buffer at pH 6.0 with 3000 equiv of H_2O_2. The residual activity was measured in 100 mM tartrate buffer [pH 3.5] containing 0.1 mM H_2O_2 and 2 mM ABTS. The residual activity refers to the corresponding VP variant incubated in the absence of H_2O_2. H_2O_2 stocks were prepared by measuring absorbance at 240 nm ($\varepsilon_{240}H_2O_2$ = 39.4 M^{-1} cm^{-1}). The protein concentrations of the purified variants were determined at 407 nm using VP extinction coefficient molar (ε_{407} = 150 000 M^{-1} cm^{-1}). The results are the means ± SD for at least three independent experiments. The dashed line indicates 50% of the residual activity. Black squares, R4-parental type; white circles, AT-AT mutant; black circles, SIth mutant; white squares, MF mutant. (B) Kinetic thermostability (T_{50}) for the different VP variants and (C) T_{50} for AT-AT (white circles), SIth (black circles), MF (white squares), and R4 parental type (black squares). The dashed line indicates 50% of the residual activity. The results are the means ± SD of at least three independent experiments.

in the 2H5 mutant of the third generation). On the other hand, Met184 was mutated previously during the directed evolution of VP to favor its functional expression in yeast (T184M).[24] Saturating both positions gave rise to an array of improved variants that contained the E83S, E83V, M184D, and M184S substitutions, yet coupled with an important drop in activity (Figures 1 and S1).

Bringing Balance between Activity and Oxidative Stability through the Exchange of Sequence Blocks in Vivo. The MF mutant obtained in generation 4 was the most stable of all the selected variants in oxidative conditions, yet at the cost of jeopardizing its activity (with a loss of 85% of the parental activity). This trade-off between activity and stability was less pronounced in other variants (e.g., 6B4 and 14H10), which also displayed considerable improvement in oxidative stability. With the aim of drawing a balance between activity and oxidative stability, several mutations were relocated in novel mutational environments by in vivo sequence block exchanges. These experiments aimed to test whether these mutations, which had been ruled out in the course of evolution and/or recombined in specific mutational contexts, could work in new mutational environments to foster epistatic interactions. After revising several domain engineering strategies found in literature,[29,32,33] we decided to prepare a simple method (DNA puzzle) that was supported by yeast homologous recombination. First, we analyzed the whole artificial evolutionary tree to identify suitable sequence blocks, (Figure 1). Most of the mutations were concentrated in distinct independent regions (comprising three segments: α[M1]-S53, C34-L165, and R151-S331) of different variants from generation 2 to generation 4 (Figure 2). Thus, 9 sequence blocks containing the different segments were amplified by high-fidelity PCR from several mutant DNA templates (i.e., 19B10 and 19F2 from generation 2; or MF, 6B4, 14H10 and 2G11 from generation 4). Each individual piece of the DNA puzzle was flanked with 50 bp overhangs to foster the in vivo annealing with each other and with the linearized vector, such that full reassembly of functional sequences could be achieved in a single transformation step in yeast (see Supporting Materials and Methods for details). After screening, the different pieces of the DNA puzzle library were sorted in terms of functionality and H_2O_2 tolerance, such that two improved variants (AT-AT and SIth) were identified. The $\Delta t_{1/2}$ of these two mutants was similar to that of the best variant from generation 4 (the MF mutant), yet with a

Table 1. Kinetic Parameters for Parental Type and Evolved Variants Expressed in *S. cerevisiae*[a]

substrate	kinetic constants	VPL2[b]	R4-parental type	MF mutant	AT-AT mutant	SI^{th} mutant
ABTS[c]	K_m (mM)	0.54 ± 0.05	0.056 ± 0.003	0.067 ± 0.005	0.095 ± 0.008	0.18 ± 0.02
	k_{cat} (s^{-1})	220 ± 30	365 ± 6	304 ± 7	420 ± 20	400 ± 20
	k_{cat}/K_m (mM^{-1} s^{-1})	410 ± 30	6480 ± 280	4510 ± 260	4400 ± 200	3200 ± 430
DMP[c]	K_m (mM)	32 ± 6	6.5 ± 0.5	48 ± 11	18 ± 3	44 ± 5
	k_{cat} (s^{-1})	98 ± 7	58 ± 1	90 ± 10	110 ± 10	60 ± 4
	k_{cat}/K_m (mM^{-1} s^{-1})	3.1 ± 0.4	9.1 ± 0.5	1.8 ± 0.2	6.0 ± 0.5	1.4 ± 0.07
Mn^{2+}	K_m (mM)	0.045 ± 0.007	0.12 ± 0.01	n.a.	1.1 ± 0.2	n.a.
	k_{cat} (s^{-1})	54 ± 1	75 ± 1	n.a.	140 ± 8	n.a.
	k_{cat}/K_m (mM^{-1} s^{-1})	1190 ± 180	630 ± 50	n.a.	121 ± 15	n.a.
RB5	K_m (mM)	0.007 ± 0.0007	0.0066 ± 0.0004	0.006 ± 0.0007	0.017 ± 0.001	0.004 ± 0.0004
	k_{cat} (s^{-1})	11.8 ± 0.5	10.6 ± 0.2	1.7 ± 0.1	7.6 ± 0.2	2.65 ± 0.06
	k_{cat}/K_m (mM^{-1}. s^{-1})	1670 ± 100	1600 ± 65	250 ± 30	426 ± 17	671 ± 48
H_2O_2-ABTS	K_m (mM)	n.d.	0.15 ± 0.02	0.17 ± 0.01	0.12 ± 0.01	0.12 ± 0.01
	k_{cat} (s^{-1})	n.d.	1120 ± 33	386 ± 6	1036 ± 21	1017 ± 23
	k_{cat}/K_m (mM^{-1} s^{-1})	n.d.	7120 ± 713	2235 ± 105	8230 ± 620	9180 ± 660

[a]VP kinetic constants were estimated in 100 mM sodium tartrate buffer containing 0.1 mM H_2O_2 at pH 3.5 for ABTS, DMP and RB5, and at pH 5.0 for Mn^{2+}. H_2O_2 kinetic constants were measured using ABTS as reducing substrate at the corresponding saturated conditions and taking into account the reaction stoichiometry (one H_2O_2 molecule is reduced for oxidation of two ABTS molecules); n.a. not active; n.d. not determined. [b]Native VPL2 expressed in *S. cerevisiae*. [c]The ABTS and DMP constants correspond to the VP low efficiency site since those for the high efficiency site cannot be measured for R4[24] and the new evolved variants.

noticeable recovery in activity (up to 46% in the AT-AT mutant). Interestingly, only 3 of the 7 mutations in MF were present in the AT-AT mutant, whose sequence blocks came from crossover events between 19B10 (D22N-T45A), 14H10 (E83G-I103V-G107S-P141A), and MF (F186L). The sequence of the SI^{th} mutant was more conserved, with only three different mutations with respect to MF (the suggested crossover events were: N11D-G35K-E40K-T45A from MF, S86R from 19F2, P141A from 6B4/MF/14H10/2G11, and F186L from MF).

Biochemical Characterization. The parental (R4) and mutant (MF [4th generation], AT-AT and SI^{th} [5th generation]) enzymes were purified to homogeneity (Reinheitszahl value: R_z (Abs_{407}/Abs_{280}) ∼ 4) and characterized biochemically. H_2O_2 inhibition can vary strongly depending on the parameters of the assay (i.e., pH, temperature, R_z of the samples, ionic strength and composition of the buffer or the inclusion of different additives).[34−36] We previously compared the oxidative stability of the R4 parental type with that of the native VP heterologously expressed in *Escherichia coli* after in vitro refolding.[24] The poor stability of the VP from *E. coli* led those experiments to be performed in the presence of polyethylene glycol.[37] Here, to better compare the variants secreted by yeast, their half-lives in the presence of H_2O_2 ($t_{1/2}$ H_2O_2) were measured at pH 6.0 and 25 °C in the absence of any additive, and with an excess of 3000 equiv of H_2O_2 (Figure 3A). Under these conditions, the $t_{1/2}$ H_2O_2 for the R4 parental type, MF, SI^{th} and AT-AT were ∼3, 40, 35, and 18 min, respectively, with improvements ranging from 6- to 13-fold. Differences were expected between the apparent $\Delta t_{1/2}$ from the supernatants and the $t_{1/2}$ H_2O_2 obtained from homogeneous purified samples because the H_2O_2/enzyme molar ratio used for screening mutant libraries was based on an estimate of the protein concentration in the culture broth. Nevertheless, a similar tendency in oxidative stability (MF ∼ SI^{th} > AT-AT > R4) was observed when the purified mutants were evaluated, validating our approach.

The kinetic thermostability was measured for the mutant offspring with T_{50} values ranging between ∼14 °C above and below that of the R4 parental type (T_{50} ∼60 °C, Figure 3B). In particular, the T_{50} for the MF, AT-AT and SI^{th} variants were ∼58, 61, and 65 °C, respectively (Figure 3C), the latter representing the strongest improvement in thermostability (5.5 °C above the parental type). This improvement could mostly be attributed to the E40K mutation (a 4.4 °C increase) introduced in the first generation 3G10 mutant and inherited in the SI^{th} mutant (Figure 1).

VP has three different catalytic sites: a Mn^{2+} binding site with three acidic residues implicated in the co-ordination of Mn^{2+} (Glu36, Glu40, and Asp175) that are common to MnP; one catalytic tryptophan residue (Trp164) involved in the oxidation of high-redox-potential compounds through a long-range electron transfer pathway (such as LiP); and the main heme access channel for the oxidation of low and medium-redox-potential substrates (such as GP) although the latter substrates can also be oxidized at the catalytic Trp, as explained below. The kinetic parameters were measured with several substrates that bind to the different catalytic centers of VP. Nonphenolic (ABTS) and phenolic (2, 6 dimethoxyphenol, DMP) substrates are oxidized at the heme access channel (with low efficiency) and at the catalytic tryptophan (with high efficiency), Mn^{2+} is oxidized at the manganese oxidation site and the azo dye Reactive black 5 (RB5) is exclusively oxidized by the catalytic tryptophan (Table 1). The R4 parental type has a 16-fold improved k_{cat}/K_m at the heme channel due to the E37K−V160A−T184M−Q202L amino acid backbone introduced in our previous directed evolution study.[24] Hence, this improvement precluded the evaluation of ABTS or DMP oxidation at the catalytic Trp164, because the kinetics at the heme channel masked their oxidation kinetics at the catalytic tryptophan.

Regardless of the substrate tested, the k_{cat}/K_m values were reduced to a greater or lesser extent, reflecting the delicate balance between the activity and oxidative stability of VP (Table 1). Oxidation at the heme access channel was slightly reduced, showing a general decrease in the substrate's affinity (ranging from a 7.3- to 1.2-fold higher K_m than the R4 parental type) but with a similar (or even enhanced) turnover rate. Still, the kinetics of the mutants in oxidizing ABTS were around 10-

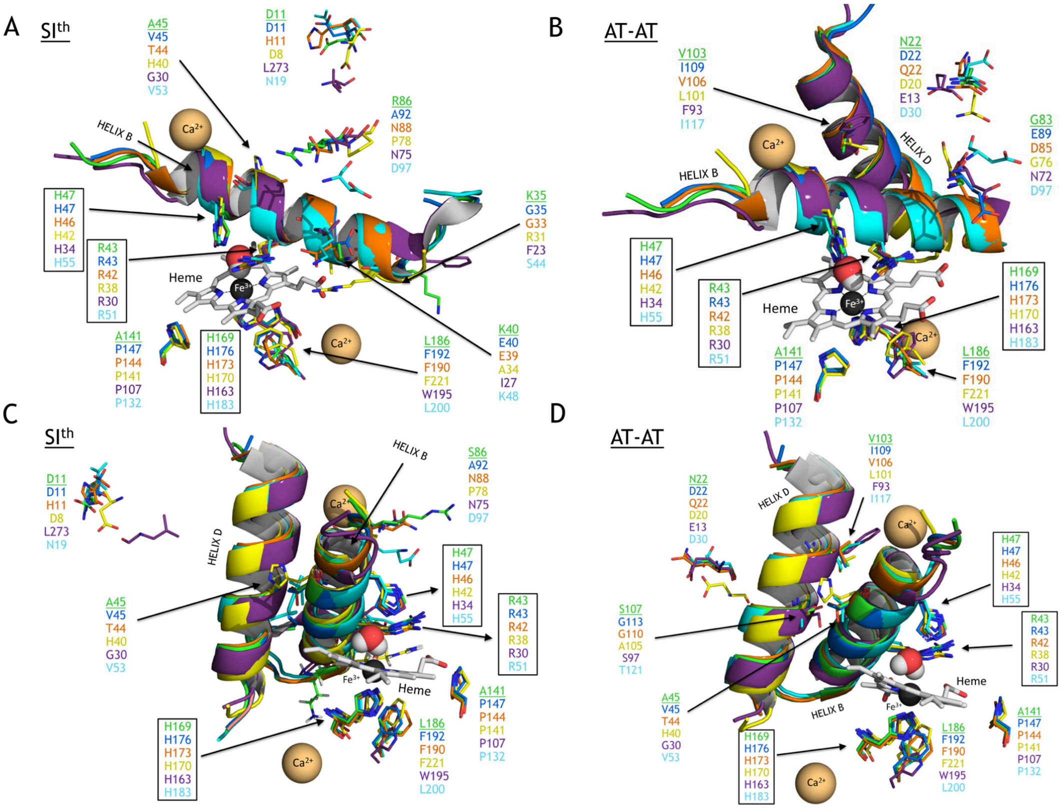

Figure 4. Multiple structural alignment of AT-AT and SIth variants together with several tolerant peroxidases vs H_2O_2. The structure of the wild-type VPL2 (purified from *P. eryngii* culture) at a resolution of 2.8 Å (1 Å = 0.1 nm) (PDB code 3FJW) was used as a template to generate a molecular model in which the newly identified mutations were mapped. The resulting model was analyzed with PyMOL Molecular Visualization System (http://pymol.org). In violet, ApX from *N. tabacum*; in orange MnP isozyme 1 from *P. chrysosporium*; in cyan, CiP from *C. cinerea*; in yellow, HRP isoform C1A from horseradish; in dark blue, LiP isoform H2 from *P. chrysosporium*; in green; VP variants. The structures are shown in cartoon mode and the heme group is highlighted with stick CPK colors, the calcium ions are represented as light-orange spheres, and the water molecule in the active site as red/white spheres. The mutated residues of AT-AT and SIth mutants are underlined and compared with the other peroxidases using a color code (the three Arg43, His47, and His169 residues conserved in all the peroxidases and the evolved variants are also shown, squared). The Ca^{2+} ions and the heme group are shown as the mean of all structures because there may be some differences in the heme or in the structural cations (Ca^{2+} ions being absent from ApX). (A,B), front view; (C,D) side view for SIth and AT-AT, respectively.

fold better than that of the native VPL2 secreted by yeast due to the aforementioned evolved amino acid backbone for total activity. The k_{cat} for RB5 at the catalytic tryptophan notably decreased (from 6- to 1.4-fold depending on the variant), although the affinity for this substrate did not change substantially. The catalytic activity at the Mn^{2+} site was practically quenched after evolution. The MF and SIth variants incorporated the stabilizing E40K mutation (with an improved T_{50} of ~5 °C, Figure 3B,C) but at the cost of collapsing the Mn^{2+} oxidation site since Glu40 is one of the three coordinating residues of Mn^{2+}. The AT-AT mutant -lacking the E40K substitution- maintained some activity at the Mn^{2+} oxidation site but with a 5-fold lower efficiency than the R4 parental variant. It is worth noting that ABTS was the substrate chosen for the colorimetric assay during screening (a compound easily recognized by both the heme channel site and the catalytic tryptophan residue) and thus, the Mn^{2+} binding pocket was not protected during evolution and its functionality was lost. Indeed, ABTS was employed in the screening when VP was evolved for secretion and activity, jeopardizing the kinetics at the Mn^{2+} due to the E37K mutation in the neighborhood of the Mn^{2+} binding site.[24] The kinetics for H_2O_2 were quite similar to that of the parental type, without further enhancement in the K_m as in the evolved R4 mutant.

Structural Alignment with Other H_2O_2-Tolerant Peroxidases. AT-AT and SIth variants were modeled using the crystal structure of wild VP purified from *P. eryngii* as a template (PDB ID: 3FJW), and they were structurally aligned together with other peroxidases with engineered oxidative stability: chloroplastic ascorbate peroxidase (ApX) from *Nicotiana tabacum*;[38] MnP isozyme 1 from *Phanerochaete chrysosporium*;[20] peroxidase from *Coprinopsis cinerea* (CiP);[17] horseradish peroxidase C1A (HRP);[19] and LiP isoform H2 from *P. chrysosporium*,[39,40] Figure 4. Overall, the protein

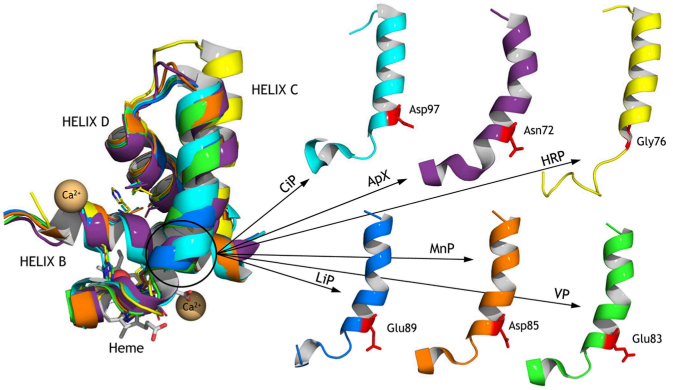

Figure 5. Relative position of VP residue 83 in a multiple structural alignment. VP position 83 (in red-sticks) is shown for the different peroxidases, with modifications in the secondary structure depending on the residue found at this position. The heme group is represented with stick CPK colors and the calcium ions as light-orange spheres. ApX, MnP, CiP, HRP, LiP, and wild-type VP (wtVP).

scaffolds for multiple alignment shared the structural arrangement of typical heme-containing peroxidases generally formed by several alpha helices surrounding the heme prosthetic group and including two structural cations, except in ApX. Following the VP numbering, the main catalytic residues are Arg43 and His47 within helix B (at the heme distal side) and His169 as the fifth Fe^{III}-ligand (at the heme proximal side).

The P141A mutation was located in a loop at the heme entrance, and it is a highly conserved residue among fungal peroxidases. Its replacement by a less bulky residue enlarges the heme access channel, allowing better substrate accommodation near the heme, as described previously for another VP variant at this residue (P141G) with improved affinity for ABTS.[41] Indeed, the P141A substitution also improved the oxidative stability of a VP-thioredoxin fusion protein.[42] The T45A mutation is located at the opposite side of the catalytic amino acids within helix B. This position shows a strong heterogeneity among the peroxidases used in the alignment (i.e., Val, Thr, His, Gly). This region limits the contact between helix D and B, such that the distance between them seems to play a key role in protein function. It is noteworthy that the same substitution was reported in the directed evolution of CiP for H_2O_2 tolerance (V53A using CiP numbering)[17], and hence, we assume that the interactions between both helices are dependent on the size and polarity of these residues. This would affect the relative position of the catalytic His and Arg residues situated in helix B, which are involved in (i) enzyme activation by H_2O_2; (ii) the interaction (directly or through a water molecule) with the ferryl oxygen in compounds I and II; and (iii) the interaction with the superoxide anion in compound III.[43] In relation to the latter, a particularly stable compound III has been associated with the resistance of heme peroxidase from *Raphanus sativus* to H_2O_2.[14] Interestingly, the G107S mutation situated between both helices provoked a strong improvement in oxidative stability and the same position in the evolved CiP was also unmasked.[17] The F186L mutation is located close to the proximal His169 and the same Phe residue was studied in MnP,[44] whereby changes to Ala or Ile reduced stability by up to 2 orders of magnitude. In fact, when the F190A variant was expressed (according to MnP numbering), secretion was reduced up to 90%, whereas the F190W mutation fully inactivated the enzyme. These results suggest that this position plays a critical role in the stability/activity trade-off. LiP, MnP, VP, and HRP contain a Phe residue at the same position, and in ApX this residue is a Trp without any attributed function, whereas the cytochrome C peroxidase has the radical at Trp191.[45−47]

Redundant mutagenesis of the Glu83 residue occurred during the evolution for oxidative stabilization (E83K, second generation; E83G, third generation), and there was an important drop in activity when it was further subjected to saturation mutagenesis (i.e., E83S/V). Glu83 is situated at the end of a loop that connects with the beginning of helix C in VP. Any subtle modification of this residue may vary the interaction with the adjacent helix, giving rise to differences in the length of the secondary structures, as can be deduced from the multiple alignment. Unlike CiP, LiP, MnP, and native VP, which retain a similar secondary organization with acidic residues at this position, HRP and ApX have an Asn and Gly residue, respectively, showing important modifications in the region that connects the loop and the helix (Figure 5). The S86R mutation was located in the middle of helix C, very close to Glu83. This position is not conserved in the other peroxidases (where Ala, Asn, Pro, or Asp residues are found), and according to our models, it may influence the attachment between helix B and D, along with I103V and the aforementioned T45A and G107S mutations. The improvement in the oxidative stability of VP due to mutations in this region was recently suggested by the preliminary analysis of a double mutated variant obtained by simultaneous substitution of the T45 and I103 residues.[48] The E40K and G35K mutations had a negative effect on Mn^{2+} kinetics, suppressing one of the three coordinating acidic residues of the Mn^{2+} sphere and affecting the environment of the binding site. These residues are conserved in MnP, VP, and LiP, yet not in the generic peroxidases as these lack the Mn^{2+} oxidation site. Inactivation of the Mn^{2+} site relaxes the oxidative stress of the enzyme, although at the cost of losing this activity. The T323I mutation (not shown in Figure 4) is placed at the C-terminal end of VP, a region with high mobility that hindered to fix the position of the last 12 residues when the VP crystal structure was determined. We can only speculate about the possible attachment of this mobile region upon mutation to enhance the stability of the protein. Moreover, although no significant differences were appreciated in the degree of glycosylation (~9%), the T323I mutation might remove the O-glycosylation site seen in the crystal structure of the homologous VP from *P. eryngii* (3FJW). Finally, the N11D and D22N mutations are located at the N-terminal end of the enzyme and they are fairly well conserved in terms of polarity within the other peroxidase scaffolds. Therefore, we cannot find a reasonable explanation as to how these changes affect the oxidative stabilization of VP.

■ CONCLUSIONS AND OUTLOOK

In the past few years, the mechanism of action of VP has been studied exhaustively, revealing at least three reactive sites (Trp164, main heme access channel, and heme-propionate channel), where electrons can be abstracted from the reducing substrate or from surrounding protein residues in the absence of substrate, in this latter scenario causing oxidative modifications that can lead to enzyme inactivation.[25−27] This phenomenon, which results in the enzyme's self-reduction, together with the generation of ROS related to the formation of compound III in the presence of excess H_2O_2, dramatically lowers the oxidative stability of VP to a few minutes, to the best of our knowledge this being the lowest H_2O_2 stability of all heme-peroxidases reported to date. Here, we have harnessed the recombination apparatus of *S. cerevisiae* to prepare several strategies that induce DNA diversity in order to study the oxidative stability in VP. Some of the structural determinants revealed in this study may be translated to other heme-containing peroxidases, especially those in which mutations are located in highly conserved regions. Nevertheless, the subtle equilibrium between activity and stability is still the biggest hurdle to circumvent. Thus, the use of in silico tools (e.g., quantum mechanics/molecular mechanics) coupled with directed evolution and hybrid approaches may help to tailor novel catalytic functions in this promiscuous biocatalyst. Finally, the appearance of the primitive ancestor of lignin-degrading oxidoreductases was linked to the end of the formation of coal deposits estimated to occur in the Permo-Carboniferous period, ~260 million years ago.[49] Interestingly, the process of in vitro evolution described here defines several stabilizing variants whose functionality at the Mn^{2+} oxidation site was lost, as also happened during the natural evolution transit of VP toward LiP. In the near future, by traveling back and forward in the temporal scale of evolution (using ancestral resurrection and directed evolution tools), we hope to gain more information about the evolutionary history of ligninolytic peroxidases.

■ MATERIAL AND METHODS

All chemical reagents were of the highest purity commercially available. The oligonucleotides used along the evolutionary process (Supporting Table 1) were purchased from Isogen Life Science (De Meern, The Netherlands). Culture media were prepared as described in the Supporting Material and Methods Section.

Directed Evolution and Hybrid Strategies. For each generation, PCR fragments were cleaned, concentrated, and loaded onto a low melting point preparative agarose gel (Bio-Rad, Hercules, CA), and then purified using the Zymoclean gel DNA recovery kit (Zymo Research, Orange, CA). PCR products were cloned under the control of GAL1 promoter of the pJRoC30 expression shuttle vector (kindly donated by Prof. F. H. Arnold from Caltech, CA), replacing the parent gene in pJRoC30. To remove the parent gene, the pJRoC30 plasmid was linearized with *Bam*HI and *Xho*I (New England Biolabs, Hertfordshire, U.K.), and the linear plasmid was concentrated and purified as described above for the PCR fragments.

Five rounds of directed evolution and hybrid approaches were carried out as described in the Supporting Material and Methods.

High-Throughput Screening (HTS) Protocol. Oxidative stability screening assay was performed as indicated in the Supporting Material and Methods.

Production and Purification of VP Variants. Selected mutants were produced and purified to homogeneity as described in the Supporting Material and Methods.

Biochemical Characterization. *Kinetic Parameters.* Kinetics were assayed with increasing substrate concentrations and fitted to Michaelis−Menten model (steady-state enzyme kinetics) using as template a hyperbolic, single rectangular, and two parameter mode. The catalytic efficiency (k_{cat}/K_m) was obtained plotting turnover rate (s^{-1}) versus substrate concentration and fitting it to a modified hyperbola with function $f(x) = (a.x)/(1 + b.x)$, where (a) is catalytic efficiency and (b) is $1/K_m$. The kinetics were measured with the following enzyme concentrations in a 200 μL final volume: 1.5×10^{-3} μM (ABTS), 1.5×10^{-2} μM (DMP), 2×10^{-2} μM (RB5), 2.5×10^{-4} μM (H_2O_2). Mn^{2+} kinetics were assayed in a final volume of 300 μL in quartz plates (Provair, leatherhead, U.K.) and 2×10^{-2} μM of VP. The following extinction molar coefficients were used: ABTS, ε_{418} = 36 000 M^{-1} cm^{-1}; DMP, ε_{469} = 27 500 M^{-1} cm^{-1}; RB5, ε_{598} = 50 000 M^{-1} cm^{-1}; Mn^{3+}-tartrate, ε_{238} = 6500 M^{-1} cm^{-1}. H_2O_2 kinetics were measured with 2 mM of ABTS. The kinetic parameters were determined in 100 mM tartrate buffer at pH 3.5 for ABTS, DMP, RB5, and H_2O_2, whereas the same buffer at pH 5.0 was employed for Mn^{2+} oxidation.

H_2O_2 Stability Assay. The purified VP samples (1 μM final concentration) were incubated for 90 min in a thermocycler at 25 °C in 100 mM phosphate buffer at pH 6.0 with 3000 equiv of H_2O_2. The residual activity was measured in 100 mM tartrate buffer pH 3.5 containing 0.1 mM H_2O_2 and 2 mM ABTS. The residual activity refers to the corresponding VP variant incubated in the absence of H_2O_2. H_2O_2 stocks were prepared measuring absorbance at 240 nm ($\varepsilon_{240}H_2O_2$ = 39.4 M^{-1} cm^{-1}). The protein concentrations of purified variants were determined at 407 nm using VP molar extinction coefficient (ε_{407} = 150 000 M^{-1} cm^{-1}).

Thermostability (T_{50}). Appropriate dilutions were prepared such that aliquots (20 μL) produced a linear response in kinetic mode. A gradient profile was constructed using a thermocycler (Mycycler, Bio-Rad, U.S.A.) for the selected mutants and the parental type, using 50 μL for each point in a gradient scale ranging from 30 to 80 °C. After a 10 min incubation, samples were removed and chilled on ice for 10 min. Thereafter, 20 μL of samples were removed and incubated for 5 min at room temperature. Finally, 180 μL of 100 mM sodium tartrate buffer [pH 3.5], 2 mM ABTS, and 0.1 mM H_2O_2 were added to the samples to measure activities. The thermostability values were calculated as the ratio between the residual activity at different temperature points and the initial activity at room temperature. The T_{50} value was determined as the transition midpoint of the inactivation curve of the protein as a function of temperature, which in our case was defined as the temperature at which the enzyme lost 50% of its initial activity after 10 min of incubation.

Protein and Homology Modeling. The crystal structure of VPL2 from *P. eryngii* at 2.8 Å resolution (1 Å = 0.1 nm, PDB ID: 3FJW) was used to generate a model to map the new mutations found with the help of the PyMOL Molecular Visualization System (Schrödinger). A homology model was generated by carrying out a structural alignment in PyMOL with the following crystal structures (PDB IDs are indicated): 3FJW, native VP from *P. eryngii* was used to model AT-AT and SIth variants; 1IYN, recombinant chloroplastic ApX from *N. tabacum* expressed in *E. coli*; 3M5Q, native MnP isozyme 1 from *P. chrysosporium*; 1H3J, native CiP from *C. cinerea*; 1W4W, recombinant HRP isoform C1A expressed in *E. coli*; and 1LLP, native LiP from *P. chrysosporium*.

■ ASSOCIATED CONTENT

Ⓢ Supporting Information

Additional description of methods used in experiments, diagram and flow chart which show experimental protocol, and table of primers used in this study. This material is available free of charge via the Internet at http://pubs.acs.org.

■ AUTHOR INFORMATION

Corresponding Author

*E-mail: malcalde@icp.csic.es.

Notes

The authors declare no competing financial interest.

■ ACKNOWLEDGMENTS

This work was supported by European Commission Projects (Peroxicats-FP7-KBBE-2010-4-26537; Indox-FP7-KBBE-2013-7-613549; COST-Action CM1303: Systems Biocatalysis) and the National Projects (Evofacel) [BIO2010-19697], (Dewry) [BIO2013-43407-R] and Hipop (BIO2011-26694). F.J.R.-D. is grateful for the award of a "Ramón y Cajal" contract of the Spanish MINECO.

■ REFERENCES

(1) Fawal, N.; Li, Q.; Savelli, B.; Brette, M.; Passaia, G.; Fabre, M.; Mathé, C.; Dunand, C. *Nucleic Acids Res.* **2013**, *41*, 441−444.

(2) Battistuzzi, G.; Bellei, M.; Bortolotti, C. A.; Sola, M. *Arch. Biochem. Biophys.* **2010**, *500*, 21−36.

(3) Poulos, T. L. *Arch. Biochem. Biophys.* **2010**, *500*, 3−12.

(4) Martínez, A. T. In *Industrial Enzymes: Structure, Function and Applications*; Polaina, J., MacCabe, A. P., Eds.; Springer: Berlin, 2007; pp 475−486.

(5) Martínez, A. T.; Ruiz-Dueñas, F. J.; Martínez, M. J.; del Río, J. C.; Gutíerrez, A. *Curr. Opin. Biotechnol.* **2009**, *20*, 348−357.

(6) Gregg, P. K.; Zhao, Y.; Kagan, V. E.; Star, A. *Adv. Drug Delivery Rev.* **2013**, *65*, 1921−1932.

(7) Salvachúa, D.; Prieto, A.; Mattinen, M. L.; Tamminen, T.; Liitiä, T.; Lille, M.; Willför, S.; Martínez, A. T.; Martínez, M. J.; Faulds, C. B. *Enzyme Microb. Technol.* **2013**, *52*, 303−311.

(8) Regalado, C.; García-Almendárez, B. E.; Duarte-Vázquez, M. A. *Phytochem. Rev.* **2004**, *3*, 243−256.

(9) Van de Velde, F.; Lourenço, N. D.; Bakker, M.; van Rantwijk, F.; Sheldon, R. A. *Biotechnol. Bioeng.* **2000**, *69*, 286−291.

(10) Valderrama, B.; Ayala, M.; Vazquez-Duhalt, R. *Chem. Biol.* **2002**, *9*, 555−565.

(11) Ayala, M.; Batista, C. V.; Vazquez-Duhalt, R. *J. Biol. Inorg. Chem.* **2011**, *16*, 63−68.

(12) Hernandez-Ruiz, J.; Arnao, M. B.; Hiner, A. N.; Garcia-Canovas, F.; Acosta, M. *Biochem. J.* **2001**, *354*, 107−114.

(13) Wariishi, H.; Gold, M. H. *FEBS Lett.* **1989**, *243*, 165−168.

(14) Gil-Rodríguez, P.; Ferreira-Batista, C.; Vázquez-Duhalt, R.; Valderrama, B. *Eng. Life Sci.* **2008**, *8*, 286−296.

(15) Ogola, H. J.; Hashimoto, N.; Miyabe, S.; Ashida, H.; Ishikawa, T.; Shibata, H.; Sawa, Y. *Appl. Microbiol. Biotechnol.* **2010**, *87*, 1727−36.

(16) Miyazaki, C.; Takahashi, H. *FEBS Lett.* **2001**, *509*, 111−4.

(17) Cherry, J. R.; Lamsa, M. H.; Schneider, P.; Vind, J.; Svendsen, A.; Jones, A.; Pedersen, A. H. *Nat. Biotechnol.* **1999**, *17*, 379−84.

(18) Cherry, J. R. *Methods Enzymol.* **2004**, *388*, 167−75.

(19) Morawski, B.; Quan, S.; Arnold, F. H. *Biotechnol. Bioeng.* **2001**, *76*, 99−107.

(20) Miyazaki-Imamura, C.; Oohira, K.; Kitagawa, R.; Nakano, H.; Yamane, T.; Takahashi, H. *Method Enzymol.* **2003**, *16*, 423−428.

(21) Mate, D.; Gonzalez-Perez, D.; Falk, M.; Kittl, R.; Pita, M.; De Lacey, A. L.; Ludwig, R.; Shleev, S.; Alcalde, M. *Chem. Biol.* **2013**, *20*, 223−231.

(22) Sun, L.; Bulter, T.; Alcalde, M.; Petrounia, I. P.; Arnold, F. H. *ChemBioChem* **2002**, *3*, 781−783.

(23) Reetz, M. T.; Wang, L. W.; Bocola, M. *Angew. Chem., Int. Ed.* **2006**, *45*, 1236−1241.

(24) Garcia-Ruiz, E.; Gonzalez-Perez, D.; Ruiz-Dueñas, F. J.; Martinez, A. T.; Alcalde, M. *Biochem. J.* **2012**, *441*, 487−498.

(25) Ruiz-Dueñas, F. J.; Martínez, M. J.; Martínez, A. T. *Mol. Microbiol.* **1999**, *31*, 223−235.

(26) Pérez-Boada, M.; Ruiz-Dueñas, F. J.; Pogni, R.; Basosi, R.; Choinowski, T.; Martínez, M. J.; Piontek, K.; Martínez, A. T. *J. Mol. Biol.* **2005**, *354*, 385−402.

(27) Ruiz-Dueñas, F. J.; Morales, M.; García, E.; Miki, Y.; Martínez, M. J.; Martínez, A. T. *J. Exp. Bot.* **2009**, *60*, 441−452.

(28) Garcia-Ruiz, E.; Mate, D. M.; Gonzalez-Perez, D.; Molina-Espeja, P.; Camarero, S.; Martinez, A. T.; Ballesteros, A. O.; Alcalde, M. In *Cascade Biocatalysis*; Riva, S., Fessner, W. D., Eds.; Wiley-VCH Verlag GmbH & Co. KGaA: Weinheim, 2014; pp 1−18.

(29) Gonzalez-Perez, D.; Molina-Espeja, P.; Garcia-Ruiz, E.; Alcalde, M. *PLoS One* **2014**, *9*, e90919.

(30) Gonzalez-Perez, D.; Garcia-Ruiz, E.; Alcalde, M. *Bioeng. Bugs* **2012**, *3*, 172−177.

(31) Zumárraga, M.; Camarero, S.; Shleev, S.; Martínez-Arias, A.; Ballesteros, A.; Plou, F. J.; Alcalde, M. *Proteins* **2008**, *71*, 250−260.

(32) Fasan, R.; Chen, M. M.; Crook, N. C.; Arnold, F. H. *Angew. Chem., Int. Ed.* **2007**, *46*, 8414−8418.

(33) Shivange, A. V.; Marienhagen, J.; Mundhada, H.; Schenk, A.; Schwaneber, U. *Curr. Opin. Chem. Biol.* **2009**, *13*, 19−25.

(34) Böckle, B.; Martínez, M. J.; Guillén, F.; Martínez, A. T. *Appl. Environ. Microb.* **1999**, *65*, 923−928.

(35) Hiner, A. N.; Hernández-Ruiz, J.; Rodríguez-López, J. N.; Arnao, M. B.; Varón, R.; García-Cánovas, F.; Acosta, M. *J. Biol. Inorg. Chem.* **2001**, *6*, 504−516.

(36) Asad, S.; Torabi, S. F.; Fathi-Roudsari, M.; Ghaemi, N.; Khajeh, K. *Int. J. Biol. Macromol.* **2011**, *48*, 566−570.

(37) Mao, L.; Luo, S.; Huang, Q.; Lu, J. *Sci. Rep.* **2013**, *3*, 3126.

(38) Kitajima, S.; Kitamura, M.; Koja, N. *Biochem. Biophys. Res. Commun.* **2008**, *372*, 918−923.

(39) Ryu, K.; Kang, J. H.; Wang, L.; Lee, E. K. *J. Biotechnol.* **2008**, *135*, 241−246.

(40) Ryu, K.; Hwang, S. Y.; Kim, K. H.; Kang, J. H.; Lee, E. K. *J. Biotechnol.* **2008**, *133*, 110−115.

(41) Morales, M.; Mate, M. J.; Romero, A.; Martínez, M. J.; Martínez, A. T.; Ruiz-Dueñas, F. J. *J. Biol. Chem.* **2012**, *287*, 41053−41067.

(42) Bao, X.; Huang, X.; Lu, X.; Li, J. J. *Enzyme Microb. Technol.* **2014**, *54*, 51−58.

(43) Berglund, G. I.; Carlsson, G. H.; Smith, A. T.; Szoke, H.; Henriksen, A.; Hajdu, J. *Nature* **2002**, *417*, 463−468.

(44) Kishi, K.; Hildebrand, D. P.; Kusters-van Someren, M.; Gettemy, J.; Mauk, A. G.; Gold, M. H. *Biochemistry* **1997**, *36*, 4268−4277.

(45) Dolphin, D.; Forman, A.; Borg, D. C.; Fajer, J.; Felton, R. H. *Proc. Natl. Acad. Sci. U.S.A.* **1971**, *68*, 614−618.

(46) Patterson, W. R.; Poulos, T. L.; Goodin, D. B. *Biochemistry* **1995**, *34*, 4342−4345.

(47) Sivaraja, M.; Goodin, D. B.; Smith, M.; Hoffman, B. M. *Science* **1989**, *245*, 738−740.

(48) Saez-Jimenez, V.; Martinez, A. T.; Ruiz-Dueñas, F. J. In *Oxizymes book of abstracts*. Proceedings of OxiZymes Vienna, July 1-4, 2014, Vienna, Austria; Obinger, C., Peterbauer, C., Eds.; Published by University of Natural Resources and Life Sciences: Vienna, Austria, 2014; p152.

(49) Floudas, D.; Binder, M.; Riley, R.; Barry, K.; Blanchette, R. A.; Henrissat, B.; Martínez, A. T.; Otillar, R.; Spatafora, J. W.; Yadav, J. S.; Aerts, A.; Benoit, I.; Boyd, A.; Carlson, A.; Copeland, A.; Coutinho, P. M.; de Vries, R. P.; Ferreira, P.; Findley, K.; Foster, B.; Gaskell, J.; Glotzer, D.; Górecki, P.; Heitman, J.; Hesse, C.; Hori, C.; Igarashi, K.; Jurgens, J. J.; Kallen, N.; Kersten, P.; Kohler, A.; Kües, U.; Kumar, T. K. A.; Kuo, A.; LaButti, K.; Larrondo, L. F.; Lindquist, E.; Ling, A.; Lombard, V.; Lucas, S.; Lundell, T.; Martin, R.; McLaughlin, D. J.; Morgenstern, I.; Morin, E.; Murat, C.; Nagy, L. G.; Nolan, M.; Ohm, R. A.; Patyshakuliyeva, A.; Rokas, A.; Ruiz-Dueñas, F. J.; Sabat, G.; Salamov, A.; Samejima, M.; Schmutz, J.; Slot, J. C.; John, F., St; Stenlid, J.; Sun, H.; Sun, S.; Syed, E.; Tsang, A.; Wiebenga, A.; Young, D.; Pisabarro, A.; Eastwood, D. C.; Martin, F.; Cullen, D.; Grigoriev, I. V.; Hibbett, D. S. *Science* **2012**, *336*, 1715−1719.

Supplemental data chapter 3

Structural determinants of oxidative stabilization in an evolved versatile peroxidase

Authors:, González-Perez, D., Garcia-Ruiz, E., Ruiz-Dueñas, F.J., Martínez, A.T., and Alcalde, M.

ACS Catal (2014) **4**, 3891-3901.

SUPPORTING INFORMATION

Structural determinants of oxidative stabilization in an evolved versatile peroxidase

David Gonzalez-Perez[†], Eva Garcia-Ruiz[‡], Francisco Javier Ruiz-Dueñas[φ], Angel T. Martinez[φ] & Miguel Alcalde[†][*]

[†]Department of Biocatalysis, Institute of Catalysis, CSIC, 28049 Madrid, Spain.

[‡]Department of Chemical and Biomolecular Engineering, University of Illinois at Urbana-Champaign, Urbana, IL 61801, USA.

[φ]Biological Research Centre, CSIC, Ramiro de Maeztu 9, 28040 Madrid, Spain.

[*]Correspondence should be addressed to: M.A. (malcalde@icp.csic.es).

SUPPORTING MATERIAL & METHODS

ABTS, DMP, RB5, manganese sulphate, *Taq* polymerase, bovine serum albumin, bovine hemoglobin and the *S. cerevisiae* transformation kit were purchased from Sigma-Aldrich (Madrid, Spain). Hydrogen peroxide 30 % (v:v) and KOD Hot Start DNA polymerase were obtained from MERCK (Madrid, Spain). The iProof High Fidelity DNA polymerase and Bio-Rad protein assay were purchased from Bio-Rad (USA). The Zymoprep Yeast Plasmid Miniprep Kit and Zymoclean Gel DNA Recovery Kit were obtained from Zymo Research (Orange, CA, USA). The *E. coli* XL2-Blue competent cells and the GeneMorph II Kit (mutazyme II polymerase) were from Stratagene (La Jolla, CA, USA), and the uracil independent and ampicillin resistance pJRoC30 shuttle vector was obtained from the California Institute of Technology (Caltech, USA). The parental type (R4 mutant) was engineered as reported in a previous work [24]. The protease-deficient *S. cerevisiae* strain BJ5465 (α ura3-52 trp1 leu2Δ1 his3Δ200 pep4::HIS3 prb1Δ1.6R can1 GAL) was obtained from LGCPromochem (Barcelona, Spain), the NucleoSpin Plasmid kit was purchased from Macherey-Nagel (Germany), and the restriction enzymes *Bam*HI and *Xho*I from New England Biolabs (Hertfordshire, UK). All chemicals were of reagent-grade purity.

Culture media

Synthetic complete (SC, minimum medium) contained 0.67% (w:v) yeast nitrogen base, 1.92 g/L yeast synthetic drop-out medium supplement without uracil, 2% (w:v) D-raffinose and 25 µg/mL chloramphenicol. YP medium contained 10 g yeast extract, 20 g peptone and ddH_2O to 650 mL. Flask expression medium contained 720 mL YP, 67 mL 1 M KH_2PO_4 buffer (pH 6.0), 111 mL 20% (w:v) D-galactose, 25 g/L ethanol, 500 mg/L bovine hemoglobin, 1 mM $CaCl_2$, 1 mL 25 g/L chloramphenicol and ddH_2O to 1000 mL. Microplate expression medium contained 720 mL YP, 67 mL 1 M

KH_2PO_4 buffer (pH 6.0), 111 mL 20% (w:v) D-galactose, 100 mg/L bovine hemoglobin, 1 ml 25 g/L chloramphenicol and ddH_2O to 1000 mL. YPD solution contained 1% (w:v) yeast extract, 2% (w:v) peptone, 2% (w:v) D-glucose and 25 µg/mL chloramphenicol. SC drop-out plates contained 0.67% (w:v) yeast nitrogen base, 1.92 g/L (w:v) yeast synthetic drop-out medium supplement without uracil, 2% (w:v) bacto agar, 2% (w:v) D-glucose and 25 µg/mL chloramphenicol. Luria-Bertani (LB) medium was prepared with 1% (w:v) peptone, 0.5% (w:v) yeast extract, 1% (w:v) NaCl and 100 µg/mL ampicillin.

Directed Evolution and hybrid strategies

First generation:

i) MORPHING: the domain mutagenesis protocol was performed in the three distinct protein segments (Leu28-Gly57; Leu149-Ala174; Ile199-Leu268) as described elsewhere [1]. The whole gene was fragmented into three different segments in individual PCR reactions. Each segment contained homologous overhangs of ~50 bp that overlapped one another to promote *in vivo* cloning in yeast. The targeted regions were subjected to random mutagenesis while the remaining segments were amplified by high-fidelity polymerases. The Leu28-Gly57 segment was selected to adjust mutational loads. Small mutant libraries of around 500 clones were screened to optimize the mutagenic conditions.

ii) Standard directed evolution: The whole R4 parental type was subjected to directed evolution by error-prone PCR. Reaction mixtures were prepared in a final volume of 50 µL containing: DNA template (0.1 ng/µL), 90 nM Forward RMLN F primer, 90 nM Reverse RMLC R primer, 0.3 mM dNTPs (0.075 mM each), 3% (v:v) dimethylsulfoxide (DMSO), 1.5 mM $MgCl_2$, 0.01 mM $MnCl_2$ and 0.05 U/µL *Taq* polymerase. Error-prone PCR was carried out under on a gradient thermocycler

(Mycycler, BioRad, USA) under the following conditions: 95ºC for 2 min (1 cycle); 94ºC for 45 s, 53ºC for 45 s, 72ºC for 2 min (28 cycles); and 72ºC for 10 min (1 cycle). The PCR product was purified, cleaned and 400 ng of total DNA used to transform *S. cerevisiae* together with 100 ng of linearized plasmid (ratio library:vector , 4:1) using the Yeast Transformation Kit. Transformed cells were plated on SC drop-out plates and incubated for 3 days at 30ºC. Subsequently, the mutant libraries were subjected to the HTS-protocol for oxidative stability (see next section).

<u>Second generation</u>:

i) epPCR + *in vivo* DNA shuffling: The best mutants obtained in the previous round by MORPHING (3G10, 1C12 and 5A9) were subjected independently to *ep*PCR. Three independent reaction mixtures (3G10, 1C12 and 5A9) were carried out to amplify the whole gene (primers RMLN and RMLC) using the same reaction conditions described in the first generation. The PCR product were purified, cleaned and 100 ng of total DNA of each gene were used to transform *S. cerevisiae* together with 200 ng of linearized plasmid (ratio library:vector , 1:2) to promote *in vivo* DNA shuffling.

ii) Site-directed mutagenesis for constructing double (T45A-E40K) and triple (E40K-T45A-P141A) variants: Directed mutagenesis was performed in *S. cerevisiae* by *in vivo* overlap extension (IVOE) [2]. For double and triple mutants, two independent gene fragments were amplified introducing the desired mutations, and thereafter reassembled *in vivo* by homologous recombination. The first fragment was amplified in a final volume of 50 µL containing: DNA template (0.2 ng/µL of 3G10 template for double mutant and 5A9 template for triple mutant), 0.3 µM Forward RMLN F primer, 0.3 µM Reverse T45A/E40K R primer, 0.3 mM dNTPs (0.075 mM each), 3% (v:v) dimethylsulfoxide (DMSO), 1.5 mM $MgSO_4$ and 0.02 U/µL KOD Hot Start DNA polymerase. The second fragment was amplified in a reaction mixture of 50 µL containing: DNA template (0.2 ng/µL of 3G10 template for double mutant and 5A9 template for triple mutant), 0.3 µM Forward T45A/E40K F primer, 0.3 µM Reverse RMLC R primer, 0.3 mM dNTPs (0.075 mM each), 3% (v:v) dimethylsulfoxide (DMSO), 1.5 mM $MgSO_4$, 0.01 mM $MnCl_2$ and 0.02 U/µL KOD Hot Start DNA polymerase.

The PCR reactions were carried out on a gradient thermocycler under the following conditions: 95°C for 2 min (1 cycle); 95°C for 20 s, 50°C for 10 s, 70°C for 15 s (28 cycles); and 70°C for 10 min (1 cycle). The PCR product were purified, cleaned and 400 ng of each fragment were used to transform *S. cerevisiae* together with 200 ng of linearized plasmid (ratio template:vector , 2:1).

Third generation:

i) MORPHING at segment G63-K94: The 3D12 mutant from second generation was divided by PCR in three independent segments: G63-K94 segment was amplified by error-prone PCR, and the segments α[M1]-D62; H95-S331 by high-fidelity polymerase.

Mutagenic PCR of G63-K94: Reaction mixtures were prepared in a final volume of 50 µL containing the following: DNA template (3D12 mutant, 0.92 ng/µL), 90 nM Forward VP Lid F primer, 90 nM Reverse VP-Lid R primer, 0.3 mM dNTPs (0.075 mM each), 3% (v/v) dimethylsulfoxide (DMSO), 1.5 mM $MgCl_2$, 0.1 Mm $MnCl_2$ and 0.05 U/µL *Taq* polymerase.

High-fidelity PCR in α[M1]-D62 Segment. Reaction mixtures were prepared in a final volume of 50 µL containing: DNA template (3D12 mutant, 0.2 ng/µL), 0.2 µM Forward RMLN F primer, 0.5 µM Reverse VP Lid -1 R primer, 0.8 mM dNTPs (0.2 mM each), 3% (v/v) dimethylsulfoxide (DMSO), and 0.02 U/µL iProof polymerase.

High-fidelity PCR in H95-S331 Segment. Reaction mixtures were prepared in a final volume of 50 µL containing: DNA template (3D12 mutant, 0.2 ng/µL), 0.2 µM Forward VP Lid +1 F primer, 0.5 µM Reverse RMLC R primer, 0.8 mM dNTPs (0.2 mM each), 3% (v/v) dimethylsulfoxide (DMSO), and 0.02 U/µL iProof polymerase.

The PCRs were performed on a gradient thermocycler using the following conditions: 94°C for 5 min (1 cycle); 94°C for 15 s, 53°C for 30 s, 72°C for 1 min (28 cycles); and 72°C for 10 min (1 cycle). The whole VP gene was reassembled *in vivo* and recombined by transformation into *S. cerevisiae* cells. The DNA transformation mixture contained the linearized plasmid (200 ng) mixed with the targeted region, as well as the segments upstream and downstream of those regions (400 ng per segment). The mutant libraries were subjected to the HTS-protocol for oxidative stability, as described below.

ii) Combinatorial saturation mutagenesis (CSM): Met262 and Met265 were subjected to CSM. Reaction mixtures were prepared in a final volume of 50 µL containing: DNA template (3D12 mutant, 0.2 ng/µL), 0.2 µM Forward primer, 0.2 µM Reverse primer (RMLN F/MET SAT R primers and MET SAT F/RMLC R for first PCR and second PCR, respectively), 0.8 mM dNTPs (0.2 mM each), 3% (v/v) dimethylsulfoxide (DMSO), and 0.02 U/µL iProof polymerase. High fidelity PCRs were carried out on the gradient thermocycler under the following conditions: 98ºC for 30 s (1 cycle); 98ºC for 10 s, 53 ºC for 30 s, 72ºC for 1 min (28 cycles); and 72ºC for 10 min (1 cycle). The whole gene was reassembled *in vivo* and recombined by transformation into *S. cerevisiae* cells and clones subjected to the HTS-protocol described below.

Fourth generation:

i) *In vivo* assembly of mutant libraries (IvAM): we followed the protocol described elsewhere with minor modifications [3]. A) Mutagenic PCR with *Taq* polymerase. Reaction mixtures were prepared in a final volume of 50 µL containing:

DNA template (0.1 ng/µL from 5H12-3G and 2H5-3G independently), 90 nM Forward RMLN F primer, 90 nM Reverse RMLC R primer, 0.3 mM dNTPs (0.075 mM each), 3% (v/v) dimethylsulfoxide (DMSO), 1.5 mM $MgCl_2$, 0.01 mM $MnCl_2$ and 0.05 U/µL *Taq* polymerase. B) Mutagenic PCR with Mutazyme II (GeneMorph II). Reaction mixtures were prepared in a final volume of 50 µL containing: DNA template (52.2 ng/µL from 3D12-2G), 0.37 µM Forward RMLN F primer, 0.37 µM Reverse RMLC R primer, 0.8 mM dNTPs (0.2 mM each), 3% (v/v) dimethylsulfoxide (DMSO), and 0.05 U/µL Mutazyme II. Error-prone PCRs were carried out using the following parameters: 95ºC for 2 min (1 cycle); 95ºC for 45 s, 50ºC for 30 s, 74ºC for 1 min (28 cycles); and 74ºC for 10 min (1 cycle).C) *In vivo* recombination of mutant libraries in *S. cerevisiae*. *Taq* polymerase libraries and Mutazyme library were added in equimolar concentrations (400 ng each) to the linearized vector (100 ng). Transformed cells were plated on SC drop-out plates and incubated for 3 days at 30ºC. Thereafter, the mutant libraries were subjected to the HTS-protocol as described below.

ii) Saturation mutagenesis at positions 83 and 184: the VP gene was amplified in two individual fragments that overlap to each other in a 40 bp overlapping area locating the degenerated codon in the central region. Reaction mixtures were prepared in a final volume of 50 µL containing: DNA template (0.2 ng/µL from 5H12-3G), 0.8 mM dNTPs (0.2 mM each), 3% (v/v) dimethylsulfoxide (DMSO), and 0.02 U/µL iProof polymerase. The primers used for saturation mutagenesis at position 83 were: 0.5 µM RMLN F forward primer, 0.5 µM Prx83SAT R reverse primer for high-fidelity PCR 1; and 0.5 µM Prx83SAT F forward primer, 0.5 µM RMLC R reverse primer for high fidelity PCR 2. The primers for saturation mutagenesis at position 184 were: 0.5 µM RMLN F forward primer, 0.5 µM Prx184SAT R reverse primer for high fidelity PCR 3; and 0.5 µM Prx184SAT F forward primer, 0.5 µM RMLC R reverse primer for high fidelity PCR 4. All PCRs were performed on a gradient using the following conditions: 98°C for 2 min (1 cycle); 98°C for 10 s, 50°C for 30 s, 72°C for 30 s (28 cycles); and 72°C for 10 min (1 cycle).The whole gene was *in vivo* reassembled transforming *S. cerevisiae* cells independently with 400 ng of PCR products 1 and 2 for saturation at position 83, or 400 ng of PCR producst 3 and 4 for position 184; plus 100 ng of linearized pJRoC30 plasmid for each construction.

Fifth generation:

19B10, 19F2 (2nd G); 6B4, MF, 2G11 and 14H10, (4th G) were chosen for DNA puzzle. The VP was fragmented in three regions: α[M1]-S53, C34-L165 and R151-S331. First PCR reaction: DNA template (0.2 ng/µL from 19B10-2G or MF-4G), 0.5 µM Forward RMLN F primer, 0.5 µM Reverse DOMREC-2R, 0.8 mM dNTPs (0.2 mM each), 3% (v:v) dimethylsulfoxide (DMSO), and 0.02 U/µL iProof polymerase. Second PCR reaction: DNA template (0.2 ng/µL from 19F2-2G, MF-4G, 6B4-4G, 14H10-4G or 2G11), 0.5 µM Forward DOMREC-1F primer, 0.5 µM Reverse DOMREC-4R, 0.8 mM dNTPs (0.2 mM each), 3% (v:v) dimethylsulfoxide (DMSO), and 0.02 U/µL iProof polymerase. Third PCR reaction: DNA template (0.2 ng/µL from MF-4G or 6B4-4G), 0.5 µM Forward DOMREC-3F primer, 0.5 µM Reverse RMLC R primer, 0.8 mM dNTPs (0.2 mM each), 3% (v:v) dimethylsulfoxide (DMSO), and 0.02 U/µL iProof polymerase. PCR reactions were performed using the following conditions: 98°C for 30 s (1 cycle); 98°C for 10 s, 50°C for 25 s, 72°C for 1 min 30 s (28 cycles); and 72°C for 10 min (1 cycle). The whole gene was reassembled *in vivo* and recombined by transformation into *S. cerevisiae*. The DNA transformation mixture contained the linearized plasmid (400 ng) mixed with the pool of fragments purified and cleaned (146 ng per segment, total amount 1,314 ng).

High-throughput screening (HTS) protocol

Individual clones were selected and cultured in sterile 96-well plates (Greiner Bio-One GmbH, Germany) containing 50 µL per well of SC minimal medium. In each plate, column number 6 was inoculated with the parental R4 mutant as an internal standard, and well-H1 (containing minimal medium supplemented with uracil) was inoculated with untransformed *S. cerevisiae* as a negative control. Plates were sealed wrapped in parafilm to prevent evaporation and incubated at 30ºC, 225 rpm and 80% relative humidity in a humidity shaker (Minitron-INFORS, Biogen, Spain). After 48 h, 160 µL of expression medium was added to each well and the plates were incubated for a further 24 h. The plates (master plates) were centrifuged for 15 min at 3,000 rpm and 4ºC (Eppendorf 5810R centrifuge, Germany) and the master plates were duplicated with the help of a robot (Liquid Handler Quadra 96-320, Tomtec, Hamden, CT, USA) by transferring 20 µL of supernatant into two replica plates: the initial activity plate (IA plate) and the residual activity plate (RA plate). Next, 180 µL of stability buffer (20 mM sodium tartrate buffer, pH 5.0: Buffer A) was added to the IA plates and 180 µL of incubation solution (Buffer A containing 0.3 mM H_2O_2) was added to the RA plates using a Multidrop robot (Multidrop Combi, ThermoFischer Scientific, Vantaa, Finland). The selective pressure was incremented up to 0.6 mM of H_2O_2 from second round onwards. Both plates were briefly stirred and incubated at room temperature for 60 min, such that the activity assessed in the RA plates was reduced by 2/3rds with respect to the initial activity of the parental type. The supernatants (20 µL) were transferred from both RA and IA plates to new plates to measure the residual and initial activity values by adding ABTS in specific buffers: 180 µL of 100 mM sodium tartrate buffer [pH 3.5] containing 2 mM ABTS and 0.1 mM H_2O_2 to estimate of residual activity; and 180 µL of 100 mM sodium tartrate buffer [pH 3.5] containing 2 mM ABTS and 0.13 mM H_2O_2

to estimate the initial activity. The plates were stirred briefly and the absorption at 418 nm ($\varepsilon_{ABTS}{}^{\bullet+}$ = 36,000 M^{-1} cm^{-1}) was recorded (end-point mode, t_0) on a plate reader (SPECTRAMax Plus 384, Molecular Devices, Sunnyvale, CA). The plates were then incubated at room temperature until a green color developed and the absorption was measured again (t_1). The relative activities were calculated from the difference between the absorption value after incubation and that of the initial measurement normalized to the parental type in the corresponding plate (Δt_1-t_0). Oxidative stability values were calculated as the ratio between residual activity and the initial activity values (RA/IA). To rule out false positives, two consecutive re-screenings were carried out. Moreover, a third re-screening was performed to determine the increase in the half-life of each selected variant ($\Delta t_{1/2}$ H_2O_2, expressed in minutes) relative to the parental R4 in different apparent molar ratios [H_2O_2] / [Enzyme].

First re-screening: Aliquots of 5 µL of the best clones were removed from the master plates and used to inoculate 50 µL of SC minimal medium in new 96-well plates. Columns 1 and 12, and rows A and H, were not used to prevent the appearance of false positives. After incubating for 24 h at 30°C, 225 rpm, and 80% relative humidity, 5 µL was transferred to the adjacent wells and incubated for a further 24 h. Finally, 160 µL of expression medium was added and the plates were incubated for another 24 h. Accordingly, each mutant was grown in 4 wells. The parental types were subjected to the same procedure (row D, wells 7-11) and the plates were assessed using the same protocols as those used for the screening described above.

Second re-screening: An aliquot from the wells with the best clones in the first re-screening was inoculated in 3 mL of YPD and incubated at 30°C and 225 rpm for 24 h, recovering the plasmids from these cultures (Zymoprep Yeast Plasmid Miniprep Kit). As the product of the zymoprep was very impure and the concentration of DNA extracted very low, the zymoprep mixtures containing shuttle vectors were transformed into super-competent *E. coli* cells (XL2-Blue, Stratagene) and plated on LB/amp plates. Single colonies were picked and used to inoculate 5 mL LB/amp media, and they were grown overnight at 37°C and 225 rpm. The plasmids were then extracted (NucleoSpin Plasmid kit, Macherey-Nagel, Germany) and *S. cerevisiae* was transformed with plasmids from the best mutants as well as with the parental type. Five colonies for each mutant were selected and re-screened as described above.

Third re-screening (determination of $\Delta t_{1/2}$ H_2O_2) : A single colony from the *S. cerevisiae* clone containing the parental R4, the new mutants and untransformed yeast were picked from a SC drop-out plate (SC supplemented with uracil for untransformed cells), used to inoculate 5 mL of minimal medium, and incubated for 48 h at 30°C and 225 rpm (Minitron-INFORS, Biogen, Spain). An aliquot of cells was removed and used to inoculate a final volume of 5 mL of minimal medium in a 50 mL falcon tube (optical density, OD_{600} = 0.3), and they were incubated until two growth phases had been completed (6-8 h, OD_{600} = 1). Thereafter, 9 mL of expression medium (500 mg/L bovine hemoglobin) was inoculated with 1 mL of this pre-culture in a 100 mL flask (OD_{600} = 0.1). After incubating for ~48 h at 30°C and 225 rpm (maximal VP activity; OD_{600} = 25-30), the cells were separated by centrifugation for 15 min at 3,000 rpm and 4°C (Eppendorf 5810R Centrifuge, Germany), and the supernatants were collected and stored at 4°C. The protein concentration was estimated from supernatants using the Bio-Rad protein assay kit (Bio-Rad, USA) with an overall standard curve ranging from 0-20 µg/mL of BSA. VP apparent concentration was calculated as the difference between the total protein content of yeast expressing VP and that in its absence (from non-transformed yeast cells -lacking VP gene- see below). The parental R4 and the mutants (final concentration 0.1 µM) were incubated at room temperature in 20 mM sodium tartrate buffer [pH 5.0] in the presence or absence of different concentrations of H_2O_2 (0.3, 0.6 mM). Aliquots (20 µL) were removed at different times and the residual/initial activities were measured in a final volume of 200 µL containing 100 mM sodium tartrate buffer [pH 3.5], 2 mM ABTS and 0.13 mM or 0.16 mM H_2O_2 (for samples incubated in the presence of 0.3 and 0.6 mM H_2O_2, respectively). The residual activity was determined relative to the corresponding mutant incubated in the absence of H_2O_2, taking into account the final concentration of H_2O_2 in each activity assay.

Production and purification of VP variants

Production of VPs in *S. cerevisiae*: A single colony from *S. cerevisiae* transformed with the parental (R4) or VP mutants (AT-AT, MF and SIth) plasmids was used to inoculate 30 mL of SC minimal medium (in a 100 mL flask) and incubated for 48 h at 30°C and 250 rpm (Micromagmix shaker). Then, OD_{600} was measured and this pre-cultured used to inoculate 120 mL of minimal medium in a 250 ml flask (OD_{600}= 0.3). They were incubated until two growth phases had been completed (6-8 h, OD_{600} = 1) and thereafter, 450 mL of expression medium (500 mg/L bovine hemoglobin) was inoculated with 50 mL of this pre-culture in a 2 litre baffled flask (OD_{600}= 0.1). The cultures were incubated for 48 h at 30°C and 225 rpm and the maximal VP activity reached (OD_{600} =28–30); the cells were recovered by centrifugation at 5,000 rpm for 30 min at 4°C (Avanti J-E centrifuge Beckman Coulter, Fullerton, CA). The supernatant was recovered and double filtered (through both a glass filter and then a nitrocellulose membrane of 0.45 µm pore size).

Purification protocol: VP crude extracts were first submitted to a fractional precipitation with ammonium sulphate: 50-65% (R4, parental type), 50-85% (AT-AT), 50-70% (SIth) and 50-75% (MF). The final pellet was recovered in 20 mM piperazine buffer (buffer P, pH 5.5), and the sample was filtered and loaded on to the FPLC (Äkta Purifier; GE

Healthcare Uppsala, Sweden) coupled with a strong anion-exchange column (HiTraP QFF; GE Healthcare Uppsala, Sweden) pre-equilibrated with buffer P. The proteins were eluted with a linear gradient from 0 to 1 M of NaCl in two phases at a flow rate of 1 ml/min: from 0 to 25% over 50 min and from 25 to 100% over 5 min. Fractions with VP activity were pooled, concentrated and dialysed against buffer P. Thereafter, samples were loaded onto a HPLC–PDA column coupled with a 10 µm high resolution anion-exchange Biosuite Q (Waters) pre-equilibrated with buffer P. The proteins were eluted on a linear gradient from 0 to 1 M NaCl at a flow rate of 1 ml/min in two phases: from 0 to 6% in 34-60 min depending of the mutant, and from 6 to 100% in 10 min. The fractions with VP activity were pooled, dialysed against 10 mM sodium tartrate buffer (pH 5.0), concentrated and stored at −20ºC. Throughout the purification protocol, the fractions were analysed by SDS/PAGE on 12% gels and the proteins were stained with colloidal Coomassie Blue (Protoblue Safe, National Diagnostics). The concentrations of all crude protein extracts were determined using the Bio-Rad protein reagent and BSA as a standard. Purified VP concentrations were determined spectrophotometrically in quarz cuvettes with extinction coefficient molar for VP at 407nm (εVP =150,000 M^{-1}. cm^{-1}).The Reinheitszahl values (*Rz*: Abs_{407}/Abs_{280}) obtained were ~4.

DNA sequencing

Plasmids containing the VP variants were sequenced on an ABI 3730 DNA Analyzer-Applied Biosystems Automatic Sequencer at the Secugen (CIB, Madrid). The following primers were designed using Fast-PCR software (University of Helsinki, Finland):

RMLN primer; 3R-direct primer (5´-GTTCCATCATCGCGTTCG-3´); 5F-reverse primer (5´-GGATTCCTTTCTTCTTGG-3´) and RMLC primer.

Supporting References

1. Gonzalez-Perez, D.; Molina-Espeja, P.; Garcia-Ruiz, E.; Alcalde, M. *PLoS One* **2014**, 9, e90919.
2. Alcalde, M. *Methods Mol. Biol.* **2010**, 634, 3–14.
3. Zumárraga, M.; Camarero, S.; Shleev, S.; Martínez-Arias, A;, Ballesteros, A.; Plou, F. J.; Alcalde, M. *Proteins* **2008**, 71, 250–260.

Supporting Figure 1. **Combination of directed evolution and hybrid strategies to engineer oxidative stability in VP.** In each generation, up to 3 independent mutant libraries were constructed and explored using conventional and focused directed evolution approaches. Solid arrows indicate the offspring produced in each generation; dotted arrows (black or grey) represent the parental types chosen in each new round. Time (expressed in min) indicates the apparent $\Delta t_{1/2}$ for each mutant calculated from *S. cerevisiae* supernatants and compared with the R4 parental type. VP activity was expressed as a percentage of the activity measured with ABTS in *S. cerevisiae* microcultures for each mutant when compared with the R4 parental type. MORPHING, mutagenic organized recombination by homologous *in vivo* grouping; *ep*PCR, error-prone PCR; IvAM, *In vivo* assembly of mutant libraries; CSM , combinatorial saturation mutagenesis. For each variant, the new mutations are underlined.

Figure S1

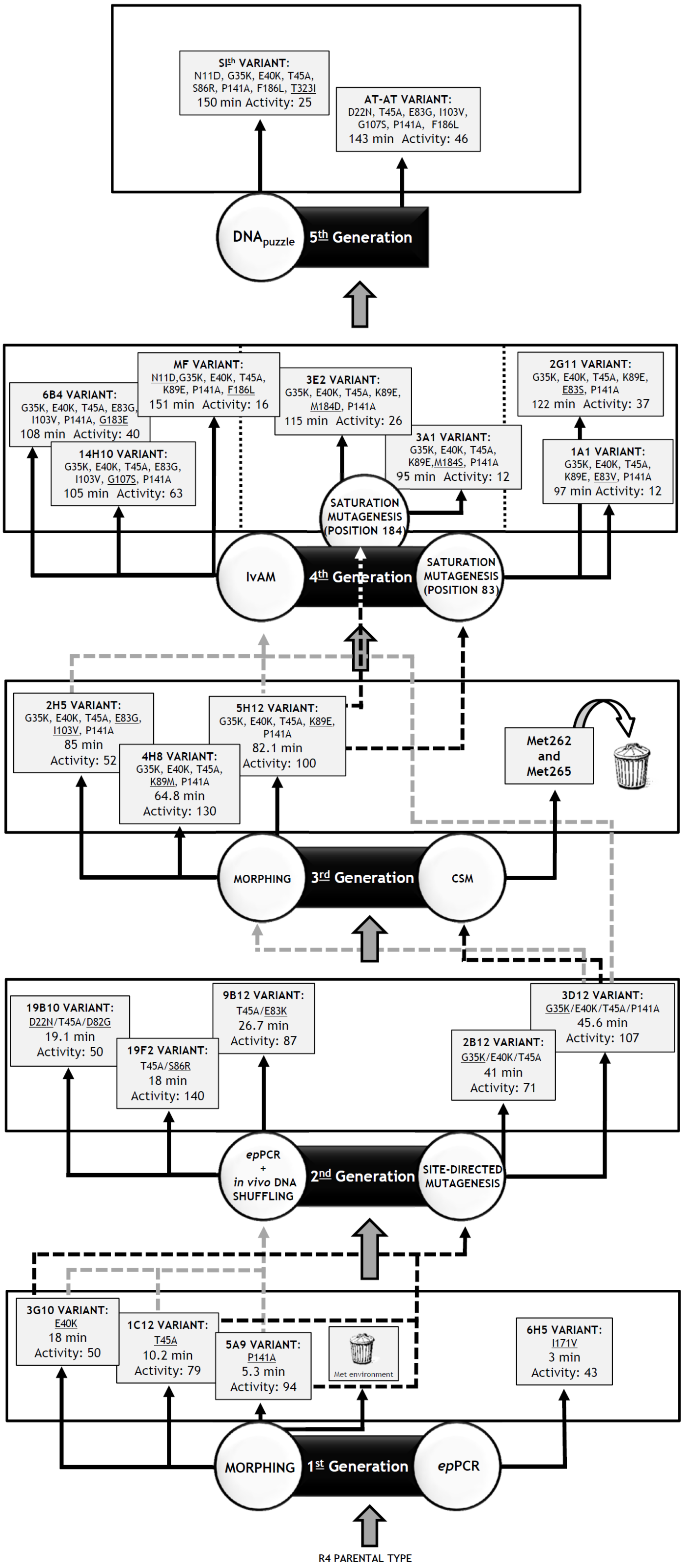
SIth VARIANT:
N11D, G35K, E40K, T45A,
S86R, P141A, F186L, T323I
150 min Activity: 25
AT-AT VARIANT:
D22N, T45A, E83G, I103V,
G107S, P141A, F186L
143 min Activity: 46
DNApuzzle
5th Generation
6B4 VARIANT:
G35K, E40K, T45A, E83G,
I103V, P141A, G183E
108 min Activity: 40
MF VARIANT:
N11D,G35K, E40K, T45A,
K89E, P141A, F186L
151 min Activity: 16
3E2 VARIANT:
G35K, E40K, T45A, K89E,
M184D, P141A
115 min Activity: 26
2G11 VARIANT:
G35K, E40K, T45A, K89E,
E83S, P141A
122 min Activity: 37
14H10 VARIANT:
G35K, E40K, T45A, E83G,
I103V, G107S, P141A
105 min Activity: 63
3A1 VARIANT:
G35K, E40K, T45A,
K89E,M184S, P141A
95 min Activity: 12
1A1 VARIANT:
G35K, E40K, T45A,
K89E, E83V, P141A
97 min Activity: 12
SATURATION MUTAGENESIS (POSITION 184)
IvAM
4th Generation
SATURATION MUTAGENESIS (POSITION 83)
2H5 VARIANT:
G35K, E40K, T45A, E83G,
I103V, P141A
85 min
Activity: 52
5H12 VARIANT:
G35K, E40K, T45A, K89E,
P141A
82.1 min
Activity: 100
4H8 VARIANT:
G35K, E40K, T45A,
K89M, P141A
64.8 min
Activity: 130
Met262
and
Met265
MORPHING
3rd Generation
CSM
19B10 VARIANT:
D22N/T45A/D82G
19.1 min
Activity: 50
9B12 VARIANT:
T45A/E83K
26.7 min
Activity: 87
3D12 VARIANT:
G35K/E40K/T45A/P141A
45.6 min
Activity: 107
19F2 VARIANT:
T45A/S86R
18 min
Activity: 140
2B12 VARIANT:
G35K/E40K/T45A
41 min
Activity: 71
epPCR + in vivo DNA SHUFFLING
2nd Generation
SITE-DIRECTED MUTAGENESIS
3G10 VARIANT:
E40K
18 min
Activity: 50
1C12 VARIANT:
T45A
10.2 min
Activity: 79
5A9 VARIANT:
P141A
5.3 min
Activity: 94
Met environment
6H5 VARIANT:
I171V
3 min
Activity: 43
MORPHING
1st Generation
epPCR
R4 PARENTAL TYPE

Table S1. Primers used in this study.

	Strategy	Primer name	Sequence	Tm (ºC)	length (bp)	Amplification (*ep*PCR/HF-PCR)	$PCR_{product}$ length (bp)
FIRST GENERATION	Distal His environment	RMLN F	5’-CCTCTATACTTTAACGTCAAGG-3'	51.1	22	HF-PCR	403
		H_2O_2BOX -1 R	5’-GTTTTCTTGGATGTCATCGAGG-3'	50.5	21		
		H_2O_2BOX N F	5’-GCATGTTGCATTCTGTTCCCCATCCTC-3'	61.3	27	*ep*PCR	180
		H_2O_2BOX C R	5’-CTCAATGGTGTCGAACGCGATGATGG-3'	61.0	26		
		H_2O_2BOX +1 F	5'-GGAGGAGGAGCTGACGGTTC-3'	56.3	21	HF-PCR	899
		RMLC R	5'-GGGAGGGCGTGAATGTAAGC-3'	55.9	20		
	Proximal His environment	RMLN F	5’-CCTCTATACTTTAACGTCAAGG-3'	51.1	22	HF-PCR	767
		HbPROX -1 R	5’-GAATGGAGTCAACAGAATCAAAAG-3'	52.3	24		
		HbPROX N F	5'-TCCCCGGACCACCTCGTG-3'	57.2	18	*ep*PCR	172
		HbPROX C R	5'-GGGTTGAATCGAATGGCATTCCAG-3'	57.4	24		
		HbPROX +1 F	5'-CGACAAGGTTGACCCATCGATTC-3'	57.1	23	HF-PCR	549
		RMLC R	5'-GGGAGGGCGTGAATGTAAGC-3'	55.9	20		
	Met environment	RMLN F	5’-CCTCTATACTTTAACGTCAAGG-3'	51.1	22	HF-PCR	919
		HbMET -1 R	5’-GATGAAGAATTGAGAATCAAAAACTC-3'	51.7	26		
		HbMET N F	5’-CTGGAATGCCATTCGATTCAACCCCC-3'	61.1	26	*ep*PCR	310
		HbMET C R	5’-GGGGTGGGGATAACATCGGAACAGTC-3'	62.7	26		
		HbMET +1 F	5'-GGCCAAGACAAGACCAAATTGATTG-3'	56.0	25	HF-PCR	266
		RMLC R	5'-GGGAGGGCGTGAATGTAAGC-3'	55.9	20		
	*ep*PCR	RMLN F	5’-CCTCTATACTTTAACGTCAAGG-3'	51.1	22	*ep*PCR	1,392
		RMLC R	5'-GGGAGGGCGTGAATGTAAGC-3'	55.9	20		
SECOND GENERATION	Site-directed mutagenesis	RMLN F	5’-CCTCTATACTTTAACGTCAAGG-3'	51.1	22	HF-PCR	478
		T45A/E40K R	5’-GAAACCGATTGCATCGTGGAAAGCCAAAC GAAGGGACTTGTGCACCTTTTCTCCACACTGG-3’	74.4	61		
		T45A/E40K F	5’-CCAGTGTGGAGAAAAGGTGCACAAGTCCCT TCGTTTGGCTTTCCACGATGCAATCGGTTTC-3’	74.4	61	HF-PCR	975
		RMLC R	5'-GGGAGGGCGTGAATGTAAGC-3'	55.9	20		
	*ep*PCR	RMLN F	5’-CCTCTATACTTTAACGTCAAGG-3'	51.1	22	*ep*PCR	1,392
		RMLC R	5'-GGGAGGGCGTGAATGTAAGC-3'	55.9	20		
THIRD GENERATION	CSM (M262/M265)	RMLN F	5’-CCTCTATACTTTAACGTCAAGG-3'	51.1	22	HF-PCR	1,141
		MET SAT R	5'-GGTCTTGTCTTGGCCAAGAAGAGC**SNN**CTT CGA**SNN**GGTAGCAGCGAAACGGTTCTGAATC-3'	76.1	61		
		MET SAT F	5'-GATTCAGAACCGTTTCGCTGCTACC**NNS**TCG AAG**NNS**GCTCTTCTTGGCCAAGACAAGACC-3'	76.1	61	HF-PCR	312
		RMLC R	5'-GGGAGGGCGTGAATGTAAGC-3'	55.9	20		
	MORPHING	RMLN F	5’-CCTCTATACTTTAACGTCAAGG-3'	51.1	22	HF-PCR	508
		VP Lid -1 R	5’-GTCAGCTCCTCCTCCGCCTAAAG-3’	60.6	23		
		VP Lid F	5’-CCACGATGCAATCGGTTTCTCTCCT-3’	59.3	25	*ep*PCR	196
		VP Lid R	5’-GACTCCAACGGCGCCAGCAAATTG-3’	60.8	24		
		VP Lid +1 F	5’-CACAACATCTCCGCCGGCGAC-3’	62.3	22	HF-PCR	788
		RMLC R	5'-GGGAGGGCGTGAATGTAAGC-3'	55.9	20		

	Strategy	Primer name	Sequence	Tm (°C)	length (bp)	Amplification (*ep*PCR/HF-PCR)	$PCR_{product}$ length (bp)
FOURTH GENERATION	IvAM	RMLN F	5'-CCTCTATACTTTAACGTCAAGG-3'	51.1	22	HF-PCR	1,392
		RMLC R	5'-GGGAGGGCGTGAATGTAAGC-3'	55.9	20		
	Saturation mutagenesis at position 83	RMLN F	5'-CCTCTATACTTTAACGTCAAGG-3'	51.1	22	HF-PCR	592
		Prx83SAT R	5'-TGGCTCCTGAGCACTGACGA T**SNN**ATCGATGCCAGCATTGGCGGG-3'	73.6	45		
		Prx83SAT F	5'-CCCGCCAATGCTGGCATCGA T**NNS**ATCGTCAGTGCTCAGAAGCCA-3'	73.6	45	HF-PCR	845
		RMLC R	5'-GGGAGGGCGTGAATGTAAGC-3'	55.9	20		
	Saturation mutagenesis at position 83	RMLN F	5'-CCTCTATACTTTAACGTCAAGG-3'	51.1	22	HF-PCR	894
		Prx184SAT R	5'-CCGGGGGTTGAATCAAATGG**SNN**T CCAGGAATCGATGGGTCAAC-3'	71.1	44		
		Prx184SAT F	5'-GTTGACCCATCGATTCCTGGA**NNS**C CATTTGATTCAACCCCCGG-3'	71.1	44	HF-PCR	542
		RMLC R	5'-GGGAGGGCGTGAATGTAAGC-3'	55.9	20		
FIFTH GENERATION	DNA_{puzzle}	RMLN F	5'-CCTCTATACTTTAACGTCAAGG-3'	51.1	22	HF-PCR	481
		DOMREC-2R	5'-AGAGAAACCGATTGCATCGTG-3'	52.4	21		
		DOMREC-1F	5'-GTGCACGAGTCCCTTCGTTTG-3'	56.3	21	HF-PCR	384
		DOMREC-4R	5'-GAGCCAAACAACCTCGGCGGG-3'	60.2	21		
		DOMREC-3F	5'-AGAATGGGTGACGCAGGCTTC-3'	56.3	21	HF-PCR	620
		RMLC R	5'-GGGAGGGCGTGAATGTAAGC-3'	55.9	20		

NNS: degenerated codon

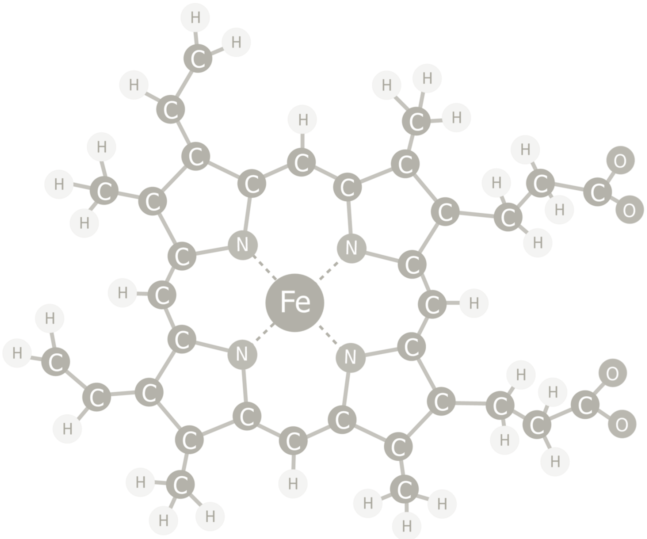

Capítulo 4:

Mutagenic Organized Recombination Process by Homologous In vivo Grouping (MORPHING) for directed enzyme evolution

En este capítulo se describe la puesta a punto de un método de evolución dirigida por dominios para introducir mutaciones aleatorias y eventos de recombinación de manera focalizada para la construcción de smart mutant libraries.

OPEN ACCESS Freely available online

PLOS | ONE

Mutagenic Organized Recombination Process by Homologous In Vivo Grouping (MORPHING) for Directed Enzyme Evolution

David Gonzalez-Perez[1], Patricia Molina-Espeja[1], Eva Garcia-Ruiz[2], Miguel Alcalde[1]*

1 Departmento de Biocatálisis, Instituto de Catálisis y Petroleoquímica, Consejo Superior de Investigaciones Científicas (CSIC), Madrid, Spain, **2** Department of Chemical and Biomolecular Engineering, University of Illinois at Urbana-Champaign, Urbana, Illinois, United States of America

Abstract

Approaches that depend on directed evolution require reliable methods to generate DNA diversity so that mutant libraries can focus on specific target regions. We took advantage of the high frequency of homologous DNA recombination in *Saccharomyces cerevisiae* to develop a strategy for domain mutagenesis aimed at introducing and *in vivo* recombining random mutations in defined segments of DNA. Mutagenic Organized Recombination Process by Homologous *IN* vivo Grouping (MORPHING) is a *one-pot* random mutagenic method for short protein regions that harnesses the *in vivo* recombination apparatus of yeast. Using this approach, libraries can be prepared with different mutational loads in DNA segments of less than 30 amino acids so that they can be assembled into the remaining unaltered DNA regions *in vivo* with high fidelity. As a proof of concept, we present two eukaryotic-ligninolytic enzyme case studies: i) the enhancement of the oxidative stability of a H_2O_2-sensitive versatile peroxidase by independent evolution of three distinct protein segments (Leu28-Gly57, Leu149-Ala174 and Ile199-Leu268); and ii) the heterologous functional expression of an unspecific peroxygenase by exclusive evolution of its native 43-residue signal sequence.

Citation: Gonzalez-Perez D, Molina-Espeja P, Garcia-Ruiz E, Alcalde M (2014) Mutagenic Organized Recombination Process by Homologous In Vivo Grouping (MORPHING) for Directed Enzyme Evolution. PLoS ONE 9(3): e90919. doi:10.1371/journal.pone.0090919

Editor: Claudio M. Soares, Instituto de Tecnologica Química e Biológica, UNL, Portugal

Received November 25, 2013; **Accepted** February 6, 2014; **Published** March 10, 2014

Funding: This work was supported by the European Comission Projects Peroxicats-FP7-KBBE-2010-4-26537 and Indox-FP7-KBBE-2013-7-613549 and the National Project (Evofacel) [BIO2010-19697]. The funders had no role in study design, data collection and analysis, decision to publish, or preparation of the manuscript.

Competing Interests: The authors have declared that no competing interests exist.

* E-mail: malcalde@icp.csic.es

Introduction

In the past two decades directed evolution strategies have had a huge impact on protein engineering and synthetic biology [1–5]. Combining directed evolution with new computational and hybrid approaches has allowed researchers to design "smart" mutant libraries to address bottlenecks in enzyme functionality, helping to maintain the balance between activity and stability, or even creating novel catalytic activities [6,7]. The use of non-adaptive evolution involving neutral genetic drift has been added to this arsenal of techniques to create polymorphic populations with the aim of enhancing protein robustness and substrate promiscuity [8–11].

Although the majority of the vast protein sequence space is probably non-functional, with 20^n possible permutations (if we exclude the introduction of non-natural amino acids), it is still far from being fully explored [12]. Advances in the field involve the use of ultrahigh-throughput screening methods and the construction of focused mutant libraries to restrict the sequence space [13,14]. Most of the available methods used to create targeted libraries are based on computational studies that identify a limited number of positions for saturation mutagenesis, combinatorial and/or iterative [15–17]. A more recent approach is to introduce ancestral consensum mutations that have been identified by phylogenetic analysis and ancestral inference in extant enzymes [18]. Despite the wide array of focused evolution methods, there remains a need for consistent domain mutagenesis/recombination strategies targeting specific protein subsets for random mutagenesis and recombination, while conserving the remaining protein regions. Although this kind of focused-indiscriminate approach has received little attention in the literature [19,20], it can effectively unmask structural determinants of specific enzymatic attributes, which can then be optimized using the aforementioned methods.

Escherichia coli is by far the most common host in directed evolution experiments of prokaryotic proteins. However, broad differences with eukaryotic cells (missing chaperones, different codon usage, lack of posttranslational modifications) preclude the use of this bacteria to engineer eukaryotic enzymes which mostly end up in misfolding and inclusion bodies formation. Alternatively, *Saccharomyces cerevisiae* is the model organism of choice for *in vitro* evolution of eukaryotic genes, permitting the development of comprehensive synthetic biology and metabolic engineering studies, particularly when dealing with the production of fuels and chemicals [21–24]. In recent years, a range of methods have been described in this yeast to construct mutant libraries with different mutational bias, to integrate multiple DNA fragments for creating combinatorial libraries or to assemble expression cassettes that generate fully autonomous artificial pathways [25–28]. The high frequency of homologous DNA recombination in *S. cerevisiae* permits to simply shuffle foreign genes creating multiple crossover events, to repair linearized vectors for *in vivo* cloning or to promote the molecular evolution of multigenic phenotypes [29–33].

Here, we present a simple, rapid and reliable random domain mutagenesis/recombination method for short fragments that is based on the physiological properties of *S. cerevisiae*. Mutagenic Organized Recombination Process by Homologous IN vivo Grouping (MORPHING) randomly introduces mutations in specific protein segments using overlapping areas to favor *in vivo* splicing and recombination in yeast. The versatility of this method was evaluated in two case studies of ligninolytic oxidoreductases. First, we used MORPHING to enhance the oxidative stability of a versatile peroxidase (VP) from the basidiomycete *Pleurotus eryngii*. VP has three different catalytic sites for the oxidation of low-, medium- and high-redox potential compounds, which makes the enzyme extremely fragile in the presence of catalytic concentrations of H_2O_2 [34]. The second enzyme studied was the unspecific peroxygenase (UPO) from the edible mushroom *Agrocybe aegerita*, a heme-thiolate peroxidase with special catalytic capacity that includes oxygen transfer reactions [35]. Despite its importance in organic synthesis, heterologous functional expression and directed evolution of this enzyme has not yet been reported. We used MORPHING to exclusively target the native UPO signal peptide for evolution towards functional expression in yeast.

Materials and Methods

VP from *Pleurotus eryngii* (the R4 mutant) was used as the parental type in the construction of the library. This R4 mutant was engineered for secretion by 4 rounds of directed evolution, resulting in expression levels of 22 mg/L [36]. The UPO1 variant (12C12) was generated by directed evolution in a previous study to functionally express the *upo1* gene (clone C1A-2) from *A. aegerita* [37] in *S. cerevisiae* (unpublished material). ABTS (2,2′-azino-bis(3-ethylbenzothiazoline-6-sulfonic acid)), *Taq* polymerase, and the *S. cerevisiae* transformation kit were purchased from Sigma-Aldrich (Madrid, Spain). The iProof High Fidelity DNA polymerase was purchased from Bio-Rad (USA). The Zymoprep Yeast Plasmid Miniprep Kit and Zymoclean Gel DNA Recovery Kit were obtained from Zymo Research (Orange, CA, USA), while NBD (5-nitro-1,3-benzodioxole) was purchased from TCI America (USA). The *Escherichia coli* XL2-Blue competent cells and the GeneMorph II Kit (mutazyme II polymerase) were from Stratagene (La Jolla, CA, USA), and the uracil independent and ampicillin resistance pJRoC30 shuttle vector was obtained from the California Institute of Technology (CALTECH, USA). The protease-deficient *S. cerevisiae* strain BJ5465 (α *ura3-52 trp1 leu2Δ1 his3Δ200 pep4::HIS3 prb1Δ1.6R can1 GAL*) was obtained from LGCPromochem (Barcelona, Spain), the NucleoSpin Plasmid kit was purchased from Macherey-Nagel (Germany), and the restriction enzymes BamHI and XhoI from New England Biolabs (Hertfordshire, UK). All chemicals were of reagent-grade purity.

Culture media

Minimal medium (SC) contained 0.67% (w/v) sterile yeast nitrogen base, 1.92 g/L sterile yeast synthetic drop-out medium supplement without uracil, 2% (w/v) sterile D-raffinose and 25 µg/mL chloramphenicol. YP medium contained 10 g yeast extract, 20 g peptone and *dd*H_2O to 650 mL. Flask expression medium contained 720 mL YP, 67 mL 1 M KH_2PO_4 buffer (pH 6.0), 111 mL 20% (w/v) D-galactose, 25 g/L ethanol, 500 or 300 mg/L bovine hemoglobin (for VP and UPO, respectively), 1 mM $CaCl_2$ for VP or 2 mM $MgSO_4$ for UPO, 1 mL 25 g/L chloramphenicol and *dd*H_2O to 1000 mL. Microplate expression medium contained 720 mL YP, 67 mL 1 M KH_2PO_4 buffer (pH 6.0), 111 mL 20% (w/v) D-galactose, 100 or 50 mg/L bovine hemoglobin (for VP and UPO, respectively), 2 mM $MgSO_4$ for UPO, 1 ml 25 g/L chloramphenicol and *dd*H_2O to 1000 mL. YPD solution contained 1% (w/v) yeast extract, 2% (w/v) peptone, 2% (w/v) sterile D-glucose and 25 µg/mL chloramphenicol. SC drop-out plates contained 0.67% (w/v) sterile yeast nitrogen base, 1.92 g/L (w/v) sterile yeast synthetic drop-out medium supplement without uracil, 2% (w/v) bacto agar, 2% (w/v) sterile D-glucose and 25 µg/mL chloramphenicol. Luria-Bertani (LB) medium was prepared with 1% (w/v) peptone, 0.5% (w/v) yeast extract, 1% (w/v) NaCl and 100 µg/mL ampicillin.

MORPHING Protocol

All the PCR products generated were cleaned, concentrated and loaded onto a low melting-point preparative agarose gel and purified using the Zymoclean Gel DNA Recovery Kit (Zymo Research). The PCR products were cloned by replacing the corresponding parental gene in pJRoC30. To remove the parental gene, the plasmid was linearized with BamHI and XhoI. The pJRoC30-R4 variant was used as a template to construct MORPHING libraries of VP, while the pJRoC30-12C12 was used as the template to construct MORPHING libraries of UPO signal peptide.

For VP MORPHING, the whole gene was fragmented into three different segments in individual PCR reactions. Each segment contained homologous overhangs of ~50 bp that overlapped one another to promote *in vivo* cloning in yeast. The targeted regions were subjected to random mutagenesis while the remaining segments were amplified by high-fidelity polymerases (**Figure S1**). The distal His environment region was selected to tune mutational loads. Small mutant libraries of around 500 clones were screened to optimize the mutagenic conditions. A similar protocol was followed for UPO MORPHING but in this case the UPO gene was split into two segments, one containing the signal peptide and the other the mature protein.

1. VP MORPHING. i) Mutagenic PCR of targeted regions: Reaction mixtures were prepared in a final volume of 50 µL containing the following: DNA template (0.1 ng/µL or 0.92 ng/µL), 90 nM Forward primer, 90 nM Reverse primer (different forward (F) and reverse (R) primers were used to amplify each region; **Table S1, Figure S1**), 0.3 mM dNTPs (0.075 mM each), 3% (v/v) dimethylsulfoxide (DMSO), 1.5 mM $MgCl_2$, increasing concentrations of $MnCl_2$ (0.01, 0.05, 0.1, 0.2, 0.4 mM) and 0.05 U/µL *Taq* polymerase. Error prone-PCRs were carried out on a gradient thermocycler (Mycycler, BioRad, USA) using the following conditions: 95°C for 2 min (1 cycle); 94°C for 45 s, 56°C for 45 s, 74°C for 45 s (28 cycles); and 74°C for 10 min (1 cycle). For the proximal His environment and Met environment, the final DNA template concentration was 0.92 ng/µL and the $MnCl_2$ concentration was set at 0.2 mM and 0.01 mM, independently for both targeted regions.

ii) High-fidelity PCR in non-mutated segments: Reaction mixtures were prepared in a final volume of 50 µL containing: DNA template (0.2 ng/µL), 0.5 µM Forward primer, 0.5 µM Reverse, (different forward (F) and reverse (R) primers were used to amplify each region; **Table S1, Figure S1**), 0.8 mM dNTPs (0.2 mM each), 3% (v/v) dimethylsulfoxide (DMSO), and 0.02 U/µL iProof polymerase. High fidelity PCRs were performed on a gradient thermocycler using the following conditions: 98°C for 30 s (1 cycle); 98°C for 10 s, 45 or 50°C for 30 s, 72°C for 1 min (28 cycles); and 72°C for 10 min (1 cycle).

iii) Reassembly of the whole gene: The whole gene was reassembled *in vivo* and recombined by transformation into *S. cerevisiae* cells using the Yeast Transformation Kit. The DNA transformation mixture contained the linearized plasmid (200 ng) mixed with the targeted region, as well as the segments upstream and downstream of those regions (400 ng per segment). Transformed cells were plated on SC drop-out plates and incubated for 3 days at 30°C. Subsequently, the mutant libraries were subjected to the HTP-protocol for oxidative stability, as described below.

2. UPO MORPHING. i) Mutagenic PCR in signal peptide: Reaction mixtures were prepared in a final volume of 50 µL containing the following: DNA template (0.92 ng/µL), 90 nM RMLN F primer, 90 nM MORPH SP R primer (**Table S1**), 0.3 mM dNTPs (0.075 mM each), 3% (v/v) dimethylsulfoxide (DMSO), 1.5 mM $MgCl_2$, 0.1 mM $MnCl_2$ and 0.05 U/µL *Taq* polymerase. Error-prone PCR was carried out on a gradient thermocycler using the following parameters: 95°C for 2 min (1 cycle); 94°C for 45 s, 50°C for 45 s, 74°C for 30 s (28 cycles); and 74°C for 10 min (1 cycle).

ii) High-fidelity PCR of non-mutated segment: Reaction mixtures were prepared in a final volume of 50 µL containing DNA template (0.2 ng/µL), 0.5 µM MORPH SP D primer, 0.5 µM RMLC R primer (**Table S1**), 1 mM dNTPs (0.25 mM each), 3% (v/v) dimethylsulfoxide (DMSO), and 0.02 U/µL iProof polymerase. High fidelity PCR was carried out on the gradient thermocycler using the following conditions: 98°C for 30 s (1 cycle); 98°C for 10 s, 55°C for 25 s, 72°C for 45 s (28 cycles); and 72°C for 10 min (1 cycle).

iii) Reassembly of the whole gene: The whole gene was reassembled *in vivo* and recombined by transformation into *S. cerevisiae* cells using the Yeast Transformation Kit. The DNA transformation mixture contained the linearized plasmid (100 ng) mixed with the targeted region, as well as the mature protein (200 ng per segment). Transformed cells were plated on SC drop-out plates and incubated for 3 days at 30°C. Subsequently, the mutant libraries were subjected to the HTP-protocol to assess activity as described below.

Directed evolution of whole UPO gene

The whole UPO gene including its signal peptide was subjected to one round of directed evolution by *In vivo* Assembly of Mutant libraries (IvAM) [27].

1. Mutagenic PCR with *Taq* polymerase. Reaction mixtures were prepared in a final volume of 50 µL containing: DNA template (0.1 ng/µL), 90 nM RMLN F primer, 90 nM RMLC R primer (**Table S1**), 0.3 mM dNTPs (0.075 mM each), 3% (v/v) dimethylsulfoxide (DMSO), 1.5 mM $MgCl_2$, 0.01 mM $MnCl_2$ and 0.05 U/µL *Taq* polymerase. Error-prone PCR was carried out under the following conditions: 95°C for 2 min (1 cycle); 94°C for 45 s, 53°C for 45 s, 74°C for 3 min (28 cycles); and 74°C for 10 min (1 cycle).

2. Mutagenic PCR with Mutazyme II. Reaction mixtures were prepared in a final volume of 50 µL containing: DNA template (56 ng/µL), 0.37 µM RMLN F primer, 0.37 µM RMLC R primer (**Table S1**), 0.8 mM dNTPs (0.2 mM each), 3% (v/v) dimethylsulfoxide (DMSO), and 0.05 U/µL Mutazyme II. Error-prone PCR was carried out using the following parameters: 95°C for 2 min (1 cycle); 94°C for 45 s, 53°C for 45 s, 74°C for 3 min (28 cycles); and 74°C for 10 min (1 cycle).

3. In vivo recombination of mutant libraries in S. cerevisiae. *Taq* polymerase library and Mutazyme library were added in equimolar concentrations (200 ng each) to the linearized vector (100 ng). Transformed cells were plated on SC drop-out plates and incubated for 3 days at 30°C. Thereafter, the mutant libraries were subjected to the HTP-protocol to assay activity as described below.

Construction of the evolved signal peptide F12Y-A14V-R15G-A21D by site-directed mutagenesis and fusion to the native *upo* gene

1. Construction of the evolved signal peptide (SP*) by site-directed mutagenesis. Reaction mixture was prepared in a final volume of 50 µL containing: DNA template (0.2 ng/µL), 0.5 µM Forward primer RMLN F, 0.5 µM Reverse primer SP* R (**Table S1**), 1 mM dNTPs (0.25 mM each), 3% (v/v) dimethylsulfoxide (DMSO), and 0.02 U/µL iProof polymerase. High fidelity PCR1 was carried out on the gradient thermocycler under the following conditions: 98°C for 30 s (1 cycle); 98°C for 10 s, 47°C for 25 s, 72°C for 15 s (28 cycles); and 72°C for 10 min (1 cycle).

2. Construction of fusion gene (evolved signal peptide plus the native upo) by In Vivo Overlap Extension (IVOE). the native *upo* was amplified by high-fidelity PCR in a final volume of 50 µL containing: DNA template (0.2 ng/µL), 0.5 µM Forward primer SP* F, 0.5 µM Reverse primer RMLC R (**Table S1**), 1 mM dNTPs (0.25 mM each), 3% (v/v) dimethylsulfoxide (DMSO), and 0.02 U/µL iProof polymerase. High fidelity PCR was carried out on the gradient thermocycler under the following conditions: 98°C for 30 s (1 cycle); 98°C for 10 s, 52°C for 25 s, 72°C for 40 s (28 cycles); and 72°C for 15 min (1 cycle). PCR fragments corresponding to the SP* and the native *upo* (200 ng each) were recombined together with the linearized vector (100 ng) by IVOE [25].

Combinatorial saturation mutagenesis experiments in VP

Reaction mixtures were prepared in a final volume of 50 µL containing: DNA template (0.2 ng/µL), 0.2 µM Forward primer, 0.2 µM Reverse primer (RMLN F/MET SAT R primers and MET SAT F/RMLC R for first PCR and second PCR, respectively, (**Table S1**)), 0.8 mM dNTPs (0.2 mM each), 3% (v/v) dimethylsulfoxide (DMSO), and 0.02 U/µL iProof polymerase. High fidelity PCRs were carried out on the gradient thermocycler under the following conditions: 98°C for 30 s (1 cycle); 98°C for 10 s, 53°C for 30 s, 72°C for 1 min (28 cycles); and 72°C for 10 min (1 cycle). The whole gene was reassembled *in vivo* and recombined by transformation into *S. cerevisiae* cells using the Yeast Transformation Kit. The DNA transformation mixture was composed of the linearized plasmid (200 ng) mixed with the mutated fragments (400 ng per fragment). Transformed cells were plated on SC drop-out plates and incubated for 3 days at 30°C. Thereafter, the mutant libraries were subjected to the HTP-protocol described below.

High-throughput oxidative stability assay of VP

Individual clones were selected and cultured in sterile 96-well plates (Greiner Bio-One GmbH, Germany) containing 50 µL per well of SC minimal medium. In each plate, column number 6 was inoculated with the parental R4 mutant as an internal standard, and well-H1 (containing minimal medium supplemented with uracil) was inoculated with untransformed *S. cerevisiae* as a negative control. Plates were wrapped in parafilm to prevent evaporation and incubated at 30°C, 225 rpm and 80% relative humidity in a humidity shaker (Minitron-INFORS, Biogen, Spain). After 48 h, 160 µL of expression medium was added to each well and the plates were incubated for a further 24 h. The plates (master plates) were centrifuged for 15 min at 3000 rpm and 4°C (Eppendorf 5810R centrifuge, Germany) and the master plates were duplicated with the help of a robot (Liquid Handler Quadra 96–320, Tomtec, Hamden, CT, USA) by transferring 20 µL of supernatant into two replica plates: the initial activity plate (IA plate) and the residual activity plate (RA plate). Next, 180 µL of stability buffer (20 mM sodium tartrate buffer, pH 5.0: Buffer A) was added to the IA plates and 180 µL of incubation solution (Buffer A containing 0.3 mM H_2O_2) was added to the RA plates using a Multidrop robot (Multidrop Combi, ThermoFischer Scientific, Vantaa, Finland). Both plates were briefly stirred and incubated at room temperature for 60 min, such that the activity assessed in the RA plates was reduced by 2/3rds with respect to the initial activity of the parental type. The supernatants (20 µL) were transferred from both RA and IA plates to new plates to measure the residual and initial activity values by adding ABTS in specific buffers: 180 µL of 100 mM sodium tartrate buffer [pH 3.5] containing 2 mM ABTS and 0.1 mM H_2O_2 to estimate of residual activity; and 180 µL of 100 mM sodium tartrate buffer [pH 3.5] containing 2 mM ABTS and 0.13 mM H_2O_2 to estimate the initial activity. The plates were stirred briefly and the absorption at 418 nm ($\varepsilon_{ABTS}{}^{\bullet +} = 36{,}000\ M^{-1}\ cm^{-1}$) was recorded (end-point mode, t_0) on a plate reader (SPECTRAMax Plus 384, Molecular Devices, Sunnyvale, CA). The plates were then incubated at room temperature until a green color developed and the absorption was measured again (t_1). The relative activities were calculated from the difference between the absorption value after incubation and that of the initial measurement normalized to the parental type in the corresponding plate (Δt_1-t_0). Oxidative stability values were calculated as the ratio between residual activity and the initial activity values (RA/IA). To rule out false positives, two consecutive re-screenings were carried out. Moreover, a third re-screening was performed to determine the increase in the apparent half-life of each selected variant ($t_{1/2}$ H_2O_2, expressed in minutes) relative to the parental R4 in different molar ratios $[H_2O_2]$/[VP in supernatants].

First re-screening: Aliquots of 5 µL of the best clones were removed from the master plates and used to inoculate 50 µL of minimal medium in new 96-well plates. Columns 1 and 12, and rows A and H, were not used to prevent the appearance of false positives. After incubating for 24 h at 30°C, 225 rpm, and 80% relative humidity, 5 µL was transferred to the adjacent wells and incubated for a further 24 h. Finally, 160 µL of expression medium was added and the plates were incubated for another 24 h. Accordingly, each mutant was grown in 4 wells. The parental types were subjected to the same procedure (row D, wells 7–11) and the plates were assessed using the same protocols as those used for the screening described above.

Second re-screening: An aliquot from the wells with the best clones in the first re-screening was inoculated in 3 mL of YPD and incubated at 30°C and 225 rpm for 24 h, recovering the plasmids from these cultures (Zymoprep Yeast Plasmid Miniprep Kit). As the product of the zymoprep was very impure and the concentration of DNA extracted very low, the zymoprep mixtures containing shuttle vectors were transformed into super-competent *E. coli* cells (XL2-Blue, Stratagene) and plated on LB/amp plates. Single colonies were picked and used to inoculate 5 mL LB/amp media, and they were grown overnight at 37°C and 225 rpm. The plasmids were then extracted (NucleoSpin Plasmid kit, Macherey-Nagel, Germany) and *S. cerevisiae* was transformed with plasmids from the best mutants as well as with the parental type. Five colonies for each mutant were selected and re-screened as described above.

Third re-screening (determination of $t_{1/2}$ H_2O_2): A single colony from the *S. cerevisiae* clone containing the parental R4, the new mutants and untransformed yeast were picked from a SC drop-out plate (SC supplemented with uracil for untransformed cells), used to inoculate 5 mL of minimal medium, and incubated for 48 h at 30°C and 225 rpm (Minitron-INFORS, Biogen, Spain). An aliquot of cells was removed and used to inoculate a final volume of 5 mL of minimal medium in a 50 mL falcon tube (optical density, $OD_{600} = 0.3$), and they were incubated until two growth phases had been completed (6–8 h, $OD_{600} = 1$). Thereafter, 9 mL of expression medium (500 mg/L bovine hemoglobin) was inoculated with 1 mL of this preculture in a 100 mL flask ($OD_{600} = 0.1$). After incubating for ~48 h at 30°C and 225 rpm (maximal VP activity; $OD_{600} = 25$–30), the cells were separated by centrifugation for 15 min at 3000 rpm and 4°C (Eppendorf 5810R Centrifuge, Germany), and the supernatants were collected and stored at 4°C. The protein concentration was estimated from supernatants using the Bio-Rad protein assay kit, (Bio-Rad, USA). VP apparent concentration was calculated as the difference between the total protein content of yeast expressing VP and that in its absence (from non-transformed yeast cells -lacking VP gene-). The parental R4 and the mutants (final concentration 0.1 µM) were incubated at room temperature in 20 mM sodium tartrate buffer [pH 5.0] in the presence or absence of different concentrations of H_2O_2 (0.3, 0.6 mM). Aliquots (20 µL) were removed at different times and the residual/initial activities were measured in a final volume of 200 µL containing 100 mM sodium tartrate buffer [pH 3.5], 2 mM ABTS and 0.13 mM or 0.16 mM H_2O_2 (for samples incubated in the presence of 0.3 and 0.6 mM H_2O_2, respectively). The residual activity was determined relative to the corresponding mutant incubated in the absence of H_2O_2, taking into account the final concentration of H_2O_2 in each activity assay. Each point represents the mean of three independent experiments performed in triplicate. Increment in apparent half-lives ($\Delta t_{1/2}$ *vs* H_2O_2) were calculated for each mutant at given molar ratio VP (supernatants) : H_2O_2.

High-throughput screening assay for UPO secretion

Individual clones were selected and inoculated in sterile 96-well plates (Greiner Bio-One GmbH, Germany) containing 50 µL per well of SC minimal medium. In each plate, column number 6 was inoculated with the corresponding parental type, and one well (H1-control) was inoculated with untransformed *S. cerevisiae* cells in minimal medium containing uracil. The plates were wrapped in parafilm to prevent evaporation and incubated at 30°C, 225 rpm and 80% relative humidity in a humidity shaker. After 48 h, 160 µL of expression medium was added to each well and the plates were incubated for 48 h. The plates (master plates) were centrifuged (Eppendorf 5810R Centrifuge, Germany) for 15 min at 3000 rpm and 4°C, and the supernatants (20 µL) were transferred from the master plate to two replica plates by a robot (Liquid Handler Quadra 96–320, Tomtec, Hamden, CT, USA), adding the reaction mixture (180 µL) together with ABTS or NBD to each replica plate. Both colorimetric assays were used for properly detecting secretion levels improvements regardless of the substrate used (ABTS is typically used for assessing peroxidative activity whereas NBD for peroxygenase activity). The reaction mixture with ABTS contained 100 mM sodium citrate/phosphate buffer [pH 4.4], 0.3 mM ABTS and 2 mM H_2O_2, while the reaction mixture with NBD contained 100 mM potassium phosphate buffer [pH 7.0], 1 mM NBD, 15% (v/v) acetonitrile and 1 mM H_2O_2. Plates were stirred briefly and the initial absorptions at 418 nm ($\varepsilon_{ABTS}{}^{\bullet +} = 36{,}000\ M^{-1}\ cm^{-1}$) and 425 nm ($\varepsilon_{NBD} = 9{,}700\ M^{-1}\ cm^{-1}$) were recorded on the plate reader (SPECTRAMax Plus 384, Molecular Devices, Sunnyvale, CA). The plates were then incubated at room temperature until a green (ABTS) or yellow (NBD) color developed, and the absorption was measured again. The values were normalized against the parental type in the corresponding plate. To rule out false positives, two re-screenings were carried out as described above for VP.

Thermostability assay (T_{50})

Appropriate dilutions of the supernatants were prepared such that aliquots (20 µL) produced a linear response in kinetic mode. A gradient profile was constructed using a thermocycler (Mycycler, Bio-Rad, USA) for the selected mutants and the parental type, using 50 µL for each point in a gradient scale ranging from 30 to 80°C. After a 10 min incubation, samples were removed and chilled on ice for 10 min. Thereafter, 20 µL samples were removed and incubated for 5 min at room temperature. Finally, 180 µL of 100 mM sodium tartrate buffer [pH 3.5], 2 mM ABTS and 0.1 mM H_2O_2 was added to the samples to measure activities. The thermostability values were calculated as the ratio between the residual activity at different temperature points and the initial activity at room temperature. The T_{50} value was determined as the transition midpoint of the inactivation curve of the protein as a function of temperature, which in our case was defined as the temperature at which the enzyme lost 50% of its initial activity after a 10 min incubation.

DNA sequencing

Plasmids containing the VP/UPO variants were sequenced on an ABI 3730 DNA Analyzer-Applied Biosystems Automatic Sequencer at the Secugen (CIB, Madrid). The following primers were designed using Fast-PCR software (University of Helsinki, Finland):

for VP: RMLN F; 3R-direct (5′-GTTCCATCATCGCGT-TCG-3′); 5F-reverse (5′-GGATTCCTTTCTTCTTGG-3′) and RMLC R (**Table S1**). For UPO: RMLN F; upo1 sec direct (5′-GAAGGCGACGCCAGTATGACC-3′); upo1 sec reverse (5′-GGTCATACTGGCGTCGCCTTC-3′) and RMLC R (**Table S1**).

Protein and homology modeling

The crystal structure of VPL2 from *P. eryngii* at 2.8 Å resolution (1 Å = 0.1 nm, PDB ID: 3FJW) was used to generate a model to map the new mutations found with the help of the PyMOL Molecular Visualization System (Schrödinger). A homology model was generated by carrying out a structural alignment in PyMOL

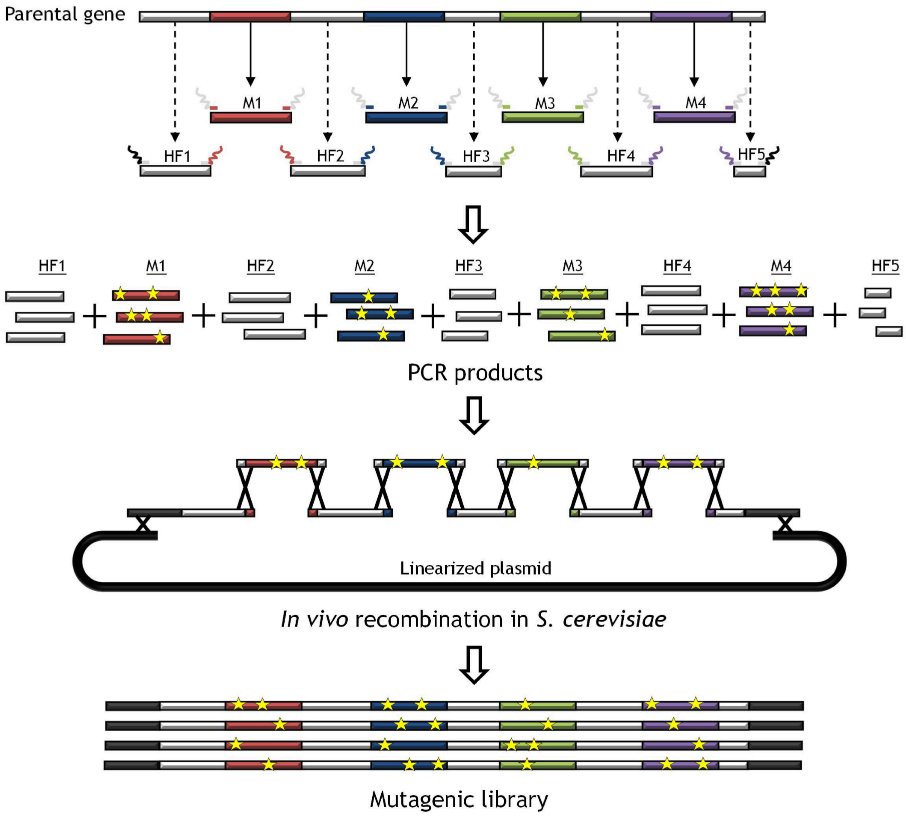

Figure 1. General approach for MORPHING. Segments subjected to random mutagenesis (M1 to M4) are shown in color and the non-mutagenized high fidelity amplified segments (HF1 to HF5) in light grey. After PCR, the pool of segments is co-transformed into *S. cerevisiae* along with the linearized vector. Overlapping areas of ~50 bp flanking each segment allow specific crossover events to occur between fragments (represented by crosses), giving rise to an autonomously repaired vector carrying a full version of the target gene with random mutations (yellow stars) only in the defined regions.
doi:10.1371/journal.pone.0090919.g001

with the following crystal structures (PDB IDs are indicated): 3FJW, native VP from *P. eryngii*; 1IYN, recombinant chloroplastic ascorbate peroxidase (ApX) from *N. tabacum* expressed in *E. coli*; 3M5Q, native manganese peroxidase (MnP) isozyme 1 from *P. chrysosporium*; 1H3J, native peroxidase from *C. cinerea* (CiP); and 1W4W, recombinant horseradish peroxidase C1A from horseradish (HRP) expressed in *E. coli*. IDENTITY and SIMILARITY percentages were obtained using SEQUENCE SIMILARITY AND IDENTITY Software (http://imed.med.ucm.es/Tools/sias.html).

Results and Discussion

MORPHING is a method of generating DNA diversity based on the high frequency of homologous recombination of *S. cerevisiae*. In a single step, this approach allows us to assemble delimited randomly mutagenized regions with the remaining, unaltered fragments of a gene. Unlike most evolution methods focused in restricted areas, mutations are randomly generated and they do not depend on the engineering of a set of spiked/degenerate synthetic oligonucleotides. By MORPHING, small segments are targeted and subjected to error-prone PCR with defined mutational frequencies, while the remaining portions of the gene are amplified using high-fidelity polymerases (**Figure 1**). Error-prone PCR methods have the drawback of codon bias although they can be modified by alternating between different polymerases in successive generations of evolution. Indeed, standard *Taq* polymerases (with a transition/transversion ratio [T_s/T_v] ranging from 2.9 to 0.8, [38]) were employed in our mutagenic experiments, although mutational bias may be altered by combining this protocol with other well-known polymerases and mutational strategies [27,36,39]. The pool of mutated/conserved fragments and the linearized plasmid are subjected to *one-pot* repair and cloned *in vivo*, giving rise to a complete autonomously replicating plasmid upon transformation in yeast, without the need for additional PCR reactions or ligation/amplification steps. The number of crossover events (*n*+1, where *n* is the number of fragments) between segments is directly proportional to the number of segments assembled, allowing several regions to be studied alone or in a combinatorial manner. Depending on the distance between mutations, crossover events can occur between the different mutations in the target fragment(s), mediated by the *S. cerevisiae* recombination machinery, fostering enrichment. The success of this method is facilitated by the high fidelity DNA splicing of fragments through the small overhangs with overlapping sequences of ~50 bp that flank each segment. These overhangs ensure the *in vivo* reconstitution of the whole gene with random mutations only in the segments specifically targeted. Under these rules, up to six recombination events between fragments can be created without significantly affecting transformation efficiencies (~10^5 clones per transformation reaction can be obtained, which are good enough to screen mutant libraries).

Engineering oxidative stability

We first used this protocol to engineer oxidative stability in an evolved VP variant, the VP-R4 mutant generated in a previous directed evolution experiment to enhance its functional expression in yeast and its stability [36]. The sensitivity of VP (EC 1.11.1.16) to peroxides is the highest reported for any peroxidase to date being strongly inhibited in the presence of catalytic concentrations of H_2O_2 due to a mechanism-based phenomenon known as suicide inactivation that is common to all peroxidases [40]. The inherent fragility of VP is explained by its complex structure. With a redox potential of over +1.2 V, three different catalytic sites (the heme domain, a catalytic tryptophan located at the protein's surface and the Mn^{2+} binding site), and two access channels, the

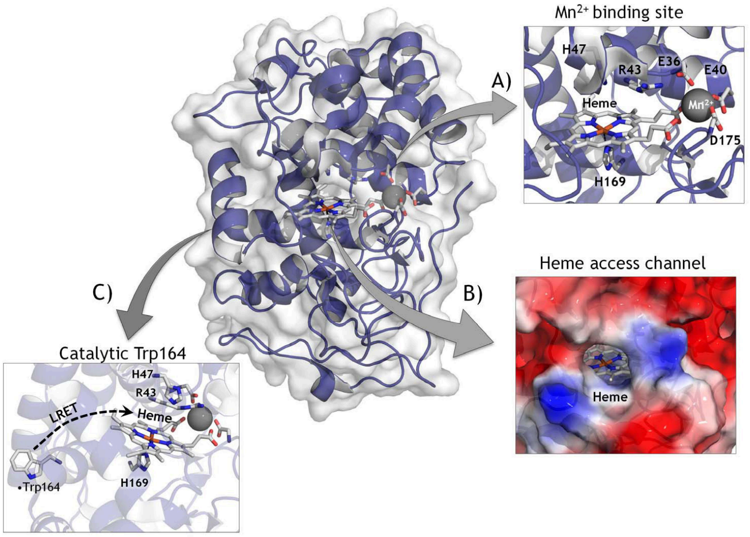

Figure 2. Overview of Versatile Peroxidase from *Pleurotus eryngii* (PDB ID: 3FJW). Heme prostetic group and catalytic residues are shown as sticks in CPK color. The three catalytic sites are shown in detail. (A) The Mn^{2+} binding site (Mn^{2+}, black sphere), the distal and proximal His (His47 and His169) the Arg43 involved in H_2O_2 reduction and the coordinating triad (Glu36, Glu40, Asp175) are depicted. (B) Heme access channel represented as electrostatics surface with heme group (stick mode) at the bottom of channel. (C) Catalytic Trp164 (LRET; long range electron transfer).
doi:10.1371/journal.pone.0090919.g002

dense production and traffic of free radicals jeopardizes the enzyme's stability and function, (**Figure 2**) [34,36].

To identify what are potentially the most H_2O_2-sensitive regions of the VP, we performed a multiple structural alignment using high- and medium-redox potential peroxidases with improved oxidative stability [39,41–43], (**Figure 3**). After careful examination of the model, three different regions (of 26, 30 and 69 amino acids each, excluding the recombination areas) in the vicinity of the heme group were targeted for random mutagenesis and recombination, (**Figures S1, S2**). The first region subjected to MORPHING was the distal His environment (L28-G57) that contains the H_2O_2 binding site within a helix that is highly conserved in all high-redox potential peroxidases. The second target region was the proximal His environment (L149-A174) located on the opposite side to the distal His, in the surroundings of the heme domain. The third region was the Met environment (I199-L268), containing three of the five putative oxidizable Met in the VP-R4 variant. Several mutational loads were assayed for each region to construct independent mutant libraries and then explore them for oxidative stability. Mutational loads were adjusted by modifying the PCR conditions in order to introduce 1 to 5 mutations per segment (including the crossover areas). The frequencies of mutation were estimated from different landscapes of mutant libraries (500 clones each), calculating the number of clones with <10% of the parental enzyme activity, and they were further verified by DNA sequencing of a random sample of mutants including active and non-active variants (**Figure 4**). Overall, an average value of T_s of 65% (A↔G, 52%; T↔C, 13%) and T_v of 35% (T↔A, 17.4%; A↔C, 8.8%; G↔C, 8.8%) was observed in the libraries under study (*i.e.* T_s/T_v ratio~1.8). Mutational frequencies of 0.5 nucleotide changes/100 bp were obtained with T_s G→A when $[MnCl_2] \leq 0.1$ mM, regardless of the DNA template concentration. In segments as short as 30 residues long (*e.g.*, the distal His environment: L28-G57), we obtained high mutational loads at $[MnCl_2] > 0.1$ mM (frequencies of ~3 mutations/100 bp). Among the high mutational variants, the 1E11 ($2T_s$, $3T_v$) and 2G4 ($3T_s$, $2T_v$) mutants incorporated 5 mutations each that inactivated the protein due to the highly conserved nature of this region (**Figure 5**).

After the initial screening and three consecutive re-screenings, several mutants with an improved increment in apparent half-life ($\Delta t_{1/2}$ *vs* H_2O_2) were identified. We found two beneficial mutations at the L28-G57 segment. The 3G10 variant showed a 2.1-fold improvement in stability *vs* H_2O_2, with a significant $\Delta t_{1/2}$ *vs* H_2O_2 of 18 min with respect to the parental type and a 5.5°C increase in the T_{50} (the temperature at which the enzyme retains 50% of its

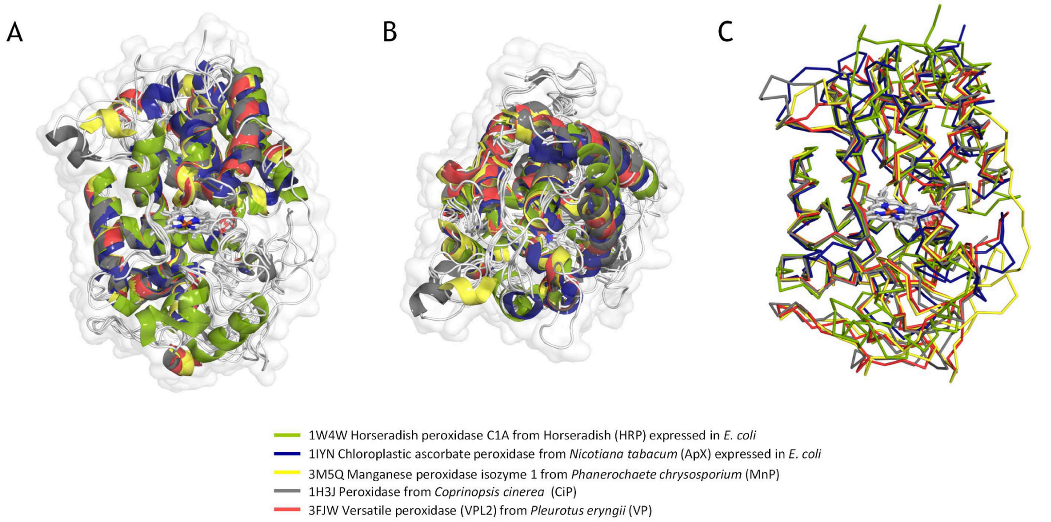

D

IDENTITY (%)

Enzyme	R4	CiP	MnP	HRP	ApX
R4	100	-	-	-	-
CiP	31.1	100	-	-	-
MnP	75.6	28.3	100	-	-
HRP	55.2	8.7	52.2	100	-
ApX	59.2	14.3	57.1	62.2	100

SIMILARITY (%)

Enzyme	R4	CiP	MnP	HRP	ApX
R4	100	-	-	-	-
CiP	37.9	100	-	-	-
MnP	80.2	33.8	100	-	-
HRP	59.5	13	56.7	100	-
ApX	63.4	18.8	61.6	66.3	100

Figure 3. Structural alignment for oxidative stability. (A, B) Front and upper view (cartoon) with the protein surfaces shown in white. (C) Structural alignment in ribbon mode. The prosthetic heme group is highlighted in CPK colors. (D) Identities and similarities for each protein scaffold using the following PDB entries for the analysis: 1W4W, horseradish peroxidase C1A (HRP) expressed in *E. coli* (green); 1IYN, chloroplastic ascorbate peroxidase (ApX) from *Nicotiana tabacum* expressed in *E. coli* (blue); 3M5Q, manganese peroxidase isozyme 1 (MnP) from *Phanerochaete chrysosporium* (yellow); 1H3J, peroxidase from *Coprinopsis cinerea* CiP (gray); and 3FJW, Versatile peroxidase (VPL2) from *Pleurotus eryngii* (red).
doi:10.1371/journal.pone.0090919.g003

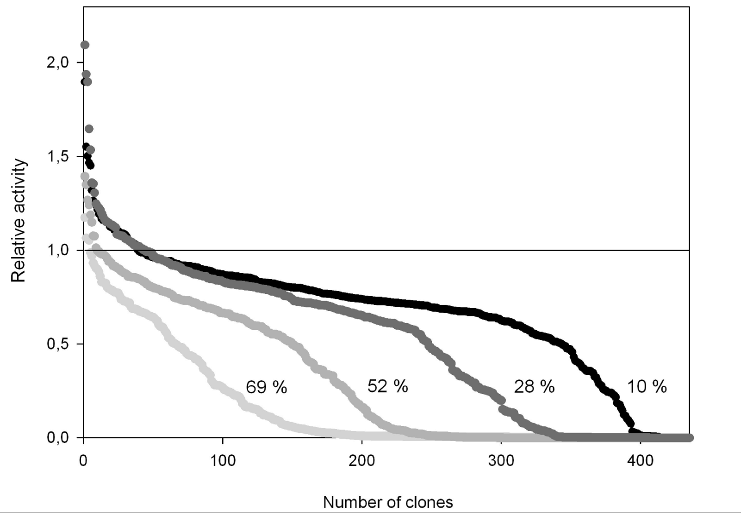

Figure 4. Mutagenic landscapes of the distal His environment (L28-G57) generated using 0.92 ng/µL of DNA template, and 0.01 mM (black), 0.1 mM (dark gray), 0.2 mM (medium gray), 0.4 mM (light gray) of $MnCl_2$, respectively. The percentages indicate the number of clones having less than 10% of the parent enzyme's activity; the solid horizontal line indicating the parental activity in the assay.
doi:10.1371/journal.pone.0090919.g004

activity after a 10 min incubation, **Figure 6**). Only one mutation, $_{GAG}$E40K$_{AAG}$, was found in 3G10 and the same mutation was introduced in 2F5 and 5D1 variants. This mutational redundancy highlights the role of this specific alteration in generating oxidative stability in VP and significantly, the highly stable CiP contains a Lys residue at the same position [39], **Figure 5**. In VP, E40 is one of three acidic residues that form the Mn^{2+} binding site (**Figure 2**) and it is plausible that closing some of the protein inlets involved in the generation of free radicals may be beneficial for VP stability, albeit at the cost of compromising this catalytic site. The $_{ACT}$T45A$_{GCT}$ mutation was discovered in both the 1C12 and 2G8 mutants, the latter of which also contained the silent $_{GCT}$A61A$_{GCC}$ mutation (**Figure 5**). While the T45A mutation did not alter thermostability ($T_{50} = 59°C$), it conferred a 1.3-fold improvement in stability and it was associated with a $\Delta t_{1/2}$ *vs* H_2O_2 of ~10 min with respect to the parental type (**Figure 6**). The same amino acid (V53A according to CiP numbering) was introduced into the evolved CiP although without improving thermostability, **Figure 5** [39]. It is likely that the only effect of introducing an Ala at this position relates with the accessibility of H_2O_2 to the internal protein structure. The $_{CCT}$P141A$_{GCT}$ mutation in the 5A9 variant arose in the L149-A174 segment (proximal His environment). Situated at the heme entrance, Pro141 is a highly conserved residue in all fungal peroxidases. However, the P141A mutation resulted in a 1.4-fold improvement in oxidative stability, producing a $\Delta t_{1/2}$ *vs* H_2O_2 of ~5 min with respect to the parental type and no change in thermostability (**Figure 6**). P141A is located in a strictly conserved region and according to our model, the substitution of Ala by Pro may widen the heme channel making easier the traffic of oxidized species and therefore limiting their harmful residence time in the inner protein structure. To further study the possible synergies between beneficial mutations E40K, T45A and P141A, a triple variant was constructed by site-directed mutagenesis doubling the $\Delta t_{1/2}$ *vs* H_2O_2 to 45 min (data not shown). This mutant was the departure point to engineer an oxidative stable VP variant by successive rounds of *in vitro* evolution (unpublished material).

No mutants were discovered in the I199-L268 segment (the Met environment), suggesting that the three oxidizable methionines in this area are not involved in the oxidative stabilization of VP. This result was corroborated by subjecting Met262 and Met265 to combinatorial saturation mutagenesis and screening. No improved variants were identified in this way and ~95% of the clones were inactive in this mutagenic landscape, indicating that these residues are very sensitive and do not tolerate changes (**Figure S3**). Similarly, Met152 in the proximal His environment was not mutated.

In this first enzyme case study, MORPHING effectively identified new structural determinants, such as the P141A mutation, that are important for oxidative stability. Significantly, the identification of the E40K and T45A mutations was in good agreement with previous findings [39], thereby validating this approach. Although each mutated segment was analyzed independently by constructing small high-quality libraries with different mutational loads, it is also feasible that different combinations of mutated segments can be prepared using the yeast's recombination machinery.

Enhancing functional UPO expression

MORPHING was also used to assess whether the secretion levels of an unspecific peroxygenase (UPO) could be enhanced in *S. cerevisiae*. UPO (EC 1.11.2.1) is a new, potentially ligninolytic, peroxidase that has attracted much research attention due to its versatility and applicability in a variety of synthetic processes [35,44]. Its peroxygenative (oxygen-transfer) activity is of particular importance as UPO can behave as a self-sufficient monooxygenase to mediate regio- and enantio-selective oxyfunctionalizations that are essential for organic synthesis. Among the array of oxygen transfer reactions catalyzed by UPO are brominations, sulphoxidations, N-oxidations, aromatic peroxygenations, alkyl

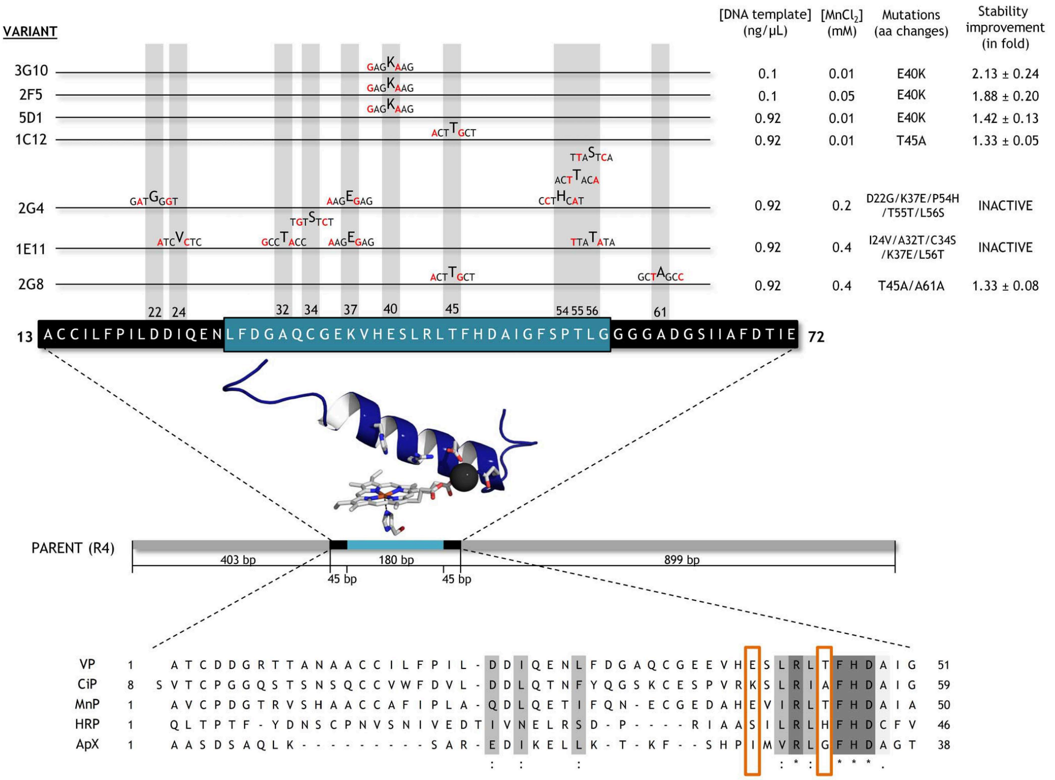

VARIANT	[DNA template] (ng/μL)	[MnCl$_2$] (mM)	Mutations (aa changes)	Stability improvement (in fold)
3G10	0.1	0.01	E40K	2.13 ± 0.24
2F5	0.1	0.05	E40K	1.88 ± 0.20
5D1	0.92	0.01	E40K	1.42 ± 0.13
1C12	0.92	0.01	T45A	1.33 ± 0.05
2G4	0.92	0.2	D22G/K37E/P54H /T55T/L56S	INACTIVE
1E11	0.92	0.4	I24V/A32T/C34S /K37E/L56T	INACTIVE
2G8	0.92	0.4	T45A/A61A	1.33 ± 0.08

Figure 5. Mutational loads, PCR conditions and selected variants used for MORPHING of the distal His environment. Point mutations are highlighted in red and the overhangs in black. Improvements in oxidative stability are indicated as the fold increase with respect to the parental type at a [H_2O_2]/[Enzyme] ratio of 3,000:1. Sequence alignments with stable peroxidase scaffolds are depicted, framing the mutations at positions 40 and 45 for VP and 53 and 48 for CiP, respectively. The MSA (multiple sequence alignment) was generated with T-coffee software: http://www.igs.cnrs-mrs.fr/Tcoffee/tcoffee_cgi/index.cgi.
doi:10.1371/journal.pone.0090919.g005

hydroxylations, double bond epoxidations and ether cleavages. Like many other ligninolytic oxidoreductases, UPO is not readily expressed in heterologous hosts so that it can be tailored by directed evolution and therefore, we recently addressed this problem by subjecting the whole UPO gene to several rounds of random mutagenesis, recombination and screening in *S. cerevisiae* (unpublished data). To further enhance the secretion of this protein, we used MORPHING to independently evolve the 43 amino acid UPO signal peptide in order to enrich the signal leader in beneficial mutations without altering the biochemical properties of the enzyme. To reliably compare the two directed evolution strategies, we exposed the signal peptide alone and the entire UPO gene (including its signal leader) to one round of directed evolution in two parallel experiments. Mutational rates for the leader library and the full-gene library were 0.5 and 0.1 nucleotide changes/100 bp, respectively. Both libraries were screened with the help of an ad-hoc dual-colorimetric assay to estimate the enzymes peroxidase (with ABTS) and peroxygenase (with NBD) activities. The mutagenic landscape generated by MORPHING revealed an increased tolerance to mutations in the signal peptide than in the whole UPO gene. Indeed, we found that when random mutagenesis of the leader and the whole UPO gene was compared, 30% and 49% of clones had <10% of parental enzyme activity on ABTS as a substrate, respectively (**Figure 7**). These results are consistent with the fact that mutations in the leader sequence only affect secretion, whereas those in the whole UPO gene may also compromise the catalytic properties. While no variants carrying mutations in the leader were identified in the whole UPO gene after one round of evolution, several independent but almost consecutive mutations were observed in three independent beneficial variants after MORPHING of the leader sequence (${}_{TTC}$F12Y${}_{TAC}$, ${}_{GCC}$A14V${}_{GTG}$ and ${}_{AGG}$R15G${}_{GGG}$). Each of these mutations individually enhanced secretion by ~20% with respect to the parental type. Although MORPHING was useful to unmask these beneficial mutations for secretion, the eukaryotic machinery of *S. cerevisiae* was unable to join these positions by homologous recombination due to their proximity. Therefore, we constructed a signal peptide containing the full set of these mutations by conventional site-directed mutagenesis looking for a synergic effect in secretion levels. The evolved signal peptide also included the beneficial mutation ${}_{GCC}$A21D${}_{GAC}$ (discovered in the earlier stages of evolution). Finally, the signal peptide of native

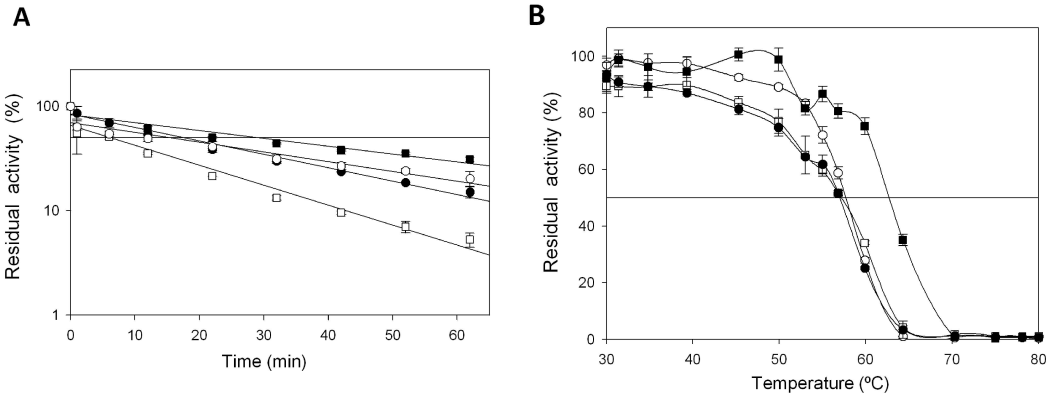

Figure 6. (A) Apparent $t_{1/2}$ *vs* H_2O_2 for the R4 parental type, 5A9 mutant (P141A), 1C12 mutant (T45A) and 3G10 mutant (E40K) in the presence of 3,000 equivalents of H_2O_2. Horizontal line indicates 50% of residual activity. (B) T_{50} profiles (kinetic thermostability) of VP variants. White squares, R4 parental type; white circle, 5A9 mutant (P141A); black squares, 3G10 mutant (E40K); black circles, 1C12 mutant (T45A). Each point represents the mean and standard deviation of three independent experiments.
doi:10.1371/journal.pone.0090919.g006

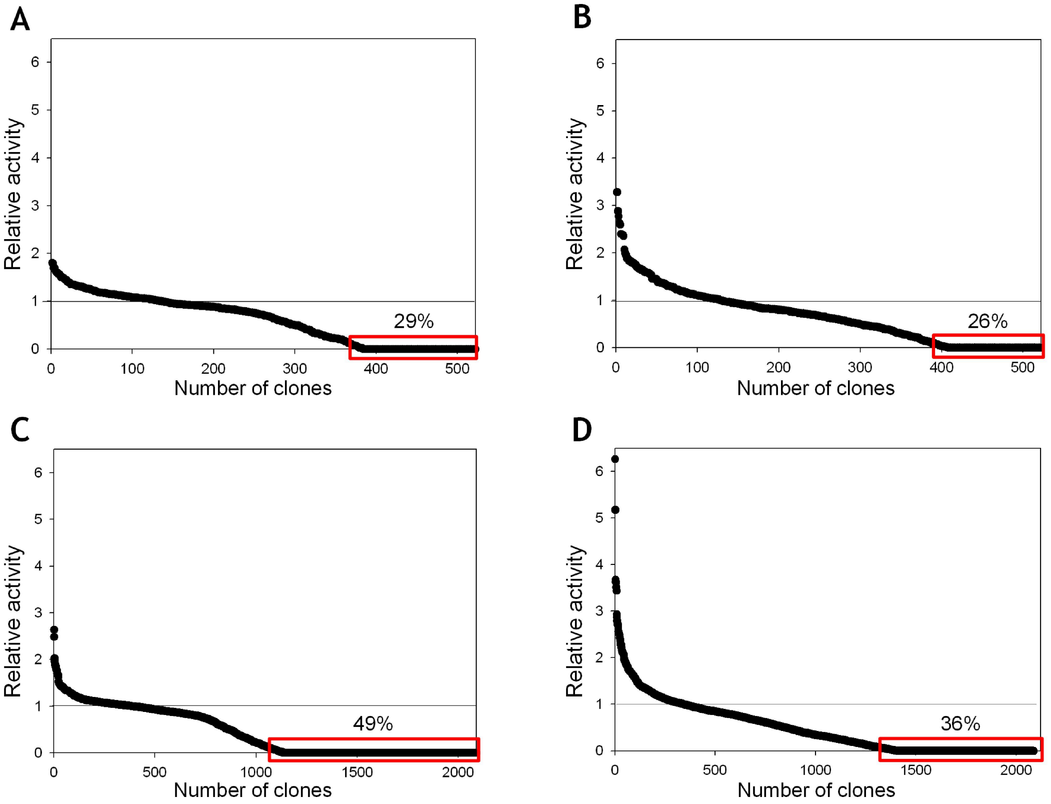

Figure 7. Mutagenic landscapes for MORPHING of the signal peptide of UPO using ABTS (A) and NBD (B) in colorimetric assays. Directed evolution landscapes of the whole UPO gene obtained with ABTS (C) and NBD (D) assays. The activity of the clones is plotted in descending order. The solid horizontal line indicates the activity of the parental type in the assay.
doi:10.1371/journal.pone.0090919.g007

UPO was replaced by the evolved signal peptide F12Y-A14V-R15G-A21D (see Materials and Methods for details), resulting in a 27-fold increase in total secretion compared to the native UPO fused to its original leader (~2±0.11 ABTS U/L and 54±5.7 ABTS U/L, respectively). F12Y-A14V-R15G-A21D mutations are located at the hydrophobic core of the leader and they may exert a beneficial effect on secretion by promoting a more suited interaction with the signal recognition particle during translocation to the endoplasmic reticulum.

This second case study demonstrates that the use of our focused mutagenesis method to direct the evolution of signal leaders is a suitable approach to promote heterologous functional expression of complex eukaryotic genes in yeast. Targeting mutational loads to leader sequences is a simple means of detecting mutations that are beneficial for secretion and that can be subsequently combined in a single signal peptide to generate potential synergies along the *S. cerevisiae* secretory pathway.

Conclusions

The random domain mutagenesis/recombination method presented here is a reliable *one-pot* approach for the construction of focused mutant libraries of eukaryotic genes in *S. cerevisiae*. In general terms, MORPHING allows the researcher to focus exclusively on the random introduction of mutations and their recombination in restricted region/s, while protecting critical domains from mutagenesis. The selection of the target regions to be evolved is as important as the mutational loads chosen for each mutant library, which can be easily varied to enrich the target segments in beneficial mutations.

The two case studies presented here validate the versatility of our method by tackling two distinct problems. While MORPHING proved useful to explore limited targeted regions, allowing us to identify several structural determinants of H_2O_2 inhibition in VP that could be applied to other high redox-potential fungal peroxidases, it also effectively decoupled secretion and catalytic activity for functional UPO expression. This approach can also be used to explore other complex problems, such as to alter substrate specificity or enantio-selectivity by subjecting several segments of the same gene to random mutagenesis, promoting their *in vivo* assembly in one transformation step. Indeed, this strategy is currently being used by our group to evolve a fungal aryl alcohol oxidase for the selective oxidation of different alcohols. Apart from structure-function relationship studies, MORPHING can be also useful when structural information is absent, *e.g.*, for the evolution of leader peptides for secretion, for the modification of promoters, or in the evolution of unknown regions of biochemical relevance that have been revealed by conventional directed evolution.

Additional advantages of this method include the reduction of the sequence space to be explored (good results can be achieved with small libraries of 400–500 clones), the conservation of certain catalytic properties while improving other traits, and the discovery of new structural/catalytic determinants that can be further optimized using focused saturation mutagenesis. The combination of MORPHING with classical directed evolution and semi-rational approaches, or with neutral genetic drift, may lead to the development of new adaptive pathways to engineer more robust eukaryotic enzymes in yeast [8,13,14].

Supporting Information

Figure S1 VP MORPHING. Three different regions of VP were targeted for random mutagenesis and recombination (L28-G57, L149-A174, and I199-L268). The VP gene is shown in blue, the α-factor prepro-leader to promote secretion in yeast in red and the shuttle vector in green. The areas of crossover between the fragments are represented by crosses. The overlapping areas between segments were created by superimposing PCR reactions in defined regions (see also **Figure S2** and **Table S1**).
(TIF)

Figure S2 Selected areas of VP subjected to MORPHING: proximal His environment (red), Met environment (yellow), and distal His environment (blue). The heme domain is depicted in stick mode and CPK colors. The amino acids delimiting mutated regions and the most relevant residues are highlighted (proximal and distal histidines; Mn^{2+} binding pocket with manganese represented as a grey sphere).
(TIF)

Figure S3 Combinatorial saturation mutagenesis landscapes at positions 262 and 265 of VP. Clone activity is plotted in descending order. The solid horizontal line indicates the activity of the parental type in the assay.
(TIF)

Table S1 Oligos used for VP and UPO MORPHING. The lengths of the PCR products and the overlapping areas are shown. NNS and SNN indicate NN(G/C) and (G/C)NN codons for the saturation mutagenesis libraries. CSM, combinatorial saturation mutagenesis; UPOsp, UPO signal peptide; IvAM, *In vivo* Assembly of Mutant libraries for the directed evolution of the whole UPO gene; epPCR, error-prone PCR; HF-PCR, high-fidelity PCR.
(TIF)

Acknowledgments

The authors thank A. T. Martínez, F. J. García-Dueñas (Centro de Investigaciones Biológicas, CIB-CSIC, Madrid, Spain) and M. Hofrichter (International Graduate School of Zittau, IHIZ, Germany) for helpful discussions.

Author Contributions

Conceived and designed the experiments: MA. Performed the experiments: DGP PME EGR. Analyzed the data: DGP PME EGR MA. Contributed reagents/materials/analysis tools: PME EGR DGP. Wrote the paper: MA.

References

1. Bershtein S, Tawfik DS (2008) Advances in laboratory evolution of enzymes. Curr Opin Chem Biol 12: 151–158.
2. Bloom JD, Arnold FH (2009) In the light of directed evolution: pathways of adaptive protein evolution. Proc Natl Acad Sci U S A 106 Suppl 1: 9995–10000.
3. Cobb RE, Si T, Zhao H (2012) Directed evolution: an evolving and enabling synthetic biology tool. Curr Opin Chem Biol 16: 285–291.
4. Romero PA, Arnold FH (2009) Exploring protein fitness landscapes by directed evolution. Nat Rev Mol Cell Biol 10: 866–876.
5. Tracewell CA, Arnold FH (2009) Directed enzyme evolution: climbing fitness peaks one amino acid at a time. Curr Opin Chem Biol 13: 3–9.
6. Lutz S (2010) Beyond directed evolution-semi-rational protein engineering and design. Curr Opin Biotechnol 21: 734–743.
7. Wong TS, Roccatano D, Schwaneberg U (2007) Steering directed protein evolution: strategies to manage combinatorial complexity of mutant libraries. Environ Microbiol 9: 2645–2659.
8. Gupta RD, Tawfik DS (2008) Directed enzyme evolution via small and effective neutral drift libraries. Nat Methods 5: 939–942.
9. Peisajovich SG, Tawfik DS (2007) Protein engineers turned evolutionists. Nat Methods 4: 991–994.
10. Bloom JD, Romero PA, Lu Z, Arnold FH (2007) Neutral genetic drift can alter promiscuous protein functions, potentially aiding functional evolution. Biol Direct 2: 17.
11. Bloom JD, Lu Z, Chen D, Raval A, Venturelli OS, et al. (2007) Evolution favors protein mutational robustness in sufficiently large populations. BMC Biol 5: 29.

12. Voloshchuk N, Montclare JK (2010) Incorporation of unnatural amino acids for synthetic biology. Mol Biosyst 6: 65–80.
13. Dalby PA (2011) Strategy and success for the directed evolution of enzymes. Curr Opin Struct Biol 21: 473–480.
14. Goldsmith M, Tawfik DS (2013) Enzyme engineering by targeted libraries. Methods Enzymol 523: 257–283.
15. Shivange AV, Marienhagen J, Mundhada H, Schenk A, Schwaneberg U (2009) Advances in generating functional diversity for directed protein evolution. Curr Opin Chem Biol 13: 19–25.
16. Reetz MT, Bocola M, Carballeira JD, Zha D, Vogel A (2005) Expanding the range of substrate acceptance of enzymes: combinatorial active-site saturation test. Angew Chem Int Ed Engl 44: 4192–4196.
17. Reetz MT, Carballeira JD (2007) Iterative saturation mutagenesis (ISM) for rapid directed evolution of functional enzymes. Nat Protoc 2: 891–903.
18. Alcolombri U, Elias M, Tawfik DS (2011) Directed evolution of sulfotransferases and paraoxonases by ancestral libraries. J Mol Biol 411: 837–853.
19. Hidalgo A, Schliessmann A, Molina R, Hermoso J, Bornscheuer UT (2008) A one-pot, simple methodology for cassette randomisation and recombination for focused directed evolution. Protein Eng Des Sel 21: 567–576.
20. Herman A, Tawfik DS (2007) Incorporating Synthetic Oligonucleotides via Gene Reassembly (ISOR): a versatile tool for generating targeted libraries. Protein Eng Des Sel 20: 219–226.
21. Hong KK, Nielsen J (2012) Metabolic engineering of *Saccharomyces cerevisiae*: a key cell factory platform for future biorefineries. Cell Mol Life Sci 69: 2671–2690.
22. Krivoruchko A, Siewers V, Nielsen J (2011) Opportunities for yeast metabolic engineering: Lessons from synthetic biology. Biotechnol J 6: 262–276.
23. Nevoigt E. (2008) Progress in metabolic engineering of *Saccharomyces cerevisiae*. Microbiol Mol Biol Rev 72: 379–412.
24. Da Silva NA, Srikrishnan S (2012) Introduction and expression of genes for metabolic engineering applications in *Saccharomyces cerevisiae*. FEMS Yeast Res 12: 197–214.
25. Alcalde M (2010) Mutagenesis protocols in *Saccharomyces cerevisiae* by In Vivo Overlap Extension. Methods Mol Biol 634: 3–14.
26. Ostrov N, Wingler LM, Cornish W (2013) Gene assembly and combinatorial libraries in *S. cerevisiae* via reiterative recombination. Methods Mol Biol 978: 187–203.
27. Zumarraga M, Camarero S, Shleev S, Martinez-Arias A, Ballesteros A, et al. (2008) Altering the laccase functionality by in vivo assembly of mutant libraries with different mutational spectra. Proteins 71: 250–260.
28. Shao Z, Zhao H, Zhao H (2009) DNA assembler, an in vivo genetic method for rapid construction of biochemical pathways. Nucleic Acids Res 37: e16.
29. Pompon D, Nicolas A (1989) Protein engineering by cDNA recombination in yeasts: shuffling of mammalian cytochrome P-450 functions. Gene 15;83(1): 15–24
30. Wingler LM, Cornish VW (2011) Reiterative Recombination for the *in vivo* assembly of libraries of multigene pathways. Proc Natl Acad Sci 13:15135–40.
31. Gonzalez-Perez D, Garcia-Ruiz E, Alcalde M (2012) *Saccharomyces cerevisiae* in directed evolution: An efficient tool to improve enzymes. Bioeng. Bugs 3: 172–177.
32. Wang T, Ma X, Zhu H, Li A, Du G, Chen J (2012) Available methods for assembling expression cassettes for synthetic biology. Appl Microbiol Biotechnol 93: 1853–1863.
33. Finney-Manchester SP, Maheshri N (2013) Harnessing mutagenic homologous recombination for targeted mutagenesis in vivo by TaGTEAM. Nucleic Acids Res 41: e99.
34. Ruiz-Dueñas FJ, Morales M, Garcia E, Miki Y, Martinez MJ, et al. (2009) Substrate oxidation sites in versatile peroxidase and other basidiomycete peroxidases. J. Exp. Bot 60: 441–452.
35. Hofrichter M, Ullrich R (2006) Heme-thiolate haloperoxidases: versatile biocatalysts with biotechnological and environmental significance. Appl Microbiol Biotechnol 71: 276–288.
36. Garcia-Ruiz E, Gonzalez-Perez D, Ruiz-Duenas FJ, Martinez AT, Alcalde M (2012) Directed evolution of a temperature-, peroxide- and alkaline pH-tolerant versatile peroxidase. Biochem J 441: 487–498.
37. Pecyna MJ, Ullrich R, Bittner B, Clemens A, Scheibner K, et al. (2009) Molecular characterization of aromatic peroxygenase from *Agrocybe aegerita*. Appl Microbiol Biotechnol 84: 885–897.
38. Wong TS, Zhurina D, Schwaneberg U (2006) The diversity challenge in directed protein evolution. Comb Chem High Throughput Screen 9(4):271–88
39. Cherry JR, Lamsa MH, Schneider P, Vind J, Svendsen A, et al. (1999) Directed evolution of a fungal peroxidase. Nat Biotechnol 17: 379–384.
40. Valderrama B, Ayala M, Vazquez-Duhalt R (2002) Suicide inactivation of peroxidases and the challenge of engineering more robust enzymes. Chem Biol 9: 555–565.
41. Miyazaki-Imamura C, Ohira K, Kitagawa R, Nakano H, Yamane T, Takahashi H (2003) Improvement of H_2O_2 stability of manganese peroxidase by combinatorial mutagenesis and high-throughput screening using in vitro expression with protein disulfide isomerase. Protein Eng 16: 423–428.
42. Ryan BJ, O'Fagain C (2007) Effects of single mutations on the stability of horseradish peroxidase to hydrogen peroxide. Biochimie 89: 1029–1032.
43. Kitajima S, Kitamura M, Koja N (2008) Triple mutation of Cys26, Trp35, and Cys126 in stromal ascorbate peroxidase confers H_2O_2 tolerance comparable to that of the cytosolic isoform. Biochem Biophys Res Commun 372: 918–923.
44. Hofrichter M, Ullrich R, Pecyna MJ, Liers C, Lundell T (2010) New and classic families of secreted fungal heme peroxidases. Appl Microbiol Biotechnol 87: 871–897.

Supplemental data chapter 4

Mutagenic Organized Recombination Process by Homologous In vivo Grouping (MORPHING) for directed evolution

Authors:, González-Perez, D., Molina-Espeja, P., Garcia-Ruiz, E., and Alcalde, M.

Plos one (2014) **9**, e90919.

Figure S1

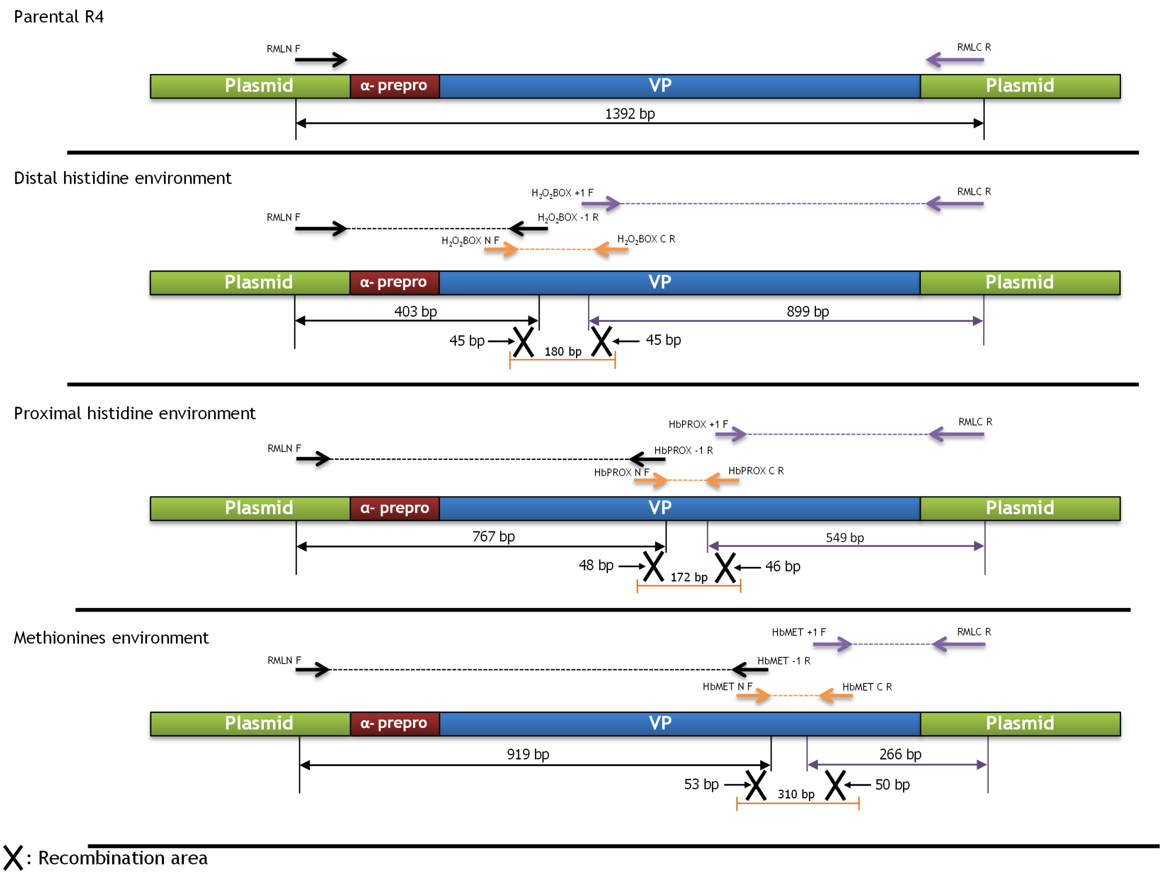

VP MORPHING. Three different regions of VP were targeted for random mutagenesis and recombination (L28-G57, L149-A174, and I199-L268). The VP gene is shown in blue, the α-factor prepro-leader to promote secretion in yeast in red and the shuttle vector in green. The areas of crossover between the fragments are represented by crosses. The overlapping areas between segments were created by superimposing PCR reactions in defined regions (see also **Figure S2** and **Table S1**).

Figure S2

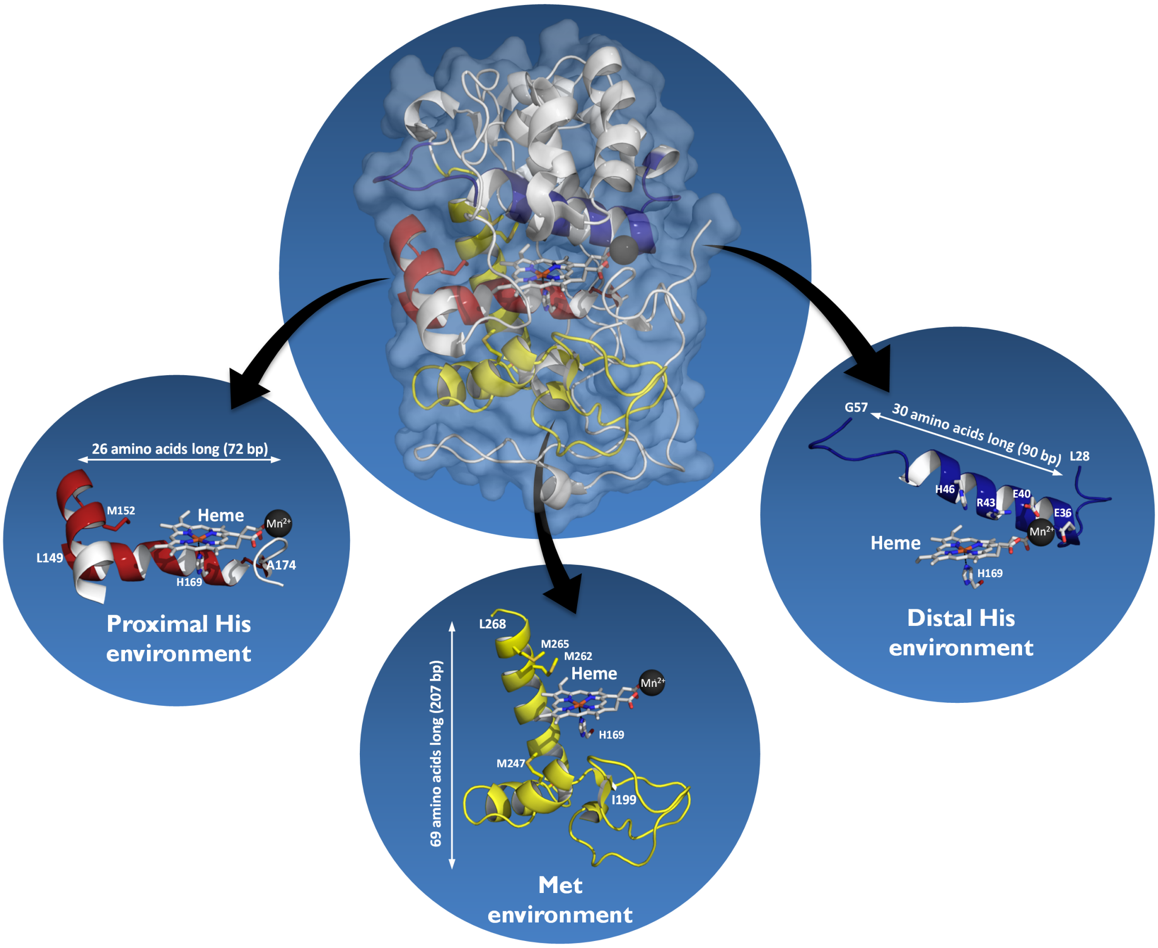

Selected areas of VP subjected to MORPHING: proximal His environment (red), Met environment (yellow), and distal His environment (blue). The heme domain is depicted in stick mode and CPK colors. The amino acids delimiting mutated regions and the most relevant residues are highlighted (proximal and distal histidines; Mn^{2+} binding pocket with manganese represented as a grey sphere).

Figure S3

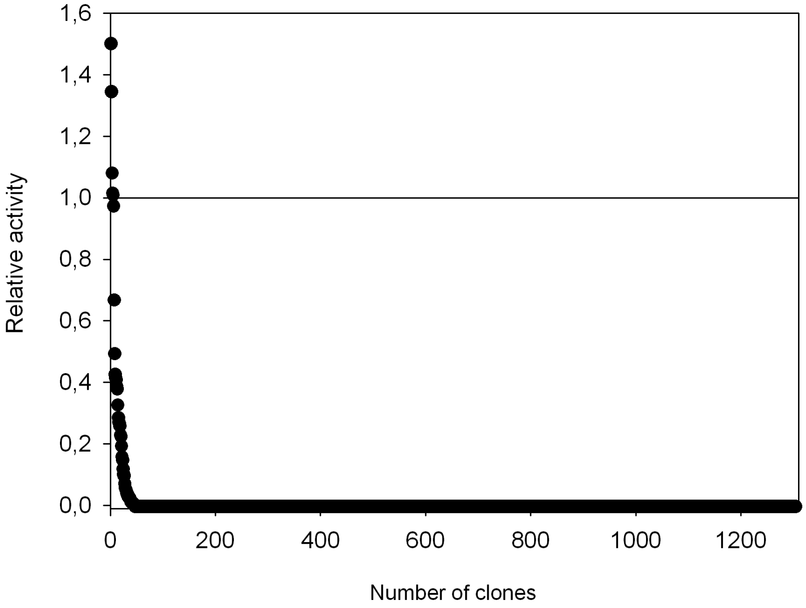

Combinatorial saturation mutagenesis landscapes at positions 262 and 265 of VP. Clone activity is plotted in descending order. The solid horizontal line indicates the activity of the parental type in the assay.

Table S1

Region	Primer name	Sequence	Tm (°C)	Base pair (bp)	Mutagenesis (*ep*PCR/HF-PCR)	PCR Product length (bp)	Overlapping areas (bp)
Distal His environment	RMLN F	5'-CCTCTATACTTTAACGTCAAGG-3'	51.1	22	NO	403	
	H_2O_2BOX -1 R	5'-GTTTTCTTGGATGTCATCGAGG-3'	50.5	21			45
	H_2O_2BOX N F	5'-GCATGTTGCATTCTGTTCCCCATCCTC-3'	61.3	27	YES	180	
	H_2O_2BOX C R	5'-CTCAATGGTGTCGAACGCGATGATGG-3'	61.0	26			45
	H_2O_2BOX +1 F	5'-GGAGGAGGAGCTGACGGTTC-3'	56.3	21	NO	899	
	RMLC R	5'-GGGAGGGCGTGAATGTAAGC-3'	55.9	20			
Proximal His environment	RMLN F	5'-CCTCTATACTTTAACGTCAAGG-3'	51.1	22	NO	767	
	HbPROX -1 R	5'-GAATGGAGTCAACAGAATCAAAAG-3'	52.3	24			48
	HbPROX N F	5'-TCCCCGGACCACCTCGTG-3'	57.2	18	YES	172	
	HbPROX C R	5'-GGGTTGAATCGAATGGCATTCCAG-3'	57.4	24			46
	HbPROX +1 F	5'-CGACAAGGTTGACCCATCGATTC-3'	57.1	23	NO	549	
	RMLC R	5'-GGGAGGGCGTGAATGTAAGC-3'	55.9	20			
Met environment	RMLN F	5'-CCTCTATACTTTAACGTCAAGG-3'	51.1	22	NO	919	
	HbMET -1 R	5'-GATGAAGAATTGAGAATCAAAAACTC-3'	51.7	26			52
	HbMET N F	5'-CTGGAATGCCATTCGATTCAACCCCC-3'	61.1	26	YES	310	
	HbMET C R	5'-GGGGTGGGGATAACATCGGAACAGTC-3'	62.7	26			50
	HbMET +1 F	5'-GGCCAAGACAAGACCAAATTGATTG-3'	56.0	25	NO	266	
	RMLC R	5'-GGGAGGGCGTGAATGTAAGC-3'	55.9	20			
CSM (M262/M265)	RMLN F	5'-CCTCTATACTTTAACGTCAAGG-3'	51.1	22	NO	1,141	
	MET SAT R	5'-GGTCTTGTCTTGGCCAAGAAGAGC**SNN**CTT CGA**SNN**GGTAGCAGCGAAACGGTTCTGAATC-3'	76.1	61			49
	MET SAT F	5'-GATTCAGAACCGTTTCGCTGCTACC**NNS**TCG AAG**NNS**GCTCTTCTTGGCCAAGACAAGACC-3'	76.1	61	NO	312	
	RMLC R	5'-GGGAGGGCGTGAATGTAAGC-3'	55.9	20			
MORPHING UPOsp	RMLN F	5'-CCTCTATACTTTAACGTCAAGG-3'	51.1	22	YES	210	
	MORPH SP R	5'-CAGAGCTATTCTCGAGAGGA-3'	50.7	20			40
	MORPH SP D	5'-GAGCCAGGATTACCTCCTGG-3'	57.7	20	NO	1,061	
	RMLC R	5'-GGGAGGGCGTGAATGTAAGC-3'	55.9	20			
IvAM	RMLN F	5'-CCTCTATACTTTAACGTCAAGG-3'	51.1	22	YES	1,231	
	RMLC R	5'-GGGAGGGCGTGAATGTAAGC-3'	55.9	20			
Evolved signal peptide and fusion gene	RMLN F	5'-CCTCTATACTTTAACGTCAAGG-3'	51.1	22	NO	104	
	SP* R	5'-CCTGTTCCCAACCTTGGTCTACGC AGTGGGGGTCGTTGCTTTTCCTGAC-3'	74.6	49			49
	SP* F	5'-CCTGTTCCCAACCTTGGTCTACGC AGTGGGGGTCGTTGCTTTTCCTGAC-3'	74.6	49	NO	1,176	
	RMLC R	5'-GGGAGGGCGTGAATGTAAGC-3'	55.9	20			

Oligos used for VP and UPO MORPHING. The lengths of the PCR products and the overlapping areas are shown. NNS and SNN indicate NN(G/C) and (G/C)NN codons for the saturation mutagenesis libraries. CSM, combinatorial saturation mutagenesis; UPOsp, UPO signal peptide; IvAM, *In vivo* Assembly of Mutant libraries for the directed evolution of the whole UPO gene; epPCR, error-prone PCR; HF-PCR, high-fidelity PCR.

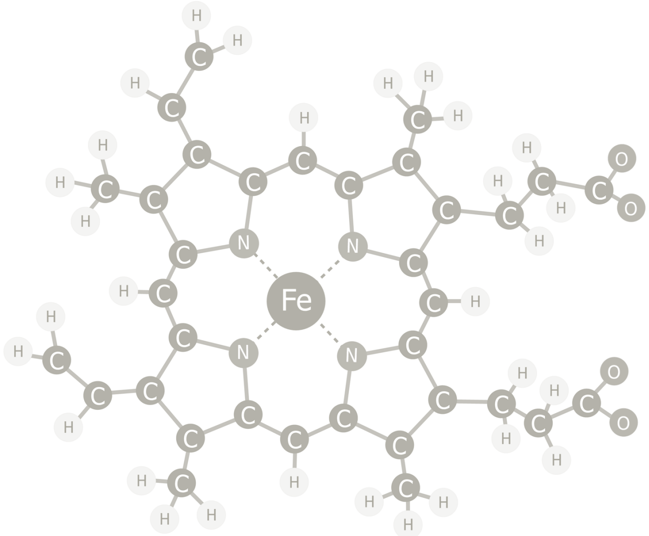

Capítulo 5:

Alkaline versatile peroxidase by directed evolution

En este capítulo se describe la obtención de una peroxidasa versátil que es activa y estable en un amplio intervalo de pH siendo la primera peroxidasa ligninolítica con estos atributos, incluyendo activación e hiperactivación alcalina, así como oxidación directa en el sitio de manganeso entre otras propiedades relevantes.

Catalysis Science & Technology

PAPER

Cite this: *Catal. Sci. Technol.*, 2016, **6**, 6625

Alkaline versatile peroxidase by directed evolution†

David Gonzalez-Perez,[a] Ivan Mateljak,[a] Eva Garcia-Ruiz,[b]
Francisco J. Ruiz-Dueñas,[c] Angel T. Martinez[c] and Miguel Alcalde*[a]

Received 12th May 2016,
Accepted 10th June 2016

DOI: 10.1039/c6cy01044j

www.rsc.org/catalysis

Ligninolytic peroxidases are involved in natural wood decay in strict acid environments. Despite their biotechnological interest, these high-redox potential enzymes are not functional at basic pH due to the loss of calcium ions that affects their structural integrity. In this study, we have built catalytic activity at basic pH in a versatile peroxidase (VP) previously engineered for thermostability. By using laboratory evolution and hybrid approaches, we designed an active and highly stable alkaline VP while the catalytic bases behind the alkaline activation were unveiled. A stabilizing mutational backbone allowed the pentacoordinated heme state to be maintained, and the new alkaline mutations hyperactivated the enzyme after incubation at basic pHs. The final mutant oxidises substrates at alkaline pHs both at the heme channel and at the Mn^{2+} site, while the catalytic tryptophan was not operational under these conditions. Mutations identified in this work could be transferred to other ligninolytic peroxidases for alkaline activation.

1. Introduction

The ligninolytic secretome from basidiomycete white-rot fungi is responsible for carbon recycling in land ecosystems.[1,2] Mostly formed by high-redox potential oxidoreductases (peroxidases and laccases), along with enzymes supplying H_2O_2 and diffusible redox active species, this consortium decomposes lignin through a complex cascade of reactions that are carried out in a strict acid environment (pH ~3 due to the release of organic acids from fungal metabolism).[3,4] Within this efficient oxidative system, high-redox potential peroxidases play a fundamental role. Indeed, it has been recently reported that the primitive ancestry of these enzymes links them to the end of coal deposits on earth during the later Carboniferous era.[5,6] Currently, they are classified in class II (secreted fungal peroxidases) of the peroxidase–catalase superfamily that is made up of manganese peroxidases (MnPs, EC 1.11.1.13), lignin peroxidases (LiPs, EC 1.11.1.14) and versatile peroxidases (VPs, EC 1.11.1.16).[7,8] Of these, the latter are considered by far the most promiscuous peroxidases found in nature due to their high redox potential (+1.4 V) and broad substrate range.[9]

The one-electron oxidation reactions carried out by VP involve three different oxidation sites and several catalytic intermediates for the transformation of low-, medium- and high-redox potential compounds.[10] Within a compact and rather small protein structure that is enriched in α-helices (~300 residues tightly packed through four disulphide bridges and two embedded structural calcium cations) VP contains a heme group with a main access channel – 9 Å in diameter – that is involved in the oxidation of low-redox potential compounds; a Mn^{2+} binding site governed by three carboxylic residues for the oxidation of Mn^{2+} to Mn^{3+}; and a catalytic Trp at the protein surface, whose activated radical permits the oxidation of both low- and high-redox potential compounds at acid pH through a long-range electron transfer (LRET) pathway to the heme.[11–13] Thus, VP not only shares catalytic attributes with MnPs for the oxidation of Mn^{2+}, but it is also capable of oxidizing the redox mediator veratryl alcohol at the catalytic Trp (like LiPs) as well as several low-redox potential compounds at the heme access channel, like generic (low-redox potential) peroxidases (GPs, EC 1.11.1.7). In addition, and unlike LiPs, VP efficiently oxidizes several high-redox potential compounds at the catalytic Trp in the absence of veratryl alcohol, and also low-redox potential substrates with high efficiency. Recently, VP was shown to oxidize several lignosulfonates in the absence of mediators, which emphasizes its pivotal role within the ligninolytic consortium.[14] Taken together, these features make VP a quite interesting model for protein designers.

One of the most attractive and intriguing challenges in VP engineering, and indeed, that of all ligninolytic peroxidases

---

[a] *Department of Biocatalysis, Institute of Catalysis, CSIC, 28049 Madrid, Spain. E-mail: malcalde@icp.csic.es; Fax: +34 915854760; Tel: +34 915854806*
[b] *Department of Chemical and Biomolecular Engineering, University of Illinois at Urbana-Champaign, Urbana, IL 61801, USA*
[c] *Center for Biological Investigations, CSIC, Ramiro de Maeztu 9, 28040 Madrid, Spain*

† Electronic supplementary information (ESI) available. See DOI: 10.1039/c6cy01044j

reported to date, is to achieve activity and stability at alkaline pHs. These features would open VP up to several biomedical purposes from the synthesis of injectable hydrogels for tissue engineering and drug delivery to enhance the chemiluminiscence signal in luminol-dependent reactions for forensic, pharmaceutical and analytical applications.[2,15–18] It is well known that the integrity of VP strongly depends on the correct attachment of the two structural Ca^{2+} located above and below the plane of the heme (in the distal and proximal domains, respectively).[19,20] The distal Ca^{2+} is fairly accessible to the solvent and it is coordinated by 7 oxygen atoms, involving two water molecules and four amino acids. By contrast, the proximal Ca^{2+} is located deep in the protein structure and it is coordinated by 8 oxygen atoms from five surrounding residues. Any subtle modification in the coordination spheres of these two cations affects the heme morphology and compromises the enzyme's functionality. Several studies have shown that both neutral/basic pH and high temperature favour Ca^{2+} loss, mostly that of the distal Ca^{2+}, leading to the hexacoordination of the heme in a low spin state (bis-histidyl heme iron complex). In this situation the heme cavity collapses, inactivating the enzyme (a phenomenon also observed in LiPs and MnPs).[21–23]

We previously performed *in vitro* evolution on the VP from the edible mushroom *Pleurotus eryngii* to improve its functional expression and thermostability in *Saccharomyces cerevisiae*.[24] After 6 generations, we obtained a VP mutant (named 2-1B) that was readily secreted by yeast and that had an 8 °C improvement in its thermostability. Notably, the 2-1B mutant was also remarkably stable, yet not active, at basic pHs. Very recently, we demonstrated that the E37K-H39R-G330R mutations in the thermostabilizing backbone were responsible for this alkaline stability, establishing new contacts while abrogating destabilizing interactions, thereby reinforcing the pentacoordinated heme state at basic pHs to avoid the calcium leakage.[25] Although the 2-1B variant retains its overall structural integrity at basic pHs; it is not active even at a neutral pH. Hence, using the stable 2-1B variant as our departure point, we have now designed the first ligninolytic peroxidase that is active at alkaline pH. We performed several rounds of directed evolution and rational mutagenesis and the final mutant obtained was characterized exhaustively to unveil the catalytic determinants underlying this unprecedented improvement.

2. Experimental

All chemical reagents were of the highest purity commercially available. Culture media were prepared as described in the ESI.†

2.1 Laboratory evolution and rational mutagenesis

All PCR fragments were cleaned, concentrated, and loaded onto a low melting point preparative agarose gel (0.75% w/v) and purified. Mutant libraries were cloned under the control of GAL1 promoter of the pJRoC30 expression shuttle vector replacing the parent gene. The pJRoC30 plasmid was linearized with *Bam*HI and *Xho*I, and the linear plasmid was concentrated and purified as described above for the PCR fragments. The parental type 2-1B mutant was previously obtained as described elsewhere.[24]

2.1.1 Mutagenic PCR (1st and 2nd generations). Reaction mixtures were prepared in a final volume of 50 μL containing DNA template (0.1 ng μL^{-1}), 90 nM forward RMLN primer (5′-CCTCTATACTTTAACGTCAAGG-3′), 90 nM reverse RMLC primer (5′-GGGAGGGCGTGAATGTAAGC-3′), 0.3 mM dNTPs (0.075 mM each), 3% (v/v) dimethyl sulfoxide (DMSO), 1.5 mM $MgCl_2$, 0.01 mM $MnCl_2$ and 0.05 U μL^{-1} *Taq* polymerase. The error-prone PCR reactions were carried out in a gradient thermocycler (Mycycler, BioRad, USA) under the following conditions: 95 °C for 2 min (1 cycle); 94 °C for 45 s, 50 °C for 45 s, 72 °C for 2 min (28 cycles); and 72 °C for 10 min (1 cycle). The PCR product was purified and cleaned and 200 ng of total DNA was used to transform *S. cerevisiae* together with 100 ng of linearized plasmid (ratio library : vector, 2 : 1) using the Yeast Transformation Kit (Sigma-Aldrich, Madrid, Spain). Transformed cells were plated on SC drop-out plates and incubated for 3 days at 30 °C. Subsequently, the mutant library was screened using the HTS-protocol for activity (see below).

2.1.2 *In vivo* assembly of mutant libraries (IvAM, 3rd generation). We followed the protocol described before with minor modifications.[26] i) Mutagenic PCR1. Reaction mixtures were prepared in a final volume of 50 μL containing DNA template (0.1 ng μL^{-1} 5B9-1G mutant), 90 nM RMLN primer, 90 nM RMLC primer, 0.3 mM dNTPs (0.075 mM each), 3% (v/v) dimethyl sulfoxide (DMSO), 1.5 mM $MgCl_2$, 0.01 mM $MnCl_2$ and 0.05 U μL^{-1} *Taq* polymerase. ii) Mutagenic PCR2. Reaction mixtures were prepared in a final volume of 50 μL containing DNA template (50.42 ng μL^{-1} 9B3-2G mutant), 0.37 μM RMLN primer, 0.37 μM RMLC primer, 0.8 mM dNTPs (0.2 mM each), 3% (v/v) dimethyl sulfoxide (DMSO), and 0.05 U μL^{-1} Mutazyme II. Error-prone PCRs were carried out using the following parameters: 95 °C for 2 min (1 cycle); 95 °C for 45 s, 50 °C for 30 s, 72 °C for 1 min 30 s (28 cycles); and 72 °C for 10 min (1 cycle). iii) *In vivo* recombination of mutant libraries in *S. cerevisiae*. Mutant libraries from PCR1 and PCR2 were added in equimolar concentrations (200 ng each) to the linearized vector (100 ng). Transformed cells were plated on SC drop-out plates and incubated for 3 days at 30 °C. Thereafter, the mutant libraries were subjected to the HTS-screening protocol (see below).

2.1.3 Saturation mutagenesis at position 182. Reaction mixtures were prepared in a final volume of 50 μL containing DNA template (2 ng μL^{-1} BB-8-3G mutant), 1 mM dNTPs (0.25 mM each), 3% (v/v) dimethyl sulfoxide (DMSO), and 0.05 U μL^{-1} *Pfu* Ultra DNA polymerase. The primers used were 0.25 μM RMLN, 0.25 μM SM182-VP R (5′-GTTGAATCGAATGGCATTCC $\underline{\text{SNN}}$ AATCGATGGGTCAACCTTGT-3′) reverse primer for PCR 1; and 0.25 μM SM182-VP F (5′-ACAAGGTTGACCCATCGATT $\underline{\text{NNS}}$ GGAATGCCATTCGATTCAAC-3′) forward primer, 0.25 μM RMLC for PCR2. Degenerate codons (N = A, T, G, C; S = G, C) are highlighted in bold and underlined. PCRs were performed on a gradient using the following conditions: 95 °C for 2 min (1 cycle); 94 °C for 45 s, 50 °C for 45 s, 72 °C for 1 min (28 cycles); and 72 °C for 10 min (1 cycle). The whole gene was *in vivo* reassembled by IVOE,[27] transforming *S. cerevisiae* cells independently with 200 ng of each PCR product and 100 ng of linearized pJRoC30 plasmid. Yeast cells were plated on SC drop-out plates and incubated for 3 days at 30 °C. Thereafter, the mutant libraries were subjected to the HTS-protocol as described below.

2.1.4 Site-directed mutagenesis (E36L-D175L-A173I). The mutant was produced by site-directed mutagenesis through IVOE.[27] Because of the distance between mutations, a double mutant was firstly designed (E36L-D175L) and used as a template for introducing the A173I mutation. The reaction mixture was prepared in a final volume of 50 μL containing DNA template (2 ng μL^{-1} BB-8-3G mutant), 1 mM dNTPs (0.25 mM each), 3% (v/v) dimethyl sulfoxide (DMSO), and 0.05 U μL^{-1} *Pfu* Ultra DNA polymerase. The primers used for site-directed mutagenesis of the double mutant were 0.25 μM RMLN, 0.25 μM E36L R reverse primer (5′-CGAAGGGACTCGCGCACCTT **TAG** TCCACACTGGGCACCGTCGA) for PCR1; 0.25 μM E36L F forward primer (5′-TCGACGGTGCCCAGTGTGGA **CTA** AAGGTGCGCGAGTCCCTTCG), 0.25 μM D175L R reverse primer (5′-GAAATCGATGGGTCAACCTT **GAG** GGCAGCGGCAATGGAGTGCG) for PCR2; and 0.25 μM D175L F forward primer (5′-CGCACTCCATTGCCGCTGCC **CTC** AAGGTTGACCCATCGATTTC), 0.25 μM RMLC for PCR3. Mutated codons are underlined and in bold. The three PCRs were performed with the following conditions: 95 °C for 2 min (1 cycle); 94 °C for 45 s, 50 °C for 45 s, 72 °C for 1 min (28 cycles); and 72 °C for 10 min (1 cycle). The whole gene was *in vivo* reassembled, transforming *S. cerevisiae* cells with 200 ng of each PCR product and 100 ng of linearized pJRoC30. Yeast cells were plated on SC drop-out plates and incubated for 3 days at 30 °C. Thereafter, the plasmid was recovered from the cells and used as template for the following PCR reactions: 0.25 μM RMLN forward primer (5′-CCTCTATACTTTAACGTCAAGG), 0.25 μM A173I R reverse primer (5′-GATGGGTCAACCTTGAGGGC **AAT** GGCAATGGAGTGCGAAGCCAG) for PCR 4; and 0.25 μM A173I F forward primer (5′-CTGGCTTCGCACTCCATTGCC **ATT** GCCCTCAAGGTTGACCCATC), 0.25 μM RMLC reverse primer (5′-GGGAGGGCGTGAATGTAAGC) for PCR 5. Mutated codons are in bold and underlined. The PCRs were performed with the following conditions: 95 °C for 2 min (1 cycle); 94 °C for 45 s, 50 °C for 45 s, 72 °C for 1 min (28 cycles); and 72 °C for 10 min (1 cycle). The whole gene was *in vivo* reassembled, transforming *S. cerevisiae* cells independently with 200 ng of PCR product 4 and 5 plus 100 ng of linearized pJRoC30 plasmid for each construction. Transformed cells were plated on SC drop-out plates and incubated for 3 days at 30 °C. Thereafter, the mutant libraries were subjected to the HTS-protocol as described below.

2.2 High-throughput screening protocol (HTS-protocol)

Individual clones were selected and cultured in sterile 96-well plates (Greiner Bio-One GmbH, Germany) containing 50 μL per well of SC minimal medium (SC-Hemin for the 1st generation). In each plate, column number 6 was inoculated with the parental 2-1B mutant as an internal standard, and well-H1 (containing minimal medium SC (or SC-Hemin in the 1st generation) supplemented with uracil) was inoculated with untransformed *S. cerevisiae* as a negative control. Plates were sealed and wrapped in Parafilm to prevent evaporation and incubated at 30 °C, 225 rpm and 80% relative humidity in a humidity shaker (Minitron-INFORS, Biogen, Spain). After 48 h, 160 μL of microplate expression medium YP-Hb (YP-EtOH in the 1st generation) was added to each well and the plates were incubated for a further 24 h. The plates (master plates) were centrifuged for 15 min at 3000 rpm at 4 °C (Eppendorf 5810R centrifuge with A-4-62 rotor, Germany) and they were duplicated with the help of a robot (Liquid Handler EVOFreedom-100, TECAN, Switzerland) by transferring 20 μL of supernatant into two replica plates: the acid activity plate (AA plate; activity at acid pH) and the basic activity plate (BA plate; activity at alkaline pH). Then, 180 μL of reaction mixture were added in each plate using a Multidrop robot (Multidrop Combi, Thermo Fischer Scientific, Vantaa, Finland). The reaction mixture for AA plates contained 100 mM citrate–phosphate buffer (pH 4.0), 2 mM ABTS and 0.1 mM H_2O_2. The reaction mixtures for BA plates contained 100 mM citrate–phosphate buffer (pH 6.0, 7.0 and 8.5 for 1st, 2nd and 3rd generation, respectively), 2 mM ABTS and 0.1 mM H_2O_2. The plates were stirred briefly and the absorption at 418 nm ($\varepsilon_{ABTS^{\cdot+}} = 36\,000\ M^{-1}\ cm^{-1}$) was recorded in kinetic mode on a microplate reader (SPECTRAMax Plus 384, Molecular Devices, Sunnyvale, CA). The improvements in the alkaline range were calculated as the ratio between BA/AA plates and normalized to the parental type in the corresponding plate. To rule out false positives, three consecutive re-screenings were carried out (including the determination of pH activity and stability profiles and thermostabilities; see the ESI†). Production and purification of VP variants: VP variants were produced and purified as described in the ESI.†

2.3 Kinetic parameters

Kinetics were assayed with increasing substrate concentrations and fitted to a Michaelis–Menten model (steady-state enzyme kinetics) using as template a hyperbolic, single rectangular, two parameter mode. The catalytic efficiency (k_{cat}/K_m) was obtained by plotting turnover rates (s^{-1}) *vs.* substrate concentration and fitting it to a modified hyperbola with the function $f(x) = (ax)/[(1 + bx)]$, where a is the catalytic efficiency and b is $1/K_m$. The kinetics were measured with the following enzyme concentrations: 1.5–0.3 × 10^{-3} μM (for ABTS), 2 × 10^{-2} μM (for RB5), 2 × 10^{-2} μM (for Mn^{2+}) and 2.5 × 10^{-2} μM (for VA). The following molar extinction coefficients were used: ABTS, $\varepsilon_{418} = 36\,000\ M^{-1}\ cm^{-1}$; RB5, $\varepsilon_{598} = 30\,000\ M^{-1}\ cm^{-1}$; VA, $\varepsilon_{310} = 9300\ M^{-1}\ cm^{-1}$; Mn^{3+}-tartrate, ε_{238}

= 6500 M^{-1} cm^{-1}. Kinetics measurements for ABTS were performed in 100 mM citrate–phosphate–borate buffer from pH 3.0 to 8.0. Kinetics measurements for RB5 and VA were performed in 100 mM citrate–phosphate buffer (pH 3.5) and those for Mn^{2+} were in 100 mM sodium tartrate buffer (pH 5.0).

2.4 pH activity profiles

The activities of purified VP variants were measured in a range of pHs with different substrates. Appropriate enzyme dilutions were prepared for each case depending on the substrate. Substrate concentrations were adjusted to be below the inhibition threshold. The reaction mixtures contained 100 mM citrate–phosphate–borate buffer with pH values ranging from 2.0 to 10.0, 0.1 mM H_2O_2 and the following substrates: 2,6-DMP (5 mM), veratryl alcohol (30 mM), reactive black 5 (0.04 mM), guaiacol (20 mM), catechol (5 mM), sinapic acid (0.25 mM), syringaldazine (0.05 mM) and ABTS ([pH 2.0 to 4.0] 0.1 mM; [pH 5.0] 0.15 mM; [pH 6.0] 0.2 mM; [pH 7.0] 0.8 mM; [pH 8.0 to 10.0] 2.4 mM for BB-8; and [pH 2.0 to 6.0] 0.4 mM; [pH 7.0 to pH 9.0] 2.4 mM for 2-1B). The manganese and VA activities were performed in UV-star plates (Greiner Bio-One GmbH, Germany). The Mn^{2+} reaction mixtures were 100 mM tartrate buffer [pH 3.0 to 5.0], 60 mM manganese sulphate, and 0.1 mM H_2O_2. The activities were recorded from triplicate experiments on a plate reader using 200 μL of final volume per reaction (20 μL of purified enzyme plus 180 μL of reaction mixture). Specific activities were determined using the following molar extinction coefficients: ABTS, ε_{418} = 36 000 M^{-1} cm^{-1}; 2,6-DMP, ε_{469} = 27 500 M^{-1} cm^{-1}; RB5, ε_{598} = 30 000 M^{-1} cm^{-1}; VA, ε_{310} = 9300 M^{-1} cm^{-1}; guaiacol, ε_{470} = 26 600 M^{-1} cm^{-1}; catechol, ε_{392} = 1460 M^{-1} cm^{-1}; sinapic acid, ε_{312} = 16 700 M^{-1} cm^{-1}; syringaldazine, ε_{525} = 65 000 M^{-1} cm^{-1}; Mn^{3+}-tartrate, ε_{238} = 6500 M^{-1} cm^{-1}. Protein concentrations were spectrophotometrically measured with ${}_{VP}\varepsilon_{407nm}$ = 150 000 M^{-1} cm^{-1}.

2.5 Ultracentrifugation experiments

Sedimentation velocity (SV) assay: purified VPs were diluted in 100 mM citrate–phosphate–borate buffer (at pH 4.0 and pH 9.0) containing 250 mM NaCl, 10 mM $MgCl_2$, 1 mM EDTA and 100 mM glycerol. Samples were loaded (320 μL) into analytical ultra-centrifugation cells. The experiments were carried out at 48 000 RPM in an XL-I analytical ultracentrifuge (Beckman-Coulter Inc.) equipped with UV-vis absorbance and Rayleigh interference detection systems. Sedimentation profiles were recorded at 403 nm. Sedimentation coefficient distributions were calculated by least-squares boundary modelling of sedimentation velocity data using the continuous distribution $c(s)$ Lamm equation model as implemented by SEDFIT 14.1.[28] Experimental S values were corrected to standard conditions (water, 20 °C, and infinite dilution) using the program SEDNTERP[29] to get the corresponding standard S values ($S_{20,w}$). Sedimentation equilibrium (SE) assay: using the same experimental conditions as in the SV experiments, short column (90 μL) SE experiments were carried out at speeds ranging from 12 000 to 18 000 rpm and at 407 nm. After the last equilibrium scan, a high-speed centrifugation run (48 000 rpm) was done to estimate the corresponding baseline offsets. Weight-average buoyant molecular weights of protein were determined by fitting a single species model to the experimental data using the HeteroAnalysis program,[30] and corrected for solvent composition and temperature with the program SEDNTERP.[29]

2.6 Protein and homology modeling

The crystal structure of VPl2 from *P. eryngii* expressed in *E. coli* at 2.11 Å resolution (1 Å = 0.1 nm, PDB ID: 3FM4) was used to generate a model to map new mutations with the help of the PyMOL Molecular Visualization System (Schrödinger).

2.7 DNA sequencing

Plasmids containing the VP variants were sequenced on an ABI 3730 DNA Analyzer (Applied Biosystems) automatic sequencer at the Secugen (CIB, Madrid) using the following primers: RMLN; 3R-direct primer (5′-GTTCCATCATCGCGTTCG-3′); 5F-reverse primer (5′-GGATTCCTTTCTTCTTGG-3′) and RMLC.

3. Results and discussion

3.1 Engineering strategy

To obtain a VP that was active at basic pHs, the 2-1B VP variant we generated previously was subjected to directed evolution by error-prone PCR in combination with hybrid approaches (Fig. 1).

Using ABTS as the reducing substrate for the screening assay, the ratio of the activity at pH 4.0 to that at neutral/basic pH was used as the selection criterion in the evolution experiment. Thus, only clones that retained ≥80% of the enzyme's activity at pH 4.0, yet displayed enhanced activity at alkaline pH, were selected for further characterization. Indeed, we used this approach to gradually increase the selective pressure during the course of the directed evolution from pH 6.0 to 8.5, while widening the pH activity profile (Fig. 2A). The yeast microfermentation conditions and the expression of the mutant libraries in 96-well plates were also adjusted to guarantee the reliable detection of VP activity under such demanding conditions. These modifications mainly affected the composition of the medium (heme supply, carbon source) as well as the stirring conditions and oxygen availability (see the ESI† for details).

We planned to precisely control the evolutionary route by using low mutational loads, 1 to 3 nucleotide changes per round of evolution, coupled to *in vivo* recombination.[31] Three consecutive re-screenings were performed to determine the pH activity and stability profiles of the new variants (in the pH range of 2.0 to 10.0) as well as the T_{50} (the temperature at which the enzyme loses 50% of its initial activity after a 10

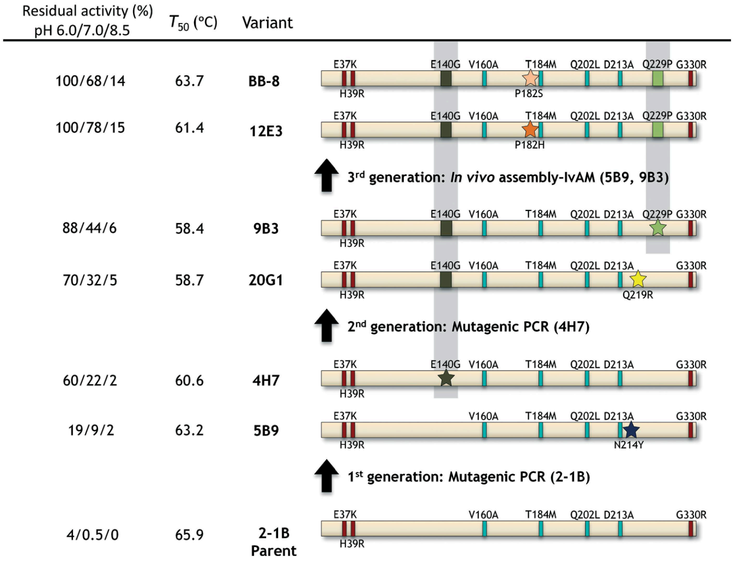

Fig. 1 Directed evolution of an alkaline VP. New mutations are depicted as stars and accumulated mutations as squares. Mutations from previous evolution campaigns[24] are shown as thin squares with the stabilizing mutational backbone in dark red. The method used for library creation and the parental types used for each generation are indicated. Residual activity (%) was calculated as the improvement in VP activity detected in *S. cerevisiae* supernatants for each mutant compared with the parental 2-1B at the corresponding pH. Measurements were made in quintuplicate with 2 mM ABTS and 0.1 mM H_2O_2 in 100 mM citrate–phosphate–borate buffer at different pHs. Thermostability (T_{50}) was estimated from the culture supernatants.

min incubation). After screening ~5000 clones in three rounds of directed evolution, the BB-8 mutant was obtained that carried the beneficial E140G, P182S and Q229P mutations.

This variant had nearly the same activity at pH 6.0 as that of the parental 2-1B variant at pH 4.0 (Fig. 2A), although unlike the 2-1B variant, the activity of BB-8 at a neutral/basic pH was readily detected. The drop in thermostability (T_{50}) identified in the first two rounds of evolution (from 66 to 58 °C, Fig. 1) was partly alleviated by including a stabilizing mutation, P182S, in the last generation, allowing BB-8 to recover ~5 °C. Given that the same position was mutated to different amino acids in two independent variants identified (12E3 and BB-8), we performed further saturation mutagenesis over this Pro182 residue. The best mutants obtained displayed a ~2-fold enhancement of activity at pH 8.0 over the original Pro182 (the 9B3 mutant from the 2nd generation). In all cases, substitution with polar residues (Tyr, Glu, His, Ser) produced similar thermostabilities, pH activity and stability profiles (Fig. 2B). Accordingly, BB-8 was selected for more exhaustive characterization.

3.2 Alkaline pH stabilization and hyperactivation

The wild-type VP ($_{wt}$VP), 2-1B and BB-8 mutants were produced, purified to homogeneity (Reinheitszahl value [Rz] [A_{407}/A_{280}], ≥2) and characterized spectroscopically and biochemically. Initially, the electronic absorption spectrum was recorded after incubating the enzymes for 72 h at pH 4.0 and 9.0 (Fig. 3A). At pH 4.0 (optimum pH for activity) the maximum absorbance of all VPs was in the Soret region (407 nm) and the two charge transference bands (CT2, 505 nm; CT1, 637 nm) were characteristic of Fe^{3+} in a high-spin (pentacoordinated) state. As observed previously,[25] the incubation of $_{wt}$VP at alkaline pH changed its spectroscopic features and these modifications were detectable even after a 1 min incubation (Fig. 3A, see inset in the first panel). The Soret maximum shifted from 407 to 413 nm and the CT bands faded, while two new shoulders arose at 532 and 565 nm that are characteristic of a low-spin (hexacoordinated and inactive) state.[32]

By contrast, the 2-1B and BB-8 mutants remained unaltered after incubation for 72 h at pH 9.0, showing a similar spectrum to that seen at pH 4.0, although with lower absorbance values. Given that both the parental 2-1B and the BB-8 mutant harbour the aforementioned stabilizing E37K-H39R-G330R backbone, they preserved the heme state (*i.e.* remaining in a pentacoordinated high-spin Fe^{3+}). In fact, the mutants were very stable in such an alkaline environment when compared to $_{wt}$VP. As such, the 2-1B and BB-8 variants retained or even increased their residual activity after incubation at pH 9.0 (see below), whereas $_{wt}$VP was fully inactive at this pH, as reported previously (Fig. 3B).[24,25] The spectroscopic changes and the poor stability of $_{wt}$VP at alkaline pH

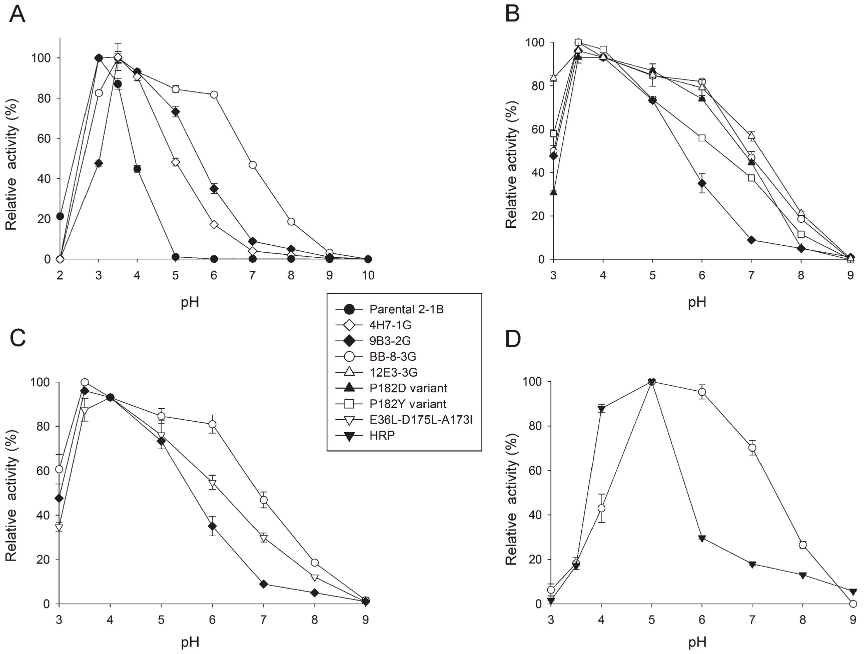

Fig. 2 Widening of the VP pH activity profile. (A) pH activity profiles for the parental 2-1B and the best mutant in each generation. Black circles, parental 2-1B; white diamonds, 4H7-1st generation; black diamonds, 9B3-2nd generation; white circles, BB-8-3rd generation. (B) pH profiles for selected mutants of saturation mutagenesis experiment at position 182. Black diamonds, 9B3-2nd generation (P182); white squares, P182Y mutant; black up triangles, P182D mutant; white up triangles, 12E3-3rd generation (P182H); white circles, BB-8-3rd generation (P182S). (C) pH activity profiles for E36L-D175L-A173I (white down triangles), 9B3-2nd generation (black diamonds) and BB-8-3rd generation (white circles) mutants. (D) pH profiles for HRP (black down triangles) and BB-8 (white circles). The concentrations of ABTS in (A)–(C) were adjusted to below the inhibitory threshold for each pH value (from pH 2.0 to 6.0, 0.4 mM and from pH 7.0 to 10.0, 2.4 mM for 2-1B; from pH 2.0 to 4.0, 0.1 mM; pH 5.0, 0.15 mM; pH 6.0, 0.2 mM; pH 7.0, 0.8 mM; pH 8.0 to 10.0, 2.4 mM for the other variants). In (D) we used 2 mM ABTS across the entire pH range as it is the concentration used for standard HRP assays. Activities were measured in 100 mM citrate–phosphate–borate buffer at different pHs with the [ABTS] indicated and 0.1 mM H_2O_2. The activity was normalized to the optimum activity value and the results shown are the means ± S.D. from three independent experiments.

are directly linked to the failure to attach the structural Ca^{2+}. Two specific ligands are involved in the coordination of Ca^{2+} (Ser170 for the proximal Ca^{2+}; Asp48 for the distal Ca^{2+}), lying adjacent to the corresponding proximal and distal His (His169 and His47, respectively). His169 is the 5th coordinating (axial) ligand of the heme group, while His47 is involved in the heterolytic cleavage of H_2O_2. It is well known that incubation at high temperature or pH provokes the release of structural Ca^{2+}, with the distal His47 concomitantly approximating to the heme and forming a bis-histidyl heme iron complex that is characteristic of a hexacoordinated low-spin inactive state.

We observed strong hyperactivation of VP mutants that was directly dependent on the length of incubation and the pH (Fig. 3B). Particularly, BB-8 was hyperactivated at pH 8.0 and 9.0, reaching a plateau after a 72 h incubation with a ~3-fold increase in residual activity. It is well known that enzyme hyperactivation can be associated with conformational changes that may occur after incubation at high temperatures or in the presence of organic co-solvents but we were not aware of such an effect by incubation at alkaline pHs. As enzyme hyperactivation might reflect a di/multimerization process, to rule out the possible formation of variant VP dimers at basic pHs, we carried out independent analytical ultracentrifugation experiments in which similar sedimentation coefficients of the mutants were obtained (sw(20,w) ~3 S) after incubation at acid (4.0) or basic pH (9.0). Further sedimentation equilibrium experiments corroborated the lack of dimerization, and a MW of ~34 000 Da for both enzymes was obtained at acid and basic pHs.

3.3 The pH activity profiles and the contribution of the Mn^{2+} binding site to direct substrate oxidation

The pH activity profiles of the purified variants were evaluated for different substrates, including some redox mediators and natural fungal metabolites at concentrations below their inhibitory thresholds (≤10-fold K_m value; Fig. 4). The low-redox potential substrates ABTS, sinapic acid and guaiacol can be oxidized at two different catalytic sites: the heme

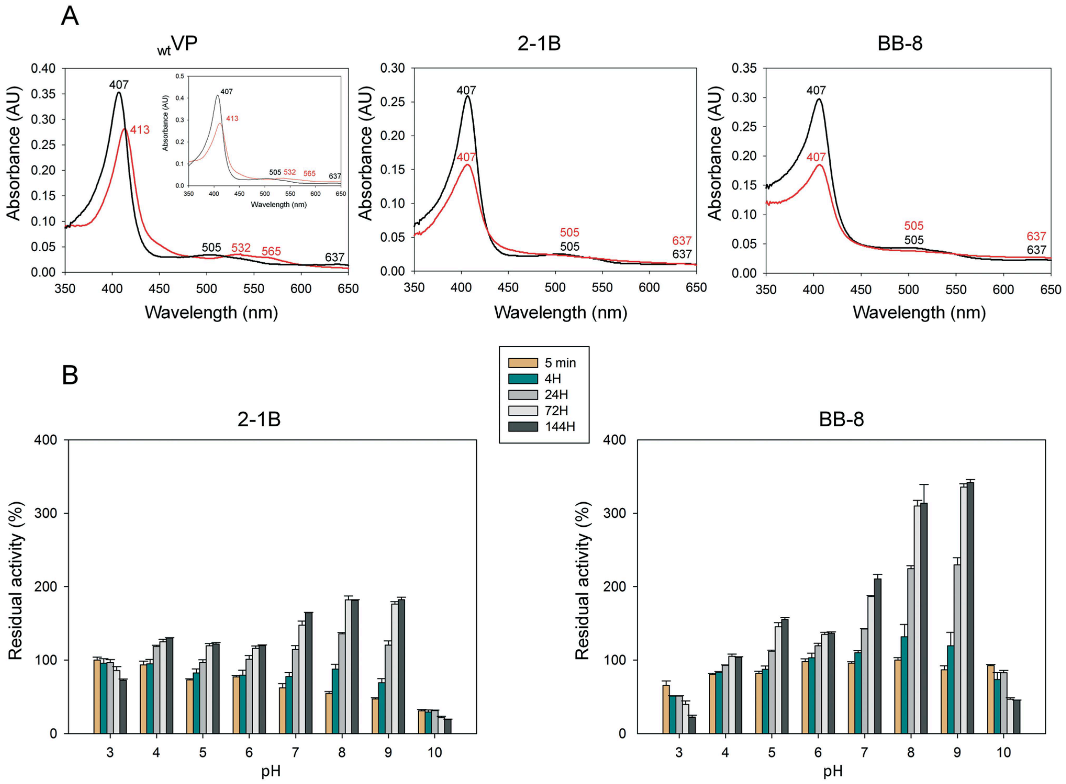

Fig. 3 VP stability at alkaline pHs. (A) Electronic absorption spectra of $_{wt}$VP and the 2-1B and BB-8 mutants. The UV-visible spectra after a 72 h incubation at pH 4.0 (black) and pH 9.0 (red) are shown. The graph for $_{wt}$VP includes an inset for the spectrum after 1 min of incubation at pH 4.0 (black) and pH 9.0 (red). (B) The pH stability profiles of the parental 2-1B and the BB-8 mutant. Enzyme samples were incubated in 100 mM citrate–phosphate–borate buffer at different pH values, and the residual activities were measured in 100 mM sodium tartrate buffer (pH 3.5) containing 2 mM ABTS and 0.1 mM H_2O_2. The results are the means ± S.D. from three independent experiments.

access channel (with low efficiency) and the catalytic Trp164 (with high efficiency). The pH profiles for these compounds were shifted and broadened towards the basic side, even detecting some activity at pH 9.0 where the parental 2-1B was inactive (Fig. 4A–C). Under acidic conditions, the veratryl alcohol (VA) and the reactive black five (RB5) high-redox potential substrates are oxidized at the Trp164 radical formed by LRET in both compounds I and II of VP after heme activation by H_2O_2.[33] However, at neutral or basic pH no oxidation of VA or RB5 was observed irrespective of the mutant tested (Fig. 4D and E). This is explained by the fact that the reduction potential of Trp164 radical decreases as the pH increases, with an estimated loss of 59 mV per unit of pH.[34] Thus, the LRET pathway from Trp164 to the heme is permanently cancelled at pH >5, diverting the oxidative route to the other two catalytic sites while suppressing the oxidation of high-redox potential compounds. It is noteworthy that the oxidation of Mn^{2+} to Mn^{3+} was drastically reduced for BB-8 (Fig. 4F), while the contribution of the Mn^{2+} binding site to the direct oxidation of low-redox potential substrates at alkaline pH (in the absence of oxidized Mn^{3+}) was evident for the first time within this enzyme superfamily. The Mn^{2+} site in VP is formed by the side chains of the three coordinating carboxylic residues (Glu36, Glu40 and Asp175), constituting a small channel that connects the protein surface to the internal propionate of the heme. In the 2-1B parental type, this catalytic site was partially suppressed for the oxidation of Mn^{2+} to Mn^{3+} due to the effect exerted by two of the mutations in the stabilizing backbone (E37K and H39R).[24,25] Moreover, the introduction of the P182S mutation in BB-8, situated in the neighbourhood of the Mn^{2+} site, negatively affected the kinetics for Mn^{2+} (see below). Conversely, we detected double slopes for the kinetics of ABTS at basic pHs, which must originate from the heme access channel and the Mn^{2+} binding site given that the catalytic Trp is inactive under such pH values.

To demonstrate this hypothesis, we inspected the structure of BB-8 and designed a triple mutant (E36L-D175L-A173I) in which the substrate cannot access the Mn^{2+} binding site (Fig. 5). As expected, the analysis of the pH activity

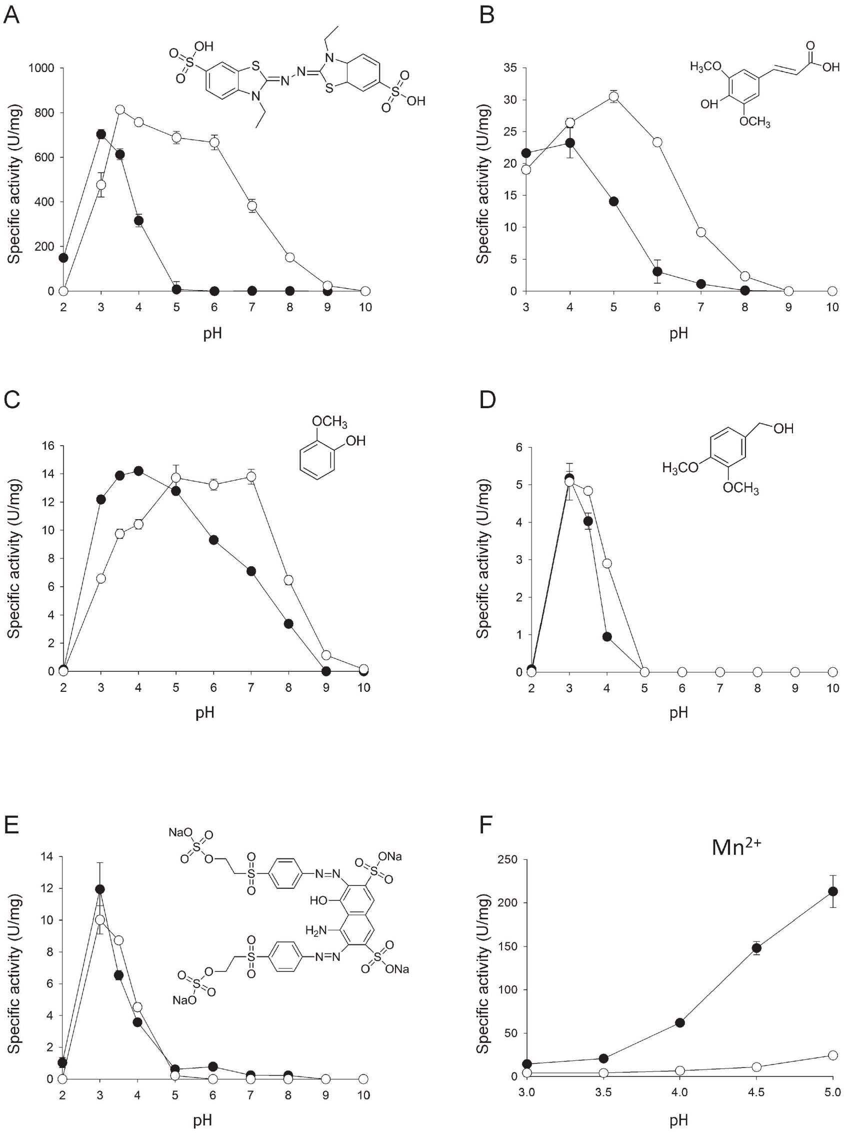

Fig. 4 pH Activity profiles. pH profiles for the parental 2-1B (black circles) and the BB-8 mutant (white circles) with ABTS (A), sinapic acid (B), guaiacol (C), VA (D), RB5 (E) and Mn^{2+} (F). Activities were measured in 100 mM citrate–phosphate–borate buffer at different pHs with a concentration of the substrate below their inhibitory threshold (see the ESI† for details) and 0.1 mM H_2O_2. VP activity was normalized to the optimum activity (U mg^{-1}) and the results shown are the means ± S.D. from three independent experiments.

profiles of BB-8 and the triple mutant confirmed the contribution of the Mn^{2+} site to the direct oxidation of ABTS at pH >6.0 (up to ~26%; Fig. 2C). We also included in these measurements the 9B3 mutant (from the 2nd generation) that lacked the P182S mutation of BB-8 to obtain a reliable breakdown of the activity at the heme channel and the Mn^{2+} site at basic pHs. While the difference between the triple mutant and 9B3 from pH >6 onwards represents the enhanced activity at the heme channel, the comparison between the E36L-D175L-A173I triple variant and BB-8 reflects that at the Mn^{2+} site. Our results are consistent with the data from an earlier rational and computational analysis of a short MnP that indicated the direct oxidation of ABTS at the Mn^{2+} site at acidic pHs.[35]

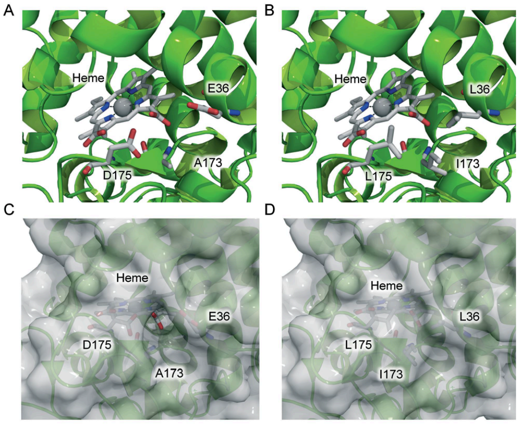

Fig. 5 Site-directed mutagenesis to block the Mn^{2+} binding site. The VP structure is shown as a green cartoon while the heme group and the residues targeted for mutagenesis are highlighted as sticks (CPK-colors), before (A) and after (B) mutagenesis to block the Mn^{2+} binding site. The bottom panel shows the protein topology in the surface mode before (C) and after (D) mutagenesis. Mutations modelled from PDB ID: 3FM4.

3.4 Kinetic parameters

Kinetic constants were assessed in the pH range from 3.5 to 8.0 (Table 1). The catalytic efficiency (k_{cat}/K_m) of BB-8 for ABTS was 5-fold higher than that of the parental 2-1B at pH 3.5. This large improvement was associated with the mutant's activity at alkaline pHs, even though the affinity and activity gradually declined (k_{cat}/K_m) as more basic pHs were reached. Still, the catalytic efficiency of BB-8 at pH 8.0 was higher than that of $_{wt}$VP at optimum pH, 3.5 (*i.e.* 1190 *vs.* 410 mM^{-1} s^{-1}, respectively).[24]

Encouraged by these results, we compared the pH activity profile of BB-8 to that of HRP (horseradish peroxidase). HRP is widely used in many analytical and biomedical applications (*e.g.*, to report biological activities linked to the production of H_2O_2, chemiluminiscence detection in western blots, *etc.*).[36] Our variant by far surpassed the activity of HRP from pH 5.0 onwards, offering an attractive solution for applications at basic pHs that require peroxidase activity (Fig. 2D). Finally, in terms of high-redox potential substrates, the kinetics for RB5 and VA were similar irrespective of the variant, while Mn^{2+} oxidation was almost completely suppressed in BB-8, with a 13-fold increase in the K_m (Table 2).

3.5 Structural analysis of mutations

The mutations found in BB-8 were mapped to the VP crystal structure (Fig. 6). The E140G mutation introduced in the first round of evolution exerted the strongest improvement in the whole study, with a ~44-fold increase in activity at pH 7.0, opening the way for evolution at alkaline pH (Fig. 1). This mutation is located at the entry to the heme access channel (Fig. 6A and B) and it seems to be the main residue responsible for the improved kinetics. Upon mutation, the heme channel is widened, facilitating the entrance and exit of bulky substrates, thereby favouring catalysis. Indeed, the gradual decrease in substrate affinity associated with higher pH values was alleviated by the E140G substitution, associated with a ~4-fold better K_m (Table 1) that enabled BB-8 to work at pH 6.0 with similar efficiency to the parental 2-1B variant at pH 3.5. Our results agree well with a previous rational experiment where the same mutation was introduced into VP, increasing catalytic efficiency by 4-fold.[13] Unfortunately, the E140G mutant in that study did not show any activity at pH >4 since it lacked the stabilizing E37K-H39R-G330R backbone that protects the enzyme against Ca^{2+} leakage. The Q229P mutation lies in a sensitive region close to the proximal Ca^{2+}. Inspection of the model suggests that this mutation affects the distance to the H-bonded Gly216, influencing the main loop of the heme access channel and modifying catalysis (Fig. 6C and D). The P182S mutation introduced in the last generation fostered activity at alkaline pHs and recovered most of the lost thermostability (~5 °C). This mutation lies in a rather labile region, between the heme access channel and in the vicinity of the Mn^{2+} binding site (Fig. 6E and F). It is likely that Pro182 exerts a destabilizing effect under alkaline conditions given that proline residues are generally indicators of protein destabilization under harsh conditions.[37] Indeed, all the mutants derived from the saturation mutagenesis at Pro182 had polar side chains introduced, providing reinforcement in this region by establishing new contacts with surrounding residues.

Moreover, potential reshaping of the Mn^{2+} binding site after mutation for the direct oxidation of substrates in the absence of Mn^{2+} cannot be ruled out. Molecular docking simulations with ABTS at the Mn^{2+} site indicates that a new

Table 1 Kinetic parameters with ABTS at different pH values

Mutant	Kinetic constants	pH 8.0	pH 7.0	pH 6.0	pH 5.0	pH 4.0	pH 3.5
BB-8	K_m (mM)	0.154 ± 0.018	0.078 ± 0.004	0.039 ± 0.005	0.013 ± 0.002	0.011 ± 0.002	0.0078 ± 0.002
	k_{cat} (s^{-1})	184 ± 6	460 ± 6	810 ± 30	840 ± 30	920 ± 30	990 ± 40
	k_{cat}/K_m (mM^{-1} s^{-1})	1190 ± 110	5910 ± 270	20 500 ± 2000	64 000 ± 9600	79 000 ± 11 700	126 000 ± 26 500
2-1B	K_m (mM)	n.m.	n.m.	n.m.	n.m.	0.17 ± 0.01	0.034 ± 0.004
	k_{cat} (s^{-1})	n.m.	n.m.	n.m.	n.m.	670 ± 20	850 ± 40
	k_{cat}/K_m (mM^{-1} s^{-1})	n.m.	n.m.	n.m.	n.m.	3900 ± 200	25 000 ± 2100

Kinetics were estimated in 100 mM citrate–phosphate–borate buffer containing 0.1 mM H_2O_2 at different pH values; n.m., not measurable.

Table 2 Kinetic parameters with Mn^{2+}, VA and RB5

Mutant	Kinetic constants	Mn^{2+}	VA	RB5
BB-8	K_m (mM)	56 ± 10	24.7 ± 1.9	0.021 ± 0.001
	k_{cat} (s^{-1})	70 ± 8	21.3 ± 0.9	20.4 ± 0.4
	k_{cat}/K_m (mM^{-1} s^{-1})	1.25 ± 0.08	0.86 ± 0.02	950 ± 30
2-1B	K_m (mM)	4.3 ± 0.3	7.14 ± 0.6	0.0055 ± 0.0006
	k_{cat} (s^{-1})	98 ± 2	2.9 ± 0.1	9.4 ± 0.4

Kinetics were estimated in 100 mM citrate–phosphate–borate buffer at pH 3.5 containing 0.1 mM H_2O_2 and for Mn^{2+} in 100 mM sodium tartrate buffer at pH 5.0.

H-bond between one of the SO^{3-} moieties of ABTS and Ser182 may more adequately orientate and direct substrate oxidation through the internal heme propionate (Fig. S1, ESI†). This data agrees well with the changes observed in the aforementioned E36L-D175L-A173I triple mutant in which the use of the Mn^{2+} site for Mn^{2+} oxidation to Mn^{3+} was rescinded. Finally, and to estimate the degree of conservation of the mutated positions, we generated a multiple sequence alignment (MSA) with an array of the most representative ligninolytic peroxidases (Fig. S2, ESI†). Interestingly, E140 and Q229 together with two of the residues in the stabilizing backbone (E37, H39) are highly conserved within this enzyme superfamily. Hence, introducing these mutations into other ligninolytic peroxidases may also influence alkaline activation/stabilization.

4. Conclusions

High-redox potential peroxidases are the product of millions of years of adaptation to achieve lignin combustion at acidic pHs. In particular, VPs are hybrid proteins that combine the best catalytic attributes of GPs, LiPs and MnPs. Very recently, we reconstructed several ancestral nodes of ligninolytic peroxidases which have been resurrected and functionally expressed in bacteria and yeast (unpublished material). All these nodes are suitable moulds that can be used as templates for protein engineering in which hot-spot mutations could be introduced, such as those discovered here or in other directed evolution campaigns.[24,38] Thus, by defining the different mechanisms of action used by VPs, we help answer key questions regarding the natural evolution of ligninolytic peroxidases, particularly as VPs were recently postulated as the evolutionary link between MnPs and LiPs.[6]

Finally, we have taken the VP from its natural biological context to make it active at alkaline pHs for the first time. Indeed, this alkaline VP is the result of the synergy between a

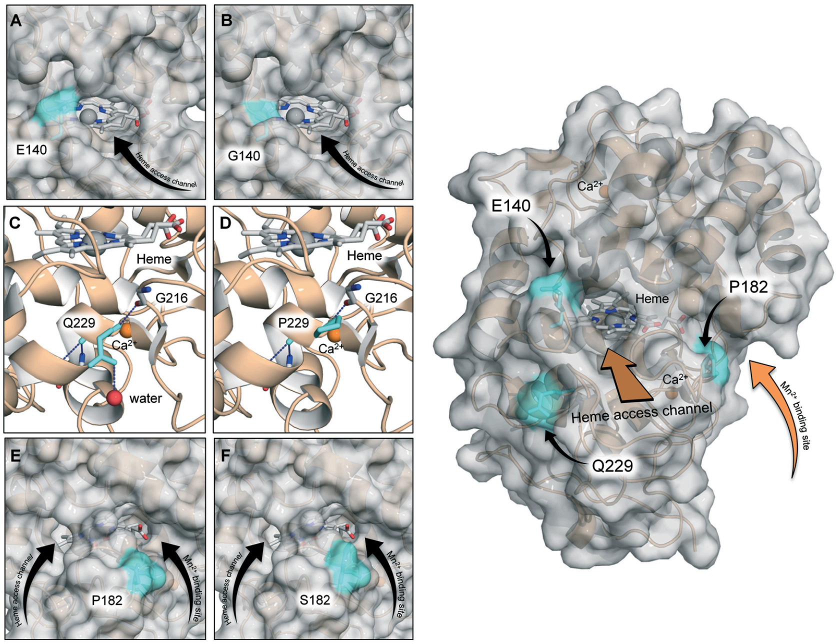

Fig. 6 Location of the mutations in alkaline VP. The mutations are highlighted in blue as sticks, the heme group is in the CPK stick mode and the structural calcium is shown as orange spheres. The protein surface is shown in transparent grey and the protein's secondary structures as a wheat cartoon. Orange arrows represent the substrate inlets. (A and B) E140G mutation, with the black arrow indicating the heme access channel. (C and D) The Q229P mutation, with the dotted blue lines showing the interactions with surrounding residues and the red sphere representing a water molecule. (E and F) P182S mutation, with black arrows showing the access to the heme channel and the Mn^{2+} site. Mutations modelled on PDB ID: 3FM4.

stabilizing backbone that maintains the integrity of the heme by avoiding calcium leakage, and mutations that allow the VP to act at basic pHs by enhancing its substrate affinity and permitting direct oxidation at the Mn^{2+} site. This biocatalyst could be tested in applications at neutral/basic pHs, ranging from organic synthesis, biomedicine, pulp biobleaching to bioremediation, as well as for the engineering of a fully consolidated microbe to produce biofuels and chemicals.[2,39]

Acknowledgements

We thank Dr Juan Roman Luque-Ortega (Laboratory of Analytical Ultracentrifugation and Macromolecular Interactions, CIB-CSIC, Madrid) for assisting in AUC assays. This research was supported by the European Commission project FP7-KBBE-2013-7-613549-INDOX, the COST-Action CM1303 and by the Spanish government (grants: BIO2013-43407-R-DEWRY and CAMBIOS-RTC-2014-1777-3).

Notes and references

1 M. E. Himmel, S. Y. Ding, D. K. Johnson, W. S. Adney, M. R. Nimlos, J. W. Brady and T. D. Foust, *Science*, 2007, **315**, 804–807.
2 M. Alcalde, *Trends Biotechnol.*, 2015, **33**, 155–162.
3 A. T. Martínez, F. J. Ruiz-Dueñas, M. J. Martínez, J. C. del Río and A. Gutiérrez, *Curr. Opin. Biotechnol.*, 2009, **20**, 348–357.
4 E. Garcia-Ruiz, D. M. Mate, D. Gonzalez-Perez, P. Molina-Espeja, S. Camarero, A. T. Martínez, A. O. Ballesteros and M. Alcalde, in *Cascade Biocatalysis: Integrating Stereoselective and Environmentally Friendly Reactions*, ed. S. Riva and W. D. Fessner, Wiley-VCH Verlag GmbH & Co. KGaA, Weinheim, Germany, 2014, ch. 1, pp. 1–18.
5 K. E. Hammel and D. Cullen, *Curr. Opin. Plant Biol.*, 2008, **11**, 349–355.
6 D. Floudas, M. Binder, R. Riley, K. Barry, R. A. Blanchette, B. Henrissat, A. T. Martínez, R. Otillar, J. W. Spatafora, J. S. Yadav, A. Aerts, I. Benoit, A. Boyd, A. Carlson, A. Copeland, P. M. Coutinho, R. P. de Vries, P. Ferreira, K. Findley, B. Foster, J. Gaskell, D. Glotzer, P. Górecki, J. Heitman, C. Hesse, C. Hori, K. Igarashi, J. J. Jurgens, N. Kallen, P. Kersten, A. Kohler, U. Kües, T. K. A. Kumar, A. Kuo, K. LaButti, L. F. Larrondo, E. Lindquist, A. Ling, V. Lombard, S. Lucas, T. Lundell, R. Martin, D. J. McLaughlin, I. Morgenstern, E. Morin, C. Murat, L. G. Nagy, M. Nolan, R. A. Ohm, A. Patyshakuliyeva, A. Rokas, F. J. Ruiz-Dueñas, G. Sabat, A. Salamov, M. Samejima, J. Schmutz, J. C. Slot, F. St John, J. Stenlid, H. Sun, S. Sun, E. Syed, A. Tsang, A. Wiebenga, D. Young, A. Pisabarro, D. C. Eastwood, F. Martin, D. Cullen, I. V. Grigoriev and D. Hibbett, *Science*, 2012, **336**, 1715–1719.
7 M. Hofrichter, R. Ullrich, M. J. Pecyna, C. Liers and T. Lundell, *Appl. Microbiol. Biotechnol.*, 2010, **87**, 871–897.
8 M. Zámocký, B. Gasselhuber, P. G. Furtmüller and C. Obinger, *Cell. Mol. Life Sci.*, 2014, **71**, 4681–4696.
9 F. J. Ruiz-Dueñas, M. Morales, E. García, Y. Miki, M. J. Martínez and A. T. Martínez, *J. Exp. Bot.*, 2009, **60**, 441–452.
10 F. J. Ruiz-Dueñas and A. T. Martínez, *Microb. Biotechnol.*, 2009, **2**, 164–177.
11 M. Pérez-Boada, F. J. Ruiz-Dueñas, R. Pogni, R. Basosi, T. Choinowski, M. J. Martínez, K. Piontek and A. T. Martínez, *J. Mol. Biol.*, 2005, **354**, 385–402.
12 F. J. Ruiz-Dueñas, M. Morales, M. J. Mate, A. Romero, M. J. Martínez, A. T. Smith and A. T. Martínez, *Biochemistry*, 2008, **47**, 1685–1695.
13 M. Morales, M. J. Mate, A. Romero, M. J. Martínez, A. T. Martínez and F. J. Ruiz-Dueñas, *J. Biolumin. Chemilumin.*, 2012, **287**, 41053.
14 V. Sáez-Jimenez, M. C. Baratto, R. Pogni, J. Rencoret, A. Gutierrez, J. I. Santos, A. T. Martínez and F. J. Ruiz-Dueñas, *J. Biolumin. Chemilumin.*, 2015, **290**, 23201–23213.
15 C. Regalado, B. E. García-Almendárez and M. A. Duarte-Vázquez, *Phytochem. Rev.*, 2004, **3**, 243–256.
16 A. T. Martínez, in *Industrial Enzymes: Structure, Function and Applications*, ed. J. Polaina and A. P. MacCabe, Springer, Berlin, 2007, ch. 27, pp. 475–486.
17 S. Sakai, Y. Yamada, T. Zenke and K. Kawakami, *J. Mater. Chem.*, 2009, **19**, 230–235.
18 P. Khan, D. Idrees, M. A. Moxley, J. A. Corbett, F. Ahmad, G. von Figura, W. S. Sly, A. Waheed and M. I. Hassan, *Appl. Biochem. Biotechnol.*, 2014, **173**, 333–355.
19 T. A. Lú-Chau, F. J. Ruiz-Dueñas, S. Camarero, G. Feijoo, M. J. Martínez, J. M. Lema and A. T. Martínez, *Bioprocess Biosyst. Eng.*, 2004, **26**, 287–293.
20 J. Verdin, R. Pogni, A. Baeza, M. C. Baratto, R. Basosi and R. Vázquez-Duhalt, *Biophys. Chem.*, 2006, **121**, 163–170.
21 G. Nie and S. D. Aust, *Arch. Biochem. Biophys.*, 1997, **337**, 225–231.
22 G. R. J. Sutherland, L. S. Zapanta, M. Tien and S. D. Aust, *Biochemistry*, 1997, **36**, 3654–3662.
23 S. J. George, M. Kvaratskhelia, M. J. Dilworth and R. N. F. Thorneley, *Biochem. J.*, 1999, **344**, 237–244.
24 E. Garcia-Ruiz, D. Gonzalez-Perez, F. J. Ruiz-Dueñas, A. T. Martínez and M. Alcalde, *Biochem. J.*, 2012, **441**, 487–498.
25 V. Sáez-Jimenez, S. Acebes, E. Garcia-Ruiz, A. Romero, V. Guallar, M. Alcalde, F. J. Medrano, A. T. Martinez and F. J. Ruiz-Dueñas, *Biochem. J.*, 2016, DOI: 10.1042/BCJ20160248, in press.
26 M. Zumárraga, S. Camarero, S. Shleev, A. Martínez-Arias, A. Ballesteros, F. J. Plou and M. Alcalde, *Proteins*, 2008, **71**, 250–260.
27 M. Alcalde, in *In Vitro Mutagenesis Protocols: Methods in Molecular Biology*, ed. J. Braman, Springer-Humana Press, Totowa, N. J., third edn., 2010, ch. 1, pp. 3–14.
28 P. Schuck, *Biophys. J.*, 2000, **78**, 1606–1609.
29 T. M. Laue, B. D. Shah, T. M. Ridgeway and S. L. Pelletier, in *Analytical ultracentrifugation in biochemistry and polymer science*, ed. S. E. Harding, A. J. Rowe and J. C. Horton, The Royal Society of Chemistry, Cambridge, UK, 1992, pp. 90–125.
30 J. L. Cole, *Methods Enzymol.*, 2004, **384**, 212–232.

31 D. Gonzalez-Perez, E. Garcia-Ruiz and M. Alcalde, *Bioeng. Bugs.*, 2012, **3**, 172–177.

32 H. L. Youngs, P. Moënne-Loccoz, T. M. Loehr and M. H. Gold, *Biochemistry*, 2000, **39**, 9994–10000.

33 F. J. Ruiz-Dueñas, R. Pogni, M. Morales, S. Giansanti, M. J. Mate, A. Romero, M. J. Martínez, R. Basosi and A. T. Martínez, *J. Biolumin. Chemilumin.*, 2009, **284**, 7986–7994.

34 O. B. Morozova and A. V. Yurkovskaya, *J. Phys. Chem. B*, 2015, **119**, 140–149.

35 E. Fernández-Fueyo, S. Acebes, F. J. Ruiz-Dueñas, M. J. Martínez, A. Romero, F. J. Medrano, V. Guallar and A. T. Martínez, *Acta Crystallogr., Sect. D: Biol. Crystallogr.*, 2014, **70**, 3253–3265.

36 F. W. Krainer and A. Glieder, *Appl. Microbiol. Biotechnol.*, 2015, **99**, 1611–1625.

37 R. Verma, T. S. Wong, U. Schwaneberg and D. Roccatano, Methods in Molecular Biology, in *Directed evolution Library Creation: Methods and Protocols*, ed. E. M. J. Gillam, J. N. Copp and D. F. Ackerley, Springer, New York, second edn., 2014, ch. 19, pp. 279–290.

38 D. Gonzalez-Perez, E. Garcia-Ruiz, F. J. Ruiz-Dueñas, A. T. Martinez and M. Alcalde, *ACS Catal.*, 2014, **4**, 3891–3901.

39 A. T. Martínez, F. J. Ruiz-Dueñas, A. Gutiérrez, J. C. del Río, M. Alcalde, C. Liers, R. Ullrich, M. Hofrichter, K. Scheibner, L. Kalum, J. Vind and H. Lund, *Biofuels, Bioprod. Biorefin.*, 2014, **8**, 819–835.

Catalysis Science & Technology

CORRECTION

View Article Online
View Journal

Cite this: DOI: 10.1039/c6cy90107g

DOI: 10.1039/c6cy90107g

www.rsc.org/catalysis

Correction: Alkaline versatile peroxidase by directed evolution

David Gonzalez-Perez,[a] Ivan Mateljak,[a] Eva Garcia-Ruiz,[b]
Francisco J. Ruiz-Dueñas,[c] Angel T. Martinez[c] and Miguel Alcalde*[a]

Correction for 'Alkaline versatile peroxidase by directed evolution' by David Gonzalez-Perez *et al.*, *Catal. Sci. Technol.*, 2016, **6**, 6625–6636.

The authors regret that Table 2 appears incorrectly in the original version of this article. A corrected version of Table 2, which features an additional row, is displayed below.

Table 2 Kinetic parameters with Mn^{2+}, VA and RB5

Mutant	Kinetic constants	Mn^{2+}	VA	RB5
BB-8	K_m (mM)	56 ± 10	24.7 ± 1.9	0.021 ± 0.001
	k_{cat} (s^{-1})	70 ± 8	21.3 ± 0.9	20.4 ± 0.4
	k_{cat}/K_m (mM^{-1} s^{-1})	1.25 ± 0.08	0.86 ± 0.02	950 ± 30
2-1B	K_m (mM)	4.3 ± 0.3	7.14 ± 0.6	0.0055 ± 0.0006
	k_{cat} (s^{-1})	98 ± 2	2.9 ± 0.1	9.4 ± 0.4
	k_{cat}/K_m (mM^{-1} s^{-1})	23 ± 1	0.4 ± 0.02	1700 ± 140

Kinetics were estimated in 100 mM citrate–phosphate–borate buffer at pH 3.5 containing 0.1 mM H_2O_2 and for Mn^{2+} in 100 mM sodium tartrate buffer at pH 5.0.

The Royal Society of Chemistry apologises for these errors and any consequent inconvenience to authors and readers.

---

[a] *Department of Biocatalysis, Institute of Catalysis, CSIC, 28049 Madrid, Spain. E-mail: malcalde@icp.csic.es; Fax: +34 915854760; Tel: +34 915854806*
[b] *Department of Chemical and Biomolecular Engineering, University of Illinois at Urbana-Champaign, Urbana, IL 61801, USA*
[c] *Center for Biological Investigations, CSIC, Ramiro de Maeztu 9, 28040 Madrid, Spain*

Supplemental data chapter 5

Alkaline versatile peroxidase by directed evolution

Authors: González-Perez, D., Mateljak, I., Garcia-Ruiz, E., Ruiz-Dueñas, F.J., Martínez, A.T., and Alcalde, M.

Catal Sci Technol (2016) **6**, 6625-6636.

Electronic Supplementary Material (ESI) for Catalysis Science & Technology.

Alkaline versatile peroxidase by directed evolution

David Gonzalez-Perez[a], Ivan Mateljak[a], Eva Garcia-Ruiz[b], Francisco J. Ruiz-Dueñas[c], Angel T. Martinez[c] and Miguel Alcalde[a*]

[a]Department of Biocatalysis, Institute of Catalysis, CSIC, 28049 Madrid, Spain.

[b]Department of Chemical and Biomolecular Engineering, University of Illinois at Urbana-Champaign, Urbana, IL 61801, USA.

[c]Center for Biological Investigations, CSIC, Ramiro de Maeztu 9, 28040 Madrid, Spain.

[*]Corresponding author: Miguel Alcalde, Department of Biocatalysis, Institute of Catalysis, CSIC, Cantoblanco, 28049 Madrid, Spain. Phone: +34 915854806; Fax: +34 915854760; malcalde@icp.csic.es.

Contents:

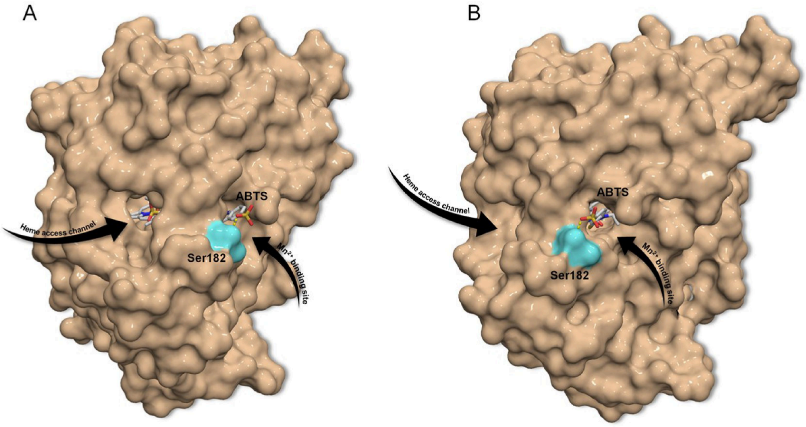

Fig. S1 Molecular Docking for ABTS at the Mn^{2+} site.

The protein is shown in the surface mode, the heme cofactor and ABTS are highlighted as stick models (CPK colors). The hydrogen bond between the SO^{3-} group of ABTS and Ser182 is represented as a yellow dash. The PDB file used for molecular docking was 3FKG. (**A**) Front view. (**B**) Side view.

Multiple structural alignment (MSA)

```
                                                          E37K H39R
AURDE-GP11        ----RPAASVCADGVTTVNNPQCCFWANVRDRFINEIFL-GVCQENVHSLVRIAFHDAIG       55
PHLRA-MnP2        -------KTTCSNG-VVVPDAVCCDFVPLASALQSEVLM-GDCGEDAHELVRLIFHDAIA       51
PHACH-MnP1        --------AVCPDG-TRVSHAACCAFIPLAQDLQETIFQ-NECGEDAHEVIRLTFHDAIA       50
BJEAD-LiP         ---AIIKRVACPDGRHTAINAACCNLFTVRDDIQRNMFDGGKCNDIAHQALRLTFHDAVA       57
PHLRA-LiP3        --ASVTRRATCPDG-TQLMNAECCALLAVRDDLQNNMFN-NECGDEAHEALRLTFHDAIA       56
PHACH-LiPH8       --------ATCSNG-KTVGDASCCAWFDVLDDIQQNLFHGGQCGAEAHESIRLVFHDSIA       51
PLEOS-MnP4        ---VPAHRAKCSKG-RTASNDACCVWFDVLDDIQENLFDGGECGEEVHESLRLTFHDAIG       56
BJEAD-VP          ---AITRRVACPDGVNTATNAACCALFAVRDDIQQNLFDGGECGEEVHESLRLTFHDAIG       57
BB8-PLEER-VP      --------ATCDDG-RTTANAACCILFPILDDIQENLFDGAQCGEKVRESLRLTFHDAIG       51
PLEOS-MnP5        -VSLPQKRATCAGG-QVTANAACCVLFPLMEDLQKNLFDDGACGEDAHEALRLTFHDAIG       58
PLEOS-VP3         -VTLPQKRATCAGG-QVTANAACCVLFPILEDLQQNLFDGGECGEEVHESLRLTFHDAIG       58
Consensus                   *  *     .  **    : . :   .     *   .:. :*: ***::.

AURDE-GP11        FSLTD----PSKGGGADGSIIMFGDTELNFHANEGIDFITAFLQPFADTVG-VTYGDAIQ       110
PHLRA-MnP2        ISQSMG---PSAGGGADGSMLIFPTVEPAFFPNLGIADSVNNLIPFLSQFPTISAGDLVQ       108
PHACH-MnP1        ISRSQG---PKAGGGADGSMLLFPTVEPNFSANNGIDDSVNNLIPFMQKHNTISAADLVQ       107
BJEAD-LiP         FSPALEAEGKFGGNGADGSIITFGNIETNFHPNIGLDEIVEIEKPFIARHN-MTPGDFLH       116
PHLRA-LiP3        ISPAMEATGQFGGGGADGSIMIFSDIETKFHPNIGLDEVVESFRPFQQRSG-MGVADFIQ       115
PHACH-LiPH8       ISPAMEAQGKFGGGGADGSIMIFDDIETAFHPNIGLDEIVKLQKPFVQKHG-VTPGDFIA       110
PLEOS-MnP4        FSPALTRQGKFGGGGADGSIMLFSDIETNFAANNGVDDIVEQQKPIAIKHQ-VSFGDFIQ       115
BJEAD-VP          ISPSIAATGKFGGGGADGSIMIFDDIEPNFHANNGVDEIINAQKPFVAKHN-MTAGDFIQ       116
BB8-PLEER-VP      FSPTLG-----G-GGADGSIIAFDTIETNFPANAGIDEIVSAQKPFVAKHN-ISAGDFIQ       104
PLEOS-MnP5        FSPSRG-----VMGGADGSVITFSDTEVNFPANLGIDEIVEAEKPFLARHN-ISAGDLVH       112
PLEOS-VP3         FSPTKG-----G-GGADGSVLTFSDPEVNFPANLGIDEIVEAQKPFLARHN-ISAGDLVQ       111
Consensus         :* :          *****:: .   *  *  * *:        *:      :  .* :
```

```
                                                     E140G                V160A
AURDE-GP11        FGAAVGLSLCPGAPT-IPAFVGRPNATMAAPDLTVPEPFDDPDKIFARMADA-GFTPVEL      168
PHLRA-MnP2        FAGAVAISNCPGAPQ-LEFLAGRPNATAPAIDGLIPEPQDDVTKILARFKDAGNFSPAEV      167
PHACH-MnP1        FAGAVALSNCPGAPR-LEFLAGRPNKTIAAVDGLIPEPQDSVTKILQRFEDAGGFTPFEV      166
BJEAD-LiP         FAGAIAVTNCPGAPT-ISFSLGRPVATRPAPDGLVPEPFHTPDQIFARMLDALEFDPLET      175
PHLRA-LiP3        FSGAVGTSNCPGAPT-LNAFIGRKDATQAAPDGLVPEPFHDVNTILARFNDAGDFDELET      174
PHACH-LiPH8       FAGRVALSNCPGAPQ-MNFFTGRAPATQPAPDGLVPEPFHTVDQIINRVNDAGEFDELEL      169
PLEOS-MnP4        FAGAVGSSNCAGGPR-IQFLAGRSNVTKPSPDHLVPEPFDSVTSILARMGDA-GFKPDEV      173
BJEAD-VP          FAGAVGVSNCPGAPQ-LSFFLGRPAATQPAPDGLVPEPFDSVTDILNRFADAGGFTTQEV      175
BB8-PLEER-VP      FAGAVGVSNCPGGVR-IPFFLGRPDAVAASPDHLVPGPFDSVDSILARMGDA-GFSPAEV      162
PLEOS-MnP5        FAGTLGVSNCPGAPQNLSFFLGRPPAKAASPIGLVPEPFDTITDILARMDDA-GFVSVEV      171
PLEOS-VP3         FAGALGVSNCPGAPR-IPFFLGRPPAKAASPIGLVPEPFDTVTDILDRMGDA-GFAAVEV      169
Consensus         *.. :. : * *.   :    **      :    :* * .    *: *. **  *   *

                                    P182ST184M       Q202L      D213A
AURDE-GP11        IHLLASHSIADQAGVDPEPQVLGAPFDSTPFSFDSQVFLEVLFEGILFPGSGPNPGELMS      228
PHLRA-MnP2        VALLASHSIARADHVDP--TLDAAPFDSTPFDFDTQIFLEVLLKGVGFPGLANNTGEVSS      225
PHACH-MnP1        VSLLASHSVARADKVDQ--TIDAAPFDSTPFTFDTQVFLEVLLKGVGFPGSANNTGEVAS      224
BJEAD-LiP         TWALIAHTVAAADDIDT--SIPRSPFDSTPELFDGQFFIETQLKGTLFPGNGPNKGEVRS      233
PHLRA-LiP3        VWFLIAHSVAAQNDIDP--AVSHAPFDSTPSVMDGQFFIETQLRGVEFIGSGGIEGVAES      232
PHACH-LiPH8       VWMLSAHSVAAVNDVDP--TVQGLPFDSTPGIFDSQFFVETQLRGTAFPGSGGNQGEVES      227
PLEOS-MnP4        VALLASHSVAAQDTIDP--KLAGHPFDSTPSDFDSQFFVETLLKGTLIPGDSLHKGQVKS      231
BJEAD-VP          VWLLASHSIAAADHVDP--TIPGSPFDSTPEIFDTQFFVETLLKGTLFPGTSGNQGEVES      233
BB8-PLEER-VP      VWLLASHSIAAADKVDP--SISGMPFDSTPGVFDSQFFIETLLKGRLFPGTAANKGEAQS      220
PLEOS-MnP5        VWLLSAHSVAAADHVDE--SIPGTPFDSTPNLFDSQIFIETQLRGISFPGTGGNHGEVQS      229
PLEOS-VP3         VWLLSSHTIAAADHVDE--SIPGTPFDSTPSIFDSQFFIETQLRGTSFPGSGGNHGEVES      227
Consensus            * :*::*    :*    :   ******  :* *.*:*. :.*  : * .   *   *


                               Q229P
AURDE-GP11        PLP-------GEFRLQSDKRFSLHNETACAWQENALSQSAMASNFQTAFTKLSLLGHDQN      281
PHLRA-MnP2        PLPVTDGTDVGELRLQSDFALARDERTACAWQSFVNEQEAMATAFKNAVKKLAVLGHNRN      285
PHACH-MnP1        PLPLGSGSDTGEMRLQSDFALAHDPRTACIWQGFVNEQAFMAASFRAAMSKLAVLGHNRN      284
BJEAD-LiP         PLA-------GEMRLQSDFLIARDNRSACEWQSFGTDHDKLTNRFQFVLETLAMVGQDPT      286
PHLRA-LiP3        PVK-------GEFRLMSDQQIARDNRTACEWQSFGTDQAKLQNRFQFIFEAMGQLGTDPT      285
PHACH-LiPH8       PLP-------GEIRIQSDHTIARDSRTACEWQSFVNNQSKLVDDFQFIFLALTQLGQDPN      280
PLEOS-MnP4        PLP-------GEFRLQSDELLARDSRTSCEWQSFISNPNSMVPKFERAMAKMATLGQNPK      284
BJEAD-VP          PLA-------GEIRLQSDADFARDSRTACEWQSFVNNQPRMQVLFKAAMQKLSILGHDLT      286
BB8-PLEER-VP      PLQ-------GEIRLPSDHLLARDPQTACEWQSMVNNQPKIQNRFAATMSKMALLGQDKT      273
PLEOS-MnP5        PLR-------GEMRLQSDHLFARDDRTSCEWQSMTNDQQKIQDRFSDTLFKMSMLGQNQD      282
PLEOS-VP3         PLA-------GEIRLQSDHLLARDSRTSCEWQSMVDNMPKIQNRFAATMLKMSLLGQNQA      280
Consensus         *:        **:*: **  :: . .::* **    .   :   *   .  :  :* :

AURDE-GP11        SLLDCSELIAQAPPATA--SQGFFPAGKTMEDLEIGCDAEAFPTTLVTQAGQPTMIPPVD      339
PHLRA-MnP2        DLVDCSAVVPVPKPATG--TPATFPASTGPQDLELTCTTEPFPTL-STAPGAQQTLIPHC      342
PHACH-MnP1        SLIDCSDVVPVPKPATG--QPAMFPASTGPQDLELSCPSERFPTL-TTQPGASQSLIAHC      341
BJEAD-LiP         NMIDCSEVIPIPRNLTS-AQIPHFPAGKTIRDVEAACPETPFPRL-PTDAGRPTAVAPVP      344
PHLRA-LiP3        TLIDCSDVLPVPPPL---STVPHFPAGITINDVEPACAETPFPTL-PTDPGPATAVAAVP      341
PHACH-LiPH8       AMTDCSDVIPQSKPIPGNLPFSFFPAGKTIKDVEQACAETPFPTL-TTLPGPETSVQRIP      339
PLEOS-MnP4        KLIDCSEVIPVPRGR---VKQPTLPAGKTIKDIEASCRKAPFPRL-PTDKGTFTSILPVP      340
BJEAD-VP          QMIDCSDVIPVPPST--AVRGSHLPAGNTLDDIEQACASTPFPTL-TADPGPATSVAPVP      343
BB8-PLEER-VP      KLIDCSDVIPTPPAL---VGAAHLPAGFSLSDVEQACAATPFPAL-TADPGPVTSVPPVP      329
PLEOS-MnP5        AMIDCSDVIPVPAAL---VTKPHLPAGKVRTDVEQACATDAFPAL-AADPGPVTSVPRVP      338
PLEOS-VP3         DLIDCSDVIPTPPAL---VGKAHLPAGKVQSDVEQACATTPFPAI-AADPGPVTAVPPVP      336
Consensus          : *** ::              :**.    *:*  *    **    :  *    :
```

S3

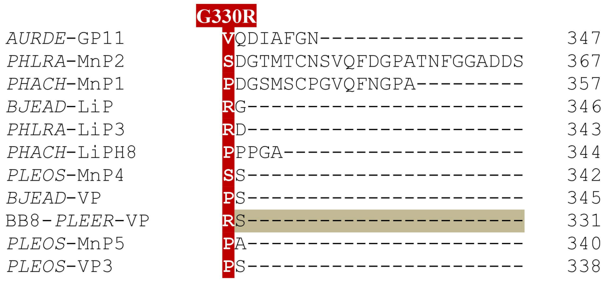

```
                     G330R
AURDE-GP11           VQDIAFGN-----------------     347
PHLRA-MnP2           SDGTMTCNSVQFDGPATNFGGADDS     367
PHACH-MnP1           PDGSMSCPGVQFNGPA---------     357
BJEAD-LiP            RG-----------------------     346
PHLRA-LiP3           RD-----------------------     343
PHACH-LiPH8          PPPGA--------------------     344
PLEOS-MnP4           SS-----------------------     342
BJEAD-VP             PS-----------------------     345
BB8-PLEER-VP         RS-----------------------     331
PLEOS-MnP5           PA-----------------------     340
PLEOS-VP3            PS-----------------------     338
```

Fig. S2 MSA of representative ligninolytic peroxidases.

Sequences were obtained from the Uniprot database and aligned together with BB-8-*PLEER*-VP (the VP mutant from *Pleurotus eryngii*, O94753; obtained in the present study) using the Clustal Omega server (http://www.ebi.ac.uk/Tools/msa/clustalo/). The accession numbers used in the MSA were: *AURDE*-GP11 (GP11 from *Auricularia delicata;* J0WUI3); *PHLRA*-MnP2 (MnP2 from *Phlebia radiata;* Q70LM3); *PHACH*-MnP1 (MnP1 from *Phanerochaete chrysosporium;* Q02567); *BJEAD-LiP* (LiP from *Bjerkandera adusta;* W8YN06); *PHLRA*-LiP3 (LiP3 from *Phlebia radiata;* Q53WT9); *PHACH*-LiPH8 (LiPH8 from *Phanerochaete chrysosporium;* P06181); *PLEOS*-MnP4 (MnP4 from *Pleurotus ostreatus;* A0A067NYV2); *BJEAD*-VP (VP from *Bjerkandera adusta;* W8YE46); *PLEPU*-MnP5 (MnP5 from *Pleurotus pulmonarius;* Q2VT17); *PLEOS*-VP3 (VP3 from *Pleurotus ostreatus;* A0A067NKY1). The mutations in the stabilizing backbone are highlighted in red, those mutations that promote functional expression in yeast in cyan, and the mutations driving activity at alkaline pHs in dark brown, orange and green.

	AURDE-GP11	*PHLRA*-MnP2	*PHACH*-MnP1	*BJEAD*-LiP	*PHLRA*-LiP3	*PHACH*-LiPH8	*PLEOS*-MnP4	*BJEAD*-VP	BB8-*PLEER*-VP	*PLEOS*-MnP5	*PLEOS*-VP3
AURDE-GP11	**100**	45.9	46.3	43.5	43.3	45.2	46.0	48.5	47.0	43.0	44.6
PHLRA MnP2	45.9	**100**	72.8	41.7	45.0	47.6	48.0	52.7	48.6	49.5	49.4
PHACH-MnP1	46.3	72.8	**100**	43.6	47.4	47.3	50.6	56.8	52.9	50.6	51.0
BJEAD-LiP	43.5	41.7	43.6	**100**	61.1	58.5	54.4	59.9	56.8	57.0	56.0
PHLRA-LiP3	43.3	45.0	47.4	61.1	**100**	63.2	50.4	58.8	54.2	52.2	53.3
PHACH-LiPH8	45.2	47.6	47.3	58.5	63.2	**100**	55.2	64.3	55.9	54.2	56.5
PLEOS-MnP4	46.0	48.0	50.6	54.4	50.4	55.2	**100**	62.6	63.1	53.7	59.5
BJEAD-VP	48.5	52.7	56.8	59.9	58.8	64.3	62.6	**100**	69.5	62.0	67.3
BB8-*PLEER*-VP	47.0	48.6	52.9	56.8	54.2	55.9	63.1	69.5	**100**	66.8	75.5
PLEOS-MnP5	43.0	49.5	50.6	57.0	52.2	54.2	53.7	62.0	66.8	**100**	81.0
PLEOS-VP3	44.6	49.4	51.0	56.0	53.3	56.5	59.5	67.3	75.5	81.0	**100**

Identity Matrix from MSA

SUPPLEMENTAL EXPERIMENTAL PROCEDURES

Reagents and strains

ABTS (2,2’-azino-bis(3-ethylbenzothiazoline-6-sulfonic acid)), 2,6-DMP (2,6-Dimethoxyphenol), Reactive black 5 (RB5), sinapic acid, guaiacol, veratryl alcohol, syringaldazine, catechol, Manganese sulphate, *Taq* DNA polymerase, bovine hemoglobin, hemin from bovine, Horseradish peroxidase (HRP) and the *S. cerevisiae* transformation kit were purchased from Sigma-Aldrich (Madrid, Spain). Hydrogen peroxide 30 % (v/v) was obtained from Merck Millipore (Darmstadt, Germany). *Pfu*-Ultra polymerase, *Escherichia coli* XL1-Blue chemocompetent cells and the GeneMorph II Kit (mutazyme II polymerase) were from Stratagene (La Jolla, CA, USA). The Zymoprep Yeast Plasmid Miniprep Kit was obtained from Zymo-Research (Orange, CA, USA). The Low melting point agarose was from Bio-Rad (Hercules, CA), the NucleoSpin and PCR clean-up kit from Macherey-Nagel (Düren, Germany) and the *Bam*HI and *Xho*I restriction enzymes from New England Biolabs (Hertfordshire, U.K.). The protease-deficient *S. cerevisiae* strain BJ5465 (α ura3-52 trp1 leu2Δ1 his3Δ200 pep4::HIS3 prb1Δ1.6R can1 GAL) was from LGCPromochem (Barcelona, Spain). The oligonucleotides used along the evolutionary process were purchased from Isogen Life Science (De Meern, The Netherlands). All chemicals were of reagent-grade purity.

Culture media

Synthetic complete (SC, minimum medium) contained 0.67% (w/v) yeast nitrogen base, 1.92 g/L yeast synthetic drop-out medium supplement without uracil, 2% (w/v) D-raffinose and 25 µg/mL chloramphenicol. SC-Hemin medium contained the recipe for SC plus bovine hemin (25 g/L) and 67 mM KH_2PO_4 buffer (pH 6.0). YP (1.55x) medium contained 10 g yeast extract, 20 g peptone and ddH_2O to 650 mL. Microplate expression medium (YP-Hb) contained 720 mL YP (1.55x), 67 mL 1 M KH_2PO_4 buffer (pH 6.0), 111 mL 20% (w/v) D-galactose, 100 mg/L bovine hemoglobin, 1 ml 25 g/L chloramphenicol and ddH_2O to 1000 mL. Microplate YP-EtOH expression medium contained 720 mL YP (1.55x), 67 mL 1 M KH_2PO_4 buffer (pH 6.0), 111 mL 20% (w/v) D-galactose, 25 g/L ethanol absolute, 1 ml 25 g/L chloramphenicol and ddH_2O to 1000 mL. YPD solution contained 1% (w/v) yeast extract, 2% (w/v) peptone, 2% (w/v) D-glucose and 25 µg/mL chloramphenicol. Flask expression medium contained 720 mL YP (1.55x), 67 mL 1 M KH_2PO_4 buffer (pH 6.0), 111 mL 20% (w/v) D-galactose, 25 g/L ethanol absolute, 500 mg/L bovine hemoglobin, 1 mM $CaCl_2$, 1 mL 25 g/L chloramphenicol and ddH_2O to 1,000 mL. SC drop-out plates contained 0.67% (w/v) yeast nitrogen base, 1.92 g/L (w/v) yeast synthetic drop-out medium supplement without uracil, 2% (w/v) bacto agar, 2% (w/v) D-glucose and 25 µg/mL chloramphenicol. Luria-Bertani (LB) medium was prepared with 1% (w/v) peptone, 0.5% (w/v) yeast extract, 1% (w/v) NaCl and 100 µg/mL ampicillin and in the case of drop-out plates LB/amp plus 2% (w/v) bacto agar.

Re-screenings

First re-screening: Aliquots of 5 µL of the best clones were removed from the master plates and used to inoculate 50 µL of SC minimal medium (SC-Hemin 1st generation) in new 96-well plates. Columns 1 and 12, and rows A and H, were not used to prevent the appearance of false positives. After incubating for 24 h at 30 °C, 225 rpm, and 80% relative humidity, 5 µL was transferred to the adjacent wells and incubated for a further 24 h. Finally, 160 µL of YP-Hb microplate expression medium (YP-EtOH for 1st generation) was added and the plates were incubated for another 24 h. Accordingly, each mutant was grown in 4 wells. The parental types were subjected to the same procedure (row D, wells 7-11) and the plates were assessed using the same protocols as those used for the HTS-screening protocol.

Second re-screening: An aliquot from the wells with the best clones in the first re-screening was inoculated in 3 mL of YPD and incubated at 30 °C and 225 rpm for 24 h, recovering the plasmids from these cultures (Zymoprep Yeast Plasmid Miniprep Kit). As the product of the zymoprep was very impure and the concentration of DNA extracted very low, the zymoprep mixtures containing shuttle vectors were transformed into super-competent *E. coli* cells (XL1-Blue, Stratagene) and plated on LB/amp plates. Single colonies were picked and used to inoculate 5 mL LB/amp media, and they were grown overnight at 37 °C and 225 rpm. The plasmids were then extracted (NucleoSpin Plasmid kit, Macherey-Nagel, Germany) and *S. cerevisiae* suspension was transformed with plasmids from the best mutants as well as with the parental type. Five colonies for each mutant were selected and re-screened as described above.

Third re-screening (determination of pH profiles, kinetic thermo-stabilities and pH stabilities): A single colony from the *S. cerevisiae* clone containing the parental 2-1B, the new mutants and untransformed yeast were picked from a SC drop-out plate (SC supplemented with uracil for untransformed cells), inoculated into 5 mL of minimal medium and incubated for 48 h at 30 °C and 225 rpm (Orbitron-INFORS, Biogen, Spain). An aliquot of cells was removed and used to inoculate a final volume of 5 mL of minimal medium in a 50 mL falcon tube (optical density, OD_{600} = 0.3), and they were incubated until two growth phases were completed (6-8 h, OD_{600} = 1). Thereafter, 9 mL of flask expression medium (500 mg/L bovine hemoglobin) was inoculated with 1 mL of this pre-culture in a 100 mL flask (OD_{600} = 0.1). After incubating for ~48 h at 30 °C and 225 rpm (maximal VP activity; OD_{600} = 25-30), the cells were separated by centrifugation for 15 min at 3,000 rpm and 4 °C (Eppendorf 5810R Centrifuge with F-34-6-38 rotor, Germany), and the supernatants were collected and stored at 4 °C.

pH activity profile: Parental type (2-1B) and the mutant winners of each round of evolution were assayed for activity in a pH range from 2 to 9. Aliquots (20 µL) of crude supernatants from *S. cerevisiae* were diluted to give a linear response in kinetic mode. Then, 180 µL of reaction mixture were added using a Multidrop station (Multidrop Combi, ThermoFischer Scientific,Vantaa, Finland). The final concentrations of reaction mixture per well were 100 mM citrate-phosphate-borate buffer at different pH (2-10), 0.1 mM of H_2O_2 and 2 mM ABTS. The absorbance was recorded at 418 nm in kinetic mode using the plate reader.

pH stability assay: Appropriate dilutions of the supernatants were prepared such that aliquots (20 µL) produced a linear response in kinetic mode. Each variant was diluted in 100 mM citrate-phosphate-borate buffer with pH ranging from 3.0-10.0. Aliquots of 20 µL were removed during 144h and measured in the presence of 180 µL of reaction. The final concentrations in the well were 100 mM citrate-phosphate-borate buffer pH 4.0, 0.1 mM of H_2O_2 and 2 mM ABTS. The absorbance was monitored at 418 nm in kinetic mode using a plate reader.

Thermostability assay (T_{50}): A gradient profile was constructed using a thermocycler (Mycycler, Bio-Rad, USA) for the selected mutants and the parental type, using 50 µL for each point in a gradient scale ranging from 30 to 80 ºC. After a 10 min incubation, samples were removed and chilled on ice for 10 min. Thereafter, 20 µL samples were removed and incubated for 5 min at room temperature. Finally, 180 µL of 100 mM sodium tartrate buffer (pH 4.0), 2 mM ABTS and 0.1 mM H_2O_2 was added to the samples to measure activities. The thermostability values were calculated as the ratio between the residual activity at different temperature points and the initial activity at room temperature.

Production and Purification of VP variants

A single colony from transformed yeast cells was used to inoculate 20 mL of SC minimal medium (in a 100 mL flask) and incubated for 48h at 30 °C and 220 rpm (Orbitron-INFORS, Biogen, Spain). Then, OD_{600} was measured and this pre-culture used to inoculate 120 mL of minimal medium in a 250 ml flask (OD_{600}= 0.3). They were incubated until two growth phases had been completed (6-8 h, OD_{600} = 1) and thereafter, 450 mL of flask expression medium (500 mg/L bovine hemoglobin) was inoculated with 50 mL of this pre-culture in a 2 litre baffled flask (OD_{600}= 0.1). The cultures were incubated for 48h at 30 °C and 230 rpm (Micromagmix shaker) and the maximal VP activity reached (OD_{600} =25–30); the cells were recovered by centrifugation at 5,000 rpm for 30 min at 4 °C (Avanti J-E centrifuge Beckman Coulter with JA-14 rotor, Fullerton, CA). The supernatant was collected and triple filtered (through filter paper, a glass fibre filter and then a nitrocellulose membrane of 0.45 µm pore size).

Purification protocol: VP crude extracts were first submitted to a fractional precipitation with ammonium sulphate (50-75%). Samples were pelleted at 12,000 rpm, 15 min and 4 °C (Avanti J-E centrifuge Beckman Coulter with JA-14 rotor). The final pellet was recovered and dialyzed in 20 mM piperazine buffer (buffer P, pH 5.5), then the sample was filtered and loaded on to the FPLC (Äkta Purifier; GE Healthcare Uppsala, Sweden) coupled with a strong anion-exchange column (HiTraP QFF; GE Healthcare Uppsala, Sweden) pre-equilibrated with buffer P. The proteins were eluted with a linear gradient from 0 to 1 M of NaCl in two phases at a flow rate of 1 ml/min: from 0 to 25% over 60 min and from 25 to 100% over 5 min. Fractions with VP activity were pooled, concentrated and dialysed against buffer P with a stirred ultrafiltration cell and an ultracell 10 kDa ultrafiltration Disc of 44.5 mm (Amincon cell, Merck

Millipore, Germany). Thereafter, samples were loaded onto a HPLC–PDA column coupled with a 10 µm high resolution anion-exchange Biosuite Q (Waters) pre-equilibrated with buffer P. The proteins were eluted on a linear gradient from 0 to 1 M NaCl at a flow rate of 1 ml/min in two phases: from 0 to 6% in 30 min, and from 6 to 100% in 5 min. The fractions with VP activity were pooled, dialysed against 10 mM sodium tartrate buffer (pH 5.0), concentrated and stored at 4 °C. Throughout the purification protocol, the fractions were analysed by SDS/PAGE on 12% gels and the proteins were stained with colloidal Coomassie Blue (Protoblue Safe, National Diagnostics). Purified VP concentrations were determined spectrophotometrically (SHIMADZU UV-1800 spectrophometer, Columbia, MD, USA) in 1 mL quartz cuvettes with molar extinction coefficient for VP at 407nm (ε_{VP} =150,000 M^{-1}. cm^{-1}).The Reinheitszahl values (R_z: Abs_{407}/Abs_{280}) obtained were above 2.

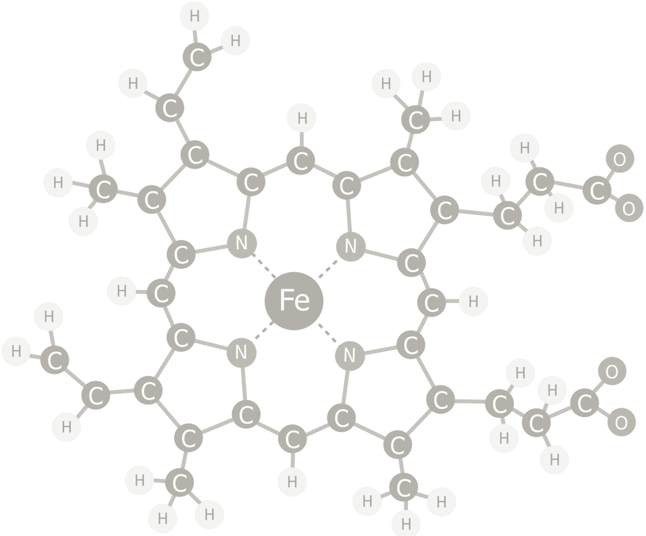

Capítulo 6:

Saccharomyces cerevisiae in directed evolution: an efficient tool to improve enzymes

En este capítulo describen las principales características de la levadura Saccharomyces cerevisiae como hospedador heterólogo y vehículo recombinante (con el que crear protocolos de diversidad genética in vivo) para experimentos de evolución dirigida.

Bioengineered Bugs 3:3, 172–177; May/June 2012; © 2012 Landes Bioscience

Saccharomyces cerevisiae in directed evolution
An efficient tool to improve enzymes

David Gonzalez-Perez, Eva Garcia-Ruiz and Miguel Alcalde*

Department of Biocatalysis; Institute of Catalysis; CSIC; Madrid, Spain

Keywords: Directed evolution, *Saccharomyces cerevisiae*, DNA recombination, random mutagenesis, IvAM, IVOE

Abbreviations: bp, base pair; CiP, *Coprinopsis cinerea* peroxidase; CLERY, combinatorial libraries enhanced by recombination in yeast; CSM, combinatorial saturation mutagenesis; epPCR, error prone-PCR; ER, endoplasmatic reticulum; FACS, fluorescence activated cell sorter; HTPS, high-throughput screening; IvAM, in vivo assembly of mutant libraries with different mutational spectra; IVOE, in vivo overlap extension; MtL, *Myceliophthora thermophila* laccase; PcL, *Pycnoporus cinnabarinus* laccase; SOE, splicing by overlap extension; StEP, staggered extension process; VP, versatile peroxidase

Over the past 20 years, directed evolution has been seen to be the most reliable approach to protein engineering. Emulating the natural selection algorithm, ad hoc enzymes with novel features can be tailor-made for practical purposes through iterative rounds of random mutagenesis, DNA recombination and screening. Of the heterologous hosts used in laboratory evolution experiments, the budding yeast *Saccharomyces cerevisiae* has become the best choice to express eukaryotic proteins with improved properties. *S. cerevisiae* not only allows mutant enzymes to be secreted but also, it permits a wide range of genetic manipulations to be employed, ranging from in vivo cloning to the creation of greater molecular diversity, thanks to its efficient DNA recombination apparatus. Here, we summarize some successful examples of the use of the *S. cerevisiae* machinery to accelerate artificial evolution, complementing the traditional in vitro methods to generate tailor-made enzymes.

Throughout evolution, natural selection promotes the survival of specific organisms at the expense of thousands with trait/s that are not optimal to live in a given environment. Alterations to genes and enzymes are generated by processes such as random mutagenesis, DNA recombination, deletion and/or insertion, augmenting the diversity in this pool. These molecular modifications are then subjected to rigorous and constant testing by environmental factors, selection processes that drive the survival or disappearance of genes and enzymes. Typically, beneficial mutations (or neutral mutations that may become beneficial) accumulate and are recombined in the offspring. After successive generations of strict selective pressure, such mutations can give rise to new phenotypes. In February 2011, the Draper prize (considered the Nobel of Engineering) was awarded to Frances Arnold and Willem Stemmer for the development of Directed Molecular Evolution. This is a tool that has revolutionized the manner in which proteins are manipulated in the laboratory in order to improve their application in distinct industrial settings. By mimicking the mutation, recombination and selection processes that occur naturally in evolution, in vitro evolution provides a means of directing the evolution of genes toward specific goals in a manner that may not occur in a natural environment[1,2] (**Fig. 1**).

Heterologous Functional Expression in *Saccharomyces cerevisiae*

The in silico analysis of genes/enzymes by computational methods is a valuable approach to engineer "smart" libraries reducing the exploration of the vast protein sequence space. This strategy can be combined with powerful tools for HTP-screening [e.g., fluorescence activated cell sorter (FACS)], providing another twist in enzyme engineering by laboratory evolution.[3-8] Still, there are 3 basic premises to carry out a laboratory evolution experiment: (1) a suitable functional expression system; (2) reliable screening assays with which to detect improvements introduced after each round of evolution; and (3) the support of in vitro or in vivo methods to create enzyme diversity. The bacteria *Escherichia coli* is by far the most widely used host in directed evolution as it has a well-described physiology and it reproduces rapidly, making experiments less time-consuming. Moreover, standardized protocols are available to manipulate this bacteria and to rapidly recover the screened variants. While these characteristics generally hold true for prokaryotic proteins, bacterial hosts are less appropriate when working with eukaryotic genes, often resulting in misfolded, deglycosylated, non-functional or altered proteins, and the accumulation of the desired enzyme in inclusion bodies.[9-11]

*Correspondence to: Miguel Alcalde; Email: malcalde@icp.csic.es
Submitted: 12/30/11; Revised: 01/28/12; Accepted: 01/31/12
http://dx.doi.org/10.4161/bbug.19544

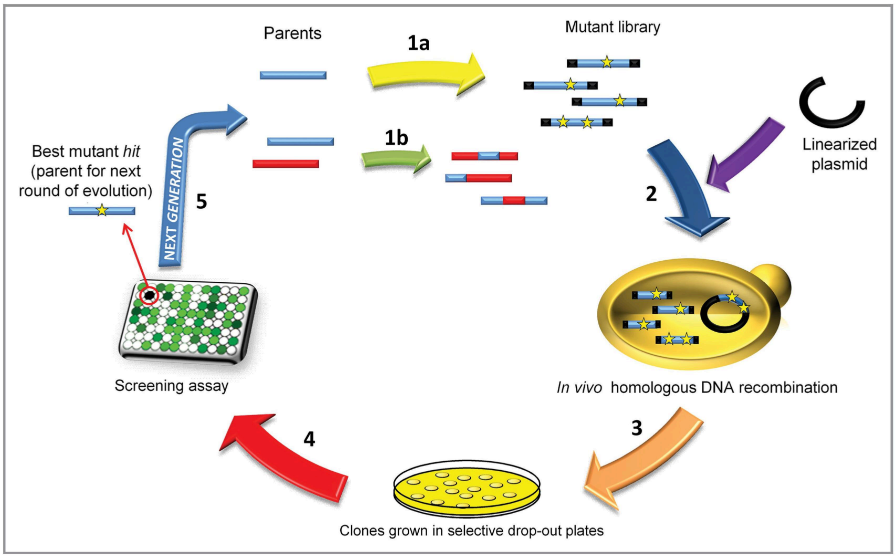

Figure 1. A typical directed evolution experiment using *Saccharomyces cerevisiae* as a eukaryotic host. The cycle of evolution begins with the generation of diversity by epPCR (1A) or in vitro DNA-recombination (1B). The mutagenic library is transformed into *S. cerevisiae* (2) and the pool of templates is further recombined by in vivo DNA shuffling. Each template contains adequate overhangs (shown in black) that overlap with the linearized plasmid, facilitating in vivo cloning to generate the autonomously replicating and repaired vector. The clones are grown on selective drop-out plates (3) and transferred to 96-well plates where the expression of mutants is induced. After secretion, the supernatants are subjected to a high throughput assay (4) to select the best enzyme variants. Generally, consecutive re-screenings are incorporated to rule out the presence of false positives. Finally, the best hits are recovered, characterized and their genes subjected to a further generation of directed evolution (5). Yellow stars indicate single mutations.

These shortcomings can be circumvented by using eukaryotic hosts such as *Pichia pastoris* or *Saccharomyces cerevisiae*. *P. pastoris* can secrete large amounts of proteins and mediate post-translational modifications. However, most vectors available for heterologous expression in *P. pastoris* are integrative—although there are a few exceptions[12]—which together with a low efficiency of integration limits their use for HTP-screening (HTPS) and laboratory evolution. Recent efforts have sought to integrate linear expression cassettes in order to express mutant libraries of hydroxynitrile lyases.[13] Nevertheless, a cumbersome mutant recovery process and poor transformation rates are still big obstacles which discourage scientists to take this approach. Fortunately, *S. cerevisiae* provides a solution to these bottlenecks as it exhibits high transformation efficiencies (from 1 × 10^6 to 1 × 10^8 transformants/μg DNA depending on the yeast strain), it performs post-translational modifications (e.g., processing of N- and C-terminal ends, glycosylation), and it possesses a fully developed secretory machinery that directs the secretion of proteins into the culture medium (bypassing the tedious lysis steps generally required when working with *E. coli* and avoiding any interference of complex lysate mixtures in the screening assays[14,15]). *S. cerevisiae* may hyperglycosylate heterologous proteins (in some cases over 50% of the enzyme molecular weight) by the addition of mannose moiteties at the Golgi compartment, a side-consequence of difficulties found during the exocytosis. This effect, although generally beneficial for protein stability—at the time that protect the enzyme from proteolytic degradation—generates a pool of isoforms which makes difficult the enzyme purification and biochemical characterization. Interestingly, in recent examples tackled in our laboratory (with high redox potential peroxidases and laccases, see below), mutations discovered by directed evolution helped us to surpass this hurdle by reducing the residence time at the Golgi, which generated new variants whose glycosylation degrees were below 10% showing a noticeable improvement in secretion yields.[16,17] It is also worth noting that multicopy episomal and bi-functional vectors are available to help identify and isolate the variants of interest screened from mutant libraries in *S. cerevisiae*. Finally, *S. cerevisiae* exhibits a high frequency of homologous DNA recombination with proof-reading activity, enabling in vivo recombination of the best mutant hits to occur at stages that prevent the incorporation of new mutations, as usually occurs in classical in vitro recombination protocols.[18] Given these many advantages, *S. cerevisiae* has begun to be heavily exploited for the functional expression of evolved eukaryotic enzymes in the laboratory.

Despite the advantages offered by *S. cerevisiae*, there are cases where the initial secretion levels of the target protein are not sufficiently high to perform artificial evolution. However, it has proved possible to adopt different strategies to considerably augment the secretion of such proteins in *S. cerevisiae*. One approach involves the introduction of random mutations in processing regions of the native gene to adjust the nascent polypeptide to the specific attributes of the proteases found in the secretory route. This approach has been successfully applied in the evolution of the laccase from the ascomycete *Myceliophthora thermophila* (MtL) in *S. cerevisiae* for functional expression.[19] The single most beneficial mutation (producing a 10-fold enhancement in total activity) was found at the C-terminal tail of MtL, and it involved the introduction of a cleavage site for the *KEX2* Golgi protease. An alternative strategy involves replacement of the signal peptide of the native protein with other signal leaders that are recognized better by *S. cerevisiae*. In particular, the construction of fusion genes with the α-factor prepro-leader from *S. cerevisiae* can drive protein secretion.[20,21] Indeed, *S. cerevisiae* can process the native signal peptide of foreign proteins in some cases, as seen with the aspartic proteinase from *Mucor pusillus* and the glucoamylase from *Aspergillus awamorii,* among other examples.[22,23] However, by replacing the native signal leader with the α-factor prepro-leader, expression can be significantly enhanced.[24] As ligninolytic enzymes are remarkably difficult to express in non-fungal systems,[18,25] our group has used this approach to enhance the expression of these interesting oxidoreductases in *S. cerevisiae*. In recent studies performed in our laboratory, the native secretion leaders of genes encoding two different high redox potential laccases (PM1L, from basidiomycete PM1, and PcL from *Pycnoporus cinnabarinus*) and one peroxidase (VP, the versatile peroxidase from *Pleurotus eryngii*) were replaced by the α-factor prepro-leader.[16,17,26] The secretion of these fusion constructs was greater than that of these enzymes with their native leader (by at least one order of magnitude). Moreover, secretion could be further augmented by subjecting the entire gene (i.e., the α-factor prepro-leader plus the mature protein) to directed evolution. This strategy allowed us to adjust both the α-factor prepro-leader and the gene encoding the mature protein to the subtleties of the yeast secretory pathway. The canonical pre-leader is involved in the orientation and insertion of the nascent polypeptide during translocation to the endoplasmic reticulum (ER). Interestingly, mutations in the hydrophobic core of the pre-leader were discovered during the evolution of PcL and PM1L that enhanced secretion several fold (A[α9]D and V[α10]D, respectively). Positions 9 and 10 of the pre-leader were further analyzed by constructing individual and double mutants containing the corresponding substitutions: A[α9]D and V[α10]D mutations exerted a 2.2-fold improvement in secretion individually but not when they were introduced together in the same variant.[16] Our results address that slightly increasing the hydrophilicity of the signal pre-leader may have beneficial effects on the interaction between the pre-leader and the signal recognition particle by improving the translocation of the polypeptide chain into the ER.[27] We also detected several interesting mutations in the pro-leader during the directed evolution of PM1L and PcL that altered the affinity for sugar anchoring (N[α23]K and S[α58]G, respectively). As these positions correspond to 2 of the 3 N-glycosylation sites in the pro-leader, they may affect ER to Golgi protein transport.[16] Recent studies demonstrated that mutations in the α-factor prepro-leader can enhance heterologous protein secretion in *S. cerevisiae* of a variety of proteins.[28] In fact, some of these mutations that increase secretion were the same as those identified for laccase fusion genes in yeast in our laboratory (position and nucleotide change). Finally, our evolved α-factor prepro-leaders were fused with native (non-mutated) laccases, enhancing secretion by up to 40-fold and thereby corroborating the significance of the mutations induced by directed evolution.[26] Taken together, these findings suggest that the directed evolution of the α-factor prepro-leader may give rise to a universal signal peptide for the heterologous expression of foreign proteins in yeast.

Exploiting the Machinery of *S. cerevisiae* for Directed Enzyme Evolution

Developing successful directed evolution experiments requires an appropriate array of molecular methods to allow the user to generate diversity. In this context, the power of *S. cerevisiae* cannot be underestimated. *S. cerevisiae* constitutes a simple and efficient vehicle to create libraries for directed evolution, exhibiting a high frequency of homologous DNA recombination with multiple recombination pathways generated by double-strand breaks.[29] A recent study reported that *S. cerevisiae* can recombine up to 38 overlapping single-stranded oligonucleotides and a linear double-stranded vector in just one transformation event.[30] Crossover areas can contain as few as 20 base pairs and as many as 200 homologous nucleotides. The importance of the length of the overlapping ends in the crossover region between the DNA fragment and the linearized plasmid to achieve high recombination efficiencies has been demonstrated. Thus, a homologous region of at least 40 base pairs appears to be necessary to obtain recombination efficiencies of over 60%.[31]

Recently, the full capacities of *S. cerevisiae* were challenged by a methodology known as *DNA assembler*, which was used to successfully assemble an entire biochemical pathway in a single step via in vivo homologous recombination.[32] In directed evolution, we use the DNA recombination machinery of *S. cerevisiae* to in vivo clone and recombine mutant libraries with the linearized vector, avoiding tedious ligation steps (**Fig. 2A**). To perform this type of experiment, it is necessary to engineer overlapping areas of approximately 40 bp of homology with the ends of the linearized vector, coupling the mutants generated to the corresponding screening assay. The number of crossover events among the inserts can also be enhanced (increasing the likelihood of recombining beneficial mutations between templates) by testing different overlapping regions with less homology to the linear vector, although the transformation efficiency may be compromised. In this context, in vivo DNA shuffling based on the *S. cerevisiae* recombination machinery is a powerful tool, speeding up the evolution process by shuffling parental genes with sequence homologies of ~70% at one point in the process where the whole autonomously replicating vector is repaired by the yeast's in vivo gap repair mechanism (**Fig. 2B**). One of the first pioneering works of in vivo DNA shuffling was reported by Cherry and coworkers to engineer oxidative stability into the low-medium redox potential peroxidase from *Coprinopsis cinerea* (CiP).[33] Although in vivo DNA shuffling relies on the proofreading device of *S. cerevisiae*, we observed better improvements

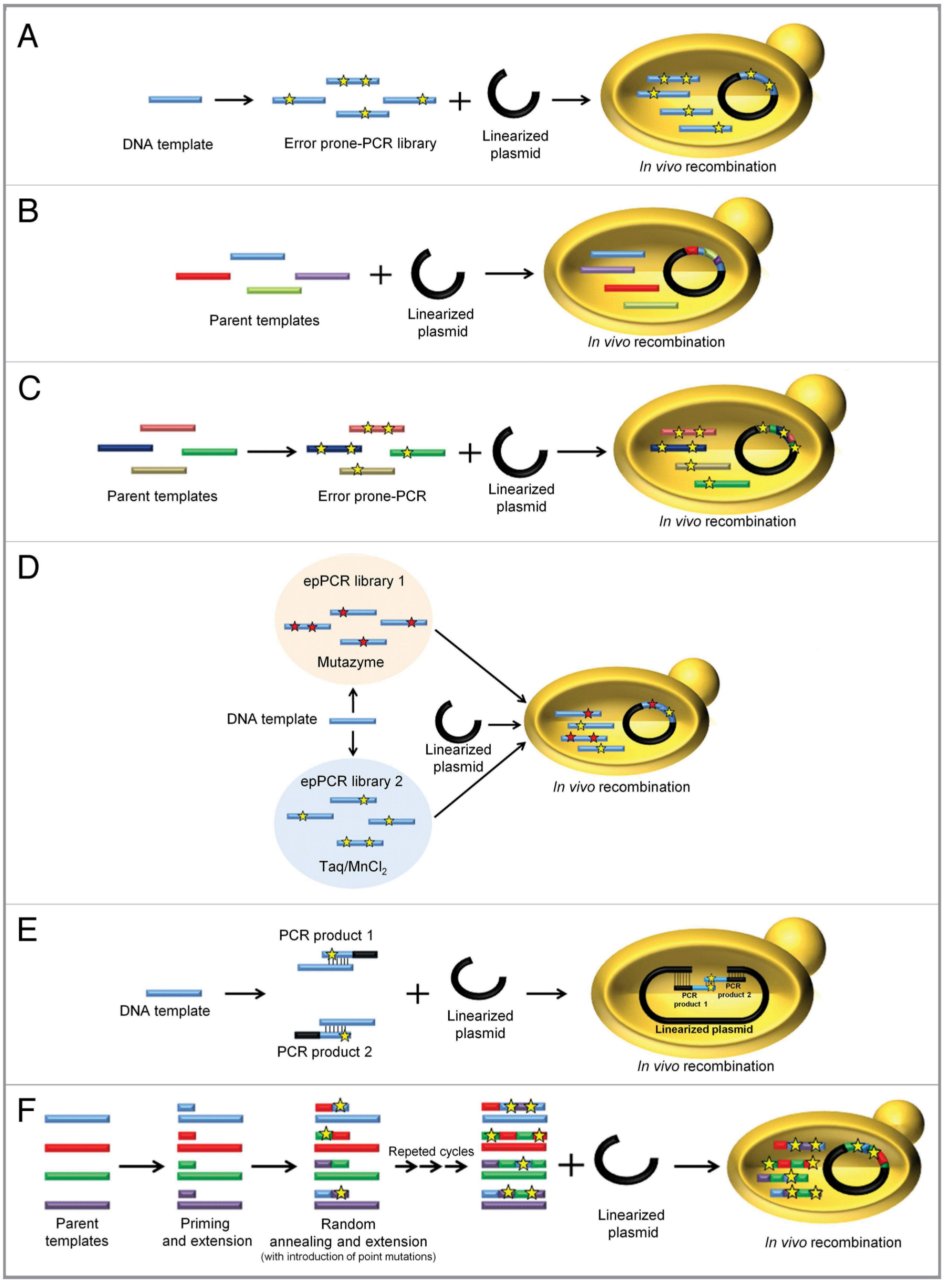

Figure 2. Different methods used to generate diversity using the *S. cerevisiae* toolbox. (A) epPCR from a single template followed by in vivo recombination in *S. cerevisiae.* (B) In vivo DNA shuffling. Several parental genes are recombined and cloned with a linearized vector into *S. cerevisiae* in a single step. (C) epPCR in conjunction with in vivo DNA shuffling. (D) IvAM (In vivo Assembly of Mutant libraries with different mutational spectra). Two or more distinct mutant libraries are generated by epPCR using polymerases with different biases. *S. cerevisiae* is transformed with the mutant libraries together with the linearized plasmid. (E) IVOE for combinatorial saturation mutagenesis or site-directed mutagenesis. The gene is amplified in two independent PCR reactions using mutagenized/degenerate primers. By engineering specific overhangs, the PCR products are then cloned into *S. cerevisiae* together with the linearized plasmid in a single transformation. (F) Mutagenic StEP (Staggered Extension Process). Several parental genes are used as templates during mutagenic StEP, promoting the random introduction of mutations during the short cycles of annealing and extension. The resulting mutant/recombined library is further shuffled by *S. cerevisiae*, together with the linearized plasmid. Stars represent single mutations.

in each cycle of evolution when error-prone PCR (epPCR) products of different templates were recombined in vivo in order to introduce new mutations in conjunction with recombination (**Fig. 2C**). In addition to our own works,[16,17,26,34,35] in vivo DNA shuffling has also been applied to other studies such as the engineering of chimeric enzymes from four different templates of Trametes C30 laccase with low and high redox potentials.[36]

Given the inherent degeneracy of the genetic code and the fact that some errors in the genetic code cause silent mutations, diversity is more fault-tolerant to point mutations. Moreover, epPCR methods (**Fig. 2A**) tend to introduce transitions (A↔G/T↔C) rather than transversion (A↔T/G↔C), limiting the mutagenic spectrum and introducing the intrinsic bias of each specific polymerase.[37] We sought to offset this tendency by designing new molecular tools based on the physiology of *S. cerevisae* (IvAM, IVOE). IvAM (In vivo Assembly of Mutant libraries with different mutational spectra) permits the combination of two or more mutant libraries created by different mutagenic approaches. The mutant libraries to be in vivo recombined can be developed by epPCR using polymerases with different biases. Despite the intrinsic bias derived from the codon usage of *S. cerevisiae*, this technique helps to enhance the mutational spectrum[34] (**Fig. 2D**). IvAM has been applied to the directed evolution of the MtL in order to confer organic co-solvent tolerance.[35] We identified two beneficial mutations in two consecutive codons during the same cycle of evolution (G614D and E615K), probably induced as a consequence of the IvAM technique. Similarly, we employed IvAM to evolve VP toward thermal stability, raising the T_{50} by 8°C in the final VP mutant.[17] IVOE (In Vivo Overlap Extension) is a simple protocol applied to semi-rational or rational approaches such as combinatorial saturation mutagenesis (CSM), site-directed mutagenesis, site-directed recombination, insertions and deletions. IVOE is based on conventional SOE (Splicing by Overlap Extension),[38] although several of the in vitro steps in SOE are missing. Our method involves the engineering of mutagenic primers that generate PCR products with homologous regions, both with one another and with the linearized plasmid. These PCR fragments are transformed into the yeast together with the linearized plasmid, promoting in vivo DNA recombination and generating a circular plasmid with the desired mutation/s (**Fig. 2E**).[39,40] We previously improved the properties of hot-spot residues in MtL by combining CSM with IVOE.[39] Moreover, in an attempt to enhance the activity and stability of PM1L using IVOE, we performed site-directed mutagenesis studies to recover beneficial mutations discarded during the evolutionary pathway. The final PM1L mutant was readily secreted by *S. cerevisiae* (~8 mg/L) in an active and stable form with regards temperature, pH range and organic co-solvents.[16] We also used IVOE to demonstrate how VP secretion was affected by linking an extra four amino acid N-terminal tail to the mature protein (EAEA). The truncated VP variant was engineered by deletion mutagenesis through IVOE, confirming that the *STE13* protease failed to process the extra N-terminal extension in the Golgi compartment of *S. cerevisiae*.[17] Another interesting application of IVOE developed in our laboratory involves the fusion of different enzymes with the α-factor prepro-leader of *S. cerevisiae*.[16,17,26] We engineered primers with homologous overhangs in order to generate fragments that were spliced in vivo to produce proteins fused to the α-factor prepro-leader, replacing the native signal peptide.

It is feasible to combine in vitro and in vivo methods for DNA-recombination to perform directed enzyme evolution. Indeed, in vitro DNA recombination and in vivo DNA shuffling were combined to increase the mutagenic spectrum of a given library (a method known as CLERY; Combinatorial Libraries Enhanced by Recombination in Yeast).[41] Similarly, we modified conventional StEP (Staggered Extension Process)[42] to enhance the likelihood of introduction of random mutations in the process (Mutagenic StEP, **Figure 2F**), and we combined this strategy with in vivo DNA shuffling in the same round of evolution to create a temperature, peroxide and alkaline-pH tolerant VP that was secreted readily by yeast (~22 mg/L).[17]

In the past decade, *S. cerevisiae* has been used widely in the directed evolution of proteins. As a host, *S. cerevisiae* possesses all the necessary cellular machinery required to secrete active and functional eukaryotic proteins. As a biomolecular toolbox, *S. cerevisiae* permits new strategies to be designed that boost and direct the evolutionary process, complementing the traditional methods used to tailor enzymes á la carte. We hope that in the near future, *S. cerevisiae* will serve as a platform to support the directed evolution of artificial operons and metabolic pathways, thereby providing us with a powerful microbial cell factory for synthetic biology.

Disclosure of Potential Conflicts of Interest

No potential conflicts of interest were disclosed.

Acknowledgments

This paper is based on research funded by EU Projects (FP7–3D-Nanobiodevices: NMP4-SL-2009–229255; FP7-KBBE-2010–4-26537: Peroxicats; COST Action CM0701) and a National project (Evofacel, BIO2010–19697).

References

1. Bloom JD, Arnold FH. In the light of directed evolution: pathways of adaptive protein evolution. Proc Natl Acad Sci U S A 2009; 106(Suppl 1):9995-10000; PMID:19528653; http://dx.doi.org/10.1073/pnas.0901522106
2. Romero PA, Arnold FH. Exploring protein fitness landscapes by directed evolution. Nat Rev Mol Cell Biol 2009; 10:866-76; PMID:19935669; http://dx.doi.org/10.1038/nrm2805
3. Dalby PA. Strategy and success for the directed evolution of enzymes. Curr Opin Struct Biol 2011; 21:473-80; PMID:21684150; http://dx.doi.org/10.1016/j.sbi.2011.05.003
4. Jäckel C, Hilvert D. Biocatalysts by evolution. Curr Opin Biotechnol 2010; 21:753-9; PMID:20850962; http://dx.doi.org/10.1016/j.copbio.2010.08.008
5. Shivange AV, Marienhagen J, Mundhada H, Schenk A, Schwaneberg U. Advances in generating functional diversity for directed protein evolution. Curr Opin Chem Biol 2009; 13:19-25; PMID:19261539; http://dx.doi.org/10.1016/j.cbpa.2009.01.019
6. Bershtein S, Tawfik DS. Advances in laboratory evolution of enzymes. Curr Opin Chem Biol 2008; 12:151-8; PMID:18284924; http://dx.doi.org/10.1016/j.cbpa.2008.01.027
7. Wong TS, Roccatano D, Schwaneberg U. Steering directed protein evolution: strategies to manage combinatorial complexity of mutant libraries. Environ Microbiol 2007; 9:2645-59; PMID:17922750; http://dx.doi.org/10.1111/j.1462-2920.2007.01411.x
8. Lutz S. Beyond directed evolution–semi-rational protein engineering and design. Curr Opin Biotechnol 2010; 21:734-43; PMID:20869867; http://dx.doi.org/10.1016/j.copbio.2010.08.011
9. Chen R. Bacterial expression systems for recombinant protein production: E. coli and beyond. Biotechnol Adv 2011; 2012. In press. PMID:21968145; http://dx.doi.org/10.1016/j.biotechadv.2011.09.013
10. Sørensen HP, Mortensen KK. Advanced genetic strategies for recombinant protein expression in Escherichia coli. J Biotechnol 2005; 115:113-28; PMID:15607230; http://dx.doi.org/10.1016/j.jbiotec.2004.08.004
11. Khow O, Suntrarachun S. Strategies for production of active eukaryotic proteins in bacterial expression system. Asian Pacific Journal of Tropical Biomedicine 2012: 159-162.
12. Lee CC, Williams TG, Wong DW, Robertson GH. An episomal expression vector for screening mutant gene libraries in *Pichia pastoris*. Plasmid 2005; 54:80-5; PMID:15907541; http://dx.doi.org/10.1016/j.plasmid.2004.12.001
13. Liu Z, Pscheidt B, Avi M, Gaisberger R, Hartner FS, Schuster C, et al. Laboratory evolved biocatalysts for stereoselective syntheses of substituted benzaldehyde cyanohydrins. Chembiochem 2008; 9:58-61; PMID:18058961; http://dx.doi.org/10.1002/cbic.200700514
14. Arnold F, Georgious G. Directed enzyme evolution: screening and selection methods. Humana Press 2003, Totowa, New Jersey (USA).
15. Arnold F, Georgious G. Directed evolution: library creation. Methods and protocols. Humana Press 2003, Totowa, New Jersey (USA).
16. Maté D, García-Burgos C, García-Ruiz E, Ballesteros AO, Camarero S, Alcalde M. Laboratory evolution of high-redox potential laccases. Chem Biol 2010; 17:1030-41; PMID:20851352; http://dx.doi.org/10.1016/j.chembiol.2010.07.010
17. Garcia-Ruiz E, Gonzalez-Perez D, Ruiz-Dueñas FJ, Martínez AT, Alcalde M. Directed evolution of a temperature-, peroxide- and alkaline pH-tolerant versatile peroxidase. Biochem J 2012; 441:487-98; PMID:21980920; http://dx.doi.org/10.1042/BJ20111199
18. Maté D, García-Ruiz E, Camarero S, Alcalde M. Directed evolution of fungal laccases. Curr Genomics 2011; 12:113-22; PMID:21966249; http://dx.doi.org/10.2174/138920211795564322
19. Bulter T, Alcalde M, Sieber V, Meinhold P, Schlachtbauer C, Arnold FH. Functional expression of a fungal laccase in *Saccharomyces cerevisiae* by directed evolution. Appl Environ Microbiol 2003; 69:987-95; PMID:12571021; http://dx.doi.org/10.1128/AEM.69.2.987-995.2003
20. Zsebo KM, Lu HS, Fieschko JC, Goldstein L, Davis J, Duker K, et al. Protein secretion from *Saccharomyces cerevisiae* directed by the prepro-alpha-factor leader region. J Biol Chem 1986; 261:5858-65; PMID:3009432
21. Shuster JR. Gene expression in yeast: protein secretion. Curr Opin Biotechnol 1991; 2:685-90; PMID:1367718; http://dx.doi.org/10.1016/0958-1669(91)90035-4
22. Hiramatsu R, Yamashita T, Aikawa J, Horinouchi S, Beppu T. The prepro-peptide of Mucor rennin directs the secretion of human growth hormone by *Saccharomyces cerevisiae*. Appl Environ Microbiol 1990; 56:2125-32; PMID:2117879
23. Innis MA, Holland MJ, McCabe PC, Cole GE, Wittman VP, Tal R, et al. Expression, glycosylation, and secretion of an *Aspergillus* glucoamylase by *Saccharomyces cerevisiae*. Science 1985; 228:21-6; PMID:17811549; http://dx.doi.org/10.1126/science.228.4695.21
24. Rourke IJ, Johnsen AH, Din N, Petersen JGL, Rehfeld JF. Heterologous expression of human cholecystokinin in Saccharomyces cerevisiae. Evidence for a lysine-specific endopeptidase in the yeast secretory pathway. J Biol Chem 1997; 272:9720-7; PMID:9092503; http://dx.doi.org/10.1074/jbc.272.15.9720
25. Pérez-Boada M, Doyle WA, Ruiz-Dueñas FJ, Martinez MJ, Martinez AT, Smith AT. Expression of *Pleurotus eryngii* versatile peroxidase in *Escherichia coli* and optimisation of in vitro folding. Enzyme Microl Tech 2002; 30:518-24; http://dx.doi.org/10.1016/S0141-0229(02)00008-X
26. Camarero S, Cañas AI, Pardo I, Molina P, Martínez AT, Martínez MJ, et al. Engineering platforms for the directed evolution of laccase from *Pycnoporus cinnabarinus*. Appl Environ Microbiol 2012; 78:1370-84; PMID:22210206; http://dx.doi.org/10.1128/AEM.07530-1
27. Romanos MA, Scorer CA, Clare JJ. Foreign gene expression in yeast: a review. Yeast 1992; 8:423-88; PMID:1502852; http://dx.doi.org/10.1002/yea.320080602
28. Rakestraw JA, Sazinsky SL, Piatesi A, Antipov E, Wittrup KD. Directed evolution of a secretory leader for the improved expression of heterologous proteins and full-length antibodies in Saccharomyces cerevisiae. Biotechnol Bioeng 2009; 103:1192-201; PMID:19459139; http://dx.doi.org/10.1002/bit.22338
29. Pâques F, Haber JE. Multiple pathways of recombination induced by double-strand breaks in *Saccharomyces cerevisiae*. Microbiol Mol Biol Rev 1999; 63:349-404; PMID:10357855
30. Gibson DG. Synthesis of DNA fragments in yeast by one-step assembly of overlapping oligonucleotides. Nucleic Acids Res 2009; 37:6984-90; PMID:19745056; http://dx.doi.org/10.1093/nar/gkp687
31. Oldenburg KR, Vo KT, Michaelis S, Paddon C. Recombination-mediated PCR-directed plasmid construction *in vivo* in yeast. Nucleic Acids Res 1997; 25:451-2; PMID:9016579; http://dx.doi.org/10.1093/nar/25.2.451
32. Shao Z, Zhao H, Zhao H. DNA assembler, an *in vivo* genetic method for rapid construction of biochemical pathways. Nucleic Acids Res 2009; 37:e16; PMID:19074487; http://dx.doi.org/10.1093/nar/gkn991
33. Cherry JR, Lamsa MH, Schneider P, Vind J, Svendsen A, Jones A, et al. Directed evolution of a fungal peroxidase. Nat Biotechnol 1999; 17:379-84; PMID:10207888; http://dx.doi.org/10.1038/7939
34. Zumárraga M, Camarero S, Shleev S, Martínez-Arias A, Ballesteros A, Plou FJ, et al. Altering the laccase functionality by *in vivo* assembly of mutant libraries with different mutational spectra. Proteins 2008; 71:250-60; PMID:17932916; http://dx.doi.org/10.1002/prot.21699
35. Zumárraga M, Bulter T, Shleev S, Polaina J, Martínez-Arias A, Plou FJ, et al. *In vitro* evolution of a fungal laccase in high concentrations of organic cosolvents. Chem Biol 2007; 14:1052-64; PMID:17884637; http://dx.doi.org/10.1016/j.chembiol.2007.08.010
36. Cusano AM, Mekmouche Y, Meglecz E, Tron T. Plasticity of laccase generated by homeologous recombination in yeast. FEBS J 2009; 276:5471-80; PMID:19694803; http://dx.doi.org/10.1111/j.1742-4658.2009.07231.x
37. Wong TS, Zhurina D, Schwaneberg U. The diversity challenge in directed protein evolution. Comb Chem High Throughput Screen 2006; 9:271-88; PMID:16724918; http://dx.doi.org/10.2174/138620706776843192
38. Horton RM, Hunt HD, Ho SN, Pullen JK, Pease LR. Engineering hybrid genes without the use of restriction enzymes: gene splicing by overlap extension. Gene 1989; 77:61-8; PMID:2744488; http://dx.doi.org/10.1016/0378-1119(89)90359-4
39. Alcalde M, Zumárraga M, Polaina J, Ballesteros A, Plou FJ. Combinatorial saturation mutagenesis by *in vivo* overlap extension for the engineering of fungal laccases. Comb Chem High Throughput Screen 2006; 9:719-27; PMID:17168677; http://dx.doi.org/10.2174/138620706779026079
40. Alcalde M. Mutagenesis protocols in *Saccharomyces cerevisiae* by *in vivo* overlap extension. In Bramman, J (Ed.), *In vitro* Mutagenesis Protocols, Towota, New Jersey US: Humana Press 2010; 634:3-14.
41. Abécassis V, Pompon D, Truan G. High efficiency family shuffling based on multi-step PCR and in vivo DNA recombination in yeast: statistical and functional analysis of a combinatorial library between human cytochrome P450 1A1 and 1A2. Nucleic Acids Res 2000; 28:E88; PMID:11024190; http://dx.doi.org/10.1093/nar/28.20.e88
42. Zhao H, Giver L, Shao Z, Affholter JA, Arnold FH. Molecular evolution by staggered extension process (StEP) in vitro recombination. Nat Biotechnol 1998; 16:258-61; PMID:9528005; http://dx.doi.org/10.1038/nbt0398-258

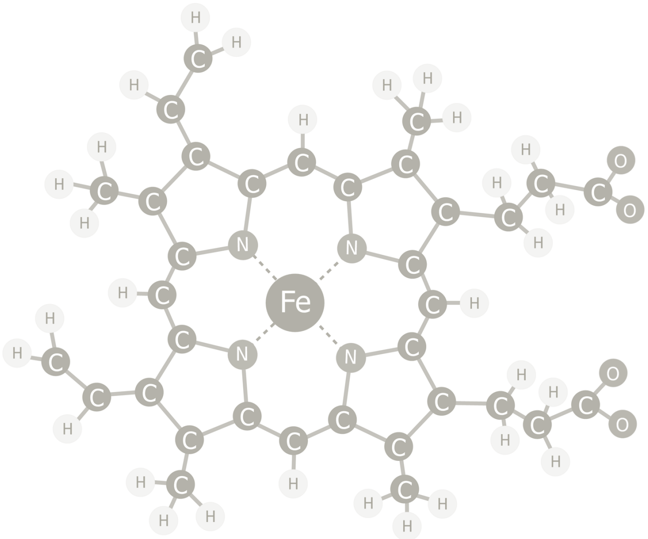

Capítulo 7:

Assembly of evolved ligninolytic genes in Saccharomyces cerevisiae

En este capítulo se describe el desarrollo de un prototipo inicial de levadura de la podredumbre blanca, incluyendo la co-expresión de enzimas ligninoliticas evolucionadas en Saccharomyces cerevisiae como proof-of-concept.

RESEARCH PAPER

Bioengineered 5:4, 1–10; July/August 2014; © 2014 Landes Bioscience

Assembly of evolved ligninolytic genes in *Saccharomyces cerevisiae*

David Gonzalez-Perez and Miguel Alcalde*

Department of Biocatalysis; Institute of Catalysis, CSIC; Madrid, Spain

Keywords: white-rot fungi, ligninolytic oxidoreductases, directed evolution, *Saccharomyces cerevisiae*, laccase, versatile peroxidase, secretome

Abbreviations: AAO, aryl alcohol oxidase; ABTS, 2,2′-azino-bis(3-ethylbenzothiazoline-6-sulfonic acid); BSA, Bovine Serum Albumin; dNTP, deoxyribonucleotide triphosphate; HRPL, high-redox potential laccase; HTS, high-throughput screening; IVOE, in vivo overlap extension; *Lac*, laccase gene; LiP, lignin peroxidase; MCS, Multiple Cloning Site; MnP, manganese peroxidase; PCR, polymerase chain reaction; PM1L, laccase from *Coriolopsis* PM1; T_{50}, the temperature at which the enzyme retains 50% of its activity after a 10 minute incubation; UPO, unspecific peroxygenase; *Vp*, versatile peroxidase gene; VP, versatile peroxidase

The ligninolytic enzymatic consortium produced by white-rot fungi is one of the most efficient oxidative systems found in nature, with many potential applications that range from the production of 2nd generation biofuels to chemicals synthesis. In the current study, two high redox potential oxidoreductase fusion genes (laccase -*Lac*- and versatile peroxidase -*Vp*-) that had been evolved in the laboratory were re-assembled in *Saccharomyces cerevisiae*. First, cell viability and secretion were assessed after co-transforming the *Lac* and *Vp* genes into yeast. Several expression cassettes were inserted in vivo into episomal bi-directional vectors in order to evaluate inducible promoter/terminator pairs of different strengths in an individual and combined manner. The synthetic white-rot yeast model harboring *Vp*(GAL1/CYC1)-*Lac*(GAL10/ADH1) displayed up to 1000 and 100 Units per L of peroxidase and laccase activity, respectively, representing a suitable point of departure for future synthetic biology studies.

Introduction

The study and engineering of the ligninolytic enzymatic consortium is generating much interest due to its enormous potential in several biotechnological applications, from bioremediation, the production of biofuels (bioethanol, biobutanol) or its use in organic synthesis, to name just a few.[1] In nature, these enzymes (mostly laccases, peroxidases and H_2O_2 supplying enzymes) are secreted by basidiomycete white-rot fungi that carry out the degradation of the lignin in plant cell walls through a complex (and still not well defined) multi-enzymatic cascade.[2] Understanding the synergies and interactions in this plastic array of high-redox potential enzymes during lignin combustion has been littered with many obstacles, including the lack of suitable functional heterologous hosts in which to perform detailed biomolecular studies.

During last decade there has been much effort to develop robust and reliable platforms for the directed evolution of ligninolytic laccases and peroxidases in the baker's yeast, *Saccharomyces cerevisiae*. This approach has allowed us to design enzymes with improved properties of biotechnological interest, including: new activities and specificities; enhanced thermostability; or even tolerance to unnatural media, such as human blood or organic co-solvents.[3-15] Through these experiments, we have witnessed the wealth of possibilities offered by *S. cerevisiae* in terms of creating DNA diversity by its physiological homologous recombination machinery,[14,16,17] and more generally, the outstanding role this yeast can play in synthetic biology studies.[18-24]

A critical issue when considering Lignocellulose Biorefineries, for the sustainable production of biofuels and biomaterials,[25] is the need to engineer artificial microorganisms with attributes tuned to the efficient use of raw plant biomass, and their subsequent exploitation as a renewable source with an industrial and energetic fate.[26,27] Important advances in the field include the transformation of chemicals (e.g., that of xylose from hemicellulose to xylitol, a C5 platform chemical) or the engineering of recombinant yeast strains able to ferment pentose sugars to produce ethanol from plant biomass.[28-30] However, in all these approaches it is indispensable to remove the recalcitrant biopolymer and obtain lignin-free hemicellulose. Typically, lignocellulosic material is pre-treated by high energy consuming and non-environmentally friendly physicochemical processes, such that the potential use of lignin derivatives in multiple sectors is misspent (including lignin-based products for manufacturing

*Correspondence to: Miguel Alcalde; Email: malcalde@icp.csic.es

Submitted: 04/14/2014; Revised: 05/07/2014; Accepted: 05/08/2014; Published Online: 05/15/2014

http://dx.doi.org/10.4161/bioe.29167

materials, surfactants and adhesives). Hence, the engineering of customized microorganisms capable of cost-effectively producing industrial chemicals and biofuels from raw materials (i.e., using whole plant biomass as the feedstock) is one of the most important goals in modern synthetic biology and metabolic engineering.

In this study, two high potential ligninolytic genes encoding a laccase (EC 1.10.3.2) and a versatile peroxidase (VP) (EC 1.11.1.16), which were previously evolved in the laboratory toward improved secretion, activity and stability, were assembled in vivo in *S. cerevisiae* using the eukaryotic biomolecular toolbox. Expression cassettes were constructed and inserted into uni- and bi-directional episomal vectors under the control of different promoters. Secretion yields and cell viability were evaluated in a simplified white-rot yeast model, thereby opening up new avenues for the engineering of a full-synthetic ligninolytic secretome for future synthetic biology studies.

Results and Discussion

Ligninolytic genes are proving to be complex targets when attempting to functionally express them in heterologous systems for metabolic engineering and synthetic biology studies (typically performed in *Escherichia coli* and/or *S. cerevisiae*). In bacteria, the main bottlenecks encountered are associated with misfolding due to the strong differences found in codon usage, missing chaperones, and the lack of post-translational modifications, all of which lead to the formation of inclusion bodies. Although the machinery of *S. cerevisiae* is closer to that of the basidiomycete white-rot fungi, serious and still unidentified shortcomings arise during the inner secretory pathway and the final exocytosis of the enzymes by yeast.

In recent years, we have circumvented many of these hurdles by undertaking exhaustive protein engineering work, including signal peptide switching and directed evolution of whole fusion proteins in order to adapt foreign genes to the subtleties of yeast. Using these approaches, we have individually expressed medium and high-redox potential laccases (HRPL),[3-11] versatile peroxidases (VP),[12-14] unspecific peroxygenases (UPO),[14,15] or even hydrogen peroxide supplying enzymes (aryl-alcohol oxidases [AAO], unpublished material). However, and taking into account the difficulties faced when expressing individual ligninolytic genes in yeast, an obvious question that arises is whether the physiology of *S. cerevisiae* can afford the functional expression of more than one of these evolved genes without suffering metabolic burdens (e.g., strong enzyme expression could drain certain metabolites from the cell or lead to the accumulation of toxic compounds), and/or expression constrains. To address this issue, our point of departure involved two evolved fusion genes, a laccase from basidiomycete PM1 and a VP from *Pleurotus eryngii*, respectively. In both cases, we had exchanged the native signal peptide with that of the α-factor prepro-leader of *S. cerevisiae* to enhance export from yeast. The laccase fusion (*Lac*) is the genetic product of 12 generations of in vitro evolution for secretion, activity, stability and tolerance to OH^- and halides,[10] whereas the *Vp* fusion is the result of 6 rounds of directed evolution for secretion, activity, thermostability and resistance to alkaline pHs,[13] **Figure 1**. Significantly, a common and unique feature of these two evolved genes is the capacity to tolerate neutral and/or alkaline pHs, at which most ligninolytic laccases and/or peroxidases reported to date are inactive. Moreover, it is worth pointing out that combining these *Vp* and *Lac* genes in the same microorganism guarantees a broader oxidative potential and substrate promiscuity: while the laccase mutant has a high redox potential (~760 mV *vs* NHE) and wide substrate specificity; the VP mutant comprises three catalytic sites for the oxidation of low-, medium-, and high-redox potential compounds, sharing common catalytic properties with lignin-peroxidases (LiP), manganese-peroxidases (MnP) and generic peroxidases.

In the first place, the culture medium was optimized by combining the different ingredients required for the individual expression of these genes (i.e., copper sources for *Lac*, Ca^{2+} and heme supplies for *Vp*), such that the health of yeast cells was not significantly affected. Thus, the *Vp* and *Lac* were co-transformed in independent high-copy episomal pJRoC30 vectors under the control of the GAL1/CYC1 promoter/terminator pair, (**Fig. S1**). From microtiter fermentations, individual clones were analyzed by means of their capacity to express both *Vp* and *Lac*. The same experiment was performed using competent cells harboring either of the two constructs and co-transforming the gene missing, however the strong background precluded the isolation of positive clones due to the limitations imposed on the screening process (data not shown). After screening the supernatants, several clones with higher, lower or similar *Vp* and *Lac* expression were found (with secretion levels up to ~100 U/L), indicating that co-expression was not harmful to the yeast (**Fig. 2A**). It is likely that the transcription and translation of *Vp* and *Lac*, although energetically expensive, did not produce an important metabolic burden on the cell with associated nucleotide and amino acid leakage.

Encouraged by these results, we employed in vivo overlap extension (IVOE)[17] to generate an array of vectors containing single and double expression cassettes ((*Vp*(GAL1/CYC1), *Vp*(GAL10/ADH1), *Lac*(GAL1/CYC1), *Lac*(GAL10/ADH1), *Vp*(GAL1/CYC1)-*Lac*(GAL10/ADH1), and *Lac*(GAL1/CYC1)-*Vp*(GAL10/ADH1)), using a pESC bi-directional vector as it harbors promoter/terminator pairs with different strengths (GAL1/CYC1, GAL10/ADH1, **Fig. 3 and 4**; **Fig. S2**). First, individual expression was evaluated by inserting the *Vp* and *Lac* genes from pJRoC30 into pESC (**Fig. 4A and B**; **Fig. S2**). However, the secretion of these enzymes proved to be lower in pESC than in pJRoC30, even for the same GAL1/CYC1 pair (**Fig. 2B and C**). Apart from the bi-directional characteristics of pESC, the only other difference of note between both vectors is that pJRoC30 comprises the FLP/FRT recombinase system associated with the stability of the copies of the 2 μm plasmid (**Fig. S1**).[31] This could represent an important difference in microfermentations, yet it may have only minor consequences in larger scale fermentations (see below). Despite the weaker secretion in pESC, sufficient quantities were available as to readily detect activity when assembling both *Vp* and *Lac* genes in the same vector (i.e., the *Vp*(GAL1/CYC1)-*Lac*(GAL10/ADH1) and *Lac*(GAL1/CYC1)-*Vp*(GAL10/ADH1) double constructs (**Figs. 2B and C and 4C and D**). Indeed, combined *Vp-Lac* constructs gave rise to similar levels of secretion for both

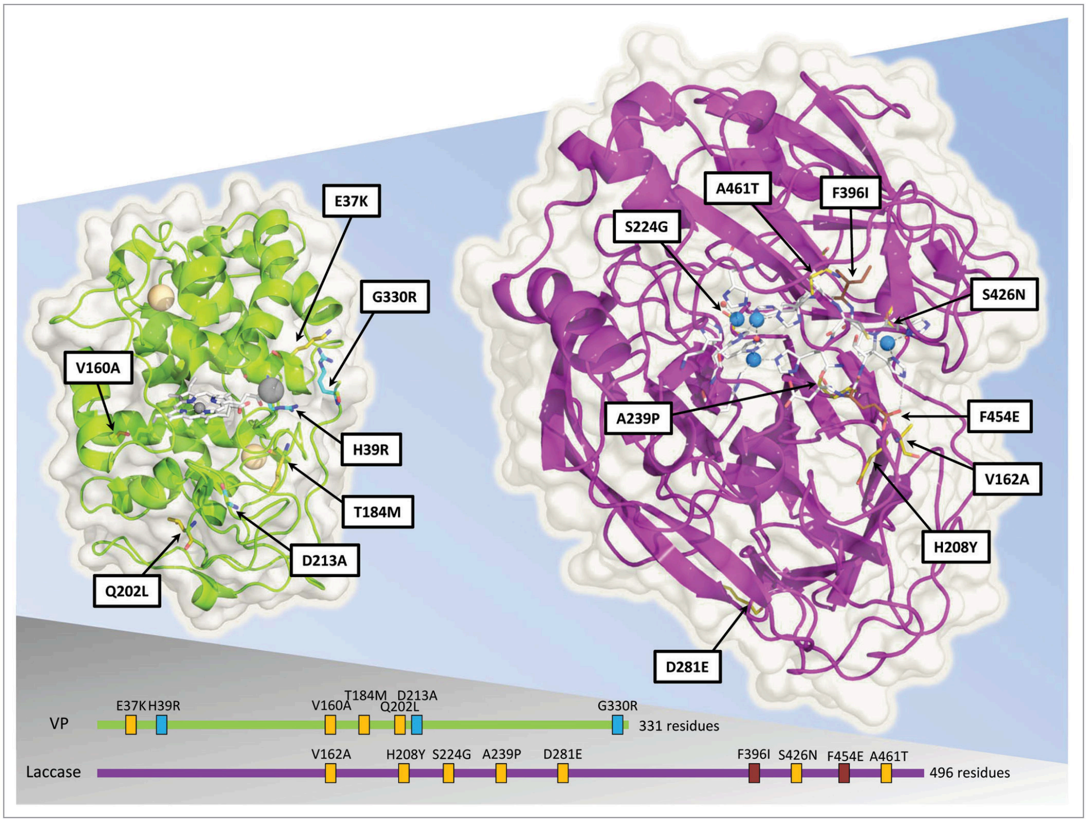

Figure 1. General overview of the evolved VP (in green) and laccase (in magenta) variants. The active sites (heme domain and copper coordination spheres) are highlighted in the CPK stick diagram. In both models, the mutations involved in secretion are shown in yellow, while the mutations that enhance thermostability (VP) are depicted in cyan and the mutations for blood tolerance (laccase) in red. In the laccase model Cu^{2+} ions are shown as blue spheres, whereas in the VP model, structural Ca^{2+} ions are shown as light-yellow spheres, with Mn^{2+} and Fe^{3+} as gray spheres. Homology models were created from PDBs ID:3FJW and ID:2HRG for the VP and laccase variants, respectively.

promoter/terminator pairs (around 30 Units/L), albeit lower than those obtained for the individual counterparts.

At this point, it is important to highlight that this set of experiments was performed in microtiter plates (i.e., ~200 µL microfermentations where stirring conditions and oxygen availability were limiting, impeding reaching the stationary phase [see Materials and Methods for details]). Since we could expect higher secretion yields when fermentations are translated to a larger scale, individual, and combined constructs were subjected to larger scale fermentation (in flask) to accurately monitor cell growth, as well as VP and laccase activity (**Fig. 5**). In all cases, the stationary phase was reached after around 50 h growth and hemoglobin was added to the expression media as a heme supply for VP as it was practically consumed by yeast after ~30 h (at the earliest logarithmic stage, when protein secretion became evident, **Fig. 5I**). Regardless of whether the plasmids harbored single or double constructs, maximal secretion was detected by the middle and/or final stages of the logarithmic phase. Indeed, the evolution of the activity profiles was quite similar in all cases, achieving a plateau at ~40 h after which VP activity slowly increased while laccase activity fell slightly. It is likely that the presence of certain metabolites released by yeast cells could negatively affect laccase activity/stability at this stage of fermentation. Independent of the promoter and vector used, the levels of expression from single constructs were quite similar (with strong secretion of 750–1500 and 600 Units/L for VP and laccase, respectively). The best double construct (*Vp*[GAL1/CYC1]-*Lac*[GAL10/ADH1]) produced strong secretion of ~1000 and 100 units/L for VP and laccase, respectively, **Figure 5A**. Nevertheless, secretion from single constructs of *Vp* were 1.25 to 2.5-fold higher than for *Lac*, which might partially explain the significant 10-fold drop in laccase activity upon co-expression with VP. It seems plausible that the pathway involved in processing the α-factor prepro-leader in yeast cannot support the heterologous co-expression of these two ligninolytic genes without sacrificing some level of secretion. Although VP and laccase joint secretion is sufficient for synthetic

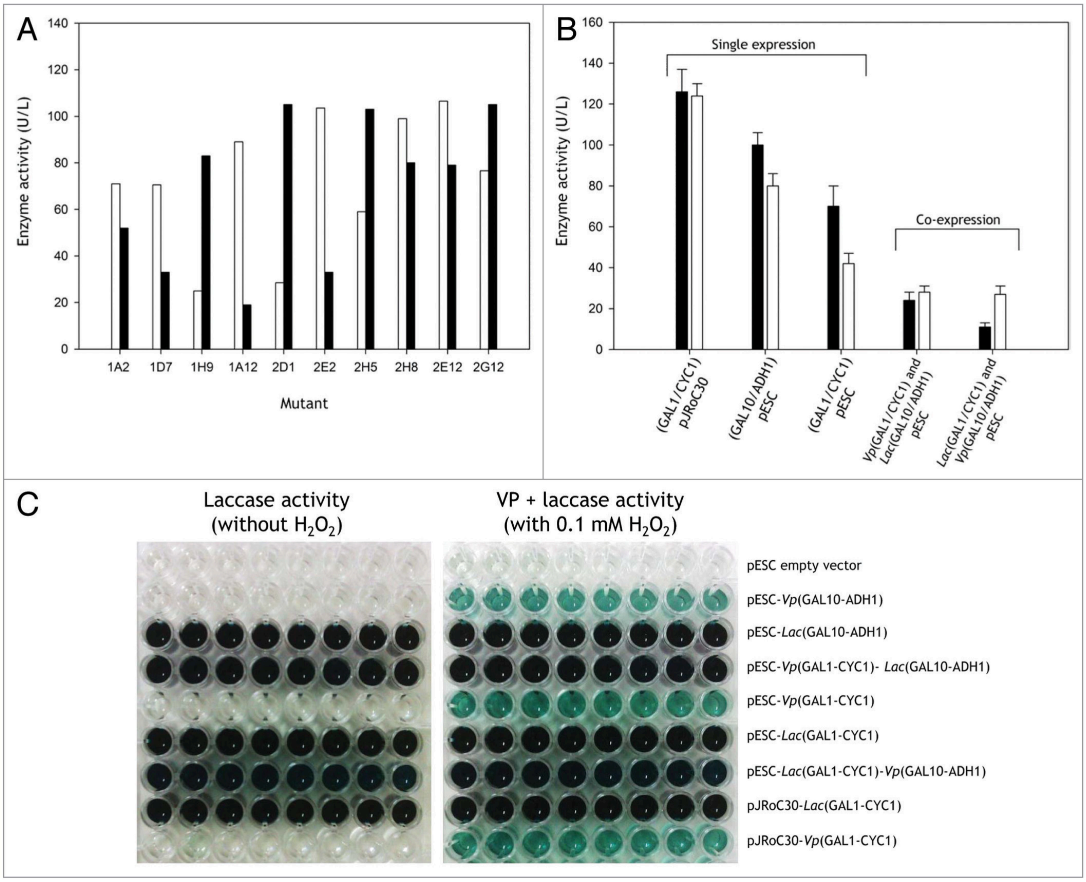

Figure 2. Secretion of *Vp* and *Lac* in the pJRoC30 and pESC shuttle vectors containing distinct expression cassettes (values obtained from microfermentations in 96-well plates). (**A**) Activities of isolated clones from co-transformation of pJRoC30-*Vp* and pJRoC30-*Lac* in yeast. (**B**) Expression of *Vp* and *Lac* from single and double constructs with different promoter/terminator pairs and vectors. Laccase activity in black, VP activity in white. Each bar represents the average of three independent fermentations including the standard deviation. (**C**) 96-well plate showing the activities of different constructs. *Vp* and *Lac* expression was assessed using the ABTS screening assay (100 mM citrate-phosphate buffer [pH 4.0] containing 3 mM ABTS). To determine the VP activity, 0.1 mM H_2O_2 was added to the ABTS assay solution. VP activities were deduced from the difference of the activities assessed in the presence (VP + laccase activity) and absence (laccase activity) of 0.1 mM H_2O_2. Each lane represents the data from 8 independent microfermentations (see Materials and Methods for details).

biology studies, possible approaches to enhance secretion could include the replacement of signal peptides by others that do not require the KEX2-StE13 proteases, the inclusion of KEX2-StE13 genes in the same pESC vector, or the engineering of chimeric peptides based on the combination of different regions of the α-factor prepro-leader and the prepro-toxin K_1 killer[32] from *S. cerevisiae* (unpublished material).

Conclusions

The current study is the first successful attempt to re-assemble a ligninolytic secretome in *S. cerevisiae*, representing a suitable starting point to develop an autonomously recombinant yeast strain capable of working directly on raw plant biomass. In this context, the most extensively investigated white-rot fungi (*Phanerochaete chrysosporium* and *Pleurotus eryngii*) have distinct extracellular enzymatic machineries to degrade lignin. While *P. chrysosporium* secretes LiP, MnP and the copper-radical glyoxal oxidase, *P. eryngii* produces MnP, VP, laccase, and aryl-alcohol oxidase. Future studies will assess the construction of a more complex artificial secretome harboring laboratory evolved versions of VP, HRPL, UPO, and AAO genes. This synthetic white rot yeast will constitute a new model organism for future synthetic biology and directed evolution developments aimed at improving the production of chemicals and biofuels, while

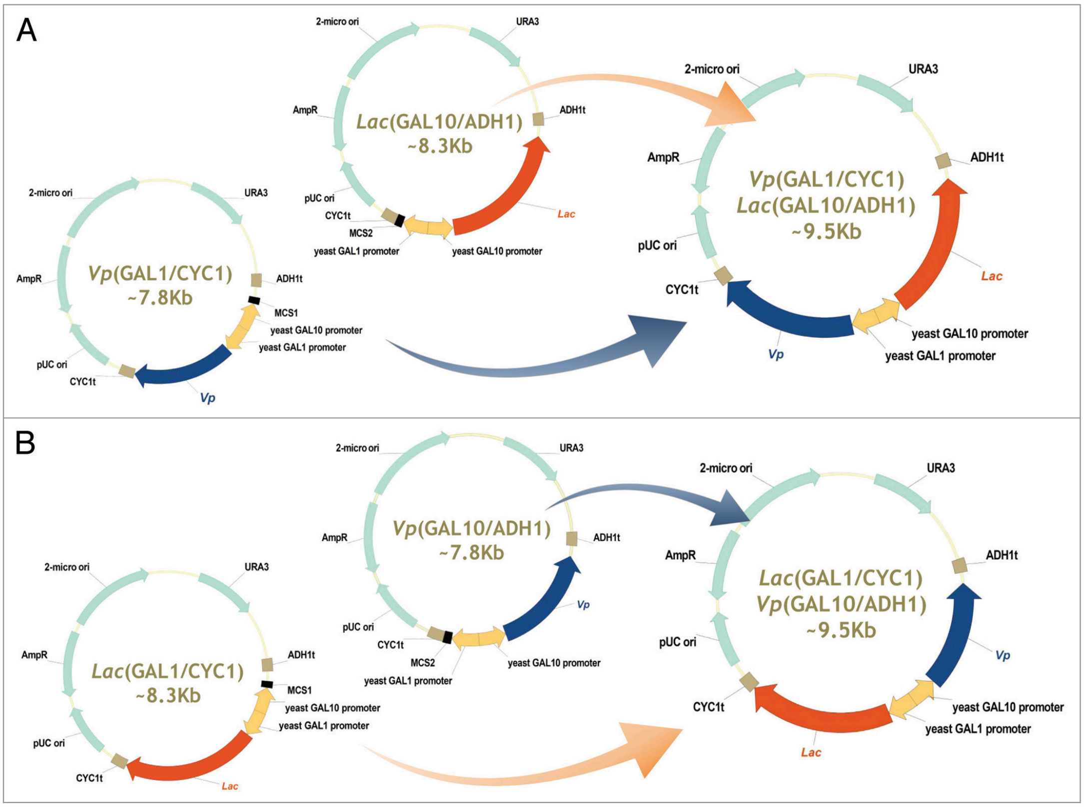

Figure 3. (**A**) *Vp*(GAL1/CYC1)-*Lac*(GAL10/ADH1) and (**B**) *Lac*(GAL1/CYC1)-*Vp*(GAL10/ADH1) expression cassettes in the pESC vector. *Vp* gene, blue boxes; *Lac* gene, red boxes; GAL1 and GAL10 promoters, orange boxes; ADH1 and CYC1 terminators, brown boxes; MCS1 and MCS2 terminators, black boxes (for further details see Materials and Methods, **Fig. 4; Fig. S1).**

providing a plastic vehicle to understand the function of the ligninolytic enzymatic consortium during natural wood decay.

Materials and Methods

Vp (2–1B variant) and *Lac* (ChU-B variant) evolved genes were obtained from previous laboratory evolution projects.[7,10,13] ABTS (2,2'-azino-bis[3-ethylbenzothiazoline-6-sulfonic acid]), Bovine hemoglobin, *Taq* polymerase and the *S. cerevisiae* transformation kit were purchased from Sigma-Aldrich. The iProof High Fidelity DNA polymerase was purchased from Bio-Rad. The Zymoprep Yeast Plasmid Miniprep Kit and Zymoclean Gel DNA Recovery Kit were obtained from Zymo Research. The *Escherichia coli* XL2-Blue competent cells and shuttle vector pESC containing two multiple cloning site (MCS1, MCS2) under the control of different promoter/terminator pairs (GAL1/CYC1, GAL10/ADH1) were from Stratagene. The uracil independent and ampicillin resistance pJRoC30 vector was obtained from the California Institute of Technology (CALTECH). The *ura3*-deficient *S. cerevisiae* strain BJ5465 (α ura3–52 trp1 leu2Δ1 his3Δ200 pep4::HIS2 prb1Δ1.6R can1 GAL1) was obtained from LGCPromochem, the NucleoSpin Plasmid kit was purchased from Macherey-Nagel, and the restriction enzymes BamHI, NheI, SpeI, SacI, and NotI from New England Biolabs. All chemicals were of reagent-grade purity.

Culture media

Minimal medium (SC) contained 0.67% (w/v) yeast nitrogen base, 1.92 g/L yeast synthetic drop-out medium supplement without uracil, 2% (w/v) D-raffinose and 25 µg/mL chloramphenicol. YP medium contained 10 g yeast extract, 20 g peptone and *dd*H_2O to 650 mL. Flask expression medium contained 720 mL YP, 67 mL 1 M KH_2PO_4 buffer (pH 6.0), 111 mL 20% (w/v) D-galactose, 25 g/L ethanol, 500 mg/L bovine hemoglobin and 1 mM $CaCl_2$ for *Vp* expression, 2 mM $CuSO_4$ for *Lac* expression, 1 mL 25 g/L chloramphenicol and *dd*H_2O to 1000 mL. Microplate expression medium contained 720 mL YP, 67 mL 1 M KH_2PO_4 buffer (pH 6.0), 111 mL 20% (w/v)

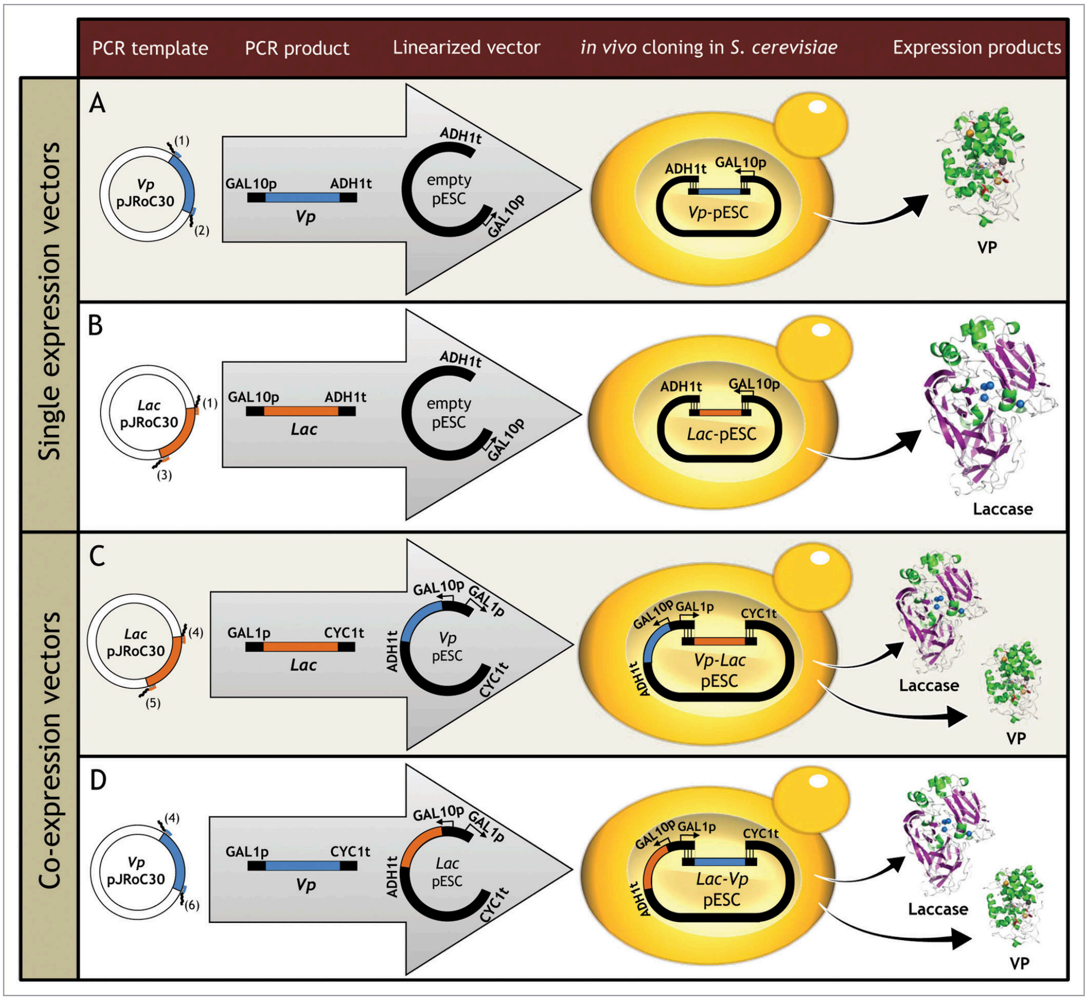

Figure 4. In vivo assembly of synthetic genes by IVOE. Each overlapping region allowed crossover events to occur between fragments giving rise to an autonomously repaired vector containing single and double expression cassettes in the correct orientation. (**A**) and (**B**) Single expression cassettes are constructed in pESC by engineering specific primers containing overhangs to foster in vivo cloning with the linearized plasmid in yeast (pJRoC30 was used as template for *Vp* or *Lac* amplifications). (**C**) and (**D**) The pESC constructs obtained in (**A**) and (**B**) were used as scaffolds to assemble *Lac* and *Vp* genes under the control of different promoter/terminator pairs. Primers used: (1)-MCS1-*Vp*/*Lac*-α-BamHI, (2)-MCS2-*Vp*-ter-NheI, (3)-MCS2-*Lac*-ter-NheI, (4)-MCS1-*Vp*/*Lac*-α-SpeI, (5)-MCS1-*Lac*-ter-SacI and (6)-MCS1-*Vp*-ter-SacI. Black arrows indicate the direction of the transcription process.

D-galactose, 100 mg/L bovine hemoglobin for *Vp*, 2 mM $CuSO_4$ for *Lac*, 1 ml 25 g/L chloramphenicol and *dd*H_2O to 1000 mL. YPD solution contained 1% (w/v) yeast extract, 2% (w/v) peptone, 2% (w/v) D-glucose and 25 μg/mL chloramphenicol. SC drop-out plates contained 0.67% (w/v) yeast nitrogen base, 1.92 g/L (w/v) yeast synthetic drop-out medium supplement without uracil, 2% (w/v) bacto agar, 2% (w/v) D-glucose and 25 μg/mL chloramphenicol. Luria-Bertani (LB) medium was prepared with 1% (w/v) peptone, 0.5% (w/v) yeast extract, 1% (w/v) NaCl, and 100 μg/mL ampicillin.

Engineering of single and double constructions

PCR products and linearized vectors were cleaned, concentrated and loaded onto a low melting-point preparative agarose gel and purified using the Zymoclean Gel DNA Recovery Kit (Zymo Research). DNA concentrations were estimated spectrophotometrically at 260 nm in 100 μL quartz cuvettes. *Vp* and *Lac* including their respective signal peptides (α factor prepro-leader) were amplified by PCR and in vivo cloned into *S. cerevisiae*. Crossover areas were engineered with overhangs of ~50 bp flanking each segment between *Vp, Lac* and linearized pESC.

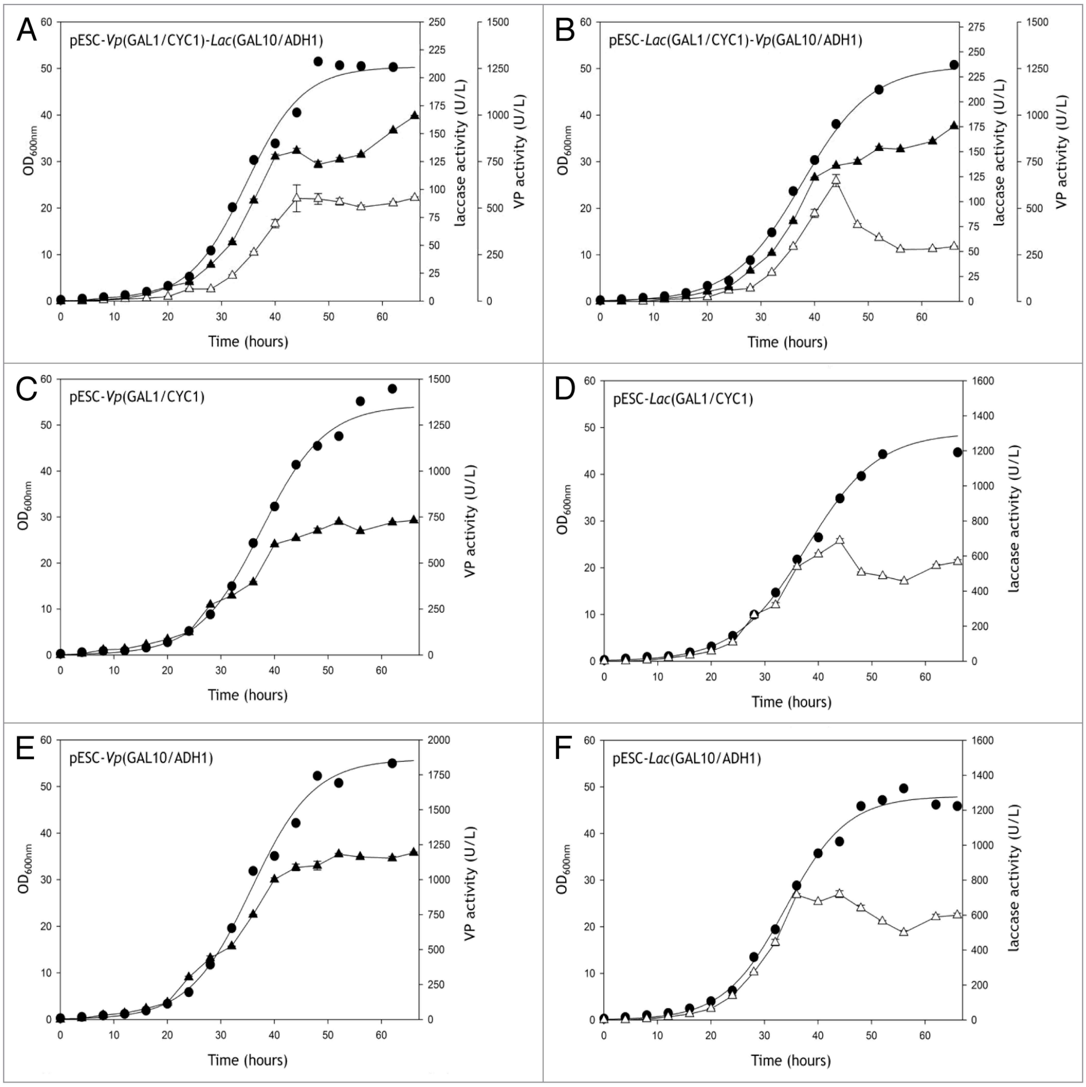

Figure 5. Large scale fermentation of single and double expression cassettes in pJRoC30 and pESC, showing the OD_{600} vs. Laccase or VP activity over time (both measured with ABTS): black circles, cell growth (OD_{600}); black triangles, VP activity; white triangles, laccase activity; white squares, background generated by the heme source (hemoglobin). Each point represents the average of three independent measurements including the standard deviation.

PCRs for in vivo cloning in MCS1-pESC (MCS1, Multiple cloning site 1)

Reaction mixtures were prepared in a final volume of 50 μL containing: DNA template (0.2 ng/μL, pJRoC30-*Vp* or pJRoC30-*Lac*), 0.5 μM MCS1-*Vp*/*Lac*-α-SpeI primer (5′-AATTTTTGAA AATTCGAATT CAACCCTCAC TAAAGGGCGG CCGCACTAGT ATGAGATTTC CTTCAATTTT TACTGCTG-3′), 0.5 μM MCS1-*Vp*/*Lac*-ter-SacI primer (5′- GATTGGAGAC TTGACCAAAC CTCTGGCGAA GAATTGTTAA TTAAGAGCTC TTACGATCTA GGGACGGGAG-3′ for *Vp* and 5′- GATTGGAGAC TTGACCAAAC CTCTGGCGAA GAATTGTTAA TTAAGAGCTC TTACTGGTCG TCAGGCGAGA G-3′ for *Lac*), 0.8 mM dNTPs (0.2 mM each), 3% (v/v) dimethylsulfoxide (DMSO), and 0.02 U/μL iProof polymerase. High fidelity PCRs were performed on a gradient thermocycler using the following

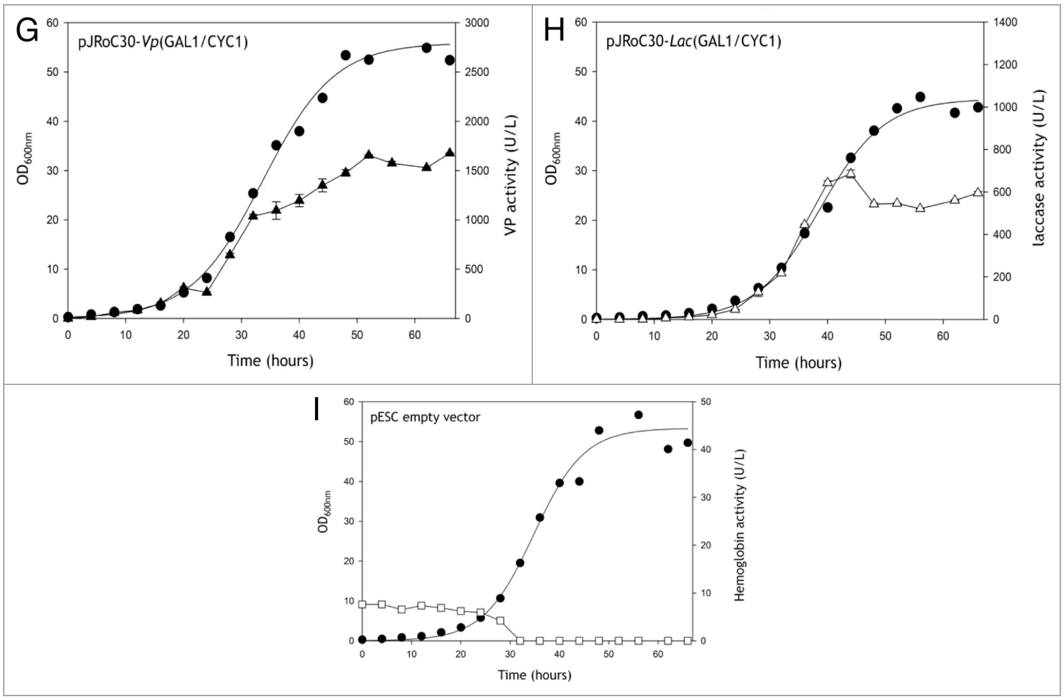

Figure 5 (Continued). See previous page for figure legend.

conditions: 98 °C for 30 s (1 cycle); 98 °C for 10 s, 55 °C for 25 s, 72 °C for 1 min 30 s (28 cycles); and 72 °C for 10 min (1 cycle). Underlined are highlighted crossover areas between genes and pESC plasmid one each other.

PCRs for in vivo cloning in MCS2-pESC (MCS2, Multiple cloning site 2)

Reaction mixtures were prepared in a final volume of 50 µL containing: DNA template (0.2 ng/µL, pJRoC30-*Vp* or pJRoC30-*Lac*), 0.5 µM MCS2-*Vp*/*Lac*-α-BamHI primer (5′-TGTTAATATA CCTCTATACT TTAACGTCAA GGAGAAAAAA CCCCGGATCC ATGAGATTTC CTTCAATTTT TACTGCTG-3′), 0.5 µM MCS2-*Vp*/*Lac*-ter-NheI primer (5′-TTCAGGTTGT CTAACTCCTT CCTTTTCGGT TAGAGCGGAT CTTAGCTAGC TTACGATCTA GGGACGGGAG-3′ for *Vp* and 5′-TTCAGGTTGT CTAACTCCTT CCTTTTCGGT TAGAGCGGAT CTTAGCTAGC TTACTGGTCG TCAGGCGAGA G-3′ for *Lac*), 0.8 mM dNTPs (0.2 mM each), 3% (v/v) dimethylsulfoxide (DMSO), and 0.02 U/µL iProof polymerase. High fidelity PCRs were performed on a gradient thermocycler using the following conditions: 98 °C for 30 s (1 cycle); 98 °C for 10 s, 55 °C for 25 s, 72 °C for 1 min 30 s (28 cycles); and 72 °C for 10 min (1 cycle). Underlined are highlighted crossover areas between genes and pESC plasmid one each other.

pESC digestion

pESC was linearized in final volume of 20µL containing: 2 µg of empty pESC vector, 100µg/mL BSA, 20 total Units of SpeI and SacI for opening MCS1 (GAL10/ADH1), or 20 total Units of BamHI and NheI for MCS2 (GAL1/CYC1) (**Figs. 3 and 4**). Digestion reactions were incubated for 1 h at 37 °C, and then enzymes heat-inactivated at 80 °C during 20 min. The products of inactivation were cleaned and purified.

Reassembly in S. cerevisiae by IVOE

Constructs were reassembled in vivo by transformation into *S. cerevisiae* cells using the Yeast Transformation Kit. The DNA transformation mixture contained 100 ng of linearized plasmid (MCS1 or MCS2) mixed with single *Vp* or *Lac* genes (400 ng per gene, ratio 1:4 vector:gene). Transformed cells were plated on SC drop-out plates and incubated for 3 d at 30 °C. Subsequently, the cloning libraries were subjected to the high-throughput protocol for laccase/VP activity.

Microfermentations and high-throughput screening (HTS) protocol for laccase/VP activity

Individual clones were selected and cultured in sterile 96-well plates (Greiner Bio-One GmbH) containing 50 µL per well of SC minimal medium. In each plate well-H1 was inoculated with *S. cerevisiae* containing pESC empty vector as a negative control. Plates were sealed to prevent evaporation and incubated at 30 °C, 225 rpm, and 80% relative humidity in a humidity shaker (Minitron-INFORS, Biogen). After 48 h, 160 µL of expression medium was added to each well and the plates were incubated for a further 24 h. The plates (master plates) were centrifuged for 15 min at 3000 rpm and 4 °C (Eppendorf 5810R centrifuge) and the master plates were duplicated with the help of a robot (EVO Freedom-100, TECAN) by transferring 20 µL of crude supernatant. Next, 180 µL of ABTS screening assay solution were added using a Multidrop robot (Multidrop Combi, ThermoFischer Scientific). The assay solution was prepared in 100 mM citrate-phosphate buffer (pH 4.0) containing 3 mM ABTS. For the determination of VP activity the assay solution was supplemented with 0.1 mM H_2O_2. The plates were stirred briefly and the absorption at 418 nm (εABTS•+ = 36 000 M^{-1} cm^{-1}) was recorded in kinetic mode on a plate reader (SPECTRAMax Plus 384, Molecular Devices). VP activities were deduced from the difference of the activities assessed in the absence (laccase activity) and in the presence (VP + laccase activity) of 0.1 mM H_2O_2.

Isolation of constructions

A 100 µL aliquot from the wells with the positive clones was inoculated in 3 mL of YPD and incubated at 30 °C and 225 rpm for 24 h, recovering the plasmids from these cultures (Zymoprep Yeast Plasmid Miniprep Kit). As the product of the zymoprep was very impure and the concentration of DNA extracted very low, the zymoprep mixtures containing shuttle vectors were transformed into super-competent *E. coli* cells (XL2-Blue, Stratagene) and plated on LB/amp plates. Single colonies were picked and used to inoculate 5 mL LB/amp media, and they were grown overnight at 37 °C and 225 rpm. The plasmids were then extracted (NucleoSpin Plasmid kit, Macherey-Nagel). Plasmids and their containing cassettes were analyzed by digestion and conventional PCR (**Fig. S2**). The plasmids were linearized with 10 units of NotI in a final volume of 20 µL containing 0.5 µg and 100µg/mL BSA of the corresponding construction. The reaction took place during 1 h at 37 °C, afterwards the enzyme was heat-inactivated and the digestion reactions analyzed in an 1% (w:v) analytical agarose gel (**Fig. S2A**). The PCR reaction mixtures for testing the presence of *Lac* and/or *Vp* were prepared in a final volume of 50 µL containing DNA template (10 ng/µL), 1.5mM $MgCl_2$, 0.09 µM forward primer, 0.09 µM reverse primer, 0.2 mM dNTPs (0.05 mM each), 3% (v/v) dimethylsulfoxide (DMSO), and 0.05 U/µL *Taq* DNA polymerase. Constructs including *Vp* or *Lac* in MCS1 were amplified using forward primer GAL10p-Binding (5′-GCGTCCATCC AAAAAAAAAG TAAGAATT-3′) and reverse primer ADH1t-binding (5′-CGACAACCTT GATTGGAGAC TTG-3′). Single constructs including *Vp* or *Lac* in MCS2 were amplified using forward primer GAL1p-Binding (5′-GTATCAACAA AAAATTGTTA ATATACCTCT ATAC-3′) and reverse primer CYC1t-binding (5′-AATAAATAGG GACCTAGACT TCAGG-3′). Double constructs were amplified using two forward primers GAL10p-Binding (5′-GCGTCCATCC AAAAAAAAAG TAAGAATT-3′) and GAL1p-Binding (5′- GTATCAACAA AAAATTGTTA ATATACCTCT ATAC-3′) plus two reverse primers ADH1t-binding (5′-CGACAACCTT GATTGGAGAC TTG-3′) and CYC1t-binding (5′-AATAAATAGG GACCTAGACT TCAGG-3′). PCRs were performed on a gradient thermocycler using the following conditions: 95 °C for 2 min (1 cycle); 94 °C for 45 s, 51 °C for 30 s, 72 °C for 1 min 30 s (28 cycles); and 72 °C for 10 min (1 cycle) (**Fig. S2B**). Whole expression vectors isolated from positive clones that contained the expected PCR products were verified by DNA sequencing using an ABI 3730 DNA Analyzer-Applied Biosystems Automatic Sequencer at the Secugen (CIB). The primers used were: GAL10p Seq (5′- GGTGGTAATG CCATGTAATA TG-3′) and ADH1t Seq (5′- GTAGACAAGC CGACAACCTT G-3′), for MCS1; GAL1p Seq (5′- CAACATTTTC GGTTTGTATT ACTTC-3′) and CYC1t Seq (5′-GGACCTAGAC TTCAGGTTGT C-3′), for MCS2. Internal primers for *Vp* were 3R-direct (5′-GTTCCATCAT CGCGTTCG-3′) and 5F-reverse (5′-GGATTCCTTT CTTCTTGG-3′). Internal primers for *Lac* were PM1FS (5′-ACGACTTCCA GGTCCCTGAC CAAGC-3′), and PM1RS (5′-TCAATGTCCG CGTTCGCAGG A-3′).

***Vp* and *Lac* expression**

Microfermentations

Individual clones were picked from a SC drop-out plate and culture in sterile 96-well plates (Greiner Bio-One GmbH) containing 50 µL per well of SC minimal medium. The following constructs were fermented: (*Vp*-(GAL1/CYC1), *Lac*-(GAL1/CYC1), *Vp*-(GAL10/ADH1), *Lac*-(GAL10/ADH1), *Vp*-(GAL1/CYC1)-*Lac*-(GAL10/ADH1), *Lac*-(GAL1/CYC1)-*Vp*(GAL10/ADH1), pJRoC30-*Vp*, pJRoC30-*Lac* and pESC empty vector). For each plate individual columns were inoculated with *S. cerevisiae* containing the different constructions. Plates were sealed to prevent evaporation and incubated at 30 °C, 225 rpm and 80% relative humidity in a humidity shaker (Minitron-INFORS, Biogen, Spain). After 48 h, 160 µL of expression medium was added to each well and the plates were incubated for a further 24 h. The plates were centrifuged for 15 min at 3000 rpm and 4 °C (Eppendorf 5810R centrifuge) and supernatants subjected to the abovementioned HTS-protocol.

Larger scale fermentations

A single colony of *S. cerevisiae* containing *Vp*-(GAL1/CYC1), *Lac*-(GAL1/CYC1), *Vp*-(GAL10/ADH1), *Lac*-(GAL10/ADH1), *Vp*-(GAL1/CYC1)-*Lac*-(GAL10/ADH1), *Lac*-(GAL1/CYC1)-*Vp*(GAL10/ADH1), pJRoC30-*Vp*, pJRoC30-*Lac*, and empty pESC was picked from a SC drop-out plate and used to inoculate 5 mL of minimal medium in a 50 mL tube. The cultures were incubated for 48 h at 30 °C and 225 rpm (Micromagmix shaker) up to saturation. An aliquot of cells was removed and used to inoculate a final volume of 5 mL of minimal medium in a 50 mL tube (Optical Density, OD_{600} = 0.3), and they were incubated until two growth phases had been completed (6–8 h, OD_{600} = 1). Thereafter, 9 mL of expression medium was inoculated with 1 mL of this pre-culture in a 100 mL flask (OD_{600} = 0.1). The flask cultures were incubated during 70 h at 30 °C and 225 rpm (OD_{600} = 45–50). Aliquots of culture were collected every 4 h to determine OD_{600} and VP/laccase activity. Activity was measured from crude supernatants, cells were separated by centrifugation for 5 min at 3000 rpm at room temperature (Eppendorf 5424 Centrifuge). The VP/laccase activities were measured with

20 μL of supernatant in a final volume of 200 μL containing 100 mM citrate-phosphate buffer (pH 4.0) with 3 mM ABTS. For VP activity, the assay solution was supplemented with 0.1 mM H_2O_2. The absorption at 418 nm (εABTS$^{\bullet +}$ = 36 000 M^{-1} cm^{-1}) was recorded in kinetic mode on a plate reader (SPECTRAMax Plus 384, Molecular Devices).

Protein and homology modeling

PyMOL Molecular Visualization System (Schrödinger) was used to generate protein models using as templates the VPl2 from *P. eryngii* (PDB ID: 3FJW) and *Trametes trogii* laccase (PDB: 2HRG, 97% sequence identity with the PM1 laccase) for VP and laccase mutants, respectively.

Disclosure of Potential Conflicts of Interest

No potential conflicts of interest were disclosed.

Acknowledgments

This work was supported by European Commission Projects (Peroxicats-FP7-KBBE-2010-4-26537; Indox-FP7-KBBE-2013-7-613549; COST-Action CM1303: Systems Biocatalysis) and the National Project (Evofacel-BIO2010-19697).

Supplemental Materials

Supplemental materials may be found here:
www.landesbioscience.com/journals/bioe/article/29167/

References

1. Garcia-Ruiz E, Mate DM, Gonzalez-Perez D, Molina-Espeja P, Camarero S, Martinez AT, Ballesteros AO, Alcalde M. Directed evoluton of ligninolytic oxidoreductases: from functional expression to stabilization and beyond. In: Cascade Biocatalysis, Riva, Fessner eds. Wiley-VCH 2014; In press.
2. Martínez AT, Ruiz-Dueñas FJ, Martínez MJ, Del Río JC, Gutiérrez A. Enzymatic delignification of plant cell wall: from nature to mill. Curr Opin Biotechnol 2009; 20:348-57; PMID:19502047; http://dx.doi.org/10.1016/j.copbio.2009.05.002
3. Bulter T, Alcalde M, Sieber V, Meinhold P, Schlachtbauer C, Arnold FH. Functional expression of a fungal laccase in *Saccharomyces cerevisiae* by directed evolution. Appl Environ Microbiol 2003; 69:987-95; PMID:12571021; http://dx.doi.org/10.1128/AEM.69.2.987-995.2003
4. Zumárraga M, Camarero S, Shleev S, Martínez-Arias A, Ballesteros A, Plou FJ, Alcalde M. Altering the laccase functionality by *in vivo* assembly of mutant libraries with different mutational spectra. Proteins 2008; 71:250-60; PMID:17932916; http://dx.doi.org/10.1002/prot.21699
5. Zumárraga M, Bulter T, Shleev S, Polaina J, Martínez-Arias A, Plou FJ, Ballesteros A, Alcalde M. *In vitro* evolution of a fungal laccase in high concentrations of organic cosolvents. Chem Biol 2007; 14:1052-64; PMID:17884637; http://dx.doi.org/10.1016/j.chembiol.2007.08.010
6. Torres-Salas P, Mate DM, Ghazi I, Plou FJ, Ballesteros AO, Alcalde M. Widening the pH activity profile of a fungal laccase by directed evolution. Chembiochem 2013; 14:934-7; PMID:23592228; http://dx.doi.org/10.1002/cbic.201300102
7. Maté D, García-Burgos C, García-Ruiz E, Ballesteros AO, Camarero S, Alcalde M. Laboratory evolution of high-redox potential laccases. Chem Biol 2010; 17:1030-41; PMID:20851352; http://dx.doi.org/10.1016/j.chembiol.2010.07.010
8. Maté D, García-Ruiz E, Camarero S, Alcalde M. Directed evolution of fungal laccases. Curr Genomics 2011; 12:113-22; PMID:21966249; http://dx.doi.org/10.2174/138920211795564322
9. Camarero S, Pardo I, Cañas AI, Molina P, Record E, Martínez AT, Martínez MJ, Alcalde M. Engineering platforms for directed evolution of Laccase from *Pycnoporus cinnabarinus*. Appl Environ Microbiol 2012; 78:1370-84; PMID:22210206; http://dx.doi.org/10.1128/AEM.07530-11
10. Mate DM, Gonzalez-Perez D, Falk M, Kittl R, Pita M, De Lacey AL, Ludwig R, Shleev S, Alcalde M. Blood tolerant laccase by directed evolution. Chem Biol 2013; 20:223-31; PMID:23438751; http://dx.doi.org/10.1016/j.chembiol.2013.01.001
11. Pardo I, Vicente AI, Mate DM, Alcalde M, Camarero S. Development of chimeric laccases by directed evolution. Biotechnol Bioeng 2012; 109:2978-86; PMID:22729887; http://dx.doi.org/10.1002/bit.24588
12. García-Ruiz E, Maté D, Ballesteros A, Martínez AT, Alcalde M. Evolving thermostability in mutant libraries of ligninolytic oxidoreductases expressed in yeast. Microb Cell Fact 2010; 9:17; PMID:20298573; http://dx.doi.org/10.1186/1475-2859-9-17
13. Garcia-Ruiz E, Gonzalez-Perez D, Ruiz-Dueñas FJ, Martínez AT, Alcalde M. Directed evolution of a temperature-, peroxide- and alkaline pH-tolerant versatile peroxidase. Biochem J 2012; 441:487-98; PMID:21980920; http://dx.doi.org/10.1042/BJ20111199
14. Gonzalez-Perez D, Molina-Espeja P, Garcia-Ruiz E, Alcalde M. Mutagenic Organized Recombination Process by Homologous *IN vivo* Grouping (MORPHING) for directed enzyme evolution. PLoS One 2014; 9:e90919; PMID:24614282; http://dx.doi.org/10.1371/journal.pone.0090919
15. Molina-Espeja P, Garcia-Ruiz E, Gonzalez-Perez D, Ullrich R, Hofrichter M, Alcalde M. Directed evolution of unspecific peroxygenase from *Agrocybe aegerita*. Appl Environ Microbiol 2014; 80:3496-507; PMID:24682297; http://dx.doi.org/10.1128/AEM.00490-14
16. Gonzalez-Perez D, Garcia-Ruiz E, Alcalde M. *Saccharomyces cerevisiae* in directed evolution: An efficient tool to improve enzymes. Bioeng Bugs 2012; 3:172-7; PMID:22572788; http://dx.doi.org/10.4161/bbug.19544
17. Alcalde M. Mutagenesis protocols in *Saccharomyces cerevisiae* by in vivo overlap extension. Methods Mol Biol 2010; 634:3-14; PMID:20676972; http://dx.doi.org/10.1007/978-1-60761-652-8_1
18. Krivoruchko A, Siewers V, Nielsen J. Opportunities for yeast metabolic engineering: Lessons from synthetic biology. Biotechnol J 2011; 6:262-76; PMID:21328545; http://dx.doi.org/10.1002/biot.201000308
19. Nevoigt E. Progress in metabolic engineering of *Saccharomyces cerevisiae.* Microbiol Mol Biol Rev 2008; 72:379-412; PMID:18772282; http://dx.doi.org/10.1128/MMBR.00025-07
20. Da Silva NA, Srikrishnan S. Introduction and expression of genes for metabolic engineering applications in *Saccharomyces cerevisiae.* FEMS Yeast Res 2012; 12:197-214; PMID:22129153; http://dx.doi.org/10.1111/j.1567-1364.2011.00769.x
21. Ostrov N, Wingler LM, Cornish VW. Gene assembly and combinatorial libraries in *S. cerevisiae* via reiterative recombination. Methods Mol Biol 2013; 978:187-203; PMID:23423898; http://dx.doi.org/10.1007/978-1-62703-293-3_14
22. Shao Z, Zhao H, Zhao H. DNA assembler, an *in vivo* genetic method for rapid construction of biochemical pathways. Nucleic Acids Res 2009; 37:e16; PMID:19074487; http://dx.doi.org/10.1093/nar/gkn991
23. Wingler LM, Cornish VW. Reiterative Recombination for the *in vivo* assembly of libraries of multigene pathways. Proc Natl Acad Sci U S A 2011; 108:15135-40; PMID:21876185; http://dx.doi.org/10.1073/pnas.1100507108
24. Wang T, Ma X, Zhu H, Li A, Du G, Chen J. Available methods for assembling expression cassettes for synthetic biology. Appl Microbiol Biotechnol 2012; 93:1853-63; PMID:22311648; http://dx.doi.org/10.1007/s00253-012-3920-8
25. Ragauskas AJ, Williams CK, Davison BH, Britovsek G, Cairney J, Eckert CA, Frederick WJ Jr., Hallett JP, Leak DJ, Liotta CL, et al. The path forward for biofuels and biomaterials. Science 2006; 311:484-9; PMID:16439654; http://dx.doi.org/10.1126/science.1114736
26. Hong KK, Nielsen J. Metabolic engineering of *Saccharomyces cerevisiae*: a key cell factory platform for future biorefineries. Cell Mol Life Sci 2012; 69:2671-90; PMID:22388689; http://dx.doi.org/10.1007/s00018-012-0945-1
27. Huang GL, Anderson TD, Clubb RT. Engineering microbial surfaces to degrade lignocellulosic biomass. Bioengineered 2013; 5:1-11; PMID:24430239
28. Oreb M, Dietz H, Farwick A, Boles E. Novel strategies to improve co-fermentation of pentoses with D-glucose by recombinant yeast strains in lignocellulosic hydrolysates. Bioengineered 2012; 3:347-51; PMID:22892590; http://dx.doi.org/10.4161/bioe.21444
29. Sun J, Wen F, Si T, Xu JH, Zhao H. Direct conversion of xylan to ethanol by recombinant Saccharomyces cerevisiae strains displaying an engineered minihemicellulosome. Appl Environ Microbiol 2012; 78:3837-45; PMID:22447594; http://dx.doi.org/10.1128/AEM.07679-11
30. Nair NU, Zhao H. Evolution in reverse: engineering a D-xylose-specific xylose reductase. Chembiochem 2008; 9:1213-5; PMID:18383056; http://dx.doi.org/10.1002/cbic.200700765
31. Andrews BJ, Proteau GA, Beatty LG, Sadowski PD. The FLP recombinase of the 2 micron circle DNA of yeast: interaction with its target sequences. Cell 1985; 40:795-803; PMID:3879971; http://dx.doi.org/10.1016/0092-8674(85)90339-3
32. Cartwright CP, Zhu YS, Tipper DJ. Efficient secretion in yeast based on fragments from K1 killer preprotoxin. Yeast 1992; 8:261-72; PMID:1514325; http://dx.doi.org/10.1002/yea.320080404

Supplemental data chapter 7

Assembly of evolved ligninolytic genes in Saccharomyces cerevisiae

Authors: González-Perez, D., and Alcalde, M.

Bioengineered (2014) **5**, 1-10.

Landes Bioscience
www.landesbioscience.com

Supplemental Material to:

David Gonzalez-Perez and Miguel Alcalde

Assembly of evolved ligninolytic genes in Saccharomyces cerevisiae

Bioengineered 2014; 5(4)
http://dx.doi.org/10.4161/bioe.29167

http://www.landesbioscience.com/journals/bioe/article/29167/

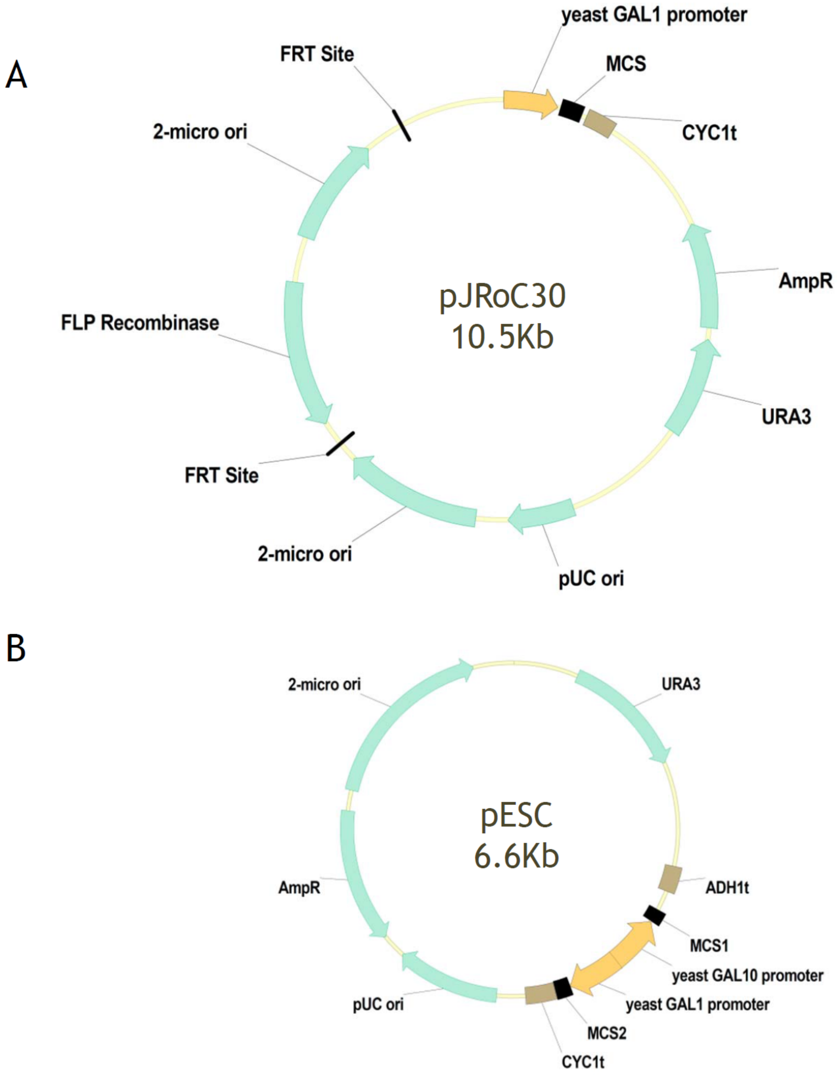

Figure S1. Shuttle vectors pJRoC30 (**A**) and pESC (**B**). In light green are highlighted the different elements of both plasmids. Promoters (GAL1 and GAL10) are shown in light orange, terminators (ADH1 and CYC1) in brown and MCS (Multiple Cloning Site) in black. pJRoC30 harbors FLP

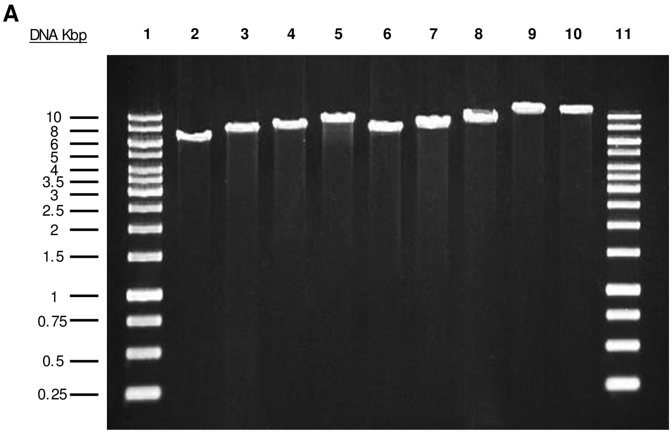

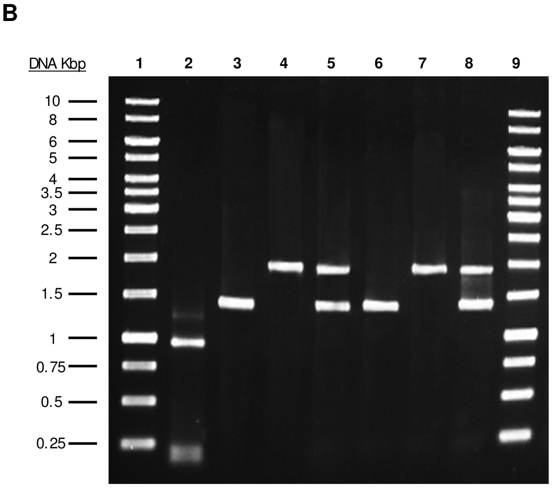

Figure S2. Analytical agarose gel of (**A**) different constructs (single and double) obtained from linearization of pESC and pJRoC30 with NotI (for details see **Materials and Methods** section), and (**B**) PCR reactions to identify the inserts of *Vp* and *Lac* in the corresponding vectors: Lanes 1A, 11A, 1Band 9B, molecular weight marker 1Kb DNA ladder; lane 2, pESC (without *Lac* and *Vp*); lane 3, pESC-*Vp*(GAL10/ADH1); lane 4, pESC-*Lac*(GAL10/ADH1); lane 5, pESC-*Vp*(GAL1/CYC1)-*Lac*(GAL10/ADH1); lane 6, pESC-*Vp*(GAL1/CYC1); lane 7, pESC-*Lac*(GAL1/CYC1); lane 8, pESC-*Lac*(GAL1/CYC1)-*Vp*(GAL10/ADH1); lane 9A: pJRoC30-*Lac*(GAL1/CYC1); lane 10A, pJRoC30-*Vp*(GAL1/CYC1). The identity of each construct was confirmed by DNA sequencing.

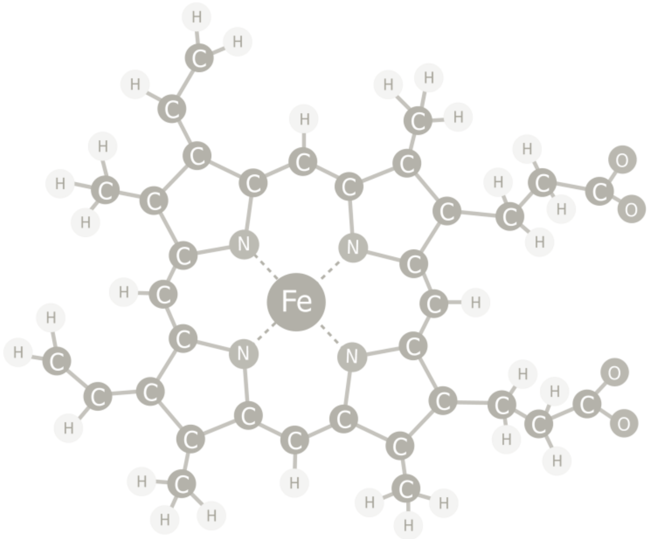

Capítulo 8:

Discusión general de resultados

Este capítulo resume los principales logros obtenidos en la Tesis Doctoral e incluye una discusión general que relaciona los resultados mostrados con el estado del arte actual y sus posibles vías de desarrollo futuro.

1. Evolución dirigida para secreción y termoestabilidad: Punto de partida para el diseño de VPs con estabilidad oxidativa mejorada y actividad a pH neutro/alcalino

El gen codificante de la VP de *P. eryngii* (variante alélica VPl2) fue sometido a evolución molecular dirigida en el transcurso del **Capítulo 2** con el fin de lograr su expresión funcional heteróloga en *S. cerevisiae*. Para adaptar la correcta expresión de la VP a la maquinaria de procesamiento y exportación de la levadura, en primer lugar su péptido señal nativo fue reemplazado por el pre-prolíder del factor alfa (un factor de apareamiento de células haploides en el ciclo vital de *S. cerevisiae*). De esta manera, la VP siguió una ruta secretora similar a la del factor alfa, al tiempo que se facilitaba su correcto plegamiento, procesamiento y exocitosis. Como sustrato para detectar la actividad oxidativa de la VP en los sobrenadantes celulares se escogió el ABTS, con lo cual se consiguió preservar la actividad de dos de los tres sitios catalíticos que posee la enzima (canal del hemo y Trp catalítico). El ABTS tiene muy buenas características para su uso en experimentos de evolución dirigida en levadura ya que presenta un límite de detección muy bajo (~5 nU/mL de VP), genera pocas interferencias con los sobrenadantes celulares y ofrece una gran estabilidad de la señal detectada; todo ello unido permite el diseño de diferentes protocolos HTS robustos y fiables (Garcia-Ruiz *et al*., 2010). Haciendo uso de este conjunto de elementos, se optimizaron las condiciones de expresión de la VP en levadura para el formato HTS (temperatura, agitación, humedad, fuente de grupo hemo, aireación, etc.), obteniéndose en el mejor de los casos unos niveles de expresión de 0,4 mg/L, que aunque bajos, fueron suficientes para comenzar una campaña evolutiva hacia secreción mejorada.

En el planteamiento de la estrategia evolutiva, el reto fue doble: en primer lugar se perseguía alcanzar una expresión funcional suficiente que permitiera llevar a cabo nuevas generaciones de evolución hacia diversos fines biotecnológicos, mientras que en segundo lugar se buscaba la mejora de la termoestabilidad de la enzima (que se afrontó en una segunda etapa del experimento evolutivo). Particularmente, el protocolo HTS de termoestabilidad fue específicamente diseñado para controlar la descompensación que resulta de mejorar la actividad enzimática a expensas de la estabilidad y viceversa (Romero and Arnold, 2009; Garcia-Ruiz *et al.,* 2010). En efecto, dicho protocolo ha sido exhaustivamente empleado en nuestro laboratorio para evolucionar otras ligninasas incluyendo lacasas y UPO (Mate *et al.,* 2010; 2016b) así como rubiscos de origen bacteriano (material no publicado).

En total, se llevaron a cabo seis rondas de evolución dirigida (9.000 clones explorados) en las que el gen de fusión (α-preprolíder)-VP se sometió a diferentes técnicas de generación de diversidad utilizando protocolos *in vivo* e *in vitro*. Las cuatro primeras generaciones se enfocaron hacia la mejora de secreción incluyendo una ronda híbrida donde se aplicó tanto el protocolo HTS para la mejora de la expresión funcional como de la termoestabilidad. En las siguientes generaciones enfocadas a aumentar la termoestabilidad de la enzima se incrementó progresivamente la presión selectiva con el fin de acelerar el proceso de evolución adaptativa (*i.e.,* la temperatura aplicada en el HTS fue incrementada de 60 ºC a 90 ºC).

Las tasas mutagénicas aplicadas junto con un uso inteligente del *in vivo* DNA *shuffling* en *S. cerevisiae* permitió una acumulación promedio de una mutación por ciclo de evolución (*i.e.*

el mutante de secreción presentó 4 mutaciones beneficiosas tras cuatro generaciones, mientras que el mutante de termoestabilidad acumuló 7 mutaciones tras seis generaciones (las 4 mutaciones de la variante de secreción más 3 nuevas mutaciones termoestabilizantes)), lo que también alivió la inclusión de mutaciones neutrales o perjudiciales.

El mutante de secreción (variante R4) mostró una mejora en la expresión funcional de la VP ~ 129 veces, con niveles de secreción próximos a los 22 mg/L en condiciones de cultivo controladas. Por su parte, el mutante de termoestabilidad (variante 2-1B) obtenido presentó una mejora de 8 ºC en su valor de T_{50} (temperatura a la cual la enzima conserva el 50% de su actividad tras una incubación de 10 min) frente al tipo parental. Ambas variantes fueron purificadas y caracterizadas en detalle, tanto bioquímica- como espectrofotométricamente revelando propiedades interesantes, y en algunos casos no esperadas, que abrieron el camino para futuras campañas evolutivas (**Figura 1**). Estas mejoras fueron particularmente:

i) El aumento en la estabilidad oxidativa del mutante de secreción R4, que estableció el punto de partida para la evolución hacia resistencia a H_2O_2.

ii) La estabilización a pH alcalinos del mutante de termoestabilidad 2-1B, que permitió emplearlo como parental para la evolución hacia actividad a pHs básicos.

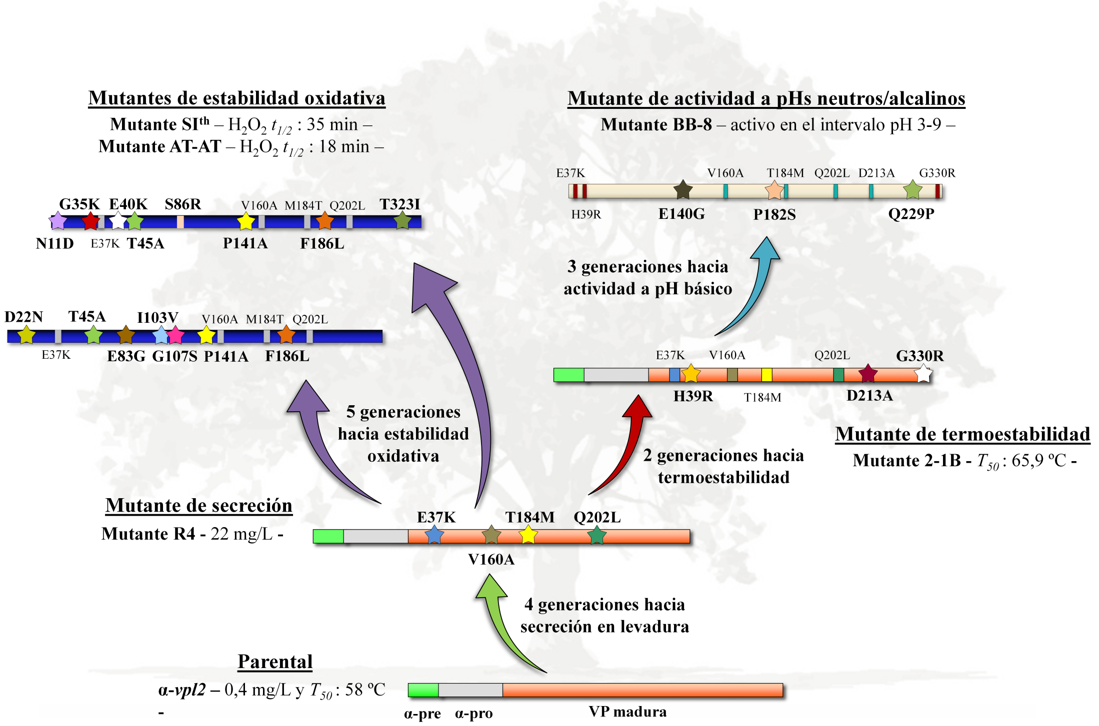

Figura 1. Diferentes rutas evolutivas recorridas en la Tesis Doctoral para el diseño de VP mejoradas en secreción, termoestabilidad, estabilidad oxidativa y actividad/estabilidad a pHs alcalinos.
Las estrellas indican aparición de nuevas mutaciones, mientras que los cuadrados denotan la acumulación de la mutación en cada caso. T_{50}: temperatura a la cual la enzima conserva el 50% de su actividad tras una incubación de 10 min. H_2O_2 $t_{1/2}$: tiempo que tarda la enzima en perder el 50% de su actividad en un tratamiento de 3.000 equivalentes de H_2O_2, pH 7,0 y 25 ºC.

El diseño de VPs que sean resistentes al daño oxidativo (como el propuesto en el primer caso) permitiría aumentar la estabilidad operacional del biocatalizador en todos los procesos biotecnológicos donde las peroxidasas encuentran aplicación. Por otro lado, la obtención de VPs activas en un amplio rango de pH (como el propuesto en el segundo caso) facilitaría su uso en un amplio espectro de aplicaciones, como *p. ej.* la solubilización de polímeros con aplicaciones biomédicas, procesos de síntesis en la industria farmacéutica, formulaciones cosméticas (como ya se ha propuesto para la LiP), o la degradación de PAHs y asfaltenos contenidos en combustibles fósiles con la intención de reducir su carácter carcinogénico tras la combustión (Ayala *et al.*, 2007b; Falade *et al.*, 2016; Sakai *et al.*, 2009).

2. Evolución dirigida de la VP hacia estabilidad oxidativa

Como se ha mencionado en la sección anterior, para llevar a cabo la mejora de la estabilidad oxidativa de la VP, se seleccionó como punto de partida la variante de secreción (mutante R4) que se obtuvo en la campaña para expresión funcional. Los principales motivos para emplear R4 como parental del proceso de evolución hacia resistencia oxidativa fueron su valor de K_m para el H_2O_2 (incrementado en 4 veces respecto al parental y que otorgó al mutante elevadas actividades específicas bajo condiciones saturantes), así como sus elevados niveles de secreción (que permitirían asumir las posibles pérdidas de actividad asociadas a la estabilización oxidativasin que el HTS perdiera fiabilidad; ver más adelante).

El daño oxidativo generado por concentraciones catalíticas de H_2O_2 es una característica muy difícil de mejorar en las peroxidasas. Esto se debe a que la oxidación de aminoácidos es un proceso que puede ocurrir tanto en la superficie de la proteína como en sus cavidades o sitios de unión a sustratos. En el caso particular de las peroxidasas, este proceso inhibitorio está estrechamente asociado al mecanismo de acción de la enzima (*i.e.* el H_2O_2 es tanto el co-sustrato/activador de la enzima como un potente inhibidor). Es por ello, que la mejora de esta característica se ha abordado fundamentalmente mediante ingeniería genética, ya sea a través de diseño racional sustituyendo aminoácidos oxidables de la proteína, como Met o Cys por otros de bajo potencial redox (Kim *et al.*, 2001; Sáez-Jiménez *et al.*, 2015a; Ogola *et al.*, 2010; Valderrama *et al.*, 2002), o bien mediante experimentos de evolución dirigida. Siendo en estos últimos en los que se ha empleado como criterio selectivo del proceso de evolución la incubación de las variantes generadas bajo altas concentraciones de H_2O_2, donde éstas son rápidamente inactivadas. Si bien este tipo de estrategias HTS permiten un cribado rápido de las librerías, no facilitan la identificación precisa de variantes mejoradas al no incluir en la ecuación una medida de actividad total en condiciones no inhibitorias. Por este motivo, en la evolución de la VP hacia estabilidad oxidativa se desarrolló un nuevo protocolo HTS basado en la determinación de la actividad inicial de las variantes con respecto a su actividad residual obtenida tras incubación en presencia de H_2O_2. En la aplicación de este HTS la presión selectiva determinada por la concentración de H_2O_2 se fue incrementando tras los ciclos sucesivos desde 0,3 mM hasta alcanzar 0,6 mM. De esta forma se consiguió aumentar la estabilidad oxidativa de la VP discriminando entre las mejoras destinadas a la estabilización oxidativa de la enzima, frente a las mejoras implicadas en los niveles de secreción, o aquéllas que afecten directamente a los parámetros cinéticos. Además, se incorporó un tercer *re-screening* en el que se analizaron los valores de T_{50} de las variantes positivas y sus vidas medias aparentes frente a H_2O_2 permitiendo una selección precisa de los clones con características mejoradas. En este proceso de evolución dirigida se exploraron un total de 15.000 clones durante cinco generaciones consecutivas.

Al contener en su estructura varios sitios catalíticos y canales, la VP soporta un alto tránsito de ROS que la hacen más sensible a la inactivación por H_2O_2. Es por ello que uno de los principales abordajes acometidos en el diseño evolutivo de la VP fue a través de la construcción de librerías inteligentes, donde las cargas de mutaciones aleatorias y los eventos de recombinación se enfocaron en regiones concretas de la proteína mientras se conservó inalterado el resto de la estructura proteica. Bajo esta premisa surgió el desarrollo del protocolo de MORPHING (*Mutagenic Organized Recombination Process by Homologous IN vivo Grouping*), lo que ha permitido la evolución enfocada de la VP y de muchas otras enzimas diseñadas mediante evolución dirigida en nuestro laboratorio (véase siguiente sección).

Así, tras un alineamiento múltiple estructural de la VP junto con diversas peroxidasas con estabilidad oxidativa mejorada, se seleccionaron tres regiones para ser sometidas a MORPHING comprendiendo: i) la parte superior de la cavidad del grupo hemo (incluyendo los aminoácidos catalíticos y su entorno), ii) la parte inferior del hemo (abarcando el entorno de la histidina proximal), y iii) una región axial al grupo hemo que contiene tres de las cuatro metioninas potencialmente oxidables en la VP (Met247, Met262 y Met265) y su entorno. La exploración de la región iii) dio lugar a un efecto inesperado, ya que no reveló ningún mutante mejorado que reemplazara alguno de los residuos de Met oxidables explorados. Cuando en rondas posteriores los residuos de Met262 y Met265 se sometieron a estudios de mutagénesis saturada combinatorial (donde se exploran las posibles combinaciones y permutaciones de los 20 aminoácidos posibles en las dos posiciones dadas) se confirmaron los resultados obtenidos mediante MORPHING, con un 95% de clones inactivos en la librería combinatorial. Esto demostró la importancia de los residuos de Met en la VP para su buen funcionamiento. Recientemente se ha descrito una variante de VP en la que únicamente la sustitución simultánea de sus cuatro metioninas dio lugar a una mejora en la estabilidad oxidativa, pero a expensas de una notable reducción en su actividad; resultados que complementan los efectos arriba descritos (Sáez-Jiménez *et al.*, 2015a).

En lo referente a los resultados del MORPHING en las regiones i) y ii), se descubrieron una serie de mutantes mejorados con substituciones en las posiciones 40, 45 y 141 de la VP. Sin embargo, las posiciones 40 y 45 se encontraron muy próximas entre sí como para permitir que la maquinaria de recombinación de *S. cerevisiae* las recombinara en un único mutante, lo cual obligó a diseñar nuevas variantes mediante mutagénesis dirigida convencional que mostraron estabilidades oxidativas mejoradas como resultado de las sinergias establecidas entre las tres mutaciones beneficiosas.

Tras cuatro rondas de evolución dirigida haciendo uso de un amplio abanico de técnicas de creación de diversidad tanto *in vitro* como *in vivo*, se obtuvo una batería de mutantes que portaban diferentes combinaciones de mutaciones beneficiosas. Tal variedad proporcionó diferencias en las propiedades mejoradas de las variantes como distintas actividades, termoestabilidades y estabilidades oxidativas. Este complejo escenario mutacional llevó a pensar en el desarrollo de una nueva técnica que permitiera explorar los posibles efectos epistáticos entre las diferentes mutaciones encontradas, con el fin de revelar la mejor combinación posible entre ellas. Teniendo este objetivo en mente, se desarrolló la técnica del DNA$_{\text{puzzle}}$, la cual toma ventaja del potencial que supone el uso de la maquinaria de recombinación de *S. cerevisiae*. De este modo, se facilitó la recombinación de bloques de secuencia evolucionados que portaban las diferentes mutaciones beneficiosas, y que se encontraban localizadas en distintos entornos mutacionales (bloques de secuencia evolucionados). El proceso de recombinación *in vivo* de los bloques de secuencia evolucionados permitió crear una única librería mutagénica que incluyó tanto la recombinación entre diferentes bloques de secuencia, como la recombinación de las distintas mutaciones contenidas en los mismos, siempre y cuando no se encontrasen a una distancia inferior a ~50 pb (donde la eficiencia de la maquinaria celular de *S. cerevisiae* ya es limitada).

Para llevar a cabo esta técnica, se hizo necesario un detallado análisis de los bloques de secuencia que mejor se adaptasen a la necesidad de alcanzar un compromiso entre actividad y estabilidad (tanto térmica como oxidativa). El gen de la VP se fragmentó mediante PCR en tres segmentos diferenciados dando lugar a la amplificación de nueve bloques de secuencia diferentes, que posteriormente se recombinaron *in vivo* en la levadura mediante un único paso de transformación. Finalmente, los clones resultantes se sometieron al protocolo HTS hacia estabilidad oxidativa seleccionando dos variantes finales que mostraron 7 y 8 mutaciones, respectivamente. En ambos casos se llegó a un consenso pleno entre los parámetros de actividad y estabilidad (oxidativa y térmica), aunque cada mutante denotó unas características diferenciales. Por ejemplo, la variante SI$^{\text{th}}$ (con 8 mutaciones) presentó una alta estabilidad oxidativa y térmica, pero actividad disminuida frente al tipo parental. A diferencia de ésta, la variante AT-AT (con 7 mutaciones) mostró inferiores estabilidades frente a la variante SI$^{\text{th}}$, pero una mayor actividad que en éste último.

Los resultados obtenidos en este trabajo fueron interpretados mediante un análisis estructural con otras peroxidasas mejoradas hacia estabilidad oxidativa, lo que permitió proponer una serie de consideraciones generales que podrían emplearse para mejorar la estabilidad oxidativa de otras peroxidasas en futuros estudios, como son:

i) Todo parece indicar que cuanto mayor es el número de canales y centros activos en la peroxidasa, más sensible es a la presencia de H_2O_2 debido al alto tránsito de ROS. Esta observación se extrae de la comparación de las propiedades de los mutantes AT-AT y SI$^{\text{th}}$: esta última variante reemplazó uno de los tres ácidos que coordinan la esfera de Mn^{2+} por un aminoácido voluminoso bloqueando parcialmente el acceso a dicho canal y aumentando su estabilidad oxidativa, mientras que la variante AT-AT aún preservó el acceso a sus tres sitios de oxidación siendo más susceptible a la inactivación suicida.

ii) En relación con el punto i), la reducción de la reactividad de la enzima parece encontrarse en estrecha relación con el aumento en la estabilidad oxidativa, probablemente debido a la reducción de la población de ROS y otros radicales. Este efecto se ha observado al modular la posición de la hélice B mediante la sustitución de las posiciones 45 y 103 de la VP en éste y otros trabajos (Cherry *et al.*, 1999;

Sáez-Jiménez *et al.*, 2015a), así como tras la substitución de la Phe proximal (Phe186).

iii) La sustitución de los residuos de Met es una estrategia de estabilización ya demostrada, pero con un efecto sumamente perjudicial sobre la actividad enzimática que se debe valorar antes de acometer dichos experimentos.

iv) El grado de compactación de la enzima parece determinar su estabilidad oxidativa, ya que puede impedir el acceso de ROS a zonas críticas de la estructura evitando su desestabilización (efecto que se puede discernir de la eliminación de sitios catalíticos y diferencias en la estructura terciaria que modulan la robustez de la proteína, éste es el caso de los resultados obtenidos tras la substitución de las posiciones 35, 40, 45, 83, 86, 103, y 107 en la VP).

3. MORPHING: Una herramienta versátil de evolución enfocada

La técnica de MORPHING encuentra sus bases en el modo que tiene de actuar la eficiente maquinaria de recombinación homóloga que posee *S. cerevisiae*. Años atrás, se desarrolló en nuestro laboratorio una técnica de recombinación de DNA en levadura que recibió el nombre de IVOE (*In Vivo Overlap Extension*), y que consiste en recombinar fragmentos de DNA mediante la ingeniería de extremos solapantes con una extensión de 40-45 pb (Alcalde, 2010), esta técnica puede ser aplicada para realizar mutagénesis dirigida, saturada, de inserción y deleción. Ciertamente, MORPHING, como la mayoría de los protocolos de creación de diversidad en levadura (véase **Capítulo 5**), se rige por los mismos principios.

Mediante el protocolo de MORPHING se pueden introducir mutaciones de manera aleatoria y eventos de recombinación en segmentos específicos, previamente determinados por el investigador en base a estudios previos (*p. ej.* haciendo un uso racional de la estructura de la enzima, o bien tras el análisis de una determinada ruta evolutiva). Mientras que los segmentos diana se amplifican por PCR mutagénica, los segmentos restantes de la proteína se obtienen mediante PCR de alta fidelidad, pero en todos los casos se planifica la inclusión de secuencias solapantes de ~40 pb (por debajo de este límite la eficiencia de recombinación se ve mermada significativamente (Hua *et al.*, 1997; Oldenburg, 1997)). Dichos brazos solapantes flanquean cada producto de PCR y se generan a partir de los propios moldes de partida (*i.e.* son secuencias extra incorporadas en los oligos cebadores). El *pool* de fragmentos resultantes de la reacción de PCR se transforma posteriormente en la levadura (junto con el plásmido linearizado) para que su maquinaria de recombinación lleve a cabo el ensamblaje del gen completo junto con la reparación y circularización del plásmido episómico, creándose la librería de mutantes que contiene las mutaciones en aquella(s) región(es) que se quiera(n) explorar quedando intactas las zonas restantes.

Además, la evolución enfocada por MORPHING permite la exploración de las regiones seleccionadas tanto de manera independiente como de manera combinatorial (*i.e.* barajando los segmentos mutagenizados para la generación de una única librería), dependiendo del abordaje que se necesite en cada caso (**Figura 2**).

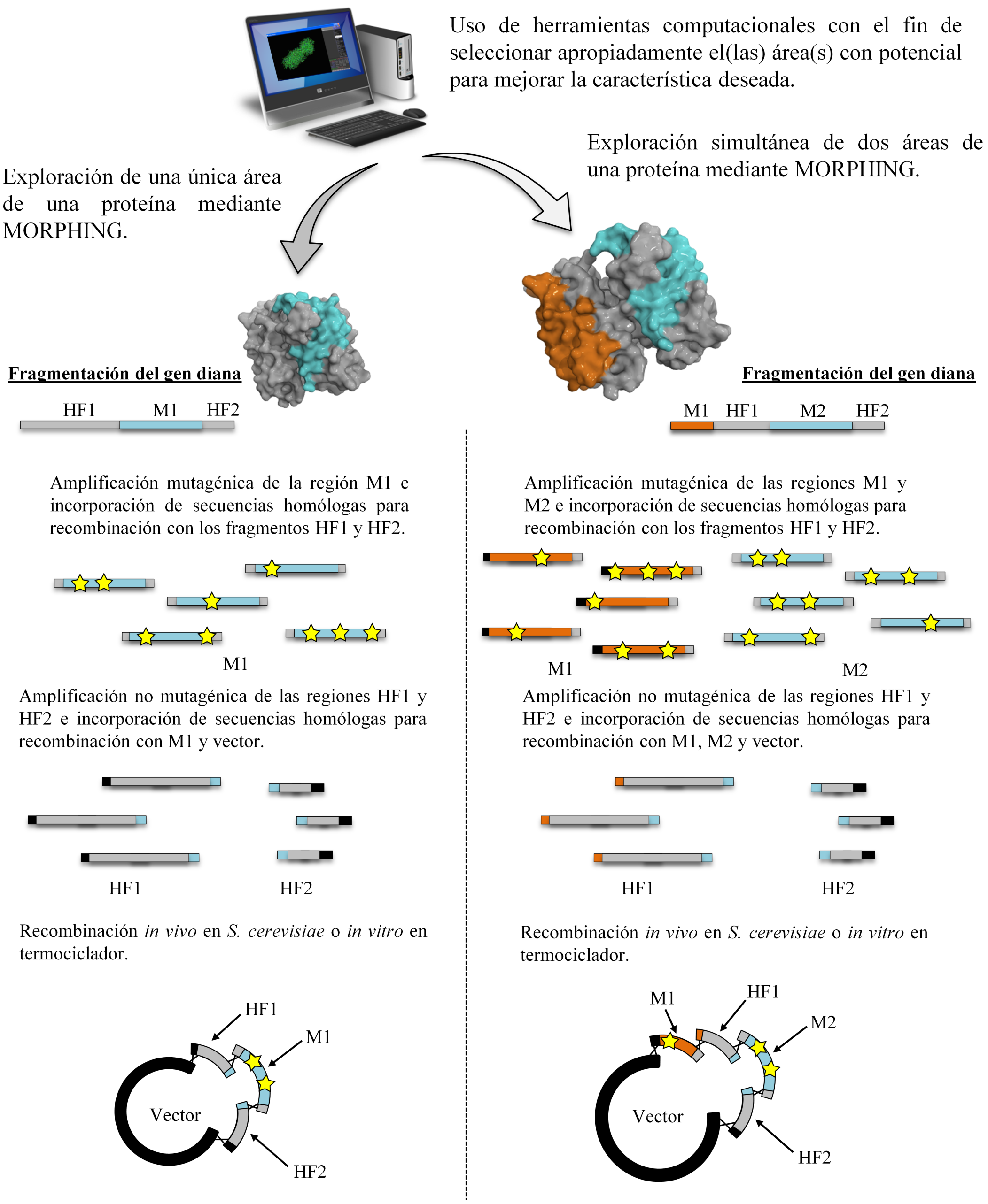

Uso de herramientas computacionales con el fin de seleccionar apropiadamente el(las) área(s) con potencial para mejorar la característica deseada.

Exploración de una única área de una proteína mediante MORPHING.

Exploración simultánea de dos áreas de una proteína mediante MORPHING.

Amplificación mutagénica de la región M1 e incorporación de secuencias homólogas para recombinación con los fragmentos HF1 y HF2.

Amplificación mutagénica de las regiones M1 y M2 e incorporación de secuencias homólogas para recombinación con los fragmentos HF1 y HF2.

Amplificación no mutagénica de las regiones HF1 y HF2 e incorporación de secuencias homólogas para recombinación con M1 y vector.

Amplificación no mutagénica de las regiones HF1 y HF2 e incorporación de secuencias homólogas para recombinación con M1, M2 y vector.

Recombinación *in vivo* en *S. cerevisiae* o *in vitro* en termociclador.

Recombinación *in vivo* en *S. cerevisiae* o *in vitro* en termociclador.

Figura 2. Esquema general del protocolo de MORPHING aplicado a la exploración de una única región o varias regiones simultáneas.
La creación de las librerías mutagénicas a través de MORPHING pretende reducir los esfuerzos experimentales invertidos en procesos HTS aumentando la posibilidad de encontrar mutantes ganadores dentro de librerías más manejables, de fácil exploración, conocidas como "*smart mutant libraries*". Esto se hace posible mediante la exploración específica de la región o regiones mutagénicas previamente seleccionadas, con ayuda de algoritmos computacionales (*p. ej.* en base a estudios de QM/MM o de dinámica molecular) u otras herramientas que puedan tener algún papel en la mejora de la característica deseada. Las estrellas indican las mutaciones introducidas mediante PCR mutagénica. Las cruces negras indican las áreas de recombinación entre fragmentos. M: regiones mutagénicas, HF: regiones amplificadas con alta fidelidad.

Una idea general de la versatilidad que ofrece el método MORPHING se puede apreciar en numerosos estudios recientes llevados a cabo en nuestro grupo, donde se ha aplicado para desenmascarar mutaciones consenso/ancestrales en la AAO (Viña-Gonzalez *et al.*, 2015; Viña-Gonzalez *et al.*, 2016), aumentar la termoestabilidad y el potencial redox de lacasas (material no publicado), mejorar la actividad de la UPO para la síntesis de metabolitos humanos de fármacos (*p.ej.* 5'- hidroxipropranolol) y mejorar su actividad peroxigenasa (Mate *et al.*, 2016b; material no publicado). Además también se ha adaptado y empleado con éxito el protocolo de MORPHING *in vitro* para enzimas expresadas funcionalmente en *E. coli* como rubiscos y β-lactamasas (material no publicado).

4. Evolución dirigida de la VP hacia actividad a pH neutro/alcalino

La oxidación de sustratos en el rango de pH neutro/alcalino es una característica ausente en todas las PODs descritas hasta la fecha debido a su baja estabilidad alcalina. Notablemente, dicha estabilidad sí fue adquirida -de manera inesperada- en el mutante de termoestabilidad de la VP (variante 2-1B) descrito en el **Capítulo 2**. Un reciente estudio sobre esta variante ha permitido revelar que su alta estabilidad alcalina se debe a la presencia de un esqueleto estabilizante formado por las mutaciones E37K, H39R y G330R (Sáez-Jiménez *et al.*, 2016). Dicho "andamiaje" permitió crear nuevas interacciones en el entorno del grupo hemo estabilizando y promoviendo el anclaje de los calcios estructurales, lo que evita en última instancia, la formación de un complejo hexacoordinado del hemo, que de otra manera, colapsaría e inactivaría la enzima (véase **apartado 3.3.3** del **Capítulo 1**). A pesar de su estabilidad alcalina, el mutante 2-1B no mostró actividad a pH neutro/alcalino en ninguno de los tres sitios catalíticos presentes en la VP. Este hecho indicó que la actividad alcalina en las PODs no solo se encuentra limitada por su estabilidad asociada a la pérdida de los calcios estructurales como se describía en la literatura hasta el momento, sino que también requiere de nuevos atributos para poder ser activa en condiciones de pH neutro o alcalino.

De esta manera, con el fin de generar actividad a pH alcalino en la VP, se escogió el mutante 2-1B como punto de partida de esta nueva ruta evolutiva. En primer lugar se diseñó un protocolo HTS dual basado en la oxidación de ABTS con el que ampliar el perfil de actividad de la enzima hacia el lado alcalino, al tiempo que se mantuviera la capacidad de oxidación a pH ácido. Para mejorar la actividad a pHs básicos se introdujo una presión selectiva mediante el incremento gradual del pH de actividad desde 6,0 unidades hasta valores de 8,5. Con los valores de actividad determinados tanto a pH óptimo (4,0) como a pH neutro/alcalino, se estableció como criterio selectivo la selección de variantes que mejoraran su actividad a pH neutro/alcalinos, mientras retuvieran una actividad a pH óptimo ≥80% con respecto al tipo parental 2-1B. Como en las rutas anteriores, se incorporó un tercer *re-screening* en el que se determinaron los perfiles de pH, estabilidades a pH, y termoestabilidades para cada variante seleccionada. Esto garantizó la correcta ejecución de la estrategia evolutiva planteada.

Tras tres generaciones de evolución dirigida y 5.000 clones analizados se obtuvo el mutante BB-8, el cual acumuló únicamente tres mutaciones adicionales sobre la secuencia del parental 2-1B (P141A, Q229P, P182S), gracias nuevamente a un preciso control de las condiciones mutagénicas. BB-8 amplió notablemente su perfil de pH mostrando actividad en la región estrictamente ácida pH 3-4 (como su parental), así como en el intervalo de pH 5-9 donde la actividad del parental es indetectable. Aunque la mejora de actividad más drástica se consiguió con el sustrato empleado durante el proceso de *screening* (ABTS), también se observó un desplazamiento en el perfil de pH para otros sustratos oxidados en el canal del hemo como guayacol y ácido sinapico. Desafortunadamente, la actividad frente a Mn^{2+} de la enzima se vio significativamente mermada debido a la introducción de una mutación en las proximidades de este sitio catalítico (P182S). Sorprendentemente, la mutación que afectó la oxidación de Mn^{2+} también aportó las primeras evidencias experimentales de su implicación en la oxidación directa de ABTS en dicho sitio a pH neutro/alcalino con un máximo de actividad a pH 6,0. La oxidación de ABTS en el sitio de unión de Mn^{2+} a pHs neutros fue un importante hallazgo, ya que hasta el momento no se había mostrado experimentalmente tal efecto en las PODs, habiendo sido solamente descrito para MnPs a pHs ácidos (Fernández-Fueyo *et al.*, 2014).

A pesar de las mejoras de actividad atribuidas al canal principal de acceso al grupo hemo, y al sitio de oxidación de Mn^{2+} para ABTS, no se apreció mejora significativa en el Trp catalítico. Es bien sabido que la oxidación de sustratos de alto potencial redox ocurre cuando el Trp164 se encuentra en forma de radical catiónico (radical triptofanil, $Trp^{\bullet+}$; Morales *et al.*, 2012; Pérez-Boada *et al.*, 2005; Sáez-Jiménez *et al.*, 2015b). Si se tiene en cuenta que el potencial redox estándar de este radical decae en función del aumento del valor de pH (Morozova and Yurkovskaya, 2015), y que su pK_a se sitúa en torno a 4,3 unidades de pH (aunque este valor puede variar ligeramente dependiendo del microambiente en el que se encuentre el radical (Solar *et al.*, 1991; Zhang and Hammarström 2011)), es razonable pensar que dicho residuo en la VP a pH alcalino se encuentra en forma de radical neutro (descargado) y con un reducido potencial redox incapaz de oxidar sustratos en estas condiciones. De esta manera, la ruta interna de transferencia electrónica de largo recorrido desde el Trp164 hacia el hemo se encontraría permanentemente bloqueada a pH > 5. La presencia de un radical neutro ha sido detectada en la VP mediante técnicas de EPR, pero aún no se ha determinado la actividad catalítica que pueda tener dicho radical (Pogni *et al.*, 2006). Entre las razones que apoyan nuestra hipótesis se encuentran: la carencia de actividad en el Trp164 para el parental (2-1B) por encima de pH 5,0 (aun siendo estable), la ausencia de mejoras frente a sustratos de alto potencial redox, y la ausencia de mutaciones localizadas en el entorno de este sitio catalítico. Sin embargo, para arrojar luz sobre este asunto sería conveniente realizar un estudio más detallado incluyendo una batería de mutantes y sustratos de bajo potencial redox susceptibles de ser oxidados en el Trp catalítico (Morales *et al.*, 2012). De esta manera, la posible ausencia de actividad a pH neutro/básico del Trp catalítico sobre sustratos de bajo potencial ayudaría a confirmar nuestra hipótesis.

Finalmente, es importante reseñar que se detectó un fenómeno de hiperactivación en la variante BB-8 tras una incubación de 72 horas a pHs alcalinos. Dicha hiperactivación fue estudiada con distintos sustratos de bajo potencial redox (ABTS, DMP, guayacol, catecol) mostrando diferentes grados de hiperactivación dependientes del sustrato testeado (ABTS~DMP>catecol>guayacol). Para determinar si se trataba de algún fenómeno de dimerización enzimática vinculada al pH se realizaron pruebas de ultracentrifugación analítica que descartaron este efecto. Por el momento se desconoce el proceso por el que se regula la hiperactivación en este mutante a pHs alcalinos, pero estudios futuros más detallados ayudarán a esclarecer el mecanismo por el que se rige dicho fenómeno.

5. Creación de un prototipo inicial de levadura de podredumbre blanca a partir del ensamblaje de genes ligninolíticos evolucionados

La creación de un primer prototipo de levadura de podredumbre blanca (WRY, *white-rot yeast*) capaz de procesar el material lignocelulósico es una meta muy interesante que puede tener cavidad en multitud de aplicaciones biotecnológicas, como la producción de biocombustibles en las biorefinerías integrales (Hong and Nielsen, 2012; Nielsen *et al.*, 2013). Además del evidente potencial industrial de este microorganismo sintético, también ofrecería la posibilidad de estudiar con un mayor control el mecanismo de acción del consorcio ligninolítico. Al tratarse de un objetivo muy ambicioso, las metas más inmediatas que se han propuesto se enfocan en la creación de un aparato ligninolítico minimizado (miniligninosoma o lignosecretoma artificial), y otro degradador de celulosa (minicelulosoma), como se recoge en la **Figura 3**.

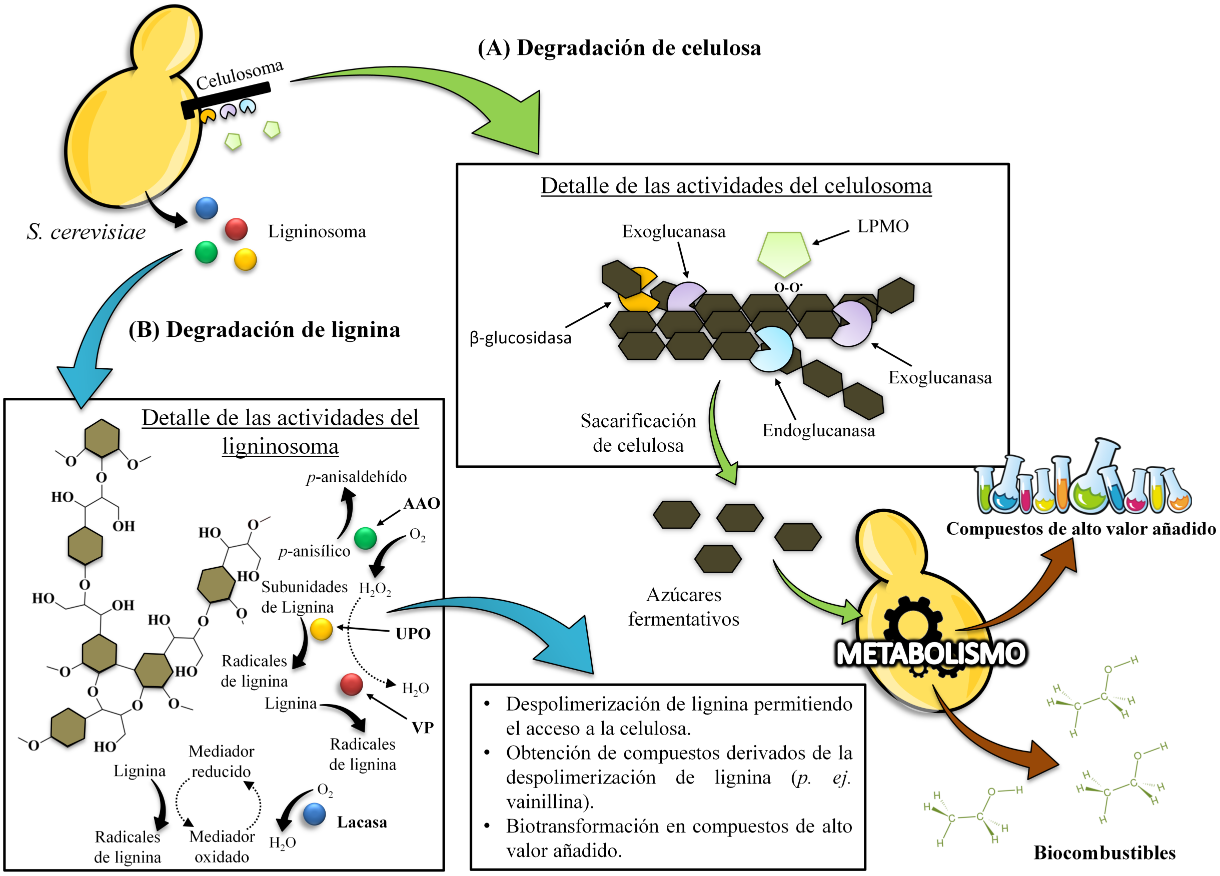

- Despolimerización de lignina permitiendo el acceso a la celulosa.
- Obtención de compuestos derivados de la despolimerización de lignina (*p. ej.* vainillina).
- Biotransformación en compuestos de alto valor añadido.

Figura 3. Esquema general de la ingeniería planeada llevar a cabo en *S. cerevisiae* para su utilización en el aprovechamiento de la biomasa lignocelulósica.

La levadura *S. cerevisiae* ha sido seleccionada como hospedador heterólogo para la expresión de estos consorcios degradadores, porque es un microorganismo modelo en biología sintética exitosamente empleado como factoría celular en la producción de biocombustibles a partir de azúcares contenidos en la biomasa vegetal. Gracias al trabajo llevado a cabo en los últimos años en nuestro laboratorio, se ha conseguido expresar funcionalmente en esta levadura una amplia representación de ligninasas de las que ahora podemos tomar ventaja para el diseño del WRY.

Algunas de las cuestiones que surgieron a la hora de comenzar a construir este prototipo de levadura fueron: ¿Es posible expresar varios genes ligninolíticos en la misma levadura sin afectar a su metabolismo, sin derivar en un exceso de consumo energético, o sin que esto sea tóxico para la célula?, ¿Existe un número límite de ligninasas que se puedan expresar heterólogamente en la levadura?, ¿Los niveles de expresión de las ligninasas serán suficientes para obtener una flujo adecuado de degradación del material lignocelulósico?. Aunque muchas de estas cuestiones se mantienen aún sin una respuesta clara, el trabajo llevado a cabo en el **Capítulo 7** ha permitido esclarecer algunos aspectos importantes.

Como prueba de concepto se abordó la expresión funcional conjunta de una lacasa del basidiomiceto PM1 (previamente evolucionada hacia expresión funcional y tolerancia a sangre humana (Mate *et al.*, 2013a)), y el mutante termoestable 2-1B de la VP (véase **Capítulo 2**), utilizando una serie de construcciones basadas en vectores bi-direccionales de la familia pESC. Con dichas construcciones se pretendía abordar la posibilidad de expresar ambos genes en la misma célula de levadura, y si esto fuera posible, estudiar de qué manera se verían afectados los niveles de expresión en cada caso. De manera paralela, también se estudió el efecto de las condiciones de cultivo en formato de microplaca y en matraz; donde las condiciones de cultivo son diferentes.

Los genes de la VP y la lacasa se clonaron bajo el control de diferentes *cassettes* de expresión incluyendo los pares promotor y terminador GAL1/ CYC1 y GAL10/ADH1. Los resultados de este trabajo mostraron que la co-expresión de ambas enzimas es posible en una única célula de levadura sin ejercer toxicidad aparente. No obstante, los niveles de co-expresión comparados con los de expresión independiente descendieron entre 4-5 veces para la co-expresión en microplaca, y entre 6-10 veces para matraz. Además, se observó de manera general que los niveles de expresión de ambos genes utilizando el *cassette* de expresión GAL10/ADH1 se vieron aumentados. La mejor construcción para expresar niveles similares de lacasa y VP en el medio de cultivo fue GAL10/Lac/ADH1-GAL1/VP/CYC1. Con estos resultados se hizo más esperanzadora la construcción de un WRY más avanzado llevando a pensar en los siguientes pasos a realizar.

La idea del miniligninosoma no es co-expresar una gran cantidad de PODs y otras ligninasas como frecuentan hacer los hongos de podredumbre blanca en la naturaleza (**Tabla 1**), sino reducirlo a una selección de genes diseñados *ad-hoc*, con propiedades mejoradas y mayor potencial biotecnológico, con lo que el efecto es doble al simplificar el modelo al tiempo que se evita un innecesario gasto energético en la levadura.

Tabla 1. Número de PODs y otras peroxidasas en los hongos de podredumbre blanca.

	Podredumbre blanca			*Podredumbre parda*	
Enzimas	*Bjerkandera adusta* (degradación selectiva)	*Phlebia brevispora* (degradación simultánea)	*Phanerochaete chrysosporium* (degradación simultánea)	*Postia placenta*	
MnP	6	6	5	0	
LiP	12	5	10	0	
VP	1	0	0	0	
GP	1	0	1	1	
	20	**11**	**16**	**1**	**Total de PODs**
HTP	4	2	2	3	
DyP	10	3	0	2	
	34	**16**	**18**	**6**	**Total de peroxidasas**
AAO	11	3	3	1	
MOX	5	6	3	4	
GOX	0	0	1	0	
CDH	1	1	1	0	
P2O	1	1	1	0	
	18	**11**	**9**	**5**	**Total GMCs**

Tabla adaptada de Ruiz-Dueñas *et al.*, 2013, Ferreira *et al.*, 2015.
PODs (peroxidasas ligninolíticas), MnP (Manganeso peroxidasa), LiP (Lignina peroxidasa), VP (Peroxidasa versátil), GP (Peroxidasa genérica), HTP (Peroxidasa hemotiolada), DyP (peroxidasa decolorante de tintes), AAO (aril-alcohol oxidasa), MOX (Metanol oxidasa), GOX (Glucosa oxidasa), CDH (Celobiosa deshidrogenasa), P2O (Piranosa 2-oxidasa).

Un ejemplo muy interesante de consorcio ligninolítico reducido podría albergar cuatro enzimas incluyendo una lacasa de alto potencial redox, una VP (evitando así la necesidad de MnPs y LiPs), una UPO, y una AAO que proporcione H_2O_2 al sistema ligninolítico. Experimentos recientes llevados a cabo en nuestro laboratorio confirman preliminarmente que la co-expresión de estos cuatro genes es posible, y no se descarta la inclusión de nuevas alternativas ligninolíticas que mejoren las prestaciones del sistema (material no publicado). Además este sistema ligninolítico podría ser mejorado mediante evolución dirigida al tener ya establecida la plataforma de evolución basada en la propia levadura.

En última estancia, se podrían activar y/o desactivar diferentes genes en los *cassettes* de expresión para estudiar las sinergias, actividades e implicaciones de las diferentes enzimas sobre ligninas modelo y/o materiales lignocelulósicos más complejos. De esta manera, el miniligninosoma ofrecería un modelo sintético de degradador selectivo de lignocelulosa, que además podría convertirse en un modelo degradador simultáneo acoplándole a modo de *gadget on/off* un minicelulosoma asociado.

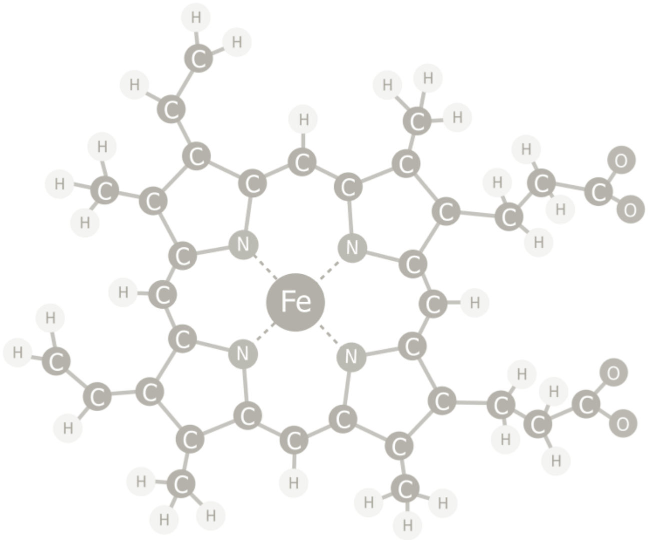

Capítulo 9:

Conclusiones / *Conclusions*

1. La VP de *P. eryngii* fue sometida a seis ciclos de evolución molecular dirigida hacia la mejora de su expresión funcional en *S. cerevisiae* y de su termoestabilidad cinética. El mutante de secreción obtenido en este proceso (variante R4, comprendiendo 4 mutaciones) mejoró su expresión funcional ~ 129 veces, lo que se tradujo en unos niveles de secreción de ~ 22 mg/L. La caracterización bioquímica de dicho mutante reveló una disminución de su afinidad por H_2O_2 y una estabilidad oxidativa mejorada, por lo que se escogió como parental para una nueva campaña evolutiva hacia estabilización oxidativa.

2. El mutante de termoestabilidad de la VP (variante 2-1B, comprendiendo 7 mutaciones) incrementó 8 ºC su valor de T_{50} respecto al parental. Además, se observó un aumento significativo en su estabilidad alcalina conferido a través de un eje estabilizante de tres mutaciones. Así, 2-1B mostró una actividad residual de más del 60 % tras 120 horas de incubación a pH 9,0, y un desplazamiento del pH óptimo de actividad frente a ABTS de pH 3,0 a pH 4,0, por lo que este mutante se escogió como parental para una nueva campaña evolutiva hacia actividad alcalina.

3. Partiendo del mutante R4, se llevaron a cabo cinco generaciones de evolución dirigida para la mejora de la estabilidad oxidativa. Para ello, se diseñó un protocolo HTS basado en el análisis de las vidas medias aparentes de los mutantes frente a H_2O_2, así como de sus actividades y termoestabilidades, lo que permitió una selección precisa de los clones con mejores características. Con la finalidad de acelerar el proceso evolutivo, el estrés oxidativo durante el HTS fue incrementado en el transcurso de la evolución hasta concentraciones de 0,6 mM de H_2O_2.

4. Durante esta ruta evolutiva, se utilizó una batería de herramientas *in vivo* e *in vitro* para la creación de diversidad genética, incluyendo el desarrollo de la técnica de MORPHING destinada a introducir mutaciones y recombinaciones en regiones específicas de la proteína manteniendo el resto de la estructura inalterada. En el último ciclo evolutivo se aplicó un nuevo método para la recombinación *in vivo* de bloques de secuencia independientes (DNA_{puzzle}), que permitió encontrar la mejor combinación posible de mutaciones beneficiosas -a partir de mutantes procedentes de diferentes etapas del proceso- alcanzando un compromiso razonable entre la actividad y la estabilidad oxidativa.

5. Los dos mejores mutantes de esta campaña evolutiva, la variante AT-AT (con 7 mutaciones) y la variante SI^{th} (con 8 mutaciones), aumentaron su estabilidad oxidativa 6 y 12 veces, respectivamente. Empleando 3.000 equivalentes de H_2O_2 (a 25 ºC y pH 7,0), la variante SI^{th} mostró una vida media de 35 min (y una termoestabilidad mejorada en ~ 6 ºC), mientras que para la variante AT-AT fue de 18 min, frente a los 3 min del parental R4.

6. Partiendo del mutante de termoestabilidad (variante 2-1B), se llevaron a cabo tres nuevas generaciones de evolución dirigida para conferir actividad a pH neutro/alcalino. Para ello, se diseñó un protocolo HTS en el que se incrementó la presión selectiva generación tras generación (de pH 6,0 a pH 8,5) al tiempo que se amplió el perfil de pH.

7. El mutante final de esta ruta (variante BB-8) acumuló tres nuevas mutaciones que le permitieron mostrar actividad en el intervalo de pH 5,0 a 9,0 frente a ABTS, donde el parental no es activo. BB-8 también mejoró la actividad a pH neutro/alcalino con los sustratos guayacol, ácido sinápico, y ligeramente con alcohol veratrílico.

8. La variante BB-8 mostró por primera vez la capacidad de oxidar directamente ABTS en el sitio de oxidación de Mn^{2+} bajo pH neutro/alcalino a costa de reducir significantemente su actividad frente a Mn^{2+}. Tras un estudio complementario basado en mutagénesis racional y *molecular docking*, dicho fenómeno se atribuyó en exclusiva a la mutación P182S localizada en la vecindad del sitio de Mn^{2+}.

9. El mutante VP de termoestabilidad 2-1B y una lacasa de alto potencial redox (evolucionada previamente para secreción en levadura y resistencia a sangre humana) se co-expresaron funcionalmente en *S. cerevisiae* mediante el uso de vectores bi-direccionales. La co-expresión de VP y lacasa se llevó a cabo en microplaca y matraz bajo diferentes *cassettes* de expresión incluyendo los pares promotor/terminador GAL1/CYC1 y GAL10/ADH1. En términos generales, la expresión de los genes individuales bajo GAL10/ADH1 fue el sistema más efectivo. Sin embargo, para la co-expresión de ambos genes con similares niveles de expresión fue necesaria la construcción GAL1/VP/CYC1-GAL10/Lacasa/ADH1.

10. Se diseñó un prototipo inicial de levadura de podredumbre blanca (WRY) con un reducido aparato degradador de lignina, que constituye una base apropiada para la construcción de un microorganismo artificial más sofisticado con potenciales aplicaciones en biología sintética. Particularmente, el WRY podría encontrar aplicación en la producción de biocombustibles a partir de material lignocelulósico en las biorefinerías integrales, además de servir como modelo de estudio del complejo proceso de degradación de lignina.

1. The VP from *P. eryngii* was subjected to six rounds of molecular evolution for functional expression and thermostability in *S. cerevisiae*. The secretion mutant obtained in this process (R4 variant, harbouring 4 mutations) improved its functional expression ~129-fold, which raised the secretion levels around 22 mg/L. The biochemical characterization of this variant showed a reduction in its affinity for H_2O_2 along with an improved oxidative stability. This mutant was selected as parental type for a new directed evolution campaign towards oxidative stabilization.

2. The termostability mutant of VP (2-1B variant, harbouring 7 mutations) enhanced its T_{50} value around 8 ºC respect to the parental type. In addition, a significant improvement was observed in its alkaline stability supported by a three mutation stabilizing backbone. Thus, 2-1B showed a residual activity over 60 % after incubation for 120 h at pH 9.0, and a shift in the optimum pH for ABTS activity (from pH 3.0 to pH 4.0). Accordingly, the mutant 2-1B was chosen as parental type for a new directed evolution campaign towards activity at alkaline pH.

3. By using as starting point R4 mutant, five generations of directed evolution were performed to improve the oxidative stability in VP. For this purpose, a HTS protocol was designed by analyzing apparent half-lives against H_2O_2 of the new mutants, as well as their activities and stabilities, allowing a precise selection of improved clones. With the aim of speeding up the evolution process, the oxidative stress during HTS was incremented along the evolution up to concentrations of 0.6 mM H_2O_2.

4. In this evolution route, an array of *in vivo* and *in vitro* tools was used for the creation of DNA diversity including the development of MORPHING. This directed evolution method was supported by the *S. cerevisiae* apparatus and allowed us to perform random mutagenesis and recombination in specific targeted areas while preserving the remaining regions of the protein. In the last cycle of evolution a new method for *in vivo* recombination of independent sequence blocks (DNA_{puzzle}) was developed allowing the selection of the best possible combination among beneficial mutations along the evolutionary process. Conversely, an appropriate trade-off between activity and oxidative stability was achieved through this method.

5. The two outcome mutants from this evolutionary campaign were AT-AT (with 7 mutations) and SI^{th} (with 8 mutations) variants, which enhanced the oxidative stability 6- and 12-fold, respectively. When both mutants were incubated in presence of 3,000 equivalents of H_2O_2, SI^{th} showed a H_2O_2 half-life of 35 min (together with a ~ 6 ºC improved thermostability) and that of AT-AT was18 min. Under the same conditions the parent´s R4 half-life was 3 min.

6. By using as starting point the thermostable mutant (2-1B variant), three new generations of directed evolution were carried out towards activity at neutral/alkaline pH. For this purpose, a HTS protocol was designed increasing the selective pressure after each generation (from pH 6.0 to pH 8.5) at the time that the pH activity profile was widened.

7. The last mutant (BB-8 variant) yielded three new mutations that conferred activity in the pH range from 5 to 9 for ABTS, where the parent type was inactive. In addition, BB-8 improved its activity under neutral/alkaline pH with the substrates guaiacol, sinapic acid, and slightly with veratryl alcohol.

8. The BB-8 variant showed for the first time the ability to oxidize directly ABTS in the Mn^{2+} binding site under neutral/alkaline pH, albeit at the cost of reducing its activity for Mn^{2+}. After rational design and molecular docking studies, this phenomenon was exclusively attributed to the mutation P182S located in the surroundings of Mn^{2+} binding site.

9. The thermostability mutant 2-1B and a high-redox potential laccase (previously evolved for secretion in yeast and human blood tolerance) were functionally expressed in *S. cerevisiae* by using bi-directional vectors. The co-expression of VP and laccase was assayed in microplate format and flask under the control of different expression cassettes including the promoter/terminator pairs GAL1/CYC1 and GAL10/ADH1. In general terms, the expression for singles genes under GAL10/ADH1 cassette was the most effective one. Nevertheless, the co-expression of both genes with similar secretion levels was observed with the construction GAL1/VP/CYC1-GAL10/Lac/ADH1.

10. An initial prototype of white-rot yeast (WRY) was designed with a reduced ligninolytic apparatus, which establishes the bases for the construction of a more sophisticated artificial microorganism with potential applications in synthetic biology. Particularly, the WRY might find application in the production of biofuels from lignocellulosic material in integral biorefineries and it could be a useful model of study to understand the complex mechanism of lignin decay.

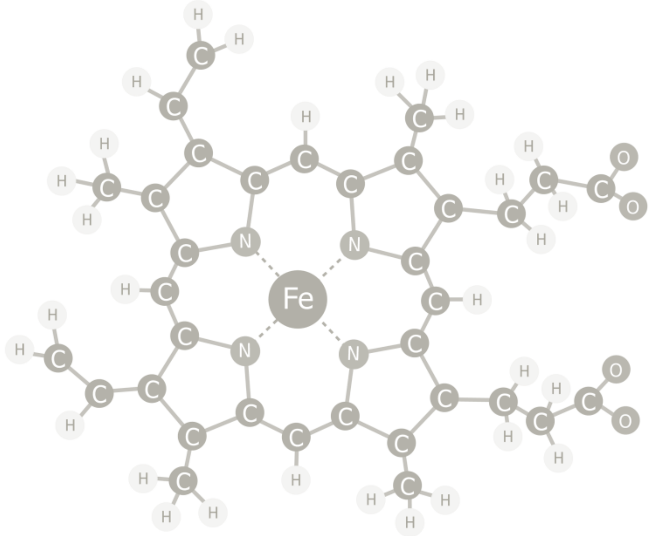

Capítulo 10:

Referencias bibliográficas

A

Abdel-Hamid, A.M., Solbiati, J.O., and Cann, I.K. (2013). Insights into lignin degradation and its potential industrial applications. *Adv Appl Microbiol* ***82***, 1-28. DOI: 10.1016/B978-0-12-407679-2.00001-6

Alcalde, M. (2010). Mutagenesis protocols in *Saccharomyces cerevisiae* by *in vivo* overlap extension. *Methods Mol Biol* ***634***, 3-14. DOI: 10.1007/978-1-60761-652-8_1

Alcalde, M. (2015). Engineering the ligninolytic enzyme consortium. *Trends Biotechnol* ***33***, 155-162. DOI: 10.1016/j.tibtech.2014.12.007

Arantes, V., Jellison, J., and Goodell, B. (2012). Peculiarities of brown-rot fungi and biochemical Fenton reaction with regard to their potential as a model for bioprocessing biomass. *Appl Microbiol Biotechnol* ***94***, 323-338. DOI: 10.1007/s00253-012-3954-y

Arnold, F.H. (2015). The nature of chemical innovation: new enzymes by evolution. *Q Rev Biophys* 48, 404-410. DOI: 10.1017/S003358351500013X

Ayala, M., Roman, R., and Vázquez-Duhalt, R. (2007a). A catalytic approach to estimate the redox potential of heme-peroxidases. *Biochem Biophys Res Commun* 357, 804-808. DOI: 10.1016/j.bbrc.2007.04.020

Ayala, M., Verdin, J., and Vazquez-Duhalt, R. (2007b). The prospects for peroxidase-based biorefining of petroleum fuels. *Biocatal Biotransform* ***25***, 114-129. DOI: 10.1080/10242420701379015

Azapagic, A. (2014). Sustainability considerations for integrated biorefineries. *Trends Biotechnol* ***32***, 1-4. DOI: 10.1016/j.tibtech.2013.10.009

B

Baldrian, P. (2006). Fungal laccases - occurrence and properties. *FEMS Microbiol Rev* ***30***, 215-242. DOI: 10.1111/j.1574-4976.2005.00010.x

Banci, L., Bertini, I., Kuan, I.C., Tien, M., Turano, P., and Vila, A.J. (1993). NMR investigation of isotopically labeled cyanide derivatives of lignin peroxidase and manganese peroxidase. *Biochemistry* ***32***, 13483-13489. DOI: 10.1021/bi00212a013

Banci, L., Bertini, I., Capannoli, C., Del Conte, R., and Tien, M. (1999). Spectroscopic characterization of active mutants of manganese peroxidase: mutations on the proximal side affect calcium binding of the distal side. *Biochemistry* ***38***, 9617-9625. DOI:10.1021/bi9825697

Bao, W., Fukushima, Y., Jensen, K.A., Moen, M.A., and Hammel, K.E. (1994). Oxidative degradation of non-phenolic lignin during lipid peroxidation by fungal manganese peroxidase. *FEBS Letters* ***354***, 297-300. DOI: 10.1016/0014-5793(94)01146-x

Bao, X., Liu, A., Lu, X., and Li, J.J. (2012). Direct over-expression, characterization and H_2O_2 stability study of active *Pleurotus eryngii* versatile peroxidase in *Escherichia coli*. *Biotechnol Lett* ***34***, 1537-1543. DOI: 10.1007/s10529-012-0940-5

Bao, X., Huang, X., Lu, X., and Li, J.J. (2014). Improvement of hydrogen peroxide stability of *Pleurotus eryngii* versatile ligninolytic peroxidase by rational protein engineering. *Enzyme Microb Technol* ***54***, 51-58. DOI: 10.1016/j.enzmictec.2013.10.003

Barr, D.P., and Aust, S.D. (1994). Conversion of lignin peroxidase compound III to active enzyme by cation radicals. *Arch Biochem Biophys* ***312***, 511-515. DOI: 10.1006/abbi.1994.1339

Beguin, P. (1994). The biological degradation of cellulose. *FEMS Microbiology Reviews* ***13***, 25-58. DOI: 10.1111/j.1574-6976.1994.tb00033.x

Blodig, W., Doyle, W.A., Smith, A.T., Winterhalter, K., Choinowski, T., and Piontek, K. (1998). Autocatalytic formation of a hydroxy group at C *beta* of Trp171 in lignin peroxidase. *Biochemistry* ***37***, 8832-8838.DOI: 10.1021/bi9727186

Bloom, J.D., and Arnold, F.H. (2009). In the light of directed evolution: pathways of adaptive protein evolution. *Proc Natl Acad Sci USA* ***106***, 9995-10000. DOI: 10.1073/pnas.0901522106

Böckle, B., Martínez, M.J., Guillén, F., and Martínez, Á.T. (1999). Mechanism of peroxidase inactivation in liquid cultures of the ligninolytic fungus *Pleurotus pulmonarius*. *Appl Environ Microbiol* ***65***, 923-928. PMID: 10049843

Bornscheuer, U.T., Huisman, G.W., Kazlauskas, R.J., Lutz, S., Moore, J.C., and Robins, K. (2012). Engineering the third wave of biocatalysis. *Nature* ***485***, 185-194. DOI: 10.1038/nature11117

Bulter, T., Alcalde, M., Sieber, V., Meinhold, P., Schlachtbauer, C., and Arnold, F.H. (2003). Functional Expression of a fungal laccase in *Saccharomyces cerevisiae* by directed evolution. *Appl Environ Microbiol* ***69***, 987-995. DOI: 10.1128/AEM.69.2.987-995.2003

Butler, A., and Carter-Franklin, J.N. (2004). The role of vanadium bromoperoxidase in the biosynthesis of halogenated marine natural products. *Nat Prod Rep* ***21***, 180-188. DOI: 10.1039/b302337k

C

Camarero, S., Galletti, G.C., and Martínez, A.T. (1994). Preferential degradation of phenolic lignin units by two white-rot fungi. *Appl Environ Microbiol* ***60***, 4509-4516. PMID: 7811086

Camarero, S., Bockle, B., Martínez, M.J., and Martínez, A.T. (1996). Manganese-mediated lignin degradation by *Pleurotus pulmonarius*. *Appl Environ Microbiol* ***62***, 1070-1072. PMCID: PMC1388814

Camarero, S., Sarkar, S., Ruiz-Dueñas, F.J., Martínez, M.J., and Martínez, A.T. (1999). Description of a versatile peroxidase involved in the natural degradation of lignin that has both manganese peroxidase and lignin peroxidase substrate interaction sites. *J Biol Chem* ***274***, 10324-10330. PMID: 10187820

Camarero, S., Pardo, I., Cañas, A.I., Molina, P., Record, E., Martínez, A.T., Martínez, M.J., and Alcalde, M. (2012). Engineering platforms for directed evolution of laccase from *Pycnoporus cinnabarinus*. *Appl Environ Microbiol* ***78***, 1370-1384. DOI: 10.1128/AEM.07530-11

Cameron, M.D., and Aust, S.D. (1999). Degradation of chemicals by reactive radicals produced by cellobiose dehydrogenase from *Phanerochaete chrysosporium*. *Arch Biochem Biophys* ***367***, 115-121. DOI: 10.1006/abbi.1999.1257

Cañas, A.I., and Camarero, S. (2010). Laccases and their natural mediators: biotechnological tools for sustainable eco-friendly processes. *Biotechnol Adv* ***28***, 694-705. DOI: 10.1016/j.biotechadv.2010.05.002

Candeias, L.P., and Harvey, P.J. (1995). Lifetime and reactivity of the veratryl alcohol radical cation: implications for lignin peroxidase catalysis. *J Biol Chem* ***270***, 16745-16748. DOI: 10.1074/jbc.270.28.16745

Carro, J., Ferreira, P., Rodríguez, L., Prieto, A., Serrano, A., Balcells, B., Arda, A., Jiménez-Barbero, J., Gutiérrez, A., Ullrich, R., *et al.* (2015). 5-hydroxymethylfurfural conversion by fungal aryl-alcohol oxidase and unspecific peroxygenase. *FEBS J* ***282***, 3218-3229. DOI: 10.1111/febs.13177

Cherry, J.R., Lamsa, M.H., Schneider, P., Vind, J., Svendsen, A., Jones, A., and Pedersen, A.H. (1999). Directed evolution of a fungal peroxidase. *Nat Biotechnol* ***17***, 379-384. DOI: 10.1038/7939

Cherubini, F. (2010). The biorefinery concept: Using biomass instead of oil for producing energy and chemicals. *Energ Convers Manag* ***51***, 1412-1421. DOI: 10.1016/j.enconman.2010.01.015

Choinowski, T., Blodig, W., Winterhalter, K.H., and Piontek, K. (1999). The crystal structure of lignin peroxidase at 1.70 Å resolution reveals a hydroxy group on the C-*beta* of tryptophan 171: a novel radical site formed during the redox cycle. *J Mol Biol* ***286***, 809-827. DOI: 10.1006/jmbi.1998.2507

Coconi-Linares, N., Magana-Ortiz, D., Guzman-Ortiz, D.A., Fernández, F., Loske, A.M., and Gómez-Lim, M.A. (2014). High-yield production of manganese peroxidase, lignin peroxidase, and versatile peroxidase in *Phanerochaete chrysosporium*. *Appl Microbiol Biotechnol 98*, 9283-9294. DOI: 10.1007/s00253-014-6105-9

Coconi-Linares, N., Ortiz-Vázquez, E., Fernández, F., Loske, A.M., and Gómez-Lim, M.A. (2015). Recombinant expression of four oxidoreductases in *Phanerochaete chrysosporium* improves degradation of phenolic and non-phenolic substrates. *J Biotechnol* ***209***, 76-84. DOI: 10.1016/j.jbiotec.2015.06.401

Colpa, D.I., Fraaije, M.W., and van Bloois, E. (2014). DyP-type peroxidases: a promising and versatile class of enzymes. *J Ind Microbiol Biotechnol* ***41***, 1-7. DOI: 10.1007/s10295-013-1371-6

Couturier, M., Navarro, D., Chevret, D., Henrissat, B., Piumi, F., Ruiz-Dueñas, F.J., Martínez, A.T., Grigoriev, I.V., Riley, R., Lipzen, A., *et al.* (2015). Enhanced degradation of softwood versus hardwood by the white-rot fungus *Pycnoporus coccineus*. *Biotechnol Biofuels* ***8***, 216. DOI: 10.1186/s13068-015-0407-8

D

Dalby, P.A. (2003). Optimising enzyme function by directed evolution. *Curr Opin Struc Biol* ***13***, 500-505. DOI: 10.1016/S0959-440X(03)00101-5

Daniel, G., Volc, J., Filonova, L., Plihal, O., Kubatova, E., and Halada, P. (2007). Characteristics of *Gloeophyllum trabeum* alcohol oxidase, an extracellular source of H_2O_2 in brown-rot decay of wood. *Appl Environ Microbiol* ***73***, 6241-6253. DOI: 10.1128/AEM.00977-07

Dashtban, M., Schraft, H., Syed, T.A., and Qin, W. (2010). Fungal biodegradation and enzymatic modification of lignin. *Int J Biochem Mol Biol* ***1***, 36-50. PMCID: PMC3180040

Delmer, D.P., and Amor, Y. (1995). Cellulose biosynthesis. *Plant Cell* ***7***, 987-1000. DOI: 10.1105/tpc.7.7.987

Dincer, I., and Rosen, M.A. (1998). A worldwide perspective on energy, environment and sustainable development. *Int J Energ Res* ***22***, 1305-1321.DOI: 10.1002/(SICI)1099-114X(199812)22:15<1305::AID-ER417>3.0.CO;2-H

Doyle, W.A., Blodig, W., Veitch, N.C., Piontek, K., and Smith, A.T. (1998). Two substrate interaction sites in lignin peroxidase revealed by site-directed mutagenesis. *Biochemistry* ***37***, 15097-15105. DOI: 10.1021/bi981633h

E

Eastwood, D.C., Floudas, D., Binder, M., Majcherczyk, A., Schneider, P., Aerts, A., Asiegbu, F.O., Baker, S.E., Barry, K., Bendiksby, M., et al. (2011). The plant cell walldecomposing machinery underlies the functional diversity of forest fungi. *Science* ***333***, 762-765. DOI: 10.1126/science.1205411

Erman, J.E., Vitello, L.B., Miller, M.A., Shaw, A., Brown, K.A., and Kraut, J. (1993). Histidine 52 is a critical residue for rapid formation of cytochrome c peroxidase compound I. *Biochemistry* ***32***, 9798-9806. DOI: 10.1021/bi00088a035

Eudes, A., Liang, Y., Mitra, P., and Loque, D. (2014). Lignin bioengineering. *Curr Opin Biotechnol* ***26***, 189-198. DOI: 10.1016/j.copbio.2014.01.002

F

Faison, B.D., and Kirk, T.K. (1983). Relationship between lignin degradation and production of reduced oxygen species by *Phanerochaete chrysosporium*. *Appl Environ Microbiol* ***46***, 1140-1145. PMCID: PMC239531

Falade, A.O., Nwodo, U.U., Iweriebor, B.C., Green, E., Mabinya, L.V., and Okoh, A.I. (2016). Lignin peroxidase functionalities and prospective applications. *Microbiologyopen* ***2016***, 1-14. DOI: 10.1007/978-3-642-12627-7_8

Fan, L.H., Zhang, Z.J., Yu, X.Y., Xue, Y.X., and Tan, T.W. (2012). Self-surface assembly of cellulosomes with two miniscaffoldins on *Saccharomyces cerevisiae* for cellulosic ethanol production. *Proc Natl Acad Sci USA* ***109***, 13260-13265. DOI: 10.1073/pnas.1209856109

Fawal, N., Li, Q., Savelli, B., Brette, M., Passaia, G., Fabre, M., Mathe, C., and Dunand, C. (2013). PeroxiBase: a database for large-scale evolutionary analysis of peroxidases. *Nucleic Acids Res* ***41***, D441-444. DOI: 10.1093/nar/gks1083

Fernández-Fueyo, E. Ruiz-Dueñas F.J., Ferreira, P., Floudas, D., Hibbett, D.S., Canessa, P., Larrondo, L.F., James, T.Y., Seelenfreund, D., Lobos, S., *et al.* (2012). Comparative genomics of *Ceriporiopsis subvermispora* and *Phanerochaete chrysosporium* provide insight into selective ligninolysis. *Proc Natl Acad Sci USA* ***109***, 5458-63. DOI: 10.1073/pnas.1119912109

Fernández-Fueyo, E., Acebes, S., Ruiz-Dueñas, F.J., Martínez, M.J., Romero, A., Medrano, F.J., Guallar, V., and Martínez, A.T. (2014). Structural implications of the C-terminal tail in the catalytic and stability properties of manganese peroxidases from ligninolytic fungi. *Acta Crystallogr D Biol Crystallogr* ***70***, 3253-3265. DOI: 10.1107/S1399004714022755

Fernández-Fueyo, E., Linde, D., Almendral, D., López-Lucendo, M.F., Ruiz-Dueñas, F.J., and Martínez, A.T. (2015). Description of the first fungal dye-decolorizing peroxidase oxidizing manganese (II). *Appl Microbiol Biotechnol* ***99***, 8927-8942. DOI: 10.1007/s00253-015-6665-3

Ferreira, P., Carro, J., Serrano, A., and Martinez, A.T. (2015). A survey of genes encoding H_2O_2-producing GMC oxidoreductarses in 10 Polyporales genomes. *Mycologia* ***107***, 1105-1119. DOI: 10.3852/15-027

Ferrer, J.C., Turano, P., Banci, L., Bertini, I., Morris, I.K., Smith, K.M., Smith, M., and Mauk, A.G. (1994). Active site coordination chemistry of the cytochrome c peroxidase Asp235Ala variant: spectroscopic and functional characterization. *Biochemistry* ***33***, 7819-7829. PMID: 8011646

Ferrer, J.L., Austin, M.B., Stewart, C., Jr., and Noel, J.P. (2008). Structure and function of enzymes involved in the biosynthesis of phenylpropanoids. *Plant Physiol Biochem* ***46***, 356-370. DOI: 10.1016/j.plaphy.2007.12.009

Finzel, B.C., Poulos, T.L., and Kraut, J. (1984). Crystal structure of yeast cytochrome c peroxidase refined at 1.7-Å resolution. *J Biol Chem* ***259***, 13027-13036.

Flohe, L., Toppo, S., Cozza, G., and Ursini, F. (2011). A comparison of thiol peroxidase mechanisms. *Antioxid Redox Sign* ***15***, 763-780. PMID: 6092361

Floudas, D., Binder, M., Riley, R., Barry, K., Blanchette, R.A., Henrissat, B., Martínez, A.T., Otillar, R., Spatafora, J.W., Yadav, J.S., *et al.* (2012). The Paleozoic origin of enzymatic lignin decomposition reconstructed from 31 fungal genomes. *Science* ***336***, 1715-1719. DOI: 10.1126/science.1221748

G

Gajhede, M., Schuller, D.J., Henriksen, A., Smith, A.T., and Poulos, T.L. (1997). Crystal structure of horseradish peroxidase C at 2.15 Å resolution. *Nat Struc Biol* ***4***, 1032-1038. DOI: 10.1038/nsb1297-1032

Garcia-Ruiz, E., Mate, D., Ballesteros, A., Martinez, A.T., and Alcalde, M. (2010). Evolving thermostability in mutant libraries of ligninolytic oxidoreductases expressed in yeast. *Microb Cell Fact* ***9***, 17. DOI: 10.1186/1475-2859-9-17

Garcia-Ruiz, E., Mate, D.M., Gonzalez-Perez, D., Molina-Espeja, P., Camarero, S., Martínez, A.T., Ballesteros, A.O., and Alcalde, M. (2014). Directed evolution of ligninolytic oxidoreductases: from functional expression to stabilization and beyond. *In: Cascade Biocatalysis*. Wiley-VCH Verlag GmbH & Co. KGaA, pp. 1-22. DOI: 10.1002/9783527682492.ch1

George, S.J., Kvaratskhelia, M., Dilworth, M.J., and Thorneley, R.N. (1999). Reversible alkaline inactivation of lignin peroxidase involves the release of both the distal and proximal site calcium ions and bishistidine co-ordination of the haem. *Biochem J* ***344*** Pt 1, 237-244. PMCID: PMC1220636

Gilmore, S.P., Henske, J.K., and O'Malley, M.A. (2015). Driving biomass breakdown through engineered cellulosomes. *Bioengineered* ***6***, 204-208. DOI: 10.1080/21655979.2015.1060379

Gil-Rodríguez, P., Ferreira-Batista, C., Vázquez-Duhalt, R., and Valderrama, B. (2008). A novel heme peroxidase from *Raphanus sativus* intrinsically resistant to hydrogen peroxide. *Eng Life Sci* ***8***, 286-296. DOI: 10.1002/elsc.200700073

Goodell, B., Qian, Y., and Jellison, J. (2008). Fungal decay of wood: soft-rot, brown-rot white-rot. *In: Development of commercial wood preservatives*, American Chemical Society, pp. 9-31. DOI: 10.1021/bk-2008-0982.ch002

Goodwin, D.C., Aust, S.D., and Grover, T.A. (1995). Evidence for veratryl alcohol as a redox mediator in lignin peroxidase-catalyzed oxidation. *Biochemistry* ***34***, 5060-5065. DOI: 10.1021/bi00015a017

Guillén, F., Martínez, A.T., and Martínez, M.J. (1990). Production of hydrogen peroxide by aryl-alcohol oxidase from the ligninolytic fungus *Pleurotus eryngii*. *Appl Microbiol Biot* ***32***, 465-469. DOI: 10.1007/BF00903784

Guimaraes, B.G., Souchon, H., Honore, N., Saint-Joanis, B., Brosch, R., Shepard, W., Cole, S.T., and Alzari, P.M. (2005). Structure and mechanism of the alkyl hydroperoxidase AhpC, a key element of the *Mycobacterium tuberculosis* defense system against oxidative stress. *J Biol Chem* ***280***, 25735-25742. DOI: 10.1074/jbc.M503076200

Gumiero, A., Metcalfe, C.L., Pearson, A.R., Raven, E.L., and Moody, P.C. (2011). Nature of the ferryl heme in compounds I and II. *J Biol Chem* ***286***, 1260-1268. DOI: 10.1074/jbc.M110.183483

H

Hammel, K.E., and Moen, M.A. (1991). Depolymerization of a synthetic lignin *in vitro* by lignin peroxidase. *Enzyme Microb Tech* ***13***, 15-18. DOI: 10.1016/0141-0229(91)90182-A

Harvey, P.J., Schoemaker, H.E., and Palmer, J.M. (1986). Veratryl alcohol as a mediator and the role of radical cations in lignin biodegradation by *Phanerochaete chrysosporium*. *FEBS Letters* ***195***, 242-246. DOI: 10.1016/0014-5793(86)80168-5

Harvey, P.J., and Palmer, J.M. (1990). Oxidation of phenolic compounds by ligninase. *J Biotechnol* ***13***, 169-179. DOI: 10.1016/0168-1656(90)90102-H

Hasunuma, T., and Kondo, A. (2012). Development of yeast cell factories for consolidated bioprocessing of lignocellulose to bioethanol through cell surface engineering. *Biotechnol Adv* ***30***, 1207-1218. DOI: 10.1016/j.biotechadv.2011.10.011

He, Y., Fang, Z., Zhang, J., Li, X., and Bao, J. (2014). De-ashing treatment of corn stover improves the efficiencies of enzymatic hydrolysis and consequent ethanol fermentation. *Bioresour Technol* ***169***, 552-558. DOI: 10.1016/j.biortech.2014.06.088

Hemsworth, G.R., Johnston, E.M., Davies, G.J., and Walton, P.H. (2015). Lytic polysaccharide monooxygenases in biomass conversion. *Trends Biotechnol* ***33***, 747-761**.** DOI: 10.1016/j.tibtech.2015.09.006

Hernández, K., Berenguer-Murcia, A., C. Rodrigues, R., and Fernández-Lafuente, R. (2012). Hydrogen peroxide in biocatalysis. a dangerous liaison. *Curr Org Chem* ***16***, 2652-2672. DOI: 10.2174/138527212804004526

Hernández-Ortega, A., Ferreira, P., and Martínez, A.T. (2012). Fungal aryl-alcohol oxidase: a peroxide-producing flavoenzyme involved in lignin degradation. *Appl Microbiol Biotechnol* ***93***, 1395-1410. DOI: 10.1007/s00253-011-3836-8

Hernández-Ruiz, J., Arnao, M.B., Hiner, A.N., Garcia-Canovas, F., and Acosta, M. (2001). Catalase-like activity of horseradish peroxidase: relationship to enzyme inactivation by H_2O_2. *Biochem J 354*, 107-114. PMCID: PMC1221634

Hiner, A.N.P., Hernández-Ruiz, J., Rodríguez-López, J.N., Arnao, M.B., Varón, R., García-Cánovas, F., and Acosta, M. (2001). The inactivation of horseradish peroxidase isoenzyme AZ by hydrogen peroxide: an example of partial resistance due to the formation of a stable enzyme intermediate. *J Biol Inorg Chem* ***6***, 504-516. DOI: 10.1007/s007750100219

Hiner, A.N.P., Raven, E.L., Thorneley, R.N.F., García-Cánovas, F., and Rodríguez-López, J.N. (2002). Mechanisms of compound I formation in heme peroxidases. *J Inorg Biochem* ***91***, 27-34. DOI: 10.1016/S0162-0134(02)00390-2

Hoegh-Guldberg, O., Mumby, P.J., Hooten, A.J., Steneck, R.S., Greenfield, P., Gomez, E., Harvell, C.D., Sale, P.F., Edwards, A.J., Caldeira, K., et al. (2007). Coral reefs under rapid climate change and ocean acidification. *Science* ***318***, 1737-1742. DOI: 10.1126/science.1152509

Hofrichter, M., Ziegenhagen, D., Vares, T., Friedrich, M., Jäger, M.G., Fritsche, W., and Hatakka, A. (1998). Oxidative decomposition of malonic acid as basis for the action of manganese peroxidase in the absence of hydrogen peroxide. *FEBS Letters* ***434***, 362-366. DOI: 10.1016/S0014-5793(98)01023-0

Hofrichter, M. (2002). Review: lignin conversion by manganese peroxidase (MnP). *Enzyme Microb Technol* ***30***, 454-466. DOI: 10.1016/S0141-0229(01)00528-2

Hofrichter, M., Ullrich, R., Pecyna, M.J., Liers, C., and Lundell, T. (2010). New and classic families of secreted fungal heme peroxidases. *Appl Microbiol Biotechnol* ***87***, 871-897. DOI: 10.1007/s00253-010-2633-0

Hong, K.K., and Nielsen, J. (2012). Metabolic engineering of *Saccharomyces cerevisiae*: a key cell factory platform for future biorefineries. *Cell Mol Life Sci* ***69***, 2671-2690. DOI: 10.1007/s00018-012-0945-1

Hosseinzadeh, P., Mirts, E.N., Pfister, T.D., Gao, Y.G., Mayne, C., Robinson, H., Tajkhorshid, E., and Lu, Y. (2016). Enhancing Mn(II)-binding and manganese peroxidase activity in a designed cytochrome c peroxidase through fine-tuning secondary-sphere interactions. *Biochemistry* ***55***, 1494-1502. DOI: 10.1021/acs.biochem.5b01299

Howes, B.D., Feis, A., Raimondi, L., Indiani, C., and Smulevich, G. (2001). The critical role of the proximal calcium ion in the structural properties of horseradish peroxidase. *J Biol Chem* ***276***, 40704-40711. DOI: 10.1074/jbc.M107489200

Hua, S.B., Qiu, M., Chan, E., Zhu, L., and Luo, Y. (1997). Minimum length of sequence homology required for *in vivo* cloning by homologous recombination in yeast. *Plasmid* 38, 91-96. DOI: 10.1006/plas.1997.1305

Huang, G.L., Anderson, T.D., and Clubb, R.T. (2014). Engineering microbial surfaces to degrade lignocellulosic biomass. *Bioengineered* ***5***, 96-106. DOI: 10.4161/bioe.27461

Hyde, S.M., and Wood, P.M. (1997). A mechanism for production of hydroxyl radicals by the brown-rot fungus *Coniophora puteana*: Fe(III) reduction by cellobiose dehydrogenase and Fe(II) oxidation at a distance from the *Hyphae*. *Microbiology* ***143***, 259-266. DOI: 10.1099/00221287-143-1-259

J

Jarosz-Wilkołazka, A., Luterek, J., and Olszewska, A. (2009). Catalytic activity of versatile peroxidase from *Bjerkandera fumosa* at different pH. *Biocatal Biotransfor* ***26***, 280-287. DOI: 10.1080/10242420701830082

Jensen, K.A., Jr., Houtman, C.J., Ryan, Z.C., and Hammel, K.E. (2001). Pathways for extracellular Fenton chemistry in the brown-rot basidiomycete *Gloeophyllum trabeum*. *Appl Environ Microbiol* ***67***, 2705-2711. DOI: 10.1128/AEM.67.6.2705-2711.2001

Jonsson, L.J., and Martin, C. (2016). Pretreatment of lignocellulose: formation of inhibitory by-products and strategies for minimizing their effects. *Bioresour Technol* ***199***, 103-112. DOI: 10.1016/j.biortech.2015.10.009

K

Kellner, H., Luis, P., Pecyna, M.J., Barbi, F., Kapturska, D., Kruger, D., Zak, D.R., Marmeisse, R., Vandenbol, M., and Hofrichter, M. (2014). Widespread occurrence of expressed fungal secretory peroxidases in forest soils. *PLoS One* ***9***, e95557. DOI: 10.1371/journal.pone.0095557

Kersten, P.J., and Kirk, T.K. (1987). Involvement of a new enzyme, glyoxal oxidase, in extracellular H_2O_2 production by *Phanerochaete chrysosporium*. *J Bacteriol* ***169***, 2195-2201. PMCID: PMC212128

Kersten, P., and Cullen, D. (2007). Extracellular oxidative systems of the lignin-degrading Basidiomycete *Phanerochaete chrysosporium*. *Fungal Genet Biol* ***44***, 77-87. DOI: 10.1016/j.fgb.2006.07.007

Kim, S., Baek, S.H., Lee, K., and Hahn, J.S. (2013). Cellulosic ethanol production using a yeast consortium displaying a minicellulosome and *beta*-glucosidase. *Microb Cell Fact* ***12***, 14. DOI: 10.1016/j.fgb.2006.07.007

Kim, Y.H., Berry, A.H., Spencer, D.S., and Stites, W.E. (2001). Comparing the effect on protein stability of methionine oxidation versus mutagenesis: steps toward engineering oxidative resistance in proteins. *Protein Eng Des Sel* ***14***, 343-347. PMID: 11438757

Kinne, M., Poraj-Kobielska, M., Ullrich, R., Nousiainen, P., Sipilä, J., Scheibner, K., Hammel, K.E., and Hofrichter, M. (2011). Oxidative cleavage of non-phenolic β-O-4 lignin model dimers by an extracellular aromatic peroxygenase. *Holzforschung* ***65***. DOI: 10.1515/hf.2011.057

Kirk, T.K., and Farrell, R.L. (1987). Enzymatic "combustion": the microbial degradation of lignin. *Annu Rev Microbiol* ***41***, 465-505. DOI: 10.1146/annurev.mi.41.100187.002341

Kishi, K., Hildebrand, D.P., Kusters-van Someren, M., Gettemy, J., Mauk, A.G., and Gold, M.H. (1997). Site-directed mutations at phenylalanine-190 of manganese peroxidase: effects on stability, function, and coordination. *Biochemistry* ***36***, 4268-4277. DOI: 10.1021/bi962627t

Knop, D., Yarden, O., and Hadar, Y. (2015). The ligninolytic peroxidases in the genus *Pleurotus*: divergence in activities, expression, and potential applications. *Appl Microbiol Biotechnol* ***99***, 1025-1038. DOI: 10.1007/s00253-014-6256-8

Koduri, R.S., and Tien, M. (1995). Oxidation of guaiacol by lignin peroxidase: role of veratryl alcohol. *J Biol Chem* ***270***, 22254-22258. DOI: 10.1074/jbc.270.38.22254

Kunishima, N., Fukuyama, K., Matsubara, H., Hatanaka, H., Shibano, Y., and Amachi, T. (1994). Crystal structure of the fungal peroxidase from *Arthromyces ramosus* at 1.9 Å resolution. Structural comparisons with the lignin and cytochrome c peroxidases. *J Mol Biol* ***235***, 331-344. DOI: 10.1016/S0022-2836(05)80037-3

L

Laberge, M., Huang, Q., Schweitzer-Stenner, R., and Fidy, J. (2003). The endogenous calcium ions of horseradish peroxidase c are required to maintain the functional nonplanarity of the heme. *Biophys J* ***84***, 2542-2552. DOI: 10.1016/S0006-3495(03)75059-0

Legras, J.L., Merdinoglu, D., Cornuet, J.M., and Karst, F. (2007). Bread, beer and wine: *Saccharomyces cerevisiae* diversity reflects human history. *Mol Ecol* ***16***, 2091-2102. DOI: 10.1111/j.1365-294X.2007.03266.x

Leitner, C., Volc, J., and Haltrich, D. (2001). Purification and characterization of pyranose oxidase from the white rot fungus *Trametes multicolor*. *Appl Environ Microbiol* ***67***, 3636-3644. DOI: 10.1128/AEM.67.8.3636-3644.2001

Liao, J.C., Mi, L., Pontrelli, S., and Luo, S. (2016). Fuelling the future: microbial engineering for the production of sustainable biofuels. *Nat Rev Microbiol* ***14***, 288-304. DOI: 10.1038/nrmicro.2016.32

Liers, C., Bobeth, C., Pecyna, M., Ullrich, R., and Hofrichter, M. (2010). DyP-like peroxidases of the jelly fungus *Auricularia auricula-judae* oxidize nonphenolic lignin model compounds and high-redox potential dyes. *Appl Microbiol Biotechnol* ***85***, 1869-1879. DOI: 10.1007/s00253-009-2173-7

Liers, C., Arnstadt, T., Ullrich, R., and Hofrichter, M. (2011). Patterns of lignin degradation and oxidative enzyme secretion by different wood- and litter-colonizing basidiomycetes and ascomycetes grown on beech-wood. *FEMS Microbiol Ecol* ***78***, 91-102. DOI: 10.1111/j.1574-6941.2011.01144.x

Liers, C., Pecyna, M.J., Kellner, H., Worrich, A., Zorn, H., Steffen, K.T., Hofrichter, M., and Ullrich, R. (2013). Substrate oxidation by dye-decolorizing peroxidases (DyPs) from wood- and litter-degrading agaricomycetes compared to other fungal and plant heme-peroxidases. *Appl Microbiol Biotechnol* ***97***, 5839-5849. DOI: 10.1007/s00253-012-4521-2

Liers, C., Aranda, E., Strittmatter, E., Piontek, K., Plattner, D.A., Zorn, H., Ullrich, R., and Hofrichter, M. (2014). Phenol oxidation by DyP-type peroxidases in comparison to fungal and plant peroxidases. *J Mol Catal B: Enzym* ***103***, 41-46. DOI: 10.1016/j.molcatb.2013.09.025

Limayem, A., and Ricke, S.C. (2012). Lignocellulosic biomass for bioethanol production: Current perspectives, potential issues and future prospects. *Prog Energ Combust* ***38***, 449-467. DOI: 10.1016/j.pecs.2012.03.002

Linke, D., Lehnert, N., Nimtz, M., and Berger, R.G. (2014). An alcohol oxidase of *Phanerochaete chrysosporium* with a distinct glycerol oxidase activity. *Enzyme Microb Technol* ***61*-62**, 7-12. DOI: 10.1016/j.enzmictec.2014.04.001

Liu, Z., Ho, S.H., Sasaki, K., den Haan, R., Inokuma, K., Ogino, C., van Zyl, W.H., Hasunuma, T., and Kondo, A. (2016). Engineering of a novel cellulose-adherent cellulolytic *Saccharomyces cerevisiae* for cellulosic biofuel production. *Sci Rep* ***6***, 24550. DOI: 10.1038/srep24550

Lu-Chau, T.A., Ruiz-Dueñas, F.J., Camarero, S., Feijoo, G., Martínez, M.J., Lema, J.M., and Martínez, A.T. (2004). Effect of pH on the stability of *Pleurotus eryngii* versatile peroxidase during heterologous production in *Emericella nidulans*. *Bioprocess Biosyst Eng* ***26***, 287-293. DOI: 10.1007/s00449-004-0365-1

M

Mao, L., Luo, S., Huang, Q., and Lu, J. (2013). Horseradish peroxidase inactivation: heme destruction and influence of polyethylene glycol. *Sci Rep* ***3***, 3126. DOI: 10.1038/srep03126

Martínez, A.T., Camarero, S., Guillén, F., Gutiérrez, A., Muñoz, C., Varela, E., Martínez, M.J., Barrasa, J.M., Ruel, K., and Pelayo, M.. (1994). Progress in biopulping of non-woody materials: Chemical, enzymatic and ultrastructural aspects of wheat-straw delignification with ligninolytic fungi from the genus *Pleurotus*. *FEMS Microbiol Rev.* ***13***, 265-274. DOI: 10.1111/j.1574-6976.1994.tb00047.x

Martínez, A.T. (2002). Molecular biology and structure-function of lignin-degrading heme peroxidases. *Enzyme Microb Technol* ***30***, 425-444. DOI: 10.1016/S0141-0229(01)00521-X

Martínez, A.T., Speranza, M., Ruiz-Dueñas, F.J., Ferreira, P., Camarero, S., Guillen, F., Martínez, M.J., Gutierrez, A., and del Rio, J.C. (2005). Biodegradation of lignocellulosics: microbial, chemical, and enzymatic aspects of the fungal attack of lignin. *Int Microbiol* ***8***, 195-204. PMID: 16200498

Martínez, A.T., Rencoret, J., Marques, G., Gutierrez, A., Ibarra, D., Jimenez-Barbero, J., and del Rio, J.C. (2008). Monolignol acylation and lignin structure in some nonwoody plants: a 2D NMR study. *Phytochemistry* ***69***, 2831-2843. DOI: 10.1016/j.phytochem.2008.09.005

Martínez, A.T., Ruiz-Dueñas, F.J., Martínez, M.J., Del Rio, J.C., and Gutiérrez, A. (2009a). Enzymatic delignification of plant cell wall: from nature to mill. *Curr Opin Biotechnol* ***20***, 348-357. DOI: 10.1016/j.copbio.2009.05.002

Martínez, A.T. (2016). How to break down crystalline cellulose. *Science* ***352***, 1050-1051. DOI: 10.1126/science.aaf8920

Martínez, D., Challacombe, J., Morgenstern, I., Hibbett, D., Schmoll, M., Kubicek, C.P., Ferreira, P., Ruiz-Dueñas, F.J., Martínez, A.T., Kersten, P., et al. (2009b). Genome, transcriptome, and secretome analysis of wood decay fungus *Postia placenta* supports unique mechanisms of lignocellulose conversion. *Proc Natl Acad Sci USA* ***106***, 1954-1959. DOI: 10.1073/pnas.0809575106

Martínez, M.J., Ruiz-Dueñas, F.J., Guillen, F., and Martínez, A.T. (1996). Purification and catalytic properties of two manganese peroxidase isoenzymes from *Pleurotus eryngii*. *Eur J Biochem* ***237***, 424-432. DOI: 10.1111/j.1432-1033.1996.0424k.x

Mate, D., Garcia-Burgos, C., Garcia-Ruiz, E., Ballesteros, A.O., Camarero, S., and Alcalde, M. (2010). Laboratory evolution of high-redox potential laccases. *Chem Biol* ***17***, 1030-1041. DOI: 10.1016/j.chembiol.2010.07.010

Mate, D.M., Gonzalez-Perez, D., Falk, M., Kittl, R., Pita, M., De Lacey, A.L., Ludwig, R., Shleev, S., and Alcalde, M. (2013a). Blood tolerant laccase by directed evolution. *Chem Biol* ***20***, 223-231. DOI: 10.1016/j.chembiol.2013.01.001

Mate, D.M., Gonzalez-Perez, D., Kittl, R., Ludwig, R., and Alcalde, M. (2013b). Functional expression of a blood tolerant laccase in *Pichia pastoris*. *BMC Biotechnol* ***13***, 38. DOI: 10.1186/1472-6750-13-38

Mate, D.M., Gonzalez-Perez, D., Mateljak I., Gomez de Santos, P. Vicente, A.I., and Alcalde, M. (2016a). The pocket manual of directed evolution: Tips and tricks. *In: Biotechnology of microbial enzymes: Production, biocatalysis and industrial applications*. G. Brahmachari, A.L. Demain and J.L. Adrio (Eds.) Elsevier (Amsterdam, The Netherlands). pp. 185-214. ISBN: 9780128037256. DOI: 10.1016/B978-0-12-803725-6.00008-X

Mate, D.M., Palomino, M.A., Molina-Espeja, P., Martin-Diaz, J., and Alcalde, M. (2016b). Improving mono(per)oxygenase activity of an unspecific peroxygenase by focused directed evolution. *Protein Eng Des Sel*. *Accepted*.

Matera, I., Gullotto, A., Tilli, S., Ferraroni, M., Scozzafava, A., and Briganti, F. (2008). Crystal structure of the blue multicopper oxidase from the white-rot fungus *Trametes trogii* complexed with *p*-toluate. *Inorg Chim Acta* ***361***, 4129-4137. DOI: 10.1016/j.ica.2008.03.091

Mendonça Maciel, M.J., Castro e Silva, A., and Telles Ribeiro, H.C. (2010). Industrial and biotechnological applications of ligninolytic enzymes of the basidiomycota: a review. *Electron J Biotech* ***13***, 14-15. ISSN 0717-3458

Miki, Y., Morales, M., Ruiz-Dueñas, F.J., Martínez, M.J., Wariishi, H., and Martínez, A.T. (2009). *Escherichia coli* expression and *in vitro* activation of a unique ligninolytic peroxidase that has a catalytic tyrosine residue. *Protein Expr Purif* ***68***, 208-214. DOI: 10.1016/j.pep.2009.06.003

Miyazaki, C., and Takahashi, H. (2001). Engineering of the H_2O_2-binding pocket region of a recombinant manganese peroxidase to be resistant to H_2O_2. *FEBS Letters* ***509***, 111-114. DOI: 10.1016/S0014-5793(01)03127-1

Miyazaki-Imamura, C., Oohira, K., Kitagawa, R., Nakano, H., Yamane, T., and Takahashi, H. (2003). Improvement of H_2O_2 stability of manganese peroxidase by combinatorial mutagenesis and high-throughput screening using *in vitro* expression with protein disulfide isomerase. *Protein Eng Des Sel* ***16***, 423-428. DOI: 10.1093/protein/gzg054

Molina-Espeja, P., Garcia-Ruiz, E., Gonzalez-Perez, D., Ullrich, R., Hofrichter, M., and Alcalde, M. (2014). Directed evolution of unspecific peroxygenase from *Agrocybe aegerita*. *Appl Environ Microbiol* ***80***, 3496-3507. DOI: 10.1128/AEM.00490-14

Molina-Espeja, P., Ma, S., Mate, D.M., Ludwig, R., and Alcalde, M. (2015). Tandem-yeast expression system for engineering and producing unspecific peroxygenase. *Enzyme Microb Technol* ***73-74***, 29-33. DOI: 10.1016/j.enzmictec.2015.03.004

Molina-Espeja, P., Canellas, M., Plou, F.J., Hofrichter, M., Lucas, F., Guallar, V., and Alcalde, M. (2016a). Synthesis of 1-naphthol by a natural peroxygenase engineered by directed evolution. *Chembiochem* ***17***, 341-349. DOI: 10.1002/cbic.201500493

Molina-Espeja, P., Viña-Gonzalez, J., Gómez-Fernández, B.J., Martín-Díaz, J., Garcia-

Ruiz, E., and Alcalde, M. (2016b). Beyond the outer limits of nature by directed-evolution. *Biotechnol Adv* 34, 754-767. DOI: 10.1016/j.biotechadv.2016.03.008

Morales, M., Mate, M.J., Romero, A., Martínez, M.J., Martínez, A.T., and Ruiz-Dueñas, F.J. (2012). Two oxidation sites for low redox potential substrates: a directed mutagenesis, kinetic, and crystallographic study on *Pleurotus eryngii* versatile peroxidase. *J Biol Chem* ***287***, 41053-41067. DOI: 10.1074/jbc.M112.405548

Morawsky, B., Quan, S., and Arnold FH. (2001). Functional expression and stabilization of horseradish peroxidase by directed evolution in *Saccharomyces cerevisiae*. *Biotechnol Bioeng.* ***76***, 99-107. DOI: 10.1002/bit.1149

Moreno, A.D., Ibarra, D., Alvira, P., Tomas-Pejo, E., and Ballesteros, M. (2015). A review of biological delignification and detoxification methods for lignocellulosic bioethanol production. *Crit Rev Biotechnol* ***35***, 342-354. DOI: 10.3109/07388551.2013.878896

Morozova, O.B., and Yurkovskaya, A.V. (2015). Modulation of the rate of reversible electron transfer in oxidized tryptophan and tyrosine containing peptides in acidic aqueous solution. *J Phys Chem B* ***119***, 140-149. DOI: 10.1021/jp511068n

Morozova, O.V., Shumakovich, G.P., Shleev, S.V., and Yaropolov, Y.I. (2007). Laccase-mediator systems and their applications: A review. *Appl Biochem Microbiol* ***43***, 523-535. DOI: 10.1134/S0003683807050055

Munk, L., Sitarz, A.K., Kalyani, D.C., Mikkelsen, J.D., and Meyer, A.S. (2015). Can laccases catalyze bond cleavage in lignin?. *Biotechnol Adv* ***33***, 13-24. DOI: 10.1016/j.biotechadv.2014.12.008

N

Nielsen, J., Larsson, C., van Maris, A., and Pronk, J. (2013). Metabolic engineering of yeast for production of fuels and chemicals. *Curr Opin Biotechnol* ***24***, 398-404. DOI: 10.1016/j.copbio.2013.03.023

Nousiainen, P., Kontro, J., Manner, H., Hatakka, A., and Sipila, J. (2014). Phenolic mediators enhance the manganese peroxidase catalyzed oxidation of recalcitrant lignin model compounds and synthetic lignin. *Fungal Genet Biol 72*, 137-149. DOI: 10.1016/j.fgb.2014.07.008

Novaes, E., Kirst, M., Chiang, V., Winter-Sederoff, H., and Sederoff, R. (2010). Lignin and biomass: a negative correlation for wood formation and lignin content in trees. *Plant Physiol* ***154***, 555-561. DOI: 10.1104/pp.110.161281

O

Octave, S., and Thomas, D. (2009). Biorefinery: Toward an industrial metabolism. *Biochimie* 91, 659-664. DOI: 10.1016/j.biochi.2009.03.015

Ogola, H.J., Hashimoto, N., Miyabe, S., Ashida, H., Ishikawa, T., Shibata, H., and Sawa, Y. (2010). Enhancement of hydrogen peroxide stability of a novel *Anabaena sp*. DyP-type peroxidase by site-directed mutagenesis of methionine residues. *Appl Microbiol Biotechnol* ***87***, 1727-1736. DOI: 10.1007/s00253-010-2603-6

Oldenburg, K. (1997). Recombination-mediated PCR-directed plasmid construction *in vivo* in yeast. *Nucleic Acids Res* ***25***, 451-452. DOI: 10.1093/nar/25.2.451

P

Packer, M.S., and Liu, D.R. (2015). Methods for the directed evolution of proteins. *Nat Rev Genet* ***16***, 379-394. DOI: 10.1038/nrg3927

Pardo, I., Vicente, A.I., Mate, D.M., Alcalde, M., and Camarero, S. (2012). Development of chimeric laccases by directed evolution. *Biotechnol Bioeng* ***109***, 2978-2986. DOI: 10.1002/bit.24588

Pardo, I., and Camarero, S. (2015). Exploring the oxidation of lignin-derived phenols by a library of laccase mutants. *Molecules* ***20***, 15929-15943. DOI: 10.3390/molecules200915929

Pardo, I., Santiago, G., Gentili, P., Lucas, F., Monza, E., Medrano, F.J., Galli, C., Martínez, A.T., Guallar, V., and Camarero, S. (2016). Re-designing the substrate binding pocket of laccase for enhanced oxidation of sinapic acid. *Catal Sci Technol* ***6***, 3900. DOI: 10.1039/C5CY01725D

Pérez, J., Munoz-Dorado, J., de la Rubia, T., and Martínez, J. (2002). Biodegradation and biological treatments of cellulose, hemicellulose and lignin: an overview. *Int Microbiol* ***5***, 53-63. DOI: 10.1007/s10123-002-0062-3

Pérez-Boada, M., Doyle, W.A., Ruiz-Dueñas, F.J., Martínez, M.J., Martínez, A.T., and Smith, A.T. (2002). Expression of *Pleurotus eryngii* versatile peroxidase in *Escherichia coli* and optimisation of *in vitro* folding. *Enzyme Microb Technol* ***30***, 518-524. DOI: 10.1016/S0141-0229(02)00008-X

Pérez-Boada, M., Ruiz-Dueñas, F.J., Pogni, R., Basosi, R., Choinowski, T., Martínez, M.J., Piontek, K., and Martínez, A.T. (2005). Versatile peroxidase oxidation of high redox potential aromatic compounds: site-directed mutagenesis, spectroscopic and crystallographic investigation of three long-range electron transfer pathways. *J Mol Biol* ***354***, 385-402. DOI: 10.1016/j.jmb.2005.09.047

Petersen, J.F.W., Kadziola, A., and Larsen, S. (1994). Three-dimensional structure of a recombinant peroxidase from *Coprinus cinereus* at 2.6 Å resolution. *FEBS Letters* ***339***, 291-296. DOI: 10.1016/0014-5793(94)80433-8

Pezzotti, F., Okrasa, K., and Therisod, M. (2004). Oxidation of chlorophenols catalyzed by *Coprinus cinereus* peroxidase with in situ production of hydrogen peroxide. *Biotechnol Prog* ***20***, 1868-1871. DOI: 10.1021/bp049750t

Pfister, T., Mirarefi, A., Gengenbach, A., Zhao, X., Danstrom, C., Conatser, N., Gao, Y.-G., Robinson, H., Zukoski, C., Wang, A., and Lu, Y. (2007) Kinetic and crystallographic studies of a redesigned manganese-binding site in cytochrome c peroxidase. *J Biol Inorg Chem* ***12***, 126- 137. DOI: 10.1007/s00775-006-0171-0

Piontek, K., Glumoff, T., and Winterhalter, K. (1993). Low pH crystal structure of glycosylated lignin peroxidase from *Phanerochaete chrysosporium* at 2.5 Å resolution. *FEBS Letters* ***315***, 119-124. DOI: 10.1016/0014-5793(93)81146-Q

Pizzul, L., Castillo Mdel, P., and Stenstrom, J. (2009). Degradation of glyphosate and other pesticides by ligninolytic enzymes. *Biodegradation* ***20***, 751-759. DOI: 10.1007/s10532-009-9263-1

Plieth, C., and Vollbehr, S. (2012). Calcium promotes activity and confers heat stability on plant peroxidases. *Plant Signal Behav* *7*, 650-660. DOI: 10.4161/psb.20065

Pogni, R., Baratto, M.C., Teutloff, C., Giansanti, S., Ruiz-Dueñas, F.J., Choinowski, T., Piontek, K., Martínez, A.T., Lendzian, F., and Basosi, R. (2006). A tryptophan neutral radical in the oxidized state of versatile peroxidase from *Pleurotus eryngii*: a combined multifrequency EPR and density functional theory study. *J Biol Chem* ***281***, 9517-9526. DOI: 10.1074/jbc.M510424200

Porter, J.L., Rusli, R.A., and Ollis, D.L. (2016). Directed evolution of enzymes for industrial biocatalysis. *ChemBioChem* ***17***, 197-203. DOI: 10.1002/cbic.201500280

Q

Quiroz-Castañeda, R.E., and Folch-Mallol, J.L. (2010). Plant cell wall degrading and remodeling proteins: Current perspectives. *Biotecnologia Aplicada* ***28***, 205-215. DOI:link

R

Ragauskas, A.J., Beckham, G.T., Biddy, M.J., Chandra, R., Chen, F., Davis, M.F., Davison, B.H., Dixon, R.A., Gilna, P., Keller, M., *et al.* (2014). Lignin valorization: improving lignin processing in the biorefinery. *Science* ***344***, 1246843. DOI: 10.1126/science.1246843

Ralph, J., Lundquist, K., Brunow, G., Lu, F., Kim, H., Schatz, P.F., Marita, J.M., Hatfield, R.D., Ralph, S.A., Christensen, J.H., *et al.* (2004). Lignins: Natural polymers from oxidative coupling of 4-hydroxyphenyl- propanoids. *Phytochem Rev* ***3***, 29-60. DOI: 10.1023/B:PHYT.0000047809.65444.a4

Regalado, V., Rodriguez, A., Perestelo, F., Carnicero, A., De La Fuente, G., and Falcon, M.A. (1997). Lignin degradation and modification by the soil-inhabiting fungus *Fusarium proliferatum*. *Appl Environ Microbiol* ***63***, 3716-3718. PMCID: PMC1389256

Renata, H., Wang, Z.J., and Arnold, F.H. (2015). Expanding the enzyme universe: accessing non-natural reactions by mechanism-guided directed evolution. *Angew Chem Int Ed Engl* ***54***, 3351-3367. DOI: 10.1002/anie.201409470

Romero, P.A., and Arnold, F.H. (2009) Exploring protein fitness landscapes by directed evolution. *Nat Rev Mol Cell Bio* ***10***, 866-876. DOI: 10.1038/nrm2805.

Rothschild, N., Hadar, Y., and Dosoretz, C.G. (1997). Lignin peroxidase isozymes from *Phanerochaete chrysosporium* can be enzymatically dephosphorylated. *Appl Environ Microbiol* ***63***, 857-861. PMCID: PMC1389116

Rowland, F.S. (2006). Stratospheric ozone depletion. *Philos T Roy Soc B* ***361***, 769-790.

Ruiz-Dueñas, F.J., Martínez, M.J., and Martínez, A.T. (1999). Molecular characterization of a novel peroxidase isolated from the ligninolytic fungus *Pleurotus eryngii*. *Mol Microbiol* ***31***, 223-235. DOI: 10.1046/j.1365-2958.1999.01164.x

Ruiz-Dueñas, F.J., Camarero, S., Pérez-Boada, M., Martínez, M.J., and Martínez, A.T. (2001). A new versatile peroxidase from *Pleurotus*. *Biochem Soc T* ***29***, 116-122. DOI: 10.1042/bst0290116

Ruiz-Dueñas, F.J., Morales, M., Perez-Boada, M., Choinowski, T., Martínez, M.J., Piontek, K., and Martínez, A.T. (2007). Manganese oxidation site in *Pleurotus eryngii* versatile peroxidase: a site-directed mutagenesis, kinetic, and crystallographic study. *Biochemistry* ***46***, 66-77. DOI: 10.1021/bi061542h

Ruiz-Dueñas, F.J., Morales, M., Mate, M.J., Romero, A., Martínez, M.J., Smith, A.T., and Martínez, A.T. (2008). Site-directed mutagenesis of the catalytic tryptophan environment in *Pleurotus eryngii* versatile peroxidase. *Biochemistry* ***47***, 1685-1695. DOI: 10.1021/bi7020298

Ruiz-Dueñas, F.J., and Martínez, A.T. (2009a). Microbial degradation of lignin: how a bulky recalcitrant polymer is efficiently recycled in nature and how we can take advantage of this. *Microb Biotechnol* ***2***, 164-177. DOI: 10.1111/j.1751-7915.2008.00078.x

Ruiz-Dueñas, F.J., Morales, M., Garcia, E., Miki, Y., Martínez, M.J., and Martínez, A.T. (2009b). Substrate oxidation sites in versatile peroxidase and other basidiomycete peroxidases. *J Exp Bot* ***60***, 441-452. DOI: 10.1093/jxb/ern261

Ruiz-Dueñas, F.J., Pogni, R., Morales, M., Giansanti, S., Mate, M.J., Romero, A., Martínez, M.J., Basosi, R., and Martínez, A.T. (2009c). Protein radicals in fungal versatile peroxidase: catalytic tryptophan radical in both compound I and compound II and studies on W164Y, W164H, and W164S variants. *J Biol Chem* ***284***, 7986-7994. DOI: 10.1074/jbc.M808069200

Ruiz-Dueñas, F.J., Lundell, T., Floudas, D., Nagy, L.G., Barrasa, J.M., Hibbett, D.S., and Martínez, A.T. (2013). Lignin-degrading peroxidases in Polyporales: an evolutionary survey based on 10 sequenced genomes. *Mycologia* ***105***, 1428-1444. DOI: 10.3852/13-059

Ryan, B.J., and O'Fagain, C. (2007). Effects of single mutations on the stability of horseradish peroxidase to hydrogen peroxide. *Biochimie* ***89***, 1029-1032. DOI: 10.1016/j.biochi.2007.03.013

Ryu, K., Hwang, S.Y., Kim, K.H., Kang, J.H., and Lee, E.K. (2008). Functionality improvement of fungal lignin peroxidase by DNA shuffling for 2,4-dichlorophenol degradability and H_2O_2 stability. *J Biotechnol 133*, 110-115. DOI: 10.1016/j.jbiotec.2007.09.008

S

Sáez-Jiménez, V., Acebes, S., Guallar, V., Martínez, A.T., and Ruiz-Dueñas, F.J. (2015a). Improving the oxidative stability of a high redox potential fungal peroxidase by rational design. *PLoS One* ***10***, e0124750. DOI: 10.1371/journal.pone.0124750

Sáez-Jiménez, V., Baratto, M.C., Pogni, R., Rencoret, J., Gutierrez, A., Santos, J.I., Martínez, A.T., and Ruiz-Dueñas, F.J. (2015b). Demonstration of lignin-to-peroxidase direct electron transfer: a transient-state kinetics, directed mutagenesis, EPR, and NMR study. *J Biol Chem* ***290***, 23201-23213. DOI: 10.1074/jbc.M115.665919

Sáez-Jiménez, V., Fernández-Fueyo, E., Medrano, F.J., Romero, A., Martínez, A.T., and Ruiz-Dueñas, F.J. (2015c). Improving the pH-stability of versatile peroxidase by comparative structural analysis with a naturally-stable manganese peroxidase. *PLoS One* ***10***, e0140984. DOI: 10.1371/journal.pone.0140984

Sáez-Jimenez, V., Acebes, S., Garcia-Ruiz, E., Romero, A., Guallar, V., Alcalde, M., Medrano, F.J., Martinez, A.T., and Ruiz-Duenas, F.J. (2016). Unveiling the basis of alkaline stability of an evolved versatile peroxidase. *Biochem J* ***473***, 1917-1928. DOI: 10.1042/BCJ20160248

Sakai, S., Yamada, Y., and Kawakami, K. (2009). Novel chitosan derivate soluble at neutral pH and *in-situ* gellable via peroxidase-catalyzed enzymatic reaction. *J Mater Chem* ***19***, 230-235. DOI: 10.1039/B812086B

Salvachúa, D., Prieto, A., Martínez, A.T., and Martínez, M.J. (2013). Characterization of a novel dye-decolorizing peroxidase (DyP)-type enzyme from *Irpex lacteus* and its application in enzymatic hydrolysis of wheat straw. *Appl Environ Microbiol* ***79***, 4316-4324. DOI: 10.1128/AEM.00699-13

Scheller, H.V., and Ulvskov, P. (2010). Hemicelluloses. *Annu Rev Plant Biol* ***61***, 263-289. DOI: 10.1146/annurev-arplant-042809-112315

Schmidt, O. (2006). Wood and tree fungi: Biology, damage, protection, and use. Berlin Heidelberg New York, Springer. DOI: 10.1007/3-540-32139-X

Sharp, K.H., Mewies, M., Moody, P.C., and Raven, E.L. (2003). Crystal structure of the ascorbate peroxidase-ascorbate complex. *Nat Struct Biol* ***10***, 303-307. DOI: 10.1038/nsb913

Shary, S., Ralph, S.A., and Hammel, K.E. (2007). New insights into the ligninolytic capability of a wood decay ascomycete. *Appl Environ Microbiol* ***73***, 6691-6694. DOI: 10.1128/AEM.01361-07

Solar, S., Getoff, N., Surdhar, P.S., Armstrong, D.A., and Singh, A. (1991). Oxidation of tryptophan and N-methylindole by $N_3^{\cdot}$, Br_2^{-}, and $(SCN)_2^{-}$ radicals in light- and heavy-water solutions: a pulse radiolysis study. *J Phys Chem* ***95***, 3639-3643. DOI: 10.1021/j100162a038

Solomon, S., Plattner, G.K., Knutti, R., and Friedlingstein, P. (2009). Irreversible climate change due to carbon dioxide emissions. *Proc Natl Acad Sci USA* ***106***, 1704-1709. DOI: 10.1073/pnas.0812721106

Strittmatter, E., Liers, C., Ullrich, R., Wachter, S., Hofrichter, M., Plattner, D.A., and Piontek, K. (2013a). First crystal structure of a fungal high-redox potential dye-decolorizing peroxidase: substrate interaction sites and long-range electron transfer. *J Biol Chem* ***288***, 4095-4102. DOI: 10.1074/jbc.M112.400176

Strittmatter, E., Wachter, S., Liers, C., Ullrich, R., Hofrichter, M., Plattner, D.A., and Piontek, K. (2013b). Radical formation on a conserved tyrosine residue is crucial for DyP activity. *Arch Biochem Biophys* ***537***, 161-167. DOI: 10.1016/j.abb.2013.07.007

Sun, Z., Wikmark, Y., Backvall, J.E., and Reetz, M.T. (2016). New concepts for increasing the efficiency in directed evolution of stereoselective enzymes. *Chemistry* ***22***, 5046-5054. DOI: 10.1002/chem.201504406

Sundaramoorthy, M., Kishi, K., Gold, M.H., and Poulos, T.L. (1994). The crystal structure of manganese peroxidase from *Phanerochaete chrysosporium* at 2.06-Å resolution. *J Biol Chem* ***269***, 32759-32767. PMID: 7806497

Sutherland, G.R., and Aust, S.D. (1996). The effects of calcium on the thermal stability and activity of manganese peroxidase. *Arch Biochem Biophys* ***332***, 128-134. DOI: 10.1006/abbi.1996.0324

T

Taboada-Puig, R., Junghanns, C., Demarche, P., Moreira, M.T., Feijoo, G., Lema, J.M., and Agathos, S.N. (2011). Combined cross-linked enzyme aggregates from versatile peroxidase and glucose oxidase: production, partial characterization and application for the elimination of endocrine disruptors. *Bioresour Technol* ***102***, 6593-6599. DOI: 10.1016/j.biortech.2011.03.018

Tanaka, H., Itakura, S., and Enoki, A. (1999). Hydroxyl radical generation by an extracellular low-molecular-weight substance and phenol oxidase activity during wood degradation by the white-rot basidiomycete *Trametes versicolor*. *J Biotechnol* ***75***, 57-70. DOI: 10.1016/S0168-1656(99)00138-8

Timofeevski, S.L., Nie, G., Reading, N.S., and Aust, S.D. (1999). Addition of veratryl alcohol oxidase activity to manganese peroxidase by site-directed mutagenesis. *Biochem Biophys Res Commun* ***256***, 500-504. DOI: 10.1006/bbrc.1999.0360

Torres-Salas, P., Mate, D.M., Ghazi, I., Plou, F.J., Ballesteros, A.O., and Alcalde, M. (2013). Widening the pH activity profile of a fungal laccase by directed evolution. *ChemBioChem* ***14***, 934-937. DOI: 10.1002/cbic.201300102

Touahar, I.E., Haroune, L., Ba, S., Bellenger, J.P., and Cabana, H. (2014). Characterization of combined cross-linked enzyme aggregates from laccase, versatile peroxidase and glucose oxidase, and their utilization for the elimination of pharmaceuticals. *Sci Total Environ* ***481***, 90-99. DOI: 10.1016/j.scitotenv.2014.01.132

U

Ullrich, R., Nuske, J., Scheibner, K., Spantzel, J., and Hofrichter, M. (2004). Novel haloperoxidase from the agaric basidiomycete *Agrocybe aegerita* oxidizes aryl alcohols and aldehydes. *Appl Environ Microbiol* ***70***, 4575-4581. DOI: 10.1128/AEM.70.8.4575-4581.2004

Upton, B.M., and Kasko, A.M. (2016). Strategies for the conversion of lignin to high-value polymeric materials: review and perspective. *Chem Rev* ***116***, 2275-2306. DOI: 10.1021/acs.chemrev.5b00345

Uzan, J., Dewilde, S., Burmester, T., Hankeln, T., Moens, L., Hamdane, D., Marden, M.C., and Kiger, L. (2004). Neuroglobin and other hexacoordinated hemoglobins show a weak temperature dependence of oxygen binding. *Biophys* J ***87***, 1196-1204. DOI: 10.1529/biophysj.104.042168

V

Valderrama, B., Ayala, M., and Vázquez-Duhalt, R. (2002). Suicide inactivation of peroxidases and the challenge of engineering more robust enzymes. *Chem Biol* ***9***, 555-565. DOI: 10.1016/S1074-5521(02)00149-7

Valderrama, B. (2010). Deactivation of hemeperoxidases by hydrogen peroxide: Focus on compound III. *In: biocatalysis based on heme peroxidases: peroxidases as potential industrial biocatalysts*, E. Torres, and M. Ayala, eds., Berlin, Heidelberg: Springer Berlin Heidelberg, pp. 291-314. DOI: 10.1007/978-3-642-12627-7_11

Vanden Wymelenberg, A., Gaskell, J., Mozuch, M., BonDurant, S.S., Sabat, G., Ralph, J., Skyba, O., Mansfield, S.D., Blanchette, R.A., Grigoriev, I.V., *et al.* (2011). Significant alteration of gene expression in wood decay fungi *Postia placenta* and *Phanerochaete chrysosporium* by plant species. *Appl Environ Microbiol* *77*, 4499-4507. DOI: 10.1128/AEM.00508-11

Vanholme, R., Demedts, B., Morreel, K., Ralph, J., and Boerjan, W. (2010). Lignin biosynthesis and structure. *Plant Physiol* ***153***, 895-905. DOI: 10.1104/pp.110.155119

Varela, E., and Tien, M. (2003). Effect of pH and oxalate on hydroquinone-derived hydroxyl radical formation during brown-rot wood degradation. *Appl Environ Microbiol* ***69***, 6025-6031. DOI: 10.1128/AEM.69.10.6025-6031.2003

Vicente, A.I., Viña-Gonzalez, J., Plou, F.J., Marquez-Alvarez, C., Ballesteros, A.O. and Alcalde M. (2016). Synthesis of C-N heteropolymeric dyes using an evolved alkaline fungal laccase secreted by *Saccharomyces cerevisiae*. *J Mol Catal B: Enzym*, *accepted.*

Viña-Gonzalez, J., Gonzalez-Perez, D., Ferreira, P., Martinez, A.T., and Alcalde, M. (2015). Focused directed evolution of aryl-alcohol oxidase in *Saccharomyces cerevisiae* by using chimeric signal peptides. *Appl Environ Microbiol* ***81***, 6451-6462. DOI: 10.1128/AEM.01966-15

Viña-Gonzalez, J., Gonzalez-Perez, D., and Alcalde, M. (2016). Directed evolution method in *Saccharomyces cerevisiae*: Mutant library creation and screening. *J Vis Exp* ***110***, e53761. DOI: 10.3791/53761

Vitello, L.B., Erman, J.E., Miller, M.A., Wang, J., and Kraut, J. (1993). Effect of arginine-48 replacement on the reaction between cytochrome c peroxidase and hydrogen peroxide. *Biochemistry* ***32***, 9807-9818. DOI: 10.1021/bi00088a036

W

Wang, X., Ullrich, R., Hofrichter, M., and Groves, J.T. (2015). Heme-thiolate ferryl of aromatic peroxygenase is basic and reactive. *Proc Natl Acad Sci USA* ***112***, 3686-3691. DOI: 10.1073/pnas.1503340112

Wariishi, H., and Gold, M.H. (1989). Lignin peroxidase compound III : Formation, inactivation, and conversion to the native enzyme. *FEBS Letters* ***243***, 165-168. DOI: 10.1016/0014-5793(89)80122-X

Whittaker, J.W. (2012). Non-heme manganese catalase--the 'other' catalase. *Arch Biochem Biophys* ***525***, 111-120. DOI: 10.1016/j.abb.2011.12.008

Williams, G.J., Zhang, C., and Thorson, J.S. (2007). Expanding the promiscuity of a natural-product glycosyltransferase by directed evolution. *Nat Chem Biol* ***3***, 657-662. DOI: 10.1038/nchembio.2007.28

Wong, D.W. (2009). Structure and action mechanism of ligninolytic enzymes. *Appl Biochem Biotechnol* ***157***, 174-209. DOI: 10.1007/s12010-008-8279-z

X

Xiao, C., and Anderson, C.T. (2013). Roles of pectin in biomass yield and processing for biofuels. *Front Plant Sci* ***4***, 67. DOI: 10.3389/fpls.2013.00067

Xu, C., Arancon, R.A., Labidi, J., and Luque, R. (2014). Lignin depolymerisation strategies: towards valuable chemicals and fuels. *Chem Soc Rev* ***43***, 7485-7500. DOI: 10.1039/C4CS00235K

Xu, F. (1996). Oxidation of phenols, anilines, and benzenethiols by fungal laccases: correlation between activity and redox potentials as well as halide inhibition. *Biochemistry* ***35***, 7608-7614. DOI: 10.1021/bi952971a

Y

Yadav, M., and Yadav, H.S. (2015). Applications of ligninolytic enzymes to pollutants, wastewater, dyes, soil, coal, paper and polymers. *Environ Chem Lett* ***13***, 309-318. DOI: 10.1007/s10311-015-0516-4

Youngs, H.L., Moënne-Loccoz, P., Loehr, T.M., and Gold, M.H. (2000). Formation of a bis(histidyl) heme iron complex in manganese peroxidase at high pH and restoration of the native enzyme structure by calcium. *Biochemistry* ***39***, 9994-10000. DOI: 10.1021/bi000679j

Z

Zakzeski, J., Bruijnincx, P.C., Jongerius, A.L., and Weckhuysen, B.M. (2010). The catalytic valorization of lignin for the production of renewable chemicals. *Chem Rev* ***110***, 3552-3599. DOI: 10.1021/cr900354u

Zamocky, M., Gasselhuber, B., Furtmuller, P.G., and Obinger, C. (2014). Turning points in the evolution of peroxidase-catalase superfamily: molecular phylogeny of hybrid heme peroxidases. *Cell Mol Life Sci* ***71***, 4681-4696. DOI: 10.1007/s00018-014-1643-y

Zhang, M.T., and Hammarstrom, L. (2011). Proton-coupled electron transfer from tryptophan: a concerted mechanism with water as proton acceptor. *J Am Chem Soc* ***133***, 8806-8809. DOI: 10.1021/ja201536b

Zhao, Y., and Zhao, B. (2013). Oxidative stress and the pathogenesis of Alzheimer's disease. *Oxid Med Cell Longev* **2013**, 316523. DOI: 10.1155/2013/316523

Zhu, Y., Zhuang, L., Goodell, B., Cao, J., and Mahaney, J. (2016). Iron sequestration in brown-rot fungi by oxalate and the production of reactive oxygen species (ROS). *Int Biodeter Biodegr* ***109***, 185-190. DOI: 10.1016/j.ibiod.2016.01.023

Zumárraga, M., Bulter, T., Shleev, S., Polaina, J., Martínez-Arias, A., Plou, F.J., Ballesteros, A., and Alcalde, M. (2007). *In vitro* evolution of a fungal laccase in high concentrations of organic cosolvents. *Chem Biol* ***14***, 1052-1064. DOI: 10.1016/j.chembiol.2007.08.010

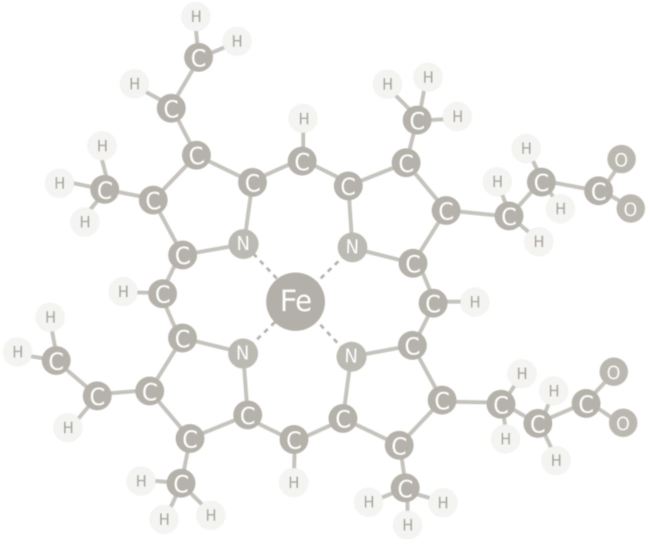

Capítulo 11:

Anexos I y II

Este capítulo incluye las secuencias de las diferentes variantes obtenidas en la Tesis Doctoral así como un breve resumen de las contribuciones científicas del doctorando.

ANEXO I

Secuencia completa del gen de fusión α-vpl2:

En la secuencia del gen de fusión se resaltan los diferentes elementos que lo componen, así como las mutaciones introducidas durante el proceso de evolución dirigida hacia expresión funcional, termoestabilidad, estabilidad oxidativa y actividad a pH neutro/alcalino.

pre-líder del factor-α (57 pb, 19 aminoácidos); **pro-líder del factor-α** (192 pb, 64 aminoácidos); **diana de corte de la proteasa KEX2** (6pb, 2 aminoácidos); **diana de corte de la proteasa STE13** (12 pb, 4 aminoácidos); **diana de restricción EcoRI** (6 pb, 2 aminoácidos); proteína madura (993 pb, 331 aminoácidos); **mutaciones de R4** (E37K-V160A-T184M-Q202L; evolución hacia expresión funcional); **mutaciones de 2-1B** (**mutaciones de R4** + H39R-D213A-G330R; evolución hacia termoestabilidad); **mutaciones de SI**th **y AT-AT** (**mutaciones de R4** + N11D-G25K-E40K-T45A-S86R-P141A-F186L-T323I, mutante SIth; **mutaciones de R4** + D22N-T45A-E83G-I103V-G107S-P141A-F186L, mutante AT-AT; evolución hacia estabilidad oxidativa); **mutaciones de BB-8** (**mutaciones de 2-1B** + E140G-P182S-Q229P; evolución hacia actividad en condiciones de pH alcalino). Los codones mostrados en gris indican la secuencia del gen antes de la mutación y los números en **negrita** representan la numeración según la secuencia de la VP madura.

1	ATG	AGA	TTT	CCT	TCA	ATT	TTT	ACT	GCT	GTT	TTA	TTC	GCA	GCA	TCC	45
1	M	R	F	P	S	I	F	T	A	V	L	F	A	A	S	15
46	TCC	GCA	TTA	GCT	GCT	CCA	GTC	AAC	ACT	ACA	ACA	GAA	GAT	GAA	ACG	90
16	S	A	L	A	A	P	V	N	T	T	T	E	D	E	T	30
91	GCA	CAA	ATT	CCG	GCT	GAA	GCT	GTC	ATC	GGT	TAC	TCA	GAT	TTA	GAA	135
31	A	Q	I	P	A	E	A	V	I	G	Y	S	D	L	E	45
136	GGG	GAT	TTC	GAT	GTT	GCT	GTT	TTG	CCA	TTT	TCC	AAC	AGC	ACA	AAT	180
46	G	D	F	D	V	A	V	L	P	F	S	N	S	T	N	60
181	AAC	GGG	TTA	TTG	TTT	ATA	AAT	ACT	ACT	ATT	GCC	AGC	ATT	GCT	GCT	225
61	N	G	L	L	F	I	N	T	T	I	A	S	I	A	A	75
226	AAA	GAA	GAA	GGG	GTA	TCT	CTC	GAG	AAA	AGA	GAG	GCT	GAA	GCT	GAA	270
76	K	E	E	G	V	S	L	E	K	R	E	A	E	A	E	90
												AAT				
271	TTC	GCA	ACT	TGC	GAC	GAC	GGA	CGC	ACC	ACC	GCA	GAT	GCT	GCA	TGT	315
91	F	A	T	C	D	D	G	R	T	T	A	D	A	A	C	105
VP madura		**1**	**2**	**3**	**4**	**5**	**6**	**7**	**8**	**9**	**10**	**11**	**12**	**13**	**14**	
								GAT								
316	TGC	ATT	CTG	TTC	CCC	ATC	CTC	AAT	GAC	ATC	CAA	GAA	AAC	CTC	TTC	360
106	C	I	L	F	P	I	L	N	D	I	Q	E	N	L	F	120
	15	**16**	**17**	**18**	**19**	**20**	**21**	**22**	**23**	**24**	**25**	**26**	**27**	**28**	**29**	
						GGA		GAG		CAC	GAG					
361	GAC	GGT	GCC	CAG	TGT	AAA	GAA	AAG	GTG	CGC	AAG	TCC	CTT	CGT	TTG	405
121	D	G	A	Q	C	K	E	K	V	R	K	S	L	R	L	135
	30	**31**	**32**	**33**	**34**	**35**	**36**	**37**	**38**	**39**	**40**	**41**	**42**	**43**	**44**	

	ACT															
406	GCT	TTC	CAC	GAT	GCA	ATC	GGT	TTC	TCT	CCT	ACT	TTA	GGC	GGA	GGA	450
136	**A**	F	H	D	A	I	G	F	S	P	T	L	G	G	G	150
	45	46	47	48	49	50	51	52	53	54	55	56	57	58	59	
451	GGA	GCT	GAC	GGT	TCC	ATC	ATC	GCG	TTC	GAC	ACC	ATT	GAG	ACT	AAT	495
151	G	A	D	G	S	I	I	A	F	D	T	I	E	T	N	165
	60	61	62	63	64	65	66	67	68	69	70	71	72	73	74	
									GAA			AGT				
496	TTC	CCC	GCC	AAT	GCT	GGC	ATC	GAT	GGA	ATC	GTC	CGT	GCT	CAG	AAG	540
166	F	P	A	N	A	G	I	D	**K**	I	V	**R**	A	Q	K	180
	75	76	77	78	79	80	81	82	83	84	85	86	87	88	89	
														ATT		
541	CCA	TTC	GTG	GCT	AAA	CAC	AAC	ATC	TCC	GCC	GGC	GAC	TTC	GTT	CAA	585
181	P	F	V	A	K	H	N	I	S	A	G	D	F	**V**	Q	195
	90	91	92	93	94	95	96	97	98	99	100	101	102	103	104	
			GGC													
586	TTT	GCT	AGC	GCC	GTT	GGA	GTC	TCC	AAC	TGC	CCT	GGT	GGT	GTC	AGG	630
196	F	A	**S**	A	V	G	V	S	N	C	P	G	G	V	R	210
	105	106	107	108	109	110	111	112	113	114	115	116	117	118	119	
631	ATT	CCT	TTC	TTC	TTG	GGT	CGC	CCG	GAT	GCC	GTG	GCC	GCC	TCC	CCG	675
211	I	P	F	F	L	G	R	P	D	A	V	A	A	S	P	225
	120	121	122	123	124	125	126	127	128	129	130	131	132	133	134	
						GAG	CCT									
676	GAC	CAC	CTC	GTG	CCA	GGG	GCT	TTT	GAT	TCT	GTT	GAC	TCC	ATT	CTT	720
226	D	H	L	V	P	**G**	**A**	F	D	S	V	D	S	I	L	240
	135	136	137	138	139	140	141	142	143	144	145	146	147	148	149	
											GTC					
721	GCC	AGA	ATG	GGT	GAC	GCA	GGC	TTC	AGT	CCC	GCC	GAG	GTT	GTT	TGG	765
241	A	R	M	G	D	A	G	F	S	P	**A**	E	V	V	W	255
	150	151	152	153	154	155	156	157	158	159	160	161	162	163	164	
766	CTC	CTG	GCT	TCG	CAC	TCC	ATT	GCC	GCT	GCC	GAC	AAG	GTT	GAC	CCA	810
256	L	L	A	S	H	S	I	A	A	A	D	K	V	D	P	270
	165	166	167	168	169	170	171	172	173	174	175	176	177	178	179	
			CCT		ACG		TTC									
811	TCG	ATT	TCT	GGA	ATG	CCA	CTT	GAT	TCA	ACC	CCC	GGA	GTT	TTT	GAT	855
271	S	I	**S**	G	**M**	P	**L**	D	S	T	P	G	V	F	D	285
	180	181	182	183	184	185	186	187	188	189	190	191	192	193	194	
								CAA								
856	TCT	CAA	TTC	TTC	ATC	GAA	ACG	CTA	CTT	AAA	GGC	AGA	CTC	TTC	CCA	900
286	S	Q	F	F	I	E	T	**L**	L	K	G	R	L	F	P	300
	195	196	197	198	199	200	201	202	203	204	205	206	207	208	209	
				GAC												
901	GGC	ACT	GCT	GCC	AAC	AAG	GGA	GAA	GCC	CAA	TCT	CCA	TTG	CAA	GGA	945
301	G	T	A	**A**	N	K	G	E	A	Q	S	P	L	Q	G	315
	210	211	212	213	214	215	216	217	218	219	220	221	222	223	224	

```
                        CAG
946     GAG ATC AGG CTT CCG TCC GAT CAC TTG TTG GCT AGA GAC CCC CAG   990
316      E   I   R   L   P   S   D   H   L   L   A   R   D   P   Q    330
        225 226 227 228 229 230 231 232 233 234 235 236 237 238 239

991     ACT GCC TGC GAA TGG CAG TCC ATG GTT AAC AAC CAA CCG AAG ATT   1035
331      T   A   C   E   W   Q   S   M   V   N   N   Q   P   K   I    345
        240 241 242 243 244 245 246 247 248 249 250 251 252 253 254

1036    CAG AAC CGT TTC GCT GCT ACC ATG TCG AAG ATG GCT CTT CTT GGC   1080
346      Q   N   R   F   A   A   T   M   S   K   M   A   L   L   G    360
        255 256 257 258 259 260 261 262 263 264 265 266 267 268 269

1081    CAA GAC AAG ACC AAA TTG ATT GAC TGT TCC GAT GTT ATC CCC ACC   1125
361      Q   D   K   T   K   L   I   D   C   S   D   V   I   P   T    375
        270 271 272 273 274 275 276 277 278 279 280 281 282 283 284

1126    CCT CCT GCC CTT GTC GGA GCG GCC CAC TTA CCG GCG GGA TTT TCT   1170
376      P   P   A   L   V   G   A   A   H   L   P   A   G   F   S    390
        285 286 287 288 289 290 291 292 293 294 295 296 297 298 299
1171    CTT AGC GAT GTA GAG CAA GCG TGC GCC GCG ACG CCT TTC CCT GCT   1215
391      L   S   D   V   E   Q   A   C   A   A   T   P   F   P   A    405
        300 301 302 303 304 305 306 307 308 309 310 311 312 313 314
                                        ACC
1216    CTT ACT GCT GAC CCA GGC CCA GTA ATT TCC GTC CCT CCC GTC CCT   1260
406      L   T   A   D   P   G   P   V   I   S   V   P   P   V   P    420
        315 316 317 318 319 320 321 322 323 324 325 326 327 328 329
        GGA
1261    AGA TCG TAA   1269
421      R   S   *
        330 331
```

ANEXO I

El desarrollo de la presente Tesis Doctoral ha dado lugar a la siguiente producción científica:

Trabajos publicados en revistas científicas SCI con relación a la Tesis Doctoral:

1. **Gonzalez-Perez, D.**, Mateljak, I., Garcia-Ruiz, E., Ruiz-Dueñas, F.J., Martinez, A.T., and Alcalde, M. (2016). Alkaline versatile peroxidase by directed evolution. *Catalysis Science & Technology* ***6***, 6625-6636.

2. Viña-Gonzalez, J., **Gonzalez-Perez, D.,** and Alcalde, M. (2015). Directed evolution method in *Saccharomyces cerevisiae*: Mutant library creation and screening. *Journal of Visualized Experiments* ***110***, e53761.

3. **Gonzalez-Perez, D.**, Garcia-Ruiz, E., Ruiz-Dueñas, F.J., Martínez, A.T., and Alcalde, M. (2014). Structural determinants of oxidative stabilization in an evolved versatile peroxidase. *ACS-Catalysis* ***4***, 3891-3901.

4. **Gonzalez-Perez, D.**, and Alcalde, M. (2014). Assembly of synthetic ligninolytic genes in *Saccharomyces cerevisiae*. *Bioengineered* ***15***, 5.

5. **Gonzalez-Perez, D.**, Molina-Espeja, P., Garcia-Ruiz, E., and Alcalde, M. (2014). Mutagenic Organized Recombination Process by Homologous *IN vivo* Grouping (MORPHING) for directed enzyme evolution. *PlOs One* ***9***, e90919.

6. Garcia-Ruiz, E., **Gonzalez-Perez, D.**, Ruiz-Dueñas, F.J., Martínez, A.T., and Alcalde M. (2012). Directed evolution of a temperature, peroxide and alkaline pH tolerant versatile peroxidase. *Biochemical Journal* ***441***, 487-498.

7. **Gonzalez-Perez, D.**, Garcia-Ruiz, E., and Alcalde, M. (2012). *Saccharomyces cerevisiae* in directed evolution: an efficient tool to improve enzymes. *Bioengineered* ***3***, 172-177.

Trabajos publicados en *proceedings* y capítulos de libro con relación a la Tesis Doctoral:

1. Mate, D.M., **Gonzalez-Perez, D.**, Mateljak I., Gomez de Santos, P. Vicente, A.I., and Alcalde, M. (2016). The pocket manual of directed evolution: Tips and tricks. *In: Biotechnology of Microbial Enzymes: Production, Biocatalysis and Industrial Applications*. G. Brahmachari, A.L. Demain and J.L. Adrio (Eds.) Elsevier (Amsterdam, The Netherlands). pp. 185-214. ISBN: 9780128037256.

2. Garcia-Ruiz, E., Mate, D.M., **Gonzalez-Perez, D.**, Molina-Espeja, P., Camarero, S., Martinez, A.T., Ballesteros, A.O. and Alcalde, M. (2014). Directed evolution of ligninolytic oxidoreductases: from functional expression to stabilization and beyond. *In*: *Cascade Biocatalysis: Integrating Stereoselective and Environmentally Friendly*

*Reaction*s. S. Riva and W.D. Fessner (Eds.). Wiley (Hoboken, New Jersey). pp. 1-18. ISBN: 978-3-527-33522-0.

3. **González-Pérez, D.**, Román, A., García-Ruiz, E., Ruiz-Dueñas, F.J., Martínez, Á.T., and Alcalde M. (2014). Screening mutant libraries of versatile peroxidase from *Pleurotus eryngii* to enhance oxidative stability. 13th European Workshop on Lignocellulosics and Pulp (EWLP-2014)-*Proceedings*. J.C. del Río, A. Gutiérrez, J. Rencoret and Á.T. Martínez (Eds.). pp 397-400. ISBN: 978-84-616-9842-4.

<u>Presentaciones orales relacionadas con la Tesis Doctoral:</u>

Gonzalez-Perez, D. (2013). “Directed evolution of versatile peroxidase (VP) towards oxidative stability”. XVI meeting of the LIGNOCEL network. Sep, 26-27. Pontevedra (Spain).

I) PEROXICATS FP-7 PROJECT “Peroxidases as biocatalyst (Peroxicats)”. Ref: FP7-KBBE-2010-4-26537:

36-Month Meeting project (2013):
Gonzalez-Perez, D. “Directed evolution of versatile peroxidase (VP) towards oxidative stability”. Nov, 18. Madrid (Spain).

30-Month Meeting project (2013):
Gonzalez-Perez, D. “Directed evolution of versatile peroxidase (VP) towards oxidative stability and co-expression of VP and laccase in *Saccharomyces cerevisiae*”. May, 28. Zittau (Germany).

24-Month Meeting project (2012):
Gonzalez-Perez, D. “Directed evolution of Versatile Peroxidase (VP) towards oxidative stability and co-expression of VP and Laccase in *Saccharomyces cerevisiae*”. Nov, 27. Seville (Spain).

18-Month Meeting project (2012):
Gonzalez-Perez, D. “Directed evolution for VP oxidative stability”. May, 25. Jena (Germany).

6-Month Meeting project (2011):
Gonzalez-Perez, D. “HTP-screening assay and diversity generation”. May, 24. Copenhagen (Denmark).

II) INDOX FP-7 PROJECT “Optimized oxidoreductases for medium and large scale industrial biotransformations (INDOX)”. Ref: FP7-KBBE-2013-7-613549.

12-Month Meeting project (2014):
Gonzalez-Perez, D. “Directed evolution of fungal laccases and versatile peroxidase”. Oct, 20. Wageningen (The Netherlands).

18-Month meeting project (2015):
Gonzalez-Perez, D. "Engineering a fungal versatile peroxidase to be active at alkaline pH by directed evolution". Apr, 9. Vienna (Austria).

Trabajos presentados en congresos en relación con la Tesis Doctoral:

1. **González-Pérez D.**, García-Ruiz E., Gómez Fernández, B.J., Ruiz-Dueñas F.J., Martínez Á.T., and Alcalde M. (2014). "Screening mutant libraries of versatile peroxidase from *Pleurotus eryngii* to enhance oxidative stability". XXXIV National Congress of the Spanish Society of Biochemistry and Molecular Biology (SEBBM-2014). Sept, 9 – 12. (Barcelona, Spain).

2. **González-Pérez, D.**, Román, A., García-Ruiz, E., Ruiz-Dueñas, F.J., Martínez, Á.T., and Alcalde, M. (2014). "Screening mutant libraries of versatile peroxidase from *Pleurotus eryngii* to enhance oxidative stability". 13th European Workshop on Lignocellulosics and Pulp (EWLP-2014). Jun, 24 – 27. Seville (Spain).

3. **Gonzalez-Perez, D.**, Molina-Espeja, P., Garcia-Ruiz, E., and Alcalde, M. (2014). "Morphing: a random domain mutagenesis method for directed evolution". 3rd Multistep Enzyme Catalyzed Processes Congress (MECP14). Jun, 7 – 10. Madrid (Spain).

4. **González-Pérez,D.**, García-Ruiz, E., and Alcalde, M. (2012). "MORPHING (Mutagenic Organized Recombination Process by Homologous *IN vivo* Grouping) for directed enzyme evolution". 2nd Multistep Enzyme-Catalyzed Processes 2012. Apr, 10 – 13. Graz (Austria).

5. Garcia-Ruiz, E., Mate, D.**, Gonzalez-Perez, D.**, Roman, A., Molina, P., Torres, P., Zumarraga, M., Camarero, S., Ballesteros, A., Plou, F.J., and Alcalde, M. (2011)."*Saccharomyces cerevisiae* in directed evolution: an efficient tool to improve enzymes". 10th International Symposium on Biocatalysis and Biotransformations (BIOTRANS). Oct, 2 – 6. Giardini Naxos (Italy).

6. Garcia-Ruiz, E., **Gonzalez-Perez, D.**, Ruiz-Dueñas, F.J., Martínez, A.T., and Alcalde, M. (2011). "Directed evolution of versatile peroxidases". 10th International Symposium on Biocatalysis and Biotransformations (BIOTRANS). Oct, 2 – 6. Giardini Naxos (Italy).

7. **González-Pérez, D.**, García-Ruiz, E., Roman, A., Ruiz-Dueñas, F.J., Martínez, A.T. and Alcalde, M. (2011). "Engineering oxidative stability in versatile peroxidase by directed evolution". XXXIV National Congress of the Spanish Society of Biochemistry and Molecular Biology. Sept, 8 – 10. Barcelona (Spain).

Otros trabajos publicados en revistas SCI del doctorando:

1. Viña-Gonzalez, J., **Gonzalez-Perez, D.**, Ferreira, P., Martínez, A.T., and Alcalde, M. (2015). Focused directed evolution of aryl-alcohol oxidase in yeast using chimeric signal peptides. *Applied and Environmental Microbiology* ***81***, 6451-6462.

2. Pita, M., Mate, D.M., **Gonzalez-Perez, D.**, Shleev, S., Fernandez, V.M., Alcalde, M., and De Lacey, A.L. (2014). Bioelectrochemical oxidation of water. *Journal of the American Chemical Society **136***, 5892–5895.

3. Molina-Espeja, P., Garcia-Ruiz, E., **Gonzalez-Perez, D.**, Ullrich, R., Hofrichter, M., and Alcalde, M. (2014). Directed evolution of unspecific peroxygenase from *Agrocybe aegerita*. *Applied and Environmental Microbiology **80***, 3496-507.

4. Mate, D.M., **Gonzalez-Perez, D.**, Falk, M., Kittl, R., Pita, M., De Lacey, A.L., Ludwig, R., Shleev, S., and Alcalde, M. (2013). Blood tolerant laccases by directed evolution. *Chemistry and Biology **20***, 223-231.

5. Mate, D.M., **Gonzalez-Perez, D.**, Kittl, R., Ludwig, R., and Alcalde, M. (2013). Functional expression of a blood tolerant laccase in *Pichia pastoris*. *BMC Biotechnology **13***, 38.

6. Álvaro-Benito, M., Sainz-Polo, M.A., **González Pérez, D.**, González, B., Plou, F.J., Fernández-Lobato, M., and Sanz Aparicio, J. (2012). Structural and kinetic insights reveal that the amino acid pair Gln-228/Asn-254 modulates the transfructosylating specificity of *Schwanniomyces occidentalis* beta-fructofuranosidase, an enzyme that produces prebiotics. *Journal of Biological Chemistry **287***, 19674-19686.

Trabajos publicados en *proceedings* no relacionados con la Tesis Doctoral:

1. Viña-González, J., **González-Pérez, D.**, Martínez, A.T., and Alcalde M. (2014). Chimeric signal peptides for the functional expression of aryl alcohol oxidase in *Saccharomyces cerevisiae*. 13th European Workshop on Lignocellulosics and Pulp (EWLP-2014)-*Proceedings*. pp 881-884. ISBN: 978-84-616-9842-4.

2. Molina-Espeja, P., **González-Pérez, D.**, Martín-Díaz, J., García-Ruiz, E., and Alcalde M. (2014). Exploring mono-oxygenase activity in mutant libraries of unspecific peroxygenase from *Agrocybe aegerita*. 13th European Workshop on Lignocellulosics and Pulp (EWLP-2014)-*Proceedings*. J.C. del Río, A. Gutiérrez, J. Rencoret and Á.T. Martínez (Eds.). pp 585-588. ISBN: 978-84-616-9842-4.

Patentes no relacionadas con la Tesis Doctoral:

1. Pita, M., Lopez de Lacey, A., Alcalde, M., Mate, D.M., **Gonzalez-Perez, D.**, and Shleev, S. (2014). Uses of laccases for water splitting. Spanish application number: PCT/ES2015/070285.

2. Alcalde, M. Molina-Espeja, P., Garcia-Ruiz, E., **Gonzalez-Perez, D.**, Ullrich, R., and Hofrichter, M. (2014). Unspecific peroxygenase with monooxygenase activity. PCT/ES2014/070113.

3. Alcalde, M., Maté, D., **González, D.**, Pita, M., López, A., Ludwig, R., and Kittl, R. (2013). High-redox potential laccase functional in blood by directed evolution, obtention methods and its applications. Spanish application number: P201330222.

Trabajos presentados en congresos no relacionados con la Tesis Doctoral:

1. Molina-Espeja, P., García-Ruiz, E., **Gonzalez-Perez, D.**, M. Mate, D., Ma, S., Ullrich, R., Hofrichter, M., Ludwig, R., and Alcalde, M. (2015). "Directed evolution of unspecific peroxygenase from *Agrocybe aegerita*". 12th International Symposium on Biocatalysis and Biotransformations (BIOTRANS). Jul, 26 – 30. Vienna (Austria).

2. Viña-Gonzalez, J., **Gonzalez-Perez, D.**, Ferreira, P., Martínez, A.T., and Alcalde, M. (2015). "Chimeric signal peptides for the focused-directed evolution of aryl alcohol oxidase from *Pleurotus eryngii*". 12th International Symposium on Biocatalysis and Biotransformations (BIOTRANS). Jul, 26 – 30. Vienna (Austria).

3. **Gonzalez-Perez, D.**, Molina-Espeja, P., García-Ruiz, E., Mate, D.M., Viña, X., Martín, J., Gomez, B.J., Vicente A.I., Mateljak, I., Ballesteros, A.O., and Alcalde, M. (2014). "Directed evolution of the ligninolytic consortium". 4th International conference on Novel Enzymes. Oct, 14 – 17. Gant (Belgium).

4. Viña-González, J., **González-Pérez, D.**, Martínez, Á.T., and Alcalde, M. (2014). "Chimeric signal peptides for the functional expression of aryl alcohol oxidase in *Saccharomyces cerevisiae*". 13th European Workshop on Lignocellulosics and Pulp (EWLP-2014). Jun, 24 – 27. Seville (Spain).

5. Molina-Espeja, P., **González-Pérez, D.**, Martín-Díaz, J., García-Ruiz, E., and Alcalde, M. (2014). "Exploring monooxygenase activity in mutant libraries of unspecific peroxygenase from *Agrocybe aegerita*". 13th European Workshop on Lignocellulosics and Pulp (EWLP-2014). Jun, 24 – 27. Seville (Spain).

6. Viña-González, J., **González-Pérez, D.**, and Alcalde, M. (2014). "Laboratory evolution platform for aryl alcohol oxidase in *Saccharomyces cerevisiae*". 3rd Multistep Enzyme Catalyzed Processes Congress (MECP14). Jun, 7 – 10. Madrid (Spain).

7. Molina-Espeja, P., **Gonzalez-Perez, D.**, and Alcalde, M. (2014). "Engineering the unspecific peroxygenase, a wide reaction range biocatalyst, by directed evolution". 3rd Multistep Enzyme Catalyzed Processes Congress (MECP14). Jun, 7 – 10. Madrid (Spain).

8. Martín-Díaz, J., García-Ruiz, E., Molina-Espeja, P., **González-Pérez, D.**, Gómez-Fernández, B.J., and Alcalde, M. (2014). "Exploring substrate promiscuity of Unspecific Peroxygenase from *Agrocybe aegerita* by neutral genetic drift". 3rd Multistep Enzyme Catalyzed Processes Congress (MECP14). Jun, 7 – 10. Madrid (Spain).

9. Santos-Moriano, P., Gomez, B.J., Martin-Diaz, J., Melchor, B., **Gonzalez-Perez, D.**, Molina, P., Viña-Gonzalez, J., Rodriguez-Colinas, B., Garcia-Ruiz, E., Mate, D.M., Fernandez-Arrojo, L., Torres-Salas, P., Plou, F.J., Alcalde, M., and Ballesteros, AO. (2013). "The Applied Biocatalysis Group at CSIC: activities in the field of bioenergy". CSIC-IMDEA workshop focused in the R&D+i technologies in the field of energy at the Madrid Region. Oct, 17. Móstoles (Spain).

10. Ballesteros, A.O., Plou, F.J., Alcalde, M., Fernandez-Arrojo, L., Torres-Salas, P., Rodriguez-Colinas, B., Garcia-Ruiz, E., Mate, D.M., Lozano, R., **Gonzalez-Perez, D.**, Molina, P., Sandoval, G., and Santos, P. (2012). "Applications of biocatalysts in sustainable chemistry. Directed evolution and semi-rational approaches". 6th International Congress on Biocatalysis (Biocat). Sep, 2 – 6. Hamburg (Germany).

11. Molina-Espeja, P., Garcia-Ruiz, E., **Gonzalez-Perez, D.**, Mate, D.M., and Alcalde, M. (2012). "Directed evolution of α-factor prepro-leader fusion genes for functional expression in *Saccharomyces cerevisiae*". 2nd Multistep Enzyme-Catalyzed Processes 2012. Apr, 10 – 13. Graz (Austria).

12. Gutiérrez-Alonso, P., Linde, D., Fernández- Arrojo, L., Rodríguez-Colinas, B., Álvaro-Benito, M., de Abreu, M., **Gónzalez-Pérez, D.**, Estévez, M., Plou, F.J., and Fernández-Lobato, M. (2010). "Production of prebiotic oligosaccharides using extracellular glycosyl hydrolases from non-conventional yeasts". 5th International Meeting on Biotechnology – Biotec2010. Sept, 29 – Oct, 1. Pamplona (Spain).

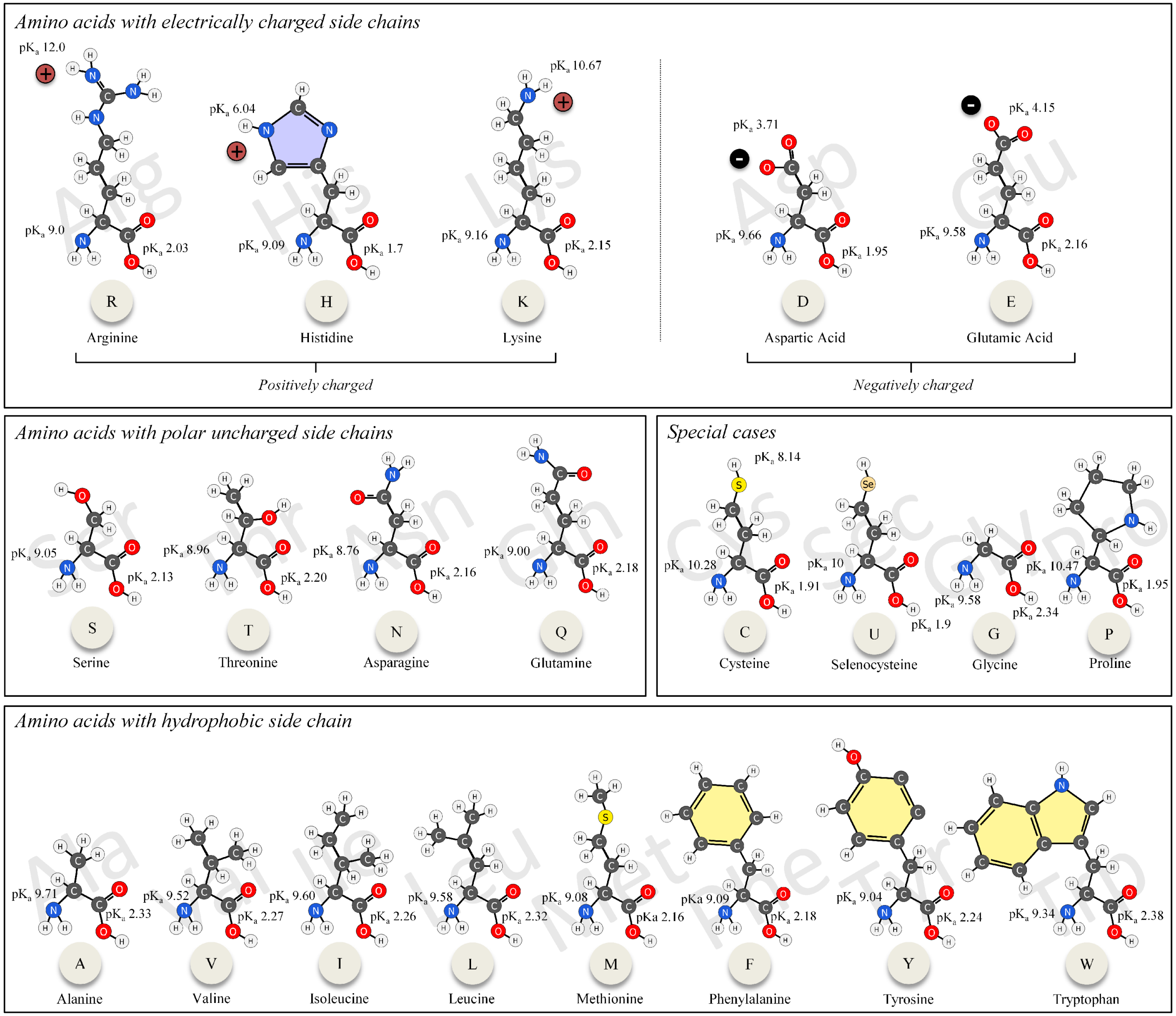

Table 1. Chemical properties of the twenty-one amino acids.

THE GENETIC CODE